

SELECTIVE CHEMISTRY TO IMPROVE ORGANIC CHEMISTRY AND DRUG
DISCOVERY

A DISSERTATION
SUBMITTED TO THE FACULTY OF
UNIVERSITY OF MINNESOTA
BY

Joseph Anthony Buonomo

IN PARTIAL FULFILLMENT OF THE REQUIREMENTS
FOR THE DEGREE OF
DOCTOR OF PHILOSOPHY

ADVISER: Prof. Dr. Courtney C. Aldrich

August 6, 2018

Acknowledgments

The following dissertation may be the culmination of my individual work during my graduate career, but that does not mean that others had no role in the development of this thesis. I would foremost like to thank the people that have allowed me to keep some semblance of sanity during these trying times, with special thanks to my wife, Tatyana Dyndikova, whom still tolerates me for reasons which I am unsure.

I also must thank my family, in particular my parents Emily T. DeMasi, Joseph Buonomo IV, and George Michael (no, not from “Wham!”) who have been supportive of my endeavors thus far. I probably would not have placed such on my education had it not been for them.

I also want to thank the friends I have made along the way, some of which I have had the pleasure of working with. In no particular order, I would like to thank Dr. Cody J. Lensing, Christopher R. Seiler, The Eiden clan (there are a lot of them), John R. Schultz, Dmitri E. Konorev, Erick J. Carlson, Malcolm S. Cole, Peter Larson, Evan M. Alexander, Dr. Skye Doering, Dr. Jacob R. Petersburg, Kellan T. Passow, Sara Coulop, Ozgun Kilic, Denise Casemore, Matthew Bockman, H. Trent West, Brittany and Luis Argueta, Johnny and Dave Nguyen, Buddy Ng, Dr. Kristen Stoltz, Kaja Rožman, and Justin “Koz” Koskovich. All of you have ensured that Minnesota is a very warm place, even if the weather doesn’t want that to be true.

I of course have to also thank my mentors throughout this entire process. In particular, I must thank my advisor Prof. Dr. Courtney C. Aldrich, without whom, I would not have had the enormous amounts of opportunities that I was granted during my studies. He gave me quite the wide berth to explore what I wanted, and to develop as an independent researcher. With his guidance I was also able to make a greater impact on my community, even on the global scale. Without his recognition of a plan that enabled my success, I would not have thrived as I have, and would likely have stalled in my growth.

I also have to thank Prof. Dr. Anthony “Tony” D. Baughn for countless hours of discussion concerning drug design/development for *M. tuberculosis* and forging a strong relationship with a collaborator’s student. Our discussions have been among the most important in terms of my development as an independent researcher at the interface of allied sciences.

I must also thank my committee members Prof. Dr. Barry C. Finzel, Prof. Dr. Carston R. Wagner, and Prof. Dr. Erin E. Carlson for their guidance during these proceedings and for taking the time to serve on my committee. Additionally, I’d like to thank my other mentors who have not served me in any sort of official capacity, namely Prof. Dr. Daniel A. Harki (University of Minnesota), Prof. Dr. David M. Ferguson (University of Minnesota), Prof. Dr. Daniel J. Weix (University of Wisconsin-Madison),

and Prof. Dr. Daniel A. Everson (California State University-Chico) without whom, I would not even have had the opportunity to thrive at the University of Minnesota.

I wish to thank the members of the Aldrich and Baughn groups, whom have been a large resource for discussion related to research and have kept me coming to work even when nothing was going right. Again, in no particular order I wish to thank Dr. Ce Shi, Dr. Feng Liu, Dr. Zheng Liu, Dr. Alvin S. Kalinda, Dr. Kishore Viswanathan, Dr. Ben Duckworth, Dr. William Fiers, Dr. Yang Li, Scott I. Brody, Malcolm S. Cole, John R. Schultz, Evan M. Alexander, Matthew R. Bockman, Dr. Yusuke Minato, Shannon L. Kordus, Joshua S. Thiede, Nicolas A. Dillon, and Michael Howe. I do wish to especially thank Dr. Surendra Dawadi for his years of mentorship and tolerance of all of my questions. I also have to thank Dr. Jennifer McCurtain, Kelsey Binder, and Prof. Dr. Ryan C. Hunter for their willingness to tolerate me as they showed me the ways of performing microbiological experiments, and their permission to use their resources.

In addition to those previously listed, I must thank my undergraduate mentees that I had during my tenure. Both, Christopher D. Brown and Kathleen J. Wang, contributed massively to success of my research and I am indebted to them for the willingness to participate in chemical research with me, even without an initial incentive to join the lab. These two individuals are certainly my peers and while I taught them things, they certainly taught me as well, a service for which I am highly grateful.

Last, but certainly not least, I have to thank my friend and co-conspirator Dr. Carter G. Eiden. Carter pushed me to exceed the limits of my mental capacity, and was the driving force behind a lot of my success. Without him, many of the pages in this manuscript would be blank, and the progress that was made would be severely diminished. He served as generator of ideas, a shoulder to lean on, de-facto captain of the soccer team, and as a mentor. His brilliance helped drive many of the works you will be reading about in this text.

Dedication

This dissertation is dedicated to my wife, Mrs. Tatyana Dyndikova. Я люблю тебя.

Abstract

Selectivity in both organic and medicinal chemistries represents the pinnacle of these scientific fields. The ability to do exactly as one intends in the most efficient manner facilitates a limited negative impact technology may impart in the environments in which it acts. As such, during these dissertation studies, I have endeavored to design new selective reactions to enable the most streamlined synthesis of organic molecules that may impart a variety of functions while simultaneously working to rationally create new drug substances that limit side effects in the patient, while also protecting the molecule from the harsh environment of an organism.

To briefly summarize the material contained herein, the first chapter comprises of the technologies I have developed for better enabled organic synthesis. These reactions can improve green chemistry initiatives to limit the negative impact on the environment, only possible because of the highly selective nature of these reactions. I expect these technologies should enable chemists who design molecules with many intended purposes, although they were designed with the intent of empowering medicinal chemists.

The second chapter of this work covers highly collaborative efforts to design improved chemotherapeutics in an effort to eradicate Tuberculosis, the leading cause of infectious disease mortality worldwide. These molecules range from selective pro-drugs that are released at the site of action by utilizing a selective targeting pro-moiety to rationally designed agents to take advantage of biological mechanism knowledge. These molecules can potentially be drugs in themselves while they certainly inform future endeavors to make new drug materials to combat Tuberculosis.

Table of Contents

Abstract	iv
Table of Contents	v
LIST OF TABLES	vi
List of Figures	xi
List of Schemes	xix
List of abbreviations	22
Preface.....	23
I. The development of chemoselective reactions through rational reagent design	26
1.1 Introduction.....	26
1.2 Development of a Catalytic Mitsunobu Reaction.....	37
1.3 Mechanistic insight provides a means to rational reagent design.....	51
1.4 Scalable preparation of hydrido-disiloxanes.....	116
1.5 Characterization of 1,3-diphenyl-disiloxane as a chemoselective reducing agent.....	122
1.6 1,3-Diphenyl-disiloxane as a multi-functional organic reducing agent.....	168
1.7 Concluding remarks	181
1.8 Methods and materials	183
II. Rationally Designed Medicinal and Chemical-Biological agents with intentional Selectivity Profiles	345
2.1 Introduction.....	345
2.2 Targeted drug delivery with a β -lactam prodrug approach	352
2.3 A paradigm shift for the design of analogs of antitubercular drug pyrazinamide	379
2.4 Rational design of a pan-acting nucleophilic probe for the characterization of the PLP-dependent proteome.....	406
2.5 Concluding remarks	433
2.6 Methods and materials	436
References.....	473
Appendix I: NMR	481
Appendix II: Coordinate outputs	576

LIST OF TABLES

Table 1.1. Development of conditions for the catalytic Mitsunobu in phosphine.....	42
Table 1.2. The effect of p-nitrobenzoic acid on the reduction of the phosphine precatalyst 1PPO. ^l	45
Table 1.3: The substrate scope of the catalytic Mitsunobu reaction.....	47
Table 1.4. The initial optimization of silane concentration in the catalytic Mitsunobu reaction.....	50
Table 1.5. Comparison of precatalyst reductions by phenylsilane at 80 °C.	54
Table 1.6. Calculated Mulliken charges of phosphine oxide precatalysts.....	55
Table 1.7. Numerical comparison between single- and double-exponential fitting of reduction curves.....	58
Table 1.8. Comparison of phosphacycle P-oxides reductions by DPDS at 25 °C.....	67
Table 1.9. Rate constants obtained through simulation.....	75
Table 1.10. Calculated Mulliken charges of silane materials.....	89
Table 1.11. Hydrogen-bonding between diphenylsilanediol and TPPO monitored by ³¹ P NMR.....	94
Table 1.12. The effect of temperature on additive studies.....	95
Table 1.13. The calculated energies and geometries of PCs with TPPO at the M06-2X level of theory.....	106
Table 1.14. The ³¹ P NMR shifts resultant upon additive addition.....	108
Table 1.15. The calculated global electronic parameters for silane materials.....	113

Table 1.16. The calculated global electronic parameters for phosphine oxide materials.	114
Table 1.17. The Direct Synthesis of Symmetrical Disiloxanes from Commercially- Available Silanes.	120
Table 1.18. The Optimization of Additive-Free Phosphine Oxide Reductions with DPDS.	126
Table 1.19. Solvent Screen of Phosphine Oxide Reductions at 110 °C.	127
Table 1.20. The Substrate Scope of Additive-Free Reductions of Phosphine Oxides by DPDS.	134
Table 1.21. Reductions of TPPO with DPDS and BNPA at 110 °C.	137
Table 1.22. Reductions of TPPO with DPDS and BNPA at 23 °C.	138
Table 1.23. DPDS-Mediated Reductions of Acyclic Phosphine Oxides at Ambient Temperature.	139
Table 1.24. Optimization of Additive-Free Catalytic Wittig Reactions with Stabilized Ylides at Ambient Temperature.	143
Table 1.25. Substrate Scope of Additive-Free Catalytic Wittig Reactions at Ambient Temperature	145
Table 1.26. Substrate Scope of Additive-Free Catalytic Appel Reactions at Ambient Temperature.	150
Table 1.27. Optimization of the catalytic Staudinger reduction with 1PPO.	152
Table 1.28. Substrate Scope of Additive-Free Catalytic Staudinger Reductions at Ambient Temperature.	153

Table 1.29. Substrate Scope of Additive-Free Catalytic Staudinger Reductions at Ambient Temperature Utilizing TPP as the Catalyst.....	155
Table 1.30. Observed Rate Constants for the Silane-Mediated Reduction of XX under Pseudo First-Order Conditions. ^a	158
Table 1.31. Optimization of catalytic Wittig reactions with TPP catalysis.....	164
Table 1.32. Substrate scope of catalytic Wittig reactions utilizing triphenylphosphine.	166
Table 1.33. Optimization of the reduction of tertiary carboxamides.....	174
Table 1.34. Optimization of the reduction of secondary carboxamides.	175
Table 1.35. Substrate scope of the reduction of tertiary carboxamides.....	177
Table 1.36. Substrate scope of the reduction of secondary carboxamides.	178
Table 1.37. Preliminary substrate scope of DPDS-mediated amine alkylation.....	180
Table 1.38. Numerical comparison between single- and double-exponential fitting of reduction curves.....	207
Table 1.39. Silane Competency Screen in Catalytic Mitsunobu Reactions.....	218
Table 1.40. Computed Mulliken charges of acyclic phosphine oxides.	227
Table 1.41. Rate constants for the reduction of acyclic phosphine oxides.....	229
Table 1.42. Stoichiometry of additives affects downfield shift in ³¹ P NMR spectra. ...	239
Table 1.43. Interactions of TPPO with miscellaneous organic molecules.	241
Table 1.44. Rate constants obtained through simulation.....	246
Table 1.45. The computed structures of silane materials studied in this report.....	265
Table 1.46. The computed structures of phosphine oxides studied in this report.....	267

Table 1.47. The calculated energies and geometries of PCs with TPPO at the B3LYP level of theory.....	274
Table 1.48. Comparison of Yields for the Synthesis of 2a when Different Balls are Employed.....	285
Table 1.49. Testing Different Sources of Ti(OiPr) ₄ . (Values Shown are % Completion).	293
Table 1.50. Silane Equivalence Screen Isolated After 16 h.....	299
Table 1.51. Silane Equivalence Screen Isolated After 24 h.....	300
Table 1.52. Silane Equivalence Screen in TBAC.....	303
Table 1.53. The reaction of 4-(trifluoromethyl)benzyl alcohol and DPDS or phenylsilane with or without benzoic acid additives.	310
Table 1.54. Catalytic and Stoichiometric Staudinger Ligation Reactions.....	336
Table 1.55. Silane dependent amide bond formation.	338
Table 2.1. The minimum inhibitory concentrations (MIC ₉₀) of compounds against Mycobacteria.....	363
Table 2.2. The MIC ₉₀ of our compounds.....	366
Table 2.3. The stability of conjugate 1 in different media as detected using LC-MS. ...	376
Table 2.4. The minimum inhibitory concentrations (MICs) of compounds against M. tuberculosis.	396
Table 2.5. The MS parameters used to detect and quantify analytes in MS experiments.	449

Table 2.6. The MS parameters used to detect and quantify analytes in MS experiments.
..... 462

List of Figures

Figure 1.1. The diversity of silane functional groups and their use as materials in organic chemistry.....	27
Figure 1.2. The classical Wittig Olefination and its catalytic counterpart using strained phosphorus heterocycles.	30
Figure 1.3. Examples of catalytic redox recycling reactions.	31
Figure 1.4. NMR spectra of selective silane reactivity.....	43
Figure 1.5. The reduction of strained phosphorus heterocycles by PhSiH ₃ at 80 °C.....	55
Figure 1.6. The single and double exponential fittings for reduction progress curves observed for the reduction of phosphine oxide precatalysts with PhSiH ₃	57
Figure 1.7. The fitting (A) and derivative (B) curves of 1PPO (left, purple), TMPPPO (center, green), and TMBPO (right, blue).....	59
Figure 1.8. The proposed kinetic mechanisms for the reduction of phosphine oxides by PhSiH ₃	61
Figure 1.9. The A) Observed reduction of TMPPPO under pseudo first order conditions with PhSiH ₃ ; B, C, D) Fitting of raw data; E) Observed reduction times to 50% and 90% completion.....	62
Figure 1.10. The reduction of phosphine oxide precatalysts with DPDS at 25 °C.....	66
Figure 1.11. The comparison of rate of reduction vs. the concentration of DPDS employed in the reduction of TPPO at 110 °C.	69
Figure 1.12. Eyring plot of the silane-mediated reduction of TMPPPO with DPDS over the temperature range of 0 – 25 °C.....	70

Figure 1.13. The Eyring plot of the silane-mediated reduction of TPPO with DPDS over the temperature range of 80 – 120 °C.	71
Figure 1.14. Graphical comparison of reaction progress curves (Figure 1.5B) and the fit obtained by the indicated parameters.....	74
Figure 1.15. The comparison of the reduction of with 1PPO no changes to the conditions in Figure 1.5 (purple, circles), phosphorus preheating (green, squares), and silane preheating (blue, triangles).	79
Figure 1.16. Reductions of 1PPO by PhSiH ₃ with or without Lewis acid additives.	83
Figure 1.17. The water cycle in PhSiH ₃ -mediated phosphine oxide reductions.....	86
Figure 1.18. Comparisson of the reduction of 1PPO by common silane reducing agents under pseudo first-order condtions at 80 °C.	88
Figure 1.19. The reduction of 1PPO by TMDSO (red) and TMDSA (blue) at 80 °C.....	91
Figure 1.20. An example of observed downfield NMR shifts in ³¹ P NMR experiments with additives.....	96
Figure 1.21. The effect of excess water on the observed rate of phosphine oxide reduction by silanes.....	97
Figure 1.22. The Hammett plot for the reduction of acyclic phosphine oxides by DPDS at 110 °C.	99
Figure 1.23. The kinetic isotope effect for the reduction of phosphine oxides with proteo- and deuterio-DPDS at 110 °C.	100
Figure 1.24. The reduction of TMPPO with <i>Si</i> , <i>Si</i> -diphenylsilannes at 80 °C.	102

Figure 1.25. The optimized PC of TPPO with A) PhSi(OH)H ₂ and B) PhSiH ₃ at the M06-2X level of theory.	105
Figure 1.26. The reduction of 1PPO using TMDSO and additives at 80 °C. A) With Brønsted acid additives; B) With Lewis acid additives.	109
Figure 1.27. The comparison of the computed nucleophilicity index at the M06-2X/6-31+G(d,p) level of theory and the reduction of phosphine oxides. A) Acyclic phosphine oxides (Figure 1.22); B) Current and previously reported phosphine oxides incorporating cyclic and acyclic phosphine oxide reagents.	115
Figure 1.28. Reaction progress curves of the reduction of TPPO, monitored by ³¹ P NMR, comparing Lemaire's system ²⁹ (blue), Beller's system ²⁵ (red), and 1.25 equiv DPDS (green).	129
Figure 1.29. Arrhenius analysis of the reduction of TPPO with DPDS over the temperature range of 80 – 120 °C.	131
Figure 1.30. The silane-mediated reduction of DIAD as conferred by the reactivity with a phosphine, leading to an unproductive catalytic Mitsunobu protocol.	148
Figure 1.31. The average reduction of BTPI with PhSiH ₃ (blue, circles) and DPDS (red, squares) under pseudo first-order conditions as monitored with ³¹ P NMR at 45 °C.	157
Figure 1.32. The Eyring plot for the reduction of BTPI with DPDS over a temperature range of 23 – 70 °C.	160
Figure 1.33. The average reduction of BTPI with DPDS at even stoichiometries at 23 °C as determined with ³¹ P NMR.	162

Figure 1.34. Representative stacked plot of ^{31}P NMR spectra obtained during a typical reduction experiment. Shown is the stacked plot of the reduction of 5PDBPO with 30 equiv PhSiH_3 at 70 °C.....	193
Figure 1.35. Progress curves of phosphine oxide reductions with phenylsilane at 25 °C.	210
Figure 1.36. Progress curves of the reduction of TMPPPO with DMDPDS at 80 °C in THF and toluene.	216
Figure 1.37. The Arrhenius plot for the reduction of TMBPO by DPDS over the temperature range 0 – 25 °C.	221
Figure 1.38. The reduction of TPPO with DPDS at 110 °C.	224
Figure 1.39. The reaction progress curves of reductions used to generate the Hammett plot in Figure 1.22.	228
Figure 1.40. Graphical comparison of reaction progress curves (Figure 1.5) and the fit obtained by the indicated parameters.....	247
Figure 1.41. A) The LC-MS trace of the reduction of S4 with TMDSO and 10 mol% $\text{Ti}(i\text{PrO})_4$, and B) The LC-MS trace of the reduction of S4 with DPDS.....	259
Figure 1.42. The comparison of silane nucleophilicity index (N) and empirically-determined initial rates of reduction with TMPPPO.....	270
Figure 1.43. The comparison of phosphine oxide nucleophilicity index (N) to empirically-observed initial rates of reduction with 5-membered phosphine oxides.....	271
Figure 1.44. The optimized PC of TPPO with A) $\text{PhSi}(\text{OH})\text{H}_2$ and B) PhSiH_3 at the B3LYP level of theory.	275

Figure 1.45. Preparation of DPDS; A) Metal balls used in the reaction, B) Formation of the active copper complex, C) Addition of phenylsilane, D) Reaction complete, E) Filtration apparatus with ice in the receiving flask.	279
Figure 1.46. The condition of used Chrome-Iron balls after one use (left) and after two uses (right).	283
Figure 1.47. Single-exponential fitting of reductions of TPPO with DPDS.	295
Figure 1.48. Arrhenius plot for TPPO showing the activation energy.	297
Figure 1.49. A) No reactivity of 3-(trifluoromethyl)-benzoic acid and phenylsilane is noted at 1.5 h, 17.5 h, or 40.5 h; B) Reactivity of 3-(trifluoromethyl)-benzoic acid and DPDS is not noted at 1.5 h or 17.5 h, however, reactivity is noted at 40.5 h.	307
Figure 1.50. The reaction of 4-(trifluoromethyl)-benzyl alcohol and DPDS at 23 °C monitored until 42 h; B) The reaction of 4-(trifluoromethyl)-benzyl alcohol, <i>p</i> -nitrobenzoic acid, and DPDS at 23 °C monitored until 42 h.	311
Figure 1.51. A) The reaction of 4-(trifluoromethyl)-benzyl alcohol and phenylsilane at 80 °C monitored until 40.5 h; B) The reaction of 4-(trifluoromethyl)-benzyl alcohol, 3-(trifluoromethyl)-benzoic acid, and phenylsilane at 80 °C monitored until 40.5 h; C) The reaction of 4-(trifluoromethyl)-benzyl alcohol and DPDS at 80 °C monitored until 40.5 h; D) The reaction of 4-(trifluoromethyl)-benzyl alcohol, 3-(trifluoromethyl)-benzoic acid, and DPDS at 80 °C monitored until 40.5 h. Large black numbers indicate the integrations of the peaks.	312
Figure 1.52. The reaction of 4-cyanobenzaldehyde and DPDS does not yield any new materials after 16.5 hours.	315

Figure 1.53. The reaction of methyl 4-nitrobenzoate and DPDS does not yield any new materials after 18 hours.....	317
Figure 1.54. The reaction of ethyl cinnamate and DPDS does not yield any new materials or isomerized materials after 16.5 hours.....	319
Figure 1.55. A) The reaction of 4-(trifluoromethyl)-benzyl azide and phenylsilane at 110 °C monitored until 21 h; B) The reaction of 4-(trifluoromethyl)-benzyl azide and DPDS at 110 °C monitored until 21 h.	321
Figure 1.55. A) The reaction of DPDS with DIAD in the presence of 3-(trifluoromethyl)-benzoic acid at 80 °C after 17 hours; B) The mixture of DPDS and diisopropyl hydrazine dicarboxylate in d8-THF.....	323
Figure 2.1. Chemotherapeutic agents with effectiveness against <i>Mtb</i> ; A) Clinically-used first line agents; B) Clinically-used reserve agents; C) Experimental agents in pre-clinical development; D) Experimental agents in development in the Aldrich Laboratory (ca. 2006-2016).	346
Figure 2.2. The extra cavity behind the 7-position of the cephalosporin bound to BlaC.	358
Figure 2.3. The potential activities of conjugate 1 in <i>Mtb</i>	368
Figure 2.4. Intracellular POA concentrations in BCG after treatment with POA and conjugate 1.	372
Figure 2.5. The intracellular acetyl CoA and malonyl CoA levels of BCG treated with POA (red) and conjugate 1 (blue) after 24 hours of treatment.	374

Figure 2.6. The BlaC-mediated release of POA from conjugate 1 without (red) and with (blue) clavulanate.....	378
Figure 2.7. The structure of pyrazinoyl CoA.....	384
Figure 2.8. Compounds synthesized via the route illustrated in Scheme 2.9.	390
Figure 2.9. The HRMS traces and mass signatures for synthetically-derived 3 (top) and cellular lysates from <i>Mtb</i> treated with POA (bottom) as detected using ESI in negative mode.....	393
Figure 2.10. The detected metabolite of POA in PZA-treated <i>Mtb</i> cellular lysates using HRMS-ESI in positive mode.	394
Figure 2.11. The assay and detection method using waning signal at 340 nm for PncA activity (top) and Michaelis-Menten curves for heteroaromatic carboxamides (bottom).	398
Figure 2.12. The binding pocket within the active site of PncA as modeled by Evan Alexander.....	400
Figure 2.13. The raw areas of POA detected in <i>Mycobacterium</i> treated with vehicle (control), PZA, POA, and 3 at 250 μ M.	403
Figure 2.14. The raw areas of CoA and acetyl CoA upon treatment of vehicle (control), titration of POA, and 3.....	404
Figure 2.15. The raw areas of pantothenate upon treatment of vehicle (control), titration of POA, and 3.....	405
Figure 2.16. The mechanism of PLP-dependent racemase Alanine racemase (Alr).	412

Figure 2.17. The proposed nitrono-quinoid intermediate formed between a modified <i>N</i> -hydroxy amino acid and PLP.....	415
Figure 2.18. The coupled assay used to assess the activity of CDB-I-143 against BioA.	418
Figure 2.19. The degree of inhibition and secondary plots used to determine the specificity constant of CDB-I-143.....	420
Figure 2.20. Time and concentration dependent inhibition of IlvE with JAB11P118. ..	429
Figure 2.21. The selective labeling of IlvE by JAB11P118 with and without a competitive inhibitor.....	430
Figure 2.22. The selective labeling of an IlvE overexpression strain in <i>E. coli</i> using varying concentrations of JAB11P118.....	432
Figure 2.23. The HPLC method used to separate and detect analytes in purified and lysate samples.....	443
Figure 2.24. The zoomed-in trace chromatogram of POA and <i>d</i> ₃ -POA using the Eclipse XDB-C8 column at 0.5 mL/min flowrate using the method defined in Figure 2.23.....	445
Figure 2.25. The HPLC method used to detect analytes with a DAD dection system. ..	447
Figure 2.26. The HPLC method used to quantify POA only in BlaC release assays.	453
Figure 2.27. A sample chromatogram for the detection of POA using the method described in this section.	454
Figure 2.28. The standard curve of MS/MS experiments for POA.	457

List of Schemes

Scheme 1.1. Phenylsilane-mediated reductions of phosphine oxides via Marsi's [2+2] transition state.	33
Scheme 1.2. The Proposed Catalytic Mitsunobu Reaction.....	39
Scheme 1.3. Synthesis and identification of cyclic phosphine oxide precatalysts.	52
Scheme 1.4. Synthesis and equilibrium of DPDS.....	65
Scheme 1.5. The mechanism of phenylsilanol generation using oxyanionic additives (top) and the mechanism of phenylsilanol generation with carboxylate additives as proposed by Denton and co-workers (bottom).....	81
Scheme 1.6. The amended transition state theory to account for our and others' observations.	92
Scheme 1.7. Putative reactivity and transition states of MDPS (top), diphenylsilane, and TPDS (bottom) with phosphine oxides.....	103
Scheme 1.8. The amended mechanistic proposal for the reduction of phosphine oxides by TMDSO/Ti(IV) reduction systems.	111
Scheme 1.9. Synthesis of hydrido-disiloxane materials from literature and this work. .	118
Scheme 1.10. The silane-mediated reduction of phosphine oxides from this and previous work.	124
Scheme 1.11. The domino synthesis of trivalent phosphines from secondary phosphine oxide DPPO.	141

Scheme 1.12. A) A generalized catalytic Mitsunobu reaction ^{REF} ; B) The desired catalytic Mitsunobu reaction (blue) utilizing phenylsilane and undesired premature reduction (red) promoted by DPDS.	147
Scheme 1.13. The literature proposed mechanisms of hydrogen atom transfer reactions.	170
Scheme 1.14. The reduction of acyclic phosphine oxides with DPDS.	226
Scheme 1.15. (A) The reduction of S4 with ring opening of the cyclopropyl side-chain with the phosphorus-centered radical as proposed by Lemaire and co-workers. ²⁹ (B) The reduction of S4 without a phosphorus-centered radical, consistent with our observations.	257
Scheme 1.16. The mechanism of titanium-catalyzed reductions of phosphine oxides with TMDSO. This scheme specifically states the reports where various intermediates have been observed.	261
Scheme 2.1. The <i>de novo</i> and salvage biosynthetic pathways for NAD ⁺ /NADH.	349
Scheme 2.2. The mechanism of PncA activation of nicotinamide/PZA to active metabolites nicotinic acid/POA.	350
Scheme 2.4. The semi-synthetic route of conjugate 1 from commercially-available 7-aminocephalosporanic acid.	360
Scheme 2.5. The Δ 2, 3 isomerization of compound 1 under basic conditions.	361
Scheme 2.6. The <i>de novo</i> biosynthetic pathway of Coenzyme A.	365
Scheme 2.7. The CoA biosynthetic pathway showing the <i>de novo</i> and salvage (starting with pantetheine) pathways.	382

Scheme 2.8. A) The half reactions catalyzed by CoaBC; and B) Proposed activation of POA by CoaBC.....	386
Scheme 2.9. The synthesis of new pyrazinoyl amide compounds.....	389
Scheme 2.10. The synthesis of CDB-I-143.	416
Scheme 2.11. The originally proposed route towards a 2 nd generation ABP for PLP-dependent enzymes.	423
Scheme 2.12. The attempted synthesis of a 2 nd generation ABP for PLP-dependent enzymes.....	425

List of abbreviations

HAT: Hydrogen atom transfer	EPR: Electron Paramagnetic Resonance
M1PPO: 3-Methyl-1-phenylphospholane-1-oxide	Mtb: <i>Mycobacterium tuberculosis</i>
TS: Transition state	TB: Tuberculosis
DFT: Density functional theory	FDA: Food and drug administration
TPPO: Triphenylphosphine oxide	RIF: Rifampicin
CWR: Catalytic Wittig Reaction	INH: Isoniazid
PMHS: Polymethyl hydrosiloxane	EMB: Ethambutol
TMDSO: 1,1,3,3-Tetramethyl-disiloxane	PZA: Pyrazinamide
5PDBP: 5-Phenyl dibenzophospole	POA: Pyrazinoic acid
1PPO: 1-Phenylphospholane-1-oxide	SAR: Structure activity relationship
5PDBPO: 5-Phenyl dibenzophospole-5-oxide	TFA: Trifluoroacetic acid
TPP: Triphenylphosphine	CoA: Coenzyme A
TMPPPO: 2,2,3-Trimethyl-1-phenylphosphetane-1-oxide	MS/MS: Tandem mass spectrometry
TMBPO: 2,2,3-Trimethyl-1 <i>n</i> -butyl-phosphetane-1-oxide	BCG: <i>Mycobacterium bovis</i> strain BCG
TMPyrPO: 2,2,3-Trimethyl-1-pyrolidyl phosphetane-1-oxide	EDC: <i>N</i> -Ethyl-(dimethylaminopropyl)-carbodiimide
THF: Tetrahydrofuran	TEA: Triethylamine
DMF: <i>N, N</i> -Dimethyl formamide	DIPEA: Di- <i>iso</i> -propylethylamine
DPDS: 1,3-Diphenyl-disiloxane	HRMS: High-resolution mass spectrometry
PNBA: <i>p</i> -Nitro benzoic acid	ESI: Electrospray ionization
BNPA: Bis-(<i>p</i> -nitrophenyl)-phosphoric acid	MIC: Minimum inhibitory concentration
TMDSA: 1,1,3,3-Tetramethyl-disiloxazide	ABPP: Activity-based protein profiling
TPDS: 1,1,3,3-Tetraphenyl-disiloxane	FAAH: Fatty acid amide hydrolase
MDPS: Methyl diphenylsilane	ABP: Activity-based probe
DHDS: 1,3-Di- <i>n</i> -hexyl-disiloxane	MBI: Mechanism-based inhibitor
DMDPDS: 1,1,3,3-Dimethyl-diphenyl-disiloxane	PLP: Pyridoxal-L-phosphate
DPPO: Diphenylphosphine oxide	DCS: D-Cycloserine
DTBPO: Di- <i>tert</i> -butylphosphine oxide	DAPA: Diaminopelargonic acid
DTBP: Di- <i>tert</i> -butylphosphine	PAL: Photo-affinity label
DIAD: Di- <i>iso</i> -propyl azo dicarboxylate	TAMRA: 5-Carboxytetramethylrhodamine
BTPI: <i>N</i> -Benzyl-1,1,1-triphenyl- λ^5 -phospanimine	IPTG: Isopropyl- β -D-1-thiogalactopyranoside
DEMS: Diethoxymethylsilane	DAD: Diode-array detector
MTHF: 2-Methyl tetrahydrofuran	ACN: Aceotnitrile
TLC: Thin layer chromatography	GDH: Glutamate dehydrogenase
UV: Ultraviolet	NAD: Nicotinamide adenosine dinucleotide
LCMS: Liquid chromatography mass spectrometry	ATP: Adenosine triphosphate
HPLC: High performance liquid chromatography	ADP: Adenosine diphosphate
MS: Mass spectrometry	HEPES: 4-(2-hydroxyethyl)-1-piperazineethanesulfonic acid
NMR: Nuclear Magnetic Resonance	PEP: Phophoenoyl pyruvate
	LDH: Lactate dehydrogenase
	PK: Phosphoenoyl pyruvate kinase
	TCEP: Tris-(2-carboxyethyl)-phosphine
	DTT: 1,4-Dithiothretol
	DMSO: Dimethyl sulfoxide
	PBS: Phospate-buffered saline

Preface

This document contains the majority of the technologies I have explored during the course of my PhD studies at the University of Minnesota. As such, the topics addressed herein vary greatly in their nature as the purpose of this dissertation is to report a breadth of new technologies relevant to modern medicinal chemists, especially those with a vested interest in the discovery of antibacterial chemotherapeutic agents. While a diverse array of medicinal chemistry-related topics is presented within these pages, the central focus of this work is of the importance of selectivity.

Selectivity, in both organic synthesis and drug development, represents the pinnacle of efficiency. Ideally, all technologies are developed to accomplish specific tasks with no “off-cycle” or “off-target” activities, other than those specifically sought by developers. In organic chemistry, this often manifests itself in the forms of side-product generation and reduced yields; while medicinal chemists and drug developers frequently struggle with removal of undesirable side-effects a new therapeutic may impart. During the course of these studies, I have pursued new technologies that hone in on optimal reactivity, using selectivity as a guiding principle. As such, I have been able to improve the nature of organic reactions as well as determine the effectiveness for the targeted delivery of chemotherapeutics.

Briefly, chapter 1 is the culmination of my efforts to impart selectivity into organic chemistry. I have done so by investigating the reduction of phosphine oxides by silane reductants. This reaction is important in its isolated form, enabling synthesis of di- and trivalent phosphines which have applications from medicinal chemistry to materials science. The full understanding of the mechanism of this reaction led to the creation of the

most active silane reductant recorded for this particular functional group conversion, while also having exquisite functional group tolerance. Additionally, this reagent can be also used to facilitate organocatalysis in reactions that can mediate the formation of a large variety of bonds. In particular, phosphine-redox mediated reactions represent an easy target for using our silane reductant. While these reactions are powerful, mild, and versatile, they frequently suffer from the generation of side-products that muddle purification and require the generation of a lot of waste in order to remove them. Phosphorus redox organocatalysis, powered by silane reduction for catalyst regeneration, alleviates these concerns by resulting in the regeneration of a simple-to-remove catalyst while minimizing byproduct formation. My efforts in studying phosphine oxide reductions has furthered this redox recycling research, allowing for unprecedented reactivity at ambient temperatures and efficient recycling. Our new reductant can also be used for other reductive processes, and the full scope of this reagent's utility still needs exploration.

The other major part of my thesis work has focused on trying to improve human health by designing new chemotherapeutic and chemical-biology tool compounds to understand and improve treatments for the number one pathogenic bacteria, *Mycobacterium tuberculosis*. My approaches to tackling this pathogen have been quite diverse. One approach has focused on a target-directed pro-drug approach using a cephalosporin as the pro-moiety. This pro-moiety facilitates the direct delivery of toxic warheads while taking advantage of what is typically a resistance mechanism. In fact, removal of this now "activating" enzyme results in susceptibility to the β -lactam targeting moiety as these molecules have the ability to act as dual warheads. In addition to imparting selectivity through a pro-drug strategy, I have had the opportunity to improve upon already

known drugs with natural selectivity for *M. tuberculosis*. These new molecules take advantage of the mechanism of action, which had been previously undetermined, to create a drug which circumvents the clinically-relevant resistance mechanism. Additionally, I have had the opportunity to design a molecule that is purposefully unselective. This particular strategy utilizes a warhead with ubiquitous activity across an important enzyme family, with the intended application to understand the selectivity of other drug substances that target this class of enzymes. Understanding the nature of a drug's selectivity can help rational drug design campaigns, while predetermining off-target effects for a particular molecule. This probe will be particularly useful in the design of therapies for a multitude of pathologies in addition to informing discovery/optimization of antitubercular chemotherapeutics.

All in all, this document recounts successes and failures in these endeavors. There will be more to each of these studies and I am proud that others in our lab are interested in carrying out more experiments for these stories. As such, for some of these projects, I am reporting what we have initially discovered with the hope of informing future campaigns. Within this text is also described the logic that facilitated rapid developments in reagent/drug optimization, much of which has to be excluded from peer-reviewed manuscripts due to space constraints.

I. The development of chemoselective reactions through rational reagent design

The material reproducing data, figures, and text from previously published manuscripts have been done so with permission from Georg Verlag Thieme and John Wiley and Sons-VCH.

1.1 Introduction

Organic compounds containing a silicon atom come in a variety of shapes, sizes, and substitution patterns, permitting the use of such compounds in a wide array of applications. To the synthetic organic chemist, silicon-containing compounds are frequently used to reap the benefits that silicon confers with regards to chemoselectivity, ease of use, and predictable behavior. In this discipline, silicon is often encountered as silyl-hydride (R_3Si-H), siloxanes ($R_2HSi-OSiR'_3$), silyl chlorides (R_3Si-Cl), and silyl ethers ($R_3Si-OCR'_3$), although all of these compounds are referred to as silanes (Figure 1.1). Probably the most widely-utilized application of silanes comes in the form of the silyl protecting group for the alcohol.¹ Silyl chlorides are utilized in a predictive manner as deprotonated alcohols can hydrolyze the Si-Cl bond, forming a much stronger silicon oxygen bond. The silyl ether is much less reactive in the majority of organic transformations compared to the bare alcohol as the liability from the hydrogen atom with a low pK_a ² is removed. However, the remarkable thing about this functional group is that its incorporation within a molecule is reversible as treatment with highly acidic conditions or fluoride cleaves the Si-O bond.¹ This example of silane usage highlights the predictable nature of the silyl chloride's reactivity, the selectivity for modifying a hydroxyl group, which can be utilized almost ubiquitously through complex total syntheses, even being utilized in the synthesis of Palau'amine,³ one of the most complex natural products ever fully synthesized by chemists.

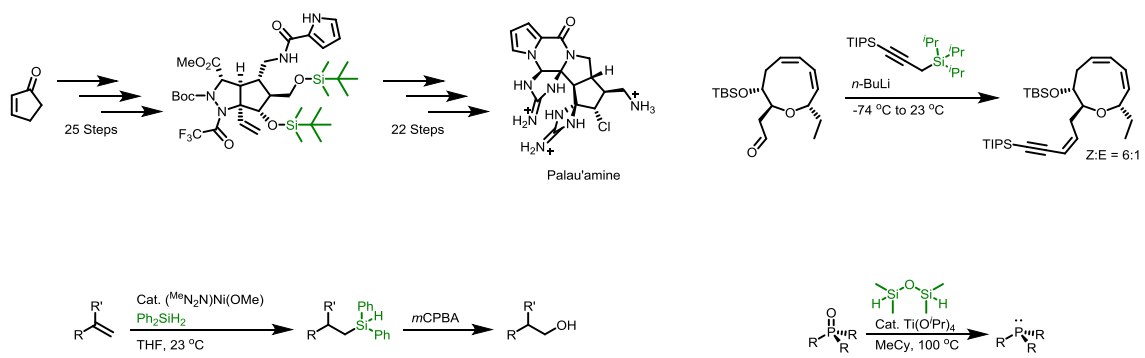


Figure 1.1. The diversity of silane functional groups and their use as materials in organic chemistry.

However, silanes containing the silyl-hydride functionality are also frequently used in synthetic organic chemistry, often finding themselves as reductants for a variety of functional groups used in many applications. Silane-mediated reductions usually occur through metal-mediated reactions⁴ or act as direct hydrogen atom transfer (HAT) reagents.⁴ These reagents have been known for their high chemoselectivity, and are capable of performing certain transformations under significantly milder conditions than other organic reducing agents (i.e. boranes), or metal hydrides (i.e. LiAlH₄). One such reaction is the reduction of phosphorus(V) oxides to phosphines, a surprisingly difficult reaction due to the strong phosphorus oxygen double bond (~110 kcal/mol⁵), however, this transformation provides a simple route to phosphorus(III) compound, called phosphines.

Phosphines are valuable reagents in synthetic organic chemistry and ubiquitous ligands in homogenous catalysis.⁶ Phosphine redox reactions including the Wittig,⁷ Staudinger,⁸ Appel,⁹ and Mitsunobu¹⁰ reactions foster a diverse array of synthetic chemistry utilizing the conversion of phosphines to phosphine oxides (P^{III} → P^V=O) as the principle thermodynamic driving force for reactivity. Despite their prominence, stoichiometric phosphine redox chemical processes lack atom economy and generate difficult-to-separate phosphine oxide waste streams. Driven by the guiding principles of sustainable chemistry, there have been significant efforts to develop catalytic redox processes to recycle phosphines or, alternatively, to design entirely new redox neutral reactions operating at either the P^{III} or P^V=O oxidation state.¹¹ For the purposes of framing the work contained herein, I will skip over the majority of the redox neutral research, as these reactions frequently lack the ease-of-use desired by today's medicinal chemists. While these processes are inherently interesting, the redox recycling approach has seemingly garnered more interest from the chemical community.

The large energy required to reduce $P^V=O$ to P^{III} presents unique challenges because typical reductants employed for this transformation ($LiAlH_4$,¹² trichlorosilane,¹³ Borohydride,¹⁴ diisobutylaluminum hydride¹⁵) are incompatible with many common functional groups.¹⁶ A key advance in the field has been the exploration of silanes exhibiting greater chemoselectivity such as phenylsilane ($PhSiH_3$)¹⁷ and diphenylsilane (Ph_2SiH_2) in conjunction with reactive, strained phosphorus heterocycles (Figure 1.2). Up until the beginnings of this work, the redox recycling approach utilizing these types of reagents had been successfully utilized in the Wittig,¹⁸ Staudinger,¹⁹ and Appel reactions,²⁰ as well as in some new synthetic applications.²¹ The catalytic Wittig reaction (CWR), the first such reaction, was pioneered by Prof. Dr. Christopher J. O'Brien utilizing the power of the selective reduction of phosphine oxides by the silane reducing agent Ph_2SiH_2 .^{18a} In his initial report, O'Brien paired the strained phosphorus heterocycle, 3-methyl-1-phenyl-phospholane-1-oxide (**M1PPO**), with diphenylsilane and heat. Both of these additions are unnecessary for typical stoichiometric Wittig reactions, with stabilized ylides, yet do not disrupt the reaction. These design criteria, were then applied more broadly with other phosphorus heterocycles to afford other redox recycling processes (Figure 1.3). However, elevated temperatures (~ 80 – 110 °C) or Brønsted acid additives are needed to achieve acceptable conversions that restrict substrate scope and have precluded widespread adoption of phosphine redox catalysis. Optimization of silane-mediated phosphine oxide reduction through semiempirical phosphine tuning and silane screening appears to have reached a plateau. We believe this is due to a dearth of advancement in terms of understanding/improving the rate-determining step, the reduction of the phosphine oxide.

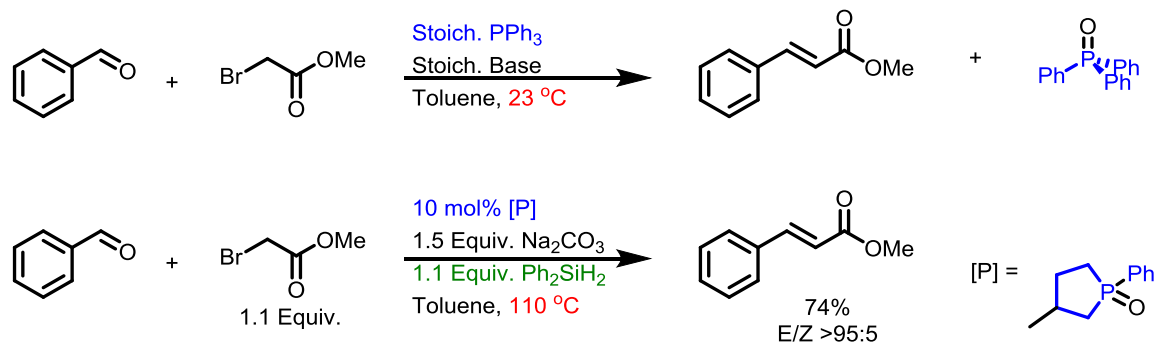


Figure 1.2. The classical Wittig Olefination and its catalytic counterpart using strained phosphorus heterocycles.

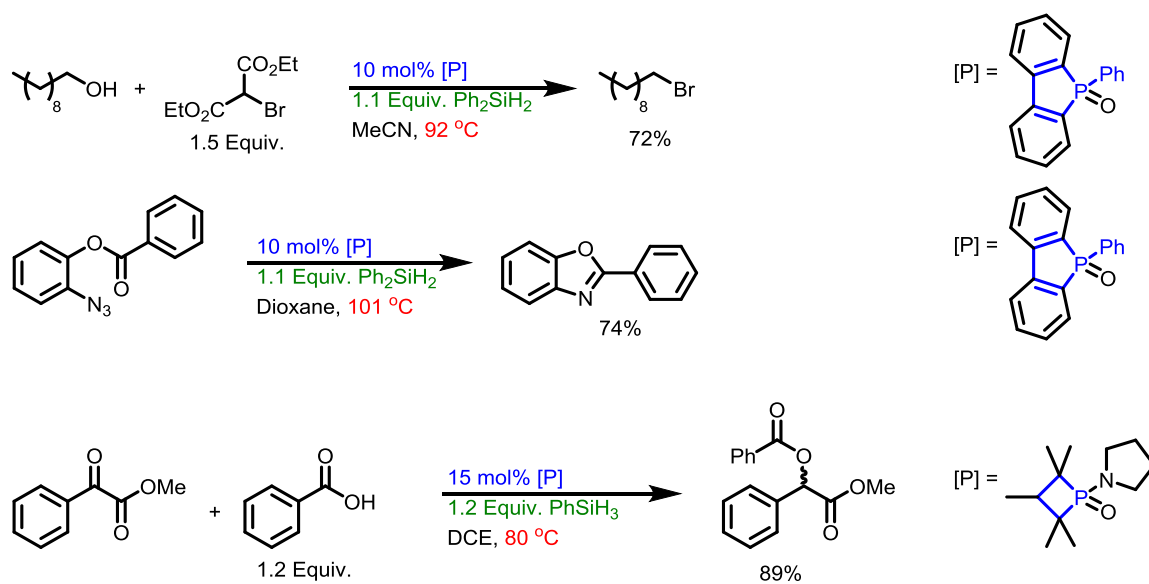
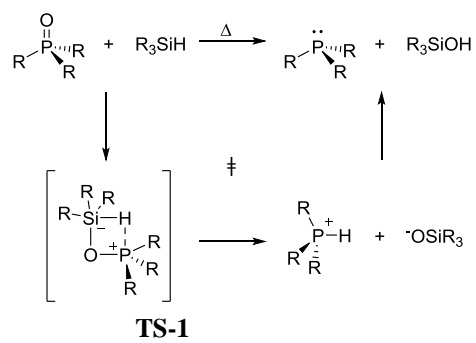


Figure 1.3. Examples of catalytic redox recycling reactions.

To briefly summarize what is believed concerning this reaction's mechanism, one scientist seems to be the driving force behind all predictions, calculations, and design behind the silane-mediated reduction of phosphine oxides. Dr. Kenneth Marsi postulated, more than forty years ago, the biomolecular reaction between phenylsilane and phosphine oxides proceeds through a 4-membered transition state (**TS-1**) to produce the *H*-phosphonium and siloxane tight ion pair (Scheme 1.1).¹⁷ Subsequent intermolecular proton transfer affords the observed phosphine and silanol products. Contemporary Density Functional Theory (DFT) calculations support **TS-1** as the rate-limiting step, yet diverge thereafter via a nonpolar mechanism.^{22,23} However, experimental validation is surprisingly limited and even fundamental parameters such as the reaction order and elementary rate constants have never been reported.



Scheme 1.1. Phenylsilane-mediated reductions of phosphine oxides via Marsi's [2+2] transition state.

Strained phosphorus heterocycle *P*-oxides lower the activation barrier for silane reduction through their higher torsional strain in the pseudotetrahedral ground state that is relieved in the trigonal bipyramidal phosphorane of **TS-1**. The influence of ring strain on reaction rates was nicely illustrated by van Delft, who showed 5-membered phospholane *P*-oxides were reduced quantitatively by diphenylsilane within 150 minutes under non-pseudo first order conditions (e.g. slight excess of silane) at 100 °C while the corresponding 6-membered phosphinane showed only 10% conversion and the 7-membered phosphepane was unreactive under identical reaction conditions.²⁰ Radosevich recently introduced the highly strained 4-membered phosphetanes for phosphine redox catalysis and demonstrated their superiority over phospholanes in a novel deoxygenative condensation of α -keto esters and carboxylic acids.^{21a} The stereoelectronic effects of the phosphorus heterocycle *P*-oxides on reactivity have been less explored, especially in the context of saturated heterocycles, but results with unsaturated dibenzophospholes suggest electron-donating substituents may increase the rate of reduction by silanes, as bis-(2,8-trifluoromethyl)dibenzophosphole *P*-oxide was reduced approximately 3-fold slower than bis-(2,8-methoxy)dibenzophosphole *P*-oxide or the parent dibenzophosphole *P*-oxide.²⁰ While this may seem counterintuitive, the oxygen atom of the phosphine oxide is predicted to first interact with phenylsilane to form a hypervalent phenylsilicate anion prior to the predicted rate-determining hydride transfer, thus, enhanced Lewis basicity of the phosphine oxide may be preferred.²² Concordant with these data, O'Brien and co-workers also experimentally showed that electron-poor 4-(trifluoromethyl)phenylsilane was a much more active reductant improving the reduction rate of **TPPO** with a Brønsted acid additive, although the opposing electron-rich silane was not shown to be a less competent reductant.²⁴ We posit further advances to realize the

ultimate goal of robust, chemoselective, additive-free, room temperature reduction of phosphine oxides has been impeded by a fundamental misunderstanding of the reaction mechanism.

Although the exact nature of the reduction is not necessarily understood, empirical studies have led to massive improvements. Improving upon the initial CWR, O'Brien further the method by lowering the temperature of the catalytic process to ambient temperatures.²⁴ To achieve this, a catalytic benzoic acid, *p*-nitrobenzoic acid (PNBA), was added to facilitate faster reduction of the phosphine oxide. The reason behind this was never truly established, but it is notable that the addition of this acidic additive to a reaction that requires basic conditions rapidly leads to phosphine oxide reduction. Additionally, this additive could be used in tandem with an acyclic phosphine oxide to facilitate the first ring-strain free catalytic redox recycling protocol.²⁴ While this additive could be used in the Wittig reaction with no measurable ill-effect, this strategy cannot necessarily be employed ubiquitously as these types of additives would interfere with Mitsunobu, Appel halogenation processes, and Staudinger reductions. However, other Brønsted acids have since found use in phosphine oxide recycling, as the phosphine oxide reduction-promoting reagent Bis-(*p*-nitrophenyl)-phosphoric acid (BNPA),²⁵ first discovered by Prof. Dr. Matthias Beller, has also found use in catalytic processes, generally derived from the group of Prof. Dr. Mecinovic.²⁶ Additionally, trifluoromethanesulfonic acid has also found limited use in these sorts of reactions.²⁷

In addition to the aforementioned Brønsted acid additives, several Lewis acids including transition metal complexes ($\text{Ti}(\text{OiPr})_4$,^{28, 29, 30} $\text{Cu}(\text{OTf})_2$ ³¹) as well as main group complexes ($\text{B}(\text{C}_6\text{F}_5)_3$,³² borinic acids,³³ fluorophosphonium salts,³⁴ $\text{In}(\text{III})$ ³⁵) have been described for silane-mediated reduction of acyclic phosphine oxides at elevated temperatures; although there are few examples that have been investigated in phosphine redox catalysis employing phosphorus

heterocycles.^{18-20, 36} These additives, again, seem to have been discovered through “brute-force” means, with limited knowledge pushing their development beyond empirical screening for reactivity. These additives seem to also lack broad utility over the entire reaction suite of phosphorus redox catalysis.

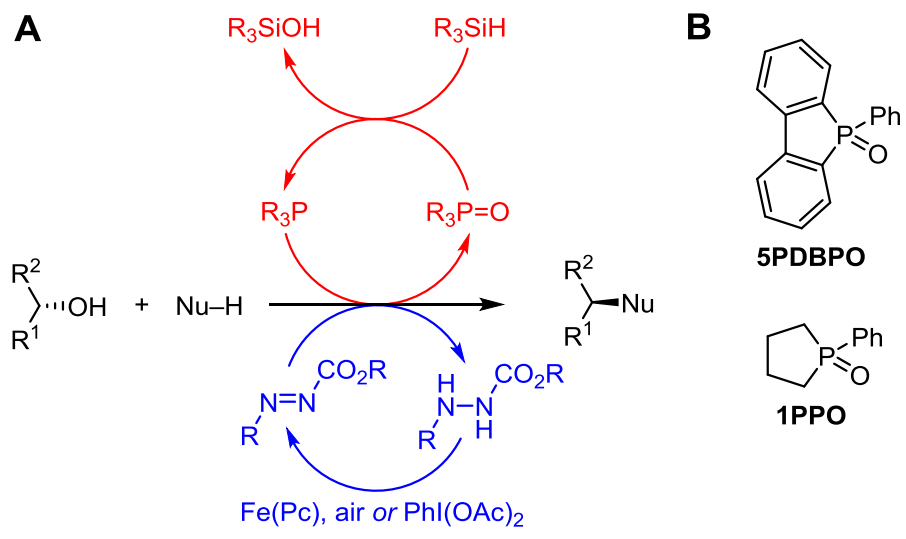
Our initial goal was to extend this concept to its use in Mitsunobu reactions, a phosphorus-mediated substitution of an alcohol synthon. This reaction has seen heavy use in the Aldrich lab specifically,³⁷ although it is frequently avoided in industrial settings due to its heavy waste stream and lack of atom economy.³⁸ The pharmaceutical round table at the green chemistry institute has placed special emphasis that a “greener” version of this reaction is in great need, as the reaction itself provides a very powerful transformation and a better version would enable many modes of discovery chemistry in industrial settings.³⁸ We elected to start with the knowledge that had been gained by others, but hoped that our present investigations would reveal the mechanism of silane-mediated phosphine oxide reduction in the context of phosphine redox catalysis. Thus we selected phenylsilane because it has emerged as a preferred reagent due to its balance of reactivity and chemoselectivity; although the related reductant diphenylsilane possesses similar attributes. Other silane reagents such as trichlorosilane¹³ and hexachlorodisilane³⁹ have been used as “chemoselective” reducing agents, but it is quite clear these reagents would be incompatible with functional groups present in Mitsunobu reactions. Moreover, phenylsilane contains three hydrides and it is generally assumed that all three can participate in phosphine oxide reduction,¹⁷ implying phenylsilanol and/or phenylsilanediol are also competent reducing agents. The simple alkoxysiloxanes (EtO)₂SiMeH and (EtO)₃SiH have also found limited use in phosphine redox catalysis while the inexpensive siloxanes polymethylhydrosiloxane (**PHMS**) and 1,1,3,3-tetramethyldisiloxane (**TMDSO**)⁴⁰ have primarily been used for phosphine oxide

reduction⁴¹ We also hoped to understand more about the Brønsted acid additives, and to get a better understanding of how to rationally design improvements to these processes in a manner that is amenable to ubiquitous application within redox recycling catalysis. Seeing that phosphine oxide reduction is the only unifying feature of these reductions, we rationalized that characterization of this reaction component should foster the most rapid improvement, hopefully leading to better Mitsunobu, Wittig, and Staudinger reactions.

1.2 Development of a Catalytic Mitsunobu Reaction

The Mitsunobu reaction is the displacement of an alcohol with a pronucleophile (Nu-H) mediated by phosphine and azocarboxylate reagents, which work in concert to activate the pronucleophile through deprotonation and convert the alcohol to a reactive alkoxyphosphonium species.¹⁰ Renowned for its mild reaction conditions and broad substrate tolerance, the Mitsunobu reaction is capable of forming C-O, C-N, C-S, C-X, and C-C bonds.⁴² However, the Mitsunobu reaction is highly under-utilized in process chemistry and manufacturing due to arduous purification from by-products and poor atom economy.⁴³ Although several innovative reagents have been developed to facilitate purification that can be removed by liquid-liquid or solid-liquid extractions,⁴⁴ the ideal Mitsunobu reaction would be catalytic in phosphine and azocarboxylate, and use innocuous reagents to recycle these catalysts.³⁸ Toward this goal, Toy and co-workers rendered the Mitsunobu catalytic in the azocarboxylate using $\text{PhI}(\text{OAc})_2$ to oxidize the hydrazine byproduct⁴⁵ while Taniguchi and co-workers developed an iron-phthalocyanine catalytic system employing oxygen as the terminal oxidant.⁴⁶ To date, a only one example of a Mitsunobu reaction catalytic in phosphine is presented in patent literature,⁴⁷ and optimization of this reaction is heavily desired.^{44, 48} Herein we report the development and optimization of the first Mitsunobu reaction catalytic in phosphorus utilizing dibenzophosphole and phospholane

precatalysts **5PDBP** and **1PPO** (Scheme 1.2B), inspired by the work in the development of the catalytic Appel¹⁹, Staudinger²⁰, and Wittig¹⁸ reactions.



Scheme 1.2. The Proposed Catalytic Mitsunobu Reaction.

Chemoselective reduction of the phosphine oxide product back to the phosphine in the presence of a reactive azo compound is required in order to complete the phosphine catalytic cycle. We initially investigated dibenzophosphole oxide **5PDBPO** as a precatalyst due to its facile reduction by silanes and ability to tune the catalyst through modification of the aryl rings.¹⁹ The coupling of 4-nitrobenzoic acid and benzyl alcohol or *p*-trifluoromethylbenzyl alcohol was studied as a model system employing stoichiometric DIAD, 10 mol% **5PDBPO** and various silanes (Table 1.1). To benchmark these results, the yield obtained using stoichiometric triphenylphosphine (**TPP**) was determined as 84% (Table 1.1, entry 1). Polymethylhydrosiloxane and triphenylsilane did not provide catalytic turnover (Table 1.1, entries 3-4). Diphenylsilane (Table 1.1, entry 5) provided the first encouraging yield of 42%, while phenylsilane (Table 1.1, entry 6) furnished an improved 63% yield. We next explored the impact of PhSiH₃ stoichiometry (Table 1.1, entries 8-11) on the outcome of the reaction. We observed that excess silane was detrimental, although it led to faster conversion. Conversely, lower equivalents of silane led to substantially slower conversion, but did result in slightly improved yields. As a control, we also measured the background reaction in the absence of PhSiH₃ confirming its vital role (Table 1.1, entry 8). The reaction of PhSiH₃ with alcohols in the presence of Lewis acids (i.e. *p*-nitrobenzoic acid) at elevated temperatures is previously known⁴⁹ and contributed to the lower yields (Figure 1.4). Thus, even the stoichiometric **TPP** reaction was lowered from 84% to 77% when PhSiH₃ was included in the reaction (Table 1.1, entries 1 and 2). Based on these considerations, we settled on 1.1 equivalents of PhSiH₃ as optimal, to minimize both reaction time and undesired reactivity. Finally, we evaluated phospholane precatalyst **1PPO** using our optimized conditions and were elated to obtain a 77% yield (Table 1.1, entry 12), identical to the stoichiometric TPP version under the same conditions.

The catalyst loading could be lowered to 5 mol% without affecting the yield, while 1 mol% still provided a respectable 54% yield (Table 1.1, entries 12-15).

Table 1.1. Development of conditions for the catalytic Mitsunobu in phosphine.^[a]

R =	[P]	X =	Silane	Y =	Product	Yield^[b]
H	TPP	110	None	-	1a	84
H	TPP	110	PhSiH ₃	1.1	1a	77
H	1	10	PHMS	1.5	1a	0
H	1	10	Ph ₃ SiH	2.0	1a	0
H	1	10	Ph ₂ SiH ₂	1.1	1a	42
H	1	10	PhSiH ₃	1.1	1a	63
H	1	10	None	-	1a	0^[c]
CF ₃	1	10	PhSiH ₃	0.5	1b	66^[d]
CF ₃	1	10	PhSiH ₃	1.5	1b	63
CF ₃	1	10	PhSiH ₃	3.0	1b	52
CF ₃	1	10	PhSiH ₃	6.0	1b	43
H	2	10	PhSiH ₃	1.1	1a	77
H	2	5	PhSiH ₃	1.1	1a	77^[e]
H	2	2	PhSiH ₃	1.1	1a	58^[f]
H	2	1	PhSiH ₃	1.1	1a	54^[g]

[a] Reactions performed on 1 mmol scale at 0.25 M [b] Isolated average of two reactions [c] Reactions with the reduced form of **5PDBPO** without silane added produced 7% of product [d] 46 h [e] Reaction at 10 mmol scale was performed with 78% yield [f] 38 h [g] 69 h

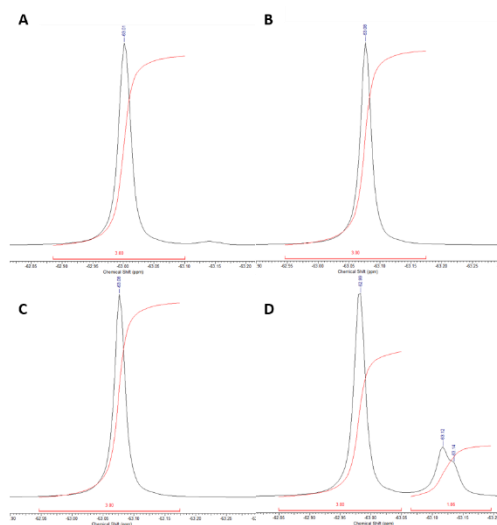
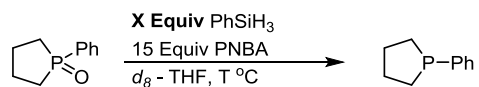


Figure 1.4. NMR spectra of selective silane reactivity; **A)** The spectrum of 4-(trifluoromethyl)benzyl alcohol heated in d_8 -THF; **B)** the reaction of 4-(trifluoromethyl)benzyl alcohol with PNBA; **C)** the reaction of 4-(trifluoromethyl)benzyl alcohol with phenylsilane; and **D)** the reaction of 4-(trifluoromethyl)benzyl alcohol with PNBA and phenylsilane. All spectra were collected after 46 h.

We speculated that the greater reactivity of catalyst **1PPO** was due to its more facile reduction by PhSiH_3 , which is the rate-limiting step in the phosphine catalytic cycle. van Delft and co-workers had indicated that **5PDBPO** and **1PPO** were nearly equivalent in reactivity as measured by reduction with Ph_2SiH_2 at 100 °C in 1,4-dioxane.¹⁹ To more rigorously study the relative reactivity of **5PDBPO** and **1PPO**, we measured their rates of reduction by ^{31}P NMR under pseudo first-order conditions (30, 15, 7.5 equiv PhSiH_3) at various temperatures ranging from 25 to 80 °C. The activation energies (E_a) were then calculated from the temperature dependence of the second-order rate constants using Arrhenius and Eyring plots. Reduction of **1PPO** was facile, even at 25 °C, as evident of its low E_a of $14.1 \pm 0.4 \text{ kcal mol}^{-1}$. Whereas **5PDBPO** was significantly less reactive with a E_a of $21.3 \pm 3.6 \text{ kcal mol}^{-1}$ and was not reduced at 25 °C even after 120 hours. These data would indicate the catalytic Mitsunobu reaction should readily occur at room temperature with **1PPO**. Unfortunately, this is not realized in practice and the catalytic Mitsunobu reaction requires elevated temperatures to achieve complete conversion. The activation energies were determined in the absence of other reagents (pronucleophile, alcohol, and DIAD), which we have shown attenuate the rate of phosphine reduction (Table 1.2).

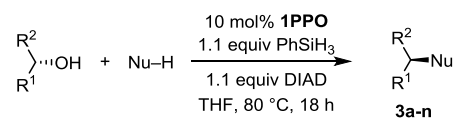
Table 1.2. The effect of *p*-nitrobenzoic acid on the reduction of the phosphine precatalyst 1PPO.^[a]

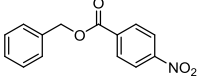
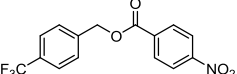
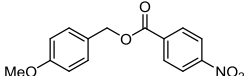
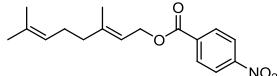
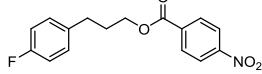
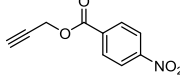
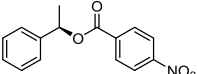
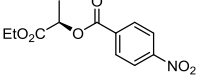
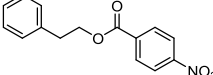
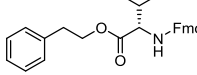
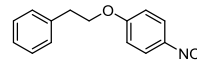
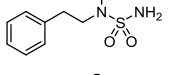
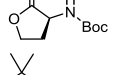
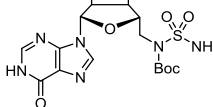
Entry	Phosphine	X =	T =	k_{obs} (s ⁻¹)	Half-life (min)	Slowing of Rate ^[b]
1	1PPO	7.5	80	0.0028	247.5	6.9
2	1PPO	15	80	0.0044	157.5	5.4
3	1PPO	30	80	0.0085	81.5	4.3
4	1PPO	30	25	0.0002	3465	5.0

[a] Reactions performed in triplicate using the procedure outlined in section 7.1.1. with 25 mg of *p*-nitrobenzoic acid (PNBA) added with the catalyst. [b] Calculated by dividing the average k_{obs} values for reductions without PNBA over average k_{obs} values for reductions with PNBA.

With optimized catalytic conditions established, we then investigated the substrate scope with a range of alcohols and pronucleophiles (Table 1.3). For comparison purposes, the yields of the stoichiometric reaction conducted at room temperature are also presented. Primary benzylic, allylic, and alkyl alcohols (Table 1.3, entries 1-6) were reacted with *p*-nitrobenzoic acid to afford the corresponding esters in moderate to good yields. The lower yield of the benzylic substrates, relative to the stoichiometric reaction, is due to competitive silane reactivity of the alcohols (Figure 1.4). Notably, the 82% yield obtained with the simple alkyl alcohol, 3-(4-fluorophenyl)propanol (Table 1.3, entry 5) was identical to the stoichiometric⁵⁰ version. Propargyl alcohol was also esterified with 84% yield (Table 1.3, entry 6), similar to its stoichiometric counterpart. Secondary alcohols were also competent substrates (Table 1.3, entries 7-8) providing respectable yields with high enantiomeric purities (er >94:6). We next examined the coupling of 2-phenylethanol with benzoic acid, aminoacid, phenol, and sulfamide pronucleophiles (Table 1.3, entries 9-12). These substrates all afforded the corresponding products in good to excellent yields compared to the stoichiometric reaction. Intramolecular reaction of Boc-protected homoserine furnished the γ -lactone in an impressive 87% yield (Table 1.3, entry 13). The background reaction lacking the phosphine catalyst was less than 2%. Reaction of 2',3'-*O*-isopropylideneinosine with Boc-protected sulfamide provided the coupled product in 70% yield (Table 1.3, entry 14) highlighting the utility of the catalytic Mitsunobu reaction with more challenging substrates.

Table 1.3: The substrate scope of the catalytic Mitsunobu reaction.^[a]

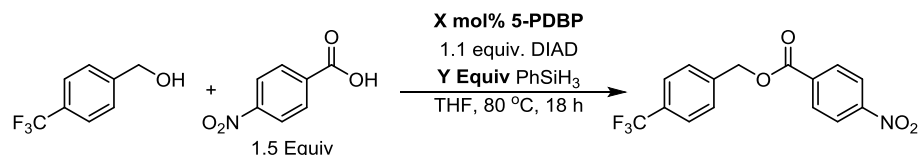


Entry	Product	Catalytic Yield[%] ^[b]	Stoichiometric Yield[%] ^[b,c]
1	 3a	77	94
2	 3b	76	92
3	 3c	61	80
4	 3d	50	50
5	 3e	82	82
6	 3f	84	90
7	 3g	69 ^[d]	77 ^[d]
8	 3h	68 ^[e]	78 ^[e]
9	 3i	76	96
10	 3j	63	83
11	 3k	51 ^[f]	85 ^[f]
12	 3l	72	90
13	 3m	87 ^[g,h]	98 ^[g]
14	 3n	70 ^[e]	93 ^[i]

[a] Reactions performed on 0.5-1.0 mmol scale at 0.25 M employing 1.5 equiv of pronucleophile, 10 mol% loadings of catalyst **2**, and 1.1 equivalents of both DIAD and PhSiH₃. Reactions were all run at 80 °C. [b] Isolated average of two reactions. [c] Reactions performed at 23 °C with 1.5 equiv of pronucleophile, TPP, and DIAD without phenylsilane for 18 h. [d] ER 94:6 [e] ER > 99.5:0.5 [f] 48 h. [g] Concentration was 0.04 M. [h] Background reaction with only Boc-Hse-OH, DIAD, and PhSiH₃ had trace yield. [i] 3 equiv N-boc sulphamide was used as the pronucleophile.

In order to improve this reaction for broader utility it would be necessary to improve the reduction of the phosphine oxide to recycle the catalyst, the rate-limiting step in the catalytic cycle. This would help improve the effective on-target percentage of the silane reducing agent. Unfortunately, in the presence of a strong pronucleophile (i.e. carboxylic acid) and elevated temperature promotes significant side reactivity. As mentioned, silanes can react with alcohols, so much so, that selectivity for product in the catalytic Mitsunobu reaction to silyl byproducts is rapidly shifted when silane is added to reactions (Table 1.4).

Table 1.4. The initial optimization of silane concentration in the catalytic Mitsunobu reaction.^[a]



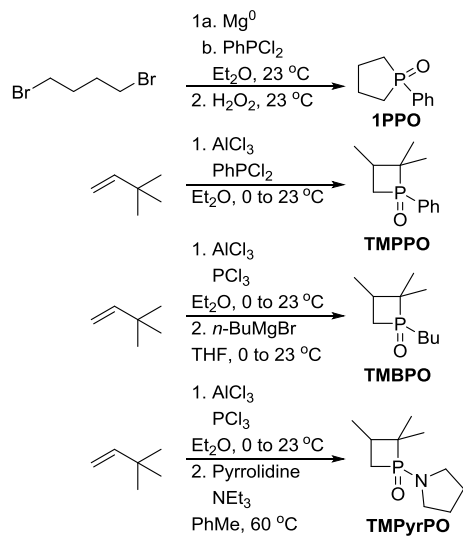
Entry	X =	Y =	Product : Silyl By-Products ^[b]	Yield ^[c]
1	10	0.5	1.2 : 1	66 ^[d]
2	10	1.5	1.15 : 1	63
3	10	3.0	1 : 1	52
4	10	6.0	1 : 1.18	43
5	5	1.5	1 : 1	55
6	5	3.0	1 : 1.65	36
7	5	6.0	1 : 2	29

[a] Reactions performed on 1.0 mmol scale in a 15 mL pressure tube at 0.25M using the general procedure for a catalytic Mitsunobu reaction. [b] Relative product distribution determined by integration of crude ¹⁹F NMR with C₆F₆ as internal standard. [c] Isolated average of two reactions after 18 h. [d] 46 h.

1.3 Mechanistic insight provides a means to rational reagent design

Knowing that the rate-determining step needed improvement, I moved to even further characterize the requirements for silane-mediated reductions of phosphine oxides. To simplify this investigation, ^{31}P NMR was used to monitor the isolated reduction reaction, and kinetics would be used to assay the reactivity of new phosphines and/or silane pairs which should then translate to improved redox recycling reactions.

To begin our mechanistic investigation, I synthesized a small series of strained phosphorus heterocycles to probe the impact of ring strain and electronics on reduction by phenylsilane. I started with the prototypical phospholane, 1-phenylphospholane-1-oxide (**1PPO**)⁵¹, and generated the isoelectronic 4-membered 2,2,3-trimethyl-1-phenylphosphetane-1-oxide (**TMPPPO**)^{52, 53} via previously-described means. Based on the hypothesis that electron-donating substituents may enhance the rate of reduction, we synthesized 2,2,3-trimethyl-1-butylphosphetane-1-oxide (**TMBPO**) and 2,2,3-trimethyl-1-pyrrolidinylphosphetane-1-oxide (**TMPPyrPO**) containing a hyperconjugatively⁵⁴ donating *n*-butyl and resonance donating pyrrolidinyl substituent, respectively (Scheme 1.3).



Scheme 1.3. Synthesis and identification of cyclic phosphine oxide pre-catalysts.

The reactivity of phenylsilane with each phosphine oxide was monitored with ^{31}P NMR at 80 °C employing phosphine oxide concentrations ($[\text{PO}] = 0.04 \text{ M}$) relevant in phosphine redox catalysis under pseudo-first order conditions ($[\text{phenylsilane}] = 0.40 \text{ M}$) as described in the methods section (Chapter 1.8). Data were gathered every 2-5 minutes and an unbiased automated integration platform, developed by Dr. Carter Eiden, was used to analyze the data in a quick and efficient manner.⁵⁵ When I first ran the reduction of TMPPO with this rate of sampling, I ended up with reduction profile that looked quite peculiar. Noticing that the curvature did not appear to be reminiscent of reactions governed by first-order kinetics. I approached Dr. Carter Eiden, a kineticist, with my intriguing data and asked for help evaluating this reaction with such a complex order. He agreed, and even agreed to help gather more data to interpret as the reaction's behavior was very abnormal and had so much information in even one curve. The reaction progress curves, gathered by Dr. Carter Eiden, shown in Figure 1.5 demonstrate the complexity of this reduction as the 4-membered phosphetane oxide **TMPO** and the 5-membered phospholane oxide **1PPO** were reduced at equal rates indicating that additional ring strain in the phosphetane does not translate into improved reactivity. On the other hand, as predicted, increasing the Lewis basicity of the phosphetane oxide by incorporation of electron-donating substituents in **TMBPO** and **TMPyrPO** led to a two- and four-fold enhancement in rate, respectively (Table 1.5). As a crude measure of Lewis basicity, I directed my undergraduate mentee, Kathleen Wang, to calculate the Mulliken charges⁵⁶ for the oxygen atom of each phosphine oxide using DFT and the M06-2X/6-31+G(d,p) basis set⁵⁷ to provide an estimate of the partial charge on the oxygen atom for this series of compounds. As summarized in Table 1.6, the calculated Mulliken charges for each of the phosphine oxides correlate nicely with the observed reactivity. While **TPPO** was calculated to be more Lewis basic than the other phosphine oxides, its

lack of ring-strain renders this compound inert under these reaction conditions, owing to the necessity of ring strain first hypothesized by O'Brien and Chass.¹⁸ Although **TMPrPO** was the most reactive phosphine oxide examined; its incompatibility in polar solvents (THF, MeCN, DMF) and tendency to over-reduce to a secondary phosphetane¹⁷ suggests it may not be an ideal precatalyst in phosphine redox reactions.

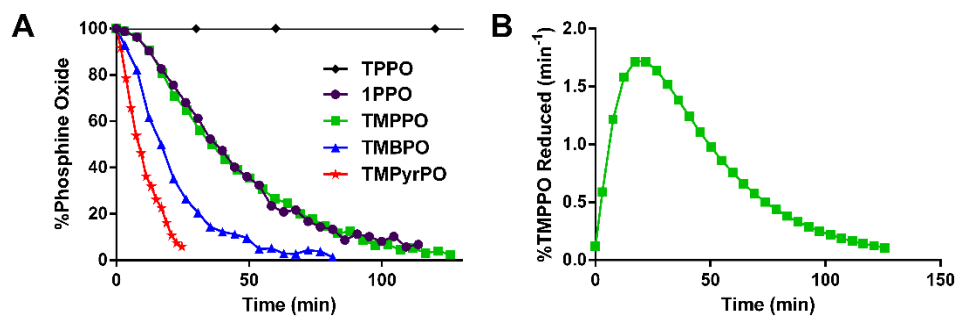
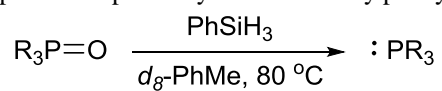


Figure 1.5. The reduction of strained phosphorus heterocycles by PhSiH₃ at 80 °C; A) The average reaction progress curves of reduction as determined with ³¹P NMR; B) The derivative curve of the reduction of TMPPO. Data collected by Dr. Carter Eiden.

Table 1.5. Comparison of precatalyst reductions by phenylsilane at 80 °C.



Entry	PO	k_{obs} (min ⁻¹) ^a	$t_{50\%}$ (min)	$t_{90\%}$ (min)
1	TPPO	n.d. ^c	n.d. ^c	n.d. ^c
2	1PPO	0.028	37.3	91
3	TMPPO	0.027	36.5	92
4	TMBPO	0.054	16.4	48
5	TMPyrPO	0.103	8.4	21

^aSee chapter 1.8; ^bCould not be determined.

Table 1.6. Calculated Mulliken charges of phosphine oxide precatalysts.^a

Entry	PO	Charge (P)^b	Charge (O)^b
1	TPPO	0.824959	-0.711251
2	1PPO	0.165482	-0.577962
3	TMPPPO	0.904052	-0.583227
4	TMBPO	1.162698	-0.675419
5	TMPrPO	1.497421	-0.769144

^aDFT calculations performed with Gaussian using the M06-2X/6-31+G(d,p) basis set; ^bAtomic units.

Intriguingly, all four reduction progress curves (Figure 1.5A) display an initial “lag phase” where the rate of reduction of the phosphine oxide increases following initiation. Such behavior is indicative of a multi-step kinetic mechanism. For added evidence against a single-step kinetic mechanism, the curves in Figure 1.5A were fit to both a single exponential and the sum of two exponentials. Upon visual inspection, it is clear the double-exponential fitting is far superior (Figure 1.6, Table 1.7), an assessment confirmed quantitatively as the variance per data point is 5 to 13-fold lower. The double exponential fitting was then used to generate derivative curves similar to the one shown in Figure 1.5B (Figure 1.7), which shows a pronounced rate increase during the early time points.

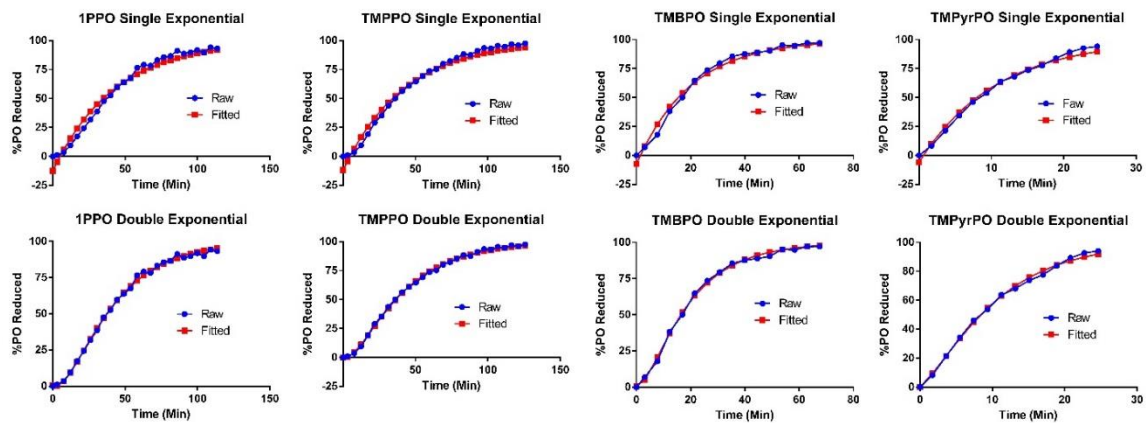


Figure 1.6. The single and double exponential fittings for reduction progress curves observed for the reduction of phosphine oxide precatalysts with PhSiH_3 . Data fitting by Dr. Carter Eiden.

Table 1.7. Numerical comparison between single- and double-exponential fitting of reduction curves.

Entry	Variance (%PO Reduced)²	# Data Points	Variance Per Data Point
1PPO-Single	612.79	26	23.57
1PPO-Double	60.93	26	2.34
TMPPPO-Single	468.99	28	16.74
TMPPPO-Double	37.93	28	1.35
TMBPO-Single	215.23	16	13.45
TMBPO-Double	35.14	16	2.20
TMPyrPO-Single	133.23	14	9.52
TMPyrPO-Double	37.09	14	2.65

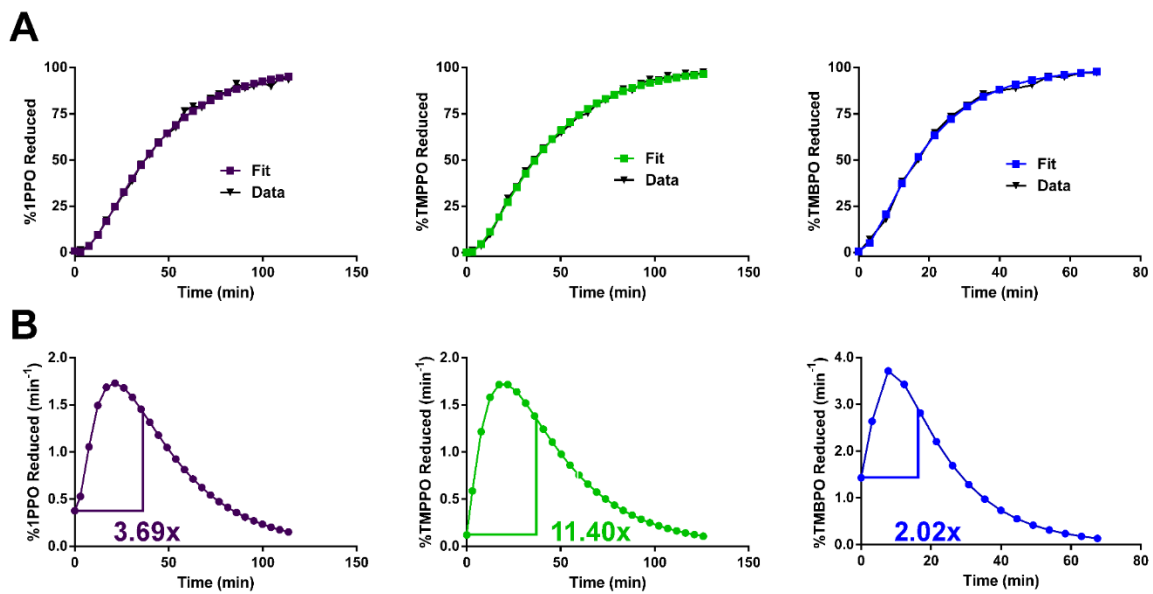
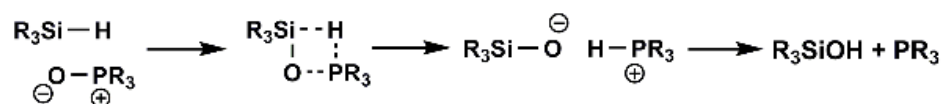


Figure 1.7. The fitting (A) and derivative (B) curves of **1PPO** (left, purple), **TMPPPO** (center, green), and **TMBPO** (right, blue).

This information was quite notable because it conflicts with the proposed single-step kinetic mechanism for reduction of phosphine oxides by phenylsilane (Figure 1.8, Mechanism I).¹⁷ We then explored whether an intermediate phosphine oxide-silane complex could explain the observed “lag” phase (Figure 1.8, Mechanism II). In order for this mechanism to be operative, the intermediate should accumulate to detectable levels given that both reaction steps are kinetically distinguishable. However, a new time-dependent resonance in ³¹P NMR besides the phosphine product was never observed during the reaction. For a sequential kinetic mechanism such as Mechanism II containing one intermediate, the normalized rate (expressed as the percent substrate remaining per unit time) should be independent of the initial variable substrate concentration leading to diagnostic superimposable reaction progress curves at different fixed substrate concentrations. However, we showed increasing the concentration of phosphine oxide, still under pseudo first-order conditions, changed the kinetic profile providing further evidence against Mechanism II (Figure 1.9).

Marsi:



Potential Mechanisms:

R = H, OH

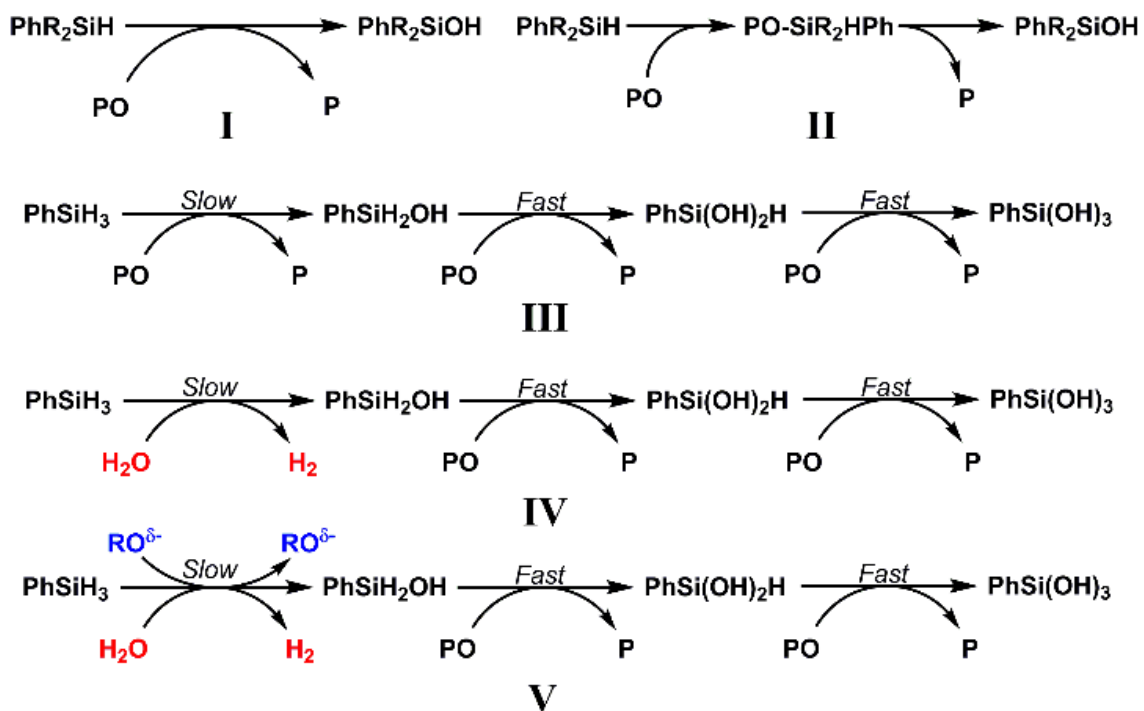


Figure 1.8. The proposed kinetic mechanisms for the reduction of phosphine oxides by PhSiH_3 .

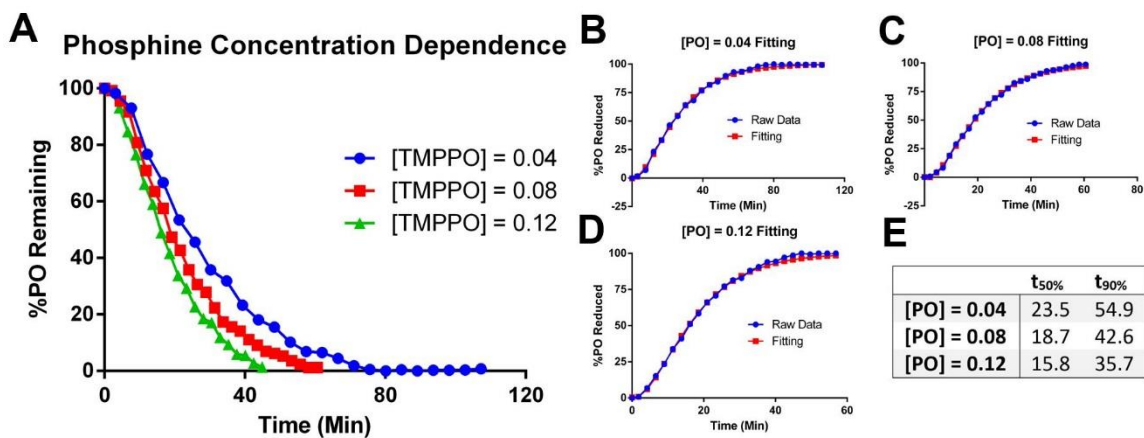
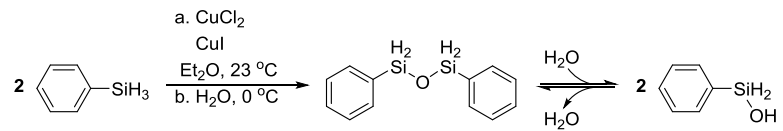


Figure 1.9. The A) Observed reduction of **TMPPO** under pseudo first order conditions with PhSiH_3 ; B, C, D) Fitting of raw data; E) Observed reduction times to 50% and 90% completion. Data collected by Dr. Carter Eiden.

Our next hypothesis to explain the biphasic kinetic profile in Figure 1.5 was the realization the silanol byproducts may reduce phosphine oxides more rapidly than phenylsilane and thus may be kinetically distinguishable leading to the proposal of Mechanism III (Figure 1.8). Recently, Fianchini, has proposed, using computational methods, that silanol byproducts are competent reducing agents with the potential to accelerate the rate of phosphine oxide reduction.⁵⁸ As the concentration of phenylsilane does not change over the course of the reaction, a dependence of the reduction rate on the concentration of phosphine oxide strongly suggests it is present at a greater or similar concentration than a rapid reductant. Seeing that silanol byproducts are the only likely culprit to act as this rapid reductant we chose to attempt to isolate this species. Silanols exist in equilibrium with the corresponding disiloxanes through self-condensation and that equilibrium favors the disiloxane species (association constants of $\sim 10^4 \text{ M}^{-1}$) except for substrates containing multiple bulky substituents, while silanediols equilibrate into complex polymeric structures.⁵⁹ Consequently, we prepared, 1,3-diphenyldisiloxane (**DPDS**) that equilibrates to phenylsilanol, the initial byproduct from one turnover of phenylsilane (Scheme 1.4).^{18a, 60} **DPDS** was evaluated against each of the cyclic phosphine *P*-oxides resulting in rapid reduction at ambient temperature (Figure 1.10). Illustrating the remarkable enhanced reactivity of **DPDS**, the electron-rich phosphetane oxides **TMBPO** and **TMPyrPO** were completely reduced within 30 minutes while **TMPPPO** and **1PPO** required 75 and 150 minutes, respectively (Table 1.7) at ambient temperature. Most significantly, **DPDS** displayed single step kinetics as evidenced by the reaction progress and derivative curves in Figure 1.7 that follow single-exponential decay. These results support Mechanism III wherein the fast step corresponds to reduction by phenylsilanol and the slow step to reduction by phenylsilane. By this mechanism, **DPDS** itself would also be a viable

reductant, but would follow the Curtin-Hammett principle, likely only reacting through its silanol form.



Scheme 1.4. Synthesis and equilibrium of DPDS.

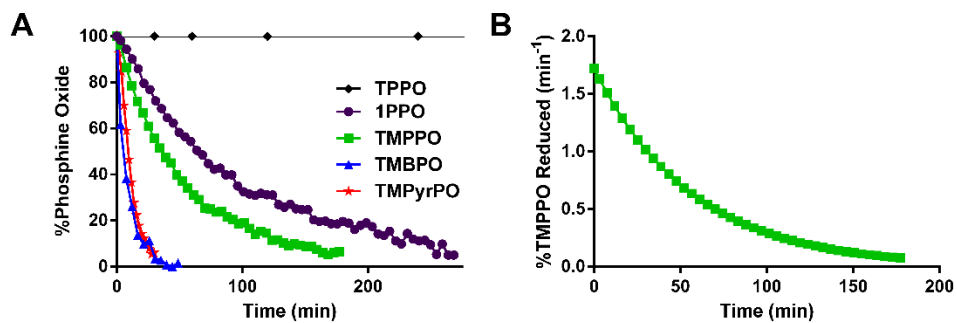


Figure 1.10. The reduction of phosphine oxide precatalysts with **DPDS** at 25 °C. A) Reaction progress curves using ³¹P NMR; B) The derivative curve of the the reduction of **TMPPO** with **DPDS**. Data collected by Dr. Carter Eiden.

Table 1.8. Comparison of phosphacycle P-oxides reductions by DPDS at 25 °C.

$$\text{R}_3\text{P}=\text{O} \xrightarrow[\text{d}_g\text{-PhMe, 25 }^\circ\text{C}]{\text{DPDS}} \text{:PR}_3$$

Entry	PO	k_{obs} (min ⁻¹) ^a	$t_{50\%}$ (min)	$t_{90\%}$ (min)
1	TPPO	n.d. ^c	n.d. ^c	n.d. ^c
2	1PPO	0.010	69.1	233
3	TMPPPO	0.018	37.9	129
4	TMBPO	0.114	5.7	20
5	TMPyrPO	0.093	9	23

^aSee Chapter 1.8; ^bCould not be determined.

To rigorously define the kinetic mechanism of **DPDS**-mediated phosphine oxide reduction, we monitored the reduction of **TMBPO** by **DPDS**. The rate exhibited a linear dependence on both **DPDS** and **TMBPO** concentration confirming the reaction is first order with respect to each substrate and second order overall furnishing a second order rate constant of (Figure 1.11). We then monitored the reaction kinetics at temperatures ranging from 0 to 25 °C to measure the energy barrier for the reaction. The activation parameters were determined by an Eyring plot (Figure 1.12), which showed a straight line over this temperature range indicating a single rate-limiting step and providing the activation parameters $\Delta H^\ddagger = 13.7 \pm 0.9$ kcal/mol, $\Delta S^\ddagger = -0.02 \pm 1.2 \cdot 10^{-4}$ kcal/mol and $\Delta G_{298K}^\ddagger = 18.8 \pm 1.9$ kcal/mol. This compares favorably against the activation parameters gathered for **TPPO** in which $\Delta H^\ddagger = 17.3 \pm 1.2$ kcal/mol, $\Delta S^\ddagger = -0.01 \pm 1.4 \cdot 10^{-4}$ cal/mol and $\Delta G_{298K}^\ddagger = 21.5 \pm 3.6$ kcal/mol (Figure 1.13). The negative values for the entropy of activation could imply an associative mechanism while the small enthalpies of activation deviate substantially from previously calculated transition states with phenylsilane.

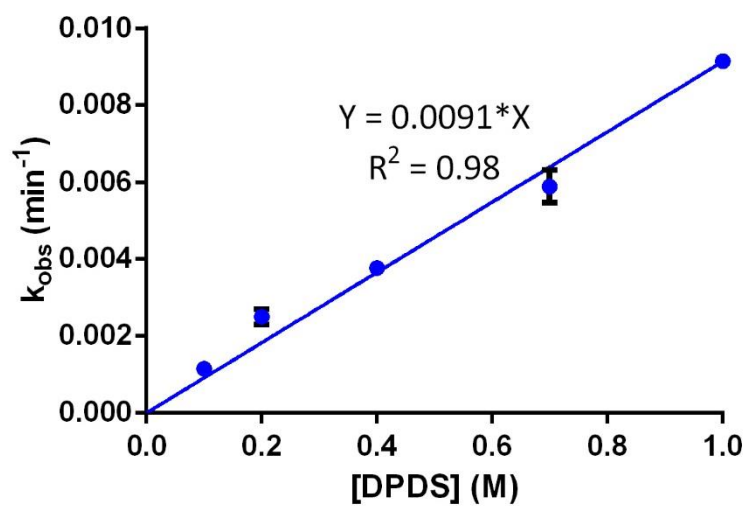


Figure 1.11. The comparison of rate of reduction vs. the concentration of **DPDS** employed in the reduction of **TPPO** at 110 °C. Data collected by Dr. Carter Eiden.

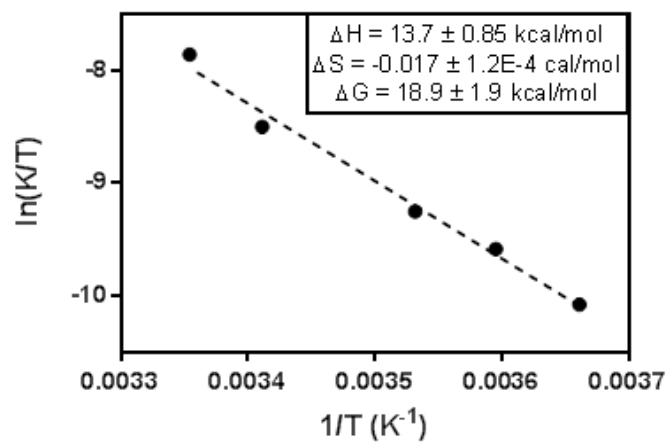


Figure 1.12. Eyring plot of the silane-mediated reduction of **TMPPO** with **DPDS** over the temperature range of 0 – 25 °C. Data collected by Dr. Carter Eiden.

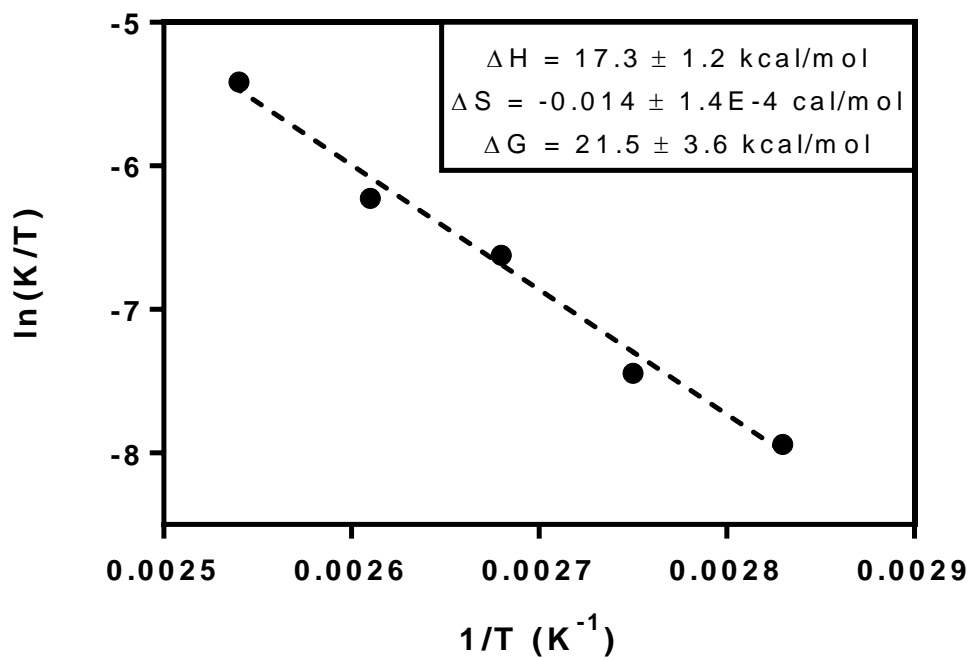


Figure 1.13. The Eyring plot of the silane-mediated reduction of **TPPO** with **DPDS** over the temperature range of 80 – 120 °C.

Although Mechanism III can account for a biphasic kinetic profile, detailed numerical investigation of the reaction progress curves in Figure 1.5 showed it could not simulate the experimental reaction progress curves. In Mechanism III, one would only expect a small increase in the rate of reduction over the initial time points; however, Figure 1.7 indicates a substantial rate increase. As detailed in the rest of this section, we evaluated the rate laws governing this kinetic scheme and show the observed increase in reaction velocity is incongruent with Mechanism III.

The rate law for Mechanism III is given by equation 1 and the initial rate of the reaction is simplified to equation 2 because the concentration of both phenylsilanol and phenylsilanediol are both zero.

$$\frac{d[P]}{dt} = k_1[PhSiH_3][PO] + k_2[PhSiH_2OH][PO] + k_3[PhSi(OH)_2H][PO] \quad (\text{eq 1})$$

$$Rate_i = k_1[PhSiH_3]_i[PO]_i \quad (\text{eq 2})$$

The theoretical maximum rate at any time point can be calculated with a few underlying assumptions of this sequential reaction wherein each silane species can contribute to the overall rate. The first assumption is that k_2 and $k_3 \gg k_1$, which allows implementation of the steady-state approximation to calculate the concentration of the intermediate phenylsilanol. Under these conditions the concentration of phenylsilanol will be low as it is consumed much faster than it is produced and importantly remain constant during most of the time course. As shown in the methods subchapter using mathematical simulations (Figure 1.14 and Table 1.9), this appears to be reasonable assumption and is supported by the experimental data from Figure 1.5 and Figure 1.10. To apply the steady-state approximation to calculate the concentration of phenylsilandiol,

it is necessary that $k_3 > k_2$, otherwise phenylsilandiol can build up during the reaction and exhibit more pronounced time-dependent changes in concentration. However, if $k_2 \leq k_3$, then its contribution to the overall rate will be diminished. Since we are attempting to calculate the maximum theoretical velocity, we will presume $k_3 > k_2$ to simplify analysis and provide an upper limit to the reaction rate.

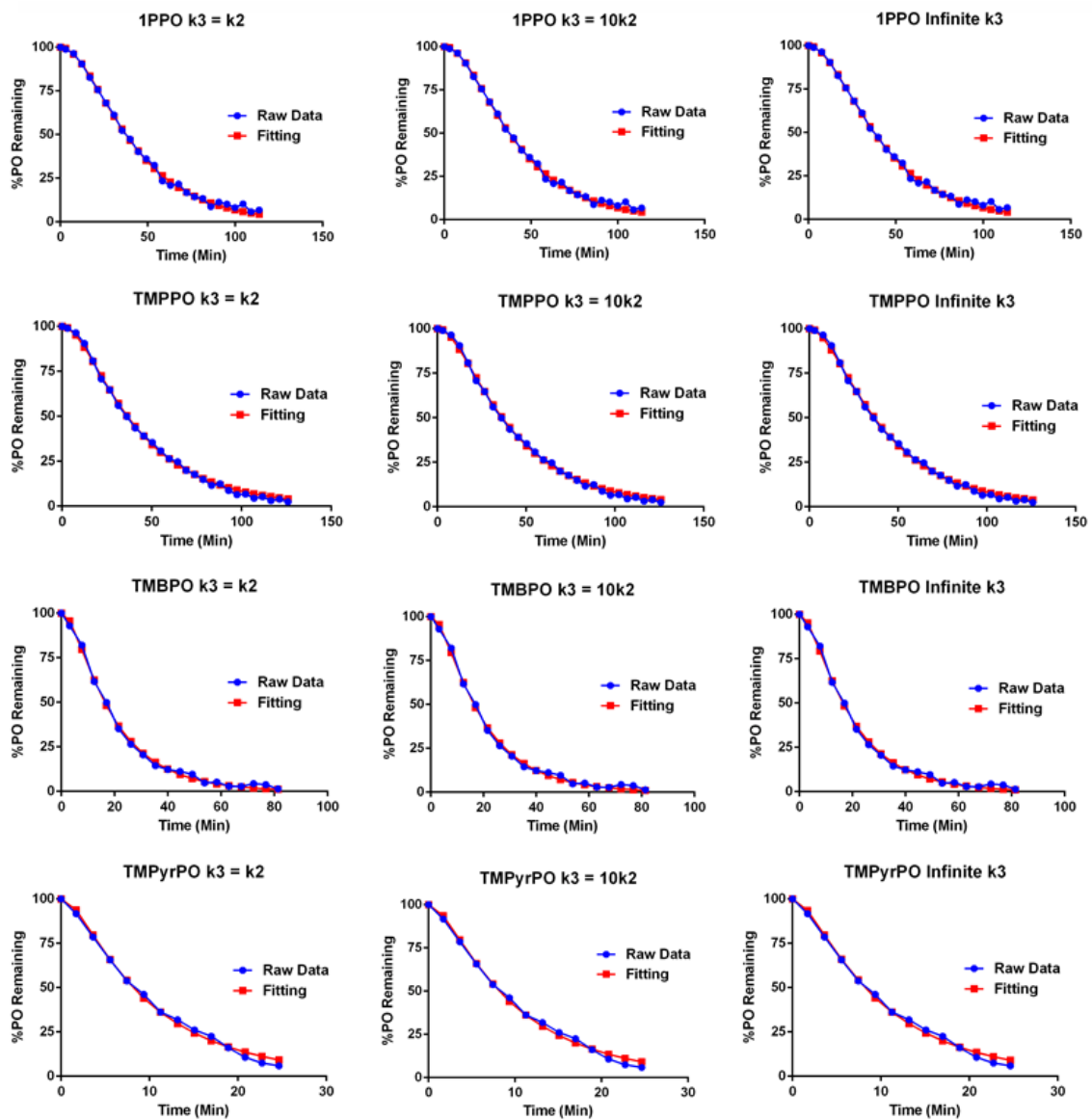


Figure 1.14. Graphical comparison of reaction progress curves (Figure 1.5B) and the fit obtained by the indicated parameters. Data fitting by Dr. Carter Eiden.

Table 1.9. Rate constants obtained through simulation.

	$k_3 = k_2$		$k_3 = 10k_2$		$k_3 = \infty$	
	k_1	k_2	k_1	k_2	k_1	k_2
1PPO	0.049	1.83	0.051	1.14	0.058	0.87
TMPO	0.038	3.01	0.039	1.90	0.040	1.67
TMBPO	0.077	8.23	0.078	5.46	0.079	5.02
TMPrPO	0.133	25.0	0.134	16.7	0.135	15.4

All rate constants are in units of ($M^{-1}s^{-1}$)

To illustrate our analysis, we elected to determine the maximum rate of Mechanism III at 50% conversion because the reaction should be at steady-state and the reaction velocity can be accurately determined at this time. Under the pseudo first-order conditions, the rate at 50% conversion is given by equation 3.

$$\frac{d[P]}{dt} = \frac{k_1[PhSiH_3]_i[PO]_i}{2} + \frac{k_2[PhSiH_2OH][PO]_i}{2} + \frac{k_3[PhSi(OH)_2H][PO]_i}{2} \quad (\text{eq 3})$$

The first term is clearly half of the initial rate presented in equation 2. To determine the value of the second term, we apply the steady-state approximation and set the derivative of the concentration of phenylsilanol with respect to time to be zero at 50% conversion as described in equation 4, leading to the equality displayed in equation 5.

$$\frac{d[PhSiH_2OH]}{dt} = \frac{k_1[PhSiH_3]_i[PO]_i}{2} - \frac{k_2[PhSiH_2OH][PO]_i}{2} = 0 \quad (\text{eq 4})$$

$$\frac{k_1[PhSiH_3]_i[PO]_i}{2} = \frac{k_2[PhSiH_2OH][PO]_i}{2} \quad (\text{eq 5})$$

Equation 5 indicates that the second term of equation 3 would be, at a maximum, equal to the half of the initial rate. The exact same strategy can then be applied to the third term of equation 3, which similarly shows the third term should be equal to half of the initial rate. From this analysis, the maximum value of the rate of phosphine formation at 50% conversion should be 1.5 times that of the initial rate, which also seems intuitively correct.

To determine the observed rate fold increase at 50% completion, we fit each of the curves in Figure 1.5A to a sum of two exponentials (Figure 1.6). This provides a very accurate estimate of the rate of reduction at 50% conversion, but struggles to precisely measure the initial rate. Therefore, we chose to use the average rate over the first two time points as an extremely

conservative estimate of the initial rate. As seen in Figure 1.7, the fold increase over initial of the rate of reduction at 50% conversion with **TMBPO**, **TMPPPO**, and **1PPO** are all larger than 1.5, with **TMPPPO** in particular displaying an 11.4-fold increase. Consequently, we conclude the rate law in Equation 1 is indeed violated and Mechanism III cannot be correct.

Because the kinetic profile for reduction of **TMBPO**, **TMPPPO**, and **1PPO** by phenylsilane does not conform to Mechanism III and **DPDS**-mediated reductions are both rapid and behave as expected with single-exponential character, we proposed Mechanism IV, where phenylsilanol is generated by the reaction of phenylsilane with water, releasing hydrogen gas. As previously discussed, it is well known that reduction of phosphine oxides by phenylsilane results in the production of both hydrogen gas and water.^{16, 17, 51} In the experimental section of his account from 1974, Marsi writes: “Initial slow evolution of hydrogen signals the onset of the reaction.” This finding is not accounted for in his proposed mechanism, although it is consistent with our novel proposal. It is also noteworthy that tri-substituted hydrido-silanes, incapable of producing hydrido-silanol species like phenylsilanol, require temperatures exceeding 250 °C to reduce phosphine oxides.^{13, 61} This empirical evidence supports our hypothesis that phenylsilane is not itself an active reductant at synthetically-practical temperatures, but requires *in-situ* pre-activation to generate the active reductant phenylsilanol.

The Role of Water, a Previously Unknown Player in the Reduction of Phosphine Oxides.

While Mechanism IV has explained all of our observations to this point, we had yet to verify the first step, wherein phenylsilane reacts with water. We thus preheated phenylsilane with wet (300 – 1000 ppm water) *d*₈-THF at 80 °C prior to the addition of phosphine oxide, reasoning that

preincubation would generate phenylsilanol and thereby increase the initial reaction rate. However, no rate increase was observed compared to the preincubation-free control (Figure 1.15), suggesting that phenylsilane does not spontaneously react with adventitious water, and implies another component of the reaction must catalyze the necessary activation step.

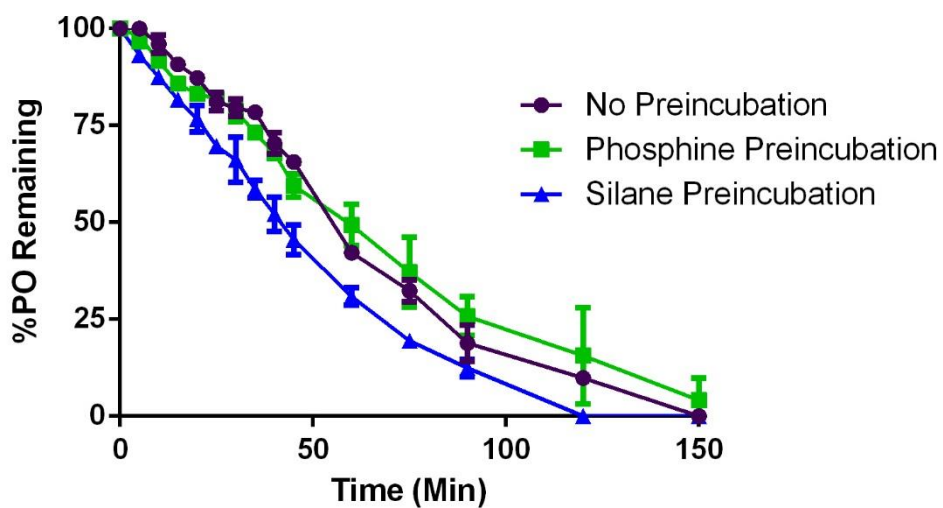
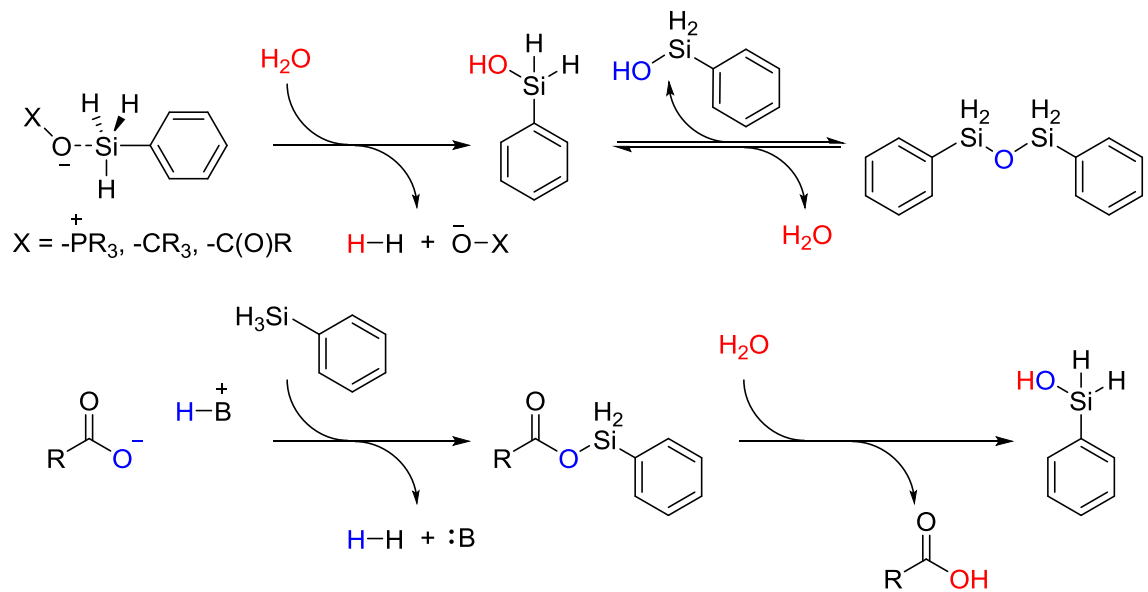


Figure 1.15. The comparison of the reduction of with **1PPO** no changes to the conditions in Figure 1.5 (purple, circles), phosphorus preheating (green, squares), and silane preheating (blue, triangles).

This was perplexing until we further investigated O'Brien's catalytic Wittig reaction, in which the addition of catalytic *p*-nitrobenzoic acid dramatically enhanced the rate of phenylsilane-mediated reduction of phospholane precatalysts.²⁴ During our own studies, we found excess benzoic acids actually decreased the rate of reduction;⁵¹ however, the addition of tetrabutylammonium *p*-nitrobenzoate to phenylsilane and **TMPPPO** at 80 °C promoted completion within 5 minutes. Benzoate activation likely proceeds via coordination to the silicon atom to form a hypervalent phenylsilicate anion (Scheme 1.5A), similar to a mechanism proposed by Denton and coworkers (Scheme 1.5B).⁶² We hypothesized that the phosphine oxide similarly activates phenylsilane through Lewis base catalysis to react with water (Scheme 1.5A) as captured in Mechanism V (Figure 1.8). The requirement of phosphine oxides for activation would also finally explain the dependence of the rate constants for the slow step of phenylsilane-mediated phosphine oxide reduction (Figure 1.9) on phosphine oxide concentration. Intriguingly, we found that Lewis bases such as amines or phosphines did not promote phenylsilanol formation.²⁴ We thus surmise Lewis bases, capable of forming an oxyanion complex with phenylsilane, are necessary to catalyze the reaction of phenylsilane with water, as a result of the natural affinity of silicon for oxygen.



Scheme 1.5. The mechanism of phenylsilanol generation using oxyanionic additives (top) and the mechanism of phenylsilanol generation with carboxylate additives as proposed by Denton and co-workers (bottom).

Returning to investigating the mechanism of phosphine oxide reduction by phenylsilane, we added Lewis acids in an attempt to directly block our proposed Lewis base activation of phenylsilane to phenylsilanol. Hindering the first step in Mechanism V should decrease the rate of reduction. Reductions of **1PPO** by phenylsilane were performed in combination with either LiCl or ZnCl₂. Compared to the no-additive positive control, both Lewis acids attenuated reduction (Figure 1.16). In particular, the more Lewis acidic ZnCl₂ completely abolished the phenylsilane-mediated reduction of **1PPO**. These results are consistent with our hypothesis and suggest the Lewis acids inhibited reduction through coordination of the phosphine oxide¹⁵ and/or adventitious water in solution, thus preventing phenylsilane pre-activation.

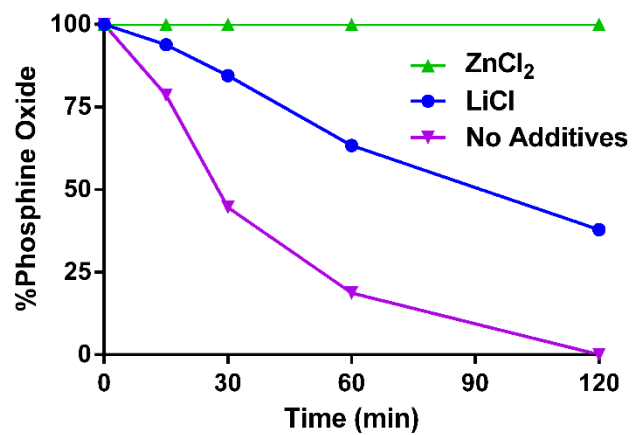


Figure 1.16. Reductions of **1PPO** by PhSiH₃ with or without Lewis acid additives.

Simulation of Mechanism V furnished an excellent fit to the curves from Figure 1.5A, providing further evidence of paradoxical phosphine oxide catalysis of silane pre-activation. These mathematical analyses also revealed substantial differences in the rate of phenylsilanol formation, defined by the rate constant k_1 , among the phosphorus heterocycles (Table 1.9) wherein **TMPPO** and **1PPO** were nearly the same while **TMBPO** and **TMPyrPO** were approximately two and four-fold higher, respectively. The relative reactivity of these compounds also correlates nearly perfectly with their oxyanionic character as measured by the Mulliken charges of the oxygen atom (Table 1.6). Unsurprisingly, we note that too strong of oxyanionic character, as found in inorganic alkoxide or hydroxide bases, is detrimental to the reaction as the silane reagent is completely consumed in a flurry of gas release. While phosphine oxides can catalyze oxidation of phenylsilane to phenylsilanol, they are much less efficient than the deprotonated forms of 4-nitrobenzoic acid (**PNBA**) or bis(*p*-nitrophenyl)phosphoric acid (**BNPA**), which are capable of quantitatively converting phenylsilane to phenylsilanol at room temperature in minutes, explaining their dramatic impact on reactivity. Optimal additives for silane pre-activation seem to be those with a finely tuned oxyanionic character. **PNBA** requires a tertiary amine base to facilitate deprotonation to generate the carboxylate oxyanion while Beller's strongly acidic **BNPA** can be deprotonated directly by the phosphine oxide.²⁵⁻²⁶

The water necessary for the pre-activation of phenylsilane is regenerated when phenylsilanetriol condenses into silyl-oxy polymers, releasing one and a half equivalents of water for each molecule of phenylsilane consumed.²⁹ This part is in accordance with the observation by Marsi, who observed production of water during the course of the reduction¹⁷ as well as Lemaire's observation of cyclic siloxane oligomers.²⁹ The initial pre-activation of phenylsilane does require

some adventitious water to initiate the reaction, thus rigorous removal of water during solvent and reagent purification should be avoided. Also notable is that the constant addition of water to the reaction should greatly affect the rate of silanol formation. Seeing as there would be more water to react with phenylsilane, thus generating phenylsilanol, the rate of reduction should increase substantially during the course of the reaction, a trend that is consistent with our data. Although water is essential, too much water is detrimental as addition of excess water greatly reduced the rate of reduction.⁵¹ The full mechanism occurring in a phosphorous recycling reaction with phenylsilane is displayed in Figure 1.17, showing the cycle of water regeneration, phenylsilanol formation as catalyzed by phosphine oxides, and reduction to the corresponding phosphine with retention of configuration.^{17, 63}

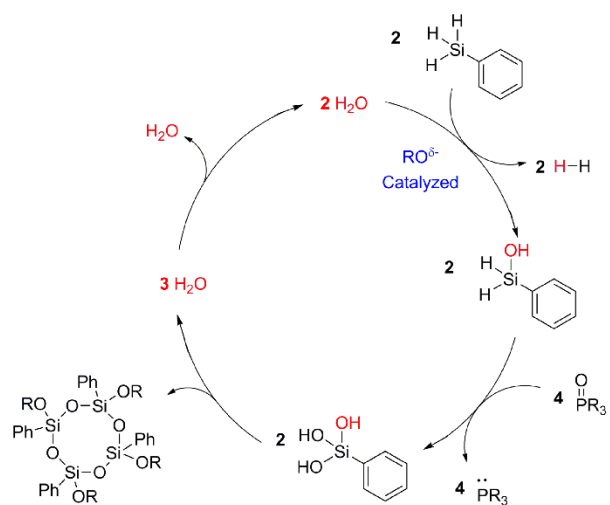


Figure 1.17. The water cycle in PhSiH_3 -mediated phosphine oxide reductions.

The significant rate enhancement gained with **DPDS** prompted further exploration into silane reactivity. We performed a screen of commercially available silicon hydride derivatives with our panel of four cyclic phosphine oxides at 80 °C. Standard mono-hydrido silanes (triethylsilane, triphenylsilane, and tris(trimethylsilyl)silane) showed null activity along with 1,1,3,3-tetramethyl disiloxane (**TMDSO**) and its polymeric counterpart polymethylhydrosiloxane (**PMHS**). Trimethoxysilane, another well-known reductant for cyclic phosphine oxides, was a competent reductant, yet it was no faster than phenylsilane (Figure 1.18). In the postulated [2+2] transition state (Scheme 1.1), the interaction between the silane and the P=O oxygen atom should be enhanced by increasing the partial positive character on the silicon atom. Indeed, O'Brien has previously shown that removing electron density on the silicon atom of a silane increased its activity.²⁴ However, to our surprise, 1,1,3,3-tetramethyldisilazane (**TMDSA**) resulted in adept reduction at 80 °C (Figure 1.18) even though **TMDSA** was expected to be inferior to **TMDSO** due to the lower electronegativity of nitrogen. As summarized in Table 1.10, calculated Mulliken charges of silanes do not correlate with known silane reactivity as exemplified with trichlorosilane, which is one of the most reactive silane reducing agents,^{13, 16} yet is calculated to be the least electron-deficient. Conversely, (MeO)₃SiH is calculated to have the most electron-deficient silicon atom, but is not the most active reducing agent in our series (Figure 1.18). To further complicate matters, we have observed a nearly 10-20 kcal/mol difference in the calculated activation energies for the reduction of **TPPO** by phenylsilane²³ or trichlorosilane²² compared to our experimentally-determined values with **DPDS**.⁶⁴ Taken together, these results indicate the substantial gap in reactivity between silanes cannot be explained by the electron density on the silicon atom and suggest an alternate transition state.

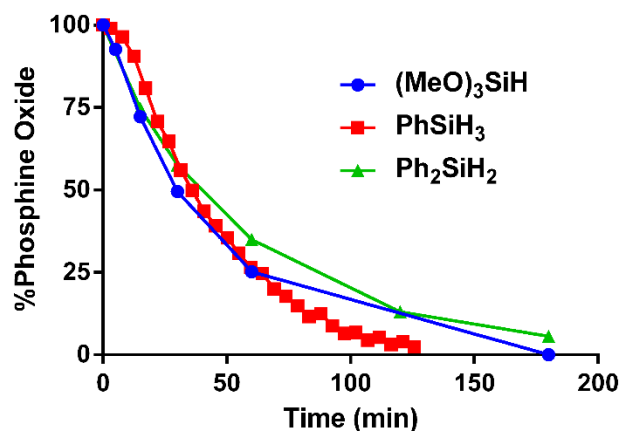


Figure 1.18. Comparisson of the reduction of **1PPO** by common silane reducing agents under pseudo first-order condntions at 80 °C.

Table 1.10. Calculated Mulliken charges of silane materials.^a

Entry	Silane	Charge (Si) ^b	Charge (H) ^b
1	Et ₃ SiH	0.742627	-0.110760
2	<i>n</i> -Hexylsilane	0.603273	-0.114822
3	TMDSO	0.823776 ^c	-0.121330
4	TMDSA	0.886715 ^c	-0.110102
5	Cl ₃ SiH	0.481423	-0.041978
6	(MeO) ₃ SiH	1.334744	-0.125532
7	Ph ₃ SiH	0.672585	-0.108150
8	Ph ₂ SiH ₂	0.799329	-0.112974
9	PhSiH ₃	0.534424	-0.103606
10	<i>p</i> -(CF ₃)-PhSiH ₃	0.524771	-0.109707
11	DPDS	0.823438 ^c	-0.120892
12	PhSiH ₂ (OH)	0.865300	-0.115566

^aDFT calculations performed with Gaussian using the M06-2X/6-31+G(d,p) basis set; ^bAtomic units; ^cAverage of two silicon centers.

We even explored the difference between tert-alkyl disiloxane and disilazane reductants, expecting neither substances to be effective, although this turned out to not be the case as the silazane (**TMDSA**) was much more active than its oxygenaceous analog (Figure 1.19). To explain the observed differences between the silazane **TMDSA** and siloxane **TMDSO**, we hypothesized that a key hydrogen bond between the silane and the oxygen atom of the phosphine oxide is required.⁶⁵ The competency of the silazane **TMDSA** is derived from its ability to serve as a hydrogen bond donor whereas the disiloxane **TMDSO**²⁰ cannot on its own participate in a hydrogen bond interaction with the phosphine oxide because it is a hydrogen bond acceptor (Scheme 1.6). Similarly, the far greater reactivity of phenylsilanol (in equilibrium with **DPDS**) as compared to phenylsilane could also be a result of its hydrogen-bond donating capacity. Unlike **DPDS**, **TMDSO** does not equilibrate to a silanol in the absence of strong Lewis or Brønsted acids.⁵⁹ Our hypothesis implies formation of a six-membered transition state (**TS-2**), in which a hydrogen-bond creates a bridge between the silanol/silazane and the phosphine oxide. As described in the next section we examined this putative transition state through NMR studies to probe silanol-phosphine oxide H-bonding, Hammett analysis, kinetic isotope effects, as well as the synthesis and evaluation of siloxanes to test the requirement for hydrido-silanol formation.

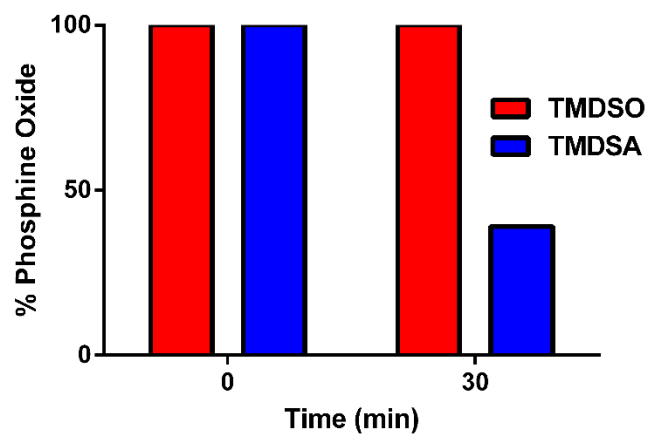
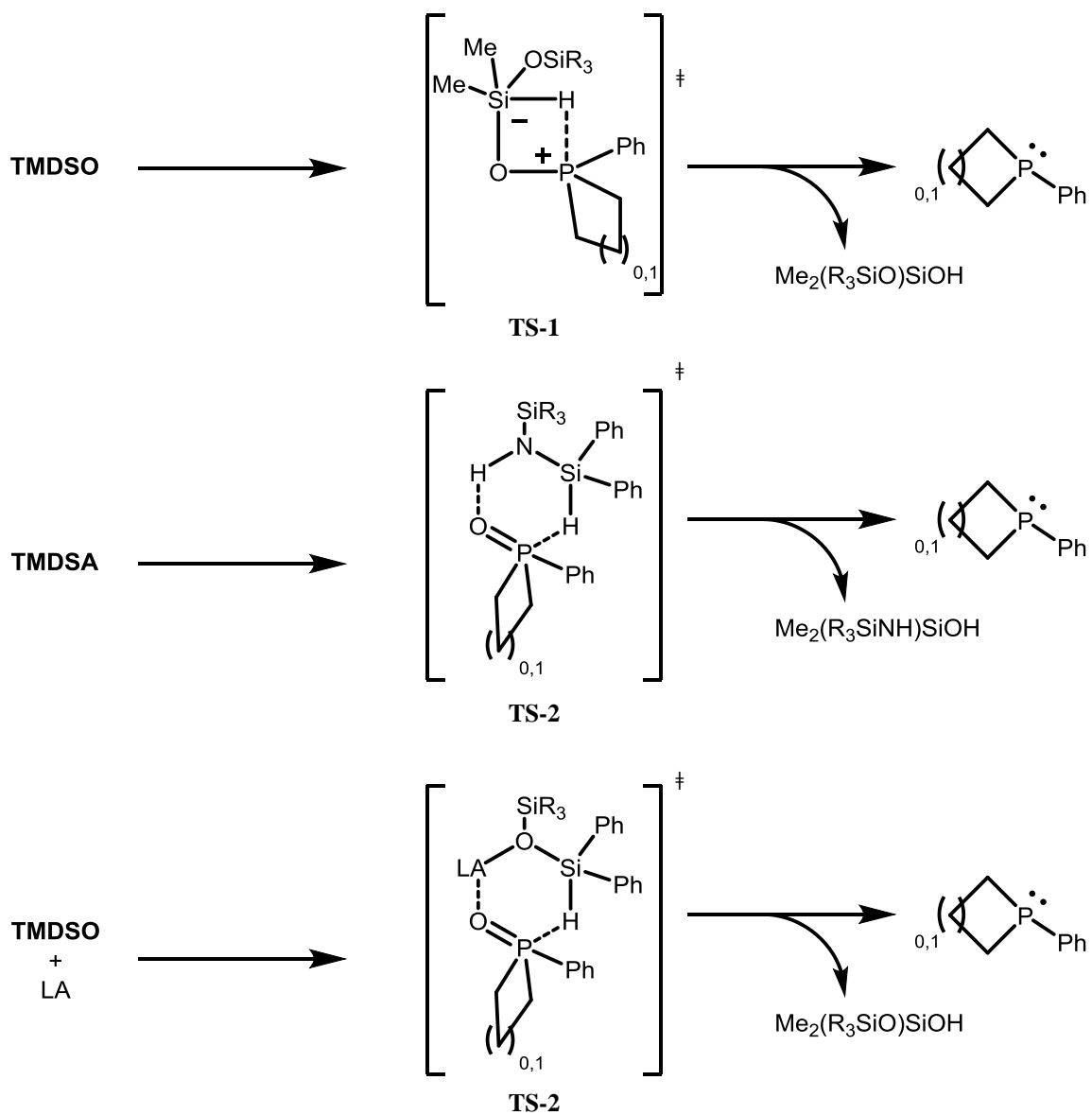


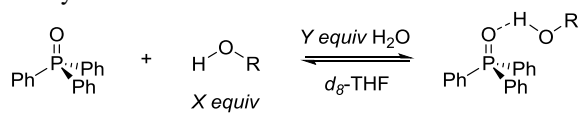
Figure 1.19. The reduction of **1PPO** by **TMDSO** (red) and **TMDSA** (blue) at 80 °C. Data collected by Dr. Carter Eiden.



Scheme 1.6. The amended transition state theory to account for our and others' observations.

The hydrogen bonding between silanols and phosphine oxides has recently been shown by Prof. Dr. Blumel and co-workers to be the primary interaction for adsorption of phosphine oxides onto silica surfaces.⁶⁵ These authors also reported a crystal structure of the **TPPO**•HOSiPh₃ adduct with a mean O···H distance of 1.8 Å. The strength of this interaction is evidenced by the lengthening of the P=O bond from 1.479 Å in pure **TPPO** to 1.503 Å in the **TPPO**•HOSiPh₃ adduct. These researchers also showed that the presence of hydrogen bonding could be shown using solid-state NMR technique as bound **TPPO** had a unique down-field shift (represented in ppm) compared to free **TPPO**.⁶⁵ This phenomenon is also recapitulated in the solution phase as Blumel and co-workers also previously demonstrated that hydrogen peroxide complexes of various phosphine oxides presented this same trend. Using solution-phase ³¹P NMR to monitor potential H-bond interactions, we confirmed **TPPO** likely interacts via hydrogen-bonding with both diphenylsilanediol (Table 1.11) and triphenylsilanol (Table 1.12) at ambient temperature in *d*₈-THF as evidenced by the same downfield shift in ³¹P NMR spectra (Figure 1.20). Also in accordance with Blümel's data, the addition of water led to a greater downfield shift detected by ³¹P NMR (Table 1.11) indicative of the tighter hydrogen-bonding network. While water can increase the strength of phosphine oxide adsorption onto silica surfaces by acting as a bridge between these two surfaces, the placement of water between a phosphine and a silyl hydride would displace the crucial P=O···H-O-Si interaction, which is consistent with our observations that addition of water reduces the overall rate of silane-mediated reduction of phosphine oxides (Figure 1.21).

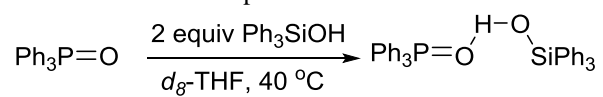
Table 1.11. Hydrogen-bonding between diphenylsilanediol and TPPO monitored by ^{31}P NMR.



Entry	X	Y	δ ppm ^a	Δ ppm ^b
1	0.0	0.0	23.69	0.00
2	0.5	0.0	24.40	0.71
3	1.0	0.0	25.20	1.51
4	2.0	0.0	26.23	2.54
5	0.0	2.0	24.50	0.81
6	0.5	2.0	25.34	1.65
7	1.0	2.0	25.78	2.09
8	2.0	2.0	26.65	2.96

^aTPP used as internal standard ($\delta = -5.41$ ppm); ^bCompared to TPPO alone.

Table 1.12. The effect of temperature on additive studies.



Entry	Temp (°C)	δ Shift (ppm)	Δ (ppm)
1	23	23.70	0.00
2	23	26.53	+2.83
3	80	26.55	+2.85

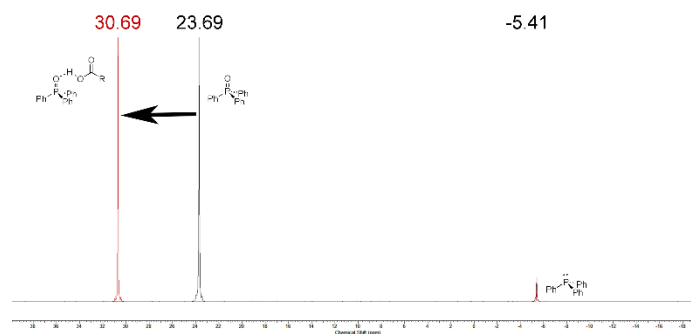


Figure 1.20. An example of observed downfield NMR shifts in ^{31}P NMR experiments with additives.

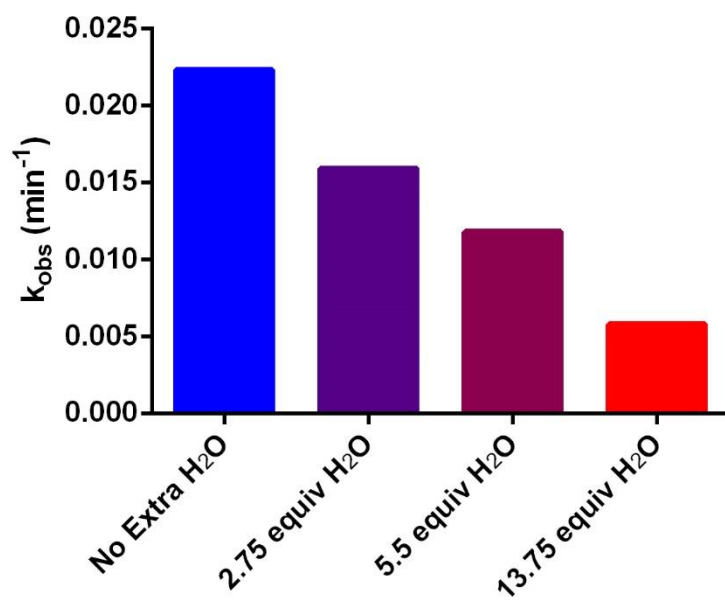


Figure 1.21. The effect of excess water on the observed rate of phosphine oxide reduction by silanes. Data collected by Dr. Carter Eiden.

To probe charge build up in the transition state we measured the rates of **DPDS**-mediated reduction of a panel of nine triphenylphosphine oxides (Figure 1.22) containing a range of electron-withdrawing and electron-donating substituents on one of the aryl rings, which were synthesized by adding aryl Grignard reagents to diphenylphosphoryl chloride. The rates for reduction (k) were monitored by ^{31}P NMR under pseudo first-order conditions (0.40 M **DPDS**, 0.04 M phosphine oxide). A plot of the relative rates $\text{Log}(k_X/k_H)$ versus the Hammett σ_P substituent constant (Figure 1.22) gave a linear fit with a slope ($\rho = -0.3951$, $R^2 = 0.9685$). The negative slope (ρ) suggests a modest build-up of positive charge at phosphorous in the rate determining step, indicative of either phosphine oxide equilibration to its ylide resonance form, or direct hydride transfer to the phosphorus center.⁶⁶ To experimentally verify that hydride transfer is the rate-limited step during phosphine oxide reductions, we also measured the primary kinetic isotope effect (KIE) for reduction of **TPPO** by **DPDS**. For this study we synthesized tetradeuterated d_4 -**DPDS** wherein all Si-H bonds were replaced with Si-D. We observed a large KIE of 5.3 at 110 °C consistent with hydride transfer as the rate-determining step (Figure 1.23).

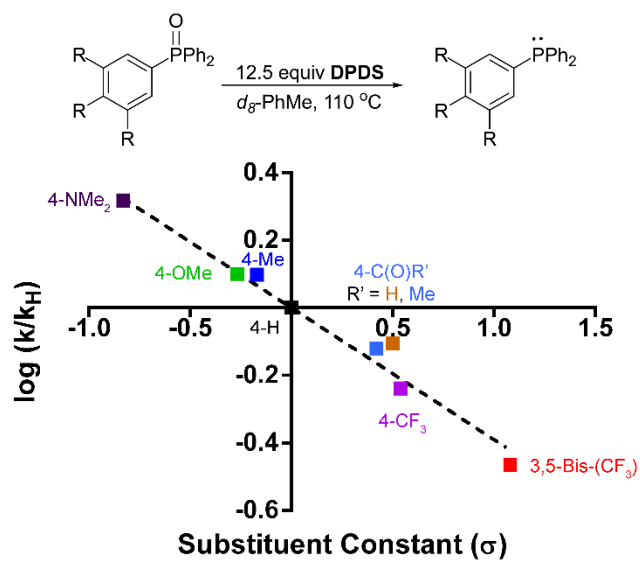


Figure 1.22. The Hammett plot for the reduction of acyclic phosphine oxides by **DPDS** at 110 °C. Data collected by Kathleen Wang.

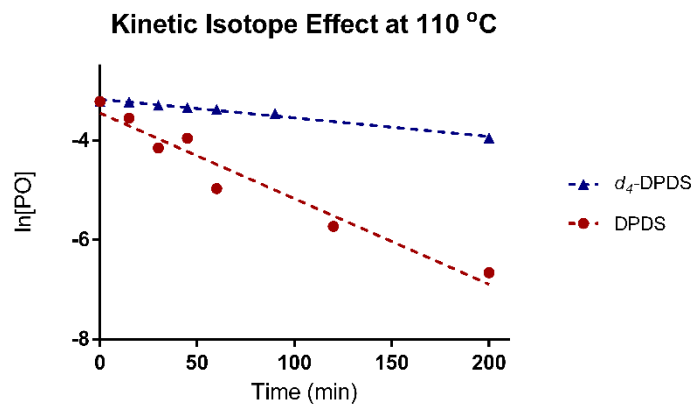


Figure 1.23. The kinetic isotope effect for the reduction of phosphine oxides with proteo- and deuterio-**DPDS** at 110 °C. Data collected by Kathleen Wang.

While the previous NMR, Hammett, and KIE studies provided valuable mechanistic information, these studies failed to provide unequivocal confirmation for **TS-2** or against **TS-1**. We thus devised and synthesized a series of *Si,Si*-diphenylsilanes to probe whether hydridosilanol ($\text{H-SiR}_2\text{OH}$) are absolutely required for reduction. Diphenylsilane, a commonly used reductant of phosphine oxides with similar kinetics as phenylsilane (Figure 1.18) was used as a benchmark for reactivity. 1,1,3,3-tetraphenyldisiloxane (**TPDS**), which equilibrates to form diphenylsilanol, should be a more rapid reductant than diphenylsilane, as it bypasses the proposed pre-activation step, much like **DPDS**. Methylidiphenylsilane (**MDPS**), on the other hand, is unable to form a hydridosilanol, and should thus provide evidence as to whether or not reduction can proceed through **TS-1** at 80 °C. The reactivity of these silanes was evaluated in the reduction of **TMPPPO**. In line with our expectations, **TPDS** was indeed faster than diphenylsilane, while **MDPS** was completely unreactive at 80 °C (Figure 1.24). As outlined in Scheme 1.7, both **TPDS** and diphenylsilane are capable of forming a hydrido-silanol, the active functional group for reduction, while **MDPS** cannot, and therefore does not lead to reduction at temperatures below 110 °C. Moreover, every tri-substituted silane, outside of those silanes containing alkoxy or chloro functionalities, which can easily hydrolyze to afford hydrido-silanols, were incompetent reducing agents at 110 °C. Trisubstituted silanes can reduce phosphine oxides at temperatures exceeding 250 °C,^{13, 16, 61} which is consistent with the higher energy **TS-1**, whereas hydrido-silanols are effective at 80 °C, presumably through **TS-2**.

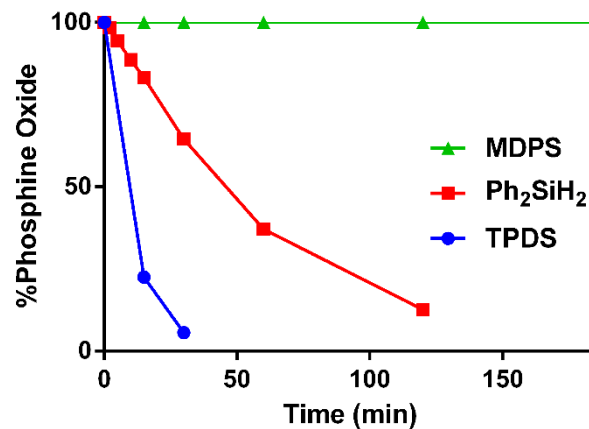
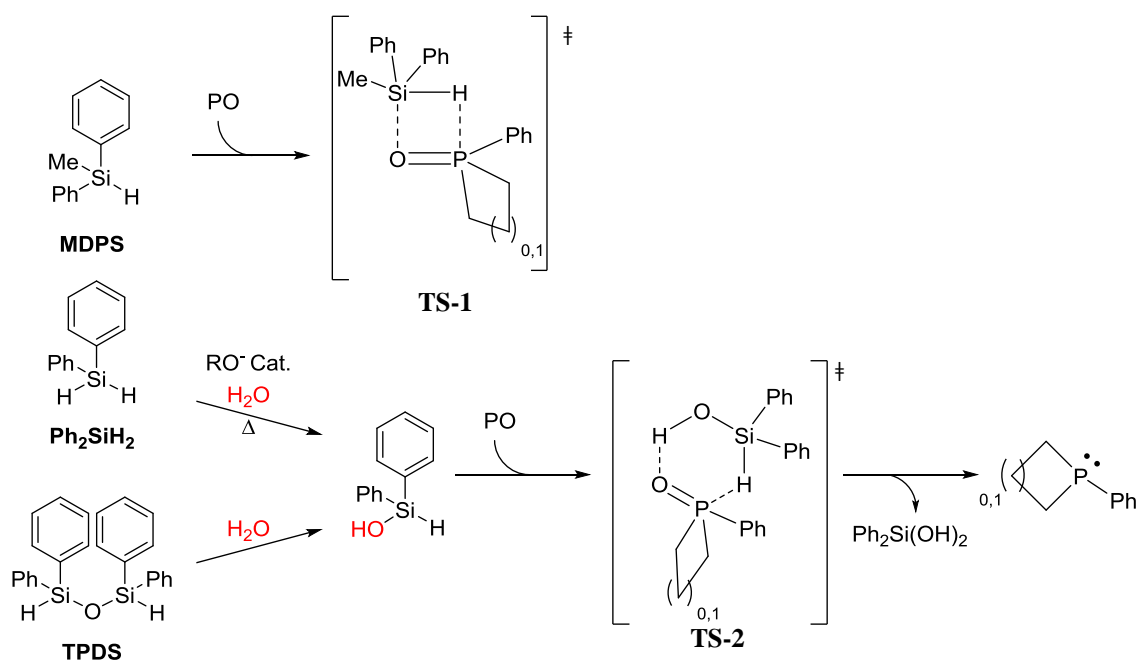


Figure 12: The reduction of **TMPPPO** with *Si, Si*-diphenylsilanes at 80 °C where [PO] = 0.04 M and [Si] = 0.40 M.

Figure 1.24. The reduction of **TMPPPO** with *Si, Si*-diphenylsilanes at 80 °C. Data collected by Dr. Carter Eiden.



Scheme 1.7. Putative reactivity and transition states of **MDPS** (top), diphenylsialne, and **TPDS** (bottom) with phosphine oxides.

The interactions of phenylsilane/phenylsilanol, and phosphines oxides were calculated by DFT employing the M06-2X/6-31+g(d,p) level of theory,⁵⁶ analogous to previous studies. Also in conjunction with other studies, these calculations were performed under the assumption that a non-polar, aprotic solvent is used for these reactions. Unsurprisingly, before engaging in either transition state, a pre-reaction complex is formed in which atoms of both molecules come in proximity of each other. However, modeling only this part of the reaction led to an interesting theoretical find in which the pre-reaction complex (PC) formed between phenylsilanol and phosphine oxides is actually favorable (Figure 1.25). In fact, this is the only such case that has been reported. The reduction in entropy is outshined by the favorable enthalpy from the formation of the hydrogen bond (Table 1.13). While these calculations are not indicative of the six-membered transition state being ultimately lower in energy, it does reflect the rapid nature of the reaction's onset. We are continuing to investigate this reaction and our proposed mechanism via computational means.

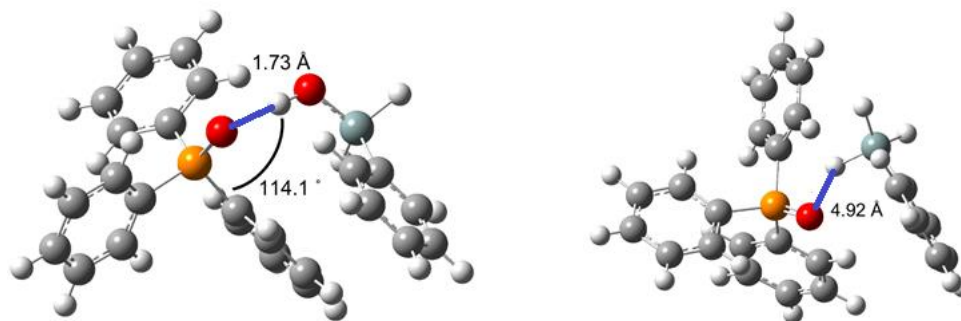


Figure 1.25. The optimized PC of **TPPO** with A) PhSi(OH)H₂ and B) PhSiH₃ at the M06-2X level of theory. Data collected by Kathleen Wang.

Table 1.13. The calculated energies and geometries of PCs with TPPO at the M06-2X level of theory.

Parameter	TPPO + PhSi(OH)H₂	TPPO + PhSiH₃	TPPO + PhSiH₃ (Freq)
ΔH (kcal/mol)	-8.3	-0.6	-0.6
ΔS (cal/mol)	-19.3	-39.7	-34.1
ΔG (kcal/mol)	-2.6	+11.2	+9.6
P=O (Å)	1.5117	1.4995	1.5117
P=O···HO-	1.7340	4.9163	2.8729
Si/P=O···H-Si (Å)			
Si-H···P (Å)	4.1240	4.2717	4.1240
Si···P (Å)	4.3157	4.6469	4.3157
P=O···H-R (°)	114.12	n.d.	108.01

In addition to gaining an understanding about the reactivity of phenylsilanes, we wished to further characterize the requirements for activating inexpensive and safe alkyl disiloxanes. Disiloxanes can react via **TS-2** only if a metallic species, Lewis acid, or hydrogen atom bridges the gap between the oxygen of the disiloxane and the phosphine oxide, or if the equilibrium is shifted such that the silanol form is favored. For example, adding acid could shift disiloxane-silanol equilibrium by promoting dissociation to the silanol monomer thereby turning the silane into an H-bond donor, or could conversely turn the phosphine oxide into the H-bond donor through protonation. Consequently, addition of a borderline Lewis acid, such as ZnCl_2 , greatly improved the rate of reduction by **TMDSO**. ZnCl_2 may operate by shifting the equilibrium in similar manner as a protic acid, and/or by coordinating to both the reductant and phosphine oxide. In support of the latter mechanism, isolated ^{31}P NMR experiments with **TPPO** confirmed ZnCl_2 caused the greatest downfield NMR shift among the Lewis acid examined while LiCl induced the smallest shift, consistent with its inability to promote reduction by **TMDSO**. Interestingly, monitoring of the interactions of protic acids and phosphosphine oxides using the same assay also indicated eventual activity (Table 1.14). As summarized in Figure 1.26, reduction rate enhancement correlated very well with the downfield shift observed in ^{31}P NMR experiments. This finding can lead to the discovery of additives that are optimized to “activate” the phosphine oxide or disiloxane to improve reductive capabilities with green silane reducing agents such as **PMHS**.

Table 1.14. The ^{31}P NMR shifts resultant upon additive addition.

$$\text{Ph}_3\text{P}=\text{O} \xrightarrow[\text{d}_8\text{-THF, 40 }^\circ\text{C}]{\text{1 or 2 equiv Acid}} \text{Ph}_3\text{P}=\text{O} \begin{array}{l} \text{H}-\text{O} \\ \diagup \quad \diagdown \\ \quad \quad \text{R} \end{array} \quad \text{R} = \begin{array}{ll} -\text{C}(\text{O})\text{CR}'_3 & -\text{C}(\text{O})\text{Ar} \\ -\text{S}(\text{O})_2\text{CH}_3 & -\text{P}(\text{O})(\text{OAr})_2 \end{array}$$

Entry	Acid	1 Equiv δ Shift (ppm)	Δ (ppm)	2 Equiv δ Shift (ppm)	Δ (ppm)
1	None	23.70	0.00	23.70	0.00
2	$\text{CH}_3\text{C}(\text{O})\text{OH}$	26.12	+2.42	27.36	+3.66
3	$\text{CHCl}_2\text{C}(\text{O})\text{OH}$	28.11	+4.41	30.22	+6.52
4	$\text{CCl}_3\text{C}(\text{O})\text{OH}$	28.79	+5.09	31.45	+7.75
5	$\text{CF}_2\text{ClC}(\text{O})\text{OH}$	31.15	+7.45	31.83	+8.13
6	$\text{CF}_3\text{C}(\text{O})\text{OH}$	30.70	+7.00	32.07	+8.37
7	PNBA	27.04	+3.34	n.d. ^a	n.d. ^a
8	$\text{CH}_3\text{SO}_3\text{H}$	31.21	+7.51	33.81	+10.11
9	BNPA	32.55	+8.85	n.d. ^a	n.d. ^a

^aSolubility limited testing this set of conditions

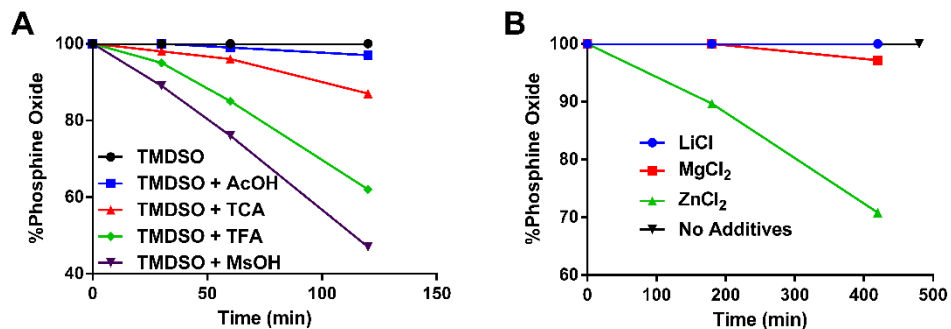
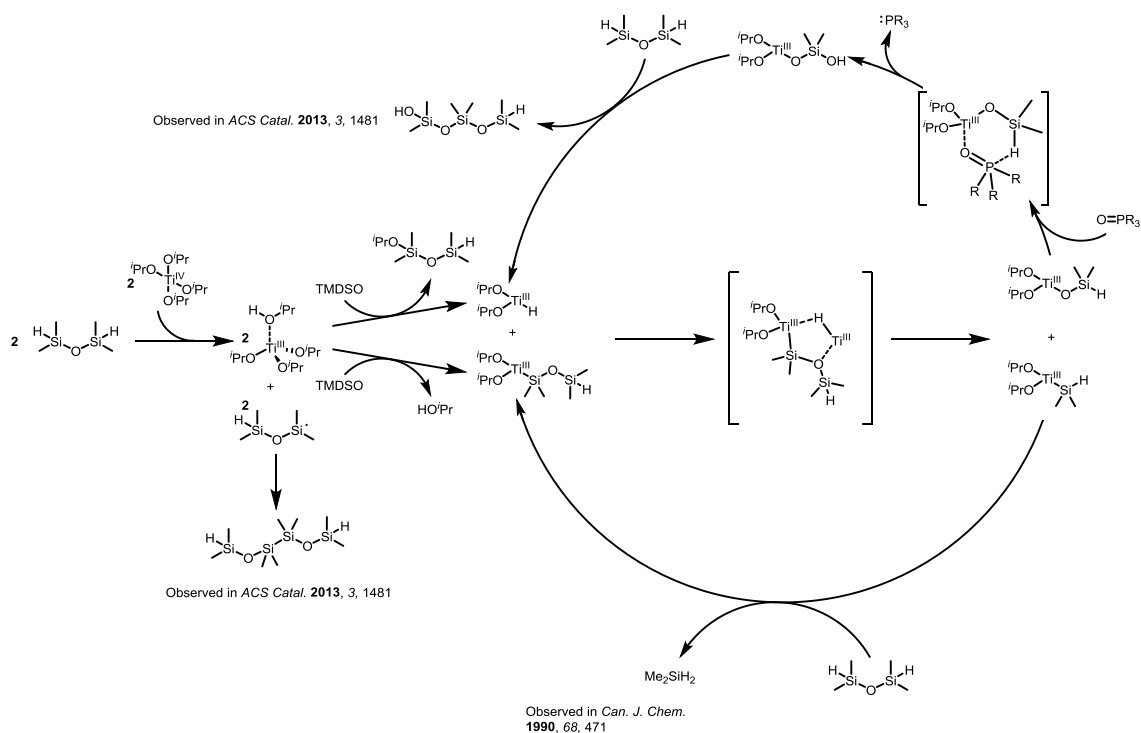


Figure 11. The reduction of **1PPO** using **TMDSO** at 80 °C.
 (A) With Brønsted acid additives where [PO] = 0.04 M, [Si] = 0.60 M, and [Acid] = 0.20 M;
 (B) With Lewis acid additives where [PO] = 0.04 M, [Si] = 0.60 M, and [M] = 0.20 M.

Figure 1.26. The reduction of **1PPO** using **TMDSO** and additives at 80 °C. A) With Brønsted acid additives; B) With Lewis acid additives.

We are also able to provide insight towards a report by Lemaire and co-workers, who used **TMDSO** to reduce phosphine oxides with titanium(IV) tetra-*iso*-propoxide as an additive and proposed a phosphorous-centered radical as a key reduction intermediate.²⁹ To test for the presence of this radical intermediate we synthesized a cyclopropanated phosphine radical clock; however, no detectable formation of ring-opened products were observed under Lemaire's conditions (Chapter 1.8). While the rates of α -scission for phosphoranyl radicals, proposed by Lemaire, is rather fast, and could account for our results, we hypothesized the Lewis acid may act through a variation of **TS-2** by activating dissociation of **TMDSO** into a monomeric silanoate and by coordinating the phosphine oxide and silanoate species via a 6-membered transition state analogous to **TS-2**. $\text{Ti}(\text{O}^i\text{Pr})_4$ is known to disproportionate **TMDSO** through a complex mechanism (Scheme 1.8), resulting in a silicon-titanium complex and release of gaseous dimethylsilane.⁶⁷ Additional reports have pointed towards an active Ti(III) species, another borderline Lewis Acid, which produces silane oligomers and reduces the phosphine oxide.^{29, 62} These combined observations suggest that a silyl-oxy Ti(III) species reduces phosphine oxides through the six-membered transition state **TS-2**, as the borderline Lewis acidic Ti(III) center substitutes for the Lewis-acidic proton (Schemes 1.6 and 1.8). Again, promoting the degradation of **PMHS** with similar, optimized, reagents might facilitate the use of this green, inexpensive, and safe silane.



Scheme 1.8. The amended mechanistic proposal for the reduction of phosphine oxides by TMDSO/Ti(IV) reduction systems.

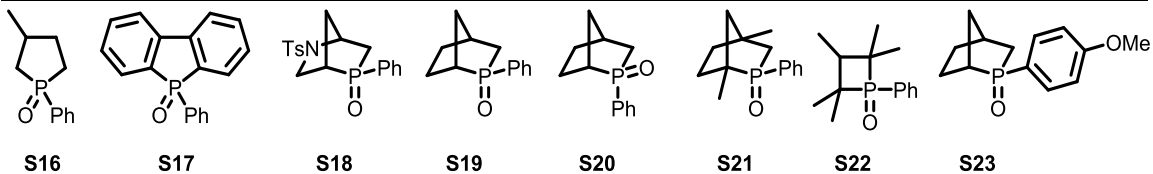
With a better understanding of the necessity for silane-mediated reductions of phosphine oxides, we hoped to be able to find a predictive model for the design of future phosphines for optimal redox catalysis. We tried to find a correlation of reaction rate to a variety of theoretical parameters from crude Mulliken charges to nucleophilicity parameters (Tables 1.15 and 1.16). As expected, we could not find any sort of correlation between silane reduction effectiveness and electronic parameters (Tables 1.10 and 1.15). However, we were surprised to find that there didn't seem to be any correlations of phosphine oxide global electronic parameters and reactivity when a larger set of phosphines were compared to each other (Table 1.16). As summarized in Figure 1.27, when phosphines of a similar nature are compared, calculated electronic parameters very tightly correlate with the rate of reduction by silane reducing agents. Yet, this assumption cannot be made when comparing silanes across scaffolds. With the current knowledge of phosphine oxide reactivity, we believe that new catalysts can easily be designed that add electron density to the oxygen atom while maintaining ring strain. These catalysts should pair well with disiloxane reducing agents, and the degree of strain necessary would be dictated by the desired application, as 4-membered phosphines lack the nucleophilicity necessary to mediate a variety of these reactions, while acyclic phosphines could be utilized in reactions which are tolerant of heating.

Table 1.15. The calculated global electronic parameters for silane materials.

Entry	Silane	μ (au)	η (au)	ω (eV)	ΔN_{max} (eV)	N (eV)
1	DHDS	-0.1623	0.3419	1.05	12.91	1.74
2	TPDS	-0.1507	0.2895	1.07	14.16	2.77
3	DPDS	-0.1550	0.2925	1.12	14.42	2.61
4	PhSiH ₃	-0.1534	0.3125	1.02	13.35	2.38
5	Ph ₂ SiH ₂	-0.1517	0.3039	1.03	13.59	2.55
6	(MeO) ₃ SiH	-0.1710	0.3668	1.08	12.69	1.17
7	PhSi(OH)H ₂	-0.1462	0.3182	0.91	12.50	2.50
8	Ph ₂ Si(OH)H	-0.1545	0.2980	1.09	14.10	2.55
9	("Hexyl)Si(OH)H ₂	-0.1688	0.3479	1.11	13.20	1.48

Table 1.16. The calculated global electronic parameters for phosphine oxide materials.

Entry	PO	μ (au)	η (au)	ω (eV)	ΔN_{max} (eV)	N (eV)
1	TPPO	-0.1605	0.3045	1.15	14.34	2.30
2	S9	-0.1316	0.2459	0.96	14.56	3.88
3	S10	-0.1619	0.2838	1.26	15.53	2.54
4	S11	-0.1727	0.2941	1.38	15.98	2.11
5	S12	-0.1802	0.2821	1.57	17.39	2.07
6	S13	-0.1861	0.2688	1.75	18.84	2.09
7	S14	-0.1813	0.2741	1.63	18.01	2.15
8	S15	-0.1556	0.2976	1.11	14.23	2.53
9	1PPO	-0.1590	0.3071	1.12	14.09	2.32
10	TMPPPO	-0.1587	0.3018	1.14	14.31	2.38
11	TMBPO	-0.1533	0.3114	1.03	13.40	2.40
12	TMPyrPO	-0.1388	0.2874	0.92	13.14	3.12
13	S16	-0.1608	0.3049	1.15	14.34	2.30
14	S17	-0.1475	0.2778	1.07	14.45	3.02
15	S18	-0.1668	0.2937	1.29	15.46	2.27
16	S19	-0.1675	0.2836	1.35	16.07	2.40
17	S20	-0.1744	0.2704	1.53	17.54	2.38
18	S21	-0.1566	0.2996	1.11	14.23	2.47
19	S22	-0.1778	0.2522	1.71	19.19	2.54
20	S23	-0.1656	0.2425	1.54	18.58	3.01



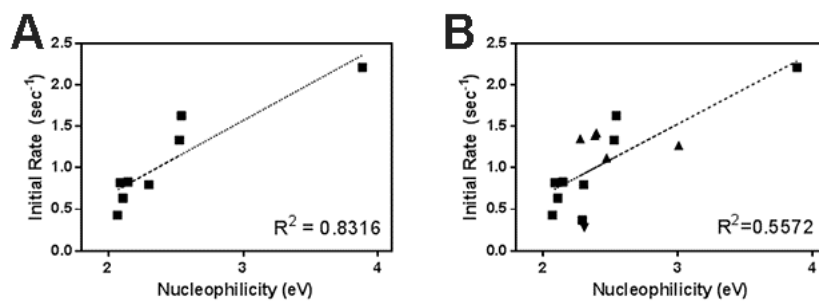


Figure 1.27. The comparison of the computed nucleophilicity index at the M06-2X/6-31+G(d,p) level of theory and the reduction of phosphine oxides. A) Acyclic phosphine oxides (Figure 1.22); B) Current and previously reported phosphine oxides incorporating cyclic and acyclic phosphine oxide reagents. Data collected by Kathleen Wang.

The combination of rational reagent synthesis and kinetic analysis led to the characterization of the entire mechanism of phosphine oxide reduction by phenylsilane, as well as the determination of the transition state of reduction by any hydridosilane. This directly led to the development of **DPDS**, an unparalleled reducing agent for phosphine oxides. Reductions of phosphine oxides by silanes, such as phenylsilane, underwent with a sigmoidal curve under pseudo-first-order conditions, data which suggested that the previously proposed mechanism was incongruous with the actual mechanism. Our results have overturned the accepted mechanism, while simultaneously explaining over 50 years of reported observations, thus enlightening our own discovery efforts. Hydrido-silanols represent supreme reducing agents which circumvent the slow activation step, as evident by the lack of a sigmoidal reaction progress curve and rapid reduction of both acyclic and cyclic phosphine oxides.⁶⁴ This work also highlights the power of reaction progress kinetic analysis and simulation to extract subtle kinetic features, which can prove crucial for prioritizing among multiple possible reaction mechanisms

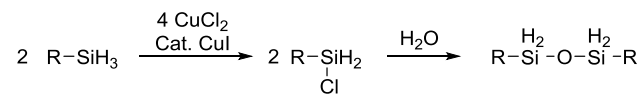
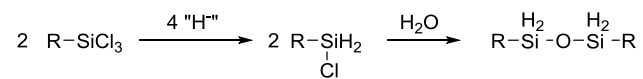
1.4 Scalable preparation of hydrido-disiloxanes

With the discovery of the reason as to why DPDS is such a powerful reductant, we decided to pursue the use of this reagent in the development of redox recycling reactions, a feat that required scaled-up synthesis of this reagent from simple, inexpensive, and widely-available starting materials.

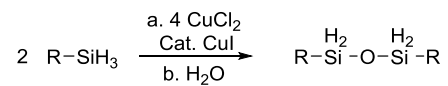
The synthesis of silanols and disiloxanes is well known as these compounds have applications in a broad range of chemistry, from the synthesis of therapeutics⁶⁸ to liquid crystals.⁶⁹ Transition-metal catalyzed oxidation of precursor silanes is the most common strategy to prepare silanols and disiloxanes,⁷⁰ but these methods lead to complete oxidation of the silane to either a

mono-, di-, or tri-silanol depending on the number of Si-H bonds.⁷¹ One report of an In(III)-catalyzed direct oxidation suggests that the mono-oxidation product can be obtained,⁷² however, this reaction was only performed on a small scale, and the reaction was not extended to phenylsilane. The generation of a full equivalent of hydrogen gas is also a safety concern. Hydrido-disiloxanes have historically been prepared through an alternative two-step sequence involving preparation and isolation of a mono-halogenated silane followed by hydrolysis (Scheme 1.9).⁷³ Synthesis of the intermediate halosilanes is challenging, as is evident by the lack of their commercial availability,⁷⁴ with multiple methods furnishing complex mixtures.⁷⁵ Consequently, much effort has been put into the synthesis of mono-halogenated silanes and two complimentary approaches have emerged that address previous synthetic deficiencies. The first of these employs concentrated HBr to displace a phenyl group on a silane with a bromide⁷⁶ while the second approach uses copper(II) chloride to directly chlorinate hydrido-silanes.⁷⁷ Zhang and co-workers^{77b} further improved on the latter copper(II) chloride halogenation through “ball-milling”. Herein, we report a one-pot experimental method for the preparation of **DPDS** and related hydrido-disiloxane reagents in high purity from commercially available silanes. This scalable procedure furnishes hydrido-disiloxanes in improved yield,^{72, 77} substantially lowers the time required to obtain product with only a single purification step.

Previous Methods: Two Purifications Necessary



This Work: Only One Purification

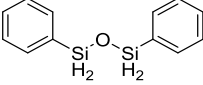
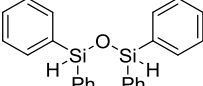
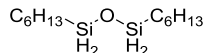
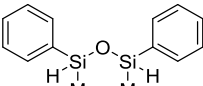


Scheme 1.9. Synthesis of hydrido-disiloxane materials from literature and this work.

The synthesis of **DPDS** begins with the complexation of CuCl_2 and catalytic CuI in diethyl ether for 30 min in the presence of either chrome or ceramic spheres. Phenylsilane is then added and the reaction is ball-milled at 350 rpm at ambient temperature under air with an overhead stirrer for 1.5 h until 100% conversion is noted by ^1H NMR to afford the intermediate chlorophenylsilane. The reaction mixture is filtered directly onto ice chips (chapter 1.8) and extracted with diethyl ether to afford **DPDS** in 93% percent yield and approximately 95% purity, which is sufficient for most applications. Distillation under high-vacuum can be performed to provide **DPDS** in >99% purity and 88% overall yield in cases where higher purity is required (Table 1.17, Entry 1). The reaction is scalable and does not require increased reaction times to obtain purified product. For example, **DPDS** is obtained in 88% yield on a 10 gram scale in less than three hours. The reaction conditions can be extended to secondary arylsilanes as well as alkylsilanes, as diphenylsilane and *n*-hexylsilane were readily converted to 1,1,3,3-tetraphenyl-disiloxane **TPDS** and 1,3-di-*n*-hexyl-disiloxane **DHDS** in 90% and 85% yield, respectively (Table 1, Entries 2-3) while a combination of these substitution patterns was also tolerated as 1,3-dimethyl-1,3-diphenyl-disiloxane **DMDPDS** was synthesized in 85% yield (Table 1.17, Entry 4).

Table 1.17. The Direct Synthesis of Symmetrical Disiloxanes from Commercially-Available Silanes.

$$\begin{array}{ccc}
 \text{R}_3\text{Si-H} & \xrightarrow[\text{Et}_2\text{O, 23 }^\circ\text{C, 2 h}]{\text{a. 2.0 equiv CuCl}_2, \text{ 0.1 equiv CuI}} & \text{R}_3\text{Si-O-SiR}_3 \\
 \mathbf{1} & & \mathbf{2} \\
 & \text{b. H}_2\text{O, 0 }^\circ\text{C, 15 min} &
 \end{array}$$

Entry	Product	Yield (%) ^a
1	2a 	93 ^{b c}
2	2b 	90
3	2c 	85 ^d
4	2d 	85

^aIsolated Yield of two trials at 15 mmol scale

^bYield was 93% before distillation (>95% purity) and 88% after distillation (99% purity)

^cYield on 90 mmol (10 gram) scale was 88% (with >95% purity)

^dThis reaction required 5 hours for step "a" before filtration onto ice

Our efficient approach utilizes mechano-chemistry in an effort to significantly reduce the reaction time from more than 8 hours (magnetic stirring) to only 1.5 hours. During the reaction CuCl_2 is reduced to a Cu(I) species, which coat the CuCl_2 particles and hinder progression of the reaction. The physical grinding during the comminution process ensures CuCl_2 is continually exposed. As such, the balls utilized should be fairly large in diameter (at least $\frac{1}{2}$ inch) to avoid the inhibition of the reaction through buildup of byproduct on the heterogeneous CuCl_2 . We explored different materials for the ball-milling procedure and found ceramic spheres were preferred over chrome ones since the reaction yield was compromised when metal balls were reused multiple times (Chapter 1.8). This is likely due to the inert nature of ceramic, as this material is chemically stable to the reaction conditions. Another advantage with respect to laboratory scale reactions utilizing transition metal catalysis is the CuCl_2 mediated mechano-chemical method does not produce a stoichiometric amount of hydrogen gas, and all byproducts are simply washed away with cold water. In addition, this protocol can be implemented in standard laboratory glassware, rather than requiring specialized ball-milling equipment.

We have described an efficient one-pot mechano-chemical procedure for the synthesis of hydrido-disiloxanes. The high yield, simple experimental set-up, and short reaction time are all ideal for laboratory scale preparations of hydrido-disiloxanes, which are valuable compounds for the chemoselective reduction of phosphine oxides. The ability to easily prepare useful quantities of hydrido-disiloxanes is expected to not only make the newly characterized reducing agent **DPDS** highly accessible for both phosphorous recycling and phosphine synthesis, but also to unleash the full potential of this entire class of under-explored reagents through stimulating further investigations into their unique reactivity.

We expect to find broad usage of **DPDS** and other hydrido-silanols in both conventional phosphine syntheses as well as future catalytic-in-phosphine reactions due to its excellent chemoselectivity and superior reducing power. Additional applications of DPDS may also be discovered, and thus a scalable synthesis was mandatory in order to discover the true potential of this novel reagent.

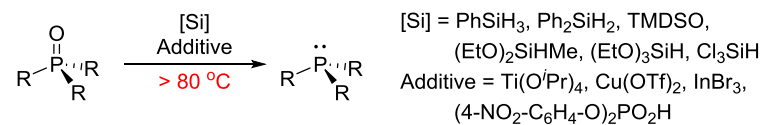
1.5 Characterization of 1,3-diphenyl-disiloxane as a chemoselective reducing agent

Trivalent phosphorus(III) compounds promote a substantial portion of synthetic organic chemistry, from classical transformations including the Wittig olefination⁷ and Mitsunobu condensation¹⁰ to contemporary metal-catalyzed bond formations such as Suzuki-Miyaura and Buchwald-Hartwig reactions.⁷⁸ Reduction of stable phosphine(V) oxides remains the most straightforward preparation of phosphines, and is often essential for the construction of easily-oxidized electron-rich phosphines.^{6, 16} Unfortunately, current methods are extremely harsh, which limits the substrate scope and precludes reaction telescoping.⁷⁹

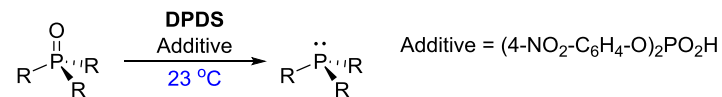
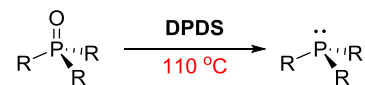
Common reducing agents such as aluminum hydrides either require prolonged heating or the addition of strong alkylating agents (e.g. MeOTf) to furnish phosphines from their corresponding oxides.⁸⁰ Such conditions are marred by indiscriminate functional group reduction and necessitate special precautions for handling on a large scale. Silanes are thus preferred due to their improved chemoselectivity,^{13, 17, 39} yet remain incompatible with many functional groups as they require elevated temperatures and additives such as $\text{Ti}(\text{O}^i\text{Pr})_4$ ²⁹ (Scheme 1.10). In a significant advance in the field, Beller and co-workers disclosed the silane-mediated reduction of phosphines employing a strong Brønsted acid along with a large excess of silane, enabling chemoselective reduction of acyclic phosphines at 110 °C even in the presence of sensitive

functional groups.²⁵ Though impressive, optimal conditions required four equivalents of silane per P=O bond, a strong Brønsted acid, and refluxing conditions (toluene, 110 °C, 24 h), leaving considerable room for improvement in regards to atom economy and reaction rate. Other Brønsted acid additives have been reported to promote silane-mediated reductions, but none of these methods have greater functional group specificity, nor the optimal atom economy of an additive-free system.^{24, 27} Specifically, laboratory-scale syntheses of phosphines would be greatly enhanced with a rapid, chemoselective, and low-temperature method for reduction of phosphine oxides, whereas industrial-scale syntheses would benefit from a more atom-economical and additive-free method to reduce waste generation and improve the ease of purification.³⁸

Previous Methods: Requires Additives **and Heat** for Reduction

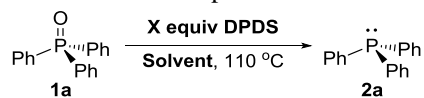


This Work: **Additive-Free and Ambient Temperature** Reductions



Scheme 1.10. The silane-mediated reduction of phosphine oxides from this and previous work.

To begin our investigation into an improved method for reduction of phosphine oxides, we selected triphenylphosphine oxide (**TPPO**) as a model substrate employing refluxing toluene as the initial reaction conditions. To render this method easy to implement, all reactions were performed without the exclusion of air or water. Consistent with precedent,^{25, 29} common silyl hydrides (PhSiH_3 , Ph_2SiH_2 , $(\text{MeO})_3\text{SiH}$, $(\text{EtO})_2\text{MeSiH}$, and **TMDSO**) were ineffective reductants as determined by ^{31}P NMR (Table 1.18, entries 1–5), with only PhSiH_3 producing an appreciable amount of triphenylphosphine (**TPP**). *n*-Hexylsilane (Table 1.18, entry 6) was also a poor reagent, at which point we noted that two of the most commonly used classes of reductants were aryl silanes (PhSiH_3 , Ph_2SiH_2) and alkyl siloxanes (**TMDSO**, **PHMS**). Since we found aryl silanes were much more effective than alkyl silanes, we hypothesized that the corresponding aryl siloxanes would be superior to alkyl siloxanes. Surprisingly, aryl siloxanes have not been explored as potential reductants for phosphine oxides. As such, we wished to apply the known reactivity of **DPDS** to determine if it could reduce acyclic phosphine oxides. To our delight, 1.5 equivalents of **DPDS** afforded a 99% isolated yield of **TPP** in 24 h (Table 1.18, entry 7). To highlight the reducing power of this new reagent, only 0.75 equivalents of **DPDS** produced an 84% isolated yield of reduced phosphine (Table 1.18, entry 8). An investigation of “green” solvents (Table 1.19) indicated that toluene (PhMe) and *tert*-butyl acetate (TBAc) were optimal for this reduction. Using TBAc for improved solubility, we consistently obtained a 99% yield of **TPP** with 1.25 equivalents of **DPDS** in 24 h (Table 1.18, Entry 11). These reaction conditions also worked well on 10 mmol scale, as the reduction of **TPPO** occurred in quantitative yield.

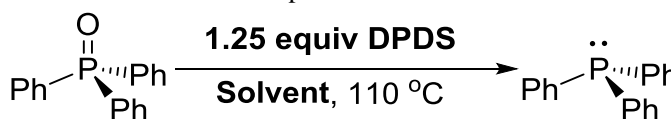
Table 1.18. The Optimization of Additive-Free Phosphine Oxide Reductions with DPDS.

Entry	Silane	X	Solvent	Yield (%) ^[a]
1	PhSiH ₃	1.5	<i>d</i> ₈ -PhMe	33 ^[b]
2	Ph ₂ SiH ₂	1.5	<i>d</i> ₈ -PhMe	0 ^[b]
3	(MeO) ₃ SiH	1.5	<i>d</i> ₈ -PhMe	<5 ^[b]
4	(EtO) ₂ MeSiH	1.5	<i>d</i> ₈ -PhMe	0 ^[b]
5	TMDSO	1.5	<i>d</i> ₈ -PhMe	0 ^[b]
6	C ₆ H ₁₃ SiH ₃	1.5	<i>d</i> ₈ -PhMe	5 ^[b]
7	DPDS	1.5	PhMe	99
8	DPDS	0.75	PhMe	84
9	DPDS	1.0	TBAC	90
10	DPDS	1.1	TBAC	95
11	DPDS	1.25	TBAC	99

^[a]Average isolated percent yields for two reactions at 0.5 mmol scale after 24 hours,

^[b]Average ³¹P NMR yield for two reactions at 0.5 mmol scale after 24 hours.

Table 1.19. Solvent Screen of Phosphine Oxide Reductions at 110 °C.



Entry	Solvent	Boiling Point	Isolated Yield ^[a]
1	Toluene	110	Quant.
2	Heptane	108	N/A ^[b]
3	Cyclohexane	80	N/A ^[c]
4	2-MeTHF	80	N/A ^[c]
5	Methyl cyclohexane	101	94
6	CPME	106	92
7	TBAc	95	99
8	Ethyl lactate	154	24
9	[Bmim] PF ₆	N/A	66

^[a]Average isolated yield of at least two reactions after 24 hours, ^[b]Phosphine oxides were not at all soluble in these reaction schemes, ^[c]The reaction mixture completely over-boiled at this temperature.

A real-time comparison of our optimized reaction with **DPDS** to those reported by Beller²⁵ and Lemaire²⁹ revealed that our system, under “dump-and-stir” conditions as described above, is the fastest of the three, concluding in about half the time as the next most rapid method (Figure 1.28). This is despite the fact that Beller’s conditions include four equivalents of silane, which causes the observed single-exponential decay of the concentration of **TPPO**. The sluggishness of Lemaire’s conditions without the exclusion of air and water is also notable. Our system is additive-free and utilizes only a slight stoichiometric excess of silane, yet it still reaches completion much more rapidly than the current state-of-the-art conditions.

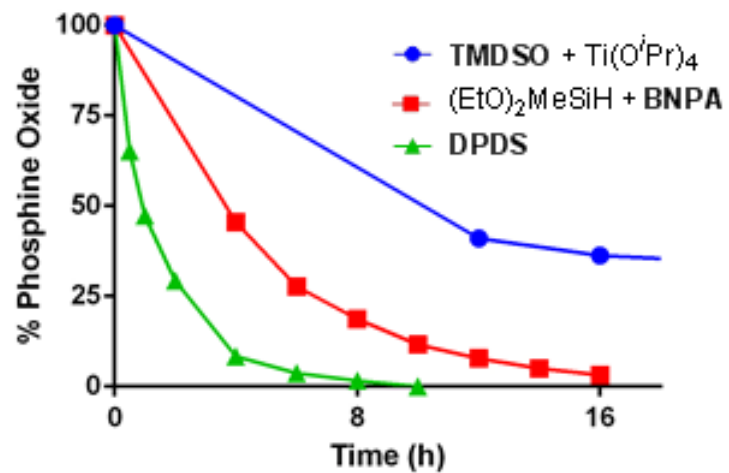


Figure 1.28. Reaction progress curves of the reduction of **TPPO**, monitored by ^{31}P NMR, comparing Lemaire's system²⁹ (blue), Beller's system²⁵ (red), and 1.25 equiv **DPDS** (green). Data collected by Dr. Carter Eiden.

We monitored the reaction kinetics at temperatures ranging from 80 to 120 °C to measure the energy barrier for the reaction. Arrhenius analysis (Figure 1.29) indicated an activation energy of 18.0 ± 1.1 kcal/mol for the reduction of **TPPO** by **DPDS**. This was surprising, as our measurements indicate a profoundly smaller energy barrier than the >40 kcal/mol calculated by Demchuk and co-workers for the reduction of **TPPO** by phenylsilane²³ as well as the 27.2 kcal/mol calculated by Krenske for the reduction of trimethylphosphine oxide with trichlorosilane.²² While decreasing the electron density of the silicon atom has been postulated to improve the rate of reduction, our disiloxane reagent would still not be as Lewis acidic as trichlorosilane.²² The drastic differences between experimental and calculated activation energies suggests that **DPDS** may reduce phosphine oxides through an alternative mechanism as previously presented. We also believe that silanes are not simple reducing agents, as **DPDS** seems to react similarly to the combination of phenylsilane and a Brønsted acid catalyst.⁸¹

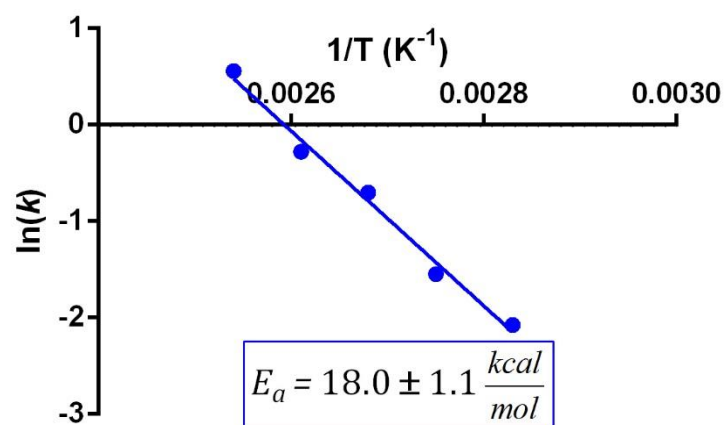
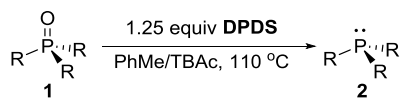


Figure 1.29. Arrhenius analysis of the reduction of **TPPO** with **DPDS** over the temperature range of 80 – 120 °C.

We next investigated the chemoselectivity of **DPDS** with a variety of substrates containing reactive functional groups (Chapter 1.8). At 110 °C, **DPDS** did not reduce aldehyde, nitro, ester, olefin, and cyano functional groups (Chapter 1.8), indicating that **DPDS** is very selective for the P=O bond. However, **DPDS** did react with unprotected alcohols to form a transiently protected compound that we and others^{21a, 51} have been unable to isolate (Chapter 1.8). This compatibility profile indicates that **DPDS** would be suitable for exploration as a reductant in redox recycling reactions,^{18-21, 24, 51} while also indicating that our reaction conditions are on par with the state-of-the-art reductions.²⁵ Satisfied with the observed chemoselectivity, we examined the scope of **DPDS** reduction with a panel of acyclic phosphine oxides. Both electron-rich and electron-deficient tertiary phosphine oxides were cleanly reduced, furnishing high yields of the corresponding phosphines (Table 1.20, entries 1–4). It is noteworthy that extremely electron-poor substrates, such as hexafluoromethyl phosphine oxide, take longer to reduce (Table 1.20, Entry 5). Tricyclohexylphosphine oxide also reacted lethargically, though the success of electron-rich triarylphosphine oxides suggests difficulties are likely due to steric concerns rather than electronic effects. Bidentate phosphine oxides were successfully reduced (Table 1.20, entries 9–12) with high fidelity in yields ranging from 75–94%. Reduction of chiral phosphine oxide derived from DIPAMP to the corresponding phosphine occurred with retention of configuration. Phosphines containing reactive functional groups such as aldehyde were also readily reduced without undesired reactivity (Table 1.20, entries 13-14). Lastly, we found secondary phosphine oxides such as diphenylphosphine oxide (**DPPO**) and di-*tert*-butylphosphine oxide (**DTBPO**) were reduced the fastest (Table 1.20, entries 14-15), with quantitative conversion to **DPPO** complete within 10 minutes. The differential reactivity between **DPPO** and **DTBPO** also points to steric

effects as a crucial indicator for the rapidity of reduction with **DPDS**. Our exploration of the scope of this reaction, in addition to our knowledge from stability studies, indicates that our new method is extremely mild while maintaining atom efficiency.

Table 1.20. The Substrate Scope of Additive-Free Reductions of Phosphine Oxides by **DPDS**.

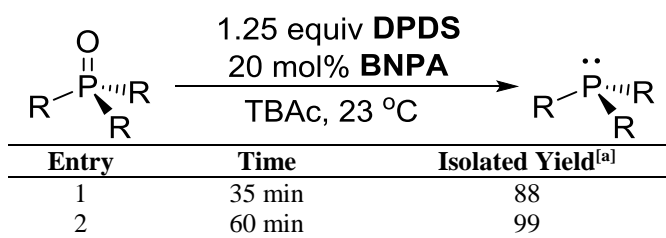


Entry	Phosphine	Yield (%) ^[a]
1		89
2		87
3		82
4		81
5		60 ^[b]
6		80 ^[b]
7		93
8		87
9 ^[c]		88
10 ^[c]		94
11 ^[c]		79
12 ^[c]		75 ^{[d],[e]}
13		97
14		96 ^[f]
15		>99 ^{[f],[g]}

^[a]Average isolated percent yields for two reactions at 0.5 mmol scale after 16-24 hours, ^[b]Reactions isolated after 48 hours, ^[c]Reactions utilized 2.5 equivalents of **DPDS** (1.25 equiv. per P=O), ^[d](*R,R*)-DIPAMP dioxide utilized as the starting material, ^[e] $[\alpha]_D^{20} = -85.6$ ($c = 0.7$), ^[f]Yield determined by ³¹P NMR, ^[g]Reactions complete within 10 minutes. ^[h]Reactions complete within 3 hours.

Having completed the development of a mild, additive-free, and atom-economical methodology for the reduction of phosphine oxides, we next attempted to create the first ambient system in order to further expand the applicable substrate scope. We observed that the addition of 20 mol% of bis-(*p*-nitrophenyl)phosphoric acid (**BNPA**),²⁵ to reductions with **DPDS** at 110 °C resulted in quantitative isolated yields within an hour (Table 1.21). This result, in combination with the success of Beller's application of **BNPA**,²⁵ indicates that with more robust phosphine oxides, the addition of **BNPA** to **DPDS**-promoted reductions at 110 °C would radically decrease the time to completion without harming the yield, and could potentially be used to lower the required temperature. We were delighted to find that addition of a combination of **BNPA** and **DPDS** to a solution of **TPPO** in EtOAc at room temperature temperature furnished **TPP** in quantitative yield after 48 hours (Table 1.22). Applying similar conditions to a range of acyclic mono- and bidentate phosphorous(V) oxides consistently afforded the product phosphines in both high yield and high specificity (Table 1.23). Additionally, the corresponding phosphines were produced in exquisite purity, frequently only requiring filtration through a plug of silica gel. Similar to the additive-free system, sterically encumbered phosphine oxides with multiple cycloalkyl substituents exhibited sluggish reactivity. At ambient temperature, we observed flawless functional group compatibility with **DPDS** and **BNPA**, as an unprotected alcohol-containing phosphine oxide was reduced to its corresponding phosphine with high fidelity. An additional benefit of the extremely gentle reaction conditions was a sharp increase in the yield of secondary phosphine **DTBP** when compared to the additive-free system (Table 1.23, Entry 15), as **DTBPO** degrades at elevated temperatures.

Table 1.21. Reductions of **TPPO** with **DPDS** and **BNPA** at 110 °C.



^[a]Average isolated yield of at least two reactions.

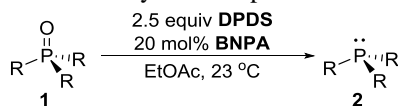
Table 1.22. Reductions of TPPO with DPDS and BNPA at 23 °C.

$$\text{R}-\overset{\text{O}}{\parallel}{\text{P}}(\text{R})_2 \xrightarrow[\text{EtOAc, 23 }^\circ\text{C}]{\substack{\text{X equiv DPDS} \\ \text{Y mol\% BNPA}}} \text{R}-\overset{\cdot\cdot}{\text{P}}(\text{R})_2$$

Entry	X equiv	Y mol%	Isolated Yield[a]
1	1.25	10	58
2	2.5	10	91
3	1.25	20	97
4	2.5	20	99

^[a]Average isolated yield of at least two reactions after 48 hours.

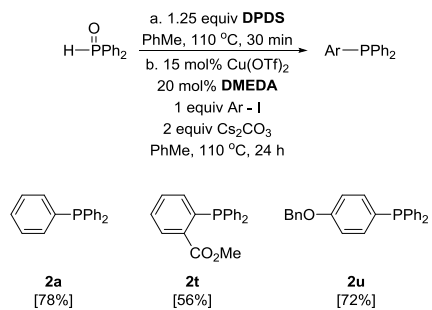
Table 1.23. DPDS-Mediated Reductions of Acyclic Phosphine Oxides at Ambient Temperature.



Entry	Phosphine	Yield (%) ^[a]
1		99
2		75
3		88
4		82
5		73
6		84 ^[b]
7		92 ^[b]
8		82 ^[b]
9		85
10 ^[c]		96 ^[d]
11 ^[c]		83
12 ^[c]		89 ^{[e],[f]}
13	H-PPh ₂	>99 ^{[g],[h],[i]}
14	H-P ^t Bu ₂	>99 ^{[g],[h]}

^[a]Average isolated percent yields for two reactions at 0.25 mmol scale after 48 hours, ^[b]Reactions isolated after 70 h, ^[c]Reactions utilized 5.0 equivalents of **DPDS** (2.5 equiv. per P=O) and 40 mol% **BNPA** (20 mol% per P=O), ^[d]Reductions with only 20 mol% **BNPA** (10 mol% per P=O) furnished 93% yields after 70 h, ^[e](*S,S*)-DIPAMP dioxide utilized as the starting material, ^[f][α]_D²⁰ = 86.2 (*c* = 0.7), ^[g]Yield determined by ³¹P NMR, ^[h]Reaction complete within 18 h, ^[i]Yield (as determined by NMR) without **BNPA** was 80% after 24 h.

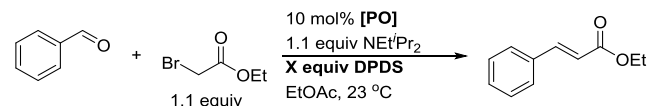
To further illustrate the utility of **DPDS**, we sought to improve Beller's domino reductive arylation reaction to prepare tertiary phosphines from secondary phosphine oxides, as it required multiple days to furnish products³¹ whereas **DPDS** can reduce **DPPO** in a matter of minutes. As shown in Scheme 1.10, **DPDS** afforded phosphines with similar yields as reported by Beller, but in a fraction of the time. These results further highlight the enhanced reactivity of **DPDS** and compatibility with telescoped reactions.



Scheme 1.11. The domino synthesis of trivalent phosphines from secondary phosphine oxide DPPO.

Since we had already characterized the reduction of both cyclic and acyclic phosphines with DPDS, while also investigating the reagent's functional group compatibility, we wished to take this new silane into a redox recycling reaction. We initially chose the Wittig reaction with stabilized ylides as a model reaction for determining the effectiveness of our precatalysts in whole reaction schemes. As summarized in Table 1, our initial catalyst, 1-phenylphospholane-1-oxide (**1PPO**)⁵¹ was highly effective compared to all of our phosphetane precatalysts (Scheme 1.3 and Table 1.24, entries 1-4) in regards to the formation of ethyl cinnamate. We attributed this difference in reactivity to the lack of nucleophilicity of the phosphetane catalysts,²¹ as the phosphorus ylide would be much more difficult to generate via S_N2 displacement of the alkyl bromide without the addition of heat. Also notable is that 2,2,3-trimethyl-1-pyrrolidyl-phosphetane-1-oxide degrades in the polar solvents we explored including EtOAc, MeCN, and THF. We also noted that at least one equivalent of **DPDS** was needed to amply promote the reaction over an 18 hour time period (Table 1, entries 5-8), while an excess of **DPDS** didn't seem to bolster the yield over this time course. As such, we selected 1 equivalent of **DPDS** as an optimal amount of reductant necessary for additive-free recycling and continued forth with EtOAc, a solvent often sourced from renewable resources.

Table 1.24. Optimization of Additive-Free Catalytic Wittig Reactions with Stabilized Ylides at Ambient Temperature.^a



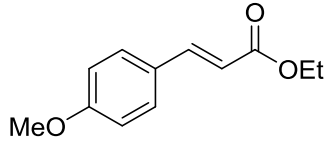
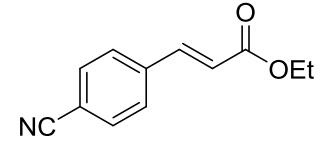
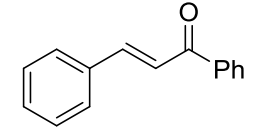
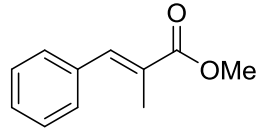
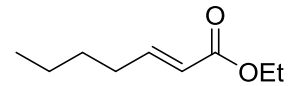
Entry	Precatalyst	X equiv	Yield ^b
1	1PPO	1.0	77 (99)
2	TMPPO	1.0	28 (77)
3	TMBPO	1.0	18 (63) ^c
4	TMPyrPO	1.0	0 ^c
5	1PPO	0.5	20 (66)
6	1PPO	0.8	44 (71)

^aCatalytic reactions performed in triplicate at 0.25 mmol scale; ^bAverage isolated yield, yields in parentheses are based on recovered starting material; ^cHeavy catalyst degradation noted.

With optimal reaction conditions in hand, we further explored the use of **DPDS** in an array of redox recycling reactions (Table 1.25). Additive-free catalytic Wittig reactions worked as expected, tolerating both electron-donating and electron-withdrawing substituents on benzaldehydes. Different stabilized ylides could also be employed to produce both di- and tri-substituted olefins while the added steric bulk diminished the yield of the tri-substituted olefin under these “dump and stir” conditions. In each case, the trans olefin was highly favored, likely due to reversible 1,4 conjugate addition of the phosphine into the α,β -unsaturated carbonyl compounds. Unfortunately, these reaction conditions are insufficient for the utilization of aliphatic aldehydes. We note, however, that no aliphatic aldehyde has been reported to be successfully utilized in catalytic Wittig reactions.^{18, 24, 82, 83} We also attempted to use pre-catalyst **1PPO** with semi-stabilized bromides (benzyl bromide), also without any success. An alternate strategy may need to be employed in which an alternate catalyst/base combination afford olefins from semi-stable alkyl bromides, as was similarly noted by O’Brien.¹⁸

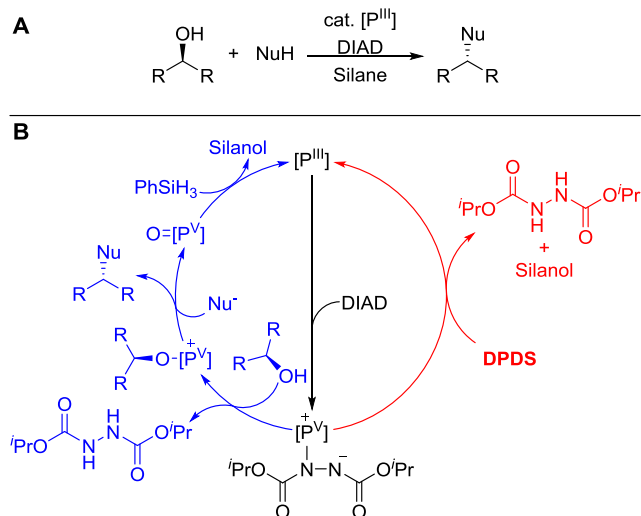
Table 1.25. Substrate Scope of Additive-Free Catalytic Wittig Reactions at Ambient Temperature.

$$\text{R-CHO} + \text{Br-CH}_2\text{-R}' \xrightarrow[\text{EtOAc, 23 }^\circ\text{C}]{\begin{array}{l} 10 \text{ mol\% } \mathbf{1PPO} \\ 1.1 \text{ equiv NEt}'\text{Pr}_2 \\ 1.0 \text{ equiv DPDS} \end{array}} \text{R-CH=CH-R}'$$

Entry	Product	Yield ^a	E/Z Ratio ^b
1		76	94:6
2		74	>95:5
3		76 ^c	>95:5
4		54 ^c	90:10
5		Trace ^d	-

^aAverage isolated yield for at least two reactions at 0.25 mmol scale after 24 h; ^bDetermined with ¹H NMR; ^c46 h; ^dLess than 2% yield, a new spot could be detected with KMnO₄ staining in thin-layer chromatography (TLC) analysis.

In addition to reactions which afford olefins and amines, we were highly interested in ambient temperature catalysis to promote the substitution of alcohols. While the previously reported methods for the catalytic Appel²⁰ and Mitsunobu⁵¹ reactions worked for their reported substrates at elevated temperatures, the power of these reactions generally lies with the fact that no heating is necessary, allowing for the incorporation of these reactions in the later stages of complex syntheses. When we first attempted a room-temperature Mitsunobu reaction, we were unable to isolate any product. We quickly discerned that the lack of product generation was due to rapid reduction of the Huisgen intermediate formed between the phosphine and diisopropyl azodicarboxylate (DIAD), which is resultant of the attack of the azodicarboxylate by the phosphine (Scheme 1.11).⁸⁴ Resulting in the formation of the unreactive hydrazine byproduct, without leading to the formation of the desired substitution product (Figure 1.30).



Scheme 1.12. A) A generalized catalytic Mitsunobu reaction^{REF}; B) The desired catalytic Mitsunobu reaction (blue) utilizing phenylsilane and undesired premature reduction (red) promoted by **DPDS**.

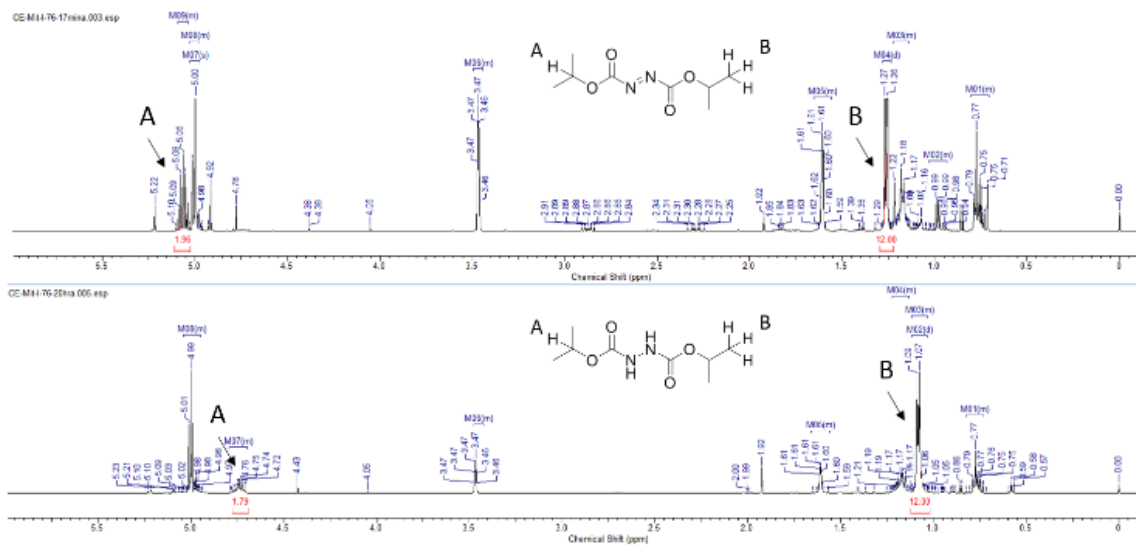
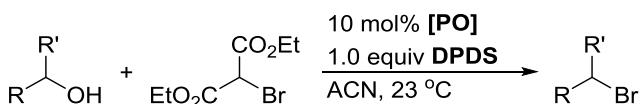
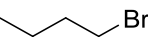
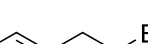
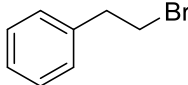
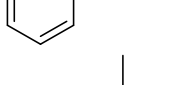
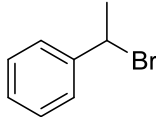
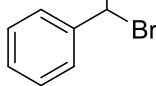


Figure 1.30. The silane-mediated reduction of DIAD as conferred by the reactivity with a phosphine, leading to an unproductive catalytic Mitsunobu protocol.

This particularly reducible phosphorus(V) intermediate is, however, not present during the course of the halogen substitution in Appel reactions. As such, we decided to use the silane-tolerant bromonium ion donor diethyl bromomalonate identified by van Delft and co-workers.²⁰ Again using 1 equivalent of **DPDS**, we were able to create an Appel reaction with similar limitations as those previously reported (Table 1.26). We noted that the use of **1PPO** could generate higher yields of bromides, but with a wide range of yields. We believe this is due to reactivity between the reduced form of the catalyst and the aliphatic bromides to form an unreactive phosphonium bromide compound which shuts down reaction progress. Use of less nucleophilic **TMPPO** garnered a bit more consistency, but did not really improve yields overall. This change likely reduced the amount of nucleophilic attack of the desired bromide product, but it seems unlikely that redox recycling in the Appel halogenation will take hold as design criteria for improved recycling catalysts directly contrasts with properties that would reduce side-product formation.

Table 1.26. Substrate Scope of Additive-Free Catalytic Appel Reactions at Ambient Temperature.

				
Entry	Product	[PO]	Yield ^a	Yield Range ^b
1		1PPO	68	62-76
2		TMPPPO	71	68-74
3		1PPO	64	55-73
4		TMPPPO	64	62-66
5		1PPO	20	18-27
6		TMPPPO	35	28-42

^aAverage isolated yield for at least two reactions at 0.25 mmol scale after 24 h; ^bThe range of yields collected for isolated catalytic Appel halogenation reactions.

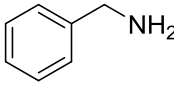
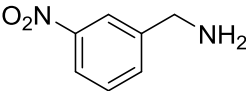
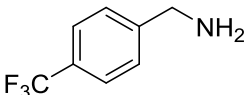
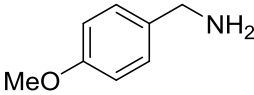
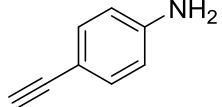
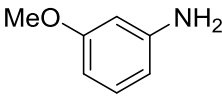
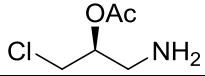
While **DPDS** could easily be utilized in ambient temperature additive-free Wittig reactions, we continued our exploration of this reagent within the suite of phosphorus redox catalysis. We found a similar dependence on the amount of **DPDS** needed for ambient-temperature recycling in the Staudinger reduction, as 1 equivalent of **DPDS** furnished the highest yield of the desired amine (Table 1.27). Summarized in Table 4, we were able to successfully employ **DPDS** in the reduction of azides even in the presence of other easily reducible functional groups which would not be tolerated using transition metal-catalyzed hydrogenation (Table 1.28, Entry 2). Again, electron donating and electron withdrawing substituents seem to have little effect on the outcome of reductions (Table 1.28, entries 1-4) as these substitutions were well tolerated, generating yields ranging from 85% to 92%. In addition to working with benzylic azides, the reaction could also be employed with aromatic azides (Table 1.28, entries 5-6) and aliphatic azides (Table 1.28, entries 7-8). Notably, alkyl chloride **4g** was reduced without racemization of the chiral center and no polymerized products were identified, a feat that could not occur with reductions occurring at higher temperatures.

Table 1.27. Optimization of the catalytic Staudinger reduction with **1PPO**.

$\text{Ph}-\text{CH}_2-\text{N}_3$			10 mol% 1PPO	$\text{Ph}-\text{CH}_2-\text{NH}_2$		
↓			X equiv DPDS	→		
↓			THF, 23 °C	↓		
Entry	X equiv	Yield ^a				
1	0.5	62				
2	0.75	77				
3	1.0	92				

^aAverage isolated yield for at least two reactions at 0.25 mmol scale after 24 h.

Table 1.28. Substrate Scope of Additive-Free Catalytic Staudinger Reductions at Ambient Temperature.

$\begin{array}{ccc} & \text{10 mol\% 1PPO} & \\ & \text{1.0 equiv DPDS} & \\ \text{R}-\text{C}(\text{R}')-\text{N}_3 & \xrightarrow{\text{THF, 23 }^\circ\text{C}} & \text{R}-\text{C}(\text{R}')-\text{NH}_2 \end{array}$		
Entry	Product	Yield ^a
1		92
2		90
3		93
4		85
5		77
6		88
7		82

^aAverage isolated yield for at least two reactions at 0.25 mmol scale after 24 h.

Unfortunately, capture of the phosphineimine was impossible when employing **DPDS** as the reductant with **1PPO** as the precatalyst. Using alternative phosphines which reduce at a slower rate would be necessary in order to capture this intermediate for tandem Staudinger reactions such as the Staudinger/aza-wittig tandem reaction.¹⁹ We do note, however, that “traceless” Staudinger ligations^{81, 85} would be unlikely to occur at room temperature as additional heat promotes the formation of the amide bond¹³ (Chapter 1.8) between the amine and the carboxylic acid. However, while exploring this reaction, we were able to identify the rates in which **DPDS** reduces acyclic phosphinimines. Most notably, this investigation did lead to the identification of conditions in which triphenylphosphine (**TPP**) is recycled during the course of Staudinger reductions (Table 1.29). The reaction works very similarly to reductions employing **1PPO**, but takes a longer time to go to completion, but is still complete within a reasonable 48 hours. Using triphenylphosphine oxide (**TPPO**) as the initial phosphorus reagent, however, did not yield any notable reactivity over the same time period, indicative of direct reduction of the phosphinimine rather than hydrolysis followed by reduction. Also, using phenylsilane and **TPP** only yielded a trace amount of product after 48 hours, and less than 20% conversion was noted after 120 hours in reactions run at ambient temperature.

Table 1.29. Substrate Scope of Additive-Free Catalytic Staudinger Reductions at Ambient Temperature Utilizing **TPP** as the Catalyst.

$\begin{array}{ccc} \text{R}' & & \text{R}' \\ & & \\ \text{R}-\text{C}-\text{N}_3 & \xrightarrow[\text{PhMe, 23 }^\circ\text{C}]{\begin{array}{l} 10 \text{ mol\% TPP} \\ 1.0 \text{ equiv DPDS} \end{array}} & \text{R}-\text{C}-\text{NH}_2 \end{array}$		
Entry	Product	Yield ^a
1		95
2		89
3		93
4		93
5		88
6		88

^aAverage isolated yield for at least two reactions at 0.25 mmol scale after 48 h.

To further characterize why **TPP** can be utilized in catalytic Staudinger reductions employing **DPDS** to recycle the catalyst, we sought to characterize the energy input needed to afford reduction. To this effect, we isolated the reduction of *N*-benzyl-1, 1, 1-triphenyl- λ^5 -phosphanimine (**BTPI**) under pseudo first-order conditions using ^{31}P NMR as we have previously reported.⁵¹ Comparing reductions of **BTPI** with **DPDS** and phenylsilane immediately indicated that phenylsilane would not be a competent reducing agent for these reactions. At 45 °C, the disiloxane shows a stark increase in compared to the corresponding silane (Table 1.30 and Figure 1.31).

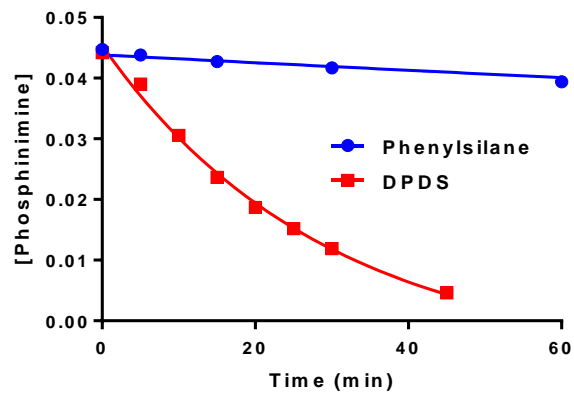


Figure 1.31. The average reduction of **BTPI** with PhSiH_3 (blue, circles) and **DPDS** (red, squares) under pseudo first-order conditions as monitored with ^{31}P NMR at 45 °C.

Table 1.30. Observed Rate Constants for the Silane-Mediated Reduction of XX under Pseudo First-Order Conditions.^a

Entry	Silane	Temperature (K)	K_{obs} (min ⁻¹) ^b
1	DPDS	296	0.010
2	DPDS	313	0.358
3	DPDS	318	0.050
4	DPDS	323	0.059
5	DPDS	343	0.189

^aReactions performed in triplicate directly in NMR tubes using *d*₈-PhMe as the solvent and freshly prepared BTPI at [BTPI]_i = 0.05 M and [Silane]_i = 0.50 M; ^bAverage values fitting to 1st order decay.

Eyring analysis of this reduction with **DPDS** (Figure 1.32) yielded the thermodynamic parameters of the transition state, indicating $\Delta H^\ddagger = 11.7 \pm 0.4$ kcal/mol, $\Delta S^\ddagger = -0.03 \pm 1.9 \cdot 10^{-4}$ cal/mol and $\Delta G_{298K}^\ddagger = 20.0 \pm 1.6$ kcal/mol. These numbers are lower than those calculated for the reduction of **TPPO** by **DPDS**,⁶⁴ recapitulated here as $\Delta H^\ddagger = 17.3 \pm 1.2$ kcal/mol, $\Delta S^\ddagger = -0.01 \pm 1.4 \cdot 10^{-4}$ cal/mol and $\Delta G_{298K}^\ddagger = 21.5 \pm 3.6$ kcal/mol, however; the free energy of activation is not actually significantly lower while the enthalpy of activation is significantly reduced.

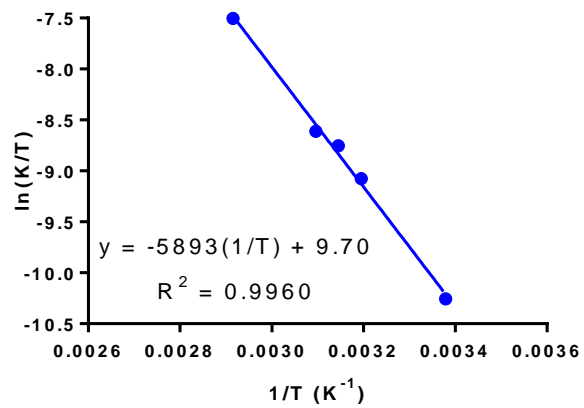


Figure 1.32. The Eyring plot for the reduction of **BTPI** with **DPDS** over a temperature range of 23 – 70 °C.

This small change in energy may very well explain the differences in reactivity between phosphinimines and phosphine oxides as only the phosphinimine is reduced at ambient temperature without an additive, although, there may be other factors at play which we cannot observe directly in these types of experiments. Additionally, we explored the reduction of **BTPI** in a 1:1 stoichiometry with **DPDS** and found that the reduction is nearly complete within 24 hours (Figure 1.33), faster than the reduction of **TPPO** with **DPDS** when **BNPA** is added.⁶⁴ Also, the reduction displays nearly ideal first-order kinetics, with no detectable intermediate in our NMR experiments. We also note that trying to identify the resting state of the catalytic reaction was difficult as the state of the phosphine changes over the course of the Staudinger reduction (Figure SX). However, the rate limiting step is surely the reduction of the phosphinimine as the formation of the phosphinimine reaches a plateau around 30 minutes into the reaction, while the reduction under pseudo first-order conditions at the same temperature (23 °C) takes approximately 4 hours to reach completion (Table 1.30).

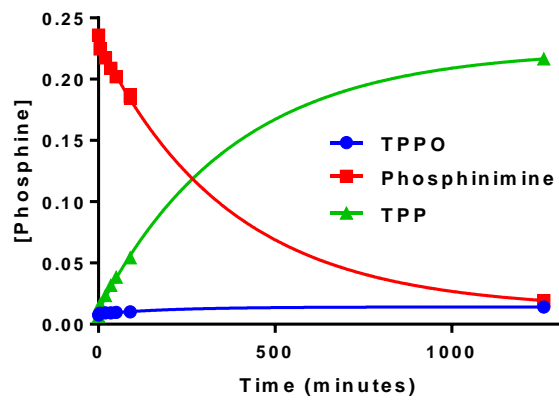
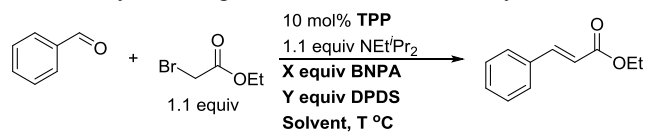


Figure 1.33. The average reduction of **BTPI** with **DPDS** at even stoichiometries at 23 °C as determined with ^{31}P NMR.

While we have demonstrated that **DPDS** can be utilized in combination with cyclic phosphine oxides in additive-free Wittig recycling reactions, we hoped to utilize much a more readily accessible phosphines, such as **TPP**, with **DPDS** in other catalytic reactions. Since these reactions, unlike the Staudinger reduction, do not go through a phosphinimine intermediate, we knew that we required a new set of optimal conditions in order to utilize **TPP** in redox recycling Wittig reactions. Knowing that acyclic phosphines require heat to be reduced without an additive, we first investigated additive-free recycling in Wittig reactions by simply adding heat to the system. As summarized in Table 1.31, optimization of such a reaction ultimately could not surpass the 65% yield mark (Table 1.31, Entry X). Addition of the additive **BNPA**, first utilized by Beller and co-workers²⁵ and later in room-temperature reductions of phosphines with **DPDS**,⁶⁴ allowed for a much more tractable reaction with **TPP**. These reactions proceeded cleanly, producing olefins with predominantly *trans* configurations with high fidelity. Unfortunately, addition of this intermediate would interfere in catalytic Mitsunobu reactions, although we had already identified that reactions with phosphinimine intermediates can only utilize **DPDS** if the amine is the desired product, and thus recycling Mitsunobu reactions would require investigation of an entirely different recycling regime.

Table 1.31. Optimization of catalytic Wittig reactions with **TPP** catalysis.

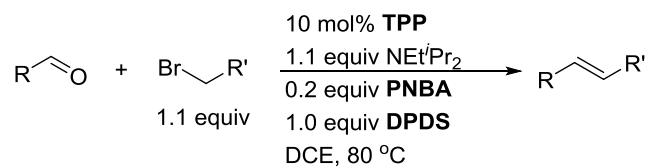


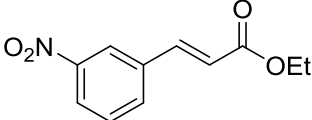
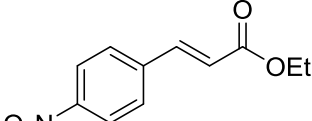
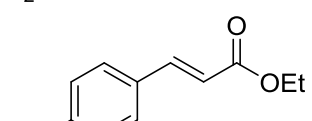
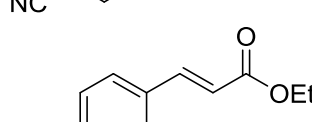
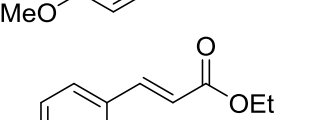
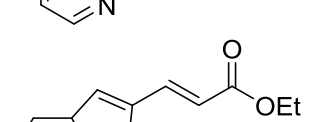
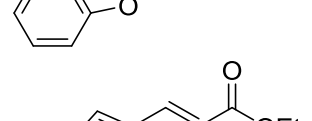
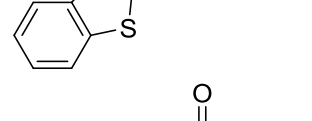
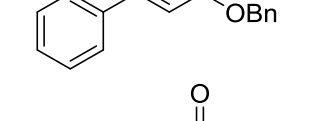
Entry	X equiv	Y equiv	Solvent	T °C	Yield	E/Z Ratio
1	0.0	1.0	THF	65	44	92:8
2	0.0	1.0	PhMe	65	59	92:8
3	0.0	1.0	PhMe	80	65	94:6
4	0.0	1.0	PhMe	110	63	93:7
5	0.1	1.0	PhMe	80	60	93:7
6	0.2	1.0	CH ₂ Cl ₂	80	67	94:6
7	0.2	1.5	CH ₂ Cl ₂	80	69	94:6

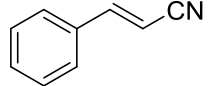
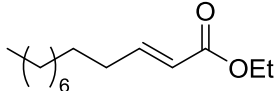
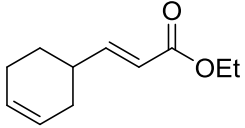
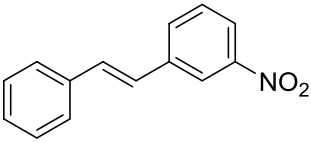
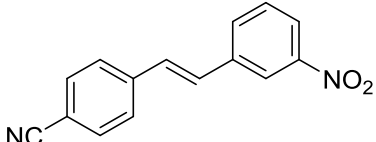
^aAverage isolated yield for at least two reactions at 0.25 mmol scale after 48 h.

For this **TPP**-catalyzed protocol, similar functional group tolerance as the additive-free reaction was noted (Table 1.32). Both electron-rich and electron-poor benzaldehydes are tolerated, although, in this case, electron-poor substrates react substantially faster, while frequently affording higher yields. Also in parallel with the additive-free system aliphatic aldehydes are unable to produce much olefin product. However, unlike our ambient temperature reaction, the synthesis of olefins with semi-stabilized ylides is possible (Table 1.32, Entry 13). While the *cis:trans* ratios are not ideal, as there is little selectivity for one isomer, the use of these types of ylides could possibly be improved with an alternate catalyst and base system.^{18, 82} We believe this reaction could be employed easily by many labs as **DPDS** is a simple reagent to synthesize, and **TPP** is easily purchased. This reaction, as well as its room-temperature equivalent offers researchers in both academic and industrial labs the ability to utilize catalytic Wittig reactions as **DPDS** is an easily accessed reagent without the need to isolate silyl chlorides or use lithium aluminum hydride to synthesize this reagent.

Table 1.32. Substrate scope of catalytic Wittig reactions utilizing triphenylphosphine.



Entry	Product	Yield ^a	E/Z Ratio ^b
1		71	11:1
2		60	14:1
3		71	14:1
4		32	>95:5
5		15	>95:5
6		58	95:5
7		82	>95:5
8		57	13:1
9		17	>95:5

10		45	3:1
11		18	95:5
12		19	>95:5
13		52	67:33
14		68	63:37

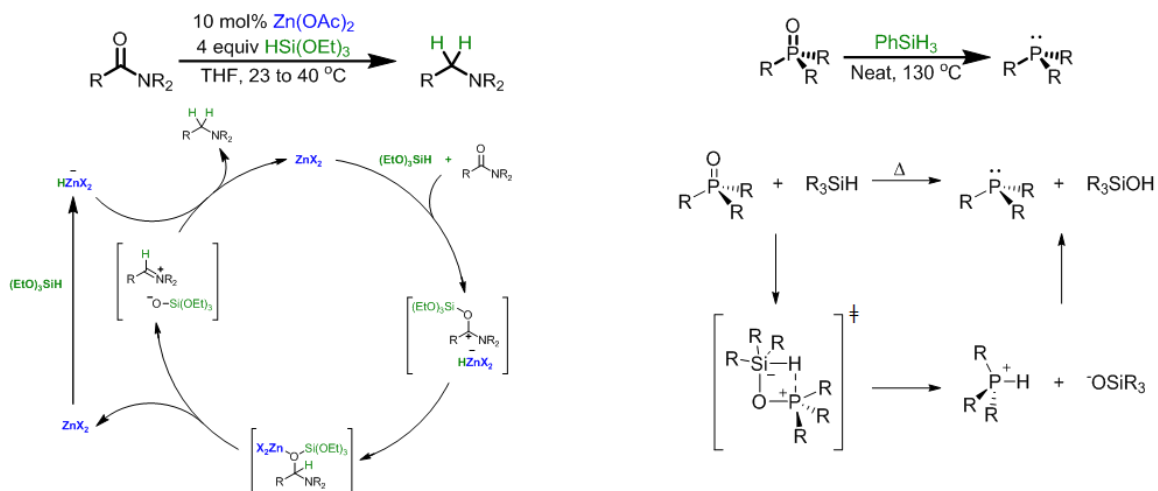
^aAverage isolated yield for at least two reactions at 0.25 mmol scale; ^bDetermined with ¹H NMR.

In conclusion, the new reducing disiloxane agent **DPDS** can be utilized in catalytic redox recycling reactions. Specifically, **DPDS** can be deployed in additive-free catalytic Wittig, Staudinger, and Appel reactions at ambient temperature with the use of phospholane precatalyst **1PPO**. This enhanced reducing agent could also be utilized in recycling reactions employing the typical phosphine **TPP** in catalytic Staudinger reductions at ambient temperature, taking advantage of the rapid reduction of phosphinimines. **TPP** was also demonstrated as a competent catalyst in Wittig reaction when **DPDS** is utilized in conjunction with a Brønsted acidic additive at elevated temperatures. **DPDS** can be further examined in other redox recycling processes to improve tandem Staudinger reactions as well as the Mitsunobu reaction, although the disiloxane and/or phosphine catalysts may need to be tuned to be less reactive in order to avoid unwanted reactivity. We expect that these reactions should be able to provide a platform for future discoveries towards greener chemistries with improved atom economy and simplified purification schemes.

1.6 1,3-Diphenyl-disiloxane as a multi-functional organic reducing agent

While **DPDS** is an excellent chemoselective reductant of phosphine oxides,⁶⁴ we wished to further explore the utility of this reagent. To this effect, we sought to utilize **DPDS** in other silane-mediated organic transformations. An obvious, and potentially very useful, application of **DPDS** is in other reductive processes falling under the broad category of metal-catalyzed hydrosilation reactions.⁴ The breadth of this field has been extensively reviewed throughout the maturation of this chemical conversion. Briefly, all of these sorts of reactions involve the transfer of a hydride and results in a new silicon-containing compound as summarized in Scheme 1.13. These processes occur over π molecular orbitals

between carbon-carbon and carbon-heteroatom bond types. While these reactions can occur spontaneously with the addition of enough thermal energy, more tractable synthetic methods often exploit multi-functional transition metal catalysts in either the homogenous or heterogeneous phases.⁴



Scheme 1.13. The literature proposed mechanisms of hydrogen atom transfer reactions.

While the act of adding a silylhydride over a π -system can be applied in many relevant processes for chemical industry, we noted that the metal-mediated hydrosilylation of carboxamides⁸⁶ as a particularly interesting transformation for the synthesis of new therapeutics, as secondary and tertiary amines are present in the vast majority of pharmacologically active substances. Additionally, the generation of amide starting materials is quite facile from a plethora of commercially-available amines and carboxylic acids, a starting material seeing more use in novel forms of powerful organic methods.⁸⁷ While the reduction of carboxamides using a silane and metal catalyst is well-known, and recently reviewed,⁸⁶ the design of these systems has been purely based on empirical observation, and the utility of these reactions is limited in scope. Limitations sometimes include a lack of functional group tolerance, but more frequently the limitations of these methods relate to the types of carboxamides that can be reduced to the corresponding amines. Generally, a single metal/silane pair can be used to reduce secondary or tertiary carboxamides, but not both. This trend is notable, as a synthetic chemist must choose wisely how they prepare their retrosynthetic analysis and judge the cost-effectiveness of their route.

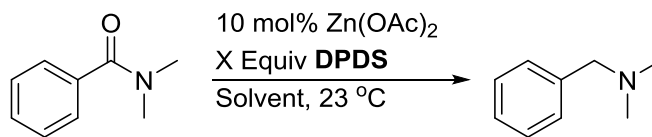
While these limitations to these methodologies do exist, there does seem to be a trend that predicts the potential reactivity of carboxamide hydrosilylation. After searching the literature, it seems apparent that oxygen-containing silane materials, such as diethoxyxymethylsilane (DEMS), are applied in the reduction of tertiary carboxamides,^{86,88} while phenylsilanes are employed in the reduction of secondary amides⁶² in tandem with

many transition metals with varying *d*-electron configurations. Recently, Matthias Beller and co-workers disclosed one such method utilizing the very inexpensive combination of $\text{Zn}^{\text{II}}(\text{OAc})_2$ and $(\text{OEt})_3\text{SiH}$ for the reduction of tertiary carboxamides which exudes high fidelity for the specific reduction in question (Scheme 1.12).⁸⁸ In their disclosure, the new method is tolerant of various easily-reduced functionalities including nitro, ester, cyano, and ketone. We noted that in their supporting information, however, was a single example in which a reduction was performed with phenylsilane, indicating that both phenylsilane and siloxycompounds would be capable of carboxamide reduction in combination with zinc. Seeing as **DPDS** contains both of these functionalities, we were hopeful that a new method would be possible that included this inexpensive metal source and could be implemented for multiple amide types.

Our starting point was to directly replace Beller's conditions with **DPDS** as a proof-of-concept that the silane could be used with zinc, even if the silane was in great excess. To our delight the reaction did work to some degree, and we could easily optimize from this point. I first opted to look at an optimal temperature and solvent before attempting to lower the amount of silane necessary for reduction. In addition, unlike other reactions within these works, I also attempted to reduce secondary and primary amides, potentially optimizing three reactions simultaneously. The initial temperature screen looked at both reductions at 23, 40, 65, and 80 °C in THF, as Beller's conditions at 40 °C had worked well in my hands. Any temperature that showed potential for reduction of either amide, would then be checked for an optimal solvent. Remarkably, the reaction seemed to reduce tertiary

and secondary amides at both 65 and 80 °C, but only worked for the reduction of tertiary amides at any other lower temperatures, similar to Beller's reaction conditions.⁸⁸ This intriguing result indicated that the reaction with **DPDS** might be temperature-tunable, in which the temperature of the reaction dictates the selectivity of the reaction for different types of carboxamide reductions.⁸⁹ As such, we continued the optimization campaigns for both carboxamide types separately, screening solvents at 23 °C for tertiary carboxamides (Table 1.33) and at 65 - 80 °C for secondary carboxamides (Table 1.34). Interestingly, the reaction works better in 2-methyl-tetrahydrofuran (MTHF), a greener solvent than THF with a higher boiling point. Being able to use this solvent allowed the latter reaction to function at 80 °C safely, and for faster reactions. It is notable that both reactions are nearly complete within 4 hours, although for the purposes of giving all potential options an equal chance, reactions were performed for 18 hours.

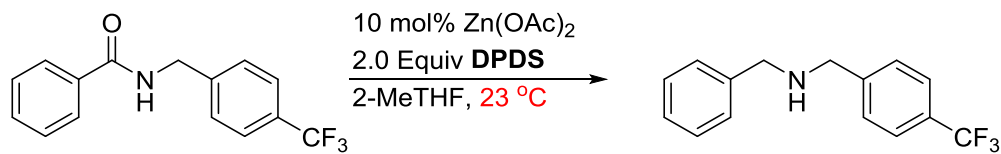
Table 1.33. Optimization of the reduction of tertiary carboxamides.



Entry	X equiv	Solvent	% Conversion ^a	Isolated Yield ^b
1	3.0	MTHF	100	99
2	2.5	MTHF	100	99
3	2.0	MTHF	100	98
4	1.5	MTHF	89	82
5	2.0	THF	78	66
6	2.0	MeCN	0	-
7	2.0	PhMe	50	-
8	2.0	EtOAc	62	48

^aDetermined with LC-MS; ^bAverage isolated yield for at least two reactions at 0.25 mmol scale.

Table 1.34. Optimization of the reduction of secondary carboxamides.

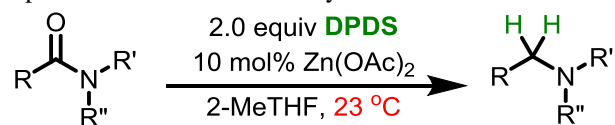


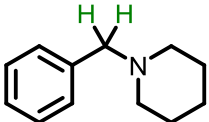
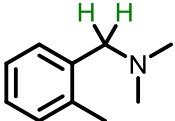
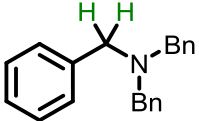
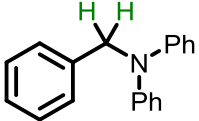
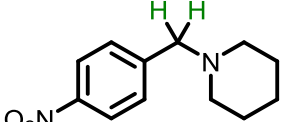
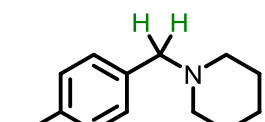
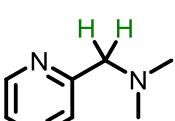
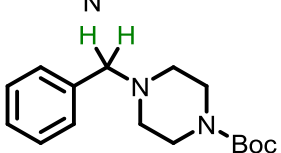
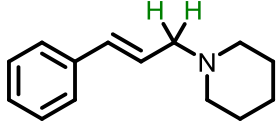
Entry	Solvent	Temperature (°C)	% Conversion ^a	Isolated Yield ^b
1	MTHF	23	0	-
2	MTHF	40	22	-
3	MTHF	65	100	92
4	MTHF	80	100	96
5	THF	65	50	-
6	MeCN	80	0	-
7	PhMe	110	36	-
8	PhMe	80	62	-

^aDetermined with LC-MS; ^bAverage isolated yield for at least two reactions at 0.25 mmol scale.

At this point, I was able to hand off the reactions to other scientists, including Kathleen Wang and Malcolm Cole, to confirm my results and to finalize the silane concentrations. In both cases, 2 equivalents of silane can be employed and the reduction works quite well. A substrate scope was then explored for both reaction types, including molecules that contain both amide types. As summarized in Tables 1.35 and 1.36, the substrate scope of this reduction is fairly broad, however, unlike Beller's reaction, our method with **DPDS** cannot tolerate cyano functionalities, and the lack of product generated in acetonitrile indicates that the silane is likely used up in some reaction with the nitrile. The reaction works with many functional groups ranging from nitro to olefin while working with benzylic, vinylic, and aliphatic amides with high yield. Interestingly, the reaction works well on modified amino acid substrates and can even perform well with a dipeptide, reducing only the tertiary amide in the molecule.⁸⁹ Notably, primary amides remain untouched at all temperatures we have explored, indicating that our system is "selective" for secondary and tertiary amides, depending on the temperature used to perform the reaction.

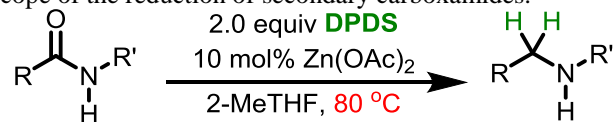
Table 1.35. Substrate scope of the reduction of tertiary carboxamides.



Entry	Product	Isolated Yield ^a
1		92
2		72
3		90
4		66
5		92
6		97
7		74
8		92
9		91

^aAverage isolated yield for at least two reactions at 0.25 mmol scale.

Table 1.36. Substrate scope of the reduction of secondary carboxamides.



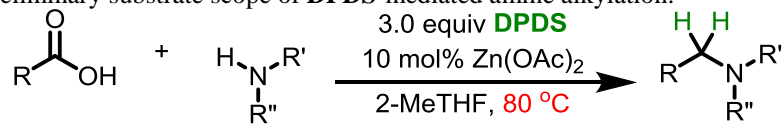
Entry	Product	Isolated Yield ^a
1		92
2		83
3		79
4		48 ^b
5		90
6		60

^aAverage isolated yield for at least two reactions at 0.25 mmol scale; ^b3 equiv of **DPDS** employed.

While the reduction of carboxamides is a useful transformation, a way to quickly improve this reaction would be to have a one-pot reductive amine alkylation protocol which can tolerate the synthesis of secondary and tertiary amines. While processes similar to this have been reported for decades,⁹⁰ they frequently combine the synthons of aldehydes and amines. For the purposes of aiding medicinal chemistry campaigns, however, I hoped to generate a reductive amine alkylation that can utilize a more commercially-available and stable synthon, the carboxylic acid.^{62,91} While this has been reported previously by multiple groups, we hoped that our **DPDS** reagent could also be used universally. The zinc system seemed like a good place to start as it was already competent at reducing carboxamides, with such an inexpensive catalyst.

Thankfully, our starting point with zinc and three equivalents of **DPDS** was capable of facilitating amide bond formation and subsequent reduction for the reaction between a primary amine and a carboxylic acid. Thankfully, being that the reaction works best in MTHF, we were able to get 100% conversion within 16 hours at 80 °C and form the corresponding secondary amine. The same could also be done for the coupling of a secondary amine and a carboxylic acid, but the requirement for heat was maintained, an unsurprising fact due to amide couplings with **DPDS** requiring thermal input.⁸⁵ This particular reaction was then checked for validity and reproducibility by other members of the lab, as it is important that this reaction can be done by other scientists other than the ones whom are developing the technology. As summarized in Table 1.37, a preliminary substrate scope has been explored and continues to expand as this publication draws nearer.

Table 1.37. Preliminary substrate scope of DPDS-mediated amine alkylation.



Entry	Product	Isolated Yield ^a
1		78
2		79
3		75
4		78
5		82
6		66

^aAverage isolated yield for at least two reactions at 0.25 mmol scale.

These results indicate that **DPDS** is in fact a very versatile reducing agent, with the potential to be utilized in wide manner of reactions which require improved chemoselectivity, or which may benefit from a multi-functional silane reagent. Even in the context of alkyl amine compounds, DPDS offers multiple angles for the synthesis of these highly desired, and highly applicable molecules from tractable synthons. We plan to flesh out the limitations of this chemistry further, to better understand the use of DPDS in the context of carboxamide reduction and amine alkylation.

1.7 Concluding remarks

All in all, the work presented in this chapter highlights the use of rational reagent design for improved chemical processes. While our initial efforts to create a catalytic Mitsunobu were fruitful, it turns out the implementation of this sort of chemistry is actually quite difficult.⁹² These efforts, driven by empirical screening, certainly need improvement; which was initially attributed to improving the rate-determining step of the redox catalysis cycle. However, upon implementation of kinetic analysis to actually vastly improve this step, the catalytic Mitsunobu at ambient temperature could still not be realized. While an optimal catalytic Mitsunobu was not realizable over this time period, other redox recycling protocols were developed with success with either zero added thermal energy, no additional chemical reagents, or both. As such, we believe the results presented herein represent a large step forward, but not quite the end of where redox recycling needs to end up for more ubiquitous usage.

We now understand the necessary components of silane-mediated reductions for phosphine oxides, and have designed **DPDS** based on those needs, although this prototypical reagent still leaves room for improvement. Thankfully, being a fully conjugated π -system, this reagent should be highly amenable to tuning via perturbation of the electronic nature of the reagent with electron-donating and electron-withdrawing functionalities. This silane modulation can be paired with phosphorus reagent design which, unfortunately, cannot be fully predicted. As presented, each phosphorus scaffold must be screened to indicate its usefulness in a given reaction, as in some cases a lack of nucleophilicity may be desired, or the rate at which its reduction occurs may need to be attenuated (as in the case of tandem Staudinger processes¹⁹). However, we expect that **DPDS** will be able to be implemented in many redox recycling schemes, which includes both classical, and novel organic transformations seeing as the reagent can be used to reduce very difficult-to-access phosphine oxides, while also maintaining a high specificity for this specific reaction type without perturbing typically reactive functional groups.

Additionally, our initial characterization of this reagent shows that the reagent can be paired with other additives in order to be useful in contexts outside of phosphine oxide reductions. We hope that symmetrical disiloxanes can be utilized in other reductive processes, or other metal-catalyzed reactions, such as the Hiyama-Denmark coupling.⁹³ We hope that **DPDS**, and reagents similar to it, can be utilized in a wide array of reactions utilizing either siloxane materials or silyl-hydrides for chemoselective reactivity. Since the synthesis of such reagents is quite facile using our mechano-chemical procedure, we expect

that these reagents should also be easily screened for their competence since they should be quite easy to access in the majority of synthetic laboratories.

1.8 Methods and materials

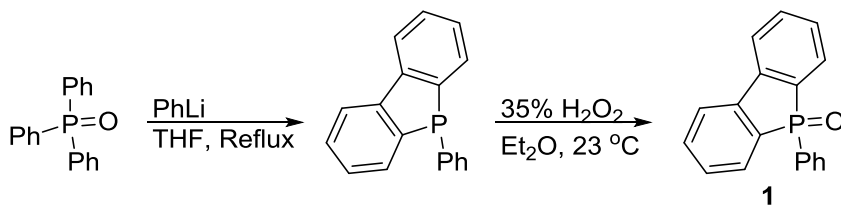
1.8.1. General Considerations

All commercially available reagents were used without further purification. Phosphine oxides **1PPO**, **TMPPPO**, **TBPO**, and triarylphosphine oxides¹ were synthesized as previously reported. 1-Chloro-2,2,3-trimethylphosphetane-1-oxide (**S1**) was prepared as described. *Si,Si,Si*-Trideutero-phenylsilane (**S8**) was also prepared as described. All disiloxanes were synthesized as described in this supporting information or using the protocol we recently reported. All phosphines were stored at -20 °C wrapped in foil to exclude light and all silanes were stored at ambient temperature in a light-shielding desiccator to exclude UV light. Benzyl azides were all prepared according to the procedure from Feringa et. al. from the corresponding benzyl bromide or benzyl chloride. Molecular sieves were activated by heating at 200 °C under reduced pressure. Tetrahydrofuran (THF), toluene, and dichloromethane (CH₂Cl₂) were dispensed from an Inert® solvent dispensing system. Deuterated THF was purchased from Sigma-Aldrich in dry 1 gram ampules and used without further drying. Deuterated chloroform, CD₂Cl₂, and toluene were purchased from Cambridge Isotopes and used without further drying from 10 gram bottles stored in a desiccator. Lithium chloride was stored in a desiccator and dried with a Bunsen burner immediately before use. Anhydrous magnesium chloride was dried and stored in a desiccator prior to use. Zinc chloride was purified in its molten form to remove water and

hydrogen chloride from the salt immediately before use. Anhydrous sodium sulfate was purchased from Fisher Chemicals and used without further purification. Pyrrolidine and piperidine were dried over calcium hydride and freshly distilled under reduced pressure immediately before use. ^1H , ^{13}C , ^{19}F , ^{29}Si , and ^{31}P NMR spectra were recorded on a Varian 400 MHz spectrometer, Bruker Avance 500 MHz spectrometer, or Varian INOVA 600 MHz spectrometer with broadband probes. High resolution mass spectra were collected on a Bruker BioTOF II mass spectrometer using PEG or PPG internal standards. Sodium formate was sometimes added in order to facilitate ionization, frequently leading to characterization of the $[\text{M} + \text{Na}^+]$ masses. Silica gel column chromatography was performed with silica gel (Dynamic Absorbents, 60A) or using a Teledyne-Isco RF-200 Combi-Flash system. Kugelrohr distillations were performed with a Buchi glass oven B-585 instrument. The experiments contained herein are not hazardous outside of the typical flammable/explosion hazards present with the usage of organic solvents, ethereal solvents such as Et_2O and THF should always be assayed for the presence of peroxy by-products. Computational experiments were performed using the resources of the Minnesota Supercomputing Institute (MSI), specifically through virtual machines running on Linux superclusters named "Itasca" and "Mesabi". Computational resources such as Gaussian09 and GaussView were provided through licenses available to the MSI.

1.8.2. Synthesis of Phosphine Precatalysts:

1.8.2.1. 5-Phenyldibenzophosphole-1-Oxide:⁹⁴

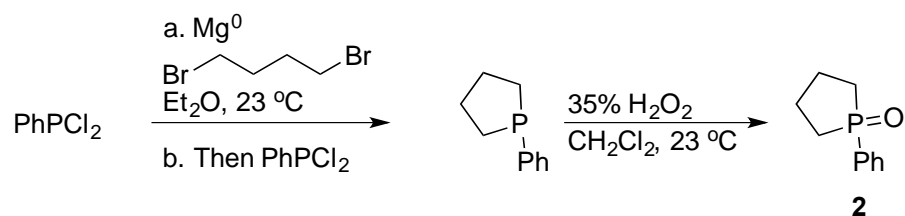


To a 3-neck 500 mL round bottom flask equipped with a stir bar and fitted with a reflux condenser and addition funnel was added triphenylphosphine oxide (11.2 g, 40.0 mmol, 1.00 equiv) and THF (240 mL). The reaction apparatus was purged with argon and the mixture was cooled to 0 °C. A 1.8 M solution of phenyllithium in di-*n*-butyl ether (45.0 mL, 81.0 mmol, 2.03 equiv) was added dropwise to the stirring solution. After complete addition of the organolithium, the reaction was heated at reflux for 46 h. After cooling to room temperature, H₂O (150 mL) was added to the reaction and the mixture was then neutralized with 3 N HCl (50 mL). The layers were separated and the aqueous layer was extracted with EtOAc (3 × 100 mL). The organic layers were combined and concentrated under reduced pressure. The residue was purified by silica gel chromatography (hexane) and then recrystallized (1:9 ethyl acetate: hexanes) to yield pure 5-phenyldibenzophosphole (5.17 g, 50%) as a white solid. All spectra and physical data matched that of previous reports. The purification step is unnecessary as the subsequent reaction is unaffected when crude material is utilized.

To a 25 mL round bottom flask equipped with a stir bar was added 5-phenyldibenzophosphole (260 mg, 1.00 mmol, 1.00 equiv) and Et₂O (5 mL). To the

reaction a 35% w/w aqueous solution of hydrogen peroxide (0.345 mL, 3.53 mmol, 3.53 equiv) was added dropwise at 23 °C. A white precipitate was noted immediately. After 30 min, the reaction was filtered and the filter cake was washed with Et₂O (20 mL). Compound **1** (178 mg, 78%) was collected from the filter as a white solid. All spectra and physical data matched that of previous reports.

1.8.2.2. 1-Phenylphospholane-1-oxide (**1PPO**):²⁰



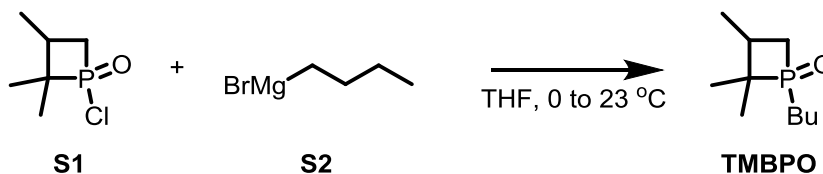
Warning: Dichlorophenylphosphine is a volatile liquid that is extremely noxious. Use only in well-ventilated areas.

To a 1000 mL round bottom flask equipped with a stir bar was added magnesium powder (50 mesh, 2.82 g, 200 mmol, 4.00 equiv) and iodine (0.350 g, 1.4 mmol, 0.28 equiv). The flask was purged with argon, and anhydrous Et₂O (250 mL) was added via cannula. The reaction was cooled to 10 °C and 1,4-dibromobutane (5.5 mL, 50 mmol, 1.00 equiv) was added dropwise. The reaction was warmed to 23 °C. After 3 h, the reaction was cooled to 0 °C and dichlorophenylphosphine (6.3 mL, 50 mmol, 1.00 equiv) was added dropwise over 40 min and a white precipitate was noted immediately upon addition of this reagent. The reaction was warmed to 23 °C and stirred overnight. The reaction was washed with H₂O (425 mL) and saturated aqueous NaCl (425 mL). The aqueous layers were combined and extracted with CH₂Cl₂ (3 × 100 mL). The organic layers were combined and

concentrated under reduced pressure to afford crude 1-phenylphospholane (6.71 g) as a yellow oil, which was carried onto the next step without further purification. **Note:** This crude mixture is also extremely noxious and should be handled in a well-ventilated area.

To a 1000 mL round bottom flask equipped with a stir bar and charged with the crude reaction mixture from above was added CH₂Cl₂ (100 mL). The reaction was cooled to 10 °C and an aqueous solution of 35% w/w hydrogen peroxide (7.94 mL, 81.7 mmol, 1.63 equiv) was added dropwise. The reaction was warmed to 23 °C. After 3 h, the reaction was washed sequentially with saturated aqueous NaHCO₃ (2 × 50 mL) and saturated aqueous NaCl (50 mL). The organic layer was dried with magnesium sulfate and concentrated under reduced pressure. The reaction was purified by silica gel chromatography (1:9 MeOH: CH₂Cl₂) and **2** was isolated as an orange oil, which solidified upon cooling at -20 °C (2.14 g, 27% over two steps). All spectra and physical data matched that of previous reports.

1.8.2.3.-*n*-Butyl-2,2,3-trimethylphosphetane-1-oxide (TMBPO):

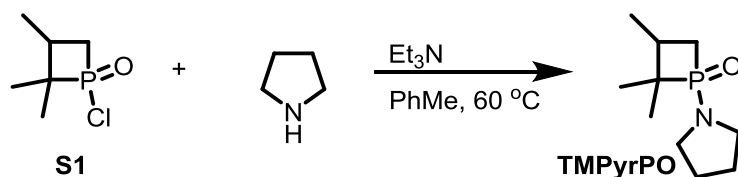


To a flame-dried two-neck round bottom flask equipped with a stir bar was added dried magnesium(0) powder (50 mesh, 0.43 g, 18 mmol), THF (2 mL), and one crystal of iodine. Stirring was initiated and a solution of bromobutane (1.6 mL, 15 mmol) in THF (13 mL) was added dropwise. When addition of the bromide was complete, the reaction was refluxed for 2 h. The reaction was then cooled to 0 °C and a solution of **S1** (1.992 g, 12

mmol) in THF (10 mL) was added dropwise to the stirring solution of **S2**. The reaction was allowed to warm to 23 °C and stirred for 16 h. After 16 h, the reaction was quenched by the addition of H₂O (25 mL). The layers were separated and the aqueous layer was washed with DCM (3 × 25 mL). The organics were combined and dried (MgSO₄). The reaction was concentrated *in vacuo* to a yellow oil and loaded onto silica gel. Purification by flash column chromatography on silica gel (40 g SiO₂, 0–10% MeOH:DCM eluent, linear gradient) afforded the title compound (1.30 g, 57%) as off-white needles: *R_f* = 0.62 (5:95 MeOH:DCM) stained with iodine. ¹H NMR (500 MHz, CDCl₃) δ 2.46-2.40 (m, 1H), 2.10-2.04 (m, 1H), 1.86-1.82 (m, 1H), 1.73-1.70 (app. m, 2H), 1.68-1.65 (m, 2H), 1.49-1.45 (m, 2H), 1.26-1.16 (app. dd, 6H), 1.03-1.02 (d, 3H), 0.97-0.94 (t, 3H); ¹³C NMR (125 MHz) δ 49.0, 37.3, 30.2, 25.9, 24.2, 23.7, 22.5, 1, 6.1, 14.4, 13.7; ³¹P {¹H} NMR (202 MHz, CDCl₃) δ 49.68. HRMS for C₁₀H₂₁NaOP [M + Na⁺] calculated 211.122; found 211.1225.

Additional purification: Preparatory TLC (5:95 MeOH:DCM) was used to purify small amounts of **TMBPO** for some syntheses of this molecule. In order to visualize this molecule with iodine, heat iodine crystals and then drop into the TLC chamber. The top spot (stains yellow with iodine) is the desired product.

1.8.2.4. 1-Pyrrolidyl-2,2,3-trimethylphospetane-1-oxide (**TMPyrPO**):



To a flame-dried round bottom flask equipped with a stir bar was added **S1** (2.16 g, 13 mmol), toluene (13 mL), triethylamine (2.2 mL, 16 mmol), and pyrrolidine (1.2 mL, 14.6 mmol) sequentially. The reaction was sealed, purged with argon, and heated to 60 °C for 24 hours. After 24 hours, the reaction was cooled to 23 °C and filtered. The cake was washed with EtOAc (10 mL). The filtrate was combined with the EtOAc wash, which were subsequently washed with 5% aqueous sodium bicarbonate (20 mL), dried (MgSO₄) and concentrated *in vacuo* to afford the title compound (1.96 g, 75%) as an orange oil and mixture of diastereomers: ¹H NMR (500 MHz, CDCl₃, Mixture of diastereomers) δ 3.33-3.23 (m, 4H), 2.65-2.60 (m, 1H), 2.14-2.06 (m, 1H), 1.91-1.88 (m, 4H), 1.58-1.53 (app. M, 1H), 1.23-1.17 (app. dd, 6H), 1.03-1.02 (d, 3H); ¹³C NMR (125 MHz) δ 52.9, 52.3, 46.6, 37.8, 37.3, 26.6, 23.2, 17.5, 14.5; ³¹P {¹H} NMR (202 MHz, CDCl₃, Mixture of diastereomers) δ 48.83, 47.73. HRMS for C₁₀H₂₀NNaOP [M + Na⁺] calculated 224.1175; found 224.1199.

1.8.2.5. 1-Cyclopropyl-2,2,3-trimethylphosphetane-1-oxide (**S4**):



To a flame-dried two-neck round bottom flask equipped with a stir bar was added dried magnesium(0) powder (50 mesh, 0.43 g, 18 mmol), THF (2 mL), and one crystal of iodine. Stirring was initiated and a solution of bromocyclopropane (1.3 mL, 15 mmol) in THF (13 mL) was added dropwise. When addition of the bromide was complete, the reaction was

refluxed for 2 h. The reaction was then cooled to 0 °C and a solution of **S1** (2.0 g, 12 mmol) in THF (10 mL) was added dropwise to the stirring solution of **S3**. The reaction was allowed to warm to room temperature and was stirred for 16 h. After 16 h, the reaction was quenched by the addition of deionized water (25 mL). The layers were separated and the aqueous layer was washed with DCM (3 × 25 mL). The organic layers were combined and dried with MgSO₄, concentrated *in vacuo* to a yellow oil, and loaded onto silica gel. Purification by flash column chromatography on silica gel (40 g SiO₂, 0–10% MeOH:DCM eluent, linear gradient) afforded the title compound (730 mg, 32%) as a yellow oil and mixture of diastereomers: $R_f = 0.60$ (5:95 MeOH:DCM) stained with iodine. ¹H NMR (500 MHz, CDCl₃, Major diastereomer) δ 2.4–2.38 (m, 1H), 2.12–2.04 (m, 1H), 1.96–1.92 (m, 1H), 1.21–1.16 (app. dd, 6H), 0.99–0.98 (d, 3H), 0.87–0.74 (m, 4H); ¹³C NMR (125 MHz, CDCl₃, Mixture of diastereomers) δ 49.0, 48.6, 46.6, 37.3, 36.9, 30.2, 25.9, 25.5, 24.3, 23.7, 22.6, 16.6, 16.1, 14.4, 14.2, 13.7, 12.1, 11.7; ³¹P {¹H} NMR (202 MHz, CDCl₃, Mixture of Diastereomers) δ 48.08 (major), 55.97 (minor). HRMS for C₉H₁₈OP [M + H⁺] calculated 173.1090; found 173.1086.

1.8.3. Reactivity of Phenylsilane with Alcohols:

1.8.3.1. Procedure: To a NMR tube was added *p*-nitrobenzoic acid (25 mg, 1.5 equiv, 0.15 mmol), *d*₈-THF (0.5 mL), 4-(trifluoromethyl)benzyl alcohol (13.7 μL, 1.0 equiv, 0.1 mmol), hexafluorobenzene (11.5 μL, 1.0 equiv, 0.1 mmol) and phenylsilane (18.5/37 μL, 1.5/3.0 equiv, 0.15/0.3 mmol). The tube was inverted three times to ensure proper mixing of the reagents and the interface between the tube and the cap was sealed with multiple

layers of paraffin wax (parafilm®) to ensure no leaks. The reaction was heated to 80 °C and monitored with ¹⁹F NMR.

1.8.4. Optimization of the Catalytic Mitsunobu Reaction:

1.8.4.1. Procedure: To a 2-dram vial equipped with a stir bar was added *p*-nitrobenzoic acid (250 mg, 1.5 equiv, 1.5 mmol) and phosphine precatalyst (0.1 equiv, 0.1 mmol). Solvent (4 mL) was added followed by benzyl alcohol (103 μL, 1.00 equiv, 1.00 mmol), DIAD (216 μL, 1.10 equiv, 1.10 mmol), and then silane (X equiv, X mmol). Reactions were sealed with a PTFE septum in the screw cap and heated to the indicated temperature. When the reaction was deemed complete (TLC), reactions were concentrated under reduced pressure and purified by silica gel chromatography

1.8.5. Optimization of Silane Stoichiometry:

1.8.5.1. Procedure: To a 15 mL pressure tube equipped with a stir bar was added *p*-nitrobenzoic acid (250 mg, 1.5 equiv, 1.5 mmol) and phosphine precatalyst (0.1 equiv, 0.1 mmol). THF (4 mL) was added followed by 4-(trifluoromethyl)benzyl alcohol (137 μL, 1.0 equiv, 1.0 mmol), DIAD (216 μL, 1.1 equiv, 1.1 mmol), hexafluorobenzene (11.5 μL, 0.1 equiv, 0.1 mmol), and then silane (X equiv, X mmol). Reactions were sealed with a PTFE septum in the screw cap and heated to the appropriate temperature. When the reaction was deemed complete, reactions were concentrated under reduced pressure and isolated by silica gel chromatography.

1.8.6. Silane Reductions of Phosphine Oxide Precatalysts for Mitsunobu Studies:

1.8.6.1. Reaction setup: To an NMR tube was added a solution of phosphine oxide (1.0 equiv, 0.01 mmol) in d_8 -THF (0.5 mL, 0.02M). Phenylsilane (9.2/18.4/37 μ L, 7.5/15.0/30.0 equiv, 0.075/0.15/0.3 mmol) was added and the tube was sealed with a cap. The tube was inverted three times to ensure proper mixing of the silane and the interface between the tube and the cap was sealed with multiple layers of paraffin wax (parafilm®) to ensure no leaks. The reaction vessels were heated to the indicated temperature and monitored by ^{31}P NMR at multiple time points as shown in Figure 1.34.

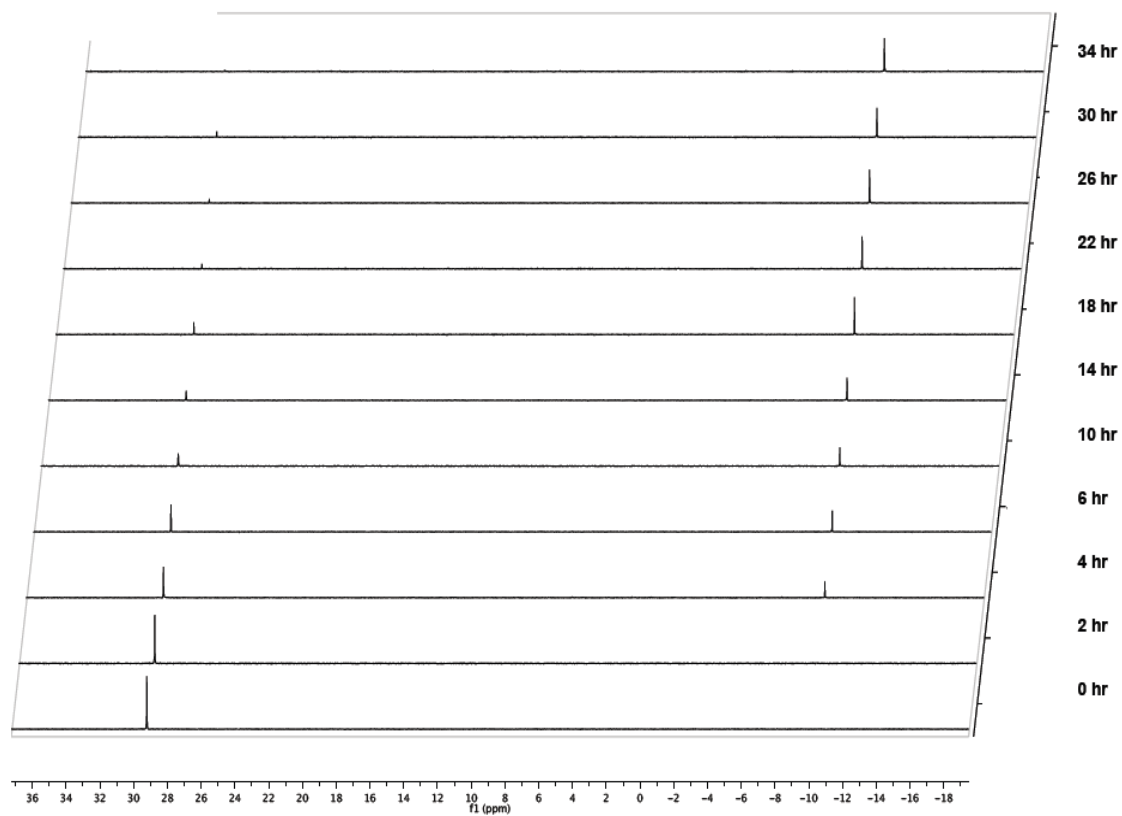


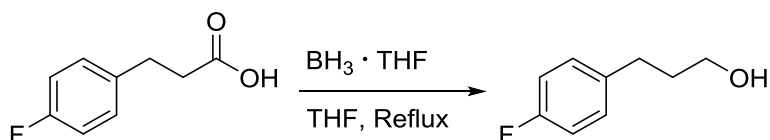
Figure 1.34. Representative stacked plot of ^{31}P NMR spectra obtained during a typical reduction experiment. Shown is the stacked plot of the reduction of **5PDBPO** with 30 equiv PhSiH_3 at 70 °C.

1.8.6.2. Time points: When using **5PDBPO** as the phosphine oxide, reactions can be effectively paused by running cold water over NMR tubes for 15-30 seconds. When using **1PPO** as the phosphine oxide, reactions can be effectively paused by running cold water over NMR tubes for 15-30 seconds followed by storage for short periods of time in a salt-water ice bath. Overnight storage (if needed) can be achieved at -20 °C as no reduction is noted at this temperature for any catalyst studied using this method.

1.8.6.3. NMR method: Tri-substituted phosphines have very long relaxation times as the ³¹P nucleus is not coupled to any other nucleus that can promote its relaxation. Because of this, we utilized a 35 second delay time between pulses and monitored each reaction with only 4 pulses per time point. While this method has been applied previously⁶, we confirmed these parameters by comparing the integration of triphenylphosphine and triphenylphosphine oxide with known concentrations.

1.8.7. Synthesis of Alcohol Substrates:

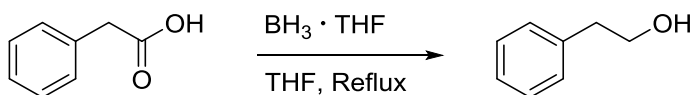
1.8.7.1. 3-(4-Fluorophenyl)propanol:⁹⁵



To a 200 mL round bottom flask equipped with a stir bar was added 3-(4-fluorophenyl)propanoic acid (4.2 g, 25 mmol, 1.0 equiv) and THF (35 mL). The flask was purged with argon and cooled to 0 °C. A 1 M solution of borane in THF (34 mL, 34 mmol, 1.4 equiv) was added dropwise over 15 min. The reaction was warmed to 23 °C. After 3 h, the reaction was cooled to 0 °C and methanol (5 mL) and H₂O (10 mL) were added to

quench the reaction. The reaction was concentrated under reduced pressure and the residue was dissolved in H₂O (20 mL). The reaction mixture was extracted with EtOAc (2 × 20 mL). The organic layers were combined and washed with saturated aqueous NaHCO₃ (40 mL) and saturated aqueous NaCl (40 mL). The combined organic layer was dried with magnesium sulfate and concentrated to give 3-(4-fluorophenyl)propanol (3.66 g, 95%) as a light yellow oil: $R_f = 0.20$ (2:8 ethyl acetate: hexanes). Spectral and physical data matched previous reports.

1.8.7.2. 2-Phenylethanol:⁹⁶



To a 100 mL round bottom flask equipped with a stir bar was added phenylacetic acid (2.45 g, 18.0 mmol, 1.00 equiv) and THF (7 mL). The flask was purged with argon, and cooled to 0 °C. A 1 M solution of borane in THF (24 mL, 24 mmol, 1.33 equiv) was added dropwise over 15 min. The reaction was warmed to 23 °C. After 3 h, the reaction was cooled to 0 °C and methanol (5 mL) and H₂O (10 mL) was added to quench the reaction. The reaction mixture was diluted with EtOAc (20 mL) and the layers were separated. The organic layer was washed with a saturated aqueous NaHCO₃ and then dried with magnesium sulfate. The reaction was concentrated to give 2-phenylethanol (2.08 g, 95%) as a colorless oil: $R_f = 0.22$ (2:8 ethyl acetate: hexanes). Spectral and physical data matched previous reports.

1.8.8. General Procedure for the Catalytic in Phosphine Mitsunobu Reaction:

To a 15 mL pressure tube equipped with a stir bar was added precatalyst **1PPO** (18 mg, 0.10 equiv, 0.10 mmol) and *p*-nitrobenzoic acid (250 mg, 1.5 equiv, 1.5 mmol). Then, THF (4 mL) was added followed by benzyl alcohol (103 μ L, 1.0 equiv, 1.0 mmol), DIAD (216 μ L, 1.1 equiv, 1.1 mmol), and phenylsilane (135 μ L, 1.1 equiv, 1.1 mmol). The reaction vessel was sealed with a #15 O-ring and heated to 80 °C for 18 h. The reaction was cooled to 23 °C and concentrated under reduced pressure. The residue was purified by column chromatography as indicated for each compound.

1.8.8.1. Alternate workup: The reaction was diluted by four-fold with ethyl acetate. The reaction mixture was washed twice with saturated aqueous NaHCO₃ (1:1 volume) and then saturated aqueous NaCl (1:1 volume). The organics were dried with anhydrous magnesium sulfate and concentrated under reduced pressure.

1.8.9. General Procedure for the Stoichiometric Mitsunobu Reaction:

To a 2-dram vial equipped with a stir bar were sequentially added triphenylphosphine (1.5 equiv), solid nucleophiles (1.5 equiv), solid alcohols (1.0 equiv) and tetrahydrofuran (0.25 *M*). If the reagents were liquids, then they were added following addition of THF. Next, diisopropyl azodicarboxylate (DIAD, 1.5 equiv) was added in a dropwise manner to initiate the reaction. The reaction vessel was sealed with a PTFE septum in the screw cap and stirred at room temperature overnight. After 18 h, the reaction was concentrated under reduced pressure. The residue was purified by silica gel chromatography as indicated for each compound.

1.8.10. Purification of Products in Table 1.3: All reactions can be monitored using standard TLC analysis. All reactions were stained with UV, iodine, KMnO₄, and/or ninhydrin.

Benzyl 4-nitrobenzoate:⁴⁵

Reactions were concentrated directly onto SiO₂. Purified using a Teledyne-Isco Combi-Flash system using a gradient from 0 to 10% ethyl acetate in hexanes. Isolated as a white to yellow solid (all had similar purity as determined by NMR): $R_f = 0.42$ (2:8 ethyl acetate:hexanes). Spectra and physical data matched previous reports.

4-Trifluoromethylbenzyl 4-nitrobenzoate:⁹⁷

Reactions were concentrated directly onto SiO₂. Purified using a Teledyne-Isco Combi-Flash system using a gradient from 0 to 10% ethyl acetate in hexanes. Isolated as a white solid: $R_f = 0.43$ (2:8 ethyl acetate:hexanes). Spectra and physical data matched previous reports.

4-Methoxybenzyl 4-nitrobenzoate:⁴⁵

Reactions were concentrated directly onto SiO₂. Purified using a Teledyne-Isco Combi-Flash system using a gradient from 0 to 10% ethyl acetate in hexanes. Isolated as a yellow solid: $R_f = 0.43$ (2:8 ethyl acetate:hexanes). Spectra and physical data matched previous reports.

Geranyl 4-nitrobenzoate:

Reactions were concentrated directly onto SiO₂. Purified using a Teledyne-Isco Combi-Flash system using a gradient from 0 to 10% ethyl acetate in hexanes. Isolated as a colorless

oil: $R_f = 0.50$ (2:8 ethyl acetate:hexanes); ^1H NMR (400 MHz, CDCl_3) δ 8.27 (d, 2H, $J = 8.9$ Hz), 8.20 (d, 2H, $J = 8.9$ Hz), 5.45 (t, 1H, $J = 7.1$ Hz), 5.07 (t, 1H, $J = 7.1$ Hz), 4.87 (d, 2H, $J = 7.1$ Hz), 2.06–2.13 (m, 4H), 1.76 (s, 3H), 1.66 (s, 3H), 1.59 (s, 3H); ^{13}C NMR (100 MHz, CDCl_3) δ 160.36, 130.68, 123.45, 117.63, 62.71, 39.51, 26.19, 25.64, 17.65; HRMS for $\text{C}_{17}\text{H}_{21}\text{NO}_4\text{Na}$ [$\text{M}+\text{Na}^+$] calculated 326.1363; found 326.1361.

3-(4-Fluorophenyl)propyl 4-nitrobenzoate:

Reactions were concentrated directly onto SiO_2 . Purified using a Teledyne-Isco Combi-Flash system using a gradient from 0 to 10% ethyl acetate in hexanes. Isolated as a colorless oil: $R_f = 0.50$ (2:8 ethyl acetate:hexanes); ^1H NMR (400 MHz, CDCl_3) δ 8.28 (d, 2H, $J = 8.9$ Hz), 8.16 (d, 2H, $J = 8.9$ Hz), 7.13–7.17 (m, 2H), 6.96 (t, 2H, $J = 8.7$ Hz), 4.37 (t, 2H, $J = 6.5$ Hz), 2.75 (t, 2H, $J = 7.4$ Hz), 2.06–2.13 (m, 2H); ^{13}C NMR (100 MHz, CDCl_3) δ 164.60, 130.62, 129.65, 123.51, 115.38, 115.18, 65.12, 31.47, 30.18; ^{19}F NMR (376 MHz, CDCl_3) δ -117.19 (s, 1F) HRMS for $\text{C}_{16}\text{H}_{14}\text{NFO}_4\text{Na}$ [$\text{M}+\text{Na}^+$] calculated 326.0799; found 326.0800.

Propargyl 4-nitrobenzoate:⁹⁸

Reactions were concentrated directly onto SiO_2 . Purified using a Teledyne-Isco Combi-Flash system using a gradient from 0 to 10% ethyl acetate in hexanes. Isolated as an off-white solid: $R_f = 0.45$ (1:9 ethyl acetate:hexanes). Spectra and physical data matched previous reports.

(R)-1-Phenylethyl 4-nitrobenzoate:⁴⁵

Reactions were concentrated directly onto SiO₂. Purified using a Teledyne-Isco Combi-Flash system using a gradient from 0 to 20% ethyl acetate in hexanes. Isolated as a yellow solid (after extensive drying): $R_f = 0.43$ (2:8 ethyl acetate:hexanes); ER > 94:6 (5:5 isopropanol:hexanes). Spectra and physical data matched previous reports.

(R)-1-Ethoxy-1-oxopropan-2-yl 4-nitrobenzoate:⁴⁵

Reactions were concentrated directly onto SiO₂. Purified using a Teledyne-Isco Combi-Flash system using a gradient from 0 to 10% ethyl acetate in hexanes. Isolated as a white to yellow solid (all had similar purity as determined by NMR): $R_f = 0.57$ (2:8 ethyl acetate:hexanes); ER > 99.5: 0.5 (5:5 isopropanol:hexanes). Spectra and physical data matched previous reports.

Phenethyl 4-nitrobenzoate:⁴⁵

Reactions were concentrated directly onto SiO₂. Purified using a Teledyne-Isco Combi-Flash system using a gradient from 0 to 10% ethyl acetate in hexanes. Isolated as a white solid: $R_f = 0.43$ (2:8 ethyl acetate:hexanes). Spectra and physical data matched previous reports.

Phenethyl *N*-fluorenylmethyloxycarbonylvalinate:

Reactions were concentrated directly onto SiO₂. Purified using a Teledyne-Isco Combi-Flash system using a gradient from 0 to 40% ethyl acetate in hexanes. Isolated as a colorless oil: $R_f = 0.31$ (2:8 ethyl acetate:hexanes); ¹H NMR (400 MHz, CDCl₃) δ 7.75 (d, 2H, $J = 7.5$ Hz), 7.59 (d, 2H, $J = 7.1$ Hz), 7.39 (t, 2H, $J = 7.1$ Hz), 7.18-7.32 (m, 7H), 5.25 (t, 1H, $J = 9.1$ Hz), 4.20-4.42 (m, 6H), 2.95 (t, 2H, $J = 6.9$ Hz), 2.05-2.13 (m, 1H), 0.90 (d, 3H, J

= 6.8 Hz), 0.81 (d, 3H, $J = 6.8$ Hz); ^{13}C NMR (100 MHz, CDCl_3) δ 171.96, 156.17, 143.90, 143.77, 141.29, 137.32, 128.81, 128.53, 127.67, 127.03, 126.66, 125.05, 119.95, 66.99, 65.64, 58.99, 47.18, 35.00, 31.25, 18.90, 17.43; HRMS for $\text{C}_{28}\text{H}_{29}\text{NO}_4\text{Na}$ [$\text{M}+\text{Na}^+$] calculated 466.1989; found 466.1995.

1-Nitro-4-phenylethoxybenzene:⁹⁹

Reactions were concentrated directly onto SiO_2 . Purified using a Teledyne-Isco Combi-Flash system using a gradient from 0 to 10% ethyl acetate in hexanes. Isolated as a yellow solid: $R_f = 0.51$ (2:8 ethyl acetate:hexanes). Spectra and physical data matched previous reports.

tert-Butyl phenethyl(sulfamoyl)carbamate:

Reactions were concentrated directly onto SiO_2 . Purified using a Teledyne-Isco Combi-Flash system using a gradient from 0 to 30% ethyl acetate in hexanes. Isolated as a white solid: $R_f = 0.13$ (2:8 ethyl acetate:hexanes); ^1H NMR (400 MHz, CDCl_3) δ 7.29–7.33 (m, 2H), 7.20–7.26 (m, 3H), 4.69 (bs, 2H), 3.96 (t, 2H, $J = 7.1$ Hz), 2.93 (t, 2H, $J = 7.1$ Hz), 1.49 (s, 9H); ^{13}C NMR (100 MHz, CDCl_3) δ 138.37, 129.46, 128.55, 126.78, 84.24, 48.74, 35.41, 28.01; HRMS for $\text{C}_{13}\text{H}_{20}\text{N}_2\text{O}_4\text{SNa}$ [$\text{M}+\text{Na}^+$] calculated 323.1036; found 323.1036.

N-tert-Butoxycarbonylhomoserine lactone:¹⁰⁰

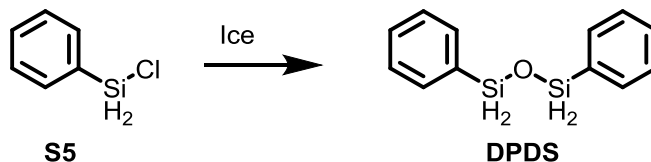
Reactions were concentrated directly onto SiO_2 . Purified using a Teledyne-Isco Combi-Flash system using a gradient from 0 to 50% ethyl acetate in hexanes. Isolated as a white solid: $R_f = 0.38$ (4:6 ethyl acetate:hexanes). Spectra and physical data matched previous reports.

tert-Butyl (2',3'-O-isopropylidene-5'-deoxyinosin-5'-yl)(sulfamoyl)lcarbamate:

Reactions were concentrated directly onto SiO₂. Purified using a Teledyne-Isco Combi-Flash system using a gradient from 0 to 100% ethyl acetate in hexanes. Isolated as a white solid: $R_f = 0.50$ (ethyl acetate); ¹H NMR (400 MHz, CDCl₃) δ 12.38 (bs, 1H), 8.27 (s, 1H), 8.05 (s, 1H), 6.07 (d, 1H, $J = 3.1$ Hz), 5.23 (dd, 1H, $J = 6.2, 2.9$ Hz), 5.07 (t, 2H, 4.7 Hz), 4.89 (dd, 1H, $J = 6.2, 2.5$ Hz), 3.50 (t, 2H, 4.7 Hz), 1.66 (s, 9H), 1.50 (s, 3H), 1.29 (s, 3H); ¹³C NMR (100 MHz, CDCl₃) δ 156.94, 155.66, 148.21, 146.48, 139.17, 124.89, 113.53, 90.01, 87.08, 84.24, 81.68, 61.88, 28.01, 27.46, 25.59; HRMS for C₁₈H₂₆N₆O₈SNa [M+Na⁺] calculated 509.1425; found 509.1451.

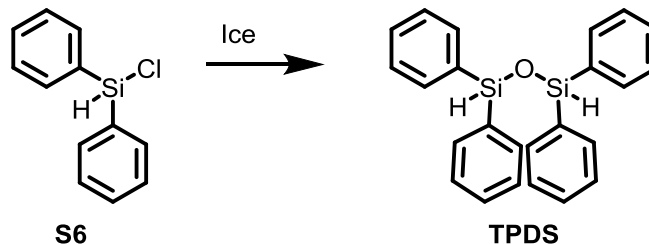
1.8.10. Synthesis of Silane Reducing Agents:

1.8.10.1. 1,3-Diphenyl-disiloxane (DPDS):



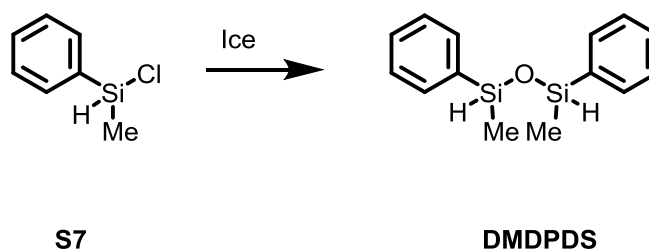
To a separatory funnel charged with partially melted ice (10 g) was added a solution of **S5** (2.0 g, 14 mmol, 2.1 mL) in diethyl ether (8 mL). The reaction was allowed to warm to 23 °C and was swirled by hand every 10 min for 1 h. Additional diethyl ether (15 mL) was then added to the reaction and the aqueous layer was drained. The ether layer was washed with H₂O (10 mL), dried (MgSO₄), and concentrated *in vacuo* to afford the crude product. Purification by Kugelrohr distillation afforded the title compound (2.6 g, 82%) as a colorless oil: bp = 155 °C at 0.8 mmHg; NMR spectra and other physical data matched previous reports.⁷³

1.8.10.2. 1,1,3,3-Tetraphenyl-disiloxane (TPDS):



To a separatory funnel charged with partially melted ice (10 g) was added a solution of **S6** (2.1 g, 9.6 mmol, 2.0 mL) in diethyl ether (8 mL). The reaction was allowed to warm to 23 °C and was swirled by hand every 10 min for 1 h. Additional diethyl ether (15 mL) was then added to the reaction and the aqueous layer was drained. The ether layer was washed with H₂O (10 mL), dried (MgSO₄), and concentrated *in vacuo* to afford the crude product. Purification by Kugelrohr distillation afforded the title compound (1.7 g, 90%) as a colorless solid: bp = 290 °C at 0.6 mmHg; NMR spectra and other physical data matched previous reports.¹⁰¹

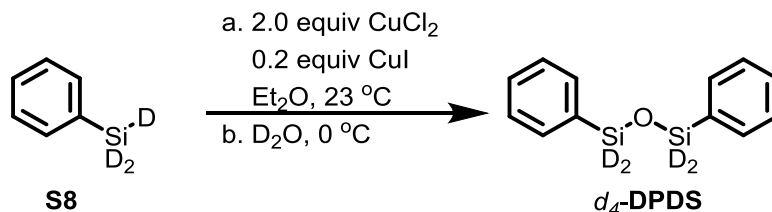
1.8.10.3. 1,3-Dimethyl-1,3-diphenyl-disiloxane (DMDPDS):



To a separatory funnel charged with partially melted ice (10 g) was added a solution of **S7** (2.2 g, 13.9 mmol, 2.1 mL) in diethyl ether (8 mL). The reaction was allowed to warm to 23 °C and was swirled by hand every 10 min for 1 h. Additional diethyl ether (15 mL) was then added to the reaction and the aqueous layer was drained. The ether layer was washed

with H₂O (10 mL), dried (MgSO₄), and concentrated *in vacuo* to afford the crude product. Purification by Kugelrohr distillation afforded the title compound (1.5 g, 81%) of a colorless oil: bp = 102 °C at 0.8 mmHg; NMR spectra and other physical data matched that of previous reports.¹⁰²

1.8.10.4. Si, Si, Si, Si-Tetradeutero-1,3-diphenyl-disiloxane (*d*₄-DPDS): JAB11P047



The synthesis of *d*₄-DPDS followed a modified version of our previously published synthesis.⁶ Briefly, a 100 mL two-neck round bottom flask was charged with CuCl₂ (1.344 g, 10 mmol), CuI (193, 1 mmol), and then 20 ¼ inch ceramic spheres. Et₂O (10 mL) was added, and the flask was fit with an overhead stirrer. The suspension was stirred at 23 °C for 30 minutes, and stirring was stopped. **S8** (555 mg, 5 mmol) was added dropwise and stirring was resumed. After 3 hours, stirring was ceased, and the reaction filtered directly onto ice chips of D₂O (10 g). The contents of the filtration flask were transferred to a separatory funnel and was allowed to warm to 23 °C and was swirled by hand every 5 min for 30 h. Additional diethyl ether (15 mL) was then added to the reaction and the aqueous layer was drained. The ether layer was washed with H₂O (15 mL), dried (MgSO₄), and concentrated *in vacuo* to afford the crude product. Purification by Kugelrohr distillation afforded the title compound (384 mg, 60%) of a colorless oil: bp = 86 °C at 0.56 mmHg.

1.8.11. Reductions of Phosphine Oxide Precatalysts:

1.8.11.1. General Procedure for NMR Experiments: To an NMR tube was added a phosphine oxide precatalyst (0.02 mmol, 0.04 M), d_8 -toluene, d_2 -DCM, or d_8 -THF (final volume of 500 μ L), and silane (7.5–15 equiv., 0.15–0.3 mmol, 0.3–0.6 M). The tube was inverted three times to ensure proper mixing of the reagents and the interface between the tube and the cap was sealed with multiple layers of paraffin wax (parafilm®) to ensure no leaks. The reaction was heated to the temperature dictated by the experiment, and monitored by ^{31}P NMR.

1.8.11.2. ^{31}P NMR Method for Monitoring the Reduction of Phosphine Oxide Precatalysts:

The NMR method is similar to the method previously reported.^{51, 64} However, a 25 second delay time was used to increase the sampling frequency with minimal error induced during integration. Spectra were also collected using a decoupled method (WALTZ 16) unless otherwise indicated to enhance the signal to noise ratios (S/N). All peaks monitored correspond to the phosphorus shifts observed for the phosphine oxide, phosphine, and any unisolable intermediates with peaks above a 3:1 S/N ratio (please see supporting section 2 for novel phosphine oxide shifts).

1.8.11.3. Data Analysis of NMR Experiments

1.8.11.3.1 Processing of Raw ^{31}P FIDs: Phosphorous NMR spectra were integrated through VNMR, ACD Labs, or, for longer time courses, with an automated processor/integrator written in Matlab. A folder containing NMR spectra is submitted to the program along with the location of a standard peak in ppm, ppm values flanking the ranges to be integrated, the type and degree of apodization, and degree of zerofilling desired. The

program then sequentially obtains the data from each folder, acquiring, apodizing, zero-filling, and inverse Fourier transforming the data through modifications to the algorithms written in MatNMR.¹⁰³ The resulting spectrum is then phased using a modified version of the algorithm developed by Liu and co-workers.¹⁰⁴ Finally, the spectrum is shifted according to the ppm of the standard provided, and the data points within the ranges provided are summed, providing the integrated totals. All spectra integrated using this program applied a 1.2 Hz Lorentzian apodization and doubled the apparent digital resolution through the addition of zeros prior to the Fourier Transform. Additionally, all were integrated twice with the standard being set one time as the starting material peak and the other time as the product peak to ensure accuracy at the tail ends of the time courses.

1.8.11.3.2 Processing the Integrated Data: Following processing of each of the time courses, the triplicate integrated values were averaged to produce the phosphine oxide reduction curves shown in Figure 1.5B & 1.10B. Each curve was then fit to both equation 1 for single exponential fitting and to equation 2 for double exponential fitting using the Microsoft Excel® add-on Solver®. This was accomplished through minimization of the sum of the variances with floating amplitude(s) and rate constant(s). An analysis of the quality of curve fitting for reductions using PhSiH₃ is shown in Figure 1.6. Variance per data point is used to measure the goodness of fit as the Pearson correlation (R^2) is not directly applicable (Table 1.5). The use of double-exponential fitting for the curves in Figure 1.6 improves the variance per data point by 3-12X.

1.8.11.3.3 Processing the Integrated Data: Following processing of each of the time courses, the triplicate integrated values were averaged to produce the phosphine oxide reduction curves shown in Figure 1B & 3B. Each curve was then fit to both equation 1 for single exponential fitting and to equation 2 for double exponential fitting using the Microsoft Excel® add-on Solver®. This was accomplished through minimization of the sum of the variances with floating amplitude(s) and rate constant(s). An analysis of the quality of curve fitting for reductions using PhSiH₃ is shown in Figure 1.6. Variance per data point is used to measure the goodness of fit as the Pearson correlation (R²) is not directly applicable (Table 1.38). The use of double-exponential fitting for the curves in Figure 1.6 improves the variance per data point by 3-12X.

Equation 1. $\%P = 100 - Ae^{-kt}$

Equation 2. $\%P = 100 - A_1e^{-k_1t} + A_2e^{-k_2t}$

Table 1.38. Numerical comparison between single- and double-exponential fitting of reduction curves.

Entry	Variance (%PO Reduced)²	# Points	Variance Per Data Point
<i>IPPO-Single</i>	612.79	26	23.57
<i>IPPO-Double</i>	60.93	26	2.34
<i>TMPPPO-Single</i>	468.99	28	16.74
<i>TMPPPO-Double</i>	37.93	28	1.35
<i>TMBPO-Single</i>	215.23	16	13.45
<i>TMBPO-Double</i>	35.14	16	2.20
<i>TMPyrPO-Single</i>	133.23	14	9.52
<i>TMPyrPO-Double</i>	37.09	14	2.65

The equations arising from the previously described fitting are then used to obtain the k , $t_{50\%}$, and $t_{90\%}$ values shown in Tables 1.5 and 1.8. The k in these figures is the rate constant obtained from fitting to equation 1, while $t_{50\%}$ and $t_{90\%}$ are obtained from setting %P in equation 2 to 50 and 90 with the amplitudes and rate constants determined from fitting.

Derivative curves were obtained through calculation of the derivative with respect to time of the exponentials resulting from fitting to equation 1 for **DPDS** reductions and equation 2 for phenylsilane reductions. Often, when fitting to equation 2, this method did not provide an accurate representation of the actual derivative for the first two data points. To overcome this problem, when necessary the slope between the first two data points (either raw or fitted) was used as the initial derivative and the slope between the first and third data points (either raw or fitted) was used as the derivative at the second time point. It is notable that this practice overestimates the initial rates.

1.8.11.3.4 Processing Data for the Reduction of **TMPyrPO**: The presence of excess reducing agent facilitates two reductions of **TMPyrPO**. One is the reduction of the phosphine oxide to the corresponding phosphetane, while the other is a reduction of the P-N bond, and it appears that these reductions can occur in either order. Reduction of the P-N bond was also noted by Radosevich and co-workers during their reduction studies while developing new catalysts for their dehydrative coupling reaction.¹⁰⁵ In the data presented for **TMPyrPO** reduction, the secondary phosphetane is quantified and used for the percentage of phosphine that has been reduced, as isolation of the intermediate

phosphetanes were impractical under pseudo first-order conditions. The amino-phosphetane was observed in the range reported by Radosevich, however quantification was much more accurate with the resonances produced by the secondary phosphetane.

1.8.11.4. Reductions of Phosphine Oxides with Phenylsilane at Ambient Temperature

1.8.11.4.1. General Procedure: To an NMR tube was added a phosphine oxide precatalyst (0.02 mmol, 0.04 M), *d*₈-toluene or *d*₈-THF (final volume of 500 μL), and phenylsilane (24.6 μL, 10 equiv., 0.2 mmol, 0.4 M). The tube was inverted three times to ensure proper mixing of the reagents and the interface between the tube and the cap was sealed with multiple layers of paraffin wax (parafilm®) to ensure no leaks. The reaction was heated to 25 °C and monitored by ³¹P NMR.

1.8.11.4.2. Results: The reductions of phosphine oxide precatalysts at 25 °C proceeded as expected. PhSiH₃ is not a powerful enough reductant to afford reduction at catalytically-relevant concentrations with minimal heat input into the system. The only exception would be with the use of **TMPyrPO**, which, as shown in Figure 1.35, does reduce completely within 6 h. However, we observed complete reduction to the secondary phosphetane, which degrades rapidly, rendering this catalyst-silane combination ineffective in reactions.

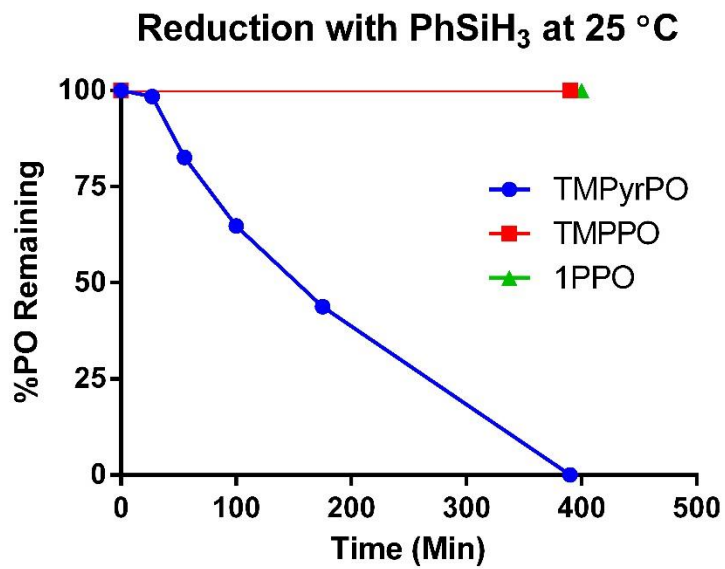


Figure 1.35. Progress curves of phosphine oxide reductions with phenylsilane at 25 °C.

1.8.11.5. Reductions of TMPyrPO Proceed with Two Steps

1.8.11.5.1. General Procedure: To an NMR tube was added *d*₈-toluene (final volume of 500 μ L), **TMPrPO** (40.2 mg, 0.2 mmol, 0.4 M) and then phenylsilane (3.07, 6.15, or 12.3 μ L, 0.025–0.1 mmol, 0.05–0.2 M) or **DPDS** (5.8, 11.5, or 23.0 mg, 0.025–0.1 mmol, 0.05–0.2 M). The tube was inverted three times to ensure proper mixing of the reagents and the interface between the tube and the cap was sealed with multiple layers of paraffin wax (parafilm®) to ensure no leaks. The reaction was heated to 25 °C and monitored by ³¹P NMR.

1.8.11.5.2. Results: As mentioned in Section 4.3.3, adding TMPyrPO to an excess of DPDS or phenylsilane causes over-reduction to the secondary phosphetane. In theory, using an excess of TMPyrPO should inhibit reduction to the secondary phosphetane. However, using 0.125 equivalent of either **DPDS** or phenylsilane still led to the formation of the secondary phosphetane rather than a mono-reduced product. This suggests the initial reduction of the phosphine oxide is slower than the rate of reduction to form the secondary phosphetane. Because the initial reduction is slower than the subsequent “over-reduction”, we believe that the data and fitting for TMPyrPO closely match the initial, slower reduction of the oxide to the amino-phosphetane.

Also noteworthy about these reductions is that fewer equivalents of silane seems to favor reduction to the amino-phosphetane, as a buildup of a phosphorus species is observed around 125 ppm, rather than around 27 ppm, which was observed in reactions with heavy excess of silane. We speculate that the species around 27 ppm is the secondary phosphetane

oxide, and are currently investigating the reactivity of phosphinic amides with silanes in greater detail.

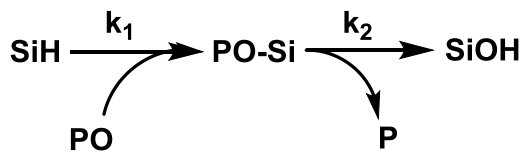
1.8.11.6. The Effect of **TMPPPO** Concentration on its Rate of Reduction

1.8.11.6.1. General Procedure: To an NMR tube was added *d*₈-toluene (451 μL), phenylsilane (49 μL, 0.4 mmol, 0.8 M), and **TMPPPO** (4.2, 8.4, or 12.6 mg). The tube was inverted three times to ensure proper mixing of the reagents and the interface between the tube and the cap was sealed with multiple layers of paraffin wax (parafilm®) to ensure no leaks. The reaction was heated to 80 °C and monitored by ³¹P NMR.

1.8.11.6.2. Results: As shown in Figure 1.9A, increasing the concentration of **TMPPPO** also increases the rate of its reduction. The trend is also demonstrated by fitting each curve to Equation 2 and then determining the number of minutes until 50% and 90% of the phosphine oxide is reduced, as shown in Figure 1.9.

This experiment was used to rule out Mechanism II in Figure 1.8. If Mechanism II were correct, the rate of phosphine oxide reduction when measured by percentage of total phosphine should stay constant regardless of the concentration of phosphine oxide as long as pseudo-first order conditions are maintained.

To help with illustrating why this information rules out Mechanism II, we will first shorten Mechanism II to the scheme below:



It is important to note that this is the *kinetic* mechanism being discussed. The real mechanism that would go through this kinetic mechanism includes phenylsilane, phenylsilanol, phenylsilanediol, and phenylsilanetriol. However, if phenylsilane reduced phosphine oxides at a similar or greater rate than phenylsilanol and phenylsilanediol, then through reduction monitoring only k_1 and k_2 for phenylsilane will be able to be extracted from the data. If small amounts of phenylsilanol or phenylsilanediol are formed and each reduce at the same speed or slower than phenylsilane, then they will have a negligible effect on the overall reduction progress because of the >10x amount of phenylsilane present.

With that established, and remembering that we are making the assumption for Mechanism II that phenylsilane is an equal or better reductant than phenylsilanol or phenylsilanediol, we can write the rate of formation of the intermediate species and phosphine formation:

$$Rate_{inter} = k_1[PO][SiH]$$

$$Rate_P = k_2[PO - SI]$$

We are under pseudo-first order conditions, so [SiH] is constant, and we can let $K_1 = k_1[SiH]$:

$$Rate_{inter} = K_1[PO]$$

$$Rate_P = k_2[PO - SI]$$

Using these equations, we can solve for [P] and [PO-Si] as a function of time, k_1 , k_2 , and the initial concentration of [PO] (written as $[PO]_0$).¹⁰⁶

$$[PO - Si] = [PO]_0 * \left(\frac{K_1}{k_2 - K_1} e^{-K_1 t} + \frac{K_1}{K_1 - k_2} e^{-k_2 t} \right)$$

$$[P] = [PO]_0 - [PO]_0 * \left(\frac{k_2}{k_2 - K_1} e^{-K_1 t} + \frac{K_1}{K_1 - k_2} e^{-k_2 t} \right)$$

If we take [P] and divide it by the initial concentration of PO, we obtain:

$$\frac{[P]}{[PO]_0} = \frac{k_2}{k_2 - K_1} e^{-K_1 t} + \frac{K_1}{K_1 - k_2} e^{-k_2 t}$$

Therefore, the left side of the equation is equal to an expression that does not have [PO]₀ in it, an expression that is only dependent on the rate constants and the time. When we drew the graphs with %PO remaining on the y-axis, what we were basically doing is dividing the concentration of phosphine oxide present by [PO]₀. The quantity represented in the reduction progress curves (Figure S3A), then, should not change regardless of the value of [PO]₀. Since changing [PO]₀ does have an effect on the rate, Mechanism II cannot be correct. It is also noteworthy that this data strongly supports Mechanism V, as the fact that phosphine oxide catalyzes the formation of phenylsilanol provides a reason for the rate to increase when [PO]₀ increases.

1.8.11.7. The Effects of Solvent on Phosphine Oxide Reductions

1.8.11.7.1. General Procedure: To an NMR tube was added a phosphine oxide precatalyst (0.02 mmol, 0.04 M), *d*₈-toluene, *d*₂-DCM, or *d*₈-THF (475 μL), and then silane (10 equiv., 0.15 mmol, 0.3 M). The tube was inverted three times to ensure proper mixing of the reagents and the interface between the tube and the cap was sealed with multiple layers of paraffin wax (parafilm®) to ensure no leaks. The reaction was heated to 80 °C and monitored with ³¹P NMR.

1.8.11.7.2. Results: The reductions of phosphine oxides with silanes can substantially vary greatly the solvent used for the reduction. The most drastic example of solvent effect is noted in the difference in reactivity when THF or toluene are used with the disiloxane **DMDPDS**. In this case, the use of toluene as the solvent significantly attenuates the rate of reduction (Figure 1.36). Fitting this data to single-exponential curves reveals that the rate of reduction is almost exactly 20-fold higher in THF than it is in toluene, which we attribute to the concentration of water in each solvent. The excess water present in a solution of THF would likely cause a shift of the equilibrium between disiloxane and silanol towards the silanol form, increasing the rate. This necessity for water indicated that water may be the primary species responsible for the production of the kinetically-relevant reductant, however, we have also observed that too much water is detrimental to reduction rates.

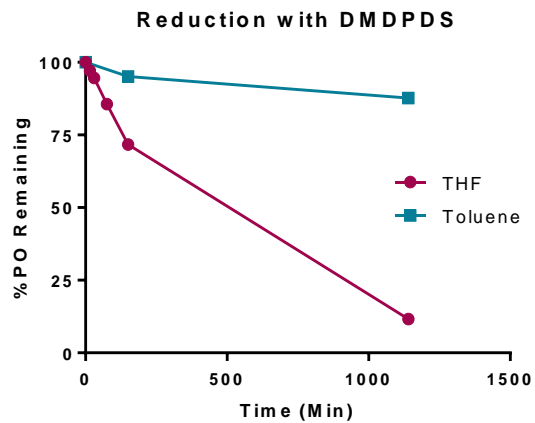


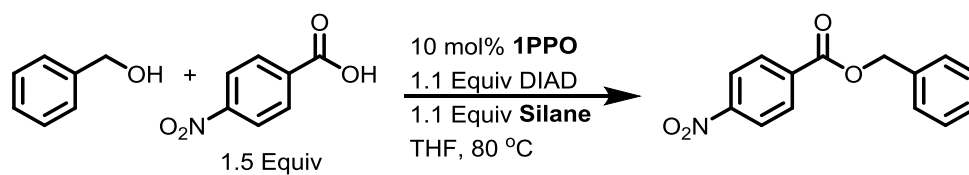
Figure 1.36. Progress curves of the reduction of **TMPPPO** with **DMDPDS** at 80 °C in THF and toluene. Data collected by Dr. Carter Eiden.

1.8.11.8. Silane Competence Screen in Catalytic Mitsunobu Reactions

1.8.11.8.1. General Procedure: To a 2 dram vial equipped with a stir bar was added *p*-nitrobenzoic acid (125 mg, 1.5 equiv, 0.75 mmol) and **IPPO** (9 mg, 0.1 equiv, 0.05 mmol). THF (2 mL) was then added followed by benzyl alcohol (57 μ L, 1.00 equiv, 0.50 mmol), DIAD (108 μ L, 1.10 equiv, 0.55 mmol), and silane (1.1 equiv, 0.55 mmol). Reactions were sealed with a PTFE septum in the screw cap and heated to 80 °C. After 24 h, the reaction was cooled and concentrated directly onto silica gel. Benzyl 4-nitrobenzoate was purified as previously described, with all spectra matching those of former reports.⁵¹

1.8.11.8.2. Results: When a sample of 14 commercially available silanes were screened for competence in a catalytic Mitsunobu reaction, only 4 of the reagents tested afforded product, as shown in Table 1.39. Phenylsilane and diphenylsilane worked as expected, but we also observed *n*-hexylsilane was a competent reducing agent in whole reaction schemes. However, further testing of *n*-hexylsilane revealed it required elevated temperatures to be a competent reducing agent.

Table 1.39. Silane Competency Screen in Catalytic Mitsunobu Reactions.



Entry	Silane	Isolated Yield
1	PhSiH ₃	81
2	Ph ₂ SiH ₂	42
3	Ph ₃ SiH	No Reaction
4	PMHS	No Reaction
5	Et ₃ SiH	No Reaction
6	ⁱ Pr ₃ SiH	No Reaction
7	(TMS) ₃ SiH	28
8	TMDSO	No Reaction
9	ⁿ HexylSiH ₃	67
10	DPDS	0

1.8.11.9. Comparison of Reduction Rates of **TMPPPO** by Standard Silanes

1.8.11.9.1. General Procedure: To an NMR tube was added *d*₈-toluene (475 μL), trimethoxysilane (25 μL, 0.2 mmol, 0.4 M), and **TMPPPO** (4.2 mg, 0.02 mmol, 0.04 M). The tube was inverted three times to ensure proper mixing of the reagents and the interface between the tube and the cap was sealed with multiple layers of paraffin wax (parafilm®) to ensure no leaks. The reactions were heated to 80 °C and monitored by ³¹P NMR.

1.8.11.9.2. Results: Figure 1.18 compares the reduction rate of **TMPPPO** (0.04 M) with phenylsilane, diphenylsilane, and trimethoxysilane (each present at 0.4 M). The rates of reduction for each silane are comparable, with trimethoxysilane and phenylsilane reducing **TMPPPO** slightly faster than diphenylsilane. With this phosphine oxide precatalyst, little rate enhancement would be gained through switching between the commonly used silane reductants.

1.8.11.10. Arrhenius and Eyring Analysis of the Reduction of **TMBPO** by **DPDS**

1.8.11.10.1. General Procedure: To an NMR tube was added a phosphine oxide precatalyst (0.02 mmol, 0.04 M), *d*₈-toluene or *d*₈-THF (465 μL), and then **DPDS** (35 mg, 7.5 equiv., 0.15 mmol, 0.3 M). The tube was inverted three times to ensure proper mixing of the reagents and the interface between the tube and the cap was sealed with multiple layers of paraffin wax (parafilm®) to ensure no leaks. The reaction was monitored with a variable temperature ³¹P NMR experiment over a temperature range from 0 to 25 °C.

1.8.11.10.2. Results: Shown in Figure 1.37, the reduction of **TMBPO** over this temperature range resulted in a linear trend evident in the Arrhenius plot. The slope of the line was

utilized to calculate the energy of activation. At 14.2 ± 0.9 kcal/mol, this energy is slightly lower than the observed energy of activation for the reduction of **TPPO** by **DPDS**, indicating that the incorporation of ring strain into phosphine oxide precatalysts certainly has an effect on this reaction. We also plotted the data utilizing Eyring theory (Figure 1.12), allowing for the calculation of $\Delta H^\ddagger = 13.7 \pm 0.9$ kcal/mol, $\Delta S^\ddagger = -0.02 \pm 1.2 \cdot 10^{-4}$ cal/mol and $\Delta G_{298K}^\ddagger = 18.8 \pm 1.9$ kcal/mol. The energies input of this reaction is certainly lower than the calculated energies for the reduction of phosphine oxides via a [2+2] mechanism.

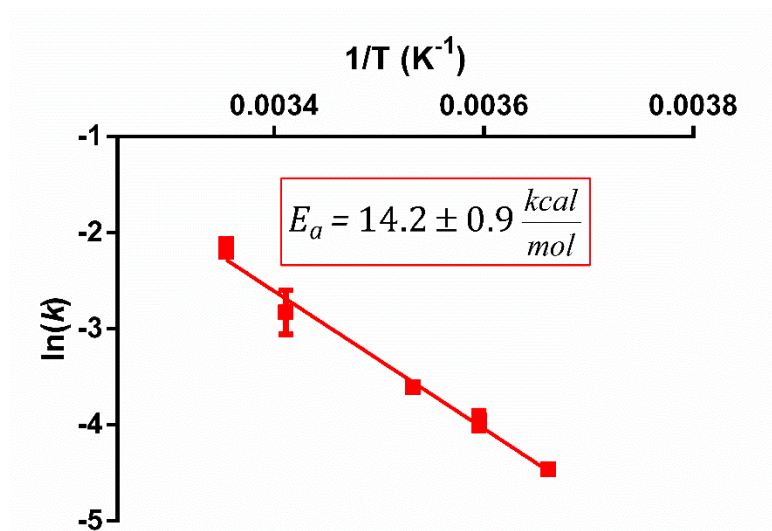


Figure 1.37. The Arrhenius plot for the reduction of **TMBPO** by **DPDS** over the temperature range 0 – 25 °C. Data collected by Dr. Carter Eiden.

1.8.11.11. Reduction of Acyclic Phosphine Oxides by **DPDS**

1.8.11.11.1. General Procedure: To an NMR tube was added *d*₈-toluene (440 μL), **DPDS** (58 mg, 0.25 mmol, 0.5 M), and phosphine oxide (0.02 mmol, 0.04 M). The tube was inverted three times to ensure proper mixing of the reagents and the interface between the tube and the cap was sealed with multiple layers of paraffin wax (parafilm®) to ensure no leaks. The reaction was heated to 110 °C and monitored with ³¹P NMR.

1.8.11.11.2. Data Fitting for Acyclic Phosphine Reductions: Under pseudo-first order conditions, rate constants for Hammett study and KIE reductions were determined by averaging the percent phosphine oxide remaining over a triplicate set of data per each time point. The logarithm of the percent product remaining was taken and a plot of ln[PO] vs. time was constructed. The slope of this line was used as a preliminary guess for *k* and an exponential decay function was fitted to the raw reaction progress data. Variance between the data and the exponential fit function $y=100*e^{(-kx)}$ was evaluated.

1.8.11.11.3. Results: As shown in Figure 1.38, **DPDS** rapidly reduces **TPPO** at 110 °C, with 100% conversion at 5 h. The kinetics of reduction fit excellently to a single exponential, as would be expected with **DPDS** as the reductant (Figure 1.11). This rate of reduction compares favorably to the rates of reduction of **TPPO** observed by Lemaire and coworkers (**TMDSO**, Ti(OiPr)₄, 100 °C, 5 h) and Beller and coworkers (HSiMe(OEt)₂, (*p*-NO₂C₆H₄O)₂PO₂H, 110 °C, >12 h).^{25, 29} Due to the lack of a titanium-based or acidic²⁹ additive, the use of **DPDS** is substantially milder than both described conditions. Additionally, **DPDS** is used at about half of the concentration of **TMDSO** used by Lemaire

and coworkers, and at the same concentration as that of $\text{HSiMe}(\text{OEt})_2$ used by Beller and coworkers. The use of **DPDS** is thus the most broadly effective set of selective reduction conditions for triphenylphosphine oxide to date.

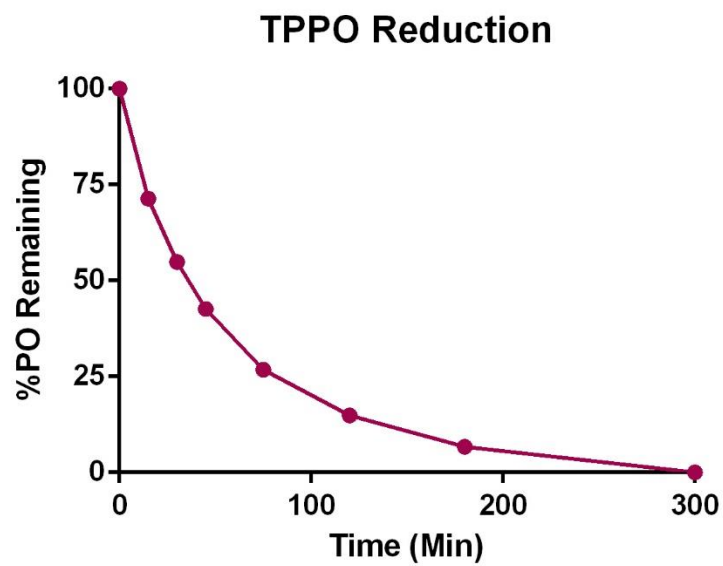
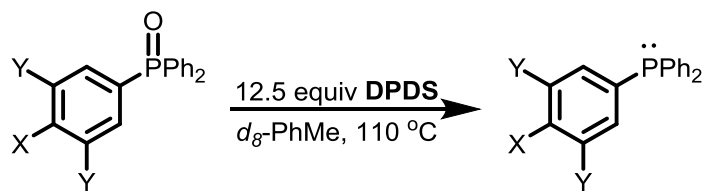


Figure 1.38. The reduction of **TPPO** with **DPDS** at 110 °C.

We then applied this reduction to a series of acyclic phosphine oxides with electronic perturbations, which vary the electronic character of the oxygen atom. As summarized in Table 1.40, the computed Mulliken charges of our series lines up well with their rate of reduction by **DPDS**. As summarized in Figure 1.22, Figure 1.39, and Table 1.41, the rate of reduction was dependent on the nature of the oxyanionic character, as the rate of reduction increased at a rate which afforded a linear Hammett plot. The negative slope of this plot indicates the buildup of a positive charge within the rate-determining step, a crucial component of understanding the reaction's mechanism.



Scheme 1.14. The reduction of acyclic phosphine oxides with **DPDS**.

Table 1.40. Computed Mulliken charges of acyclic phosphine oxides.

Substrate	Mulliken charge on P	Mulliken charge on O
TPPO	0.165482	-0.577962
X = N(Me) ₂ (S9)	0.195433	-0.647214
X = OMe (S10)	0.044019	-0.624292
X = CF ₃ (S11)	0.468533	-0.588180
Y = CF ₃ (S12)	0.364637	-0.565905
X = CHO (S13)	0.427478	-0.592717
X = C(O)Me (S14)	0.437315	-0.582638
X = CH ₃ (S15)	0.320644	-0.558752

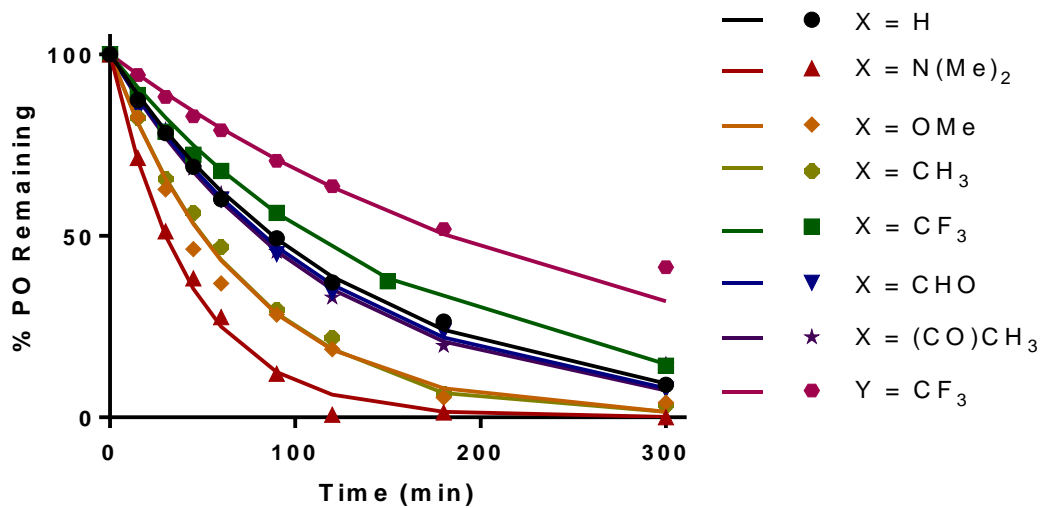


Figure 1.39. The reaction progress curves of reductions used to generate the Hammett plot in Figure 1.22. Data collected by Kathleen Wang.

Table 1.41. Rate constants for the reduction of acyclic phosphine oxides.

Substrate	Substituent Constant σ^{107}	Rate Constant (min^{-1})
TPPO	0	0.0111
S9	-0.83	0.0231
S10	-0.268	0.0140
S11	0.54	0.0064
S12	1.08	0.0038
S13	0.42	0.0139
S14	0.5	0.0084
S15	-0.179	0.0087

1.8.11.11.4. Determination of the Kinetic Isotope Effect with *d*₄-**DPDS**

1.8.11.11.4.1. General Procedure: To a set of two Shigemi tubes were added **TPPO** (1.12 mg, 0.004 mmol) and **DPDS** (11.6 mg, 0.05 mmol, 12.5 eq) or *d*₄-**DPDS** (11.8 mg, 0.05, mmol, 12.5 eq) in *d*₈-toluene (88 μL) per tube. The reactions were heated to 110 °C without stirring, and ³¹P NMR spectra were collected every 10 minutes for the first two hours, then every hour until the reaction had run for 5 hours.

1.8.11.11.4.2. Results: With the results of our Hammett study, we understood that our rate-determining step included the buildup of positive charge which we hypothesized could be indicative of the formation of the internal salt via resonance with the phosphine oxide or could be the positive charge on the phosphorous during the hydrogen atom transfer (HAT). To determine if the HAT step was rate-determining, we utilized a deuterated silane reagent such that any significant difference in reduction rate would implicate the HAT as the rate-determining step. Performance of these reductions with hydrido- and deuterio-**DPDS** indicated a primary kinetic isotope effect of 5.3 at 110 °C, as the rate of reduction was dropped by over 5-fold at this elevated temperature as illustrated in Figure 1.23 ($k_H = 0.0197$; $k_D = 0.0037$).

1.8.11.11.5. Eyring Analysis of the Reduction of **TPPO** by **DPDS**: Having access to the raw data for the reduction of **TPPO** over a range of temperatures, we performed Eyring analysis (Figure 1.13) on this reduction as well. Running that data through an alternate set of calculations allows for the calculation of $\Delta H^\ddagger = 17.3 \pm 1.2$ kcal/mol, $\Delta S^\ddagger = -0.01 \pm$

$1.4 \cdot 10^{-4}$ cal/mol and $\Delta G_{298K}^{\ddagger} = 21.5 \pm 3.6$ kcal/mol. These values are still lower than those previously calculated.

1.8.11.12. Determination of Reaction Order for Reductions by **DPDS**

1.8.11.12.1. General Procedure:

To an NMR tube was added *d*₈-toluene (475 μL), **DPDS** (0.1 M – 0.75 M), and **TPPO** (5.6 mg, 0.02 mmol, 0.04 M). The tube was inverted three times to ensure proper mixing of the reagents and the interface between the tube and the cap was sealed with multiple layers of paraffin wax (parafilm®) to ensure no leaks. The reactions were heated to 110 °C and monitored by ³¹P NMR.

1.8.11.12.2. Results: As evident in Figure 1.11, the rate of reduction scales linearly with the concentration of **DPDS** employed. As such, it is easy to say that this reaction is in fact first order with respect to the silane reagent, and that our reagent does not undergo a more complex process than we have described.

1.8.11.13. Determination of the Effect Water has on Reductions by **DPDS**

1.8.11.13.1. General Procedure:

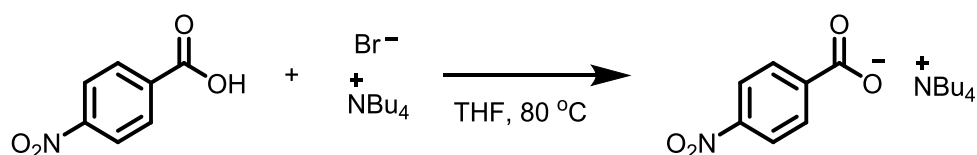
To an NMR tube was added *d*₈-toluene (475 μL), **DPDS** (35 mg, 7.5 equiv., 0.15 mmol, 0.3 M), **TMPPO** (4.2 mg, 0.02 mmol, 0.04 M), and water was added to each tube (0.00 – 13.75 equiv). The tube was inverted three times to ensure proper mixing of the reagents and the interface between the tube and the cap was sealed with multiple layers of paraffin wax (parafilm®) to ensure no leaks. The reactions were heated to 25 °C and monitored by ³¹P NMR.

1.8.11.13.2. Results: As summarized in Figure 1.21, the addition of water is detrimental to the overall rate of reduction. We believe this is due to the ability of water to form a stronger hydrogen bond to the phosphine oxide, thus out competing with the hydrogen-bond acceptor necessary for reduction via a 6-membered transition state.

1.8.12. In-Situ Activation of Silanes to Silanols:

1.8.12.1. Activation of Silanes with to Silanols with Carboxylate Additives

1.8.12.1.1. Synthesis of Tetra-*n*-butyl ammonium-*p*-nitrobenzoate:



To a round bottom flask equipped a stir bar was added *p*-nitrobenzoic acid (500 mg, 3.0 mmol), tetrabutylammonium bromide (1.0 g, 3.0 mmol), and THF (10 mL). The reaction was fitted with a reflux condenser and heated to 80 °C for 28 h. The reaction was cooled to 23 °C and concentrated *in vacuo*. The residue was taken up in cold toluene (15 mL), filtered, and concentrated *in vacuo* to afford the title compound (1.00 g, 82%) as a yellow solid: NMR spectra and other physical data matched that of previous reports.¹⁰⁸

1.8.12.1.2. General Procedure: To an NMR tube was added **TMPPO** (4.3 mg, 1.0 equiv., 0.02 mmol, 0.04 M), *d*₈-THF (475 μL), PhSiH₃ (25 μL, 10.0 equiv., 0.2 mmol, 0.4 M), and tetra-*n*-butyl ammonium-*p*-nitrobenzoate (25.3 mg, 3.0 equiv, 0.06 mmol, 0.12 M). The tube was inverted three times to ensure proper mixing of the reagents and the interface between the tube and the cap was sealed with multiple layers of paraffin wax (parafilm®) to ensure no leaks. The reaction was heated to 80 °C and monitored by ³¹P NMR.

1.8.12.1.3. Results: Within five minutes of heating to 80 °C, all of the phosphine oxide precatalyst **TMPPPO** had been reduced. Vigorous bubbling was observed, suggesting that hydrogen gas is rapidly evolved. This indicates that the oxyanion *p*-nitrobenzoate rapidly converts PhSiH₃ to silanol, promoting extremely rapid reduction of **TMPPPO**. This result explains the observations of O'Brien²⁴ as he discovered the addition of a catalytic amount of benzoic acid to his catalytic Wittig reaction containing DIPEA lowers the necessary temperature for reduction to 25 °C from 80 °C. In that reaction, DIPEA abstracts the proton with the lowest *pK_a* from the benzoic acid, forming DIPEA-HCl (which actually also increases the rate of reduction, but significantly less than carboxylate) and benzoate, which we demonstrated drastically increases the rate of reduction.

1.8.12.2. Activation of Disiloxanes with Protic Acids

1.8.12.2.1 General Procedure: To an NMR tube was added **1PPO** (3.7 mg, 1.0 equiv., 0.02 mmol, 0.04 M), *d*₈-THF (440 μL), **TMDSO** (53.0 μL, 15.0 equiv., 0.3 mmol, 0.6 M), and acid (5.0 equiv., 0.1 mmol, 0.2 M). The tube was inverted three times to ensure proper mixing of the reagents and the interface between the tube and the cap was sealed with multiple layers of paraffin wax (parafilm®) to ensure no leaks. The reaction was heated to 80 °C and monitored by ³¹P NMR.

1.8.12.2.2. Results: As stated previously, **TMDSO** was completely ineffective at reducing phosphine oxide precatalysts at 80 °C without additives. However, upon the addition of a Brønsted acid, **TMDSO** successfully reduced **1PPO** within the two hour period this

reduction was monitored (Figure 1.26). With equimolar amounts of AcOH and TFA added, TFA induced significantly more reduction. As siloxanes have been shown to equilibrate significantly more towards silanols in acidic or basic aqueous solutions as opposed to pH neutral solutions,^{109,110} we believe that reduction is occurring because **TMDSO** is equilibrating between **TMDSO** and dimethylsilanol. The presence of TFA likely shifts the equilibration towards silanol more so than AcOH, which results in faster **1PPO** reduction. Alternatively, the stronger acid may be getting deprotonated by the phosphine oxide, facilitating a hydrogen bond to the oxygen in the disiloxane reducing agent. In general, the lower the pK_a of the acid, the more reduced product was observed.

1.8.12.3. Activation of Disiloxanes with Lewis Acids

1.8.12.3.1. General Procedure: To an NMR tube was added **1PPO** (3.6 mg, 0.02 mmol, 0.04 M), d_8 -THF (447 μ L), **TMDSO** (53 μ L, 0.3 mmol, 0.6 M), and LiCl, MgCl₂, ZnCl₂, or Na₂SO₄ (0.1 mmol, 0.2 M). The tube was inverted three times to ensure proper mixing of the reagents and the interface between the tube and the cap was sealed with multiple layers of paraffin wax (parafilm®) to ensure no leaks. The reaction was heated to 80 °C and monitored by ³¹P NMR for 7 h.

1.8.12.3.2. Results: As shown in Figure 1.26, MgCl₂, ZnCl₂, and Na₂SO₄ all induced some reduction at 7 hours, with ZnCl₂ superior at promoting the reduction of **1PPO**. The use of a divalent cation seems to facilitate the formation of the six-membered transition state similarly to the hydrogen-bonding capabilities of a silanol. However, the monovalent cations of sodium sulfate seemed capable of promoting reduction to some extent. This may

be due to an adjustment to the balance of the water in the reaction, as too much water would slow reduction and may coordinate too heavily to the monovalent (and smaller) cations which blocks formation of the six-membered transition state. The effect that sodium sulfate has on reduction may also synergize with titanium additives, thus leading to lower temperatures necessary for reduction, as observed by Lemaire and co-workers.²⁹ While divalent cations may be acting as proton surrogate, it is also possible that the addition of zinc may be altering the equilibrium of TMDSO more towards the active silanol reductant. Because Zn^{2+} is neither a “hard” nor “soft” Lewis acid,¹¹¹ it is difficult to determine if the zinc is forming a relatively covalent bond with TMDSO/phosphine oxide, or if the additive is acting as a coordinating species. Seeing how the “hard” Lewis acids facilitate less reduction, it is likely that simple coordination is not all that is at play.

1.8.12.4 Circumventing Disiloxane-Silanol Equilibria with Disilazanes

1.8.12.4.1. General Procedure: To an NMR tube was added **1PPO** (3.7 mg, 1.0 equiv., 0.02 mmol, 0.04 M), d_2 -DCM (458 μ L), and **TMDSA** (42.0 μ L, 15.0 equiv., 0.3 mmol, 0.6 M). The tube was inverted three times to ensure proper mixing of the reagents and the interface between the tube and the cap was sealed with multiple layers of paraffin wax (parafilm®) to ensure no leaks. The reaction was heated to 80 °C and monitored with ³¹P NMR.

1.8.12.4.2. Results: While silanols act as sufficient hydrogen-bond donors to stabilize the six-membered transition state, the very fact that these molecules exist in an equilibrium with a non-reactive entity inherently leads to sub-optimal reductive potential. One way to circumvent this shortcoming would be through the use of a reagent that lacks this

deactivation pathway, but still maintains the hydrogen-bond donor which is critical for the formation of the six-membered transition state. 1,1,3,3-tetramethyl disilazane (**TMDSA**) represents a commercially-available solution, and when tested in isolated reduction studies, the reagent was a competent reductant without an additive, unlike its disiloxane counterpart. As shown in Figure 1.19 **TMDSA** is effective at 80 °C, with approximately 60% of reaction completion within 30 minutes, whereas **TMDSO** is inert for at least 14 hours (not shown). The presence of a permanent hydrogen-bond donor indicates that the reagent does not need any time to equilibrate to be active. Unfortunately, **TMDSA** represents the only commercially-available hydrido-disilazane, and lacks the stability needed to be used in full reaction schemes. The design of a stabilized disilazane reagent may afford an even further improved reductant for phosphorus recycling, beyond even **DPDS**.

1.8.12.5. Blocking Activation of Phenylsilane to Phenylsilanol with Lewis Acids

1.8.12.5.1. General Procedure: To three separate NMR tubes was added **1PPO** (0.02 mmol, 0.04 M), *d*₈-THF (475 μL), and then PhSiH₃ (25 μL, 0.2 mmol, 0.4 M). To one of the tubes was added LiCl (4 mg, 0.1 mmol, 0.2 M) and to another was added ZnCl₂ (6.8 mg, 0.05 mmol, 0.1 M). All three tubes were inverted three times to ensure proper mixing of the reagents and the interface between the tubes and their respective caps were sealed with multiple layers of paraffin wax (parafilm®) to ensure no leaks. The reactions were heated to 80 °C and monitored by ³¹P NMR.

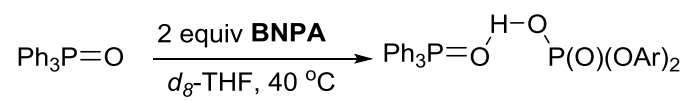
1.8.12.5.2. Results: As demonstrated in Figure 1.16, the addition of ZnCl₂ completely abolished reduction of **1PPO** and the addition of LiCl significantly slowed it. Taking into context the results in Figure 12, where addition of ZnCl₂ enhanced reduction substantially, it is likely that the observed reduction stoppage with ZnCl₂ and PhSiH₃ is due to blocking the activation of PhSiH₃ to phenylsilanol. We proposed that phosphine oxide catalyzed the formation of phenylsilanol from phenylsilane through donation of electron density from the phosphine oxide into the silicon atom, causing an increased chance of a reaction with water. LiCl and ZnCl₂ likely form Lewis acid-base pairs with the phosphine oxide, dramatically decreasing the potential for electron density donation into phenylsilane. The difference in potency between LiCl and ZnCl₂ is likely due to the greater Lewis acidity of ZnCl₂.

1.8.12.6. Investigation of Coordination to **TPPO**

1.8.12.6.1. General Procedure: To a 1-dram vial was added TPPO (70 mg, 0.25 mmol, 1 equiv), TPP (6.5 mg, 0.025 mmol, 0.1 equiv) as an internal standard, other solid reagents (0.05 – 2.5 mmol, 0.1 – 10 equiv), solvent (*d*₈-THF or *d*₈-PhMe, 500 mL), and then liquid reagents (0.05 – 2.5 mmol, 0.1 – 10 equiv). The vessel was mixed vigorously with a vortex mixer set to its highest setting. The reaction was heated to the desired temperature (between 23 – 80 °C) and monitored by ³¹P NMR with 16 one-second delay scans. The WALTZ 16 decoupling parameter was still used to ease deconvolution. The reactions were checked after 1 to 45 minutes, and 5 minutes was deemed an appropriate amount of time for universal reaction monitoring.

1.8.12.6.2. Interactions with Additives: We note that NMR shift of phosphine oxide coordination is not affected by different temperatures (Table 1.12), but is affected by the saturation of the interactions. As such, adding additional substrate pronounces the downfield shift of the observed phosphorus signal rather than producing two distinct NMR resonances corresponding to coordinated and uncoordinated oxygen atoms (Table 1.42). Understanding the nature of this assay, we decided to pursue characterizing interactions between phosphine oxides and acids in 1:1 and 1:2 stoichiometric ratios. As summarized in Table 1.14, various carboxylic acids can interact with phosphine oxides, characterized by a downfield shift in the ^{31}P NMR spectrum. These downfield shift these acids promote lines up very well with their ability to promote reduction as well as their pK_a . Additionally, other acids such as methanesulfonic acid and **BNPA** also cause a downfield shift. To our delight, the downfield shift resultant of additive addition aligns well with the rate of reduction for phosphine oxides with disiloxanes in the presence of these functional groups (Figure 1.26). Generally speaking, it would seem that lower pK_a predicates potential effectiveness of the additive in these reductions. Yet, **BNPA** bucks this trend, producing the greatest reactivity and greatest downfield shift. The strong correlation of reactivity to downfield shift indicates that this assay may be very effective for the discovery of acidic additives for disiloxane-mediated phosphine oxides.

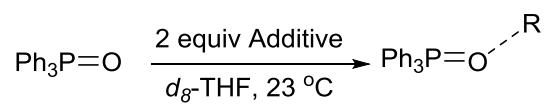
Table 1.42. Stoichiometry of additives affects downfield shift
in ^{31}P NMR spectra.



Entry	X Equiv	δ Shift (ppm)	Δ (ppm)
1	0	23.70	0.00
2	0.2	26.13	+2.43
3	0.4	27.77	+4.07
4	1.0	32.55	+8.85

Additionally, we investigated the downfield shift of phosphine oxides with neutral hydrogen-bond donors. Both alcohols and silanols can effectively cause a downfield NMR shift, but to a much lesser extent than carboxylic acids (Table 1.14). However, much like the results reported by Blumel and coworkers, the addition of water seems to strengthen this interaction as the addition of 2 equivalents of water always generated a larger downfield shift indicative of a better hydrogen-bonding interaction. The addition of water did not cause downfield shifts of the same magnitude, and molecules such as phenylsilane (which lacks H-bond donors) do not perturb the system in any notable fashion (Table 1.43).

Table 1.43. Interactions of TPPO with miscellaneous organic molecules.

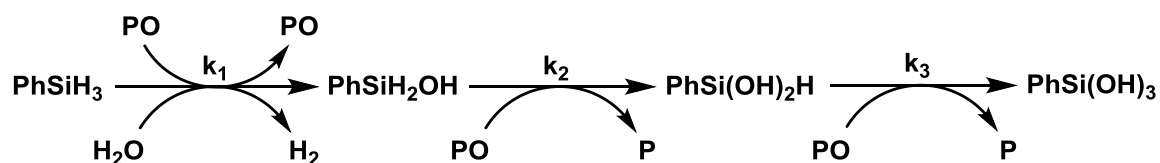


Entry	Additive	δ Shift (ppm)	Δ (ppm)
1	None	23.70	0.00
2	TMDSO	23.76	+0.06
3	PhSiH ₃	23.68	-0.02
4	DPDS	24.05	+0.35
5	Benzyl Alcohol	27.17	+3.47

Addition of Lewis acidic metals also correlates with the reactivity of disiloxanes towards phosphine oxides. Addition of the weak Lewis acid LiCl caused a modest 3.79 ppm downfield shift and only mildly promoted reactivity of **TMDSO** (Figure 1.26), while borderline Lewis acid ZnCl₂ caused a very significant downfield shift of 17.35 ppm while simultaneously being better suited to facilitate reduction with **TMDSO** (Figure 1.26).

1.8.13. Mathematical Modeling of Reaction Progress Curves

1.8.13.1. Procedure: An Excel spreadsheet was used to model the reaction progress curves from Figure 1 for **TMPyrPO**, **TMBPO**, **TMPPPO**, and **1PPO** to Mechanism V (shown below, with PO being the phosphine oxide and P the reduced phosphine).



To begin, the initial values for the concentrations of each of the components were set to 0.4 for [PhSiH₃], 0.04 for [PO], and 0 for all of the others. The only exception is the concentration of water, which we assume for the sake of this exercise does not change, and is thus not included in the equations. We then calculated the derivatives of the concentrations of each of the components with respect to time, according to the equations below (the initial rate constants were estimated).

$$\frac{d[\text{PhSiH}_3]}{dt} = -k_1[\text{PO}][\text{PhSiH}_3]$$

$$\frac{d[\text{PhSiH}_2\text{OH}]}{dt} = k_1[\text{PO}][\text{PhSiH}_3] - k_2[\text{PO}][\text{PhSiH}_2\text{OH}]$$

$$\frac{d[PhSi(OH)_2H]}{dt} = k_2[PO][PhSiH_2OH] - k_3[PO][PhSi(OH)_2H]$$

$$\frac{d[PhSi(OH)_3]}{dt} = k_3[PO][PhSi(OH)_2H]$$

$$\frac{d[PO]}{dt} = -k_2[PO][PhSiH_2OH] - k_3[PO][PhSi(OH)_2H]$$

$$\frac{d[P]}{dt} = k_2[PO][PhSiH_2OH] + k_3[PO][PhSi(OH)_2H]$$

The calculated derivatives at 0 seconds were used to determine the concentration of each species that would be present at 0.1 seconds. The derivatives of the concentrations of each species was then calculated for $t = 0.1$ seconds, which was used to determine the concentration of each species at 0.2 seconds. This process was continued, each time with 0.1 second iterations of time. The calculated concentration curves of phosphine oxide were overlaid with the curves from Figure 1.5B, and the iterative process was continued for as long as the concentration of phosphine oxide in each of the Figure 1.5B curves stayed above 5% of the initial concentration.

We then utilized Excel Solver to solve for the rate constants. This was done by minimization of the sum of the variance between the experimental concentration of phosphine oxide at each data point (Figure 1.5B) and the simulated concentration of phosphine oxide at the closest time point calculated. The rate constants were allowed to float, with the exception of choosing k_3 to be a fixed multiple of k_2 . This produced two solutions of k_1 and k_2/k_3 for each phosphine oxide reduction curve, but one was ruled out

through knowledge of the concentration of PhSiH₃ throughout the reductions. The process was repeated for each phosphine oxide reduction curve for $k_3 = k_2$, $k_3 = 10k_2$, and $k_3 = \infty$.

1.8.13.2. Results: As we had previously been able to eliminate various mechanisms with kinetics, we chose to confirm that the final proposed mechanism did in fact result in adept fitting of our experimental reduction curves (Figure 1.40). While this could have been accomplished through a fitting program, the degree of control that is available through setting up the equations by oneself made the use of Excel and Excel Solver quite attractive. Unsurprisingly, when fitting the simulation to the data from Figure 1.5B while letting all three of k_1 , k_2 , and k_3 float, we obtained an infinite number of solutions, as the data is not precise enough to differentiate between k_2 and k_3 . We were able to avoid this problem by setting k_3 to be a fixed multiple of k_2 . We wanted to limit the number of analyses as the relationship between k_2 and k_3 had to be manually defined, and thus decided to run the simulation with $k_3 = k_2$, $k_3 = 10k_2$, and $k_3 = \infty$. These were chosen because a wide range of ratios was desired and it seemed unlikely that k_3 would be slower than k_2 due to the decreased electron density on silicon of phenylsilanediol as opposed to phenylsilanol. For each of these simulations, two solutions were obtained, one with k_1 fast and k_2 slow, and one with k_2 fast and k_1 slow. We were able to eliminate all solutions that had k_1 fast and k_2 slow as we have observed many times that following complete reduction of phosphine oxide, most of the phenylsilane remains. If k_1 is fast and k_2 slow, the reduction finishes with almost complete conversion of phenylsilane to phenylsilanol, so this possibility was ruled out. We thus successfully obtained a single pair of rate constants for each ratio of k_2

and k_3 /phosphine oxide combination, which are shown in Table 1.44. A graphical comparison each of the simulations with the data modeled is shown in Figure 1.39.

Table 1.44. Rate constants obtained through simulation.

	$k_3 = k_2$		$k_3 = 10k_2$		$k_3 = \infty$	
	k_1	k_2	k_1	k_2	k_1	k_2
IPPO	0.049	1.83	0.051	1.14	0.058	0.87
TMPPPO	0.038	3.01	0.039	1.90	0.040	1.67
TMBPO	0.077	8.23	0.078	5.46	0.079	5.02
TMPyrPO	0.133	25.0	0.134	16.7	0.135	15.4

All rate constants are in units of ($M^{-1}s^{-1}$)

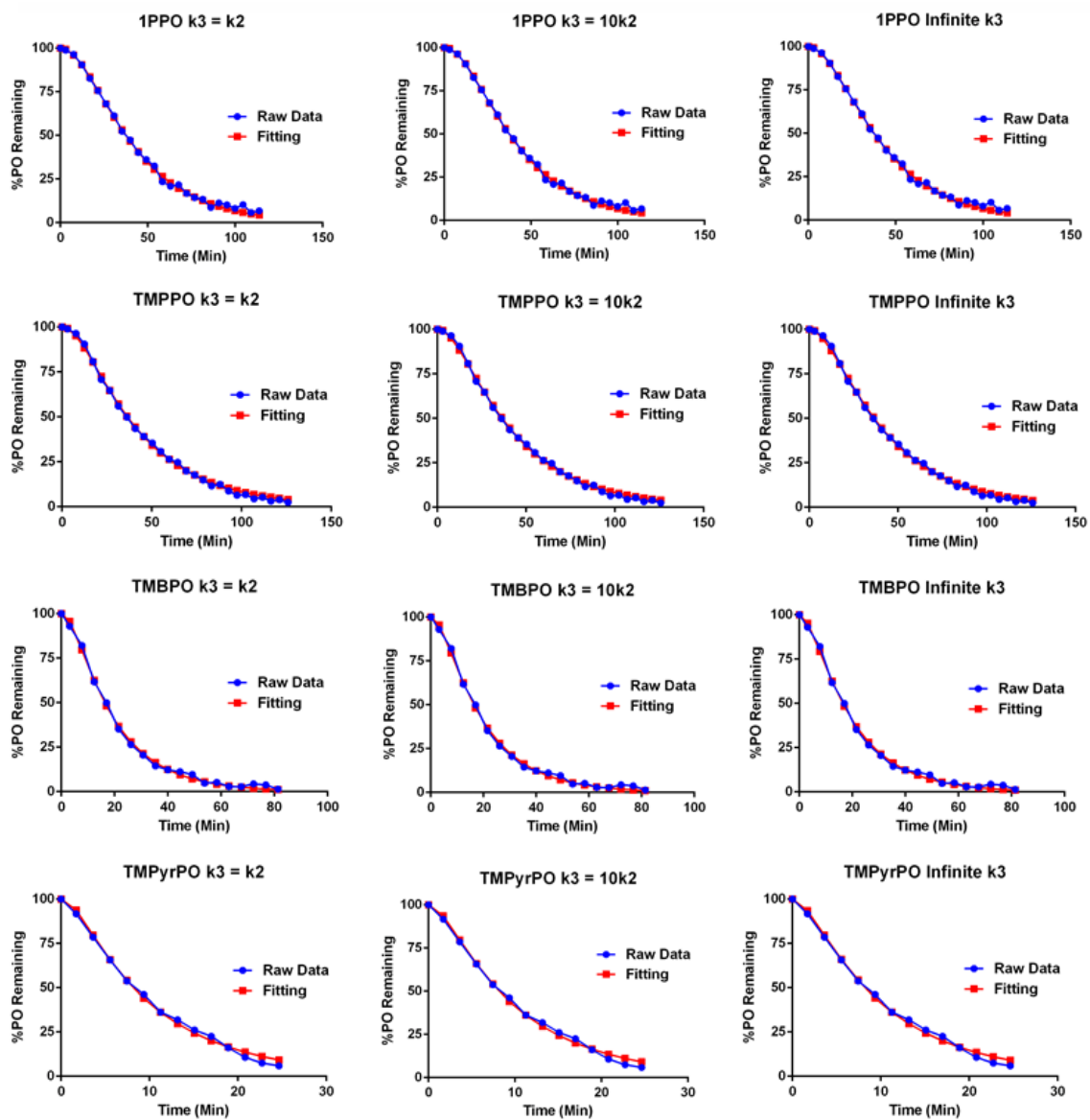


Figure 1.40. Graphical comparison of reaction progress curves (Figure 1.5) and the fit obtained by the indicated parameters. Data fitting by Dr. Carter Eiden.

Figure 1.40 demonstrates that fitting the mechanism was quite successful, the simulation curves mirror the actual data quite nicely, demonstrating that the proposed mechanism for phenylsilane reduction could produce the data in Figure 1.7. This is not a proof, as other mechanisms could certainly also fit the data, but Mechanisms I-III were successfully able to be ruled out with numerical analysis, and Mechanism V successfully matches the data.

We were also interested in using this data to monitor the rates of each of the steps separately. This would allow for a comparison of which phosphine oxides activate phenylsilane to phenylsilanol the fastest as well as which are reduced the fastest by phenylsilanol/phenylsilanediol. Clearly, with our method of analysis, we cannot differentiate between k_3 and k_2 , nor use the absolute values of the rate constants, as they change based on the relationship chosen between k_3 and k_2 . However, the data can still be used quite effectively, as the relative rates of the different phosphine oxides can be compared since the trends stay the same regardless of the relationship between k_3 and k_2 . Two key points are illustrated by Table 1.44.

1. **IPPO** activates phenylsilane to phenylsilanol faster than **TMPPPO** but is reduced by the produced silanols slower than the phosphetane.
2. The phosphetanes follow a clear trend demonstrating adding electron density to the phosphine oxide causes both faster activation of phenylsilanol and faster reduction by silanols

The first point confirms the expected differences in reactivity between **IPPO** and **TMPPPO** based on the reduction curves in Figure 1.5 and Figure 1.10. The two phosphine oxides are reduced at similar rates in Figure 1.5, while in Figure 1.10, **TMPPPO** is reduced

nearly twice as fast as **1PPO**. The difference in Figure 1.10 suggests silanols reduce **TMPPPO** faster than **1PPO** (based on the Arrhenius equation, which is an oversimplification), indicating that the similar rates observed in Figure 1.5 would be a result of faster phenylsilane activation by **1PPO**. This is interesting because **1PPO** and **TMPPPO** likely have fairly similar amounts of electron density on the phosphine oxide, meaning the differences in ring strain/steric hindrance are causing the differing rates of the steps. With further exploration, this knowledge could be used in future design of phosphine oxide precatalysts.

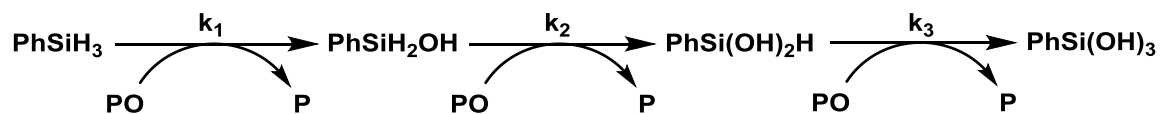
The second point, that adding electron density to the phosphine oxide causes both faster activation and reduction, provides further support for our theory that oxygen-based Lewis basicity is necessary for phenylsilanol formation. Also, the greater the degree of oxyanionic character, the more facile the activation of phenylsilane. It is important to note, for future phosphine design, that greater electron density on the phosphine oxide also causes faster reduction with silanols.

As a final point, Figure 1.10 shows **TMBPO** and **TMPyrPO** are reduced at similar rates, and Table 1.44 suggests they are not. It is important to remember that when we are monitoring **TMPyrPO** reduction, we are actually observing the presence of the secondary phosphetane, which requires two reductions. This is likely why a “lag phase” exists in Figure 1.10 for **TMPyrPO**. Analyzing the rates of reduction in Figure 1.10 when 50% of the phosphine oxide is already reduced reveals **TMPyrPO** is being reduced at a faster rate

at that point, suggesting **TMPyrPO** should have a larger rate constant of reduction than **TMBPO**.

1.8.13.3. Mathematical Argument against Mechanism III (Figure 1.8):

This is a mathematical proof that if one translates kinetic mechanism Mechanism III in Figure 1.8 to the data in Figure 1.5, Mechanism III cannot accurately describe the data regardless of the kinetic constants chosen. Mechanism III is shown below.



In the above mechanism, PO refers to unreduced phosphine oxide, and P the reduced phosphine. From the above mechanism we can write the rate of reduction as the change in [PO] with respect to time:

$$\frac{d[P]}{dt} = k_1[\text{PhSiH}_3][\text{PO}] + k_2[\text{PhSiH}_2\text{OH}][\text{PO}] + k_3[\text{PhSi(OH)}_2\text{H}][\text{PO}]$$

Due to the fact that we are operating in pseudo-first order conditions with an excess of phenylsilane:

$$[\text{PhSiH}_3] = [\text{PhSiH}_3]_i$$

Now, at time $t = 0$, it is also known that:

$$[\text{PhSiH}_2\text{OH}]_i = [\text{PhSi(OH)}_2\text{H}]_i = 0$$

The initial rate of phosphine formation is thus:

$$\text{Rate}_i = k_1[\text{PhSiH}_3]_i[\text{PO}]_i$$

To prove that the maximum rate at 50% PO reduced is 3/2 the initial rate of reduction, we first write the rate of reduction where half the PO has already been reduced.

$$\frac{d[P]}{dt} = \frac{k_1[PhSiH_3]_i[PO]_i}{2} + \frac{k_2[PhSiH_2OH][PO]_i}{2} + \frac{k_3[PhSi(OH)_2H][PO]_i}{2}$$

Evaluating the above equation term by term, it is clear that the first term is equal to half of the initial rate. To evaluate the second term, we note that this term would be at a maximum when the concentration of phenylsilanol is at a maximum. From the proposed mechanism, the concentration of phenylsilanol will reach a maximum at the time its rate of formation equals its rate of consumption, or where the derivative of the concentration of phenylsilanol is zero. We then write the derivative of the concentration of phenylsilanol with respect to time at 50% PO reduced.

$$\frac{d[PhSiH_2OH]}{dt} = \frac{k_1[PhSiH_3]_i[PO]_i}{2} - \frac{k_2[PhSiH_2OH][PO]_i}{2}$$

Setting that derivative to 0, we obtain:

$$\frac{k_1[PhSiH_3]_i[PO]_i}{2} = \frac{k_2[PhSiH_2OH][PO]_i}{2}$$

This means the second term can, at a maximum, be equal to half the initial rate.

We can apply the same strategy to the third term. The concentration of phenylsilanediol will also be at a maximum when its rate of formation equals its rate of consumption. The derivative of phenylsilanediol at 50% PO reduced is:

$$\frac{d[PhSi(OH)_2H]}{dt} = \frac{k_2[PhSiH_2OH][PO]_i}{2} - \frac{k_3[PhSi(OH)_2H][PO]_i}{2}$$

Again setting the derivative to 0:

$$\frac{k_2[PhSiH_2OH][PO]_i}{2} = \frac{k_3[PhSi(OH)_2H][PO]_i}{2}$$

Now, we have already shown that the maximum the term on the left in the equation above could be is half of the initial rate. Since they are equal, this is also the maximum that the term on the right could be, and we have now shown that the maximum all three terms can be is just half the initial rate. Adding up all of them, we find that the maximum rate of phosphine oxide reduction following this mechanism at 50% PO reduced is just 3/2 the initial rate, providing strong evidence via Figure 5 and Table S2 that this mechanism is incorrect.

$$\begin{aligned}\frac{d[P]}{dt} &= \frac{k_1[PhSiH_3]_i[PO]_i}{2} + \frac{k_2[PhSiH_2OH][PO]_i}{2} + \frac{k_3[PhSi(OH)_2H][PO]_i}{2} \\ &= \frac{3}{2}Rate_i\end{aligned}$$

It is also worth mentioning again that the derivative curves were created as described in Figure 1.7, which deliberately overestimates the initial rate. This means that the values listed in Table 1.5 are most likely an underestimation of the actual rate increase at 50% reduction.

1.8.14. Testing for a Phosphorous-Centered Radical Intermediate:

1.8.14.1. Procedure for the Reduction of S4 with DPDS: To an NMR tube was added **S4** (3.6 mg, 0.02 mmol, 0.04 M), *d*₈-toluene (450 μL), and **DPDS** (53 mg, 7.5 equiv., 0.15 mmol, 0.3 M). The tube was inverted three times to ensure proper mixing of the reagents and the interface between the tube and the cap was sealed with multiple layers of paraffin wax (parafilm®) to ensure no leaks. The reaction was heated to 25 °C and monitored by ³¹P NMR and ¹H NMR. After 4 h, the crude reaction mixture was poured from the NMR

tube into a 1 dram vial. Aqueous hydrogen peroxide (30 %, 200 μL) was then added to the reaction mixture and the reaction was shaken on an orbital shaker for 10 minutes at 25 $^{\circ}\text{C}$ in which a color change to bright yellow was observed. The crude mixture was then diluted with DCM (3 mL) and samples were diluted another 1000-fold with acetonitrile. Samples were analyzed with an LC-MS using a C-18 column and an electrospray ionization source in positive mode. The ions corresponding to $m/z = 173$ and 175 were extracted from the total ion source to monitor the presence of the cyclopropyl and *n*-propyl compounds, respectively.

1.8.14.2. Procedure for the Reduction of **S4** with **TMDSO** without any Additives: To an NMR tube was added **S4** (3.6 mg, 0.02 mmol, 0.04 M), *d*₈-toluene (482 μL), and then **TMDSO** (17.7 μL , 5.0 equiv., 0.10 mmol, 0.2 M). The tube was inverted three times to ensure proper mixing of the reagents and the interface between the tube and the cap was sealed with multiple layers of paraffin wax (parafilm®) to ensure no leaks. The reaction was heated to 80 $^{\circ}\text{C}$ and monitored by ^{31}P NMR and ^1H NMR. After 4 h, the crude reaction mixture was poured from the NMR tube into a 1 dram vial. Aqueous hydrogen peroxide (30 %, 200 μL) was then added to the reaction mixture and the reaction was shaken on an orbital shaker for 10 minutes at 25 $^{\circ}\text{C}$ in which a color change to bright yellow was observed. The crude mixture was then diluted as in section 1.8.14 and monitored by LC-MS using a C-18 column and an electrospray ionization source in positive mode. The ions corresponding to $m/z = 173$ and 175 were extracted from the total ion source to monitor the presence of the cyclopropyl and *n*-propyl compounds, respectively.

1.8.14.3. Procedure for the Reduction of **S4** with **TMDSO** with the Addition of $\text{Ti}(i\text{OPr})_4$:

To an NMR tube was added **S4** (3.6 mg, 0.02 mmol, 0.04 M), d_8 -toluene (481.7 μL), **TMDSO** (17.7 μL , 5.0 equiv., 0.10 mmol, 0.2 M), and then $\text{Ti}(i\text{OPr})_4$ (0.6 μL , 0.1 equiv., 0.002 mmol, 0.004 M). The tube was inverted three times to ensure proper mixing of the reagents and the interface between the tube and the cap was sealed with multiple layers of paraffin wax (parafilm®) to ensure no leaks. The reaction was heated to 80 °C and monitored by ^{31}P NMR. After 4 h, the crude reaction mixture was poured from the NMR tube into a 1 dram vial. Aqueous hydrogen peroxide (30 %, 200 μL) was then added to the reaction mixture and the reaction was shaken on an orbital shaker for 10 minutes at 25 °C in which a color change to bright yellow was observed. The crude mixture was then diluted as in section 1.8.14 and monitored by LC-MS using a C-18 column and an electrospray ionization source in positive mode. The ions corresponding to $m/z = 173$ and 175 were extracted from the total ion source to monitor the presence of the cyclopropyl and *n*-propyl compounds, respectively.

1.8.14.4. LC-MS Methodology for product detection:

An Agilent 1100 series HPLC stack was utilized with an Agilent Zorbax 300 SB-C18 column (150 x 0.5 mm, 5 μm) as the stationary phase at 25 °C. The mobile phase consisted of 0.1% formic acid in water (A) and 0.1% formic acid in acetonitrile (B) with a flow rate of 15 $\mu\text{L}/\text{min}$. The mass spectrometry was performed by an Agilent MSD SL Iontrap in positive mode with the acquisition parameters shown in Figure 1.41. The exact ion current for $m/z = 173 \pm 1$ and

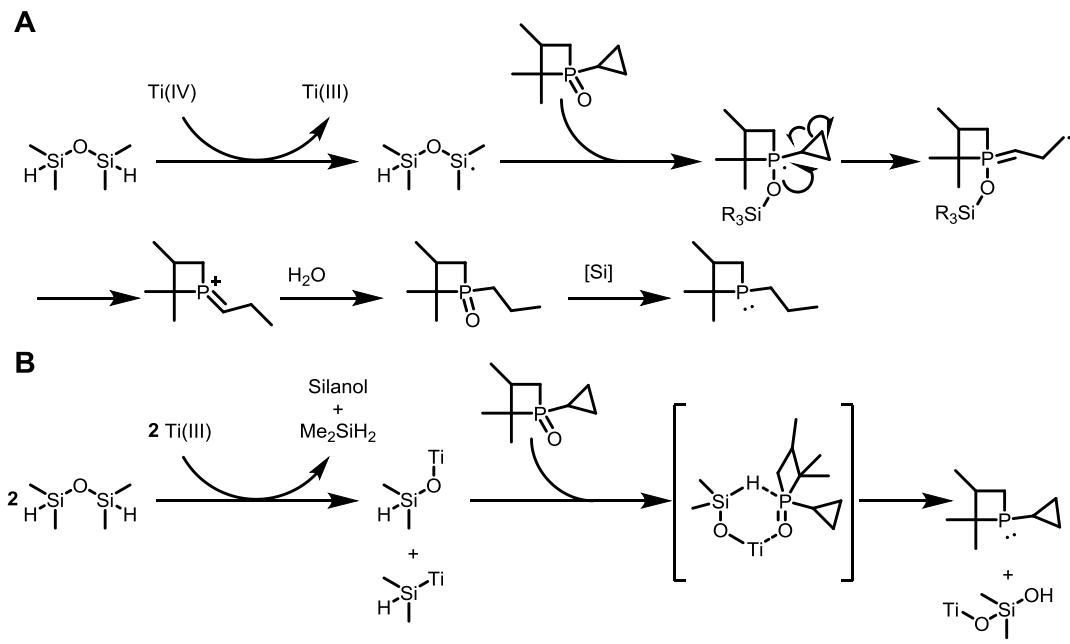
$m/z = 175 \pm 1$ were isolated from the total ion current corresponding to the mass to charge ratios of **S4** and 1-*n*-propyl-2,2,3-trimethylphosphetane-1-oxide, respectively.

1.8.14.5. Results: These experiments all utilized the “radical clock” of a cyclopropyl ring adjacent to the potential location of a radical center. Since cyclopropyl represents the fastest known radical clock, we imagined that if a radical was induced during the reduction of our phosphine **S4**, we would see the presence of a new peak by either NMR methods or mass spectrometry. The reaction, which would only occur in the presence of a radical (Scheme 1.15), would produce a new peak by NMR and the presence of the unique cyclopropyl peaks would disappear in favor of an *n*-propyl¹ side chain.¹¹² Mass-spectrometry analysis would also show a new peak at $[M+2]$,² corroborating the existence of the *n*-propyl compound. Unfortunately, the ¹H NMR spectra were inconclusive when titanium was added, and so this method was unable to discern if the cyclopropyl ring did indeed open. However, the MS analysis was successfully able to discern the presence of product. Shown in Figure 1.41, both reductions with **DPDS**, and **TMDSO** with $\text{Ti}(i\text{OPr})_4$ produce the phosphine with the cyclopropyl intact, in contrast to the result expected based

¹ While the phosphonium ylide would be present for a brief time, the presence of water in the solvent would lead to an oxidation event as previously observed.¹⁰⁶ An excess of silane would lead to another round of reduction, resulting in the production of 1-*n*-propyl-2,2,3-trimethylphosphetane.

² Above the 0.01% integration of $m/z = 175$ due to natural isotope abundance of C^{13} (1%) for 9 carbons.

on the mechanism proposed by Lemaire and co-workers.²⁹ A peak corresponding to $m/z = 175$ was observed, although the intensity was approximately 0.01% of the peak corresponding to $m/z = 173$, which is approximately equal to the natural frequency of two carbons with a mass of 13 AMUs in a 9-carbon compound (natural isotope abundance).

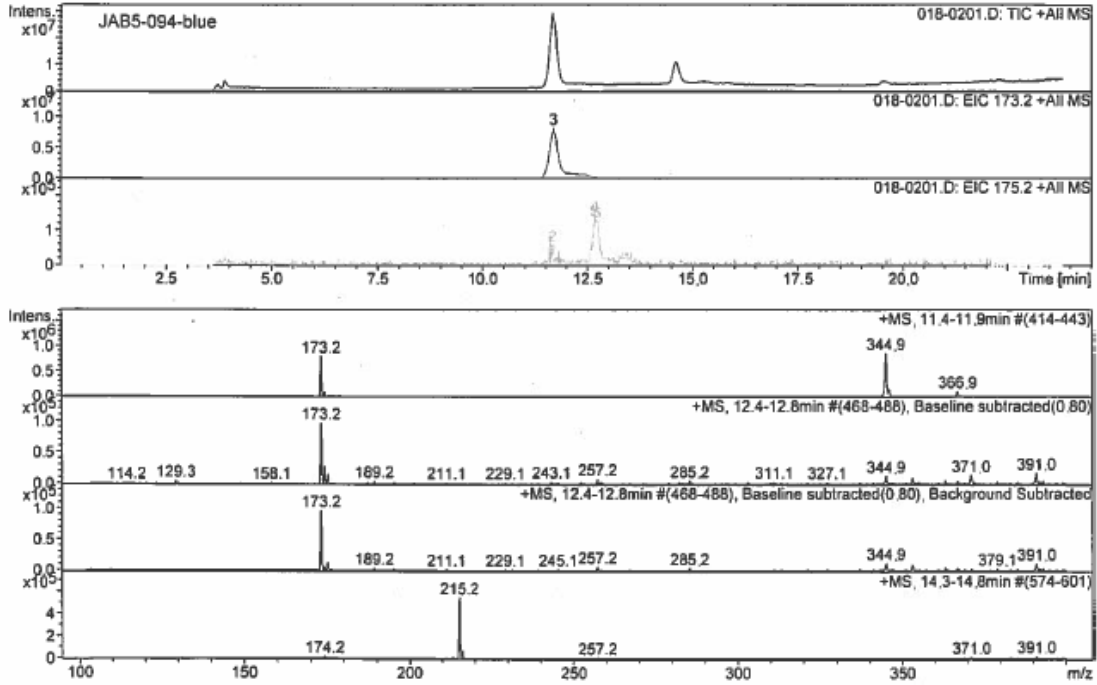


Scheme 1.15. (A) The reduction of **S4** with ring opening of the cyclopropyl side-chain with the phosphorus-centered radical as proposed by Lemaire and co-workers.²⁹ (B) The reduction of **S4** without a phosphorus-centered radical, consistent with our observations.

Analysis Name 018-0201.D
 Acquisition Date 03/11/2016 09:03:14 AM Operator Joseph Buonomo
 Method 160310A.M Instrument LC-MSD-Trap-SL
 Comment

Acquisition Parameters

Mass Range Mode	Std/Normal	Ion Polarity	Positive	Alternating Ion Polarity	off
Ion Source Type	ESI	Capillary Current Control	off	Auto MS/MS	off
Accumulation Time	300000 μ s	Trap Drive	40.0	Multiplier Voltage	2274 Volt
Averages	12 Spectra	Octopole RF Amplitude	152.8 Vpp		
Dry Heat	on	Capillary Exit	113.5 Volt		
Neb. Gas	on	Skimmer	40.0 Volt		
Dry Gas	on	Dry Temp (Set)	200 °C		
High Voltage	on	HV Capillary	3400 V		
		Scan Begin	103 m/z		
		Scan End	400 m/z		



Analysis Name 020-0201.D
 Acquisition Date 03/10/2016 04:15:22 PM Operator Joseph Buonomo
 Method 160310A.M Instrument LC-MSD-Trap-SL
 Comment

Acquisition Parameters

Mass Range Mode	Std/Normal	Ion Polarity	Positive	Alternating Ion Polarity	off
Ion Source Type	ESI	Capillary Current Control	off	Auto MS/MS	off
Accumulation Time	300000 μ s	Trap Drive	29.9	Multiplier Voltage	2274 Volt
Averages	8 Spectra	Octopole RF Amplitude	120.2 Vpp		
Dry Heat	on	Capillary Exit	102.8 Volt		
Neb. Gas	on	Skimmer	40.0 Volt		
Dry Gas	on	Dry Temp (Set)	200 °C		
High Voltage	on	HV Capillary	3400 V		
		Scan Begin	103 m/z		
		Scan End	400 m/z		

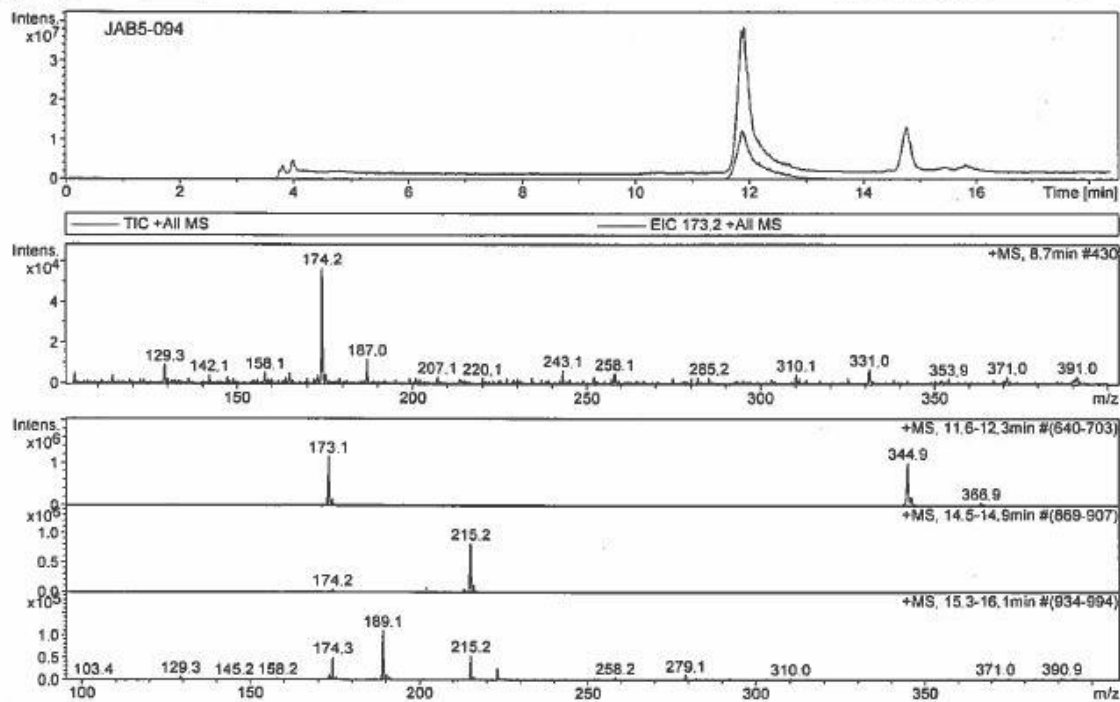
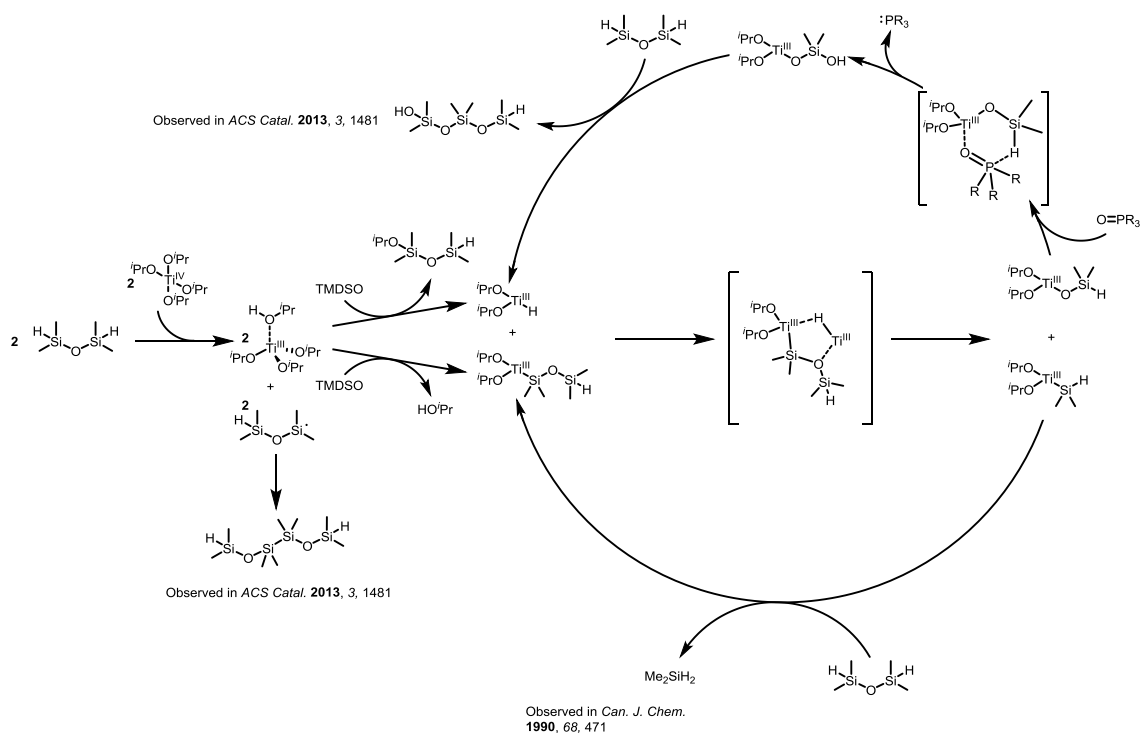


Figure 1.41. A) The LC-MS trace of the reduction of **S4** with **TMDSO** and 10 mol% **Ti(*i*PrO)₄**, and B) The LC-MS trace of the reduction of **S4** with **DPDS**.

These results indicated the need for a new mechanism to be proposed, one in which a phosphorus-centered radical is avoided and that accounts for the observations we and others^{107, 113} have made with titanium additives. We propose that the reductions proceed with the formation of our six-membered transition state and utilizes the titanium in place of the proton.

1.8.14.6 Discussion: The titanium-catalyzed reduction of phosphine oxides lacks a phosphorus-centered radical, prompting the need for a new mechanism to describe the reduction process. Previous studies utilized NMR, gas chromatography, mass spectrometry, X-ray crystallography, and EPR; while we utilized NMR and a novel radical clock reagent to track the nature of the single-electron transfer previously described. The updated mechanism, shown in Scheme 1.16, includes the findings of our studies in addition to the previously described byproducts and intermediates.



Scheme 1.16. The mechanism of titanium-catalyzed reductions of phosphine oxides with **TMDSO**. This scheme specifically states the reports where various intermediates have been observed.

The work of Samuel and co-workers⁶⁷ seems to accurately describe the disproportionation of **TMDSO** by bis-cyclopentadienyl titanium complexes. This study used a combination of X-ray crystallography, NMR, IR, and GC studies to identify intermediates and the nature of the metal complexes. These data indicate that siloxanes, specifically **TMDSO**, are capable of forming intermediates which include a Si-O-Ti motif, which we propose facilitates the reduction of phosphine oxides (Scheme 1.16). Samuel and co-workers also collected the gas released, identifying that the reaction of **TMDSO** with a titanium complexes produces dimethylsilane.

Lemaire and coworkers²⁹ also conducted several ²⁹Si NMR studies that revealed multiple species that cannot be accounted for by the mechanism proposed by Samuel. We presume these to be due to Lemaire using this system to reduce phosphine oxides. The Si-Si bond, observed by Lemaire, is easily explained as a small amount of **TMDSO** acts as a suicide reagent allowing for the activation of Ti(IV) to Ti(III), Samuel's dimethyltitanocene released methane during this reduction rather than the presumed alcohol which is derived from the alkoxymetal complex. Since the titanium is catalytic in respect to the amount of **TMDSO**, it only makes sense that only a small amount of the silyl silane would ever be observed in NMR. While the presence of a titanium hydride was not necessarily observed in Lemaire's EPR studies, it is notable that these studies were conducted at concentrations 32-fold less than the catalytically-relevant system. Stoichiometric studies by Samuel confirmed that multiple titanium(III) hydride species are possible, as these complexes could be isolated and studied by both NMR and X-ray

crystallography. However, the non-stoichiometric studies by Samuel would indicate that the titanium hydride may be short-lived or that it may mostly exist as a dinuclear titanium complex with the high valency (through ethoxide bridging ligands),⁶⁷ corroborated by the observations of Lemaire's EPR studies.²⁹

The new mechanism we propose takes into account the observations in titanium-catalyzed disproportionation, the ²⁹Si NMR studies, and the lack of a phosphorus radical as noted in our radical clock experiments. In addition, this mechanism also implies that two equivalents of silylhydride are required for reduction. Because **TMDSO** contains two silylhydride centers, only one equivalent should be enough to reduce one equivalent of phosphine oxide and the reaction should never be able to go to completion with less than one equivalent of **TMDSO** (Note: a slight excess promotes faster completion). The new mechanism also utilizes the titanium as if it was a "large proton" in the six-membered transition state which leads to phosphine oxide reduction and eventually linear silanol oligomers. These linear chains can cyclize to form 8 to 10-membered rings as observed by both Samuel and Lemaire.

1.8.15. Computational Modeling of Silane and Phosphine Oxide Materials:

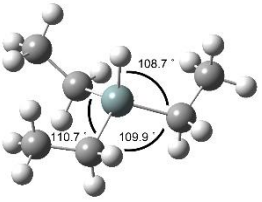
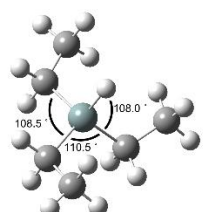
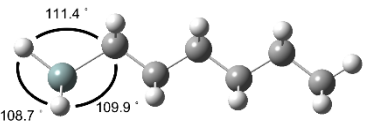
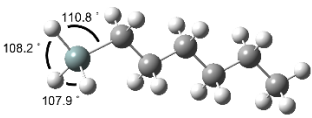
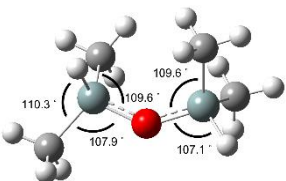
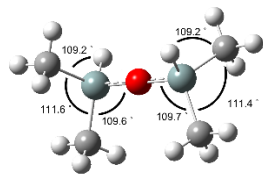
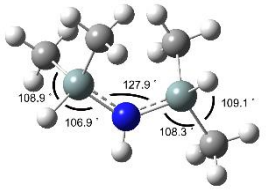
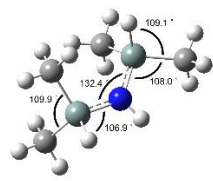
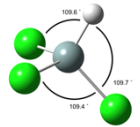
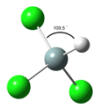
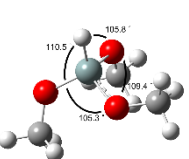
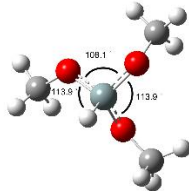
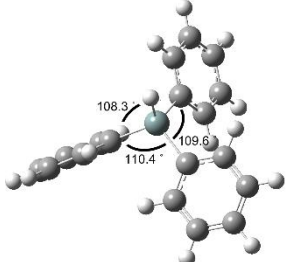
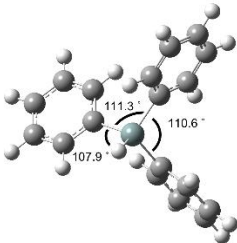
1.8.15.1. General Procedure: All density functional theory (DFT) calculations were performed using Gaussian09¹¹⁴ on a Linux supercomputer. Electronic parameters were calculated from structures optimized at the M06-2X/6-31+G(d,p)⁵⁷ and B3LYP/6-31+G(d,p)¹¹⁵ levels of theory in benzene using the default SCRF model. Vibrational mode

analysis was used to confirm each optimized structure represented potential energy minima.

Coordinate outputs are logged at the end of this document in the appendix.

1.8.15.2 Results of Geometry Minimizations: The computed structures of silane materials and phosphine oxide materials are shown in Table 1.45 and Table 1.46, respectively. Each entry depicts the optimal geometry as calculated at both levels of theory, and highlights the differences in bond angles around critical components of either material type. These structures were then used to calculate Mulliken charges (Tables 1.6 and 1.10) which can be used to compare materials of a similar type at the same level of theory, as well as global electronic parameters that are more robustly comparable across reagent classes and levels of theory.

Table 1.45. The computed structures of silane materials studied in this report.

Entry	Silane	M06-2X optimized geometry	B3LYP optimized geometry
1	Et ₃ SiH		
2	<i>n</i> -Hexylsilane		
3	TMDSO		
4	TMDSA		
5	Cl ₃ SiH		
6	(MeO) ₃ SiH		
7	Ph ₃ SiH		

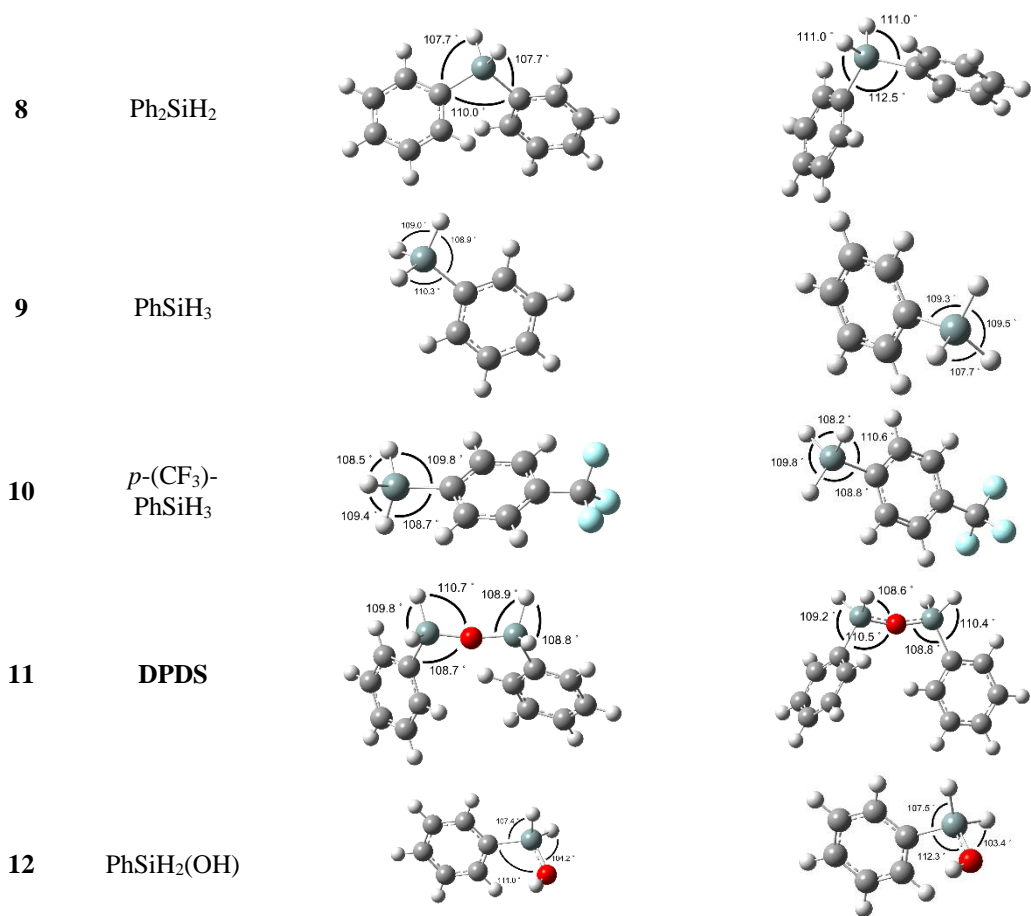
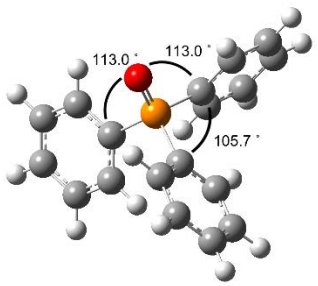
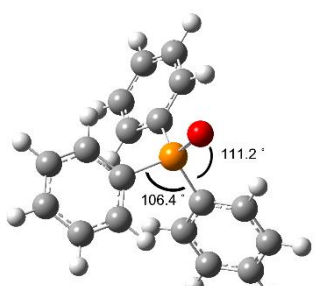
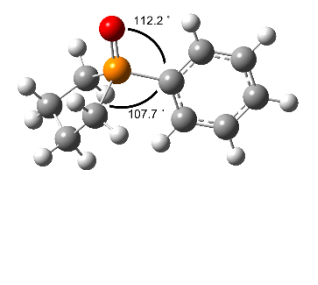
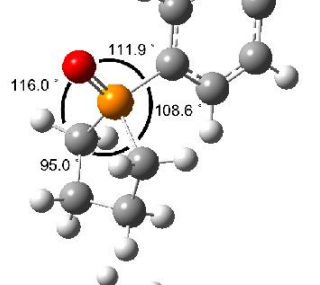
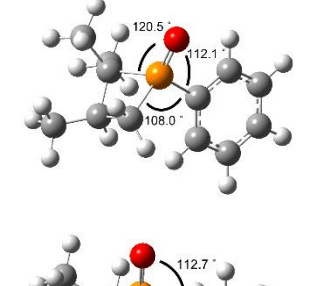
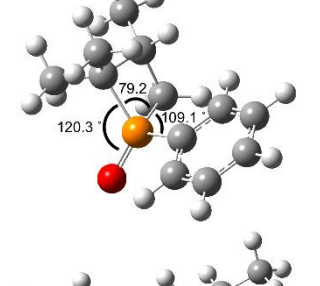
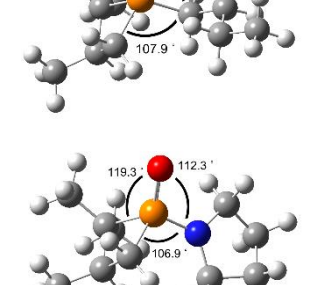
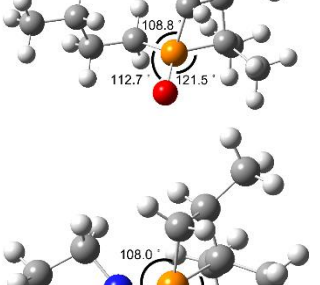
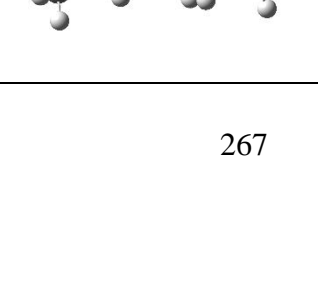
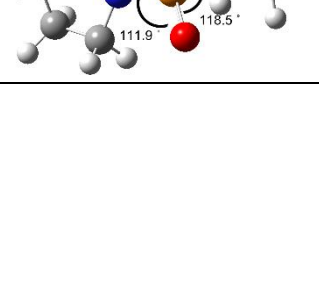


Table 1.46. The computed structures of phosphine oxides studied in this report.

Entry	PO	M06-2X optimized geometry	B3LYP optimized geometry
1	TPPO		
2	IPPO		
3	TMPPPO		
4	TMBPO		
5	TMYPPO		

1.8.15.3. Global Computational Trends

1.8.15.3.1. Comparison of Empirical Data: To compare computed trends between phosphine oxides in the Hammett series and the cyclic phosphine oxides in the literature,⁸² initial rates for the Hammett series were calculated using the same fitting function and initial rate equation for consistency's sake.

Fitting function: $Y = Y_0 + A_1 \cdot \exp[-(X-X_0)/t_1]$

Initial rate: $R = -(A_1/t_1) \cdot \exp(X_0/t_1)$

1.8.15.3.2. Computation of Reactivity Indices: All reactivity indices, including global electronic properties, were computed using the following equations, determined with values generated with relevant chemical species at the M062X/6-31+G(d,p) level of theory.¹¹⁶

Chemical Electron Potential: $\mu = \frac{E_{HOMO} + E_{LUMO}}{2}$

Chemical Hardness: $\eta = E_{LUMO} - E_{HOMO}$

Global Electrophilicity: $\omega = \frac{\mu^2}{2\eta}$

Maximum amount of electronic charge accepted by electrophile: $\Delta N_{max} = -\frac{\mu}{\eta}$

Nucleophilicity index: $N = E_{HOMO}(substrate) - E_{HOMO}(tetracyanoethylene)$

1.8.15.3.3. Results: The calculations of both silanes (Table 1.15) and phosphine oxides (Table 1.16) are shown. These values were then used to determine if a correlation could be found that computationally links catalyst/reductant design to activity. Unfortunately, no such correlation could be found for silanes, as summarized in Figure 1.42. For phosphine

oxides, the computational parameter nucleophilicity index (N), correlates very well with purported activity within a phosphine scaffold, nearly matching the Hammett plot (Figures 1.22 and 1.27). The same could also be said for five-membered phosphines (Figure 1.43), however, the trend is less apparent when a broad set of phosphine oxides is compared (Figure 1.27). With that said, a vanilla example of a certain catalyst scaffold is all that is needed to have an idea of designing new catalysts, since phosphine oxides within the same series are comparable.

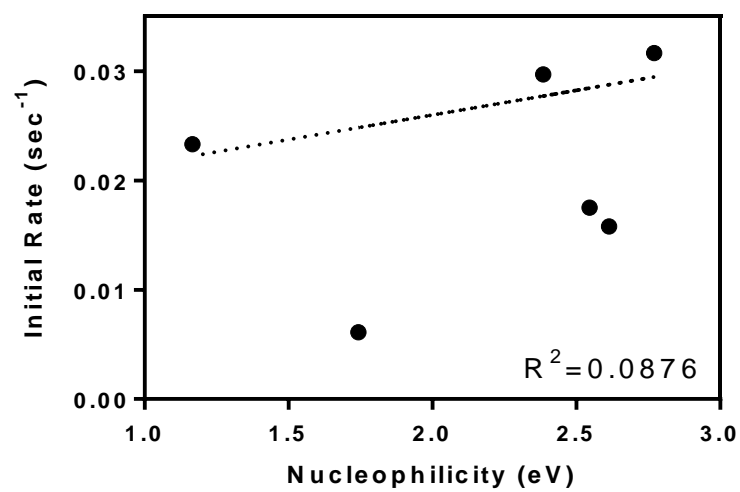


Figure 1.42. The comparison of silane nucleophilicity index (N) and empirically-determined initial rates of reduction with **TMPPPO**. Data collected by Kathleen Wang.

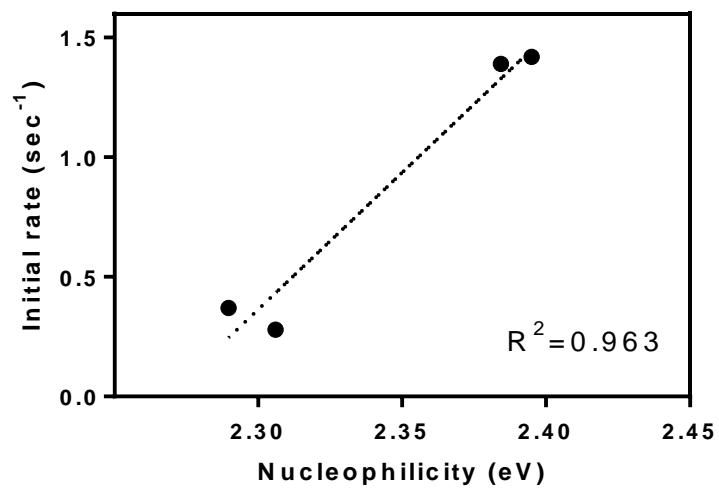


Figure 1.43. The comparison of phosphine oxide nucleophilicity index (N) to empirically-observed initial rates of reduction with 5-membered phosphine oxides. Data collected by Kathleen Wang.

1.8.16. Computational Modeling of Reaction Intermediates:

1.8.16.1. Modeling the Pre-Reaction Complex

1.8.16.1.1. General Procedure: Pre-reaction complexes (PCs) for the reduction of triphenylphosphine oxide with phenylsilane and the reduction of triphenylphosphine oxide with phenylsilanol were calculated using DFT at the M06-2X/6-31+G(d,p) and B3LYP/6-31+G(d,p) levels of theory. Structures were preliminarily optimized at the HF/3-21G, B3LYP/3-21G, B3LYP/6-31G, and B3LYP/6-31+G levels of theory before the final optimizations at target levels of theory were performed. For these calculations, additional keywords were included to model solvent effects in benzene using the PCM model, and an additional keyword was included to specify an ultrafine grid. Vibrational analysis was used to confirm that optimized structures were at energetic minima.

In addition, the silanol OH functional group in the optimized geometry of the **TPPO** + phenylsilanol PC was replaced with just an H, and a frequency calculation was performed for this structure. This was done to simulate the thermodynamics of **TPPO** + phenylsilane in the exact conformation and geometry of the **TPPO** + phenylsilanol PC. The basis set and functional used for the frequency calculations was consistent with the level of theory the original optimization was run at.

Coordinate outputs are logged at the end of this supporting document in the appendix.

1.8.16.1.2. Thermodynamic Equations: Gaussian provides $E_{electronic}$ and E_{ZPE} in atomic units, and values for entropy in cal/mol in the output of frequency calculations. E_{trans} and E_{rot} are $3RT/2$ each and $\Delta(PV)$ is approximately -0.6 kcal/mol.

$$U(T) = E_{electronic} + E_{ZPE} + E_{trans} + E_{rot}$$

$$\Delta H = \Delta U + \Delta(PV)$$

$$\Delta G = \Delta H - T\Delta S$$

1.8.16.1.3. Results of Modeling the Interaction of **TPPO** with Phenylsilane and Phenylsilanol: The modeling to determine PCs proceeded by limiting interactions within a sphere of 5 Å. This was difficult to do for structures with phenylsilane, as repulsive forces made minimization difficult. As such, we elected to calculate energies *de novo* and by replacing atoms in the minimized structures with phenylsilanol, denoted by the addition of “Freq” in its entries in Tables 1.13 and 1.47. As summarized in Figures 1.25 and 1.44, the geometries show that the phenylsilane cannot make a specific interface that is favorable, until a covalent interaction occurs. However, the phenylsilanol reductants easily associate with each other, resulting in a PC that is stabilized through a hydrogen-bond culminating in the first computed PC that is energetically favorable.

Table 1.47. The calculated energies and geometries of PCs with **TPPO** at the B3LYP level of theory.

Parameter	TPPO + PhSi(OH)H ₂	TPPO + PhSiH ₃	TPPO + PhSiH ₃ (Freq)
ΔH (kcal/mol)	-14.3	-0.61	-0.07
ΔS (cal/mol)	-27.8	-40.5	-47.2
ΔG (kcal/mol)	-6.0	+11.5	+14.0
P=O (Å)	1.5207	1.5093	1.5207
P=O \cdots HO-Si/P=O \cdots H-Si (Å)	1.7064	3.7933	2.8767
Si-H \cdots P (Å)	5.2718	4.7807	5.2718
Si \cdots P (Å)	5.1368	5.2347	5.1368
P=O \cdots H-R (°)	128.96	n.d.	131.27

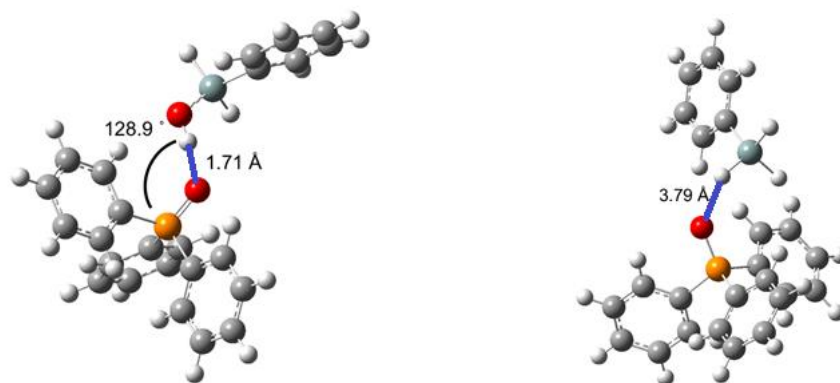


Figure 1.44. The optimized PC of **TPPO** with A) PhSi(OH)_2 and B) PhSiH_3 at the B3LYP level of theory. Data collected by Kathleen Wang.

1.8.17. Stability of Phosphine Oxide Precatalysts:

Although it has been previously established that the phosphine oxide **1PPO** is stable for months at -20 °C,¹ it is noteworthy that this is not necessarily true for all of these cyclic phosphines. While **1PPO** seems to be stable at room temperature for a few days, the four-membered phosphetanes **TMPPPO**, **TMBPO**, and **TMPyrPO** all have different stabilities which do not seem to follow a trend. Similarly to **1PPO**, the precatalysts were all stored in clear vials wrapped with aluminum foil to exclude light. The purity of samples and presence of degradation was monitored by ¹H and ³¹P NMR spectroscopy at 1 day, 3 days, 7 days, 14 days, 30 days, 90 days, and 180 days (when applicable).

TMBPO is the least stable precatalyst we have studied to date, and shows signs of degradation within two weeks of storage at -20 °C (storage at -80 °C was also ineffective at stopping degradation). **S4** (only used in supporting experiments) had a similar stability profile, potentially indicating that trialkyl phosphetanes are unstable and incompatible for use in reactions (trialkyl phospholanes may be a suitable substitute). **TMPyrPO** seems to have limited stability at room temperature, with degradation noted after 3 days, but degrades only slightly after 6 months when stored at -20 °C. **TMPPPO** has a similar stability profile as **1PPO**, as it does not degrade when stored at -20 °C (monitored for 180 days), nor when stored at room temperature in a desiccator for 90 days. **1PPO** is very stable when stored at -20 °C with the exclusion of light, as catalyst batches retained purity for at least 18 months.

1.8.18. The Balls for the Ball-Milling Strategy:

The balls used to enhance the reaction rate to form the chlorosilane intermediate were purchased from VXB.com (part numbers in parentheses) and degreased (using CH_2Cl_2) prior to use. For small scale reactions (1 mmol), 1000 $\frac{1}{2}$ mm diameter tungsten-carbide balls (0-5MMTUNGSTENBALLS) were employed in a small vial with a $\frac{1}{4}$ inch stir bar used to stir the reaction. The tungsten carbide balls are easily recycled. For larger reactions, $\frac{1}{2}$ inch diameter chrome iron (KIT8597) or ceramic (KIT12927) balls were used. Sometimes, with the iron balls, a yellow (not pale yellow) crude material was obtained and distillation could be needed, although the product would often appear >95% pure by NMR. The iron balls could be reused, although the propensity to obtain this yellow crude material became greater. We found that the ceramic balls were better for recycling and could be used many times, similarly to the tungsten-carbide balls.

1.8.19. Synthesis of Disiloxane Materials:

1.8.19.1. General Procedure of Ball-Milling Process:

To a 2-neck 500 mL round bottom flask was added 35 $\frac{1}{2}$ inch metal or ceramic spheres. Then, CuCl_2 (12.1 g, 90 mmol, 2.0 equiv), CuI (857 mg, 4.5 mmol, 0.1 equiv), and Et_2O (60 mL). An overhead stirrer was fitted to the vessel and the reaction was stirred at 30% speed for 30 min. Phenylsilane (5.54 mL, 45 mmol, 1.0 equiv) was added dropwise and a color change was noted immediately. After about 1.5 h, the reaction was complete (completion is noted when the balls are caked with greyish solid). The reaction was filtered directly onto ice (45 g) and washed with 30 mL Et_2O . The ether and ice were swirled every 5 min for 15-45 min, until the ice was melted. The layers were separated and the organic

layer was washed with cold deionized water (2×30 mL) and then dried with MgSO_4 . The solvent and excess phenylsilane were evaporated at 40 °C at reduced pressure (22 Torr). **DPDS** was obtained as a colorless to pale-yellow oil (4.80 g, 20.9 mmol) in 93% yield. Generally, disiloxanes were at least 95% pure.

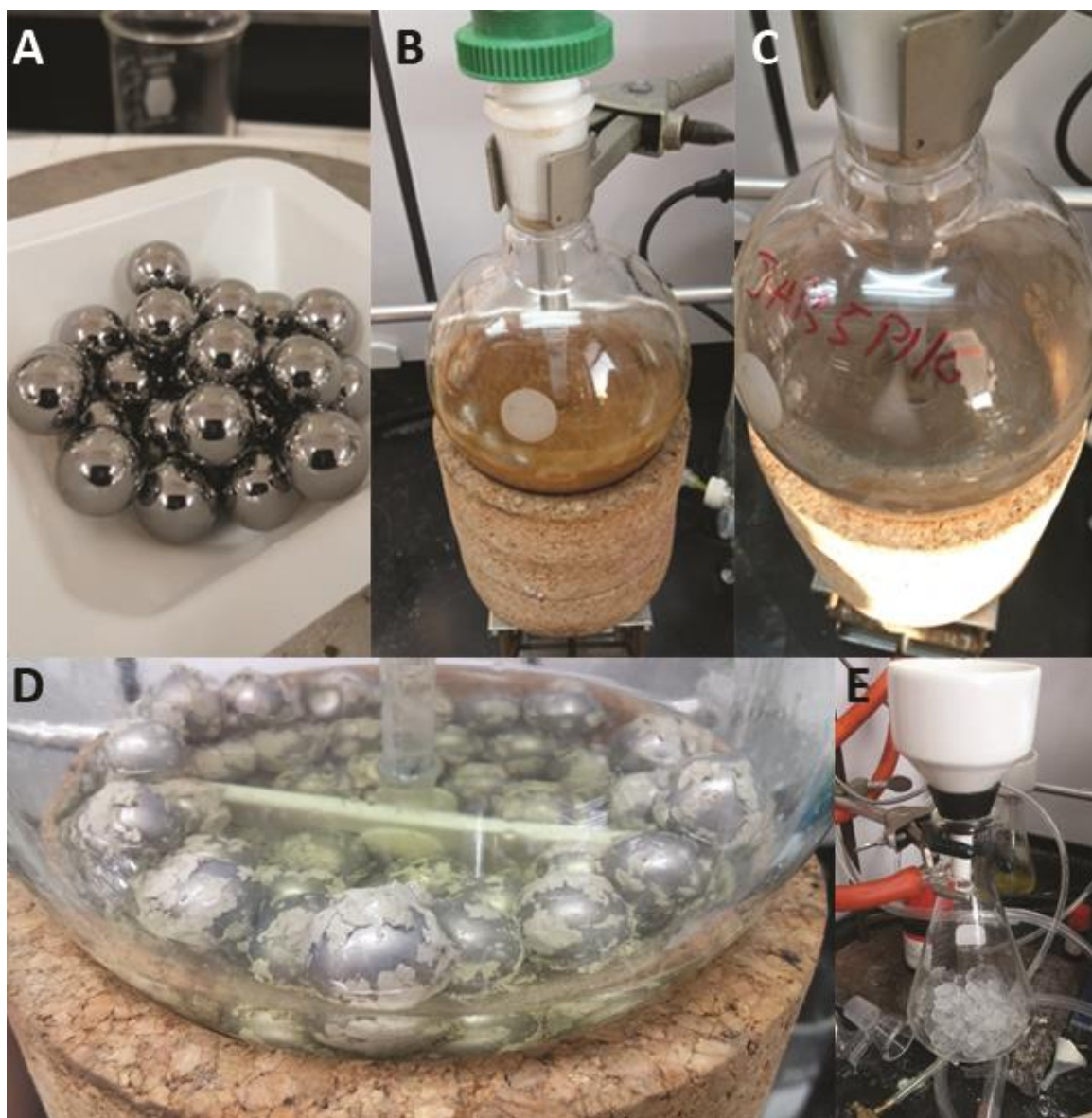


Figure 1.45. Preparation of DPDS; A) Metal balls used in the reaction, B) Formation of the active copper complex, C) Addition of phenylsilane, D) Reaction complete, E) Filtration apparatus with ice in the receiving flask.

1.8.19.2. Procedure of Reactions without Balls (Magnetic Stirring):

To a 2-dram vial, equipped with a ¼ inch magnetic stir-bar was added CuCl₂ (1.21 g, 9 mmol, 2.0 equiv), CuI (85.7 mg, 0.45 mmol, 0.1 equiv), and Et₂O (6 mL). The reaction vessel was sealed with a screw cap and stirred at 750 rpm for 30 min. Phenylsilane (554 µL, 4.5 mmol, 1.0 equiv) was added dropwise and a color change was noted immediately. The reaction was monitored by ¹H NMR for completeness. After 16 h, the reaction was filtered directly onto ice (5 g) and washed with 10 mL Et₂O. The ether and ice were swirled every 5 min for 5-15 min, until the ice was melted. The layers were separated and the organic layer was washed with cold deionized water (2 × 15 mL) and then dried with MgSO₄. The solvent and excess phenylsilane were evaporated at 40 °C at reduced pressure (22 Torr). **DPDS** was obtained as a colorless oil (414 mg, 1.8 mmol) in 80% yield.

1.8.19.3. Procedure of Reactions without Balls (Overhead Stirring):

To a 2-neck 500 mL round bottom flask was added CuCl₂ (12.1 g, 90 mmol, 2.0 equiv), CuI (857 mg, 4.5 mmol, 0.1 equiv), and Et₂O (60 mL). An overhead stirrer was fitted to the vessel and the reaction was stirred at 30% speed for 30 min. Phenylsilane (5.54 mL, 45 mmol, 1.0 equiv) was added dropwise and a color change was noted immediately. The reaction was monitored by ¹H NMR for completeness. After 20 h, the reaction was filtered directly onto ice (45 g) and washed with 10 mL Et₂O. The ether and ice were swirled every 5 min for 15 min, until the ice was melted. The layers were separated and the organic layer was washed with cold deionized water (2 × 15 mL) and then dried with

MgSO₄. The solvent and excess phenylsilane were evaporated at 40 °C at reduced pressure (22 Torr). **DPDS** was obtained as a pale yellow oil (3.639 g, 15.8 mmol) in 70% yield.

1.8.20. Additional Purifications of Disiloxanes in Table 1.17:

1,3-Diphenyl-disiloxane [17962-59-3] (**DPDS**)⁷³: Reactions were performed at 1, 15, 45, and 90 mmol scales. Additional purification (if needed) was achieved by distillation under reduced pressure (bp. 76°C at 580 mTorr). The title compound was obtained as a colorless to pale-yellow oil (9.1 g, 39.6 mmol) in 88% yield. ¹H NMR (CDCl₃) δ 7.53 (d, *J* = 7.6 Hz, 4H), 7.37 (t, *J* = 7.6 Hz, 2H), 7.32 (t, *J* = 7.2 Hz, 4H), 5.06 (s, 4H); ¹³C NMR (CDCl₃) δ 134.10, 130.54, 128.13; HRMS (ESI) Calc. C₁₂H₁₄NaOSi₂ [*M* + Na] 253.0475, Found 253.0471.

1,1,3,3-Tetraphenyl-disiloxane [15545-80-9] (**TPDS**)^{73, 101}: Reactions were performed at 15 mmol scale. The title compound was obtained as a colorless solid (2.58 g, 6.75 mmol) in 90% yield; mp. 48–49 °C [Lit.² mp. 46–49 °C]. ¹H NMR (CDCl₃) δ 7.48 (d, *J* = 6.9 Hz, 8H), 7.34 (t, *J* = 7.4 Hz, 4H), 7.27 (t, *J* = 7.7 Hz, 8H), 5.52 (s, 2H); ¹³C NMR (CDCl₃) δ 134.33, 130.24, 127.96; HRMS (ESI) Calc. C₂₄H₂₃OSi₂ [*M* + H] 383.1282, Found 383.1280.

1,3-Di-*n*-hexyl-disiloxane [1203611-82-8]: Reactions were performed at 1 and 15 mmol scales. Additional purification (if needed) was achieved by distillation under reduced pressure (bp. 76°C at 580 mTorr). The title compound was obtained as a colorless to pale yellow oil (1.57 g, 6.38 mmol) in 85% yield. ¹H NMR (CDCl₃) δ 4.52 (t, *J* = 2.6 Hz, 4H), 1.36–1.22 (m, 20H), 0.82 (t, *J* = 6.9 Hz, 6H); ¹³C NMR (CDCl₃) δ 32.34, 31.55, 22.92,

22.54, 14.47, 14.10; HRMS (ESI) Calc. C₁₂H₃₀NaOSi₂ [M + Na] 269.1727, Found 269.1732.

1,3-Dimethyl-1,3-diphenyl-disiloxane [6689-22-1] (DMDPS)¹⁰²: Reactions were performed at 15 mmol scale. Additional purification (if needed) was achieved by distillation under reduced pressure (bp. 102 °C at 800 mTorr). The title compound was obtained as a colorless to pale yellow oil (1.64 g, 6.35 mmol) in 85% yield. ¹H NMR (CDCl₃) δ 7.40 (dt, *J* = 7.9, 1.4 Hz, 4H), 7.25-7.19 (m, 6H), 4.98 (dd, *J* = 2.9, 1.1 Hz, 2H), 0.27 (d, *J* = 3.1 Hz, 6H); ¹³C NMR (CDCl₃) δ 32.34, 31.55, 22.92, 22.54, 14.47, 14.10; HRMS (ESI) Calc. C₁₄H₁₈NaOSi₂ [M + Na] 281.0788, Found 281.0799.

1.8.21. Procedure for Cleaning Balls for Recycling:

After the reaction is completed, the balls are removed from the filter and are separated from the excess copper salts also remaining on the filter paper. The balls are soaked in 50:50 acetone:water and are scrubbed by hand until the balls appear clean. The balls are then washed with water and acetone. The balls are then dried on a paper towel and stored in a closed container. Before reuse, the balls are washed with acetone and CH₂Cl₂ immediately prior to use. An image of the chrome-iron balls after washing is shown in Figure 1.46.

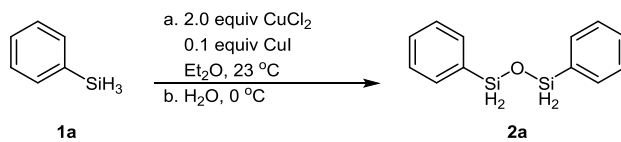


Figure 1.46. The condition of used Chrome-Iron balls after one use (left) and after two uses (right).

1.8.22. Comparison of Yields with Different Balls:

The general procedure was used for each reaction and the type of balls used was varied. In each trial, either all-new or all-used balls were utilized for the reaction. As summarized in Table 1.48, the reaction yield was nearly the same for new chrome iron and new ceramic spheres. However, upon recycling, the yield stayed constant for the ceramic balls while a drop-off was noted for the recycled iron balls. This drop in yield was further exacerbated by an additional recycling step, and the initially purity of the crude material was also lower. For optimal performance, chrome iron balls should be retired after two uses. Ceramic balls, while more stable to the chemical conditions, did have longevity issues due to the mechanical force exerted on the balls during reactions as microfractures eventually resulted in the physical breaking of the ceramic material after repeated use, although this process was generally slower than the rate of “degradation” of the chrome iron balls.

Table 1.48. Comparison of Yields for the Synthesis of 2a when Different Balls are Employed.



Entry	Ball Material	Previous Number of Uses ^a	Yield ^b
1	Ceramic	0	93
2	Ceramic	1	91
3	Ceramic	2	90
4	Chrome Iron	0	91
5	Chrome Iron	1	88
6	Chrome Iron	2	80

^aBalls recycled as indicated in section 2.4, ^bIsolated crude yield of two reactions at 45 mmol scale prior to additional purification.

1.8.23. Synthesis of Phosphine Oxides:

1.8.23.1. General Procedure for Oxidation of Phosphines: To a stirring solution of phosphine (2.0 mmol, 1 equiv) in 10 mL Et₂O or CH₂Cl₂ was added H₂O₂ (30% aqueous solution, 5 mL). The reaction was stirred under Schotten-Baumann conditions for 30 minutes to 16 hours. The reactions were filtered, and washed with Et₂O to afford phosphine oxides in yields ranging from 69 to 99%.

1.8.23.2. General Procedure for Grignard Reactions with Diphenylphosphinic chloride: A roundbottom flask equipped with a teflon-coated stirbar was charged with magnesium (-90 mesh, 144 mg, 6.0 mmol, 1.2 equiv). The reaction flask and metal was flame-dried under reduced pressure, and the vessel was allowed to cool to 23 °C. After cooling, a solution of I₂ (20 mg) and aromatic bromides (5.5 mmol, 1.1 equiv) in anhydrous THF (5.5 mL) was added. The reaction vessel was heated to 60 °C with vigorous stirring. After 1.5 hours, the reaction was cooled to 0 °C and diphenylphosphinic chloride (954 µL, 5.0 mmol, 1.0 equiv) was added in a dropwise manner. The reaction was stirred and allowed to warm to 23 °C slowly. After 18 hours, the reaction was again cooled to 0 °C and 6.0 mL of 2.0 N NaOH was added to quench the reaction. The reaction layers were separated, and the aqueous layer was washed with EtOAc (3 x 10 mL). The organic layers were combined and concentrated directly onto silica gel for column chromatography to afford phosphine oxides in yields ranging from 73 to 92%.

1.8.23.3. Purification of Phosphine oxides:

(4-(Dimethylamino)phenyl)diphenylphosphine oxide¹¹⁷: The reagent was prepared according to the procedure in section 2.2. The crude mixture was purified by column chromatography with 10% methanol in CH₂Cl₂ to afford the title compound as a white solid. All physical data and spectra matched literature reports.

(4-methoxyphenyl)diphenylphosphine oxide¹¹⁸: The reagent was prepared according to the procedure in section 2.2. The crude mixture was purified by column chromatography with 10% methanol in CH₂Cl₂ to afford the title compound as an off-white solid. All physical data and spectra matched literature reports.

(4-(Trifluoromethyl)phenyl)diphenylphosphine oxide¹¹⁸: The reagent was prepared according to the procedure in section 2.2. The crude mixture was purified by column chromatography with 10% methanol in CH₂Cl₂ to afford the title compound as a white solid. All physical data and spectra matched literature reports.

(3,5-Bis(trifluoromethyl)phenyl)diphenylphosphine oxide: The reagent was prepared according to the procedure in section 2.2. The crude mixture was purified by column chromatography with 10% methanol in CH₂Cl₂ to afford the title compound as a brown solid. ¹H NMR (CDCl₃, 500 MHz) δ 8.15 (d, *J* = 11.4 Hz, 2H), 8.04 (s, 1H), 7.69 – 7.61 (m, 6H), 7.54 (dd, *J* = 7.6, 2.7 Hz, 4H); ¹³C (CDCl₃, 126 MHz) δ 132.9, 132.0, 131.9, 131.1, 130.3, 129.1, 129.0, 125.7; ³¹P (CDCl₃, 202 MHz) δ 50.32; ¹⁹F (CDCl₃, 470 MHz) δ -62.89; HRMS (ESI) Calc. C₂₀H₁₃F₆NaOP [M + Na] 437.0500, Found 437.0501.

Tris-(3,5-(trifluoromethyl)phenyl)phosphine oxide¹¹⁹: The reagent was prepared according to the procedure in section 2.1. and filtered directly to afford a white solid. All physical data and spectra matched literature reports.

[1,1'-biphenyl]-2-yl)dicyclohexylphosphine oxide¹²⁰: The reagent was prepared according to the procedure in section 2.1. and filtered directly to afford a white solid. All physical data and spectra matched literature reports.

(2',6'-dimethoxy-[1,1'-biphenyl]-2-yl)dicyclohexylphosphine oxide: The reagent was prepared according to the procedure in section 2.1. and filtered directly to afford an off-white solid. ¹H NMR (CDCl₃, 500 MHz) δ 7.80 (dd, *J* = 10.4, 8.5 Hz, 1H), 7.44 (t, *J* = 8.7 Hz, 1H), 7.37 (t, *J* = 8.7 Hz, 1H), 7.25 (t, *J* = 8.4 Hz, 1H), 7.08 (dd, *J* = 7.3, 3.5 Hz, 1H), 6.54 (d, *J* = 8.4 Hz, 2H), 3.61 (s, 6H), 1.67 – 1.62 (m, 8H), 1.54 – 1.49 (m, 4H), 1.27 – 1.19 (m, 2H), 1.10 – 1.00 (m, 6H); ¹³C (CDCl₃, 126 MHz) δ 137.1, 136.3, 132.8, 132.0, 131.3, 129.0, 125.7, 123.9, 121.7; ³¹P (CDCl₃, 202 MHz) δ 50.32; HRMS (ESI) Calc. C₂₆H₃₅NaO₃P [M + Na] 449.2211, Found 449.2187.

1,2-Bis(diphenylphosphino oxide)ethane¹²¹: The reagent was prepared according to the procedure in section 2.1. and filtered directly to afford a white solid. All physical data and spectra matched literature reports.

rac-2,2'-Bis(diphenylphosphino oxide)-1,1'-binaphthene²⁹: The reagent was prepared according to the procedure in section 2.1. and filtered directly to afford a white solid. All physical data and spectra matched literature reports.

(9,9-Dimethyl-9H-xanthene-4,5-diyl)-bis-diphenylphosphine oxide: The reagent was prepared according to the procedure in section 2.1. and filtered directly to afford a white solid. ^1H NMR (CDCl_3 , 500 MHz) δ 7.54 (d, $J = 7.1$ Hz, 2H), 7.34 – 7.30 (m, 11H), 7.22 – 7.19 (m, 9H), 6.91 (t, $J = 7.2$ Hz, 2H), 6.70 (dd, $J = 7.5$ Hz, 2H), 1.63 (s, 6H); ^{13}C (CDCl_3 , 126 MHz) δ 153.0, 134.2, 132.1, 131.4, 130.6, 128.1, 123.0, 34.1, 33.0; ^{31}P (CDCl_3 , 202 MHz) δ 30.13; HRMS (ESI) Calc. $\text{C}_{39}\text{H}_{32}\text{NaO}_3\text{P}_2$ [$\text{M} + \text{Na}$] 633.1719, Found 633.1790.

1,2-Bis [(2-methoxyphenyl)(phenylphosphine oxide)] ethane²⁵: The reagent was prepared according to the procedure in section 2.1. and filtered directly to afford a white solid. All physical data and spectra matched literature reports.

[4-(Dimethoxymethyl)phenyl]diphenylphosphine oxide: The reagent was prepared according to the procedure in section 2.2. The crude mixture was purified by column chromatography with 5% methanol in CH_2Cl_2 to afford the title compound as a colorless oil. ^1H NMR (CDCl_3 , 500 MHz) δ 7.68 – 7.65 (m, 6H), 7.55 (t, $J = 6.5$ Hz, 4H), 7.46 (t, $J = 6.5$ Hz, 4H), 5.42 (s, 1H), 3.34 (s, 6H); ^{13}C (CDCl_3 , 126 MHz) δ 142.1, 132.9, 132.1, 132.0, 128.5, 126.9 (d, 12.7 Hz), 126.9 (d, 11.8 Hz), 102.5, 52.9; ^{31}P (CDCl_3 , 202 MHz) δ 28.91; HRMS (ESI) Calc. $\text{C}_{21}\text{H}_{21}\text{NaO}_3\text{P}$ [$\text{M} + \text{Na}$] 375.1121, Found 375.1112.

4-(Diphenylphosphine oxide)-benzaldehyde: The reagent was prepared according to the procedure in section 2.2. The crude mixture was purified by column chromatography with 5% methanol in CH_2Cl_2 to afford the title compound as a colorless oil. ^1H NMR (CDCl_3 , 500 MHz) δ 10.09 (s, 1H), 7.97 (d, $J = 7.4$ Hz, 2H), 7.87 (t, $J = 8.7$ Hz, 2H), 7.68 (t, $J = 8.7$ Hz, 4H), 7.59 (t, $J = 7.9$ Hz, 2H), 7.50 (t, $J = 7.2$ Hz, 4H); ^{13}C (CDCl_3 , 126 MHz) δ

191.6, 132.8, 132.4, 132.1, 132.0, 129.4, 128.8, 128.7; ^{31}P (CDCl_3 , 202 MHz) δ 28.57; HRMS (ESI) Calc. $\text{C}_{19}\text{H}_{15}\text{NaO}_2\text{P}$ [$\text{M} + \text{Na}$] 329.0702, Found 329.0731.

1,1'-Bis(diphenylphino oxide)ferrocene: The reagent was prepared according to the procedure in section 2.1. and filtered directly to afford an orange solid. ^1H NMR (CDCl_3 , 500 MHz) δ 7.51 – 7.33 (m, 20H), 4.61 (s, 4H), 4.20 (s, 4H); ^{13}C (CDCl_3 , 126 MHz) δ 134.2, 133.3, 131.7, 131.4, 131.3, 128.4, 74.1, 74.0, 73.5, 73.4; ^{31}P (CDCl_3 , 202 MHz) δ 28.50; HRMS (ESI) Calc. $\text{C}_{34}\text{H}_{29}\text{FeO}_2\text{P}_2$ [$\text{M} + \text{H}$] 587.0987, Found 587.0998.

1.8.24. NMR Studies of Silane Reductions:

1.8.24.1. Real-Time Reaction Monitoring of Silane-Based Reducing Conditions:

1.8.24.1.1. General Procedure for DPDS Reduction: To an NMR tube was added *d*₈-toluene (425 μL), **DPDS** (72 mg, 0.31 mmol, 0.63 M), and **TPPO** (70 mg, 0.25 mmol, 0.5 M). The tube was inverted three times to ensure proper mixing of the reagents and the interface between the tube and the cap was sealed with multiple layers of paraffin wax (parafilm®) to ensure no leaks. The reaction was heated to 110 °C and monitored with ^{31}P NMR.

1.8.24.1.2. General Procedure for TMDSO/Ti(OiPr)₄ Reduction²⁹: To an NMR tube was added *d*₈-toluene (500 μL), **TMDSO** (115 μL , 0.65 mmol, 1.06 M), **Ti(OiPr)₄** (15.4 μL , 0.052 mmol, 0.084 M), and **TPPO** (145 mg, 0.52 mmol, 0.84 M). The tube was inverted three times to ensure proper mixing of the reagents and the interface between the tube and the cap was sealed with multiple layers of paraffin wax (parafilm®) to ensure no leaks. The reaction was heated to 110 °C and monitored with ^{31}P NMR.

1.8.24.1.3. General Procedure for HSiMe(OEt)₂/BNPA Reduction²⁵: To an NMR tube was added *d*₈-toluene (500 μL), HSiMe(OEt)₂ (40 μL, 0.25 mmol, 0.46 M), (*p*-NO₂C₆H₄O)₂PO₂H (**BNPA**, 1.6 mg, .0047 mmol, 0.009 M), and **TPPO** (17.4 mg, 0.062 mmol, 0.116 M). The tube was inverted three times to ensure proper mixing of the reagents and the interface between the tube and the cap was sealed with multiple layers of paraffin wax (parafilm®) to ensure no leaks. The reaction was heated to 110 °C and monitored with ³¹P NMR.

1.8.24.1.4. Results: These reductions were run using the exact reactant concentrations reported by Beller²⁵ and Lemaire²⁹ to provide an accurate comparison of **DPDS**-mediated reduction to dump-and-stir versions of their optimized systems. We did choose to heat the **TMDSO**/Ti(OiPr)₄ system to 110 °C instead of the reported 100 °C to normalize the temperatures that the reaction mixtures were heated to (presumably this would increase the rate of reduction).

As shown in Figure 1.28, reduction using **DPDS** solely is by far the swiftest, completing in 10-12 h with greater than 90% conversion at 4 h. The HSiMe(OEt)₂/BNPA reduction system was the next quickest, proceeding via first-order kinetics to furnish complete reduction in 16-18 h, which is very close to the reported rate.²⁵ The **TMDSO**/Ti(IV) trials, on the other hand, struggled to perform at the reported rates under our conditions which did not strictly eliminate water and air from the reaction mixture. Figure 1.28 only shows time points for the **TMDSO**/Ti(IV) system after 10 hours because cooling the reaction any earlier resulted in unreacted **TPPO** crashing out.

It is worth noting that reductions using $\text{HSiMe}(\text{OEt})_2$ and **BNPA** require 4 equivalents of silane to proceed at the rate in Figure 1.28. Beller and coworkers note the production of H_2 over the course of the reaction caused by reaction of the silyl hydride with a proton source, which causes low yields when less equivalents of silane are used. Our proposed system using **DPDS** requires only 1.25 equivalents of silane and eschews additional additives, making it far more atom-economical while still achieving complete reduction in around 60% of the time

We were also quite surprised to see the **TMDSO**/Ti(IV) system not finish. To ensure that we were not misrepresenting the performance of this system, we tried multiple sources of $\text{Ti}(\text{OiPr})_4$. The data shown in Figure 1.28 is from three concurrent trials with a never-before opened bottle of $\text{Ti}(\text{OiPr})_4$ from Strem Chemicals, Inc., which we have observed to be the best provider of our transition metals. Individual results with different sources of $\text{Ti}(\text{OiPr})_4$ are shown in Table 1.49.

Table 1.49. Testing Different Sources of $\text{Ti}(\text{OiPr})_4$. (Values Shown are % Completion).

Time (h)	Trial A	Trial B	Trial C	Trial D	Trial E	Trial F
10	62	59	56			
12				60	55	61
14						61
16	69	62	60			
32	76	67	66			
48	81	70	69	79	65	

Trials A-C are the concurrent trials with fresh $\text{Ti}(\text{OiPr})_4$ from Strem that are used in Figure 1. Trial D is with an older bottle of $\text{Ti}(\text{OiPr})_4$ from Strem stored in a desiccator, and Trials E & F are with an older bottle of $\text{Ti}(\text{OiPr})_4$ from Sigma-Aldrich stored in a desiccator.

1.8.24.2. Arrhenius Analysis:

1.8.24.2.1. General Procedure for Arrhenius Analysis of **TPPO** Reduction with **DPDS**: To three NMR tubes was added *d*₈-toluene (440 μL), **DPDS** (58 mg, 0.25 mmol, 0.50 M), and **TPPO** (5.6 mg, 0.2 mmol, 0.04 M). The tubes were inverted three times to ensure proper mixing of the reagents and the interface between the tube and the cap was sealed with multiple layers of paraffin wax (parafilm®) to ensure no leaks. The reactions were heated to the temperature indicated and monitored with ³¹P NMR.

4.2.2 Data Analysis:

The phosphine oxide reduction time courses were fit to equation 1 to determine the rate constants (*k*) of reduction with each catalyst at each temperature.

Equation 1. $\%P = -Ae^{-kt}$

Figure 1.47 shows the time course analysis and fitting to Equation 1 for **TPPO**.

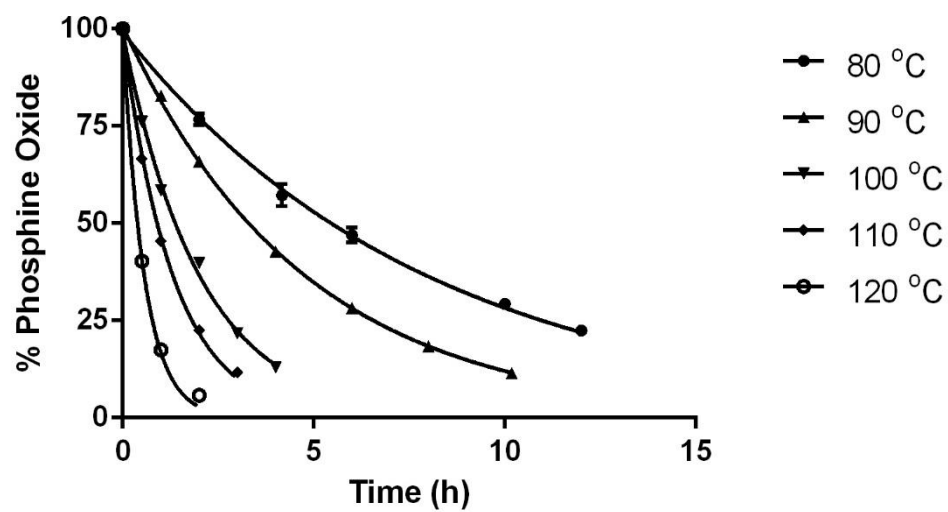


Figure 1.47. Single-exponential fitting of reductions of **TPPO** with **DPDS**.

The k values obtained from Figure S1 was then used to generate Arrhenius plots to determine the activation energy of each reaction. Equation 2 shows the linearized form of the Arrhenius equation.

$$\textbf{Equation 2. } \ln(k) = -\frac{E_a}{R} * \frac{1}{T} + \ln(A)$$

Now, for our analysis, k is actually equal to a rate constant (call it k_1) times the concentration of **DPDS**, since we are running these analyses using a large excess of **DPDS**. Equation 3 describes this.

$$\textbf{Equation 3. } \ln(k_1 * [\textbf{DPDS}]) = -\frac{E_a}{R} * \frac{1}{T} + \ln(A)$$

The natural logarithm on the left of Equation 3 can be split to provide Equation 4.

$$\textbf{Equation 4. } \ln(k_1) + \ln([\textbf{DPDS}]) = -\frac{E_a}{R} * \frac{1}{T} + \ln(A)$$

The natural logarithm of the concentration of **DPDS** is constant. This means that if we were doing full Arrhenius analysis, without accounting for the $\ln([\textbf{DPDS}])$ term, we would obtain an incorrect value for the parameter A. Since we are only interested in determining the energy of activation, however, this is not an issue.

Fitting the k values obtained from Figure 1.46, we generate Arrhenius plots for **TPPO** as in Figures 1.48 This provides an estimate of the activation energy for reduction.

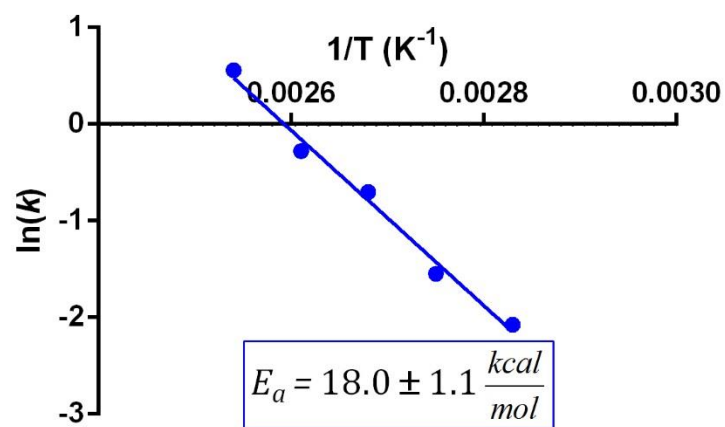


Figure 1.48. Arrhenius plot for **TPPO** showing the activation energy.

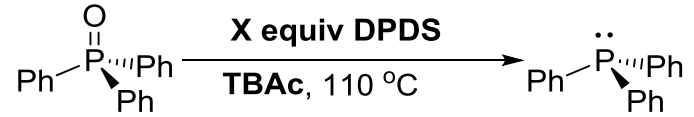
1.8.25. Optimization of Additive-Free Reductions of Acyclic Phosphines:

1.8.25.1. Silane Equivalence Screening:

1.8.25.1.1. General Procedure: To a 2-dram vial equipped with a ¼" teflon-coated stir bar was added triphenylphosphine oxide (**TPPO**, 140 mg, 0.5 mmol, 1.0 equiv), toluene (1 mL, 0.5 M), and then **DPDS** (See tables for equivalence screen). The reaction was sealed with a pressure-relief cap (Chemglass: CG-4912-02) and heated to 110 °C. After 16-24 hours, the reactions were cooled to ambient temperature and then loaded directly onto silica gel (using approx. 10 mL acetone to wash the reaction vessel) for chromatography to yield compound **TPP**.

1.8.25.1.2. Results: Unsurprisingly, adding more **DPDS** resulted in faster reduction and higher yields of desired product. Quantitative yields could be achieved easily with a slight excess of **DPDS** (Table 1.50). However, high yields could still be achieved with less than one equivalent of **DPDS**, which was not surprising since **DPDS** contains two silicon centers (Tables 1.50 and 1.51). When the reaction is performed overnight (16 hours), quantitative yields are achieved with an equivalence of **DPDS** corresponding to 1.25 times **TPPO** (Table 1.50), while a 24 hour reaction gave the same yield with only 1.1 equivalence of **DPDS** (Table 1.51). Unfortunately, at either of these times, using equal stoichiometry or lower equivalence of **DPDS** did not afford higher than 95% yield. In order to achieve our desired goal of reductions that occur with high fidelity, we sought to use 1.25 equivalence of **DPDS** as our optimized conditions in toluene. These conditions were carried through to the next optimization of solvent.

Table 1.50. Silane Equivalence Screen Isolated After 16 h.


Reaction: $\text{Ph}-\text{P}(=\text{O})(\text{Ph})_2 \xrightarrow[\text{TBAc, 110 } ^\circ\text{C}]{\text{X equiv DPDS}} \text{Ph}-\text{P}(\text{Ph})_2$

Entry	Concentration (M)	Equiv DPDS	Isolated Yield ^[a]
1	0.25	0.75	78
2	0.25	1.0	78
3	0.25	1.5	99
4	0.25	2.0	Quant.
5	0.5	0.75	82
6	0.5	1.0	89
7	0.5	1.1	95
8	0.5	1.25	Quant.
9	0.5	1.5	Quant.
10	0.5	2.0	Quant.

^[a]Average isolated yield of at least two reactions.

Table 1.51. Silane Equivalence Screen Isolated After 24 h.

$$\text{Ph}-\overset{\text{O}}{\parallel}{\text{P}}(\text{Ph})_2 \xrightarrow[\text{PhMe, 110 }^\circ\text{C}]{\text{X equiv DPDS}} \text{Ph}-\ddot{\text{P}}(\text{Ph})_2$$

Entry	X equiv	Isolated Yield ^[a]
1	0.75	84
2	1.0	93
3	1.1	97
4	1.25	Quant.

^[a]Average isolated yield of at least two reactions.

While screening silane equivalence, we also investigated the requirements for optimal reactivity concerning concentration of the phosphorus oxide (Table 1.50). Overall, yields are better with more concentrated reactions. The reaction is also much more consistent when reducing at higher initial concentrations. Because of this reactivity, we chose to continue using highly concentrated reactions. It is noteworthy, however, that most phosphine oxides (including **TPPO**) are not soluble in toluene unless the reactions are heated.

1.8.25.2. Solvent Screening:

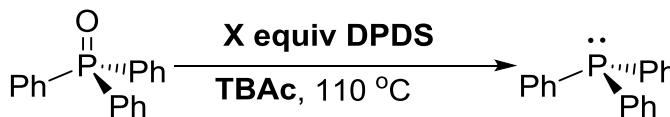
1.8.25.2.1.1. General Procedure: To a 2-dram vial equipped with a ¼" teflon-coated stir bar was added triphenylphosphine oxide (**TPPO**, 140 mg, 0.5 mmol, 1.0 equiv), **solvent** (1 mL, 0.5 M), and then **DPDS** (144 mg, 0.625 mmol, 1.25 equiv) The reaction was sealed with a pressure-relief cap (Chemglass: CG-4912-02) and heated to 110 °C. After 18 hours, the reactions were cooled to ambient temperature and then loaded directly onto silica gel (using approx. 10 mL acetone to wash the reaction vessel) for chromatography (see SI section 8.1) to yield compound **TPP**.

1.8.25.2.1.2. Alternative Workup Procedure for Ionic Liquid [Bmim]PF₆: After the reaction was cooled, the ionic liquid was extracted with Et₂O (3 x 7 mL) and the crude material was evaporated (156.4 mg). The crude material was again taken up in Et₂O and concentrated directly onto silica gel for chromatography (see SI section 8.1) to yield compound **TPP**.

1.8.25.2.2. Results: We investigated a range of “green” solvents, in addition to those used in other phosphine oxide reductions.^{25,29} Unsurprisingly, **TPPO** was unable to dissolve in heptane and cyclohexane boiled off at the high temperature, and thus neither of these solvents could be utilized at 110 °C. The ionic liquid [Bmim]PF₆ was capable of facilitating reduction (Table 1.19), however a side reaction is clearly occurring which results in a white precipitate, a yellow solution, and a “fishy” odor in reactions before workup. We also investigated ethyl lactate, which is sourced from renewable resources. Unsurprisingly, the yield of the reduction was quite low, likely due to **DPDS** consumption through side reactivity with the abundant (and unprotected) alcohol. Methyl cyclohexane, cyclopentyl methyl ether (CPME), and *tert*-butyl acetate (TBAC) were all competent solvents, and TBAC solubilized **TPPO** without heat, while methyl cyclohexane is already known to be poor at solubilizing phosphine oxides.²⁹

Because TBAC can easily solubilize phosphine oxides and reaction yields were comparable to reductions in toluene, we chose this solvent as the optimal solvent for reductions. TBAC is also attractive as a solvent because it lacks volatile organic compound (VOC) regulations from the United States Environmental Protection Agency. We opted to revisit a brief silane equivalence screen with the newly chosen solvent (Table 1.52) with similar results as those achieved with toluene.

Table 1.52. Silane Equivalence Screen in TBAc.


$$\text{Ph}-\overset{\text{O}}{\parallel}{\text{P}}(\text{Ph})_2 \xrightarrow[\text{TBAc, 110 } ^\circ\text{C}]{\text{X equiv DPDS}} \text{Ph}-\overset{\cdot\cdot}{\text{P}}(\text{Ph})_2$$

Entry	X equiv DPDS	Isolated Yield ^[a]
1	0.75	67
2	1.0	90
3	1.1	95
4	1.25	99

^[a]Average isolated yield of at least two reactions after 24 hours.

1.8.26. General Procedure of Additive-Free Phosphine Oxide Reductions:

To a 2-dram vial equipped with a ¼” teflon-coated stir bar was added phosphine oxides (0.1-0.5 mmol, 1.0 equiv), *tert*-butyl acetate (0.5 M), and then **DPDS** (0.125-0.625 mmol, 1.25 equiv). The reaction was sealed with a pressure-relief cap (Chemglass: CG-4912-02) and heated to 110 °C. After 16-24 hours, the reactions were cooled to ambient temperature and then loaded directly onto silica gel (using approx. 10 mL acetone to wash the reaction vessel) for chromatography (see SI section 8) to yield phosphines.

1.8.26.1. Alternate Workup: When working on a large enough scale, it may be necessary to destroy excess unreacted **DPDS**. This is easily accomplished by stirring the reaction with an equal volume of 2.0 M NaOH for 15 minutes (**Warning:** Rapid gas evolution). The reaction layers were separated and the organic layer was concentrated onto silica gel to remove soluble silanol byproducts from desired phosphines.

1.8.26.2. Determination of yields by ³¹P NMR: For secondary phosphine oxides, the reaction was set up in an NMR tube using the procedure from section 3.1.1. The reaction was cooled to 23 °C by running cold water over the tubes for 30 seconds. The reaction was checked by ³¹P NMR for conversion at 10, 30, 60, 90, 120, 180, 240, and 300 minutes. Reactions with di-*tert*-butyl phosphine oxide were monitored for 24 hours, at which point a degradant was noted to dominate the reaction mixture as no productive change in conversion was noted after 180 minutes.

1.8.27. Optimization of Room-Temperature Silane-Mediated Reductions of Phosphine Oxides:

1.8.27.1. Representative Procedure: To a 2-dram vial equipped with a ¼” teflon-coated stir bar was added triphenylphosphine oxide (**1a**, 70 mg, 0.25 mmol, 1.0 equiv), **BNPA** (17 mg, 0.05 mmol, 0.2 equiv), ethyl acetate (0.5 mL, 0.5 M), and then **DPDS** (144 mg, 0.625 mmol, 2.5 equiv) The reaction was sealed with a cap and stirred at 23 °C for 48 hours. The reaction was then diluted to 3 mL with additional ethyl acetate and 1.5 mL of 2.0 N NaOH was added to quench the reaction (**Warning:** Gas evolution possible). After stirring for 15 minutes, the layers were separated and the organic layer was concentrated onto silica gel to remove soluble silanol byproducts from desired phosphines using chromatography to yield pure phosphine **2a**.

1.8.27.2. Results: Our initial attempt to create a room-temperature reduction protocol combined our novel system with the phosphoric acid additive **BNPA** found to be highly effective by Beller and co-workers. Addition of **BNPA** to reductions with **DPDS** was beneficial, promoting reduction at 110 °C to completion within 2 hours (Table 1.21). Encouraged by this result, we continued with ethyl acetate as the solvent for this ambient temperature reaction, as this solvent is sourced from renewable resources. Unfortunately, only a slight excess of **DPDS** and 10 mol% loading of the additive did not furnish a reaction with high yields. This was quickly alleviated by either A) adding more additive and/or B) adding excess **DPDS**. As summarized in Table 1.22, either of these strategies resulted in a drastic increase in yield. In fact, adding more **BNPA** was the most effective way to increase the yield, as this additive likely only interacts with the silane to activate this reducing agent. Increasing both **DPDS** and **BNPA** resulted in a reaction that was done in a reasonable

amount of time which was general for a variety of phosphines. As such, reductions employing 2.5 equivalents of **DPDS** and 20 mol% of **BNPA** were selected as the optimal conditions with highly consistent results.

1.8.28. Silane Compatibility Studies:

1.8.28.1. Reactivity of DPDS with carboxylic acids

1.8.28.1.1. General Procedure: To an NMR tube was added 3-(trifluoromethyl)-benzoic acid (19 mg, 0.1 mmol), *d*₈-THF or *d*₈-Toluene (0.5 mL), and then DPDS (53 mg, 0.22 mmol). The tube was sealed with a cap and inverted three times to ensure proper mixing of the reagents and the interface between the tube and the cap was sealed with multiple layers of paraffin wax (parafilm®) to ensure no leaks. The reaction was heated to 80 °C and monitored by ¹⁹F NMR.

1.8.28.1.2. Results: Minor reactivity of **DPDS** and carboxylic acid was observed (Figure 1.49) after 40 hours. With phenylsilane, no change was not observed in ¹⁹F NMR spectra or ¹H NMR spectra when compared to the initial spectra after 40 hours of heating. Due to the lack of substantial reactivity at 80 °C within 18 hours, we believe **DPDS** can easily be employed in reactions that contain carboxylic acids.

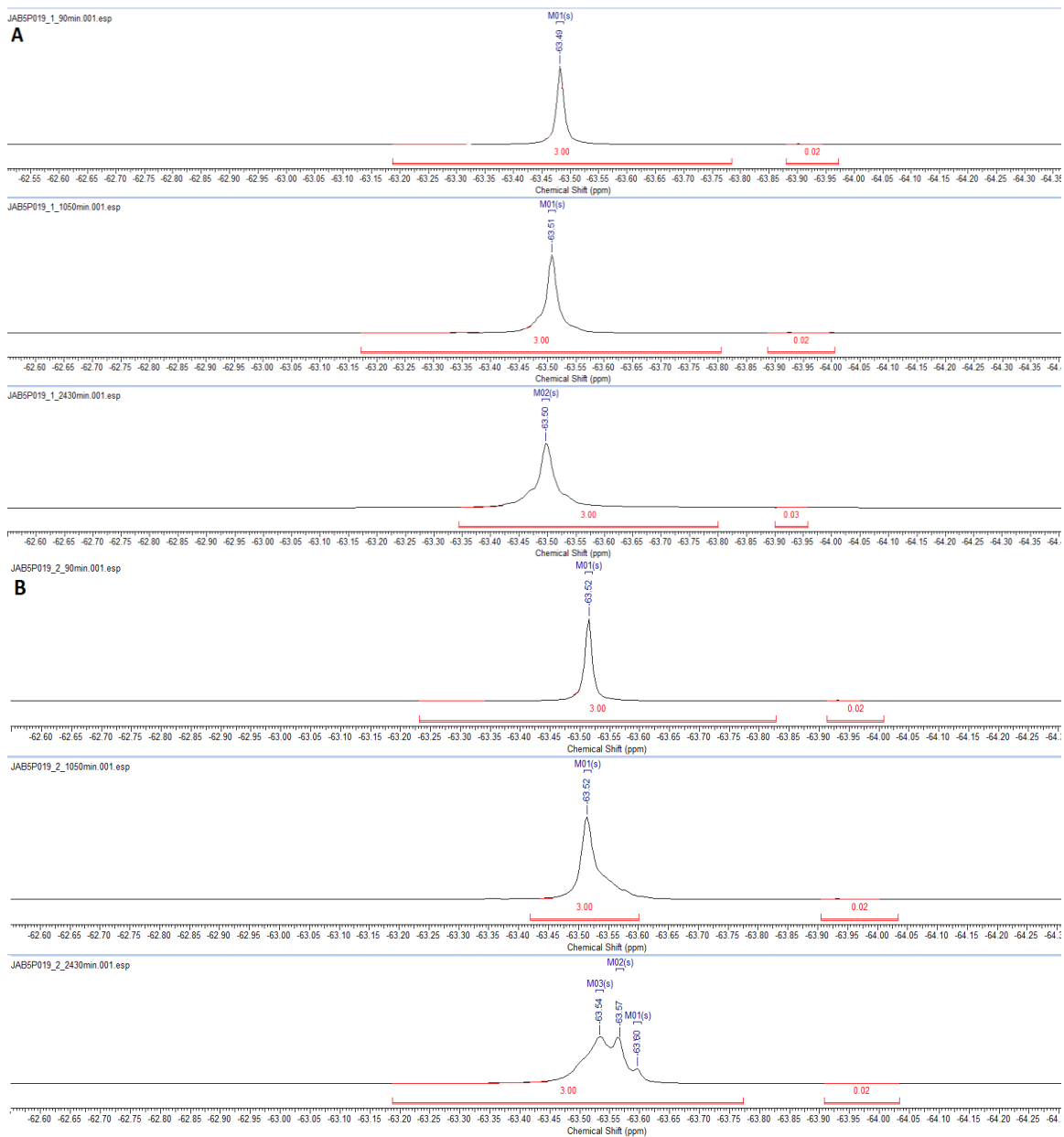


Figure 1.49. A) No reactivity of 3-(trifluoromethyl)-benzoic acid and phenylsilane is noted at 1.5 h, 17.5 h, or 40.5 h; B) Reactivity of 3-(trifluoromethyl)-benzoic acid and DPDS is not noted at 1.5 h or 17.5 h, however, reactivity is noted at 40.5 h.

1.8.28.2. Reactivity of **DPDS** with alcohols

1.8.28.2.1.1. General Procedure of Alcohol Compatibility: To an NMR tube was added *d*₈-THF (0.5 mL), 4-(trifluoromethyl)-benzyl alcohol (13.7 μL, 1.0 equiv, 0.10 mmol), hexafluorobenzene (11.5 μL, 1.0 equiv, 0.1 mmol) and **DPDS** (53 mg, 2.2 equiv, 0.22 mmol). The tube was inverted three times to ensure proper mixing of the reagents and the interface between the tube and the cap was sealed with multiple layers of paraffin wax (parafilm®) to ensure no leaks. The reactions were either left at room temperature or heated to 80 °C and monitored by ¹⁹F NMR.

1.8.28.2.1.2 General Procedure of Alcohol Compatibility with Benzoic Acids: To an NMR tube was added 3-(trifluoromethyl)-benzoic acid (19 mg, 1.0 equiv, 0.10 mmol) or *p*-nitrobenzoic acid (16 mg, 1.0 equiv, 0.10 mmol), *d*₈-THF (0.5 mL), 4-(trifluoromethyl)-benzyl alcohol (13.7 μL, 1.0 equiv, 0.10 mmol), hexafluorobenzene (11.5 μL, 1.0 equiv, 0.1 mmol) and **DPDS** (53 mg, 2.2 equiv, 0.22 mmol). The tube was inverted three times to ensure proper mixing of the reagents and the interface between the tube and the cap was sealed with multiple layers of paraffin wax (parafilm®) to ensure no leaks. The reactions were either left at room temperature or heated to 80 °C and monitored with ¹⁹F NMR.

1.8.28.2.2. Results: Previously, we reported that phenylsilane was unreactive with benzyl alcohols at elevated temperature unless a carboxylic acid such as **PNBA** was added to the reaction mixture. Due to the increased reductive potential of **DPDS** at least in terms of phosphine oxide reduction, we wanted to test whether **DPDS** reacted with alcohols and whether **PNBA** could affect the rate of that reaction. No reactivity was observed between

DPDS and the benzyl alcohol at ambient temperature for 42 hours, even in the presence of benzoic acid (Figure 1.50 and Table 1.53, entries 1–4). However, significant reactivity was observed at 80 °C (Figure 1.51), as no alcohol is observed within 40.5 hours (Table 1.53, entries 9–12). This reaction also proceeds, albeit more slowly, at 80 °C without the presence of benzoic acid (Table 1.53, entries 9–10).

Table 1.53. The reaction of 4-(trifluoromethyl)benzyl alcohol and **DPDS** or phenylsilane with or without benzoic acid additives.

Entry	Benzoic Acid	Silane	T (°C)	Time (Min)	% Alcohol Remaining
1	None	DPDS	23	1080	>95
2	None	DPDS	23	2520	>95
3	<i>p</i> -Nitrobenzoic acid	DPDS	23	1080	>95
4	<i>p</i> -Nitrobenzoic acid	DPDS	23	2520	>95
5	None	PhSiH ₃	80	1050	>95
6	None	PhSiH ₃	80	2430	>90
7	3-(Trifluoromethyl)-benzoic acid	PhSiH ₃	80	1050	79
8	3-(Trifluoromethyl)-benzoic acid	PhSiH ₃	80	2430	25
9	None	DPDS	80	1050	57
10	None	DPDS	80	2430	16
11	3-(Trifluoromethyl)-benzoic acid	DPDS	80	1050	25
12	3-(Trifluoromethyl)-benzoic acid	DPDS	80	2430	0



Figure 1.50. The reaction of 4-(trifluoromethyl)-benzyl alcohol and **DPDS** at 23 °C monitored until 42 h; B) The reaction of 4-(trifluoromethyl)-benzyl alcohol, *p*-nitrobenzoic acid, and **DPDS** at 23 °C monitored until 42 h.

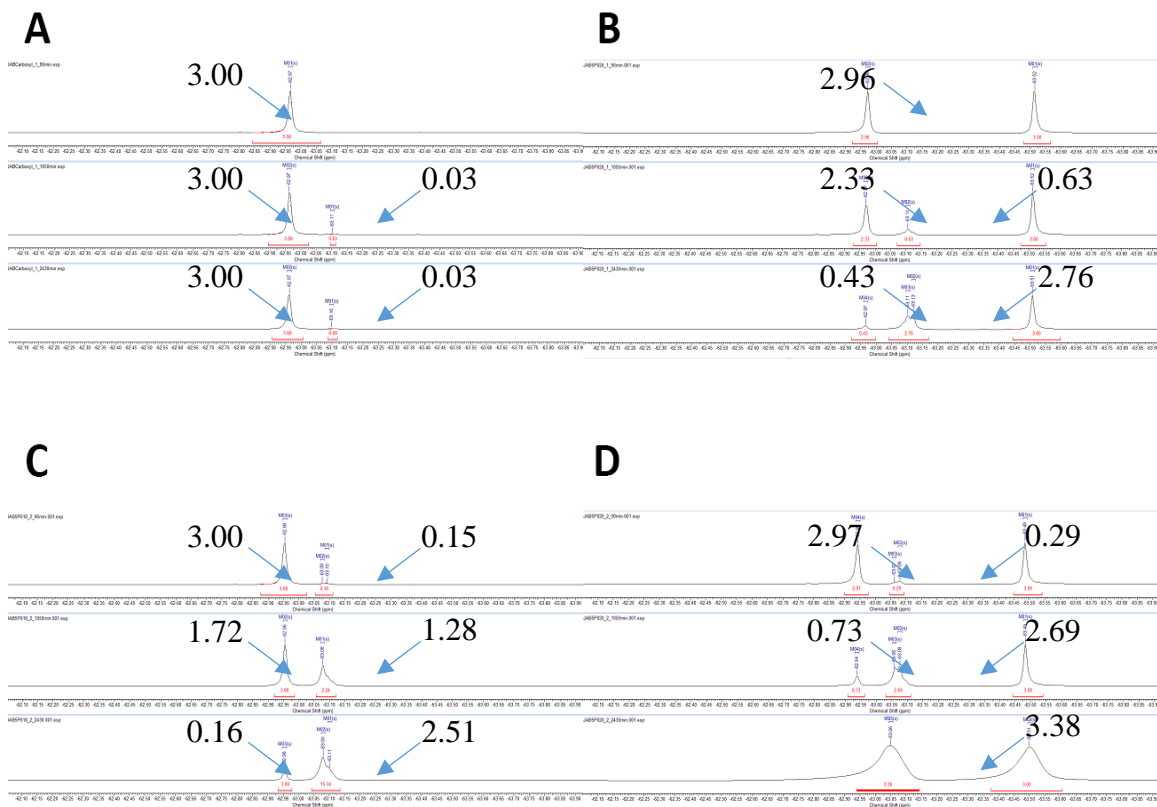


Figure 1.51. A) The reaction of 4-(trifluoromethyl)-benzyl alcohol and phenylsilane at 80 °C monitored until 40.5 h; B) The reaction of 4-(trifluoromethyl)-benzyl alcohol, 3-(trifluoromethyl)-benzoic acid, and phenylsilane at 80 °C monitored until 40.5 h; C) The reaction of 4-(trifluoromethyl)-benzyl alcohol and **DPDS** at 80 °C monitored until 40.5 h; D) The reaction of 4-(trifluoromethyl)-benzyl alcohol, 3-(trifluoromethyl)-benzoic acid, and **DPDS** at 80 °C monitored until 40.5 h. Large black numbers indicate the integrations of the peaks.

1.8.28.2.3 Recovery of alcohols which have reacted with **DPDS**

1.8.28.2.3.1. General Procedure: To an NMR tube was d_8 -PhMe (0.25 mL), 4-(trifluoromethyl)-benzyl alcohol (17 μ L, 1.0 equiv, 0.125 mmol), hexafluorobenzene (11.5 μ L, 1.0 equiv, 0.8 mmol) and **DPDS** (43 mg, 1.5 equiv, 0.1875 mmol). The tube was inverted three times to ensure proper mixing of the reagents and the interface between the tube and the cap was sealed with multiple layers of paraffin wax (parafilm®) to ensure no leaks. The reactions were either left at room temperature or heated to 110 °C. After 18 hours, the reaction was diluted by two-fold and the reaction was monitored by ^{19}F NMR. The mixture was then either concentrated onto silica gel directly, or treated with 2.0 N NaOH for 15 minutes before column chromatography.

1.8.28.2.3.2. Results: Unsurprisingly, the ^{19}F NMR spectrum produced from the crude reaction mixtures were complex, as about 55% of the starting alcohol remained. The reaction loadeds directly onto silica gel did not result in the isolation of the silyl ether compound. However, 82% of the starting alcohol was recovered unchanged. Reactions that were treated with base also did not allow for isolation of the proposed silyl ether compound; however, these reactions resulted in 100% recovery of the starting alcohol, indicating that this transient silyl ether formation is easily reversed during the course of our normal workups for reductions of phosphine oxides.

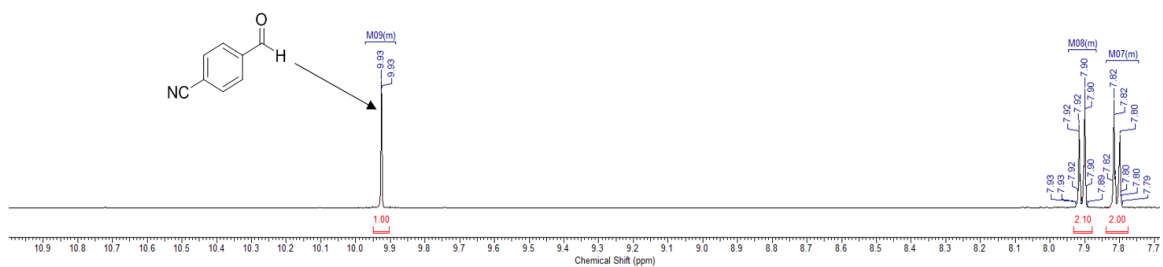
1.8.28.3. Reactivity of **DPDS** with aldehyde and cyano functional groups

1.8.28.3.1. General Procedure: To an NMR tube was added 4-cyanobenzaldehyde (13.1 mg, 1.0 equiv, 0.10 mmol), d_8 -PhMe (0.5 mL), and **DPDS** (53 mg, 2.2 equiv, 0.22 mmol).

The tube was inverted three times to ensure proper mixing of the reagents and the interface between the tube and the cap was sealed with multiple layers of paraffin wax (parafilm®) to ensure no leaks. The reaction was heated to 110 °C and monitored with ¹H NMR.

8.3.2. Results: Much like our results obtained when **DPDS** was reacted with carboxylic acids, no reduction of the benzaldehyde was observed. As shown in Figure 1.52, the reduction of the aldehyde or cyano group is not observed after 16.5 hours at 110 °C.

JABSP026_90min.003.esp



JABSP026_990min.003.esp

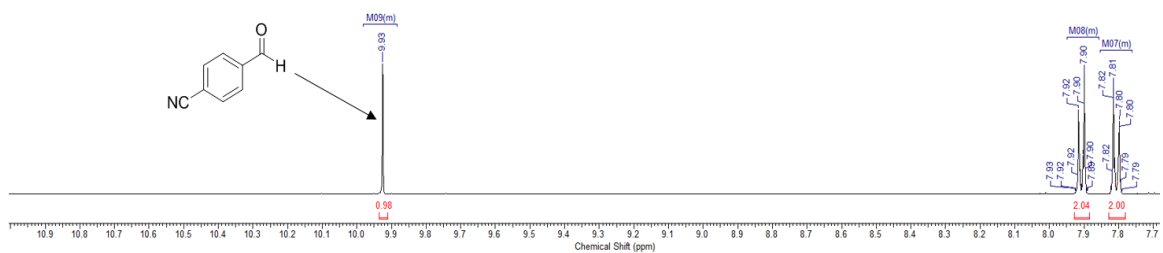


Figure 1.52. The reaction of 4-cyanobenzaldehyde and **DPDS** does not yield any new materials after 16.5 hours.

1.8.28.4. Reactivity of **DPDS** with ester and nitro functional groups

1.8.28.4.1. General Procedure: To an NMR tube was added methyl 4-nitrobenzoate (18.1 mg, 1.0 equiv, 0.10 mmol), *d*₈-PhMe (0.5 mL), and **DPDS** (53 mg, 2.2 equiv, 0.22 mmol). The tube was inverted three times to ensure proper mixing of the reagents and the interface between the tube and the cap was sealed with multiple layers of paraffin wax (parafilm®) to ensure no leaks. The reaction was heated to 110 °C and monitored with ¹H NMR.

1.8.28.4.2. Results: Much like our results obtained when **DPDS** was reacted with carboxylic acids, no reduction of the benzaldehyde was observed. As shown in Figure 1.53, the reduction of the ester or nitro group is not observed after 18 hours at 110 °C.

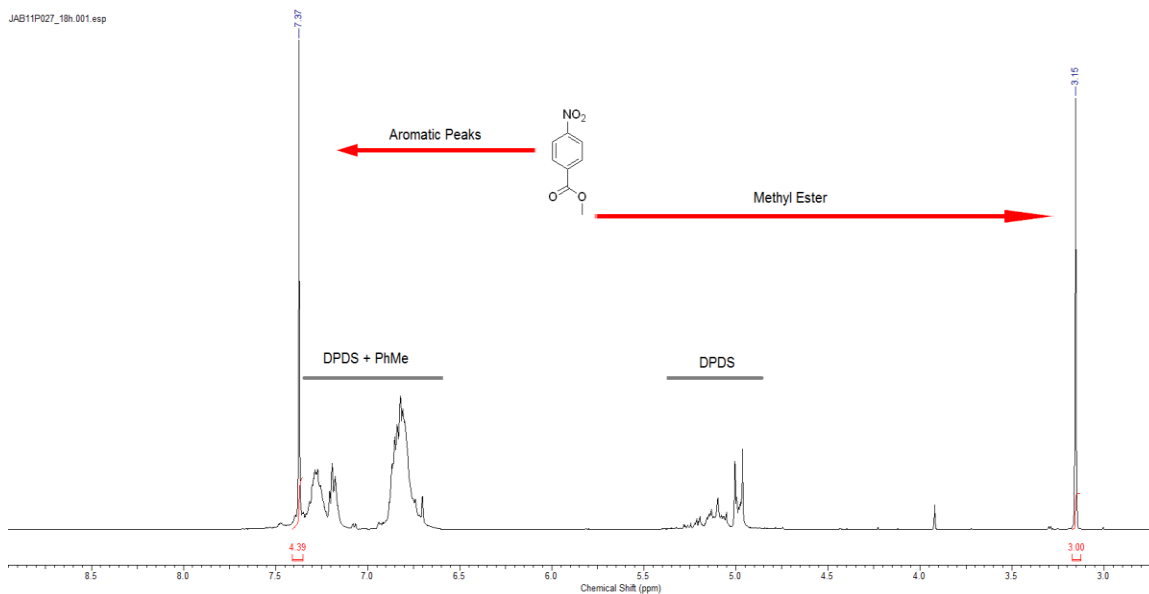


Figure 1.53. The reaction of methyl 4-nitrobenzoate and **DPDS** does not yield any new materials after 18 hours.

1.8.28.5. Reactivity of **DPDS** with α,β -unsaturated esters

1.8.28.5.1. General Procedure: To an NMR tube was added ethyl cinnamate (17.6 mg, 1.0 equiv, 0.10 mmol, 25:1 *E:Z* ratio), *d*₈-PhMe (0.5 mL), and **DPDS** (53 mg, 2.2 equiv, 0.22 mmol). The tube was inverted three times to ensure proper mixing of the reagents and the interface between the tube and the cap was sealed with multiple layers of paraffin wax (parafilm®) to ensure no leaks. After 16.5 h, the reaction mixture was cooled to ambient temperature and evaporated directly onto silica gel. The reaction was purified with a Teledyne-Isco Combi-Flash RF-200 system with 0.02:0.98 EtOAc: hexanes. Ethyl cinnamate was isolated as a colorless oil.

1.8.28.5.2. Results: Much like our results obtained when **DPDS** was allowed to react with other functional groups, no reactivity was noted. As shown in Figure 1.54, the reduction of the ester or olefin is not observed after 16.5 hours at 110 °C. In addition, isomerization of the olefin was not noted as the final product retained the initial 25:1 *E:Z* ratio.

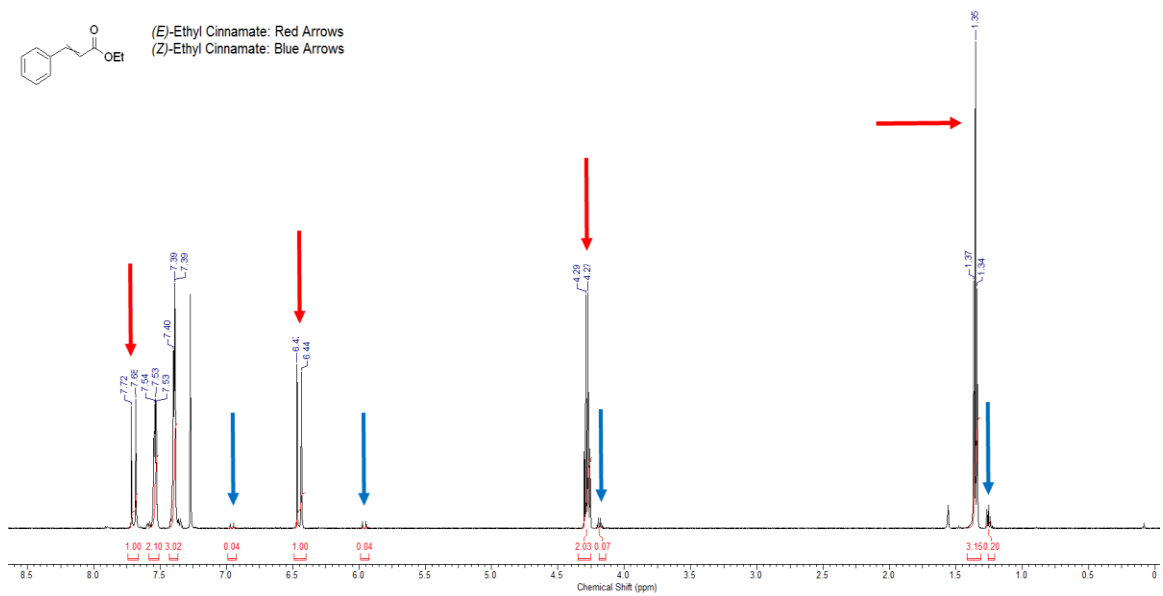


Figure 1.54. The reaction of ethyl cinnamate and **DPDS** does not yield any new materials or isomerized materials after 16.5 hours.

1.8.28.6. Reactivity of **DPDS** with azides

1.8.28.6.1. General Procedure: To an NMR tube was added 4-nitrobenzoic acid (16.7 mg, 0.1 mmol, 1.0 equiv), *d*₈-toluene (500 μL), 4-(trifluoromethyl)-benzyl azide (20.1 mg, 0.1 mmol, 1.0 equiv), and then phenylsilane (12.3 μL, 0.1 mmol, 1.0 equiv) or **DPDS** (17.7 mg, 0.073 mmol, 0.73 equiv). The tube was inverted three times to ensure proper mixing of the reagents and the interface between the tube and its cap was sealed with multiple layers of paraffin wax (parafilm®) to ensure no leaks. The reaction was heated to 110 °C. After 21 hours, the reaction cooled to room temperature and monitored by ¹⁹F NMR.

1.8.28.6.2. Results: The reduction of an azide with phenylsilane was possible, although the reaction proceeded very slowly. While only less than 15% of the azide reacted within 21 hours (Figure 1.55), this indicates that silanes in general react with azides, a feature that would not be detrimental to Staudinger reduction or ligation reactions. **DPDS** is also not a more active reductant than phenylsilane (Figure 1.55).

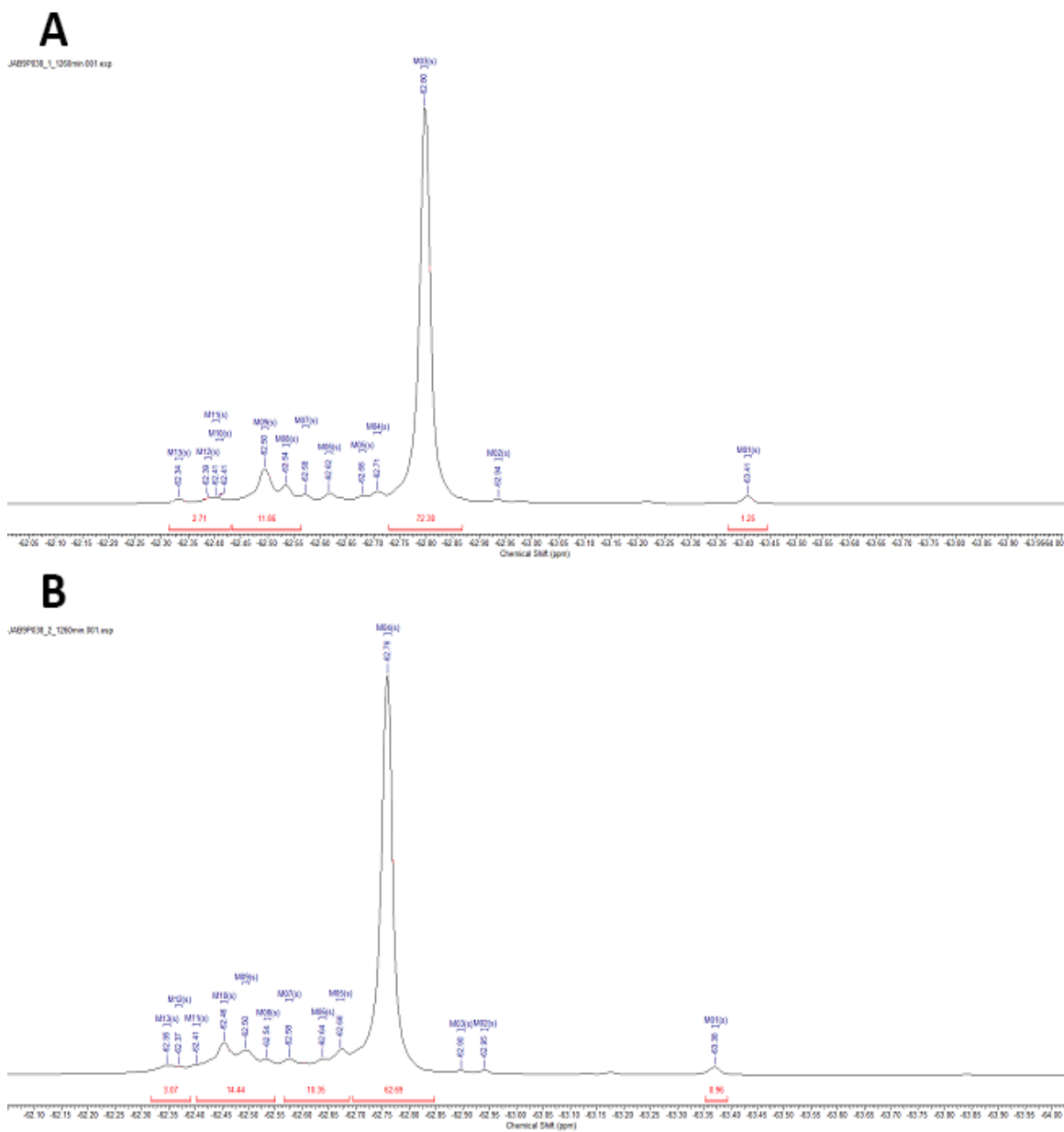


Figure 1.55. A) The reaction of 4-(trifluoromethyl)-benzyl azide and phenylsilane at 110 °C monitored until 21 h; B) The reaction of 4-(trifluoromethyl)-benzyl azide and **DPDS** at 110 °C monitored until 21 h.

1.8.28.7. Reactivity of **DPDS** with DIAD

1.8.28.7.1. General Procedure: To an NMR tube was added DIAD (4.9 μ L, 1.0 equiv, 0.025 mmol), *d*₈-THF (0.5 mL), 3-(trifluoromethyl)-benzoic acid (4.7 mg, 1.0 equiv, 0.025 mmol), and **DPDS** (13 mg, 2.3 equiv, 0.056 mmol). The tube was inverted three times to ensure proper mixing of the reagents and the interface between the tube and the cap was sealed with multiple layers of paraffin wax (parafilm®) to ensure no leaks. The reaction was heated to 80 °C and monitored by ¹H NMR through observation of a shift in ppm of the methine and methyl protons.

1.8.28.7.2. Results: No reduction of DIAD by **DPDS** was observed after 17 hours (Figure 1.56A). The addition of benzoic acid was performed to more closely mimic the conditions of a Mitsunobu reaction. The methine protons and methyl protons show no shift to the hydrazine product, which is shown in Figure 1.56B for direct comparison between these reagents.

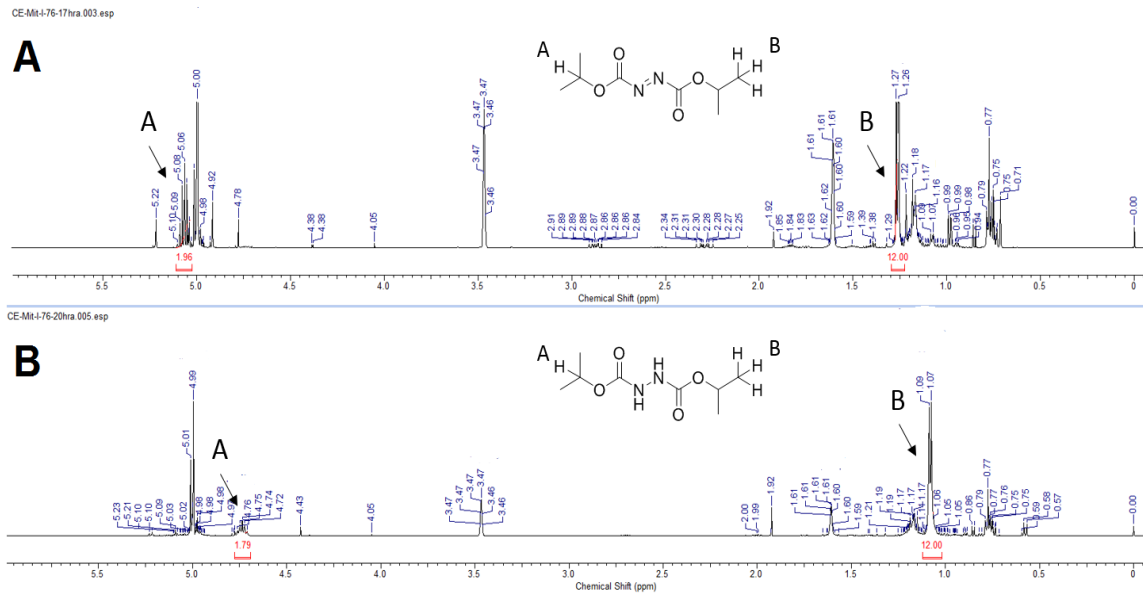


Figure 1.55. A) The reaction of **DPDS** with **DIAD** in the presence of 3-(trifluoromethyl)-benzoic acid at 80 °C after 17 hours; B) The mixture of **DPDS** and diisopropyl hydrazine dicarboxylate in d₈-THF.

1.8.29. Purification of Phosphines in Tables 1.20 and 1.23:

Triphenylphosphine¹²²: Purified with a Teledyne-Isco Combi-Flash RF-200 system with 100% hexanes. Isolated as a white solid: m.p. = 79-80 °C; all other physical data and spectra matched literature reports.

(4-(Dimethylamino)phenyl)diphenylphosphine⁷: Purified with a Teledyne-Isco Combi-Flash RF-200 system with 10:90 EtOAc: hexanes. Isolated as a white solid: all physical data and spectra matched literature reports.

(4-(Methoxy)phenyl)diphenylphosphine¹²³: Purified with a Teledyne-Isco Combi-Flash RF-200 system with 1:9 EtOAc: hexanes. Isolated as a white solid: all physical data and spectra matched literature reports.

(4-(Trifluoromethyl)phenyl)diphenylphosphine¹²⁴: Purified with a Teledyne-Isco Combi-Flash RF-200 system with 100% hexanes. Isolated as a white solid: all physical data and spectra matched literature reports.

(3,5-Bis(trifluoromethyl)phenyl)diphenylphosphine¹²⁵: Purified with a Teledyne-Isco Combi-Flash RF-200 system with 100% hexanes. Isolated as a white solid: all physical data and spectra matched literature reports.

Tris-(3,5-(trifluoromethyl)phenyl)phosphine¹²⁶: Purified with a Teledyne-Isco Combi-Flash RF-200 system with 100% hexanes. Isolated as a white solid: all physical data and spectra matched literature reports.

Tricyclohexylphosphine¹²⁷: Purified with a Teledyne-Isco Combi-Flash RF-200 system with 100% hexanes. Isolated as a white solid: all physical data and spectra matched literature reports.

[1,1'-biphenyl]-2-yl)dicyclohexylphosphine¹²⁸: Purified with a Teledyne-Isco Combi-Flash RF-200 system with 1:9 EtOAc: hexanes. Isolated as a white solid: all physical data and spectra matched literature reports.

(2',6'-dimethoxy-[1,1'-biphenyl]-2-yl)dicyclohexylphosphine¹²⁹: Purified with a Teledyne-Isco Combi-Flash RF-200 system with 1:9 EtOAc: hexanes. Isolated as a white solid: all physical data and spectra matched literature reports.

1,2-Bis(diphenylphosphino)ethane²⁵: Purified with a Teledyne-Isco Combi-Flash RF-200 system with 1:9 EtOAc: hexanes. Isolated as a white solid: all physical data and spectra matched literature reports.

rac-2,2'-Bis(diphenylphosphino)-1,1'-binaphthene²⁹: Purified with a Teledyne-Isco Combi-Flash RF-200 system with 1:9 EtOAc: hexanes. Isolated as a white solid: all physical data and spectra matched literature reports.

(9,9-Dimethyl-9H-xanthene-4,5-diyl)-bis-diphenylphosphine¹³⁰: Purified with a Teledyne-Isco Combi-Flash RF-200 system with 1:9 EtOAc: hexanes. Isolated as a white solid: all physical data and spectra matched literature reports.

1,2-Bis [(2-methoxyphenyl)(phenylphosphino)] ethane²⁵: Purified with a Teledyne-Isco Combi-Flash RF-200 system with 1:9 EtOAc: hexanes. Isolated as a white solid. All physical data and spectra matched literature reports. For reductions at elevated temperature

employing *R,R* **1m** as the substrate: the product had optical rotation $[\alpha]_D^{20} = -85.6$ ($c = 0.7$, CHCl_3). For reductions at room temperature employing *S,S* **1m** as the substrate: the product had optical rotation $[\alpha]_D^{20} = 86.2$ ($c = 0.7$, CHCl_3).

[4-(Dimethoxymethyl)phenyl]diphenylphosphine: Purified with a Teledyne-Isco Combi-Flash RF-200 system with 1:9 EtOAc: hexanes. Isolated as a white solid. ^1H NMR (CDCl_3 , 500 MHz) δ 7.33 (d, $J = 7.6$ Hz, 2H), 7.23 (s, 12H), 5.29 (s, 1H), 3.24 (s, 6H); ^{13}C (CDCl_3 , 126 MHz) δ 138.7, 137.6, 137.1, 137.0, 133.9, 133.7, 133.5, 128.8, 128.6, 128.5, 126.9, 126.8, 103.0, 52.9; ^{31}P (CDCl_3 , 202 MHz) δ -5.81; HRMS (ESI) Calc. $\text{C}_{21}\text{H}_{22}\text{O}_2\text{P}$ [M + H] 337.1352, Found 337.1368.

4-(Diphenylphosphino)benzaldehyde: Purification was not performed for this compound. The product was assessed for conversion and purity by ^{31}P NMR only. ^{31}P NMR (d_8 -PhMe, 202 MHz) δ -4.48.

(2,5-Dihydroxyphenyl)diphenylphosphine: Purified with a Teledyne-Isco Combi-Flash RF-200 system with 2:8 EtOAc: hexanes. Isolated as a white solid. ^1H NMR (d_8 -THF, 500 MHz) δ 10.38 (s, 1H), 7.82 (s, 1H), 7.61 – 7.56 (m, 4H), 7.46 (td, $J = 7.8, 3.1$ Hz, 2H) 7.39 – 7.36 (m, 4H), 6.72 (dd, $J = 8.9, 2.7$ Hz, 1H), 6.59 (dd, $J = 8.8, 5.5$ Hz, 1H), 6.38 (dd, $J = 13.9, 2.9$ Hz, 1H); ^{13}C (d_8 -THF, 126 MHz) δ 156.9, 149.8, 149.7, 133.3, 131.9, 131.8, 130.4, 128.3, 121.9, 118.8, 118.7, 116.7, 112.0, 111.2; ^{31}P (d_8 -THF, 202 MHz) δ -16.52; HRMS (ESI) Calc. $\text{C}_{18}\text{H}_{16}\text{O}_2\text{P}$ [M + H] 295.0882, Found 295.0880.

1,1'-Bis(diphenylphino)ferrocene¹³¹: Purified with a Teledyne-Isco Combi-Flash RF-200 system with 1:9 EtOAc: hexanes. Isolated as an orange solid: all physical data and spectra matched literature reports.

1.8.30. Domino Reactions of Secondary Phosphine Oxides:

1.8.30.1. General Procedure: To a 2-dram vial equipped with a ¼" teflon-coated stir bar was added diphenylphosphine oxide (**1p**, 101 mg, 0.5 mmol, 1.0 equiv), toluene (1.0 mL), and **DPDS** (144 mg, 0.625 mmol, 1.25 equiv) The reaction was sealed with a cap, purged with argon, and heated at 110 °C for 30 minutes. The reaction was then cooled to 23 °C and a stream of argon was maintained over the reaction mixture. Then, Cu(OTf)₂ (27 mg, 0.075 mmol, 0.15 equiv), *N, N*-dimethylethylenediamine (DMEDA, 11 µL, 0.1 mmol, 0.2 equiv), CsCO₃ (320 mg, 1.0 mmol, 2.0 equiv), and aryl iodides (0.5 mmol, 1 equiv) were added as a solution in 0.5 mL PhMe. The reaction was resealed while maintaining an atmosphere of argon, and was again heated to 110 °C. After 18 hours, the reaction was cooled to 23 °C and diluted to 3 mL with EtOAc. While stirring, 1.5 mL of 2.0 N NaOH was added, and the mixture was stirred for 15 minutes. The layers were separated and the organic layer was further diluted to 15 mL with EtOAc. The organic layer was then washed with 1.0 N HCl (15 mL), saturated aqueous NaHCO₃ (15 mL), and then a brine solution (15 mL). The organic layer was then dried with MgSO₄, filtered, and concentrated. The residue was purified by column chromatography to afford phosphines **2a**, **2t**, and **2u**.

1.8.30.2. Results: Unsurprisingly, this reaction is sensitive to air and/or water.³¹ As such it is necessary to maintain an inert atmosphere during the course of these reactions. Yields

for the synthesis of **2a** from **1p** and iodobenzene varied heavily depending on the reaction's atmosphere as reactions under air afforded only 36% of desired product, while reactions maintaining an inert atmosphere produced **TPP** in 78% yield.

1.8.30.3. Purification of Products in Scheme 1.11:

Triphenylphosphine¹²²: Purified with a Teledyne-Isco Combi-Flash RF-200 system with 100% hexanes. Isolated as a white solid; m.p. = 79-80 °C; all other physical data and spectra matched literature reports.

Methyl-2-(diphenylphosphino)benzoate¹³²: Purified with a Teledyne-Isco Combi-Flash RF-200 system with 1:9 EtOAc: hexanes. Isolated as a white solid: all physical data and spectra matched literature reports.

4-(Benzyloxy)phenyl)diphenylphosphine¹³³: Purified with a Teledyne-Isco Combi-Flash RF-200 system with 1:9 EtOAc: hexanes. Isolated as a white solid: all physical data and spectra matched literature reports.

1.8.31. Optimization of Disiloxane Stoichiometry in Redox Recycling Reactions

1.8.31.1. General Procedure: To a 2-dram vial equipped with a stir bar was added **IPPO** (4.5 mg, 0.025 mmol, 0.1 equiv), toluene (1 mL), benzaldehyde (25.5 μ L, 0.25 mmol, 1.0 equiv), ethyl bromoacetate (30.4 μ L, 0.275 mmol, 1.1 equiv), Hünig's base (47.5 μ L, 0.275 mmol, 1.1 equiv), and **DPDS** (60 mg, 0.25 mmol, 1.0 equiv). The reaction was sealed and stirred at 23 °C for 24 h. The reaction was then diluted with CH₂Cl₂ or acetone (5 mL) and loaded directly onto silica gel (200 mg). Individual purifications proceeded as specified.

1.8.31.2 Optimization of Silane Concentration: As **DPDS** had been previously determined to be compatible with aldehydes, the only optimization we deemed required was the number of equivalents of **DPDS**. When less than one equivalent of **DPDS** was added, the yields diminished. Table 1.24 shows the dependence of yield based on the amount of silane added. Unsurprisingly, increased silane concentration improved the yield due to faster reduction kinetics for increased turnover within the 18 hour time span. It is noteworthy that only 0.8 equivalents of **DPDS** did furnish a 46% yield in the synthesis of the trisubstituted olefin after 48 hours. Because the BRSM yield was high for our reactions, we chose the 1.0 equivalent of **DPDS** as optimal conditions for our experiments and would opt to wait 24 hours before workup.

The same trend was noted for the catalytic Staudinger reduction and catalytic Appel using the cyclic precatalyst **1PPO**. Adding excess **DPDS** did not have any real positive effect on the reaction, and only wasted more material than was necessary.

1.8.32. Reductions of Phosphinimines

1.8.32.1. Reductions of Acyclic Phosphinimines

5.1.1 ³¹P NMR Method: The NMR method is similar to the method previously reported.¹ However, a 25 second delay time was used to increase the sampling frequency with minimal error induced during integration. Spectra were also collected using a decoupled method (WALTZ 16) unless otherwise indicated to enhance the signal to noise ratios (S/N).

1.8.32.1.2. Synthesis of Phosphinimines: To a 1-dram vial was added triphenylphosphine (32.75 mg, 0.125 mmol, 0.25 M), *d*₈-toluene (500 μL), and then benzylazide (15.6 μL, 0.25

mmol, 0.25 M). The vial was mixed using a vortex to ensure proper mixing of the reagents and the interface between the tube and the cap was sealed with multiple layers of paraffin wax (parafilm®) to ensure no leaks. The reaction was heated to 60 °C and monitored with ³¹P NMR, although reactions are complete at approximately 90 minutes.

1.8.32.1.3. Reductions of Phosphinimines with DPDS: To an NMR tube was added phosphinimine solution as defined in section 5.2 (100 μL, 0.025 mmol, 0.05 M), *d*₈-toluene (342 μL, final volume is 500 μL), and then **DPDS** (57.5 mg, 0.25 mmol, 0.5 M). The tube was inverted three times to ensure proper mixing of the reagents and the interface between the tube and the cap was sealed with multiple layers of paraffin wax (parafilm®) to ensure no leaks. The reaction was heated to the desired temperature and monitored with ³¹P NMR. To ensure accuracy during time points, reactions were chilled to -10 °C to stall the reaction for data collection.

1.8.32.1.4. Reductions of Phosphinimines with Phenylsilane: To an NMR tube was added phosphinimine solution as defined in section 5.2 (100 μL, 0.025 mmol, 0.05 M), *d*₈-toluene (363 μL, final volume is 500 μL), and then phenylsilane (37 μL, 0.25 mmol, 0.5 M). The tube was inverted three times to ensure proper mixing of the reagents and the interface between the tube and the cap was sealed with multiple layers of paraffin wax (parafilm®) to ensure no leaks. The reaction was heated to the desired temperature and monitored with ³¹P NMR. To ensure accuracy during time points, reactions were chilled to -10 °C to stall the reaction for data collection.

1.8.32.1.5. Results: We started by monitoring the reduction of an acyclic phosphinimine with **DPDS** at five temperatures (± 0.5 °C) over a range of 23 – 70 °C. Reductions were

$$k_{obs} = \frac{\ln([Phosphine]) - c}{time} \quad (1)$$

$$k = \frac{k_{obs} - c}{[phenylsilane]} \quad (2)$$

$$\ln(k) = \frac{-E_a}{R} \times \frac{1}{Temperature} + \ln(A) \quad (3)$$

$$\ln(k) = \frac{-\Delta H^\ddagger}{R} \times \frac{1}{Temperature} + \frac{\ln k_B}{h} + \frac{\Delta S^\ddagger}{R} \quad (4)$$

performed under pseudo first-order conditions and were carried out in triplicate. The rate of reduction for individual reactions were calculated as pseudo first-order rate constants by creating linear plots of raw data (Equation 1). The observed rate constants (k_{obs}) of individual trials were then averaged and a second-order rate constant (k) was obtained by calculating the slope of the line generated by the plot of k_{obs} vs. the concentration of reducing agent (Equation 2). These second-order rate constants at each temperature were then utilized in an Arrhenius plot and a line was fit (Equation 3) to determine the coefficient (A) and energy of activation (E_a) for reduction. This Arrhenius analysis determined the energy of activation to be 12.4 ± 0.4 kcal/mol while Eyring analysis (Equation 4) shown in Figure 1.32 also agreed with this finding as $\Delta H^\ddagger = 21.9 \pm 3.6$ kcal/mol, $\Delta S^\ddagger = 21.9 \pm 3.6$ kcal/mol, and $\Delta G^\ddagger = 21.9 \pm 3.6$ kcal/mol.

While the Arrhenius and Eyring analyses of the reduction with DPDS indicate that the reduction can readily occur at room temperature, these energies are not overly different from our results with phosphine oxides. However, unlike our studies with phosphine oxides, the reduction of a phosphinimine with phenylsilane can readily occur with the addition of heat. At room temperature, the reduction is very sluggish (Table 1.30), so much so that phenylsilane would not be applicable for the design of a catalytic Staudinger reduction without an additive.

1.8.32.2. Reactivity of **DPDS** with DIAD

1.8.32.2.1. General Procedure: To an NMR tube was added DIAD (4.9 μ L, 1.0 equiv, 0.025 mmol), *d*₈-THF (0.5 mL), 3-(trifluoromethyl)-benzoic acid (4.7 mg, 1.0 equiv, 0.025 mmol), and **DPDS** (13 mg, 2.3 equiv, 0.056 mmol). The tube was inverted three times to ensure proper mixing of the reagents and the interface between the tube and the cap was sealed with multiple layers of paraffin wax (parafilm®) to ensure no leaks. The reaction was heated to 80 °C and monitored by ¹H NMR through observation of a shift in ppm of the methine protons and terminal methyl protons. After 2.5 h, the NMR tube was cooled to 23 °C, opened, and **TMPPPO** (1 mg, 0.2 equiv, 0.005 mmol) was added. The tube was resealed, mixed, heated to a desired temperature, and monitored by ¹H NMR.

1.8.32.2.2. Results: No reduction of DIAD by **DPDS** was observed prior to **TMPPPO** addition.⁶⁴ The addition of benzoic acid was attempting to model the conditions of the Mitsunobu reaction. However, 90 min following addition of **TMPPPO**, significant reduction of DIAD was observed when heated to 80 °C, and, 20 hours following the

addition of **TMPPPO**, no DIAD remained (Figure 1.30) at room temperature (23 °C). **TMPPPO**, following addition, would be quickly reduced to a phosphine, where it could attack DIAD, forming a P-N bond. However, due to the lack of an alcohol, this species is unproductive, and does not lead to any further reactivity.¹³⁴ The addition of only 0.2 equivalents of **TMPPPO** confirms that the ¹H shift observed is not just due to P-N bond formation, but rather must be a phosphine-mediated reduction of DIAD by **DPDS**. We speculate that **DPDS** reduces the P-N bond, similarly to the reactivity observed with other phosphinimines.

1.8.33. Investigation of the Catalytic Staudinger Ligation with Triphenylphosphine

1.8.33.1 Limited Activation Occurs with Additives Reported by Ashfeld & Coworkers⁸⁵

1.8.33.1.1. General Procedure: To an NMR tube was added **TPPO** (4.2 mg, 0.015 mmol, 0.03 M), *d*₈-toluene (500 mL), **PNBA** (30 mg, 0.18 mmol, 0.36 M), and PhSiH₃ (19 mL, 0.15 mmol, 0.3 M) followed by *N*-benzylmethylamine (19 μL, 0.15 mmol, 0.3 M). The tube was inverted three times to ensure proper mixing of the reagents and the interface between the tube and its cap was sealed with multiple layers of paraffin wax (parafilm®) to ensure no leaks. The reaction was heated to 60 °C and monitored by ³¹P NMR.

1.8.33.1.2. Results: Phosphorous NMR was taken after 16 hours, after which 49% reduction of the TPPO was observed. This NMR tube is meant to provide a “best-case” scenario for the reaction reported by Ashfeld, as in it all of the azide would have been reduced to amine, producing carboxylate in combination with **PNBA**. The carboxylate formed would obviously produce substantially more reduction, as demonstrated

previously. However, even though reduction was observed, obtaining only 49% of triphenylphosphine after 16 hours means that a full equivalent of **TPPO** would not be reduced over this time period even if the all phosphine-imine formed instantly performed the aza-Wittig, and was thus converted to TPPO. With the mechanism reported by Ashfeld, and assuming the conditions reported are realistic (they are not, again this is a best-case scenario for reduction), the maximum possible amount of turnover that could be obtained would be twice the catalyst loading. Since Ashfeld and coworkers report substantially higher amounts of turnover, this experiment provides strong evidence that the reaction does not go through their proposed mechanism.

1.833.2. Investigation of Ashfeld's Conditions⁸⁵

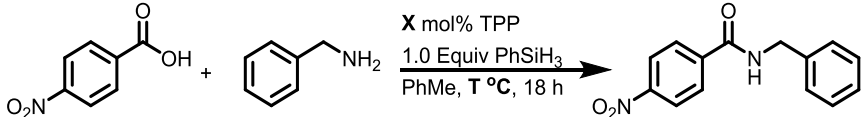
1.8.33.2.1. General Procedure of Catalytic Staudinger Ligations: To a 2-dram vial equipped with a stir bar was added 4-nitrobenzoic acid (50a mg 0.3 mmol, 1.0 equiv.), **TPP** (13 mg, 0.05 mmol, 0.17 equiv.) or **TPPO** (13.8 mg, 0.05 mmol, 0.17 equiv.), toluene (1 mL), benzyl azide (45 μ L, 0.36 mmol, 1.2 equiv.) followed by phenylsilane (36 μ L, 0.3 mmol, 1.0 equiv.). The reaction was sealed and stirred at various temperatures. After 18 h, the reaction was diluted with acetone (5 mL) and loaded directly onto silica gel (200 mg). Purification by flash column chromatography (0–50% EtOAc:hexanes eluent, step-wise gradient, 10% EtOAc incremental increase every 6 column volumes) afforded the product.

1.8.33.2.2. General Procedure of Stoichiometric Staudinger Ligations: To a 2-dram vial equipped with a stir bar was added 4-nitrobenzoic acid (50.1 mg, 0.3 mmol, 1.0 equiv.), **TPP** (88mg, 0.33 mmol, 1.1 equiv.) toluene (1 mL), and then benzyl azide (45 μ L, 0.36

mmol, 1.2 equiv.). The reaction was sealed and stirred at various temperatures. After 18 h, the reaction was diluted with acetone (5 mL) and loaded directly onto silica gel (200 mg). Purification by flash column chromatography (0–50% EtOAc:hexanes eluent, step-wise gradient, 10% EtOAc incremental increase every 6 column volumes) afforded the product.

1.8.33.2.3. Results: The reaction as reported by Ashfeld works well enough, though we were unable to reproduce the yields reported in their communication (Table 1.54). Since substantially greater than 34% turnover is being observed, it is not likely that **TPPO** is the main species being reduced by the silanes. Using **TPPO** as the precatalyst significantly lowered the yield of the reaction, even with increasing the reaction time from 18 to 24 hours.

Table 1.54. Catalytic and Stoichiometric Staudinger Ligation Reactions.



Entry	Phosphine	X =	Silane	Temp. (°C)	Isolated Yield
1	TPP	17 mol%	Yes	60	62
2	TPPO	17 mol%	Yes	60	23 ³
3	TPP	17 mol%	Yes	110	65
4	TPP	17 mol%	No	60	0 ⁴
5	TPP	110 mol%	No	23	0 ⁵
6	TPP	110 mol%	No	60	0
7	TPP	110 mol%	No	110	0

³ Reaction for 24 hours

⁴ Obtained 16% yield of primary amine

⁵ Obtained quantitative yield of primary amine

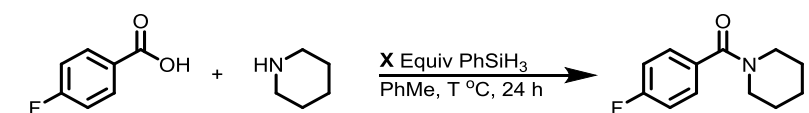
In addition to the previous results, we desired to test whether the reaction would succeed with a stoichiometric amount of phosphine, but removing the silane. Regardless of the temperature used, using a slight excess of **TPP** lead to none of the desired ligated product. If the mechanism proposed by Ashfeld were at play, the reaction should proceed smoothly once the phosphine imine is formed. However, at 60 °C the ligated product cannot be isolated when no silane is added. It is likely that the Staudinger ligation only occurs when the carboxylate is attached to the phosphine imine generated, as in the case of the reagents utilized by Bertozzi and co-workers in bioorthogonal reactions.¹³⁵

1.8.33.3. Silane-Mediated Amide Couplings

1.8.33.3.1. General Procedure of Silane-Mediated Amide Bond Formation: To a 2-dram vial equipped with a stir bar was added 4-fluorobenzoic acid (35 mg 0.25 mmol), toluene (1 mL), piperidine (0.3 mmol) and phenylsilane (See table S6 for equivalence). The reaction was sealed and stirred at various temperatures. Aliquots (50 μ L) of each reaction were pulled for analysis by ¹⁹F NMR before workup. After 20 h, the reaction was diluted with acetone (5 mL) and loaded directly onto silica gel (200 mg). Purification by flash column chromatography (0–20% EtOAc:hexanes eluent, step-wise gradient, 5% EtOAc incremental increase every 6 column volumes) afforded the product.

1.8.33.3.2. Results: The reactions of amines and carboxylic acids proceeds to the amide when a silane and heat are added to the reaction mixture. The reaction to form the amide results in quantitative yields when an excess of phenylsilane is added to reactions heated to 80 °C or above (Table 1.55).

Table 1.55. Silane dependent amide bond formation.



Entry	X =	T =	Isolated Yield
1	1.0	110	87
2	1.5	110	Quant.
3	2.0	110	Quant.
4	1.5	80	Quant.
5	1.5	37	Trace
6	1.5	23	Trace
7	0.0	80	0

1.8.33.3.3. Silane Screen in Amide Coupling Reactions

1.8.33.3.3.1. General Procedure of Silane Screen in Amide Couplings: To a 2-dram vial equipped with a stir bar was added 4-nitrobenzoic acid (50.1 mg, 0.3 mmol, 1.0 equiv.), toluene (1 mL), 4-methoxybenzyl amine (46.6 μ L, 0.36 mmol, 1.2 equiv.), and then silane (0.3 mmol, 1.0 equiv.). The reaction was sealed and stirred at 60 °C. After 18 h, the reaction was diluted with acetone (5 mL) and loaded directly onto silica gel (200 mg). Purification by flash column chromatography (0–50% EtOAc:hexanes eluent, step-wise gradient, 10% EtOAc incremental increase every 6 column volumes) afforded the product. NMR Spectra and other physical data matched previous reports.¹³⁶

1.8.33.3.3.2. Results: Similar to the results obtained previously,¹³⁷ the amide couplings with phenylsilane proceeded smoothly and formed product in similar amounts as Ashfeld's ligation reaction. The reaction with 1.0 equivalent phenylsilane alone at 60 °C (comparable to Ashfeld's report) produced the benzyl benzoyl amine in approximately 50% yield, while the reactions with trimethoxysilane and diethoxymethylsilane did not produce any amide product. It seems that the phenyl substituent on the silane is necessary for the formation of the "activated" ester which is necessary to form the amide. Unfortunately, we were unable to isolate the acyloxysilane intermediate that we and others propose is necessary for the amide coupling reaction.

1.8.33.4. Remarks on the Catalytic Staudinger Ligation: While the reaction observed by Ashfeld and co-workers is feasible, however, the likelihood that the reaction occurs via the mechanism proposed in the original communication is low. Since the reaction works

significantly better employing the phosphine at beginning, it is likely that the phosphine imine actually what is being reduced by the silane, giving the amine and triphenylphosphine. The carboxylic acid can react with the silane to become activated for coupling with the nucleophilic amine, kicking out a silanol and the amide product. Having the amine intermediate, carboxylic acid, and the silanol certainly indicate that the **TPP** could be recycled under these conditions, while the stoichiometric reactions indicate that the **TPP** is only involved in the reduction of the azide rather than the amide bond formation. Ashfeld's reaction was likely serendipitous and likely proceeds via the mechanism proposed by Denton and co-workers.⁸¹

1.8.34. General Procedures

1.8.34.1. Catalytic Wittig Reactions with 1-PPO and DPDS: To a 2-dram vial equipped with a stir bar was added all solid reagents (Aldehyde: 0.25 mmol, 1 equiv; Bromide: 0.275 mmol, 1.1 equiv), followed by **1PPO** (4.5 mg, 0.025 mmol, 0.1 equiv), toluene (1 mL), all liquid reagents (Aldehyde: 0.25 mmol, 1 equiv; Bromide: 0.275 mmol, 1.1 equiv), Hünig's base (47.5 μ L, 0.275 mmol, 1.1 equiv), and **DPDS** (60 mg, 0.25 mmol, 1.0 equiv). The reaction was sealed and stirred at 23 °C for 24-48 h. The reaction was then diluted with CH₂Cl₂ or acetone (5 mL) and loaded directly onto silica gel (200 mg). Individual purifications proceeded as specified.

1.8.34.2. Catalytic Wittig Reactions with TPP and DPDS: To a 2-dram vial equipped with a stir bar was added all solid reagents (Aldehyde: 0.25 mmol, 1 equiv; Bromide: 0.275 mmol, 1.1 equiv), followed by **TPP** (6.6 mg, 0.025 mmol, 0.1 equiv), C₂H₄Cl₂ (1 mL),

Hünig's base (47.5 μ L, 0.275 mmol, 1.1 equiv), and **DPDS** (60 mg, 0.25 mmol, 1.0 equiv). The reaction was sealed and stirred at 80 °C for 24-48 h. The reaction was then diluted with DCM or acetone (5 mL) and loaded directly onto silica gel (200 mg). Individual purifications proceeded as specified.

1.8.34.3. Catalytic Staudinger Reductions with **1-PPO** and **DPDS**: To a 2-dram vial equipped with a stir bar was added all solid reagents (Azide: 0.25 mmol, 1.0 equiv), **1PPO** (4.5 mg, 0.025 mmol, 0.1 equiv), toluene (1 mL), all liquid reagents (Azide: 0.25 mmol, 1.0 equiv), and then **DPDS** (57.5 mg, 0.25 mmol, 1.0 equiv). The reaction was sealed and stirred at ambient temperature (23 °C) for 24 h. The reaction was diluted with acetone, and the vessel was washed with acetone (7.5 mL) and loaded directly onto silica gel (200 mg). Purification by flash column chromatography (0–50% EtOAc:hexanes eluent, step-wise gradient, 10% EtOAc incremental increase every 6 column volumes) afforded the product.

1.8.34.4. Catalytic Staudinger Reductions with **TTP** and **DPDS**: To a 2-dram vial equipped with a stir bar was added all solid reagents (Azide: 0.25 mmol, 1.0 equiv), **TTP** (6.6 mg, 0.025 mmol, 0.1 equiv), toluene (1 mL), all liquid reagents (Azide: 0.25 mmol, 1.0 equiv), and then **DPDS** (57.5 mg, 0.25 mmol, 1.0 equiv). The reaction was sealed and stirred at ambient temperature (23 °C) for 48 h. The reaction was diluted with acetone, and the vessel was washed with acetone (7.5 mL) and loaded directly onto silica gel (200 mg). Purification by flash column chromatography (0–50% EtOAc:hexanes eluent, step-wise gradient, 10% EtOAc incremental increase every 6 column volumes) afforded the product.

1.8.34.5. Catalytic Appel Halogenation Reactions with **DPDS**: To a 2-dram vial equipped with astir bar was added **1PPO** (4.5 mg, 0.025 mmol, 0.1 equiv.) or **TMPPPO** (5.4 mg, 0.025 mmol, 0.1 equiv.), MeCN (1 mL), alcohol (0.25 mmol, 1.0 equiv.), diethyl bromomalonate (64 μ L, 0.375 mmol, 1.5 equiv.), and then **DPDS** (60 mg, 0.25 mmol, 1.0 equiv.). The reaction was sealed and stirred at ambient temperature (23 $^{\circ}$ C) for 24 h. The reactions were purified as specified.

1.8.34.6. Carboxamide Reductions of Tertiary Amides with Zn^{2+} and **DPDS**: To a 2-dram vial equipped with astir bar was added **1PPO** (4.5 mg, 0.025 mmol, 0.1 equiv.) or **TMPPPO** (5.4 mg, 0.025 mmol, 0.1 equiv.), MeCN (1 mL), alcohol (0.25 mmol, 1.0 equiv.), diethyl bromomalonate (64 μ L, 0.375 mmol, 1.5 equiv.), and then **DPDS** (60 mg, 0.25 mmol, 1.0 equiv.). The reaction was sealed and stirred at ambient temperature (23 $^{\circ}$ C) for 24 h. The reactions were purified as specified.

1.8.34.7. Carboxamide Reducions of Secondary Amids with Zn^{2+} and **DPDS**: To a 2-dram vial equipped with astir bar was added **1PPO** (4.5 mg, 0.025 mmol, 0.1 equiv.) or **TMPPPO** (5.4 mg, 0.025 mmol, 0.1 equiv.), MeCN (1 mL), alcohol (0.25 mmol, 1.0 equiv.), diethyl bromomalonate (64 μ L, 0.375 mmol, 1.5 equiv.), and then **DPDS** (60 mg, 0.25 mmol, 1.0 equiv.). The reaction was sealed and stirred at ambient temperature (23 $^{\circ}$ C) for 24 h. The reactions were purified as specified.

1.8.34.8. One-Pot Reductive Amine Alkylations with **DPDS**: To a 2-dram vial equipped with astir bar was added **1PPO** (4.5 mg, 0.025 mmol, 0.1 equiv.) or **TMPPPO** (5.4 mg, 0.025 mmol, 0.1 equiv.), MeCN (1 mL), alcohol (0.25 mmol, 1.0 equiv.), diethyl

bromomalonate (64 μ L, 0.375 mmol, 1.5 equiv.), and then **DPDS** (60 mg, 0.25 mmol, 1.0 equiv.). The reaction was sealed and stirred at ambient temperature (23 $^{\circ}$ C) for 24 h. The reactions were purified as specified.

1.8.35. Purification of Olefin Products:Ethyl (E)-cinnamate: NMR Spectra and other physical data matched previous reports.¹³⁸

Diphenyl-propen-3-one: NMR Spectra and other physical data matched previous reports.¹³⁹

Ethyl (E)-*p*-methoxycinnamate: NMR Spectra and other physical data matched previous reports.¹⁴⁰

Ethyl (E)-*p*-cyanocinnamate: NMR Spectra and other physical data matched previous reports.¹³⁹

Methyl (E)-3-(*p*-cyanophenyl)-2-methylpropenoate: NMR Spectra and other physical data matched previous reports.¹⁴¹

1.8.36. Purification of Amine Products: All purification were performed using a Teledyne Isco Retrieve[®] Flash chromatography Instrument using an isocratic eluent with 60:40 hexanes: EtOAc supplanted with 5% triethylamine.

Benzylamine: NMR Spectra and other physical data matched previous reports.¹⁴²

3-Nitrobenzylamine: NMR Spectra and other physical data matched previous reports.¹⁴²

9.3. 4-(Trifluoromethyl)benzylamine: NMR Spectra and other physical data matched previous reports.¹⁴²

9.4. 4-Methoxybenzylamine: NMR Spectra and other physical data matched previous reports.¹⁴²

9.5. 4-Ethynylaniline: NMR Spectra and other physical data matched previous reports.¹⁴²

9.6. 3-Methoxyaniline: NMR Spectra and other physical data matched previous reports.¹⁴²

9.7. 1-Amino-3-chloropropan-2-ol Hydrochloride: NMR Spectra and other physical data matched previous reports.¹⁴³

1.8.37. Purification of Bromide Products

1-Bromobutane: Purification by fractional distillation under reduced atmosphere (22 mmHg). Unreacted butanol and acetonitrile was removed at approximately 5–7 °C and 1-bromobutane was obtained at approximately 14–15 °C as a colorless oil (52 mg, 76% yield). All spectra and physical data matched previous reports.¹⁴⁴

1-Bromo-2-phenylethane: Reactions were loaded directly onto silica gel (250 mg). Purification by flash column chromatography (0–20% EtOAc:hexanes eluent, step-wise gradient, 5% EtOAc incremental increase every 6 column volumes) afforded the title compound (70.5 mg, 73%) as a pale yellow oil. All spectra and physical data matched previous reports.¹⁴⁵

1-Bromo-1-phenylethane: Reactions were loaded directly onto silica gel (250 mg). Purification by flash column chromatography (0–20% EtOAc:hexanes eluent, step-wise gradient, 5% EtOAc incremental increase every 6 column volumes) afforded the title compound (25 mg, 27% yield) as a pale yellow oil: $R_f = (1:4 \text{ EtOAc:hexanes})$. All spectra and physical data matched previous reports.¹⁴⁶

II. Rationally Designed Medicinal and Chemical-Biological agents with intentional Selectivity Profiles

2.1 Introduction

Tuberculosis (TB) has plagued mankind for millennia and is currently the leading cause of infectious disease mortality and morbidity worldwide, being responsible for over 1.8 million deaths in 2015.¹⁴⁷ It is primarily caused by *Mycobacterium tuberculosis* (*Mtb*), an extremely slow-growing bacillus that requires extended periods of treatment and is impervious to most conventional anti-bacterials.¹⁴⁸ The introduction of antibiotics combined with public practices specifically aimed to prevent the transmission of TB led to a near-eradication of the disease from industrialized nations in the 20th century.¹⁴⁹ However, the last approved first-line drug for TB chemotherapy, Rifampin, was introduced in 1968. Combined with the necessary treatment time, the dearth of new antibiotics has led to the development of multiple drug-resistant TB strains.¹⁵⁰ In fact, reports over the last half century confirm the development of resistance to all first- and second-line antitubercular agents. The first line agents (Figure 2.1), rifampicin (RIF), isoniazid (INH), ethambutol (EMB), and pyrazinamide (PZA), are all administered simultaneously for the first 2 months of treatment.¹⁴⁸ Then, INH and RIF are administered simultaneously for the remainder of the treatment regimen, lasting up to 24 months.¹⁵¹ This long treatment period often results in non-compliance, exacerbating the development of resistance and facilitating continuous spread of the pathogen.

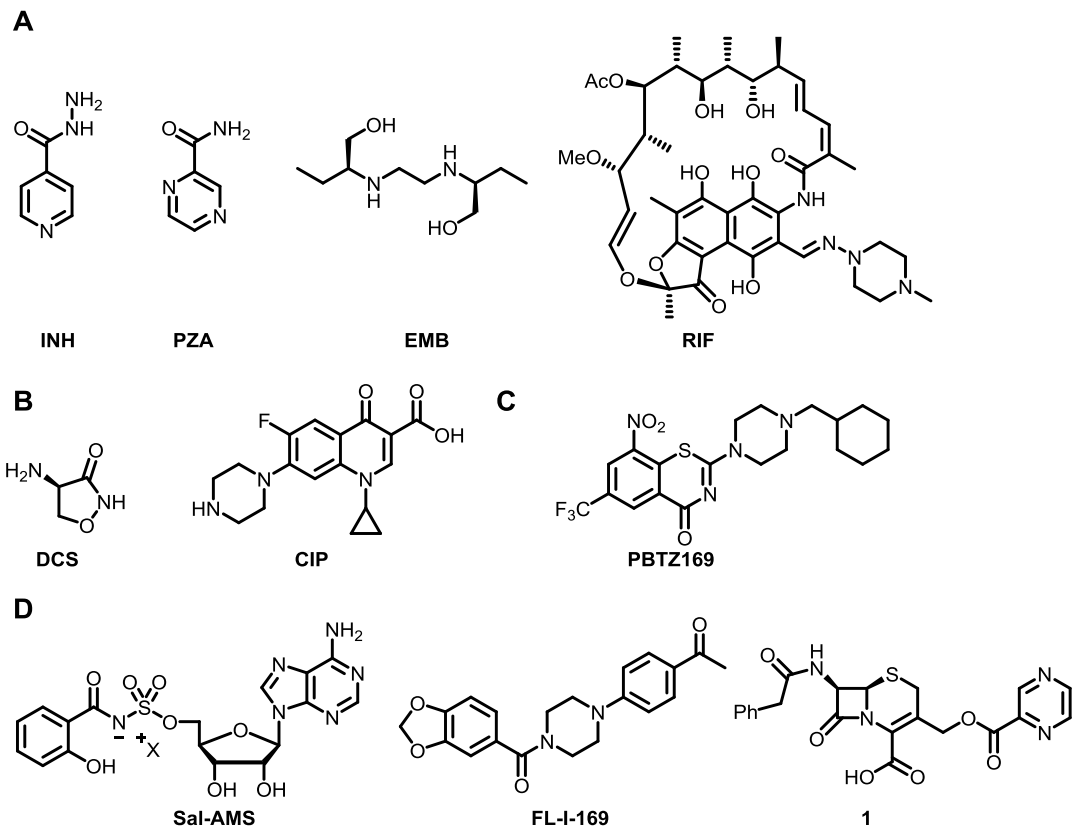
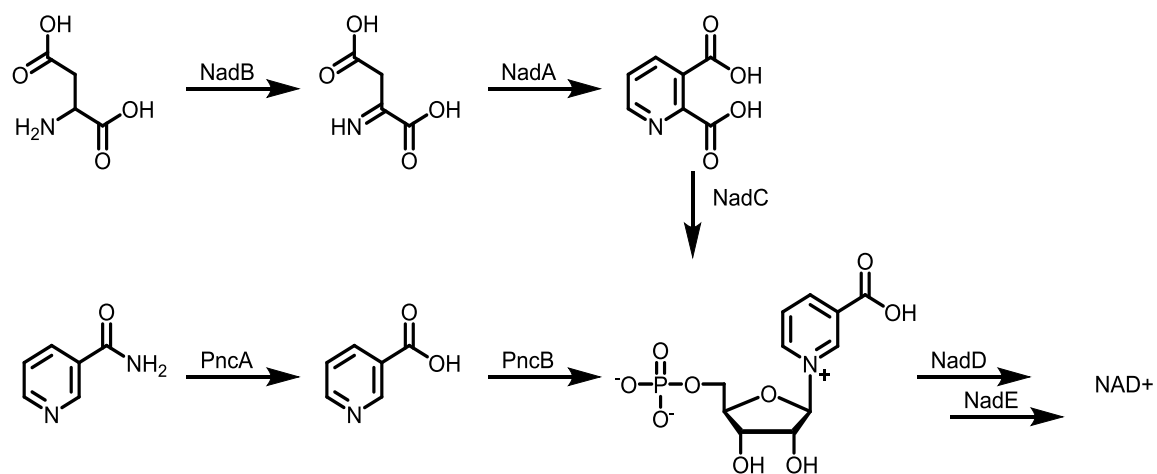


Figure 2.1. Chemotherapeutic agents with effectiveness against *Mtb*; A) Clinically-used first line agents; B) Clinically-used reserve agents; C) Experimental agents in pre-clinical development; D) Experimental agents in development in the Aldrich Laboratory (ca. 2006-2016).

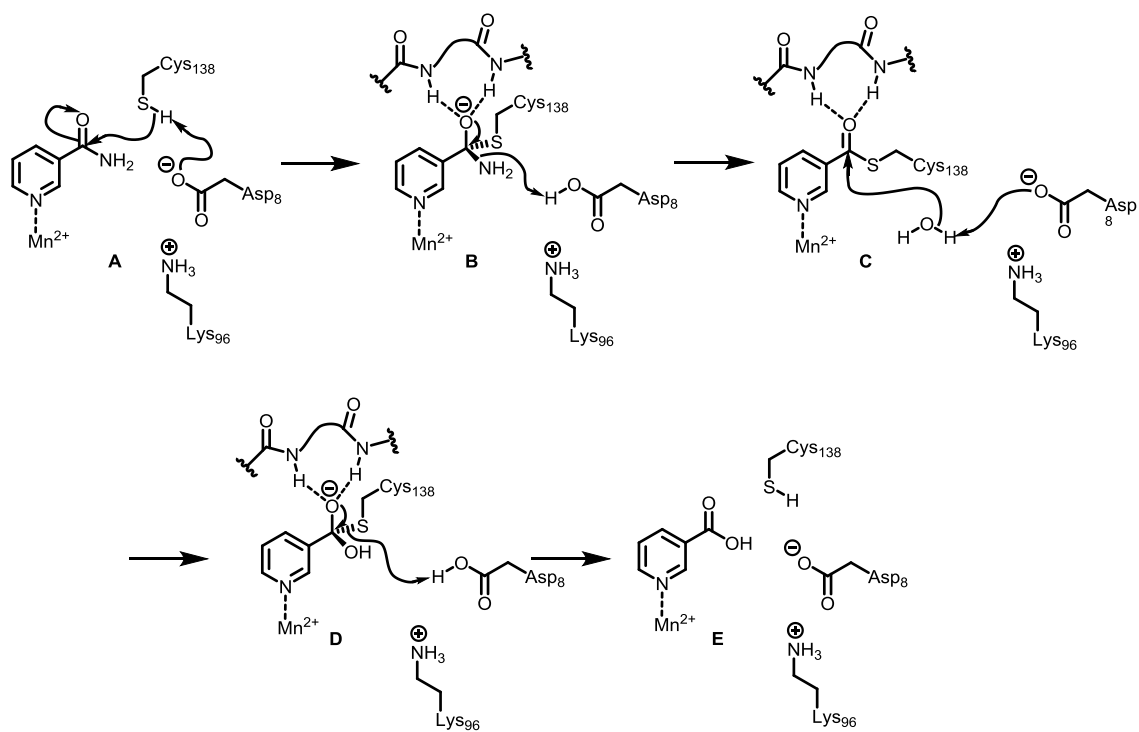
The antitubercular agent PZA is arguably the most important drug within the frontline cocktail of treatment. PZA, unlike any of the other molecules, is specifically active in non-replicating *Mtb*, especially those residing in macrophages. This unique activity helps shorten the course of treatment substantially, promoting as short as a 6 month treatment in drug susceptible strains versus the necessary 1+ years needed for treatment without PZA. PZA is a remarkable drug in that it is significantly more potent *in vivo* compared to *in vitro*. Intriguingly, in order to study the compound, lower pH is necessary to achieve a minimum inhibitory constant (MIC).¹⁵² While this vital molecule has been used extensively in combination therapies, the development of resistance to PZA is quite substantial, and unlike other front-line chemotherapeutics, there is no replacement for PZA.

Resistance to PZA happens very readily, as PZA is actually only a pro-drug of the active metabolite.¹⁵³ This activation step is actually performed by *Mtb*'s encoded nicotinamidase, PncA (Scheme 2.1). This enzyme's natural function is to act as the first step of the salvage pathway for the biosynthesis of the coenzyme NADH. However, PZA is also acted upon by PncA, being cleaved into ammonia and the active metabolite pyrazinoic acid (POA) as shown in Scheme 2.2.¹⁵⁴ POA, unlike PZA, is not active *in vivo*, as the body of mammals clears the molecule quite rapidly.¹⁵⁵ Inhibitors of xanthine oxidase can be used to increase total body drug exposure, renal excretion is also quite rapid. Decades ago, the pharmaceutical industry attempted to circumvent PncA-mediated activation by generating a pyrazinoyl ester which would be activated to the desired metabolite by the host or pathogen.¹⁵⁶ Unfortunately, this simple esterification strategy, as

in 1-propyl-pyrazinoate, did not yield a replacement for PZA as cleavage of the ester was too rapid, and improper exposure to POA was achieved.



Scheme 2.1. The *de novo* and salvage biosynthetic pathways for NAD⁺/NADH.



Scheme 2.2. The mechanism of PncA activation of nicotinamide/PZA to active metabolites nicotinic acid/POA.

In our efforts to identify new drug substances for *M. tuberculosis*, we also envisioned that a replacement for PZA is absolutely essential to combating global infection. While many drug discovery campaigns are ongoing in the Aldrich laboratory, many of which involve rationally-designed inhibitors for novel drug targets, my approach to drug discovery has been less focused on *ab initio* campaigns, but rather has been directed at modifying POA to be more amenable for treatment. As outlined in this chapter, I've taken multiple directions in order to accomplish this goal. First, I endeavored to make a more selectively activated prodrug, using a β -lactam targeting pro-moiety. This molecule, **1** (Figure 2.1), was evaluated for its effectiveness against bacterial pathogens, assayed for its ability to release POA, and assessed for its stability in mammalian serum.

In addition to improving prodrug development for POA, I've also had the pleasure of working closely with Prof. Dr. Anthony Baughn and his trainees to attempt to elucidate the mechanism of action for POA. While still not completely understood, we've endeavored to elucidate at least the major contributor to POA's antimycobacterial activity, cell-killing unique only to *Mycobacteria*. During these studies, we uncovered an additional bioactivation step which has never been hypothesized. With the knowledge of an additional bioactivation step, we were able to synthesize molecules that look much like the activated molecules, generating new amide compounds that retain the pyrazinoyl core, but with entirely novel structure-activity relationship (SAR) off the amide nitrogen.

Both of these studies highlight the necessity of high selectivity for a desired drug to perform optimally. In the case of the TB treatment, this is decidedly valuable as the drug

treatment regimen is seemingly chronic such that side effects are highly likely to manifest within the patient if the drug lacks selectivity. However, not every instance of a drug discovery campaign calls for selective substances. Frequently, a non-selective molecule is desirable for use as a tool when one intends to learn more about basic biology, biochemistry, and the interactions of families of drug targets, rather single drug targets. These probe molecules can inform scientists about potential liabilities during drug development, assist in target identification and validation, or allow for systemic modulation of a family of biological factors which promote similar cellular processes. While this tool molecule will itself never become a viable drug, its existence is warranted in that such molecules help inform drug discovery to alleviate a wide variety of pathologies ranging from chronic pain, to cancer, to battling infectious diseases. During my studies, I've also been able to develop a molecule which is deliberately unselective, but can be proved as a valuable asset in the discovery and characterization of a very “druggable” enzyme class. These examples of compound development for biological processes, while seemingly unrelated, expose the gamut of desired reactivity for a given molecule. These stories highlight the practicality of rationally-designed chemical entities, and expose the range of impact well-thought medicinal and biological chemistries can have when one intends to improve human health.

2.2 Targeted drug delivery with a β -lactam prodrug approach

Although already stated, treatment of TB is certainly shorter when PZA is an effective chemotherapeutic.¹⁵¹ While the exact manner in which PZA acts is unknown, it

is well known that PZA must be activated, via hydrolysis, to POA.¹⁵³ POA, the active metabolite, can then exert its action. Thus, the central dogma of PZA, is that one must always be able to access the 2-carboxylic acid in order to make a viable antitubercular agent. While the host is capable of converting PZA to POA,¹⁵⁵ the most efficacious delivery of POA involves on-site delivery of the active metabolite, via PncA-mediated activation. Unfortunately, the fact that this enzyme is non-essential for pathogen survival plays a large role in *Mtb*'s ability to evade POA's action. Treatment of patients with POA (rather than PZA) is unfortunately not an alternative therapy, as POA lacks the efficacy needed to treat the pathology, likely due to rapid clearance of the drug.¹⁵⁵ Thus, it is absolutely necessary to develop another vehicle to deliver this vital drug to its site of action, while circumventing the resistance garnered by loss-of-function mutations of PncA.

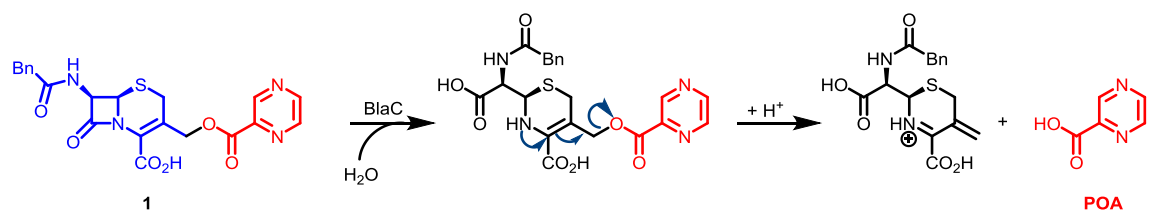
While previous methods to circumvent PncA-mediated activation have centered on esterification, these compounds have no target-directing moieties to facilitate the on-site activation deemed mandatory by the host's rapid metabolism and excretion of POA. Simple esters are cleaved whenever they come in contact with the body's esterases present ubiquitously in serum and tissues.¹⁵⁷ This lack of on-site delivery can be alleviated by appending a targeting moiety to the drug, likely through an ester linkage. This strategy has been applied for the treatment of a variety of pathologies, although bacterial infection has generally been targeted through siderophore conjugates or β -lactam conjugates. Siderophores are Fe^{III}-chelating molecules, created by all orders of life, which facilitate the uptake of iron from the environment.¹⁵⁸ In bacteria, these secondary metabolites are

biosynthesized, exported, and then imported with high selectivity in order for pathogens to acquire iron in deficient settings. The specificity garnered by these transporters has facilitated selective targeting of pathogens,¹⁵⁹ however, these moieties are generally difficult to make, work with, and semisynthetic strategies utilizing over-expression would still be a challenge. Particularly in *Mtb*, the siderophores produced, known as mycobactins,¹⁶⁰ contain moieties that would make synthetic modifications very difficult while also lacking a suitable location from which to append a pyrazinoyl functional group.

While the use of siderophores as a targeting moiety has been known for decades,¹⁶⁰ another promoiety that has also been well studied is the use of a β -lactam to foster drug release only in the presence of β -lactam hydrolyzing enzymes known as β -lactamases.¹⁶¹ These enzymes are produced by bacteria to counteract β -lactam containing antibiotics/antibacterials which target cell-wall biosynthesis,¹⁶² thereby inhibiting their growth and proliferation. This resistance mechanism has helped fuel drug resistance to many of the drugs we use for the treatment of infection, contributing to extensively- and totally-drug resistant strains of certain pathogens.¹⁶³ While these enzymes and compounds can come in multiple forms,¹⁶⁴ the most relevant system utilized in targeting therapeutics involves the use of the cephalosporin-type β -lactam compound with serine-based hydrolases.¹⁶⁵

As such, we hoped to apply this strategy for the delivery of POA to *Mtb*, utilizing its germ-line encoded β -lactamase, encoded by the gene *BlaC*.¹⁶⁶ The proteinaceous product of this gene, BlaC, is a serine hydrolase with a very large binding surface which grants this

protein the ability to cleave an extended spectrum of these β -lactam compounds. BlaC is also the reason why β -lactam antibacterials are an ineffective regimen for the treatment TB as removal of this gene leads to bacteria which are heavily susceptible to β -lactam compounds.¹⁶⁷ This enzyme could thus provide a platform that can be utilized for targeted delivery¹⁶⁸ of POA, directly at the site of action, without the need for PncA, a criterion not met by basic esters that have been previously studied.¹⁰ Much like the literature precedent, we also chose the cephalosporin nucleus for our initial studies, taking advantage of spontaneous release of POA upon β -lactam bond cleavage by BlaC, shown in scheme 2.3.



Scheme 2.3. The spontaneous release of POA after lactam bond cleavage by BlaC.

The conjugate we have envisioned is solely a prototype, although we expect to gain enough information with this molecule to be able to move forward with our ultimate goal of developing a new, stable, and orally bioavailable POA prodrug with targeted release. The key design criteria of our ultimate conjugate are: 1) the β -lactam promoiety should be devoid of intrinsic antibacterial activity to prevent disruption of commensal bacteria; 2) the conjugate should be stable and orally bioavailable; and 3) POA should be selectively released by *Mtb* and not by the host or other commensal microorganisms. To achieve selective antibacterial activity, we have chosen to start with a phenylacetyl modification off of the exocyclic amine, a modification that does not enhance antibacterial activity,¹⁶⁸ however, this may conflict with our second aim as the orally-available either contain D-amino acyl or α -oximino acyl substitution patterns off of the exocyclic amine,¹⁶⁹ which can enhance antibacterial properties. Our initial studies will forego this consideration for the time being. The last goal seems relatively straightforward to accomplish, as our desired hydrolase is an extended-spectrum β -lactamase (ESBL) that contains an extra cavity (Figure 2.2) behind the 7-position of the cephalosporin nucleus when the compound is bound to the enzyme.^{168, 170} This larger binding site can accommodate a small functional group (i.e. methoxy) installed at the 7α position which precludes binding to the vast majority of β -lactamases.¹⁶⁸

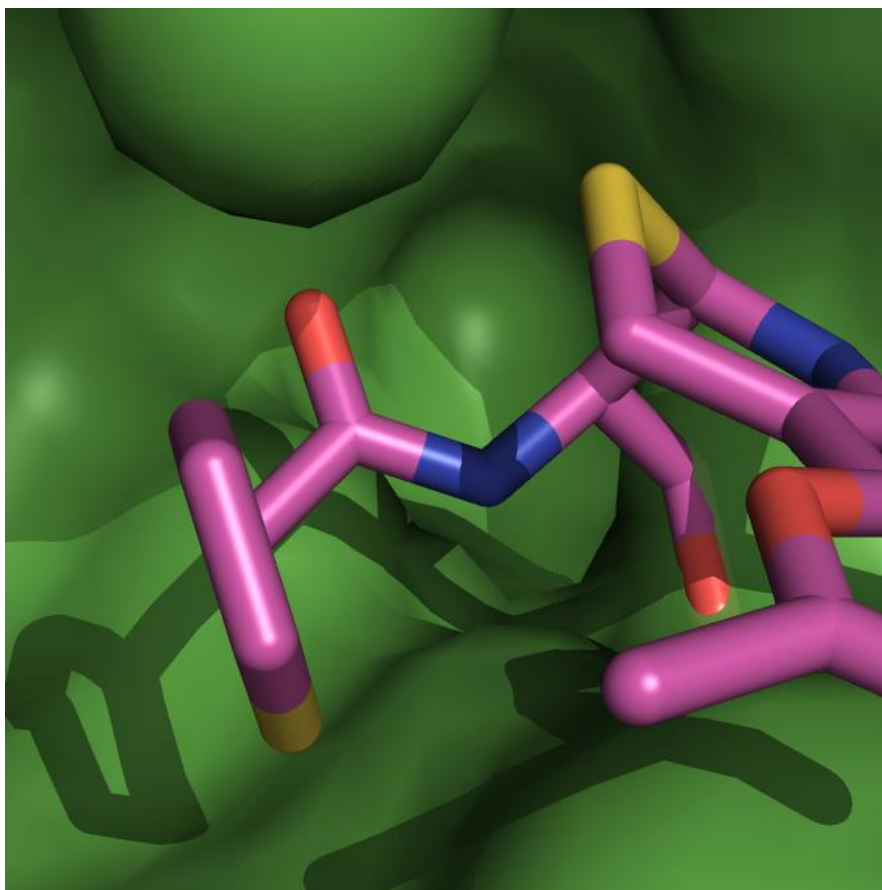
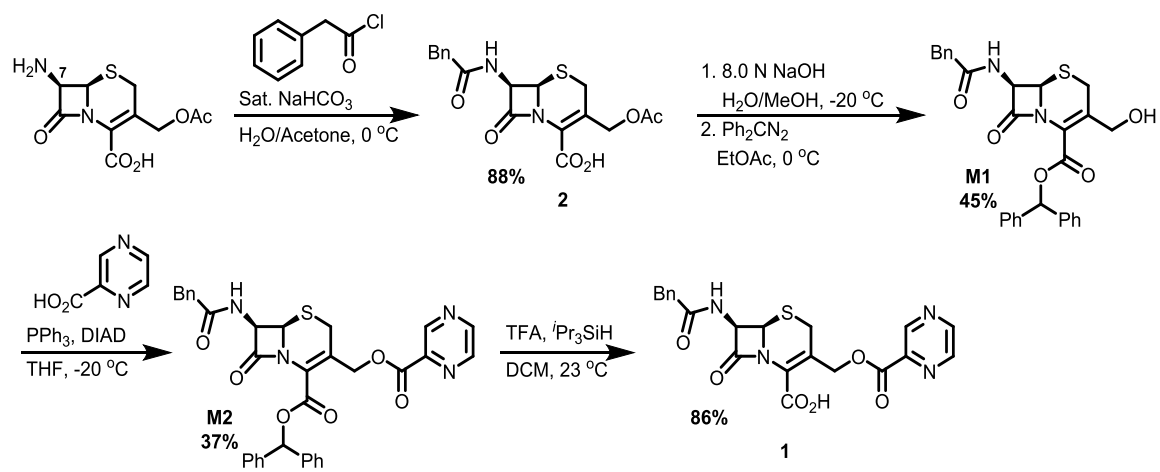
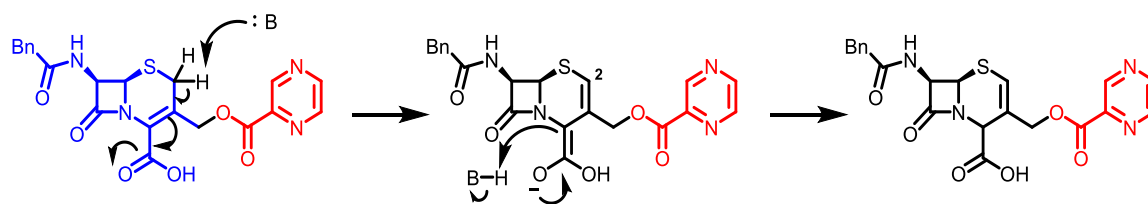


Figure 2.2. The extra cavity behind the 7-position of the cephalosporin bound to BlaC.¹⁷¹

Intuitively, we began with the synthesis of conjugate **1**, a feat that has been accomplished by myself, but optimized by Malcolm Cole, another student in the Aldrich laboratory. The synthetic route, shown in Scheme 2.4, utilizes previously established semi-synthetic chemistry to install the N⁷-phenylacyl group and add/remove protecting groups necessary to complete the synthesis.¹⁷² Compound **2**, isolated after the first semi-synthetic step, was to be used as a control molecule to gauge the effectiveness (if any) of the bare cephalosporin compound as an antibacterial compound. Deprotection of the C^{3'} acetyl ester under heavily basic conditions followed by benzhydryl protection of the carboxylic acid under acidic conditions afforded an alcohol intermediate.¹⁷³ Then, a Mitsunobu reaction that was heavily optimized connected the pyrazinoyl warhead to the pro-moiety. While only a 35% yield, these reaction conditions were selective for the desired transformation, limiting undesired $\Delta 2, 3$ isomerization which yields an inert compound (Scheme 2.5).¹⁶⁸ Deprotection of the benzhydryl protection with highly acidic conditions (TFA/CH₂Cl₂) in the presence of a cation scavenger afforded compound **1**. This synthesis can be scaled up to generate hundreds of milligrams at a time, enough for collaborators to characterize our prototypical compound. We found that the cephalosporin nucleus is very hardy and is seemingly amenable to modification.



Scheme 2.4. The semi-synthetic route of conjugate 1 from commercially-available 7-aminocephalosporanic acid.



Scheme 2.5. The $\Delta^{2,3}$ isomerization of compound **1** under basic conditions.

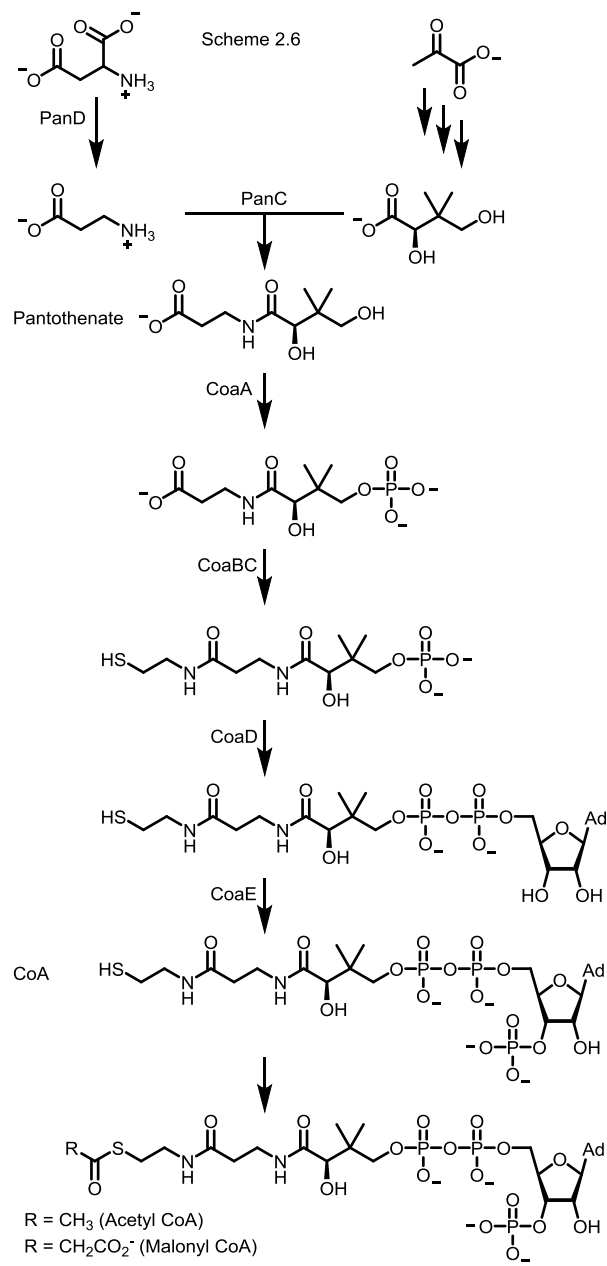
With plenty of molecule in hand, we moved forward with testing the molecule against living cells. I initially tested these molecules in pathogenic bacteria frequently encountered in the clinic such as *S. aureus*, *P. aeruginosa*, *A. baumannii*, and *E. coli*. In each case, compounds **1**, **2**, and POA were all ineffective when tested up to 800 $\mu\text{g/mL}$ (Table 2.1). This is likely due to the presence of intrinsic β -lactam resistance present with each strain, while POA is already known to be highly selective for *Mycobacteria*. It is notable that the activity of these compounds is frequently recovered when combined with a substoichiometric amount of the β -lactamase inhibitor clavulanate. These compounds were then handed off to the Baughn group, specifically Dr. Yusuke Minato, for testing in *Mycobacteria*. Notably, our compound is active in both *Mtb* and the closely related *Mycobacterium bovis* (BCG), even though BCG lacks the *pncA* gene (Table 2.1).¹⁷⁴ This demonstrates a lack of need for PncA in order to deliver POA. Even more intriguing, however, is that our compound is also active at neutral pH, unlike PZA which requires acidification in order to be efficacious.

Table 2.1. The minimum inhibitory concentrations (MIC₉₀) of compounds against Mycobacteria.^a

MIC ₉₀ (mM)	PZA ^b	POA	1	2
<i>M. tuberculosis</i> (+ <i>pncA</i>)	0.4	1.6	0.4	1.0
<i>M. bovis</i> (- <i>pncA</i>)	0.4	0.8	0.4	1.0

^aMIC₉₀ determined after 10 days of drug treatment with cultures grown in Middlebrook 7H9, pH 6.8; ^bpH 5.8

With known activity in *Mtb*, we then decided to probe the molecule's mechanism with some selective genetic manipulation. As such, we first desired to see if a strain with intrinsic POA resistance also displayed resistance to conjugate **1**. This strain, while still unpublished, was discovered through transposon insertion screening with a loss-of-function transposon insertion in the *panD* conferring resistance to POA, but only light resistance to PZA.¹⁷⁵ The *panD* gene encodes for *Mtb*'s aspartate decarboxylase which converts aspartic acid to β -alanine, a central metabolite necessary for the *de novo* biosynthesis of coenzyme A (CoA),¹⁷⁶ as shown in Scheme 2.6. Our molecule was evaluated against this Δ *panD* strain of *M. tuberculosis* and was found to be more effective against this strain of *Mtb* than either PZA or POA (Table 2.2). Furthermore, conjugate **1** was found to be cidal towards *Mtb* lacking PanD with a minimum bactericidal concentration (MBC₉₉) of 440 μ M, 2-fold greater than its MIC₉₀. This result was quite perplexing as we expected to at minimum see some resistance to our molecule, if the targeting moiety truly had no effect on *Mtb* growth. However, this result was welcomed as we realized that our conjugate can successfully dodge confirmed resistance to POA which is not derived from PncA loss-of-function, an unexpected capability of our prodrug.



Scheme 2.6. The *de novo* biosynthetic pathway of Coenzyme A.

Table 2.2. The MIC₉₀ of our compounds.^a

MIC₉₀ (μM)	PZA^b	POA	1	2
<i>Mtb</i> (WT)	400	1,600	440	1,000
<i>Mtb</i> (Δ <i>panD</i>)	800	>6,500	220	1,000
<i>Mtb</i> (Δ <i>blaC</i>)	400	2,400	55	110

^aMIC₉₀ determined after 10 days of drug treatment with cultures grown in Middlebrook 7H9, pH 6.8;
^bpH 5.8.

In order to determine how much of an effect the β -lactam pro-moiety had on cells, we also studied our conjugate in the context of an *Mtb* strain that lacks a functional BlaC enzyme. This strain, graciously provided by Prof. Dr. Martin Pavelka (University of Rochester), was utilized to evaluate our molecules, although this would not necessarily preclude POA release. Unsurprisingly, our molecule was highly effective against this strain of *Mtb*, as expected based on the work previously reported by Prof. Pavelka (Table 2.2).¹⁶⁷ This demonstrates that BlaC is not necessary for the molecule's activity as the β -lactam can act through its own intended mechanism of cell-wall disruption via irreversible inhibition of Penicillin binding proteins (Figure 2.3),¹⁶¹ while also releasing POA indicating that our molecule can act as a dual therapeutic, a trait that should potentially reduce the frequency of resistance; a frequency that has yet to be determined. While *in vitro* assays are suggestive that the molecule may contain activity dependent on both parts of the conjugate, we hoped that the POA portion of the observed activity should dominate as the principle driver of antimycobacterial action of compound 1. We believed that the β -lactam contribution should be abolished by the presence of BlaC. In reality, this may not be the case, but since the conjugate is about as effective as PZA, and the cephalosporin is much more active in a *Mtb* that lacks BlaC, we expected to be able to determine that the molecule's activity was due to the payload, rather than the targeting moiety. We also wished to determine if the β -lactam pro-moiety conferred greater cell penetration in a similar vein as PZA and pyrazinoyl ester compounds.

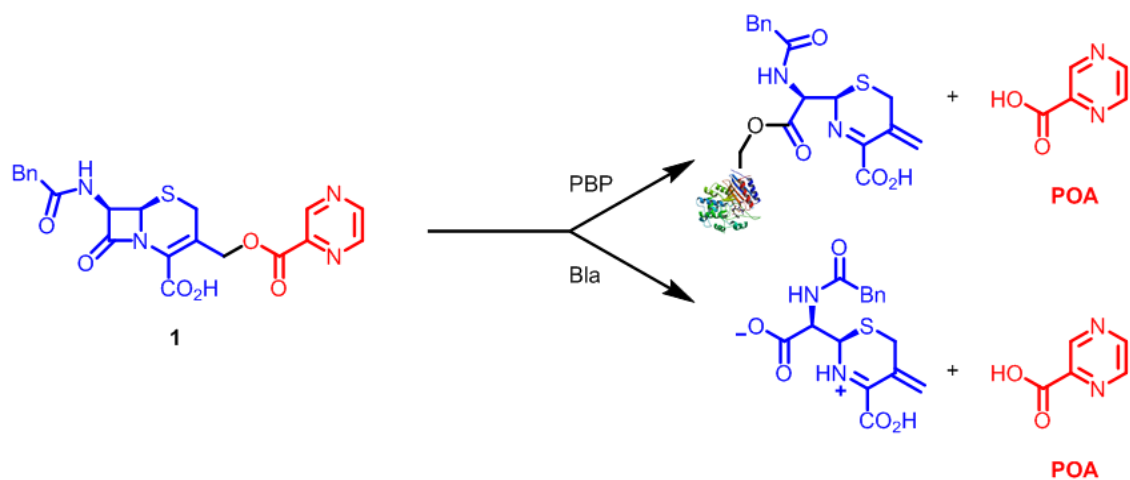


Figure 2.3. The potential activities of conjugate **1** in *Mtb*.

In order to determine a proper way to assess POA's contribution to compound **1**'s activity in *Mtb*, I've had the opportunity to collaborate extensively with Prof. Anthony Baughn and his group. Throughout the years in their research program, Prof. Baughn and co-workers have had the opportunity to establish that some of the debated mechanisms of action are highly unlikely, using genetics as a major tool to drive these conclusions.¹⁷⁷ While the exact mechanism continues to elude researchers within the field, there does seem to be a consensus as to what qualities the phenotype of treatment should possess. To this effect, we can actually utilize this knowledge to assay the effectiveness of the POA however, a few facts from the Baughn lab's research, and our own efforts, all of which remains unpublished, indicate that the effect on CoA levels may not be the most optimal way to assess POA's activity after release.

The phenotype presented upon PZA treatment, that seems to have found a consensus among the many groups working towards elucidating this drug's mechanism, revolves around the modulation of the *de novo* biosynthetic pathway (Scheme 2.6) of CoA, in which global CoA levels (CoA, acetyl CoA, malonyl CoA) are depleted as well as pantothenate, a key intermediate in the biosynthetic pathway.¹⁷⁸ This cellular response, while postulated to be attributed to by multiple factors, seems to be universally observed and agreed upon as an indicator of POA activity. As such, we decided to characterize these metabolites using liquid chromatography coupled to tandem Mass-spectrometry (MS/MS)¹⁷⁹ to determine the exact quantities of these molecules within cells. This targeted

metabolomics approach also gives us the opportunity to quantify how much, if any, of our pro-drug and drug are penetrating cellular membranes.

While it is outside of the scope of this work to describe another student's thesis, it is important to highlight that cell-wall disruption and POA treatment appear to be very synergistic.¹⁸⁰ While I cannot comment on all of the data leading to this hypothesis, it appears that variance of *Mtb*'s Sigma factor E (SigE) due to cell wall damage leads to greater susceptibility, manifesting as synergy between POA and the disrupter.¹⁸⁰ Since the β -lactam conjugate combines POA and a known cell-wall inhibitor,¹⁶⁵ it would not be surprising to receive inconclusive results from MS/MS studies. β -Lactams have been shown to increase cofactors, such as CoA, in response to cell wall damage. This should complicate our attempt to profile the effect of the conjugate on the metabolome.¹⁸¹ While this conundrum exists, we hoped that the data gathered in these experiments would be indicative of POA treatment, with a phenotype resembling that which has been reported.

Even with the daunting challenge of parsing the nature of compound **1** via targeted metabolomics data, it was important to be properly prepared for these experiments. As such, I prepared standard curves of each compound and ensured that the compounds we intended to study were separable, while we sought the limit of detection for each molecule. Our metabolites of interest included CoA, Acetyl CoA, Malonyl CoA, and our conjugate in positive mode using MS/MS. We also investigated the *de novo* biosynthesis of CoA intermediate, pantothenate, and searched for POA in negative mode of MS/MS studies. For each polarity, an internal standard was used for quantification and quality control purposes.

For positive mode, a β -lactam, ampicillin, was chosen to most accurately quantify our conjugate, should it get into cells, while negative mode utilized d_3 -POA as an internal standard. The mass transitions used for quantification are summarized in Table 2.5. As an example of a standard curve experiment, the quantification of POA is shown in Figure 2.26, compared to its trideuterated internal standard. In this experiment, we determined that the limit of quantification is about 15 nM, while our input of the conjugate is much higher, we hoped to detect and quantify accurately all of the POA that may enter cells.

Armed with an effective mass-spectrometry and chromatography method, we then compared cellular samples of *Mycobacterium bovis* (BCG) treated with our conjugate for 4 and 24 hours at 0.2 mM and 0.8 mM, as well as samples treated with POA at 1.0 mM. To start, the presence of POA was quite apparent in every sample and varied based on the time point analyzed (Figure 2.4). POA treatment seemed to reach a maximal intracellular concentration quite rapidly, and surprisingly declined from the 4 hour time point to the 24 hour time point. However, the opposite trend was true for the conjugate, reflecting the need for enzymatically-derived POA release. Additionally, the conjugate could not be detected intracellularly, indicating that POA release and stronger MIC is not due to increased penetration of the pro-drug, but is likely due to the synergy eluded to earlier.

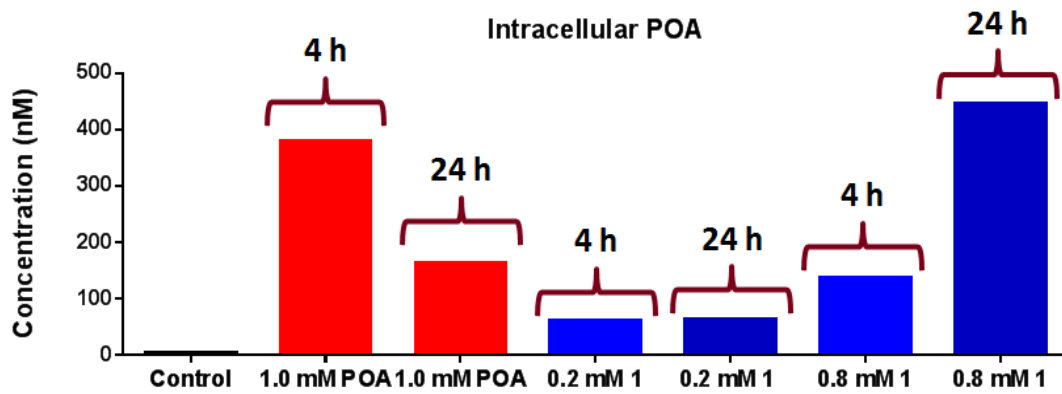


Figure 2.4. Intracellular POA concentrations in BCG after treatment with POA and conjugate 1.

While we were able to see that POA was released, we were unable to recapitulate the full effect of POA, as evidenced by the lack of CoA species drop with conjugate treatment (Figure 2.5). Thankfully, the phenotype we characterized for POA treatment alone, did mirror the results previously reported. However, our conundrum is not at all surprising when one weighs the notion that our molecule is not limited to the mechanism of the payload as the delivery vehicle is already known to be antibacterial, and is actually effective on its own against *Mtb* at high enough concentrations. Unfortunately, β -lactams have been reported to increase CoA levels in bacteria,¹⁸¹ causing greater conflict with our studies, than initially expected.

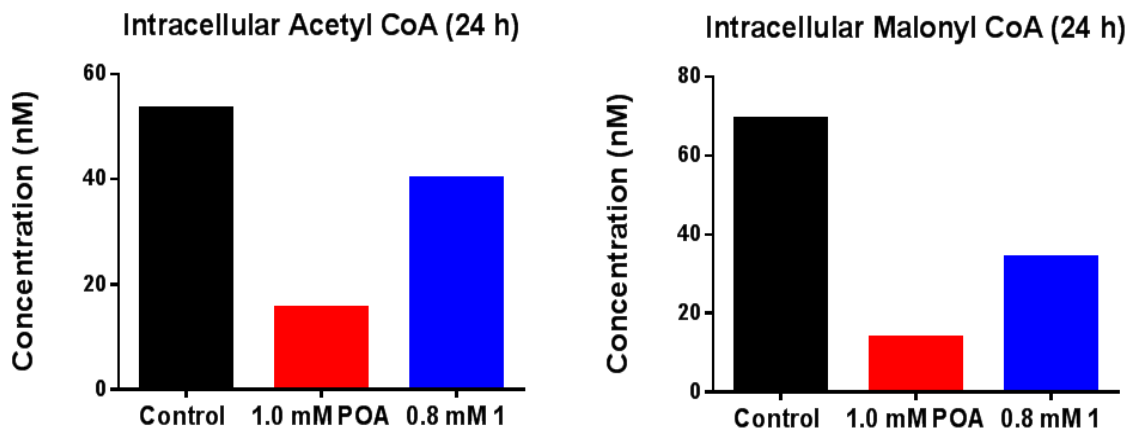
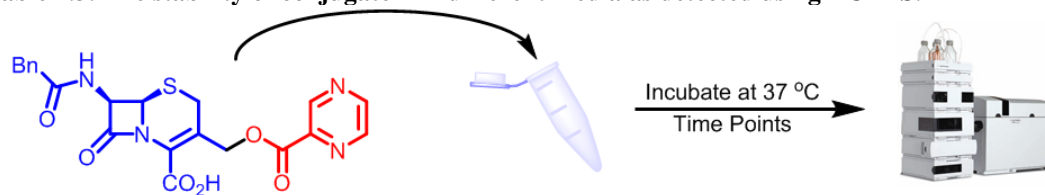


Figure 2.5. The intracellular acetyl CoA and malonyl CoA levels of BCG treated with POA (red) and conjugate **1** (blue) after 24 hours of treatment.

While we were not able to completely get a grasp of conjugate **1**'s complex mechanism of action, we did wish to continue on with this prototypical molecule to determine if we had met our criterion of selective warhead release. To assay this property of our molecule we opted to monitor the stability of **1** in aqueous media, at both acidic (pH 1.3) and neutral (pH 7.4) conditions to assess potential liabilities in aqueous conditions.¹⁸² Additionally, we monitored the stability of **1** in plasmas derived from female mice, rats, and humans to assess if non-specific esterases have the capacity to foster POA release in mammals relevant to preclinical animal models utilized in our and collaborators' laboratories.¹⁸³ As summarized in Table 2.3, our conjugate is very stable in the studied media out to 120 minutes, with even 50% of the parent compound remaining in simulated gastric fluid after 120 minutes, owing to the remarkable acid stability noted for cephalosporin molecules.¹⁸⁴

Table 2.3. The stability of conjugate 1 in different media as detected using LC-MS.



Entry	Media	pH	% Remaining at 120 minutes
1	50 mM HEPES	7.4	> 95%
2	Simulated Gastric Fluid	1.3	50%
3	Female Mouse Plasma	7.4	>95%
4	Female Rat Plasma	7.4	>95%
5	Female Human Plasma	7.4	>95%

While the conjugate seems to be stable to aqueous media, we wished to determine the conditions necessary for POA release, to confirm that BlaC does facilitate the desired degradation. As such, we determined the amount of POA released by BlaC turnover with or without the presence of clavulanate, a known inhibitor of BlaC.¹⁸⁵ As shown in Figure 2.6, the presence of BlaC leads to rapid evolution of POA, a trait that is inhibited by the addition of clavulanate. This indicates that BlaC release is the primary method for POA release, while the actual rate of release is still being determined by Malcolm Cole. In addition, we will also test the selectivity, or lack thereof, for cleavage using a panel of β -lactamases covering a wide range of enzymes capable of this transformation to determine what pro-moiety scaffold is necessary for optimal selectivity for *Mtb*.¹⁶⁸

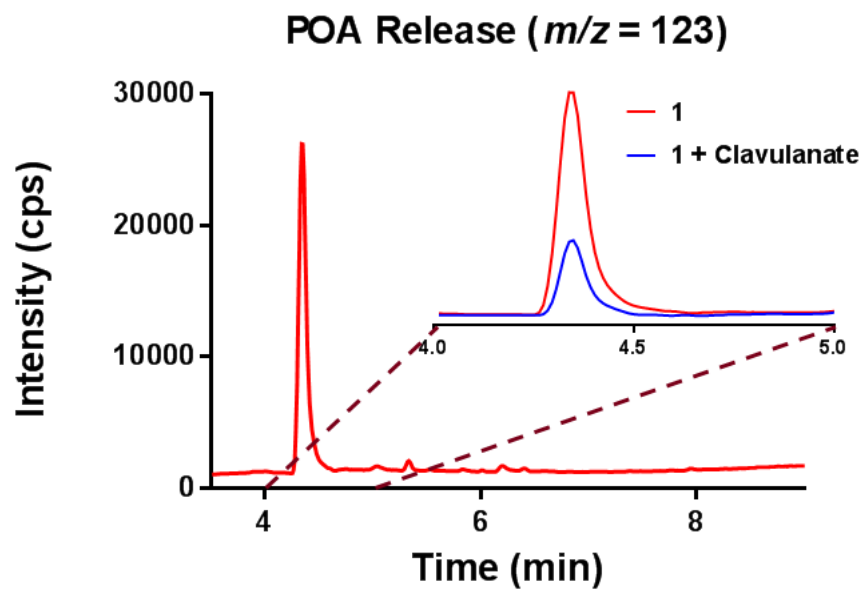


Figure 2.6. The BlaC-mediated release of POA from conjugate **1** without (red) and with (blue) clavulanate. Data collected by Malcolm Cole.

Taken together, these results indicate that conjugate **1** is a great prototype for a new drug, yet the molecule presented herein is certainly not that drug. The β -lactam targeting system does have the ability to release drug when desired, but the specific conjugate is not as acid stable as we would like, and its pharmacology seems to be heavily affected by the targeting moiety, an aspect that will likely translate to poor pharmacokinetic properties, unless modifications are made using the knowledge we have gained about β -lactam drugs through the decades.¹⁸⁶ The underlying pharmacology of conjugate **1** is also much more complex than expected. Yet, this complexity will likely lend itself to better properties for the treatment of such a complex pathogen, adding more channels necessary to confer resistance. The ability for conjugate **1** to act as a dual warhead, should reduce the possibility of spontaneous resistance, and has even already been shown to circumvent a known resistance mechanism compared to the warhead used in mono-therapy applications. Future endeavors should seek to stabilize the molecule under acidic conditions, further garner selectivity for BlaC, and/or attempt to utilize transport mechanisms to yield a bioavailable drug which adheres to the tenets of our prodrug design.

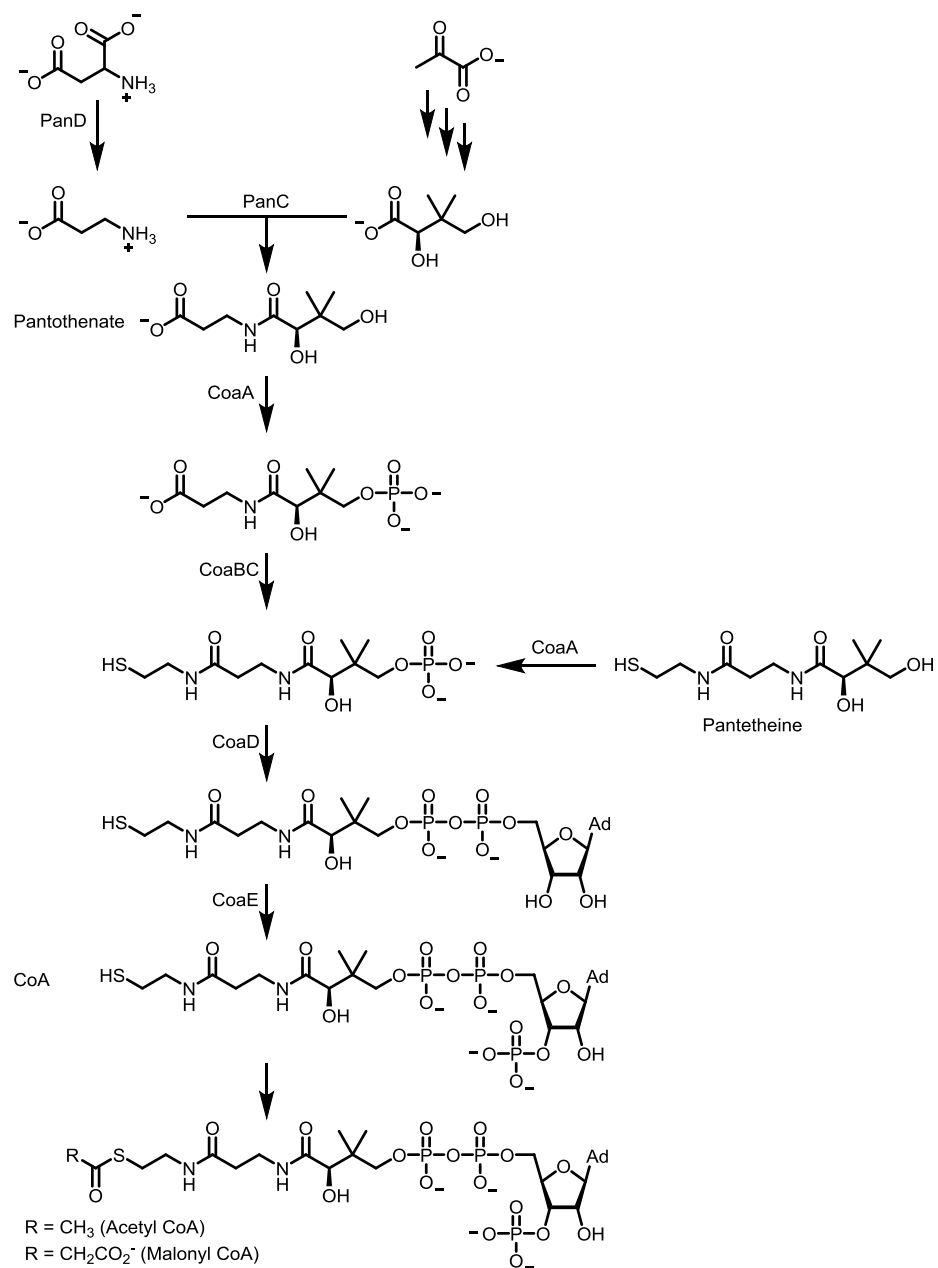
2.3 A paradigm shift for the design of analogs of antitubercular drug pyrazinamide

While we worked on the development of MS methods for targeted metabolomic studies, Prof. Baughn also asked us to follow-up on a hunch he had regarding the mechanism of PZA. However, before getting to the hypothesis Prof. Baughn had regarding PZA/POA's mechanism of action, it is important to discuss some of the findings his and other groups have had while studying this molecule. While already summarized over

multiple review articles,¹⁵³ the mechanism of PZA/POA (from here on, referred to solely as POA) is certainly complex, while central metabolism is frequently identified as being disrupted by the molecule. Other theories, such as POA targeting trans-translation, have been debunked,¹⁸⁷ and will not be discussed here. Yet other potential targets of the drug, such as the proteasome subunit ClpC1,¹⁵⁵ remain with unknown implications as novel techniques to rapidly screen genetic manipulations continue to be developed. Deconvolution of these data is an ongoing process. While there has been much speculation as to what drives POA activity, multiple groups, including the Baughn group, have isolated some form of inhibition within the *de novo* biosynthetic route of CoA as the potential source of POA's antitubercular activity.

The theories presented regarding the way POA acts on this pathway are not necessarily contradictory, however, the interpretation of these results has led to some contention as to what is truly happening upon drug treatment. What can be easily stated are the observations made by the groups studying the interactions of POA and *Mycobacteria*. As a notable contribution to the field, Prof. Dr. Thomas Dick and Prof. Dr. Veronique Dartois have jointly proposed that binding to the aspartate decarboxylase enzyme PanD (Schemes 2.6 and 2.7) is important for whole cell inhibition.¹⁵⁵ Indeed, this research program has even gone to the lengths to characterize the kinetics of binding, and have worked with genetic knockouts of the enzyme, showing resistance to POA. While their findings point to PanD as a key piece to unraveling POA activity, some of their own data as well as data gathered by the Baughn group conflict with the necessity of PanD

binding.¹⁸⁸ It is important to restate, however, that $\Delta panD$ strains do display *in vitro* resistance to POA even though binding to PanD has not been demonstrated to inhibit the enzyme's function.^{155, 180} This certainly conflicts with the notion that $\Delta panD$ strains are unable to confer resistance in *in vivo* infection models, but does indicate the necessity of such experiments when conducting investigations with such a complex pathogen.



Scheme 2.7. The CoA biosynthetic pathway showing the *de novo* and salvage (starting with pantetheine) pathways.

Furthermore, the fact that PanD is considered a target of POA should indicate that addition of any excess of downstream intermediates in the biosynthesis pathway would antagonize the drug's activity. While this is true for the majority of drugs, antagonism of POA with CoA biosynthetic intermediates is not as straightforward as one would imagine.¹⁸⁸ Addition of exogenous pantothenate, β -alanine, and pantetheine all do antagonize POA activity, but the antagonism noted with PZA treatment is significantly less pronounced, though PZA is solely a prodrug of POA. Even more perplexing is the fact that the addition of pantothenate and β -alanine is about 4-fold more antagonistic than adding pantetheine, even though all of these metabolites fuel CoA biosynthesis after the PanD-catalyzed step (Scheme 2.7). This finding is most peculiar especially when coupled with the fact that we have been unable to find an absolute target of POA.

Sensing the potential for incorporation of POA into the metabolome, Prof Dick's researchers attempted to characterize what they believed to be the most likely candidate molecule for POA integration. This molecule, pyrazinoyl CoA (Figure 2.7), was synthesized and cellular lysates were investigated for the abundance of such a molecule. However, pyrazinoyl CoA was never detected by MS in targeted metabolomics studies, while it did seem like a likely candidate for POA integration as the amounts of typically-anticipated CoA species should drop, and more pantothenate would be necessary to make up for a loss of functional CoA acyl carriers. However, the proposal of pyrazinoyl CoA ignores the patterns of antagonism reported by the Baughn group,¹⁸⁸ yet does open up the thought process that POA, much like other known drugs, is an antimetabolite.

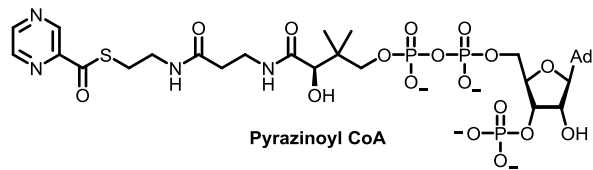
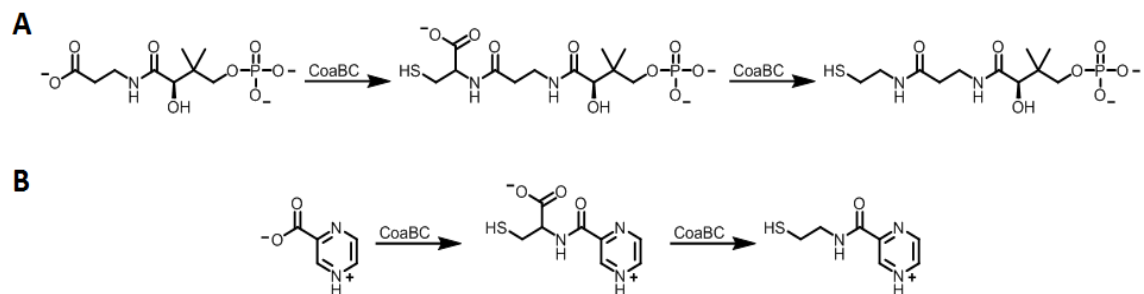


Figure 2.7. The structure of pyrazinoyl CoA.

In this sense, the word “antimetabolite” does not refer to a molecule which blocks metabolism, but actually refers to a molecule that is incorporated by biological machinery and converted to an active inhibitor. Examples of this strategy have found use in many pathologies, however, this potential mechanism prior to Dick’s work had never been postulated for POA. This hypothesis also correlates with our unpublished data previously disclosed in this thesis as intracellular POA levels are depleted over the course of drug treatment. Knowing about the way central metabolites affect POA treatment, we then hypothesized that it is possible for POA to be acting as an antimetabolite, but that its incorporation would be much earlier in the biosynthesis of CoA rather than modifying the terminal sulfhydryl of the cofactor. Our hypothesis for POA as an antimetabolite has POA incorporated by the enzyme CoaBC (Scheme 2.8), being converted to either the pyrazinoyl cysteine or pyrazinoyl cysteamine compounds which then go on to inhibit *Mycobacterial* growth. If *Mtb* were to use this machinery to further activate POA, then POA would compete with pantothenate for binding to the protein, and excess pantothenate would block this activation step. However, once activated by *Mtb*, this new molecule could act at a variety of places within cells, even within the same pathway, leading to an inhibition of CoA synthesis and depleting global CoA levels.

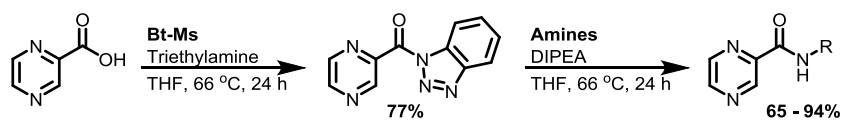


Scheme 2.8. A) The half reactions catalyzed by CoaBC; and B) Proposed activation of POA by CoaBC.

In order to test such a hypothesis, two approaches were simultaneously surveyed. The first approach involved direct detection of the molecule via MS, and to test if the proposed metabolites even have antimycobacterial activity. This part of the project relied on synthetic and analytical chemistry skills, making new molecules for testing within whole cell assays, as analytical standards, and for characterization of a new drug-like substance. The alternate approach involves an ongoing investigation using genetic manipulation of the bacteria to confirm with both over- and under-expression strains that the bioactivation is both specific to one enzyme, and to identify the targets of the new chemical entities. These orthogonal approaches are both needed to confirm our hypothesis of POA acting as an antimetabolite. Unfortunately, I will only really be able to discuss the first such approach in detail as this has been my contribution to the project and we are still awaiting the generation of the necessary strains of *Mtb* with the desired genetic modulations.

In order to detect and determine if POA is modified within *Mtb*, I synthesized a few standards for MS experiments. At first, I tried using 1-ethyl-3-(3-dimethylaminopropyl) carbodiimide (EDC), but found the low yields unsatisfactory for the synthesis of great enough quantities required for many of the whole-cell studies planned as my best yield using this reagent was 21%. To alleviate this short-coming, I turned to chemistry developed by the late Prof. Dr. Alan Katritsky,¹⁸⁹ which is specifically suited for the formation of amide bonds from heavily withdrawn carboxylic acids. POA, a carboxylic acid adjacent to the electron poor pyrazine heterocycle, certainly lacks the reactivity required of traditional

amide coupling reagents, such as EDC, but works just fine with Katritsky's system (Scheme 2.9). This methodology was then applied to make a small series of pyrazinoyl compounds (Figure 2.8) to assess potential antimycobacterial activity of this scaffold while also serving as synthetic standards to confirm further bioactivation of POA.



Scheme 2.9. The synthesis of new pyrazinoyl amide compounds.

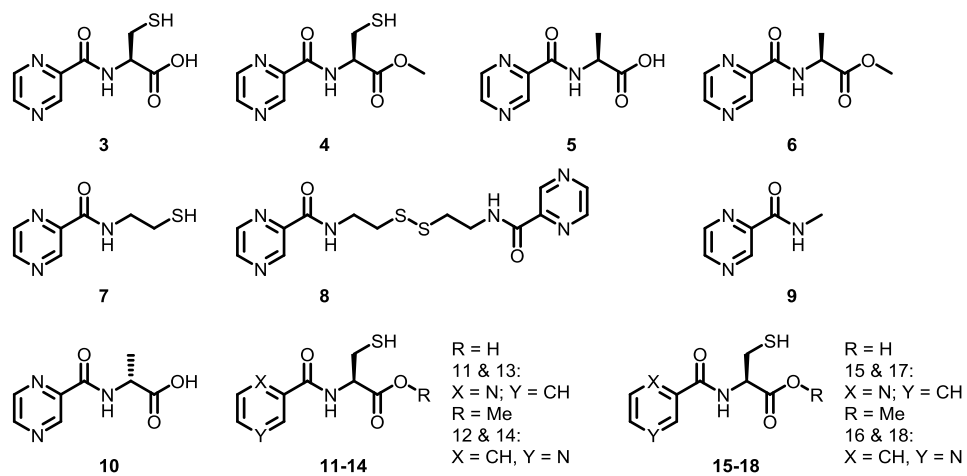


Figure 2.8. Compounds synthesized via the route illustrated in Scheme 2.9.

With a few new compounds synthesized as in Figure 2.8 I was then able to make new LC and MS methods to detect potential metabolites of POA. I was able to use these standards for two types of MS, tandem MS, described earlier, in which we would be able to quantify these new chemical motifs, and high-resolution MS (HRMS), to confirm absolute identity of compounds detected in lysate experiments. Having been given prepared lysate samples from cultures of *Mtb*, I then prepared these samples further by concentrating the lysate and dissolving the samples in MS-grade solvents. This facilitated HRMS studies in which samples could be shot on directly to the mass-spectrometer, or in which a short column could be added to further filter out noisy signals. The latter was chosen to simplify our initial readout, although direct infusions would later turn out to be fine for detecting any additional metabolites. Shown in Figure 2.9, we were delighted to be able to detect our desired compound, **3**, on an Orbitrap Velos instrument in negative mode, using electrospray ionization (ESI). We were able to identify the splitting pattern which included the parent mass, its disulfide, and the unique fragment resulting from cleave of the C_{sp}²-C_{sp}² bond between the nitrogenous heterocycle and the carbonyl of compound **3**. When a sample generated from an *Mtb* lysate was investigated, an identical mass signature was detected at the same retention time of 0.85 minutes. Additionally, adding both the synthetic standard and the lysate simultaneously did not affect the chromatogram, nor the mass signature. This confirmed the presence of **3** in samples treated with POA, while untreated samples lacked this specific metabolite. Additionally, we also looked for, and detected, the presence of additional metabolites in positive mode, which further validated

our hypothesis (Figure 2.10). The metabolite detected in positive mode is derived from compound **7**, the proposed metabolite generated by CoaBC action upon POA.

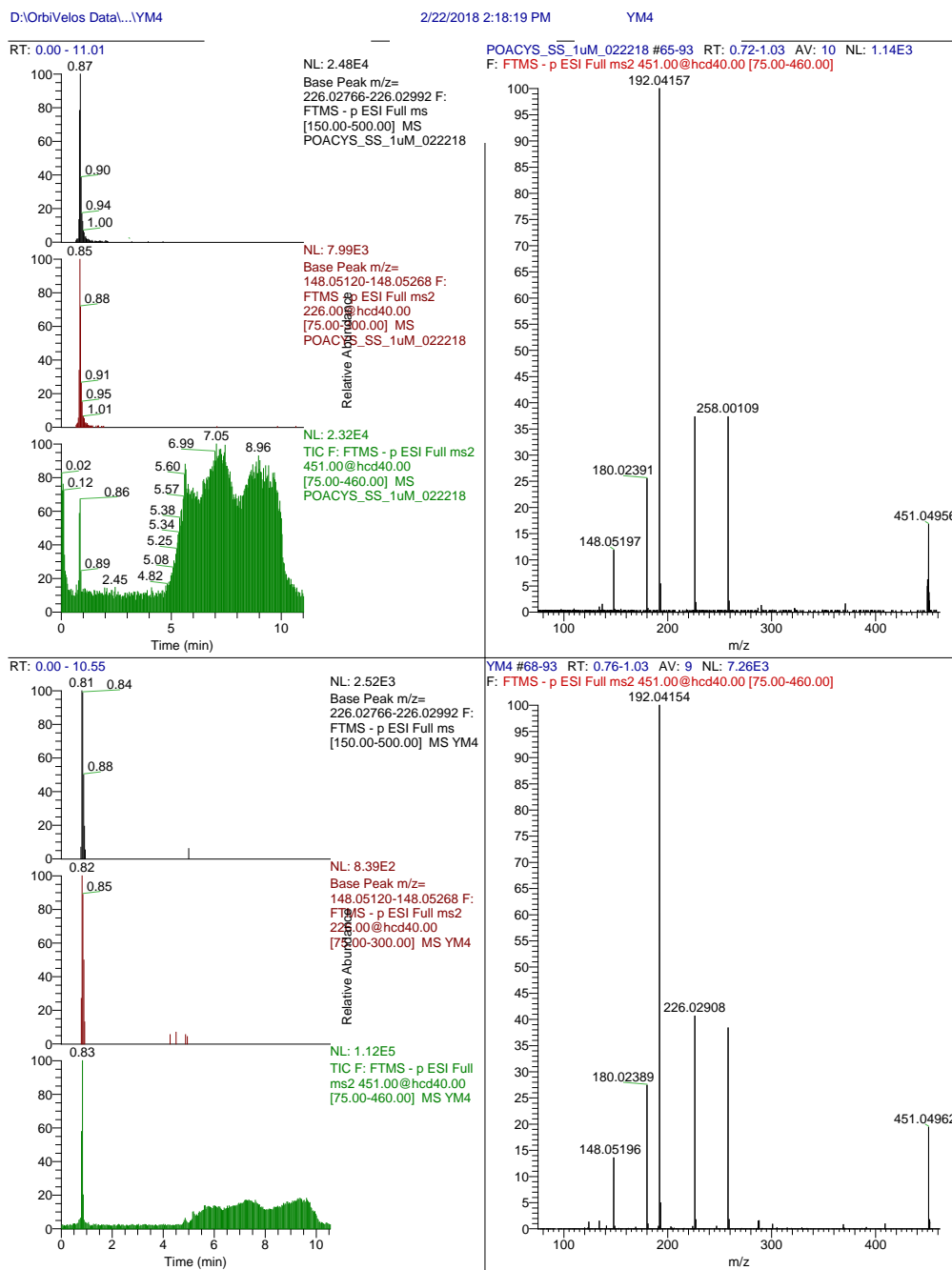


Figure 2.9. The HRMS traces and mass signatures for synthetically-derived **3** (top) and cellular lysates from *Mtb* treated with POA (bottom) as detected using ESI in negative mode.

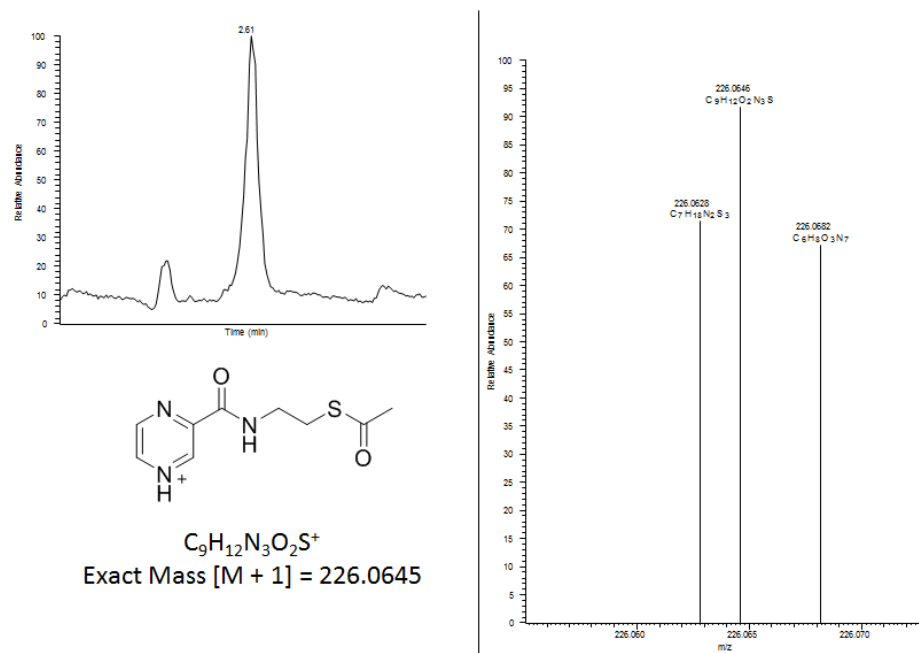


Figure 2.10. The detected metabolite of POA in PZA-treated *Mtb* cellular lysates using HRMS-ESI in positive mode.

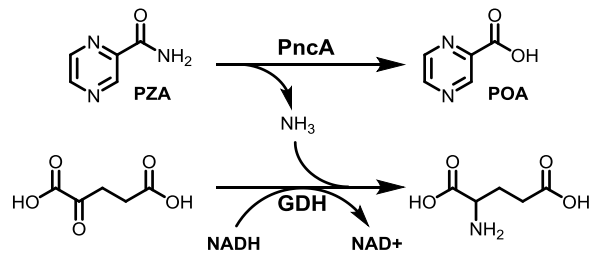
With the ability to detect metabolites directly using HRMS, we also wished to characterize if these molecules possessed antimycobacterial properties, and what the effect of these molecules might be. With a small sample of the molecules generated, Dr. Yusuke Minato, of the Baughn group, evaluated these molecules in *Mtb*, while I counter screened these molecules in other pathogenic bacteria. Intriguingly, much like our parent compound, POA, these molecules tend to exude the need for lower pH for activity in *in vitro* experiments, yet we were able to circumvent that need for a few of these analogs. Unfortunately, to date, only the six analogs presented in Table 2.4 have been evaluated for their antitubercular activity, while not a single compound has displayed antibacterial activity in *E. coli*-K12, *A. baumannii*-AB5075, *P. aeruginosa*-PA14, or *S. aureus*-USA300, even tested out to 800 µg/mL. With considerable activity in *Mtb*, these molecules display the same sort of specificity and potency for *Mtb*, noted with the parent drug, while also circumventing the necessary PncA-mediated activation step, much like pyrazinoyl esters. However, these molecules represent a paradigm shift in SAR for the drug scaffold as decades of study have been devoted to modification of the heterocyclic component of the molecule. This is due to the central dogma of PZA, in which a carboxylic acid must be present for antitubercular activity. We believe our new molecules lack this part of PZA's mechanism, and thus act via a novel mechanism of action.

Table 2.4. The minimum inhibitory concentrations (MICs) of compounds against *M. tuberculosis*.^a

Entry	Compound	pH	MIC ₉₀ (mM)	Entry	Compound	pH	MIC ₉₀ (mM)
1	PZA	5.8	0.4	8	5	5.8	2.0
2	PZA	7.0 ^b	>13.0	9	5	6.8	>2.0
3	POA	5.8	0.8	10	6	5.8	0.5
4	3	5.8	1.2	11	6	6.8	0.5
5	3	6.8	>1.2	12	7	5.8	1.1
6	4	5.8	0.4	13	8	5.8	0.5
7	4	6.8	0.4	14	9	5.8	>11.5

^aMICs measured after 10 days in Middlebrook 7H9 media using wild-type virulent strain H37Rv; ^bValue determined after 14 days as in *Antimicrob. Agents Chemother.* **2015**, *59*, 7320.

In order to separate our molecules from this canon philosophy, we wished to both biochemically and analytically confirm that compounds such as **3** do not simply act as dipeptide prodrugs of POA. This reaction could not be impossible for the many peptidases in *Mtb*. At this point, I recruited Evan Alexander, a highly capable chemical biologist in the Aldrich lab, to assist with these studies. Before initiating this project, Evan had already expressed, purified, and studied some of the specificity of nicotinamidase PncA (Figure 2.11).¹⁹⁰ With this assay already known in the lab, I handed off molecules **3** – **8** for their evaluation against PncA.



Michaelis-Menten Curves for Various Substrates

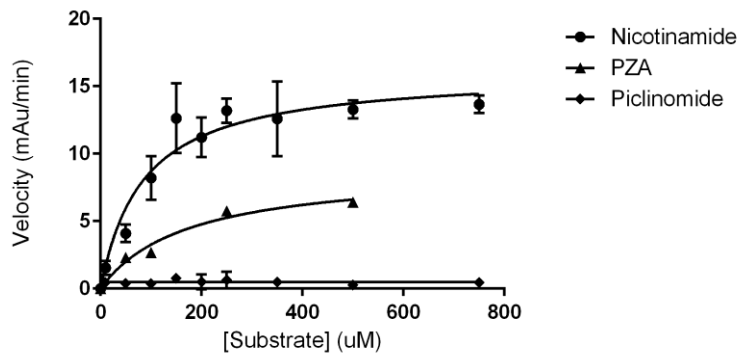


Figure 2.11. The assay and detection method using waning signal at 340 nm for PncA activity (top) and Michaelis-Menten curves for heteroaromatic carboxamides (bottom). Data collected by Joseph Ahenkorah.

While these compounds could be substrates for PncA, it would be highly unlikely to ever detect ammonia released from these molecules. This, in turn, required detection of the pyrazinoate that would be liberated from the amide compounds. Again using MS, our compounds were compared to PZA using purified PncA, but rather than adding another enzyme to detect activity spectrophotometrically, the protein was removed using an acetonitrile crash, and samples were loaded directly onto the instrument. Monitoring at [M-1 = 123] (still in negative mode ESI), we were unable to detect POA release when any of our novel compounds were incubated with PncA, even at 750 μ M. This result, while encouraging, was unsurprising given what is known about the binding pocket of PncA. Figure 2.12 shows a model of the active site, generated by Evan Alexander, which highlights the limits of the cavity, showing that the catalytic residues really do define the depth to which a molecule can extend into the protein.

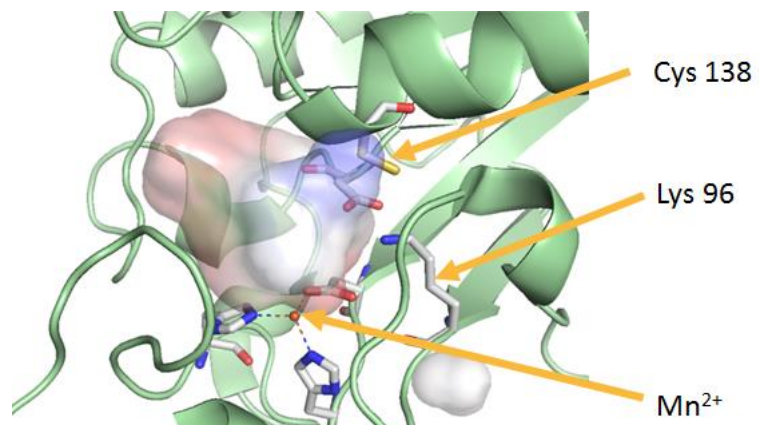


Figure 2.12. The binding pocket within the active site of PncA as modeled by Evan Alexander.

While the results with purified PncA indicated hope that our compounds act in an entirely novel manner, we could not discount the potential that *Mtb* may cleave these dipeptides using some other means. As such, we again turned to studying the whole-cell lysate of *Mtb* treated with specifically compound **3**, a molecule with favorable activity, yet most resembles a natural dipeptide. Again, using a similar procedure described earlier, we intended to detect and quantify the initial molecule, POA, and CoA biosynthetic intermediates using MS/MS on a triple quadrupole linear trap mass spectrometer in both positive and negative modes. Much to our delight, POA was undetected in cultures treated with **3**, but readily seen in those treated with either PZA or POA (Figure 2.13). While also detecting POA, we opted to quantify the changes to changes to CoA, acetyl CoA, and pantothenate in order to better understand if these molecules match POA's resultant phenotype. Again, we were pleased to see the overall reduction of both CoA and acetyl CoA (Figure 2.14). Thankfully, POA's activity against these metabolites scaled quite nicely with the dose administered, and our compound seemed similar, if not more active, at similar concentrations. However, compound **3** did deviate from POA in that pantothenate levels did not drop. In fact, treatment with **3** caused a slight (not significant) increase in pantothenate when compared to controls, while POA acted exactly as expected based on literature precedent (Figure 2.15).¹⁵⁵ These results certainly point to **3** acting within the CoA biosynthetic pathway which we are currently investigating. As eluded to earlier, we are seeking over- and under-expression strains of each piece of the biosynthetic machinery, while also working on generating mutant strains which display resistance to **3**. However,

these experiments have yet to yield fruit, and at this time, we await these materials in order to more fully characterize these new chemical entities. In the meantime, I have worked on scale-up and can safely make over 1 gram of final compounds per batch, and we have filed for legal protection to ensure these new chemical entities can be further developed into drugs if these promising results translate to *in vivo* experiments.

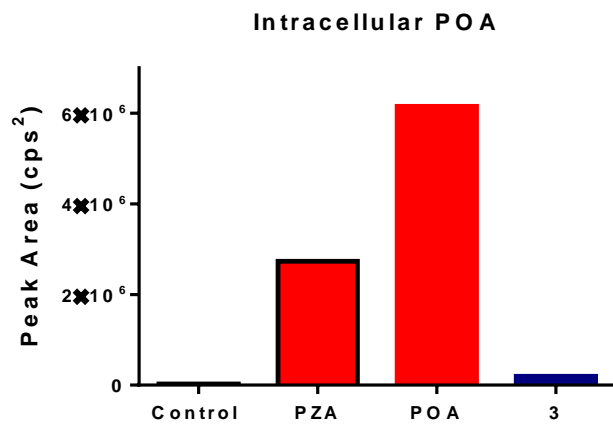


Figure 2.13. The raw areas of POA detected in *Mycobacterium* treated with vehicle (control), PZA, POA, and **3** at 250 µM.

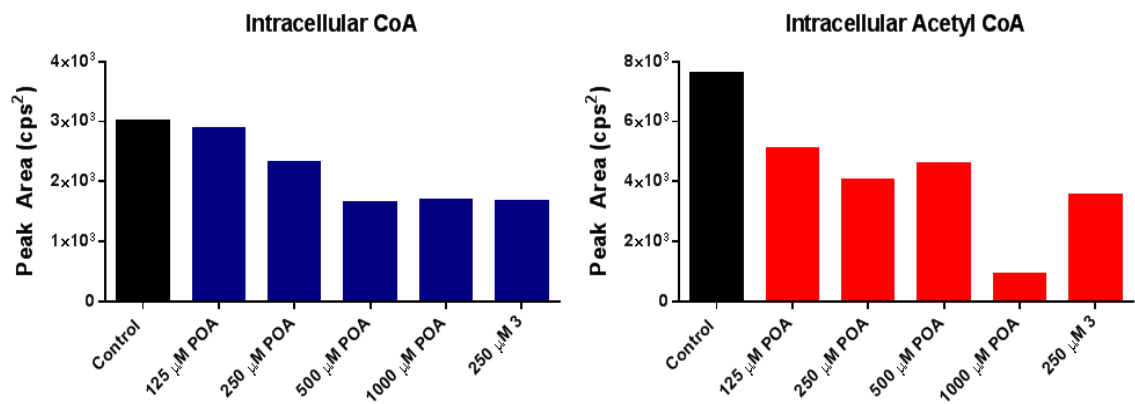


Figure 2.14. The raw areas of CoA and acetyl CoA upon treatment of vehicle (control), titration of POA, and **3**.

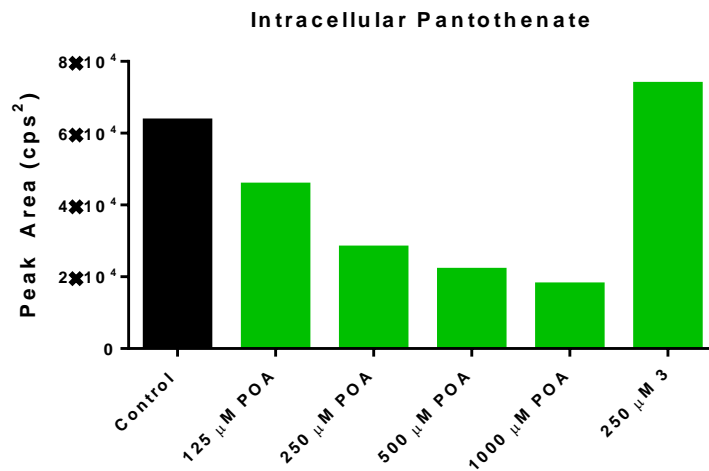


Figure 2.15. The raw areas of pantothenate upon treatment of vehicle (control), titration of POA, and 3.

Currently we are continuing to characterize these molecules in order to gather the necessary information for *in vivo* experiments. As for *in vitro* experiments remaining on the docket, we are seeking determination of the frequency of mutation, characterization of our molecules in CoaBC over- and under-expression strains, characterization of our molecules in CoaD over- and under-expression strains, and evaluation of our molecules against purified CoA biosynthetic machinery. These pieces of data are what remains before publication of these molecules, although we hope to move into *in vivo* infection models, to determine efficacy. We also hope to characterize the pharmacokinetic and pharmacodynamics properties of these molecules to determine the best molecules with which to move forward into efficacy studies, and to determine what prodrug strategy, if any, is necessary to ensure proper animal exposure to these drug candidates.

2.4 Rational design of a pan-acting nucleophilic probe for the characterization of the PLP-dependent proteome

While the development of selective chemotherapeutics is always desired, frequently, when we develop so-called “selective” agents, we intend to focus on the ability of a drug to bind to an intended target compared to its ability to bind related proteins. Determination of the selectivity profile of a pharmacologically-active substance is key to understanding how a molecule achieves an observable activity. Additionally, understanding potential liabilities of active compounds is important to avoid unnecessary investment, be that time and/or money, in a molecule that can result in an unnecessary outcome *in vivo*.

Unfortunately, this task can be difficult when one must investigate the entire proteome for potential binding, however, if one breaks up the proteome into related families the task becomes much easier. Seemingly the poster-child of enzymes in which selectivity is highly important for garnering a desired phenotype is the kinase family.¹⁹¹ Many inhibitors developed for a member of this class of enzymes lack selectivity for their intended target, however, this does not mean that these molecules automatically make for poor drug candidates, especially when a multi-action pharmacology is desired. It is also notable to mention that off-target activities of drug-like substances frequently spell doom for the potential of these molecules to advance to clinical testing.

Some drug discovery campaigns begin with a screen of massive amounts of molecules in an attempt to cover a greater chemical diversity. In modern times such screening usually begins with a purified protein target, generally a validated drug target, although whole-cell screening is still employed and is rapidly regaining popularity.¹⁹² In the case of screens against a purified protein, chemical “hit” compounds, are validated with an orthogonal assay, and confirmed for on-target activity. Yet, to discern if a molecule is actually selective, another process must go on, generally involving other, related, proteins. Continuing to use the development of kinase inhibitors as an example, this process involves counter-screening against other purified enzymes, a time and resource intensive process. Fortunately, libraries that span the “kinome” have been generated for regular screening, utilizing a miniaturization process that speeds up the turnaround time for results when screening against literally hundreds of proteins. While more optimal than what would have

been used even ten years ago, this still uses much more time, effort, and material, than focusing solely on one protein, and is essential for drug discovery campaigns. This model of counter screening has been used for decades, and similar libraries/testing services have been developed for other families of drug targets, such as G-protein coupled receptors (i.e. neuro-receptors). Some pieces of data require counter screens, such as monitoring whole-cell activity against unrelated cell types or species of bacteria, as previously encountered in this thesis.

In an effort to skirt this resource-intensive process, alternate strategies to characterize small molecule interactions with a target protein family have been extensively researched. Likely the most successful approach, pioneered by Prof. Dr. Benjamin Cravatt¹⁹³ and Prof. Dr. Matthew Bogoy,¹⁹³ has focused on the characterization of enzymatic classes that are susceptible to mechanism-based inhibition. This technique, commonly referred to activity-based protein profiling (ABPP), can rapidly increase the understanding of a drug-like substance's selectivity profile for a family of enzymes in a whole-cell system in one fell swoop.¹⁹⁴ Though extensively reviewed in the recent literature, I will briefly explain this technique, the technologies that underlie its capacity to function, and cover an example to illustrate the power of this technique. Currently, ABPP has been most extensively studied using molecules that react with nucleophilic proteins such as serine/threonine hydrolases and proteases, cysteine proteases, and in some rare instances ABPP has been utilized to characterize alternate enzyme classes such as histidine kinases.

¹⁹⁵

Briefly, ABPP can be applied to a wide range of protein families with a known mechanism. To date, protein families that have been well characterized via these means contain nucleophilic residues that interact with a pan-inhibitor of sorts. In the case of serine proteases, originally characterized by Cravatt, an electrophilic warhead is allowed to react with the nucleophilic serine residue in an irreversible fashion. This irreversible warhead is then, somehow, linked to a chemical handle that can be utilized in bio-orthogonal chemical reactions such as the copper-catalyzed Huisgen cyclization (“click reaction”) developed by Prof. Dr. K. Barry Sharpless¹⁹⁶ or the Bertozzi-Staudinger ligation pioneered by Prof. Dr. Carolyn Bertozzi.¹⁹⁷ The electrophilic warhead utilized depends on the class of enzyme being studied, and may be as simple as a substituted fluorophosphonate for serine proteases.¹⁹⁸ This universally-acting compound, after it is allowed to react with proteins in an unspecific manner, can then be modified using one of these bio-orthogonal for imaging or enrichment purposes. During the early characterization of this technique by Cravatt, in concert with Prof. Dr. Dale Boger, the selectivity of a new class of fatty-acid amide hydrolase (FAAH) inhibitors was easy to study in single whole cell-lysate experiments.¹⁹⁸ To succinctly summarize how the technique was utilized in this optimization campaign, when a band on the gel disappeared, that meant the protein was inhibited, and thus, when more than one band on a gel went missing, this indicated a lack of selectivity for FAAH. This approach can be used with many classes of enzymes, and frequently pan-inhibitory probes are designed to look like certain substrates/xenobiotics rather than bind across the entirety of an enzyme class. In the case of FAAH, the comparator activity-based probe

(ABP) closely mimicked the natural substrate arachidonic acid, while unrelated studies have used β -lactones or β -lactams, to study unrelated serine hydrolases which act upon penicillin-containing molecules.^{199, 200}

In tandem with structural-information gathered via X-ray crystallography, this technique can rapidly inform an SAR campaign as it hones in on a selected target, while not requiring isolation, purification, and assay development for the related protein(s) that initial hit molecules may have inhibited. ABPP rapidly allows for the acquisition of proteomic data without excessive effort from the scientists, yet garners the same sort of information gleaned from counter screening. Most importantly, this approach can identify proteins not necessarily postulated to be affected by the molecule in question.

While this technique has the power to inform many types of drug discovery campaigns, it is hampered by the need for a pan-acting warhead which covalently labels proteins within a family. Additionally, to date, this technique has only been utilized with electrophilic probes to characterize entire protein families, although a “reverse polarity” technique has been recently reported utilizing a hydrazine warhead to unselectively label cellular electrophiles, and thus far has only been characterized with post-translationally modified enzymes.²⁰¹ However, potential enzymatic drug targets are not only nucleophilic proteins, and there is currently no known way to gauge the selectivity of a molecule for nucleophilic mechanism-based inhibitors (MBIs), or any enzyme that contains an active-site electrophile.

A key enzymatic class that is susceptible to mechanism-based inhibition via its active-site electrophile is the PLP-dependent enzyme class.²⁰² PLP-dependent enzymes utilize the coenzyme pyridoxal phosphate, an essential dietary vitamin frequently consumed as vitamin B6. This family of proteins is responsible for a wide array of biochemical activity, however, for simplicity, the mechanism of a racemase is shown in Figure 2.16.²⁰³

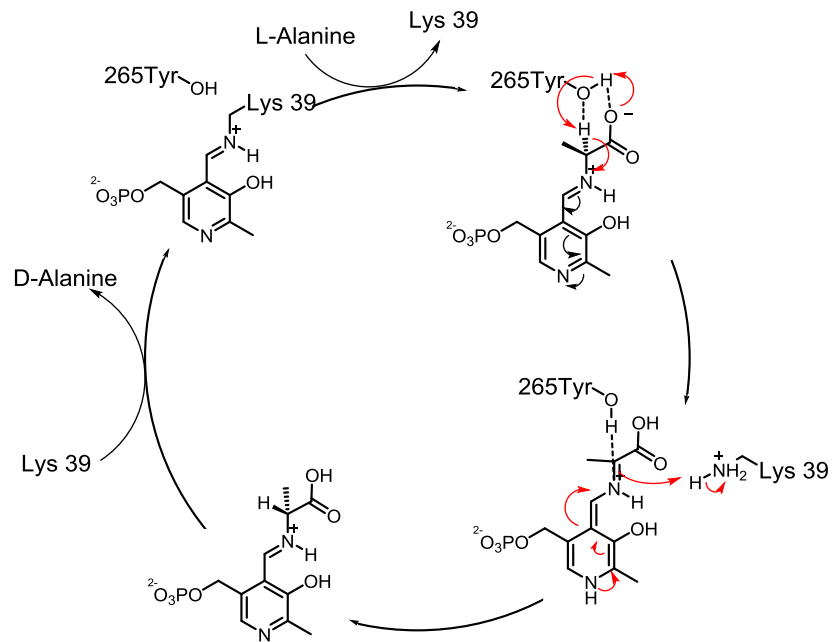


Figure 2.16. The mechanism of PLP-dependent racemase Alanine racemase (Alr).

PLP-dependent enzymes have materialized as viable drug targets for a variety of pathologies ranging from neurological disorders to fighting infectious diseases. While multiple FDA-approved drugs target a PLP-dependent enzyme as part of their principle mechanism of action, the actual pharmacology exuded by these drugs is not necessarily explainable solely by the action of the intended enzymatic target. For instance, the antitubercular drug D-cycloserine (DCS) is intended to treat infection by tuberculosis, with a known mechanism of action due to non-covalent inhibition of D-Alanine-D-alanine ligase (Ddl) and mechanism-based inhibition of the PLP-dependent enzyme Alanine racemase (Alr).²⁰⁴ However, the side-effects in humans manifests itself as psychosis in otherwise healthy patients, limiting the use of this drug in the clinic for its FDA-approved use. This suite of side effects can be attributed to non-specific binding with multiple identifiable protein targets (i.e. metabotropic glutamate receptor 4, and the N-Methyl-D-aspartate receptor), yet the effect that DCS has on the brain is not fully understood, and may be due to activity PLP-dependent enzymes such as GABA transaminase, the putative target of the FDA-approved antiepileptic agent Vigabatrin (Sabril®).²⁰⁵ In order to better characterize drugs like DCS, and this overall important class of drug targets, we envisioned that the reverse polarity ABPP strategy may be a viable approach to studying these enzymes and the selectivity of molecules intended to inhibit them.

Prior to the initiation of this work, no report of reverse polarity ABPP had been publically released.²⁰¹ As such when the first probe was designed, I based the molecule off of known inhibitors of PLP-dependent enzymes. While hydrazines/hydrazides have been

known for decades to inhibit these sorts of enzymes,^{206, 207} their potency has often been lacking for drug targets, and many of these molecules show reversible binding kinetics.²⁰⁸ Additionally, these molecules are not mechanism-based inhibitors as they strictly interact with the carbonyl of PLP in a non-specific manner and the enzyme does not interact with the hydrazone adduct in any manner. While this nucleophilic warhead may be able to serve as a mediator of PLP-dependent enzyme profiling, the initial hope would be to have a molecule that is specific for the PLP cofactor, which would force interaction with the protein, solidifying selectivity for the desired cofactor. To this effect, a report from 1979 would serve as the basis for the design of my probe, as *N*-hydroxy amino acids serve as mechanism based probes of racemase-type enzymes.²⁰⁹

As a proof-of-concept, I started with an *N*-hydroxy alanine scaffold, hoping that the lack of functionality on the β carbon would confer the most universal binding while still closely mimicking the natural substrates. This molecule, synthesized under my direction by another one of my undergraduate mentees Christopher (Chris) Brown, would likely function via the mechanism outlined in Figure 2.16, forming a stable nitron functional group (Figure 2.17), labeling the cofactor irreversibly. This initial molecule, known internally as CDB-I-143, was synthesized using standard chemistries starting with pyruvic acid. The Steglich esterification²¹⁰ proceeded with a low yield likely due to the heavily withdrawing nature of the α -keto substituent. Nevertheless, once the ester bond was formed, reductive amination, using Borch conditions, afforded the racemic amine (Scheme 2.10) for our initial characterization.

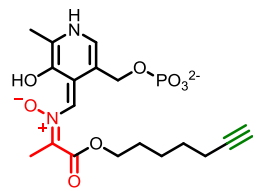
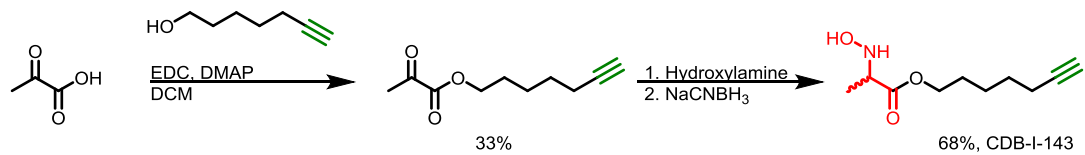


Figure 2.17. The proposed nitrono-quinoid intermediate formed between a modified *N*-hydroxy amino acid and PLP.



Scheme 2.10. The synthesis of CDB-I-143 as performed by Christopher Brown.

With this molecule in hand, I opted to first characterize the molecule as an inhibitor of a PLP-dependent enzyme. Familiar to the Aldrich group, I chose diaminopelargonic acid (DAPA) synthase from *M. tuberculosis* called BioA.²¹¹ This enzyme, a transaminase, catalyzes an important amination in the *de novo* biosynthetic route of biotin by *Mtb*. Additionally, prior to working with the enzyme, our lab had already established enzymatic assays to assay the effectiveness of inhibitors we have developed for this enzyme.²¹² Our previous knowledge of the enzyme indicated the protein has high specificity as to what can bind to the cofactor, and is quite slow at catalyzing its desired reaction as well as its own demise when an MBI is introduced. Using the coupled assay depicted in Figure 2.18, I was able to discern the nature of inhibition by CDB-I-143.

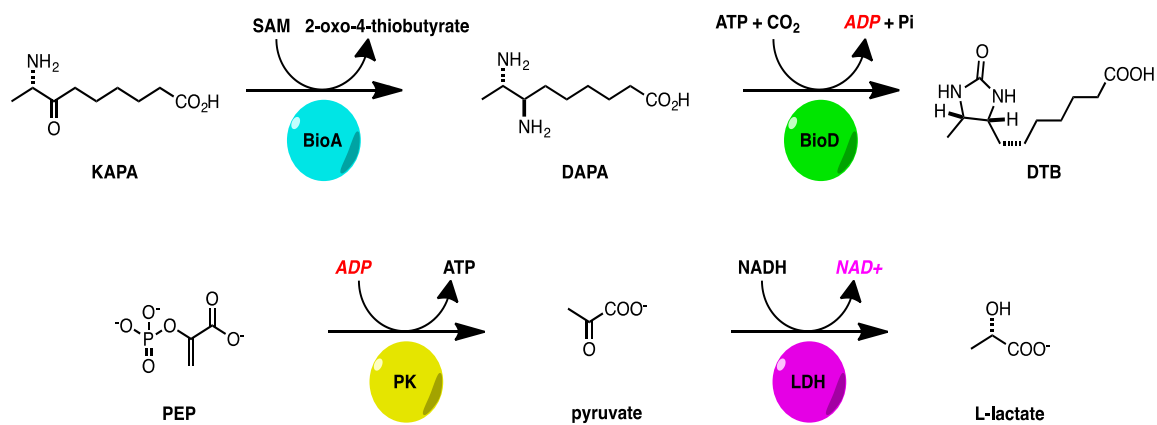


Figure 2.18. The coupled assay used to assess the activity of CDB-I-143 against BioA.

Notably, the molecule displays time-dependent inhibition, and seems to be unable to be competed out of the enzymatic pocket after preincubation. To summarize the effect of CDB-I-143, its specificity constant, defined as the rate of inactivation over the rate of the initial binding event (k_{inact}/k_i), was determined by determining the percent of inhibition after preincubation times varying between 5 and 45 minutes. The secondary plot, shown in Figure 2.19, can then be fit to a line giving the value $k_{inact}/k_i = 355 \text{ Min}^{-1}\text{M}^{-1}$, a value that is actually quite similar to a molecule made by a former post-doctoral scholar in our group, Dr. Ce Shi, which is reportedly optimized for activity against BioA.²¹³

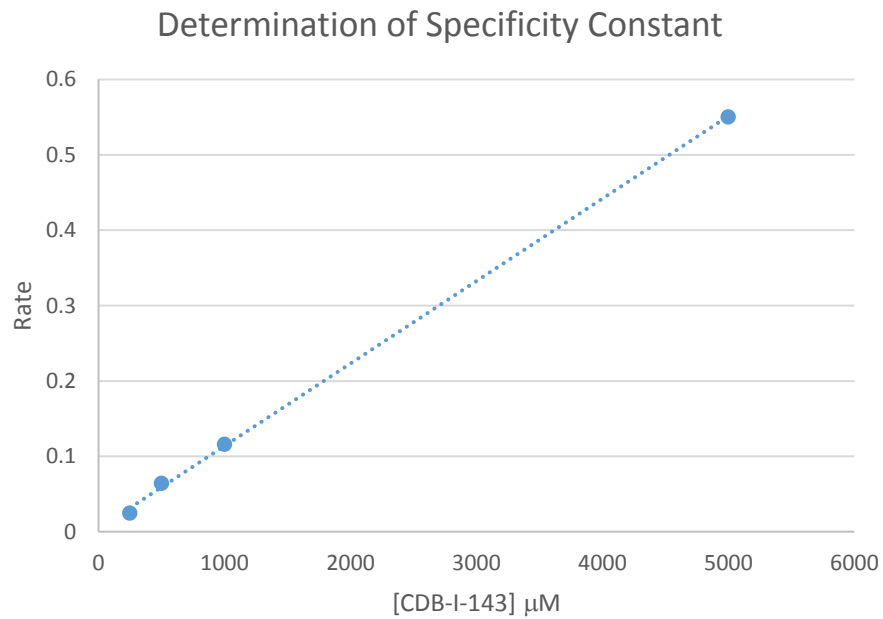
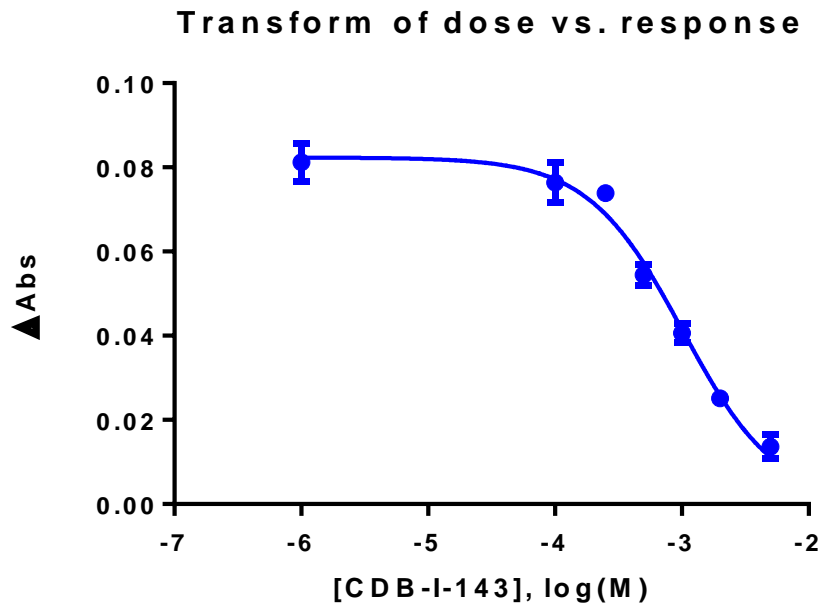


Figure 2.19. The degree of inhibition and secondary plots used to determine the specificity constant of CDB-I-143.

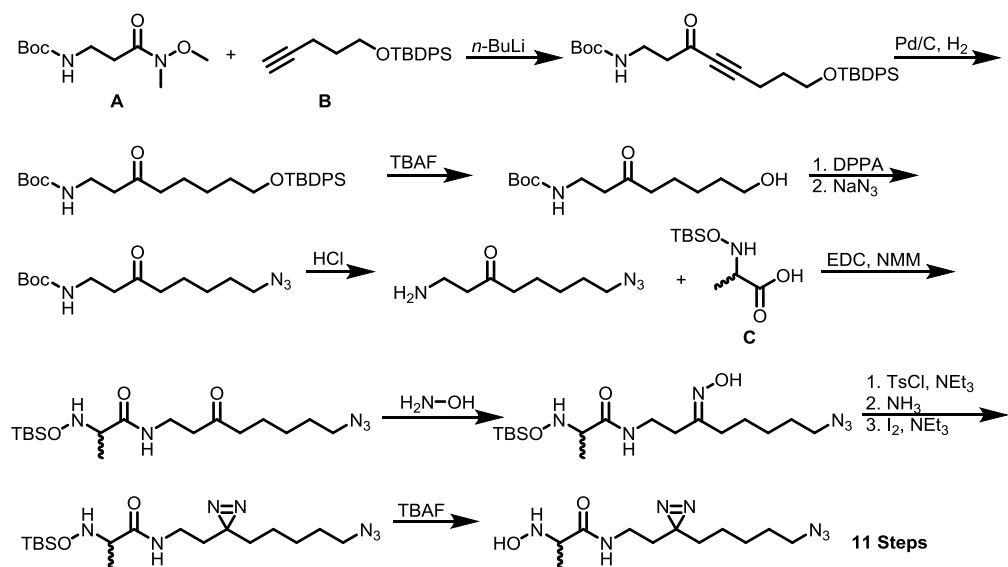
This result prompted a bit further study with CDB-I-143, but also indicated that a more stable amide analog should be generated. To this effect, Chris once again got to work, however, when he attempted to make the amide analog using the same route, the Borch conditions⁹⁰ never yielded the α -*N*-hydroxy amino amide compound. As a second reducing condition, Chris tried to use hydrogen with a Palladium catalyst, but only ended up generating the amine compound, finding a great way to make racemic alanine.²¹⁴ To alleviate this short-coming, Chris attempted multiple routes, all of which included starting with *N*-hydroxy alanine, without being able to bear the desired compound by the end of his tenure within the lab.

Even without a more stable amide compound, I used CDB-I-143 in preparation of whole-cell lysate proteomic experiments. These experiments, while informative about the workflow of ABPP, did not ultimately yield publishable images, however, it was apparent in experiments using two unrelated purified enzymes (BioA and BlaC) that the probe only bound to one of these enzymes. The results of this effort, which are not shown in this text made a few things quite clear: 1) CDB-I-143 does not bind to serine hydrolase BlaC, indicating the *N*-hydroxy alanine warhead does not bind to proteins without specificity; 2) Labeling the cofactor of the protein is not necessarily sufficient for gathering proteomic data, instead one should attempt to label the protein; 3) Copper-catalyzed “click” chemistry¹⁹⁶ will work with our alkyne probe bound to the PLP coenzyme, indicating appropriate linker length; and 4) A next generation probe should use the same warhead for

targeting our desired enzyme class, but should also contain a moiety that can be induced to react directly with the protein to facilitate higher yields in enrichment experiments.

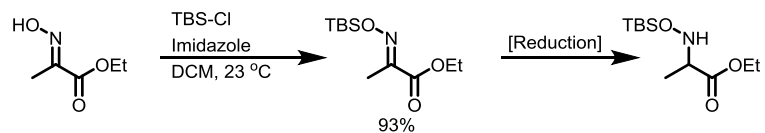
Having learned about the necessity of what is needed for a probe in these studies, I then designed a next generation probe that includes a photo-inducible covalent interaction with proteins. This technique, known as photo-affinity labeling (PAL), has been used with regularity when studying the interface of chemistry and biology.²¹⁵ Even in the Aldrich lab, PAL has been used to discern the specificity of molecules studied in the lab.²¹⁶ While this field has been extensively reviewed in the literature, the main highlight that should be addressed is that PAL is not simple, and that optimization of the PAL moiety is often needed to ensure both binding and suitable kinetics of reactivity with the protein. Luckily, others have done much of the heavy lifting, and it was fairly straightforward to pick a PAL that matched our needs, while still being synthetically feasible. As such, I chose the diazirine as the PAL of choice, continuing to use about the same alkyl-type linker region between the bio-orthogonal handle and targeting warhead. With this probe, the ABP should retain the targeting aspect of CDB-I-143, yet should be capable of binding directly to the protein with rapid kinetics when 365 nm light is shined on a sample.

Synthesis of this molecule would be arduous from typical commercially-available starting materials. Shown in Scheme 2.11, the originally proposed route encompassed 11 synthetic steps, and was assigned to both, Kathleen Wang, and a first-year graduate student Scott Brody.



Scheme 2.11. The originally proposed route towards a 2nd generation ABP for PLP-dependent enzymes.

Unfortunately neither of these scientists were able to put much of a dent into the synthesis before we discovered that a reagent containing both an alkyne and PAL moiety was available for purchase. While this would shorten the synthesis considerably, this wouldn't necessarily make the molecule appear out of thin air, as Chris' experiments years prior had indicated that making an α -*N*-hydroxy amino amide would be much more difficult than making the corresponding α -amino amide. To alleviate the problems noted by Chris, I opted to try to install the *N*-hydroxy moiety before the amide coupling. To this effect, I tried a few routes which included silicon protecting groups for the hydroxyl group. Summarized in Scheme 2.12, these routes all failed, as either the reduction failed for the protected oxime, or the protecting groups were not robust enough to survive hydrolysis of the ester moiety. This was peculiar, but would later be used to my advantage.



Reductions Attempted and Outcome:

Pd/C + H₂: No reduction

Raney Ni + H₂: No reduction

Na(CN)BH₃ + HCl: No reduction + Protecting group loss

NaBH₄ + AcOH: No reduction + Protecting group loss

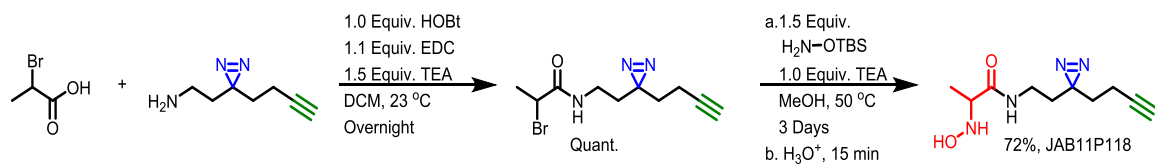
BH₃: No reduction with Et₂O or THF complexes

BH₃ + HCl: Reduction + Protecting group loss

BH₃ + AcOH: Reduction + Proteting group loss

Scheme 2.12. The attempted synthesis of a 2nd generation ABP for PLP-dependent enzymes.

While the reductive amination type synthetic route would ultimately not work, I was inspired by one of Chris' proposed routes that he was never able to pursue. In this direction, the final step would be a nucleophilic substitution with hydroxylamine using 2-bromopropionic acid as the carbon skeleton of the targeting warhead. When I attempted the synthesis using this route I found that the reaction with the secondary bromide would go, however, an *O*-protected hydroxylamine would be optimal for selectivity and ease of purification. Using the route summarized in Scheme 2.13, I was able to generate JAB11P118, the 2nd generation PLP-dependent enzyme pan-probe for ABPP. After nearly three years from conceptualization, a molecule was ready that should be usable for our purposes.



Scheme 2.13. The synthesis of JAB11P118.

At this point, JAB11P118 was handed off to Scott Brody for further characterization. Although these results are still quite preliminary, I wish to highlight the potential of this molecule that I fantasized about for quite a long time during my tenure in the Aldrich lab. Scott was able to show that this molecule is capable of inhibiting another PLP-dependent enzyme (Figure 2.20), IlvE, an amino acid synthetase that generates branched chain amino acids via transaminase activity.²¹⁷ In addition to studies with purified enzymes, Scott has also had the time to perform other necessary control studies before taking JAB11P118 into unknown samples. One such study performed showed that enzyme labeling can be competed away by other inhibitors. In this study, a cocktail of three potential inhibitors were preincubated with purified IlvE before JAB11P118 was added to the sample.²¹⁸ The inhibitors; DCS, β -chloroalanine, and *N*-hydroxy alanine, were incubated in 10-fold excess for 30 minutes to irreversibly label PLP, blocking the ability for JAB11P118 to bind. Then, this sample and no-drug control were treated with JAB11P118 and copper-catalyzed click chemistry was utilized to label proteins with a TAMRA fluorophore.²¹⁹ Shown in Figure 2.21, the lack of fluorescent signal in pre-treated samples continued to indicate that JAB11P118 only labels with specificity.

Time & Concentration Dependent Inactivation

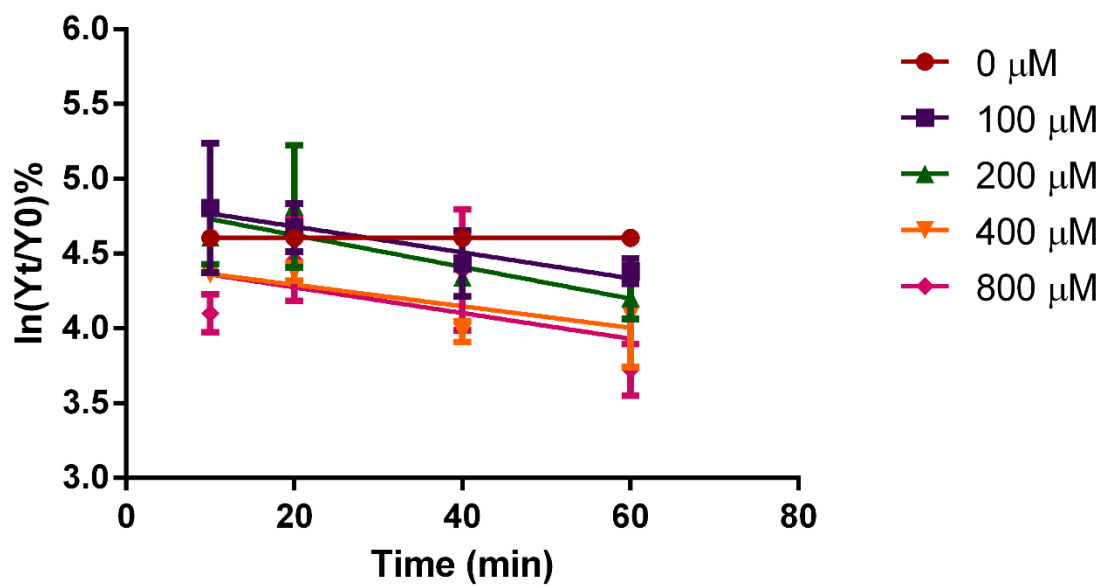


Figure 2.20. Time and concentration dependent inhibition of IlvE with JAB11P118. Data collected by Scott Brody.

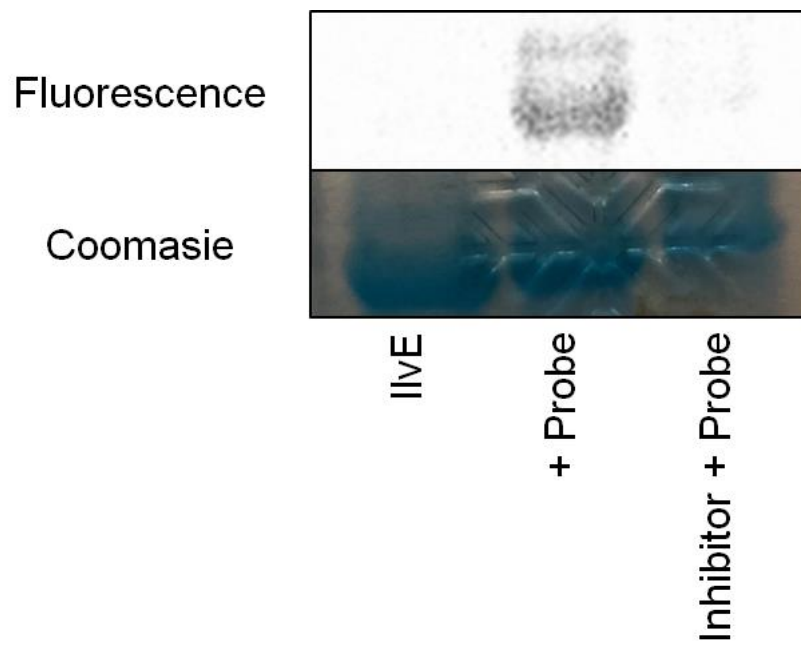


Figure 2.21. The selective labeling of IlvE by JAB11P18 with and without a competitive inhibitor. Data collected by Scott Brody.

As such, JAB11P118 has been taken into lysate experiments²²⁰ with a strain of *E. coli* overexpressing IlvE. Shown in Figure 2.22, our probe selectively labels proteins, labeling IlvE quite well as indicated by fluorescent imaging. Additionally, other bands can be noted in the wells that have sufficient labeling, indicating that a high concentration of the probe is needed in order to label proteins. These bands don't just recapitulate the coomassie staining in which higher abundance proteins are labeled unselectively via reaction with the PAL. This finding is extremely encouraging, as we can trust the probe not to label proteins in high abundance that lack PLP-dependent action or other electrophilic residues. What has yet to be fleshed out at this point, however, is MS-based confirmation of proteins. The samples generated thus far have focused on adding fluorophores to proteomic samples, rather than an enrichment handle (i.e. biotin) to perform affinity purification of labeled samples. While this optimization is not necessarily easy, this workflow has been utilized by thousands of researchers, and its robustness for producing the desired enrichment results is unparalleled.²²⁰

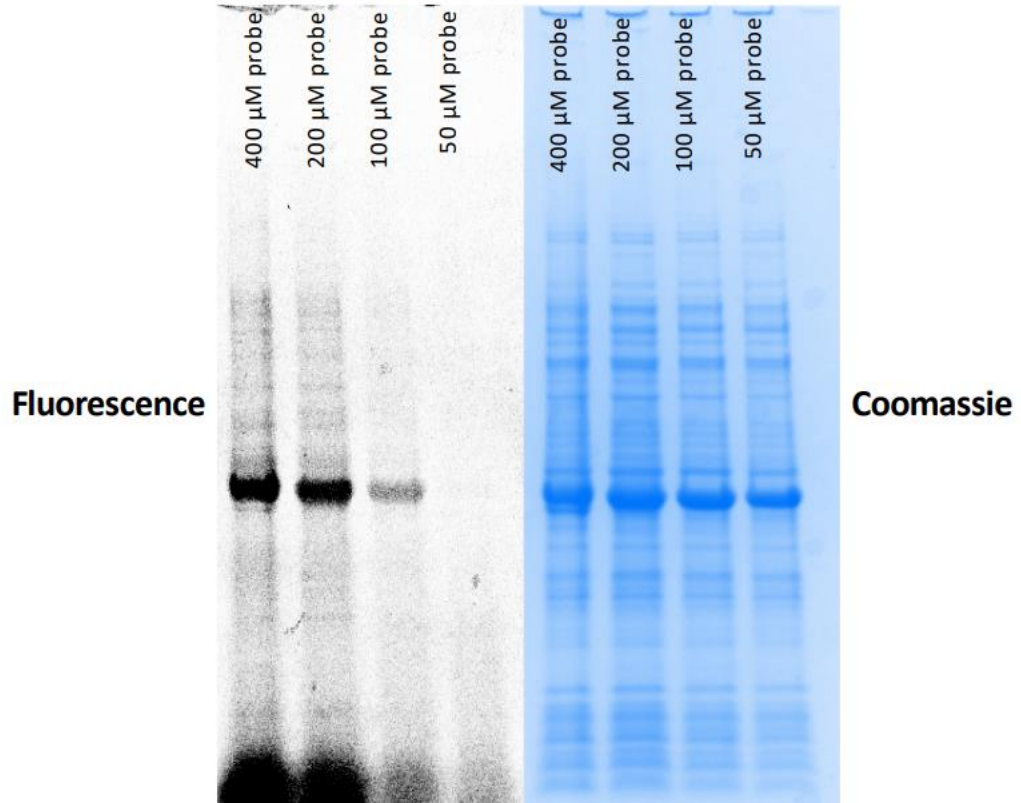


Figure 2.22. The selective labeling of an IlvE overexpression strain in *E. coli* using varying concentrations of JAB11P118. Data collected by Scott Brody.

While JAB11P118 appears to be a promising probe towards understanding the PLP-dependent proteome, there are more experiments necessary to prepare this story for publication. Currently, we are optimizing enrichment studies using a tri-functional azide probe that can be used for affinity-purification and gel-electrophoresis imaging of the same exact lysate sample. This optimization should yield proteomic samples which can be analyzed with MS to identify proteins that our probe binds to, facilitating an understanding of the PLP-proteome. We will also use JAB11P118 to investigate a variety of known PLP-dependent enzyme inhibitors, namely, we intend to investigate DCS both bacterial and mammalian tissues in order to better characterize this highly intriguing drug. At this time, these studies are still planned, and we hope to submit an initial report which characterizes this reverse polarity ABP. The bulk of this additional characterization will be performed by others in the pursuit of their own degrees, however, it felt necessary to cover this topic as the idea, design, and initial synthesis was derived from my own curiosity.

2.5 Concluding remarks

While the efforts presented in this chapter are still ongoing, the labor presented herein represents much of the proof-of-concept work necessary to begin much more arduous characterization of these systems. These molecules exhibit the breadth of work one encounters during their pursuit of new drug materials. While the emphasis of the Aldrich group, and much of the work that has been exhibited, has remained on the discovery of new drug materials for the eradication of *Mtb*, we've also branched out from

focusing on therapeutics to gaining new tools which can be used to identify, validate, and study new drug targets.

The β -lactam prodrug, **1**, highlights the necessity of understanding how known drugs interact with the body. By building a better prodrug, it is very likely that this conjugate can deliver the actually toxic warhead at the site of action, limiting full-body exposure, reducing first-pass metabolism aimed at ejecting the drug, and in this case, circumvent known resistance mechanisms. Likely, this strategy can find use in alternate applications in the treatment of pathologies derived from infectious agents. Currently ongoing in our laboratories is the identification of such moieties that lack selectivity for *Mtb*, yet are effective against the microbe. Such warheads may be presently known to be toxic when administered chronically, but these properties should very well be alleviated by the addition of the β -lactam promoiety. We also note that, in the case of *Mtb*, these molecules have the potential to not only act as target-directed pro-drugs, but also as dual warhead molecules that can even promote synergy within itself.

My research has also highlighted the importance of understanding a molecule's pharmacology. As highlighted within this text, characterization of the mechanism behind POA's action yielded an unforeseen development that POA is in fact an antimetabolite-type drug. POA is bioactivated by *Mtb* to an active antimycobacterial compound, one that we were able to identify and synthetically generate. While characterization of molecules that resemble these activated entities is still ongoing, we now know a rational route towards the design of molecules which have similar activity against *Mtb* which may replace PZA

in regions of the world with endemic resistance. For now, no resistance has been isolated or characterized, and the exact manner in which these molecules act is still unclear, much like the parent molecule. Our effort, however, does point us in the right direction for elucidating the mechanism of this very important drug while also yielding a new drug scaffold with which to develop new chemotherapeutics.

Also discussed in this chapter was an entirely unrelated project to developing new antitubercular agents, in the development of a new ABP for PLP-dependent enzymes. This project was initiated by the desire to characterize the known TB drug DCS, but ultimately was a foray into a new frontier for chemical biology. The design of this nucleophilic probe meant to characterize a specific coenzyme was conceived when no such molecule had existed. This concept unfortunately took much time in order to manifest itself as a usable probe, since multiple generations of molecules were designed and then synthesized in order to find a chemical moiety that is amenable to use by both experts and trainees. With a molecule that targets the coenzyme that is also then capable of directly labeling the enzyme in place, we can now move to advance the characterization of molecules which target PLP-dependent enzymes, many of which were approved by the FDA before such rigorous testing was required for an application to go into human patients.

While these projects presented within this chapter are seemingly unrelated, each one hopes to address the nature and importance of selectivity in drug discovery programs. The first project presented really emphasizes the need for selectivity, as this prodrug strategy would fail if any basic serum esterase were able to cleave the promoiety from the

warhead. Selective release with a β -lactam promoiety ensures the drug 1) gets to the site of action; 2) limits exposure of the drug to metabolic enzymes which deactivate the molecule; and 3) promotes on-target activity of the drug, should any off-target effects exist. The second part of this work potentially explains the reason for PZA/POA's selectivity for *Mtb*, but also takes advantage of this selective molecule as a framework for another selective drug. The last part presented actually highlights a case in which a lack of selectivity isn't necessarily a negative quality of a molecule. The development of this probe was based on the need for ubiquitous binding of the targeting moiety to an entire family of proteins, but only that specific family. The specificity for PLP-dependent enzymes is necessary to then understand how other molecules, anything from new chemical matter to FDA-approved entities, interact with this family of proteins. This new molecule can garner a new appreciation for the selectivity, or lack thereof, a molecule has to exert its pharmacological outcome. Taken together, this body of work has attempted to utilize selectivity for the rational design of new chemotherapeutics for a wide range of potential pathologies.

2.6 Methods and materials

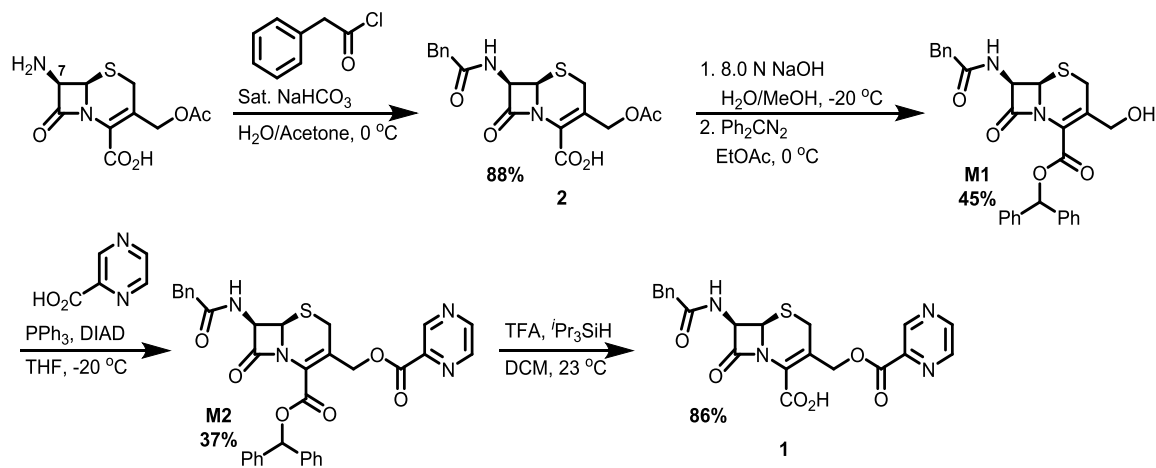
2.6.1. General Remarks

All commercially available reagents were used without further purification. Molecular sieves were activated by heating at 200 °C under reduced pressure. Tetrahydrofuran (THF), toluene, and dichloromethane (CH_2Cl_2) were dispensed from an Inert® solvent dispensing system. Deuterated chloroform, CD_3CN , and d_6 -DMSO were purchased from Cambridge Isotopes and used without further drying from 10 gram bottles

stored in a desiccator. Piperidine were dried over calcium hydride and freshly distilled under reduced pressure immediately before use. ^1H , ^{13}C , ^{19}F , and ^{31}P NMR spectra were recorded on a Varian 400 MHz spectrometer, Bruker Avance 500 MHz spectrometer, or Varian INOVA 600 MHz spectrometer with broadband probes. High resolution mass spectra were collected on a Bruker BioTOF II mass spectrometer using PEG or PPG internal standards. Sodium formate was sometimes added in order to facilitate ionization, frequently leading to characterization of the $[\text{M} + \text{Na}^+]$ masses. Silica gel column chromatography was performed with silica gel (Dynamic Absorbents, 60A) or using a Teledyne-Isco RF-200 Combi-Flash system. Kugelrohr distillations were performed with a Buchi glass oven B-585 instrument. The experiments contained herein are not hazardous outside of the typical flammable/explosion hazards present with the usage of organic solvents, ethereal solvents such as Et_2O and THF should always be assayed for the presence of peroxy by-products.

Pathogenic bacterial strains were graciously supplied by either the laboratory of Prof. Dr. Anthony Baugh, or Prof. Dr. Ryan Hunter. Biosafety-level 3 experiments were all performed by the Baughn laboratory according to their protocols. All reagents used in these and other biological experiments are described in each experimental section.

2.6.2. Synthesis of β -Lactam conjugate **1**



To a 500 mL round bottom flask equipped with a stir bar was added 7-aminosephalosporanic acid (9.00 g, 33.2 mmol, 1 equiv), acetone (75 mL), and saturated NaHCO₃ (225 mL). The slurry was stirred until gas evolution ceased, upon which the reaction was cooled to 0 °C. Phenylacetyl chloride (4.75 mL, 36.3 mmol, 1.1 equiv) was added in a dropwise manner over 15 minutes. The reaction was stirred and allowed to warm slowly to 23 °C. After 16 hours, the reaction was diluted with 100 mL of EtOAc, and the layers were separated. The aqueous layer was acidified with 2.0 N HCl (500 mL) and the reaction was with EtOAc (3 x 500 mL). The organic layer was evaporated under reduced pressure and the resultant gum was suspended in Et₂O (200 mL). After 15 minutes of stirring, the suspension was filtered to yield compound **2** (11.66 g, 88%) as an off-white solid. Physical and spectrographic data matched previous reports.¹⁷³

To a 100 mL round bottom flask equipped with a stir bar was added **2** (2.334 g, 6 mmol, 1.00 equiv) and a solution of water (12 mL) and MeOH (9 mL). The suspension was cooled to -20 °C and a cooled solution (stored on ice) of 15% NaOH (2.4 mL) was added over 40 minutes and the reaction was allowed to continue stirring at -20 °C. After

20 minutes the reaction was neutralized to a pH of 6 with slow addition of 10% HCl (~1.0 mL). Then, a solution of diphenyl diazomethane (1.222, 6.30 mmol, 1.05 equiv) in EtOAc (6 mL) was added to the reaction and an addition 1.2 mL of 10% HCl was added over 90 minutes. The reaction was warmed to 0 °C and stirred for 2 hours, upon which the reaction mixture was filtered and washed with EtOAc (100 mL) to afford compound **M1** (1.390 g, 45%) as a snow-white solid. Physical and spectrographic data matched previous reports.²²¹

To a 100 mL round bottom flask charged with **M1** (1.000 g, 1.89 mmol, 1.0 equiv) was added pyrazinoic acid (259 mg, 2.09 mmol, 1.1 equiv), and anhydrous THF (38 mL). The flask was sealed, purged with argon, and cooled to -20 °C. Triphenylphosphine (550 mg, 2.09 mmol, 1.1 equiv) was added, the flask was resealed, and the vessel was fitted with an argon balloon. After dissolution of the solid, diisopropyl azodicarboxylate (DIAD, 410 µL, 2.09 mmol, 1.1 equiv) was added in a dropwise manner over 20 minutes and the mixture was stirred for 2 hours. The mixture was diluted with EtOAc (40 mL), poured into ice water (80 mL), and the layers were separated. The aqueous layer was extracted with EtOAc (2 x 80 mL) and the organic layers were combine and evaporated directly onto SiO₂. Purification using a Teledyne Isco Repi-Sep Combi-Flash Rf-200 MPLC afforded compound **M2** (421.8 mg, 36%) as a white solid. NMRs did show some impurity as triphenyl phosphine oxide readily co-elutes with **M2**. The product was carried forward to deprotection without further isolation and characterization: $R_f = 0.10$ (50:50 hexanes: EtOAc).

To a 50 mL round bottom charged with **M2** (270 mg, 0.435 mmol, 1 equiv) was added CH₂Cl₂ (18.9 mL) and the reaction was cooled to 0 °C. With stirring, both TFA (16.7 mL, 217.5 mmol, 500 equiv) and triisopropylsilane (TIPS, 890 μL, 4.35 mmol, 10 equiv) were added simultaneously and the reaction was allowed to stir at 0 °C. After 15 minutes, the reaction mixture was evaporated under reduced pressure, using both PhMe and Et₂O as azeotropes to remove excess TFA. The crude mixture was evaporated onto celite and purified using a Teledyne Isco Repi-Sep Combi-Flash Rf-200 MPLC equipped with a Cyano-functionalized silica gel column using a gradient of 0 – 100% MeOH in CH₂Cl₂ to afford conjugate **1** (170.2 mg, 86%) as a tan-colored solid; ¹H NMR (500 MHz, *d*₆-DMSO) δ 13.80 (br, 1H), 9.24 (d, 1H, *j* = 1.5 Hz), 9.11 (d, 1H, *j* = 8.3 Hz), 8.92 (d, 1H, *j* = 2.4 Hz), 8.84 (s, 1H), 7.30 (d, 4H, *j* = 8.4 Hz) 7.24 (d, 1H, *j* = 7.1 Hz), 5.69 (dd, 1H, *j* = 8.3, 4.8 Hz), 5.24 (ABq, 2H, *j* = 135 Hz, *j*(AB) = 12.8 Hz), 5.06 (d, 1H, *j* = 4.8 Hz), 3.75 (d, 1H, *j* = 17.8 Hz), 3.64 (d, 1H, *j* = 17.7 Hz), 3.54 (ABq, 2H, *j* = 35 Hz, *j*(AB) = 13.9 Hz); ¹³C NMR (125 MHz, *d*₆-DMSO) δ 171.42, 166.98, 148.66, 147.84, 146.21, 145.99, 143.31, 143.03, 136.28, 129.48, 128.70, 126.96, 123.13, 71.84, 60.19, 59.51, 57.86, 42.05, 26.04, 22.86; HRMS for C₂₁H₁₈N₄NaO₆S⁺ [M+Na⁺] calculated 477.0839; found 477.0847.

2.6.3. General procedure for the assessment of minimum inhibitory constants

Susceptibility was determined by measuring the optical densities of cultures (OD₆₀₀) for three separate experiments. The MIC was defined as the concentration of drug compound for which growth was inhibited by at least 90% compared to a no-drug control.

2.6.3.1. MIC testing in Mycobacteria

Susceptibility testing in Mycobacteria was carried out using *M. tuberculosis* strain H37Rv and *M. bovis* strain BCG. Cultures were grown in Middlebrook 7H9 medium (Difco) supplemented with 10% (v/v) oleic acid-albumin-dextrose-catalase (Difco), 0.2% (v/v) glycerol, and 0.05% tyloxapol. Each strain was first grown to mid-exponential phase in defined media and diluted to an OD₆₀₀ of 0.01 in 5 mL of culture medium adjusted to the desired pH in 30 mL square Nalgene bottles (Fisher). Compounds were added to the media in concentrations ranging between 0.5 – 1600 µg/mL as indicated. Cultures were incubated at 37 °C with shaking on a rotary platform at 100 rpm for 10 days (unless otherwise indicated).

2.6.3.2. MIC testing in other pathogens

Susceptibility testing in ESKAPE pathogens included *E. coli* strain K12, *A. baumannii* strain AB5075, *P. aeruginosa* strains PAO1 and PA14, *A. xylosoxidans* strain MN-001, and *S. aureus* strain USA300. Cultures were grown in cation-adjusted Mueller-Hinton broth (Sigma) without any additional components or adjustment to pH. Each strain was then grown to the end of mid-exponential phase (OD₆₀₀ = 0.6 – 0.8) and diluted to an OD₆₀₀ of 0.01 in 200 mL of culture medium in a clear-bottom 96-well plate (Corning). Compounds were added to the media in concentrations ranging between 0.5 – 1600 µg/mL as indicated. Cultures were incubated at 37 °C without shaking for 16 – 18 hours. Control antibacterial compounds were added as follows: *E. coli* – Zosyn; *A. baumannii* – Rifampicin; *P. aeruginosa* – Tetracycline; *A. xylosoxidans* – Zosyn; and *S. aureus* – Tetracycline.

2.6.4. HPLC method for detection of 1, POA, and other metabolites

2.6.4.1. HPLC Method for MS/MS studies

Reverse-Phase HPLC was performed on a Shimadzu Nexera X2 instrument (Shimadzu Corporation, Kyoto, Japan) equipped with a Zorbax Eclipse XDB-C8, 5 micron, 4.6 x 150 mm column (Agilent Technologies, Santa Clara, CA). The mobile phase consisted of 5 mM aqueous ammonium acetate, pH unadjusted, with 2% acetonitrile as the aqueous component (A) and 100% acetonitrile as the organic component (B). Solvents used were at least mass-spectrometry grade, and were prepared within 72 hours of use. Elution was performed following the gradient shown in Figure 2.21 at a flow rate of 0.5 mL/min. Detection of mass transitions and polarities for MS experiments are described in section 2.6.5.

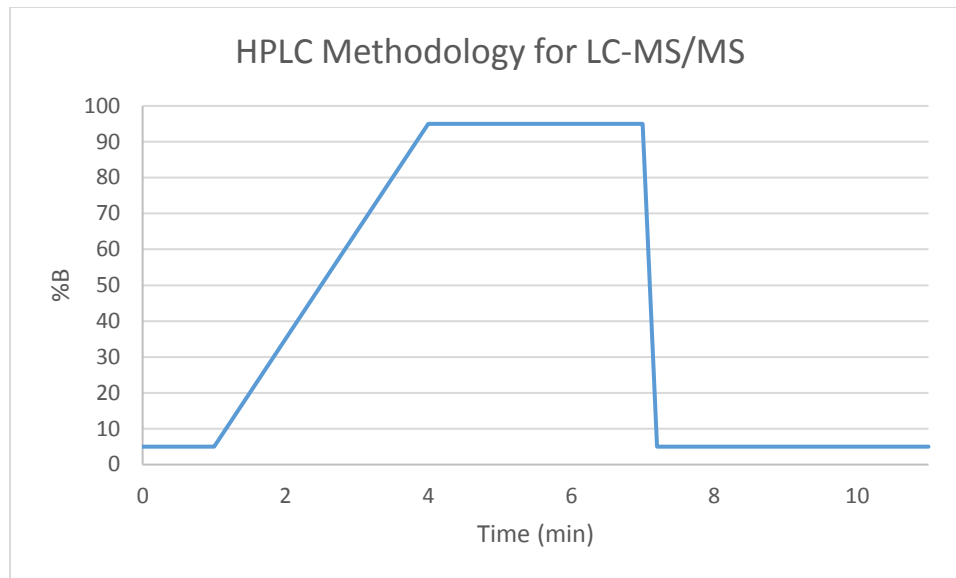


Figure 2.23. The HPLC method used to separate and detect analytes in purified and lysate samples.

An example of a chromatogram is shown in Figure 2.24 for POA and its tris-deuterated standard d_3 -POA to illustrate a once-difficult analyte to retain on columns within the Aldrich lab.

Method Development and Validation

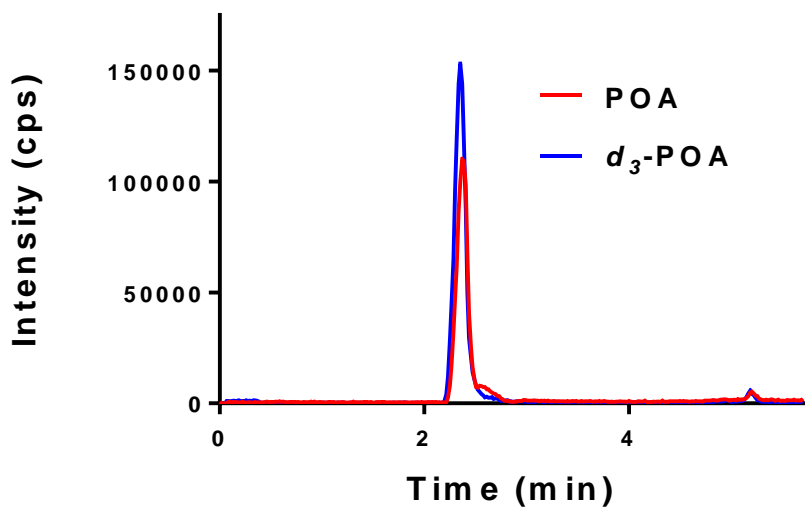


Figure 2.24. The zoomed-in trace chromatogram of POA and d_3 -POA using the Eclipse XDB-C8 column at 0.5 mL/min flowrate using the method defined in Figure 2.23.

2.6.4.2. HPLC coupled to a diode array detector (DAD)

Reverse-Phase HPLC was performed on an Agilent 1260 instrument (Agilent Technologies, Santa Clara, CA) equipped with a Kinetex-C18, 2.6 micron, 4.6 x 100 mm column (Phenomenex, Torrance, CA). The mobile phase consisted of 0.1% (v/v) aqueous formic acid as the aqueous component (A) and 0.1% (v/v) formic acid solution in acetonitrile as the organic component (B). Solvents used were at least mass-spectrometry grade, and were prepared within 72 hours of use. Elution was performed following the gradient shown in Figure 2.25 at a flow rate of 0.4 mL/min. The DAD was set to monitor at wavelength 254 nm with 360 nm acting as a reference wavelength.

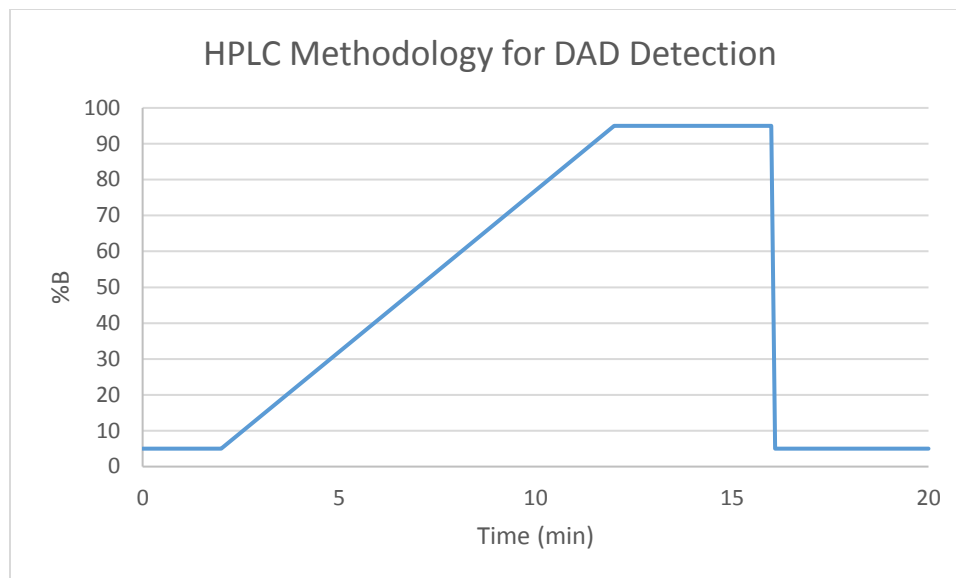


Figure 2.25. The HPLC method used to detect analytes with a DAD detection system.

2.6.5. MS methods for the detection of 1, POA, and other metabolites

MS/MS development was performed using ESI in either positive or negative mode using an ABSciEx QTRAP 5500 (Sciex Ltd, Framingham, MA) linear trap triple quadrupole mass spectrometer set to ± 4500 V monitoring the desired masses ± 0.5 Da. Dr. Bruce Witthuhn assisted with direct infusions used to determine the power for detecting unique mass transitions for each metabolite, analyte, and internal standard. Each transition for each analyte is summarized in Table 2.5, and these typical settings were used for all studies.

Table 2.5. The MS parameters used to detect and quantify analytes in MS experiments.

Entry	Compound^a	Retention (min)^b	DP (V)^c	CE (V)^d	CXP (V)^e	Q1 (Da)	Q3 (Da)
1	POA	2.50	-35	-20	-17	123	79
2	<i>d</i> ₃ -POA	2.51	-35	-20	-17	126	82
3	Pantothenate	3.34	-35	-25	-17	218	88
4	Ampicillin	1.72	+35	+20	+17	350	106
5	CoA	0.6	+35	+30	+17	768	261
6	Acetyl CoA	0.98	+35	+36	+17	810	303
7	Malonyl CoA	0.66	+35	+30	+17	854	347
8	1	2.29	+49	+10	+17	485	333

^aSynthetically-derived or purchased compounds; ^bRetention for purified compound; ^cDeclustering potential; ^dCollision energy; ^eExit potential.

2.6.6. General procedure for aqueous and serum stability assays

2.6.6.1. HPLC method

The HPLC method employed in these studies is described in section 2.6.4.2. Conjugate **1** elutes at retention time 2.85 minutes, while POA elutes at retention time 2.50 minutes. Single quad mass spectrometry was also added as an additional detection method to confirm peak identities. For compound **1**, reliable masses detected in positive mode include m/z [M+H] = 453 and the dimeric compound at m/z [M+H] = 907. For POA, the compound could be reliably detected at m/z [M+H] = 125.

2.6.6.2. Stability assays and sample preparation^{182, 183}

Both serum and aqueous stability studies were performed with known protocols within the laboratory. Briefly, **1** (50 μ M) was incubated at 37 °C in simulated gastric fluid (pH 1.3), 50 mM HEPES (pH 7.4), CD-1 female pooled mouse plasma, Sprague-Dawley female pooled rat plasma, and female pooled human plasma (BioChemed, Winchester, VA) in triplicate experiments. “Buffer” (980 μ L) was heated to 37 °C for five minutes, and then 20 μ L of a 10.0 mM DMSO solution was added, the mixtures were briefly vortexed (3-5 s), and incubated at 37 °C. 100 μ L aliquots were removed from the experiment at 0, 10, 30, 60, 120, 240, and 360 minutes and immediately quenched with the addition of 100 mL of pure CAN. The samples were vortexed, centrifuged (60 s at 15,000 x g) and 140 μ L of the supernatant were added to HPLC vials with a conical insert. Samples were analyzed using the method previously described with a 50 μ L injection volume.

2.6.7. General procedure for the determination of POA release with BlaC

2.6.7.1 Transformation of BlaC Plasmid¹⁷⁰

After receipt of properly ligated *blaC*-pet28b plasmid, which encodes for BlaC without the first 40 amino acids, from the Blanchard laboratory at Einstein Medical Center, the plasmid was transformed into *E. coli* BL21-DE3 cells that are engineered to more effectively express protein. The standard heat shock protocol was used again for transformation (Biolabs, N. E, 2017). The resulting cell culture was diluted 10-fold, plated on LB-KAN (50 µg/mL) and grown overnight at 37° C. A single colony was picked from the resulting plate and used for all further expression and purification of BlaC.

2.6.7.2. BlaC expression and purification¹⁷⁰

A 5mL starter culture was then used to inoculate 1 L LB media containing 50 µg/mL kanamycin. The culture was shaken at 250 rpm and 37° C until OD₆₀₀ reached 0.7 (approximately 5 hours). The culture was induced with IPTG (0.5 mM) and incubated at 18° C for 18 hours. The resulting cell culture was centrifuged at 5000 x g for 25 mins. The cell pellet obtained was resuspended in 20 mL lysis buffer (25 mM Tris-HCl, 300 mM NaCl, pH 7.5). The cells were lysed using sonication (40% amplitude, 2 minute on/5 minute off, 4 cycles). The insoluble fraction was centrifuged at 42,000 x g for 45 min. The supernatant was collected, 2 mL Ni-NTA resin was added and the mixture was incubated for 15 min. at 4° C. The mixture was then passed through a sintered glass filter and the resin was washed with 10 mL wash buffer (25 mM Tris-HCl, 250 mM NaCl, 20 mM imidazole, pH 7.5). BlaC was then eluted with 2.5 mL elution buffer (25 mM Tris-HCl, 250 mM NaCl, 250 mM imidazole, pH 7.5). A buffer exchange was performed using an

Amicon centrifugation filter to store the BlaC in storage buffer (25 mM Tris-HCl, 250 mM NaCl, pH 7.5) and thrombin was added and incubated for 24 hours to cleave the His₆ N-terminal tag. Size exclusion chromatography was performed using a Superdex 200 Hi-Load 26-60 column (Amersham Pharmacia Biotech) using 25 mM Tris-HCl, containing 300 mM NaCl, pH 7.5 as elution buffer. Protein was then stored at -80 °C in a solution containing buffer with 25% glycerol. The yield for expression and purification was determined by nanodrop to be 9 mg/L.

2.6.7.3. LC-MS Biochemical Assay

2.6.7.3.1. LC-MS method

Reverse-Phase HPLC was performed on an Agilent 1260 instrument (Agilent Technologies, Santa Clara, CA) equipped with a Zorbax Eclipse XDB-C8, 5 micron, 4.6 x 150 mm column (Agilent Technologies, Santa Clara, CA). The mobile phase consisted of 0.1% (v/v) aqueous formic acid as the aqueous component (A) and 0.1% (v/v) formic acid solution in acetonitrile as the organic component (B). Solvents used were at least mass-spectrometry grade, and were prepared within 72 hours of use. Elution was performed following the gradient shown in Figure 2.26 at a flow rate of 0.8 mL/min. The DAD was set to monitor at wavelength 254 nm with 360 nm acting as a reference wavelength and an Agilent 6120 single quadrupole mass spectrometer (Agilent Technologies, Santa Clara, CA) set to monitor the single ion $m/z = 123$ Da in negative mode. A sample chromatogram is shown in Figure 2.27.

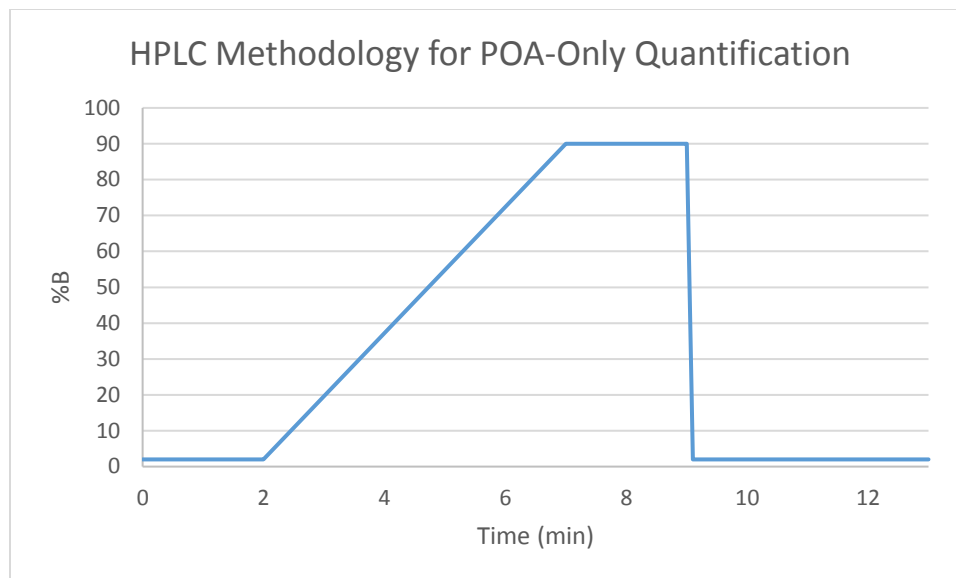


Figure 2.26. The HPLC method used to quantify POA only in BlaC release assays.

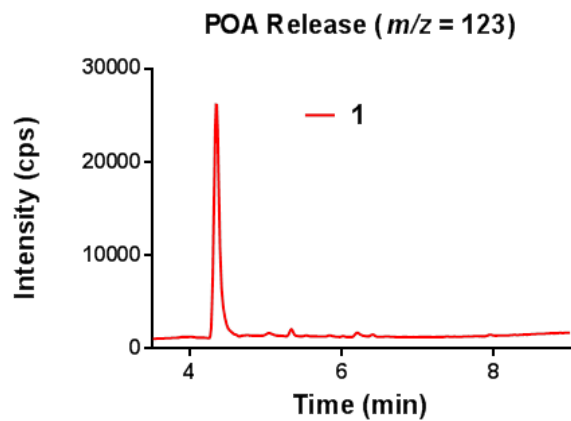


Figure 2.27. A sample chromatogram for the detection of POA using the method described in this section.

2.6.7.3.2. BlaC release assay

Assay components, including 50 mM NH₄OAc, **1** (100 μM), and BlaC (1 μM) were combined to a total volume of 60 μL and incubated for 30 min at 23 °C (for inhibited replicates, enzyme and clavulanate (100 μM) were pre-incubated for 30 min at 23 °C prior to substrate addition). 60 μL of acetonitrile was added to precipitate protein, and the mixture was centrifuged for 10 min at 4,000 rpm at 4 °C. Following centrifugation, 24 μL of supernatant were removed and diluted with 108 μL 8:5:5 water: MeOH: ACN. Release of pyrazinoic acid was analyzed by HPLC using the method described in section 2.6.7.3.1 with confirmation by MS with a single quadrupole mass spectrometer set to single ion monitoring at $m/z = 125$.

2.6.8. General procedure for targeted metabolomics

2.6.8.1. Cell lysate preparation

A culture of *Mtb* is grown to its mid-exponential phase in Middlebrook 7H9 media. Then, 10 million colony forming units (cfus) are removed and placed on an agar plate embedded with the desired treatment condition. After 24 hours, the cells are harvested, taken up in 40:40:20 MeOH:ACN:H₂O, lysed, and the crude lysate is filtered through a 3 kDa amicon filter to remove cellular debris. The lysate is allowed to decontaminate according to BSL3 standards, and stored at -80 °C.

2.6.8.2. Sample preparation

A 200 μL sample of the cellular lysate is taken into a new vessel that can be fitted to a rotary evaporator. The sample is then evaporated under reduced pressure (300 mTorr)

at 40 °C for 2 minutes. The sample is then taken up in 5 mM aqueous ammonium acetate with 2% ACN containing 1 μ M ampicillin and 1 μ M d_3 -POA at 10-fold greater concentration (20 μ L) and transferred to a sample vial containing a conical insert for analysis by HPLC-MS/MS.

2.6.8.3. Data analysis

The data was gathered and analyzed in Analyst software (ABSciex). Samples were compared to a standard curve generated for each metabolite of interest on the day of the experiment to account for instrument drift. Standard curves covered 15 nM to 5 mM ranges for each compound, and values of raw area were compared to the known internal standard. Figure 2.28 shows an example of a standard curve generated for POA. Areas gathered in lysate experiments were plotted against the standard curve generated to determine the final concentrations of analytes in lysate experiments.

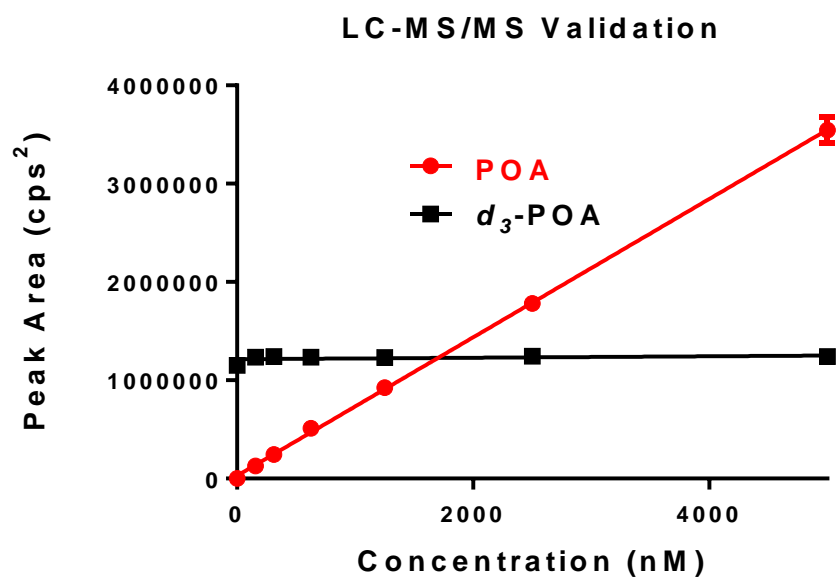


Figure 2.28. The standard curve of MS/MS experiments for POA.

2.6.9. Synthesis of pyrazinoyl amide compounds

2.6.9.1. Synthesis of 1-pyrazinoyl-benzotriazole¹⁸⁹

To a 100 mL round bottom flask equipped with a stir bar was added pyrazinoic acid (POA, 620 mg, 5 mmol, 1.0 equiv), 1-(methanesulfonyl)-benzotriazole (985 mg, 5 mmol, 1 equiv), THF (25 mL), and then triethylamine (1.04 mL, 7.5 mmol, 1.5 equiv). The reaction was stirred and heated to reflux (~70 °C) for 18 – 24 hours. The reaction was cooled and then concentrated *in vacuo*. Then, the mixture was dissolved in CHCl₃ (25 mL) and washed with a saturated solution of NaHCO₃ (3 x 25 mL) followed by drying with MgSO₄. The organic layer was evaporated under reduced pressure and the mixture was taken up in Et₂O (100 mL). The solution was heated to reflux (40 °C) for 20 minutes and the precipitate was filtered and then dried under reduced pressure to yield 1-pyrazinoyl-benzotriazole (866.2 mg, 78%) as a pink solid; physical properties and spectra matched previous reports.

2.6.9.2. Synthesis of pyrazinoyl amides

To a 50 mL round bottom flask equipped with a stir bar was added 1-pyrazinoyl-benzotriazole (225 mg, 1 mmol, 1 equiv), L-cysteine (133.1 mg, 1.1 mmol, 1.1 equiv), THF (10 mL), and *N,N*-diisopropylethylamine (Hünig's base, 440 µL, 2.5 mmol, 2.5 equiv). The reaction was heated to reflux (~70 °C) for 16 – 48 hours and then cooled. The reaction was then concentrated *in vacuo* and purified as specified.

2.6.9.3. Purification of pyrazinoyl amide compounds

2.6.9.3.1. Compounds **3**, **5**, **10**, **11**, **13**, **15**, **17**: The reaction concentrate was taken up in 50:50 water: MeCN with 0.1% formic acid (20 mg/mL) and purified using reverse-Phase

HPLC on preparatory scale. HPLC was performed on an Agilent 1260 instrument (Agilent Technologies, Santa Clara, CA) equipped with a Phenomenex Gemini C18, 10 micron, 21.2 x 250 mm column (Phenomenex, Torrance, CA). The mobile phase consisted of 0.1% (v/v) aqueous formic acid as the aqueous component (A) and 0.1% (v/v) formic acid solution in acetonitrile as the organic component (B). Solvents used were at least HPLC grade, and were prepared within 72 hours of use. Elution was performed following the gradient shown in Figure 2.25 at a flow rate of 21 mL/min. The DAD was set to monitor at wavelength 254 nm with 360 nm acting as a reference wavelength.

2.6.9.3.2. Compounds 4, 6, 7, 9, 12, 14, 16, 18: The reaction concentrate was dissolved in EtOAc and concentrated onto SiO₂. The compounds were purified with a Teledyne Isco Combi-Flash RF 200 system using a gradient from 90:10 hexanes: EtOAc to 0:100 hexanes: EtOAc with a 10% increase in EtOAc every six column volumes.

2.6.9.3.3. Compound 8: The reaction concentrate was dissolved in EtOAc and filtered. The precipitate was dried further *in vacuo* to yield compound **8** as a white solid.

2.6.9.4. Characterization of biologically-evaluated pyrazinyl amides:

N-Pyrazinoyl-L-cysteine: ¹H (500 MHz, *d*₆-DMSO) δ 13.17 (br, 1H), 9.22 (s, 1H), 8.96 (s, 1H), 8.93 (s, 1H), 8.80 (s, 1H), 4.69 (q, 1H, *j* = 4.5 Hz), 3.09–3.04 (m, 2H), 2.09 (s, 1H); ¹³C (125 MHz, *d*₆-DMSO) δ 171.67, 163.25, 148.42, 144.53, 143.96, 54.86, 25.69.

N-Pyrazinoyl-L-cysteine-methyl ester: ¹H (500 MHz, CDCl₃) δ 9.39 (s, 1H), 8.79 (s, 1H), 8.60 (br, 2H), 5.09 (dt, 1H, *j* = 7.6 Hz), 3.84 (s, 3H), 3.14 (m, 2H), 1.46 (t, 1H, *j* = 8.9 Hz); ¹³C (125 MHz, CDCl₃) δ 170.15, 162.88, 147.70, 144.46, 142.85, 53.72, 52.97, 26.94.

N-Pyrazinoyl-L-alanine: ^1H (500 MHz, CDCl_3) δ 9.40 (s, 1H), 8.78 (d, 1H, $j = 1.8$ Hz), 8.57 (s, 1H), 8.21 (br, 1H), 4.83 (t, 1H, $j = 7.2$ Hz), 1.62 (d, 3H, $j = 7.2$ Hz); ^{13}C (125 MHz, CDCl_3) δ 163.13, 147.86, 144.46, 142.77, 17.96.

N-Pyrazinoyl-L-alanine-methyl ester: ^1H (500 MHz, CDCl_3) δ 9.40 (s, 1H), 8.77 (d, 1H, $j = 1.8$ Hz), 8.56 (s, 1H), 8.27 (br, 1H), 4.82 (quin, 1H, $j = 7.3$ Hz), 3.80 (s, 3H), 1.56 (d, 3H, $j = 6.7$ Hz); ^{13}C (125 MHz, CDCl_3) δ 172.98, 162.58, 147.48, 144.44, 142.69, 52.64, 48.12, 29.72, 18.46.

N-Pyrazinoyl-cysteamine: ^1H (500 MHz, CDCl_3) δ 9.41 (s, 1H), 8.77 (d, 1H, $j = 2.1$ Hz), 8.55 (s, 1H), 3.69 (m, 2H), 2.81 (m, 2H), 1.46 (t, 1H, $j = 7.9$ Hz); ^{13}C (125 MHz, CDCl_3) δ 163.12, 147.44, 144.48, 142.61, 42.35, 24.62.

N,N'-Di-pyrazinoyl-cystamine: ^1H (500 MHz, d_6 -DMSO) δ 9.18 (s, 2H), 9.08 (t, 2H, $j = 5.5$ Hz), 8.87 (s, 2H), 8.73 (s, 2H), 3.63 (q, 4H, $j = 6.5$ Hz), 2.98 (t, 4H, $j = 6.9$ Hz); ^{13}C (125 MHz, d_6 -DMSO) δ 163.39, 148.05, 145.06, 143.90, 38.76, 37.35.

N-Pyrazinoyl-methylamine: Purified as specified in section 2.6.9.3.2. All spectra and physical properties matched previous reports.²²¹

2.6.10. MS methods for the detection of 3, 5, 7, and 8: MS/MS development was performed using ESI in either positive or negative mode using an ABSciEx QTRAP 5500 (Sciex Ltd, Framingham, MA) linear trap triple quadrupole mass spectrometer set to ± 4500 V monitoring the desired masses ± 0.5 Da. Dr. Bruce Witthuhn assisted with direct infusions used to determine the settings for detecting unique mass transitions for each

metabolite, analyte, and internal standard. Each transition for each analyte is summarized in Table 2.6, and these typical settings were used for all studies.

Table 2.6. The MS parameters used to detect and quantify analytes in MS experiments.

Entry	Compound^a	Ret (min)^b	DP (V)^c	CE (V)^d	CXP (V)^e	Q1 (Da)	Q3 (Da)
1	3	4.94	-35	-22	-17	226	148
2	5	4.30	-35	-20	-17	194	122
3	7	5.87	-35	-21	-17	182	122
4	8	5.21	+35	+21	+17	365	182

^aSynthetically-derived compounds; ^bRetention for purified compound; ^cDeclustering potential; ^dCollision energy; ^eExit potential.

2.6.11. Assessment of PncA activity on novel compounds

2.6.11.1. Acquisition of genetic material

A synthetic gene encoding for *pncA* was ordered from integrated DNA technologies (Coralville, IA). Restriction enzymes, and plasmid buffers were ordered from New England Biolabs (Ipswich, MA). All biological buffers and reagents were obtained from Sigma-Aldrich (St. Louis, MO). DNA isolation kits (Qiagen Sciences, Germantown, MD), *E. coli* DH5 alpha and BL21DE3 competent cells were prepared as described (Biolabs, N. E, 2017).

2.6.11.2. Cloning of PncA into pet28b(+)

Codon optimization was performed for gene expression in *E. coli* using the protocols from integrated DNA technologies (Integrated DNA Technologies, IA, 2017). *PncA* was ligated into a pet28b(+) plasmid using protocols portrayed by Biolabs, N. E, 2017. The pet28b(+) plasmid was linearized using the restriction endonucleases XhoI and NdeI. XhoI recognized the DNA sequence CTCGAG and cleaves after C-1 (Therriault et al., 1985). NdeI recognizes the DNA sequence CATATG and cleaves after A-1 (Watson et al., 1983). The ends of *pncA* was also cut using the same restriction endonucleases to compliment the plasmid sticky ends. Using T4 DNA ligase in the presence of linear pet28b(+) and *pncA* yielded cyclized plasmids containing the gene of interest. Heat inactivation at 65° C of restriction endonucleases and ligase was performed after every step.

2.6.11.3. Transformation of PncA plasmids

After conformation of properly ligated *PncA*-pet28b the plasmid was transformed into *E. coli* BL21-DE3 cells that are engineered to more effectively express protein. The standard heat shock protocol was used again for transformation (Biolabs, N. E, 2017). The resulting cell culture was diluted 10-fold, plated on LB-KAN (50 µg/mL) and grown overnight at 37° C. A single colony was picked from the resulting plate and used for all further expression and purification of *pncA*.

2.6.11.4. PncA expression and purification¹⁹⁰

A 5mL starter culture with *E. coli* overexpressing *pncA* was then used to inoculate 1 L LB media containing 50 µg/mL kanamycin. The culture was shaken at 250 rpm and 37° C until OD₆₀₀ reached 0.8 (approximately 6 hours). The culture was induced with IPTG (0.5 mM) and incubated at 16° C for 18 hours. The resulting cell culture was centrifuged at 5000xg for 20 mins. The cell pellet obtained was resuspended in 20 mL lysis buffer (50 mM HEPES, 250 mM NaCl, 5 mM imidazole, pH 7). The cells were lysed using sonication (50% amplitude, 1 minute on/1 minute off, 4 cycles). The insoluble fraction was centrifuged at 42,000xg for 45 min. The supernatant was collected, 2 mL Ni-NTA resin was added and the mixture was incubated for 15 min. at 4° C. The mixture was then passed through a sintered glass filter and the resin was washed with 10 mL wash buffer (50 mM Tris, 250 mM NaCl, 60 mM imidazole, pH 8). PncA was then eluted with 2.5 mL elution buffer (50 mM Tris, 250 mM NaCl, 250 mM imidazole, pH 8). A buffer exchange was performed using an Amicon centrifugation filter to store the PncA in storage buffer (20 mM Tris, 250 mM NaCl, pH 7.4) at -20 °C. The yield for expression and purification was

determined by nanodrop to be 10 mg/L. Relative purity of the protein was determined by SDS-PAGE.

2.6.11.5. Continuous Coupled Biochemical Assay¹⁹⁰

Initial velocities were determined by monitoring change in absorbance at 340 nM from the conversion of NADH to NAD⁺ by glutamic dehydrogenase (GDH). GDH utilizes ammonia to convert alpha-ketoglutarate to glutamate. The cofactor NADH is used and NAD⁺ is generated as a byproduct. Therefore, as *PncA* converts pyrazinamide to pyrazinoic acid, the ammonia generated is used by GDH, coupling amide hydrolysis to NAD⁺ generation. The typical assay uses 5 mM alpha-ketoglutarate, 8 units of GDH, 200 μM NADH, 35 nM *PncA* and varying concentrations of amide substrates. The reaction is run in 100 μL assay buffer (100 mM HEPES, pH 7.5) in a 96 well clear bottom plate (Corning) in triplicate. Enzyme activities were calculated using the molar extinction coefficient of NADH ($\epsilon_{340} = 6220 \text{ M}^{-1}\text{cm}^{-1}$) and GraphPad Prism® was used to graph Michaelis-Menten curves to determine K_M and k_{cat} values.

2.6.11.6. LC-MS Biochemical Assay

The LC-MS based assay was decided upon to test analogs that were altered off the pyrazine amide; thus, when hydrolyzed by *PncA*, would not yield the necessary ammonia for use in the coupled assay. The output of this assays is pyrazinoic acid which can be detected by the 123 m/z [M-H] anion. The typical assay uses 30 nM *PncA*, and varying substrate concentrations. The assay is performed in 100 μL buffer (20 mM Tris, pH 7.5). The reactions were initiated with addition of *PncA* then allowed to incubate at room

temperature for 10 minutes. After incubation the reaction is terminated with addition of 900 μ L crash solution (1:1 ACN:MeOH). The resulting mixture is then vortexed for 10 seconds and centrifuged at 5000 rpm for 5 minutes. 100 μ L of the supernatant is then collected, filtered and submitted for LC-MS.

2.6.12. Synthesis of CDB-I-143 and JAB11P118

2.6.12.1. Synthesis of CDB-I-143

To a 25 mL round bottom flask charged with pyruvic acid (0.75 mL, 10.65 mmol, 1.0 equiv) and equipped with a magnetic stir bar was added CH_2Cl_2 (10 mL), 4-(dimethylamino)-pyridine (0.130 g, 1.06 mmol, 0.1 equiv), and 6-heptyne-1-ol (2.74 mL, 20.00 mmol, 1.9 equiv). Then, while stirring at 0 $^\circ\text{C}$, EDC-HCl (2.416 g, 11.71 mmol, 1.1 equiv) was added slowly in a batch-wise manner. The reaction was warmed to 23 $^\circ\text{C}$ and allowed to stir at this temperature. After 3 hours, the reaction contents were poured out and the reaction vessel was cleaned with 10 mL of CH_2Cl_2 . The combined organic layers were washed with 0.5 M HCl (20 mL) and saturated NaHCO_3 (20 mL), dried over MgSO_4 , and evaporated. The crude material was checked by NMR to be pure hept-6-yn-1-yl-2-oxo-propionate (0.6606 g, 33% yield) as a colorless oil: $R_f = 0.4$ (90:10 hexanes: EtOAc); ^1H NMR

To a 100 mL round bottom flask charged with hept-6-yn-1-yl-2-oxo-propionate (0.2000 g, 1.09 mmol, 1.0 equiv) and equipped with a magnetic stir bar was added hydroxylamine monohydrate (109 mg, 1.64 mmol, 1.5 equiv), EtOH (20 mL), and then pyridine (4 mL). The reaction was heated to 85 $^\circ\text{C}$ for 2 hours and then cooled. Water (25

mL) was added and the reaction was extracted with CH₂Cl₂ (4 x 25 mL), dried over MgSO₄, and the solvent was evaporated under reduced pressure yielding the oxime product as a viscous oil contaminated with a bit of pyridine: $R_f = 0.6$ (85:15 hexanes: EtOAc). The crude material was carried on without further purification or characterization to the next step.

To a 100 mL round bottom flask charged with oxime (207 mg, 1.01 mmol, 1.00 equiv) and equipped with a magnetic stir bar was added AcOH (10 mL) and THF (5 mL). The reaction was cooled to 0 °C with stirring while Na(CN)BH₃ (79 mg, 1.26 mmol, 1.25 equiv) was added slowly. The reaction was allowed to warm to 23 °C and stirred for 24 hours. 2 N NaOH (10 mL) was then added to the reaction slowly and the aqueous mixture was extracted with CH₂Cl₂ (4 x 25 mL), dried with MgSO₄, and evaporated under reduced pressure. Purification on Teledyne Isco Combi-Flash RF® system afforded CDB-I-143 (137 mg, 68%) as a white solid: $R_f = 0.4$ (85:15 hexanes: EtOAc); ¹H NMR (400 MHz, *d*₆-DMSO) δ 12.19 (s, 1H), 4.11 (t, 2H, *j* = 6.5 Hz), 2.7 (t, 1H, *j* = 2.6 Hz), 2.12 (td, 2H, *j* = 6.7 Hz), 1.89 (s, 3H), 1.62 (quin, 2H, *j* = 6.9 Hz), 1.46 – 1.42 (m, 4H), 1.23 (s, 1H); ¹³C NMR (100 MHz, *d*₆-DMSO) δ 164.43, 148.15, 84.78, 71.66, 65.02, 27.98, 25.09, 18.02, 10.95; HRMS for C₁₀H₁₇NNaO₃⁺ [M+Na⁺] calculated 222.1101; found 222.1109.

2.6.12.2. Synthesis of JAB11P118

To a 20 mL scintillation vial equipped with a magnetic stir bar was added was added CH₂Cl₂ (4 mL), 2-bromo propionic acid (30.6 mg, 0.20 mmol, 1.0 equiv), 2-β-(but-3-yn-1-yl)-3H-diazirin-3-yl-ethan-1-amine (30.1 mg, 0.22 mmol, 1.1 equiv), triethylamine (22 μL, 0.30 mmol, 1.5 equiv), and 1-hydroxybenzotriazole (HOBt, 30.6 mg, 0.20 mmol, 1.0

equiv). The reaction vessel was wrapped with foil to exclude light and the mixture was cooled to 0 °C with stirring. EDC-HCl (42 mg, 0.22 mmol, 1.1 equiv) was then added, the vessel was sealed, and allowed to warm to 23 °C. After 18 hours, the reaction was diluted to 20 mL total volume with CH₂Cl₂ and then washed with cold (stored at 4 °C) 1.0 N HCl (20 mL), saturated NaHCO₃ (20 mL), and dried with anhydrous MgSO₄, and evaporated under reduced pressure. The crude material was checked by NMR and contained some HOBt impurity. The crude material was not further isolated nor characterized and was carried onto the next synthetic step.

To a 2-dram vial charged with the crude material from the previous synthetic step (54.2 mg, 0.20 mmol, 1.0 equiv) and equipped with a stir bar was added methanol (2 mL), triethylamine (22 μL, 0.30 mmol, 1.5 equiv), and then *O*-^t-Butyldimethylsilylhydroxylamine (44.1 mg, 0.30 mmol, 1.5 equiv). The reaction vessel was again covered in foil to exclude light and heated to 50 °C. After 71 hours, the solvent and volatile components were evaporated under reduced pressure. The crude reaction mixture was dissolved in CH₂Cl₂ (10 mL) and then treated 2.0 N HCl (10 mL). The mixture was stirred vigorously under Schotten-Baumann conditions for 15 minutes and then the organic layer was isolated, dried with MgSO₄, and evaporated under reduced. Purification on Teledyne Isco Combi-Flash RF® system (with UV detection turned off) afforded JAB11P118 (32.3 mg, 72%) as a white solid: $R_f = 0.2$ (90:10 hexanes: EtOAc); ¹H NMR (500 MHz, CDCl₃) δ 6.47 (br, 1H), 4.41 (q, 1H, $j = 7$ Hz), 3.15 (q, 2H, $j = 6.9$ Hz), 2.03 (m, 3H), 1.90 (d, 3H, $j = 7.1$ Hz), 1.73 (t, 2H, $j = 6.7$ Hz), 1.67 (t, 2H, $j = 6.8$ Hz), 1.26 (s, 1H); ¹³C NMR (125

MHz, CDCl₃) δ 169.32, 82.62, 69.50, 45.19, 35.06, 32.32, 26.69, 26.24, 23.17, 13.23;
HRMS for C₁₀H₁₇N₄O₂⁺ [M+H⁺] calculated 225.1346; found 225.1341.

2.6.13. Assessment of CDB-I-143 binding to BioA

2.6.13.1. BioA and BioD acquisition²¹²

Both BioA and BioD purified proteins were graciously supplied by both Dr. Feng Liu and Dr. Carter Eiden which were expressed and purified according to the published procedure.

2.6.13.2. General continuous assay setup for BioA

To a black 384-well plate with a clear bottom (Corning) was added 69 μ L total of LDH (20 units), Phospho-enoylppyrivate (PEP, 20 mM), PK (96 units), NADH (113 nM), TCEP (5 mM), *S*-adenosyl methionine (SAM, 50 mM), KAPA (625 μ M), and ATP (50 mM). Then 1 μ L of preincubated solutions (varying times) of CDB-I-143 (varying concentration) with BioA (1 μ M final concentration) and BioD (15 μ M final concentration) were added to initiate the reaction and the plate was added to the plate reader. UV absorbance at 340 nm ($\epsilon_{340} = 6220 \text{ M}^{-1} \text{ cm}^{-1}$) was monitored to determine the use of NADH in this coupled assay system. 100 nM of FL-1-169 (Figure 2.1; graciously supplied by Dr. Feng Liu) was used as a positive control for full inhibition of BioA.

2.6.14. Expression and purification of IlvE²¹⁸

A 5mL starter culture with *E. coli* overexpressing *IlvE* was then used to inoculate 1 L LB media containing 50 μ g/mL kanamycin. The culture was shaken at 250 rpm and 37° C until OD₆₀₀ reached 0.6 (approximately 3 hours). The culture was induced with IPTG

(0.1 mM) and incubated at 16 °C for 18 hours. The resulting cell culture was centrifuged at 4000 x g for 15 mins at 4 °C. The cell pellet obtained was resuspended in 20 mL lysis buffer (20 mM HEPES, 200 units of DNase, Complete® protease inhibitor tablet-EDTA free (Roche), pH 7.5). The cells were lysed using sonication (50% amplitude, 30 seconds on/30 seconds off, 5 cycles). The insoluble fraction was centrifuged at 42,000xg for 60 min. The supernatant was collected, 2 mL Ni-NTA resin was added and the mixture was incubated for 15 min. at 4° C. The mixture was then passed through a sintered glass filter and the resin was washed with 10 mL wash buffer (20 mM HEPES, 500 mM NaCl, 1 mM DTT, pH 7.5). IlvE was then eluted with 2.5 mL elution buffer (20 mM HEPES, 300 mM imidazole, 1 mM DTT, pH 7.5). A buffer exchange was performed using an Amicon centrifugation filter to store the IlvE in storage buffer (20 mM HEPES, 300 mM NaCl, pH 7.5) at -20 °C. The yield for expression and purification was determined by nanodrop to be 10 mg/L. Size exclusion chromatography was performed using a Superdex 200 Hi-Load 26-60 column (Amersham Pharmacia Biotech) using 20 mM HEPES, containing 300 mM NaCl, pH 7.5 as elution buffer. Protein was then stored at -80 °C in a solution containing buffer with 25% glycerol.

2.6.15. General continuous assay setup for IlvE²¹⁸

To a clear 96-well plate with a clear, flat, bottom (Corning) was added 180 µL total of GDH (8 units), PLP (40 nM), L-glutamate (15 mM), NADH (160 nM), NH₄Cl (1 mM), and α-ketocaproate (2 mM). Then 20 µL of preincubated solutions (varying times) of CDB-I-143 or JAB11P118 (varying concentration) with IlvE (40 nM final concentration) were

added to initiate the reaction and the plate was added to the plate reader. UV absorbance at 340 nm ($\epsilon_{340} = 6220 \text{ M}^{-1} \text{ cm}^{-1}$) was monitored to determine the use of NADH in this coupled assay system.

2.6.16. General procedure for labeling protein and cellular lysates with JAB11P118

2.6.16.1. Generation of cellular lysates²²⁰

Following a similar procedure as described in section 2.6.14, cellular lysates were generated from over-expression strains with or without IPTG induction. The resulting cell culture was centrifuged at 4000 x g for 15 mins at 4 °C. The cell pellet obtained was resuspended in 20 mL lysis buffer (20 mM HEPES, 200 units of DNase, Complete® protease inhibitor tablet-EDTA free (Roche), pH 7.5). The cells were lysed using sonication (50% amplitude, 30 seconds on/30 seconds off, 5 cycles). The insoluble fraction was centrifuged at 42,000xg for 60 min. The supernatant was collected and buffer exchange was performed using amcon-type filtration with centrifugation (3 cycles), exchanging into phosphate-buffer saline (PBS) solution.

2.6.16.2. Labeling samples²²⁰

The cellular lysate or purified protein samples were each concentrated to 6 mg/mL of protein content, confirmed using a nano-drop UV-spectrophotometer. Then, JAB11P118 (200 μM) is added and the solution is vortexed (power level 3) for 3 seconds to mix the components. The mixtures are allowed to stand at 23 °C for 1 hour. Then, each sample is irradiated with UV light at 365 nm (hand lamp, long wave) for 1 hour at 4 °C. Then to the mixtures is added TAMRA-N₃ (final concentration 1 mM), TCEP (final concentration 1

mM), TBTA (1:4 DMSO:^tBuOH, final concentration 1 mM), and Cu^{II}SO₄ (final concentration 1 mM). The solution is vortexed (power level 9) and allowed to stand at 23 °C for 1 hour with vortex mixing every 30 minutes. The proteins will begin to precipitate and the solution will appear cloudy. The samples are then diluted to 2 mg/mL protein content and analyzed via gel electrophoresis (SDS-PAGE). Labeling was monitored with a Typhoon (GE) gel imager set to excite at 532 nm and detect at 670 nm for TAMRA fluorophore and cross-examined with coomassie staining to confirm protein content.

References

- ¹ A) E. J. Corey, A. Venkateswarlu, *J. Am. Chem. Soc.* **1972**, *94*, 6190-6191; B) *Protective Groups in Organic Synthesis* (Eds. T. W. Green, P. G. M. Wuts), John Wiley & Sons, New York, **1999**.
- ² A) W. N. Olmstead, Z. Margolin, F. G. Bordwell, *J. Org. Chem.* **1980**, *45*, 3295-3299; B) F. G. Bordwell, R. J. McCallum, W. N. Olmstead, *J. Org. Chem.* **1984**, *49*, 1424-1427; C) F. G. Bordwell, *Acc. Chem. Res.* **1998**, *21*, 456-463.
- ³ K. Namba, K. Takeuchi, Y. Kaihara, M. Oda, A. Nakayama, A. Nakayama, M. Yoshida, K. Tanino, *Nat. Comm.* **2015**, *6*, 8731.
- ⁴ A) S. Diez-Gonzalez, S. P. Nolan, *Org. Prep. Proceed. Int.* **2007**, *39*, 523-559; B) X. Du, Z. Huang, *ACS Catal.* **2017**, *7*, 1227-1243; C) J. V. Obligacion, P. J. Chirik, *Nat. Rev. Chem.* **2018**, *2*, 15-34.
- ⁵ L. S. Bartell, L.-S. Su, H. Yow, *Inorg. Chem.* **1970**, *9*, 1903-1912.
- ⁶ *A Guide to Organophosphorus Chemistry* (Ed. L. D. Quin), John Wiley & Sons, New York, **2000**.
- ⁷ A) G. Wittig, G. Geissler, *Liebigs Ann. Chem.* **1953**, *580*, 44-57; B) G. Wittig, U. Schollkopf, *Chem. Ber.* **1954**, *87*, 1318-1330; C) B. E. Maryanoff, A. B. Reitz, *Chem. Rev.* **1989**, *89*, 863-927; D) P. A. Byrne, D. G. Gilheany, *Chem. Soc. Rev.* **2013**, *42*, 6670-6696.
- ⁸ H. Staudinger, J. Meyer, *Helv. Chim. Acta* **1919**, *2*, 635-646.
- ⁹ I. Downie, J. Holmes, J. Lee, *Chemistry and Industry*, **1966**, *22*, 900-903; B) R. Appel, *Angew. Chem. Int. Ed.* **1975**, *14*, 801-811; C) V. de Andrade, M. de Mattos, *Curr. Org. Syn.* **2015**, *12*, 309-327.
- ¹⁰ O. Mitsunobu, M. Yamada, T. Mukaiyama, *Bull. Chem. Soc. Jpn.* **1967**, *40*, 935-939; b) O. Mitsunobu, M. T. Yamada, *Bull. Chem. Soc. Jpn.* **1967**, *40*, 2380-2382.
- ¹¹ A) T. W. Campbell, J. J. Monagle, V. S. Foldi, *J. Am. Chem. Soc.* **1962**, *84*, 3673-3677; B) R. M. Denton, J. An, B. Adeniran, *Chem. Commun.* **2010**, *46*, 3025-3027.
- ¹² A) P. D. Henson, K. Naumann, K. Mislow, *J. Am. Chem. Soc.*, **1969**, *91*, 5645; B) T. Imamoto, T. Takeyama, T. Kusumoto, *Chem. Lett.* **1985**, *14*, 1491-1492.
- ¹³ A) H. Fritzsche, U. Hasserodt, F. Korte, *Chem. Ber.* **1964**, *97*, 1988-1993; B) H. Fritzsche, U. Hasserodt, F. Korte, G. Friese, K. Adrian, *Chem. Ber.* **1965**, *98*, 171; C) L. Horner, W. D. Balzer, *Tetrahedron Lett.* **1965**, *17*, 1157-1162.
- ¹⁴ S. Sowa, M. Stankevič, A. Szmigielska, H. Malusznska, A. E. Koziol, K. M. Pietrusiewicz, *J. Org. Chem.* **2015**, *80*, 1672-1688.
- ¹⁵ C. A. Busacca, R. Raju, N. Grinberg, N. Haddad, P. James-Jones, H. Lee, J. C. Lorenz, A. Saha, C. H. Senanayake, *J. Org. Chem.* **2008**, *73*, 1524-1531.
- ¹⁶ D. Héroult, D. H. Nguyen, D. Nuel, G. Buono, *Chem. Soc. Rev.* **2015**, *44*, 2508.
- ¹⁷ K. L. Marsi, *J. Org. Chem.* **1974**, *39*, 265.
- ¹⁸ A) C. J. O'Brien, J. L. Tellez, Z. S. Nixon, L. J. Kang, A. L. Carter, S. R. Kunkel, K. C. Przeworski, G. A. Chass, *Angew. Chem. Int. Ed.* **2009**, *48*, 6836-6839; B) C. J. O'Brien, Z. S. Nixon, A. J. Holohan, S. R. Kunkel, J. L. Tellez, B. J. Doonan, E. E. Coyle, F. Lavigne, L. J. Kang, K. C. Przeworski, *Chem. Eur. J.* **2013**, *19*, 15281-15289; C) E. E. Coyle, B. J. Doonan, A. J. Holohan, K. A. Walsh, F. Lavigne, E. H. Krenske, C. J. O'Brien, *Angew. Chem. Int. Ed.* **2014**, *53*, 12907-12911; D) Z. Lao, P. H. Toy, *Beilstein J. Org. Chem.* **2016**, *12*, 2577-2587.
- ¹⁹ A) H. A. van Kalker, J. J. Bruins, F. P. J. T. Rutjes, F. L. van Delft, *Adv. Synth. Catal.* **2012**, *354*, 1417-1421; B) H. A. van Kalker, C. te Grotenhuis, F. S. Haasjes, C. R. A. Hommersom, F. P. J. T. Rutjes, F. L. van Delft, *Eur. J. Org. Chem.* **2013**, 7059-7066.
- ²⁰ H. A. van Kalker, S. H. A. M. Leenders, C. R. A. Hommersom, F. P. J. T. Rutjes, F. L. van Delft, *Chem. Eur. J.* **2011**, *17*, 11290-11295.
- ²¹ A) W. Zhao, P. K. Yan, A. T. Radosevich, *J. Am. Chem. Soc.* **2015**, *137*, 616-619; B) K. Fourmy, A. Voituriez, *Org. Lett.* **2015**, *17*, 1537-1540.
- ²² A) E. H. Krenske, *J. Org. Chem.* **2012**, *77*, 1-4; B) E. H. Krenske, *J. Org. Chem.* **2012**, *77*, 3969-3977.
- ²³ O. M. Demchuk, R. Jasinski, K. M. Pietrusiewicz, *Heteroat. Chem.* **2015**, *26*, 441-448.

- ²⁴ C. J. O'Brien, F. Lavigne, E. E. Coyle, A. J. Holohan, B. J. Doonan, *Chem. Eur. J.* **2013**, *19*, 5854-5858.
- ²⁵ Y. Li, L.-Q. Lu, S. Das, S. Pisiewicz, K. Junge, M. Beller, *J. Am. Chem. Soc.* **2012**, *134*, 18325-18329
- ²⁶ D. C. Lenstra, F. P. J. T. Rutjes, J. Mecinović, *Chem. Commun.* **2014**, *50*, 5763-5766.
- ²⁷ M.-L. Schirmer, S. Jopp, J. Holz, A. Spannenberg, T. Werner, *Adv. Synth. Catal.* **2016**, *358*, 26-29.
- ²⁸ S. C. Berk, S. L. Buchwald, *J. Org. Chem.* **1993**, *58*, 3221.
- ²⁹ A) M. Berthod, A. Favre-Réguillon, J. Mohamad, G. Mignani, G. Docherty, M. Lemaire, *Synlett*, **2007**, 2007, 1545-1548; B) C. Petit, A. Favre-Reguillon, B. L. Albela, L. Bonneviot, G. Mignani, M. Lemaire, *Organometallics* **2009**, *28*, 6379-6382; C) C. Petit, E. Poli, A. Favre-Réguillon, L. Khrouz, S. Denis-Quanquin, L. Bonneviot, G. Mignani, M. Lemaire, *ACS Catal.* **2013**, *3*, 1431-1438.
- ³⁰ T. Coumbe, N. J. Lawrence, F. Muhammad, *Tetrahedron Lett.* **1994**, *35*, 625-628.
- ³¹ Y. Li, S. Das, S. Zhou, K. Junge, M. Beller, *J. Am. Chem. Soc.* **2012**, *134*, 9727-9732.
- ³² A) J.-M. Denis, H. Forintos, H. Szelke, G. Keglevich, *Tetrahedron Lett.* **2002**, *43*, 5569-5571; B) M. Mehta, I. G. de la Arada, M. Perez, D. Porwal, M. Oesterich, D. W. Stephan, *Organometallics*, **2016**, *35*, 1030-1035.
- ³³ A. Chardon, O. Maubert, J. Rouden, J. Blanchet, *ChemCatChem*, **2017**, *9*, 4460-4464.
- ³⁴ G. Keglevich, Z. Baan, I. Hermecz, T. Novak, I. L. Odinets, *urr. Org. Chem.* **2007**, *11*, 107-126.
- ³⁵ L. Pehlivan, E. Metay, D. Delbrayelle, G. Mignani, M. Lemaire, *Tetrahedron*, **2012**, *68*, 3151-3155.
- ³⁶ A) L. Wang, Y. Wang, M. Chen, M.-W. Ding, *Adv. Synth. Catal.* **2014**, *356*, 1098-1104; B) L. Wang, M. Sun, M.-W. Ding, *Eur. J. Org. Chem.* **2017**, *2017*, 2568-2578.
- ³⁷ R. V. Somu, H. I. Boshoff, C. Qiao, E. M. Bennett, C. E. Barry, 3rd, C. C. Aldrich, *J. Med. Chem.* **2006**, *49*, 31-34.
- ³⁸ D. J. C. Constable, P. J. Dunn, J. D. Hayler, G. R. Humphrey, J. L. Leazer, Jr., R. J. Linderman, K. Lorenz, J. Manley, B. A. Pearlman, A. Wells, A. Zaks, T. Y. Zhang, *Green Chem.* **2007**, *9*, 411-420.
- ³⁹ K. E. DeBruin, G. Zon, K. Naumann, K. Mislow, *J. Am. Chem. Soc.* **1969**, *91*, 7027-7030.
- ⁴⁰ J. Pesti, G. L. Larson, *Org. Proc. Res. Dev.* **2016**, *20*, 1164-1181.
- ⁴¹ D. F. J. Hamstra, D. C. Lenstra, T. J. Koenders, F. P. J. T. Rutjes, J. Mecinovic, *Org. Biomol. Chem.* **2017**, *15*, 6426-6432.
- ⁴² A) O. Mitsunobu, *Synlett*, **1981**, 1-28; B) D. L. Hughes, *Org. React.* **1992**, *42*, 335-656; C) K. C. Kumara Swamy, N. N. Bhuvan Kumar, E. Balaraman, K. V. P. Pavan Kumar, *Chem. Rev.* **2009**, *109*, 2551-2651.
- ⁴³ J. S. Carey, D. Laffan, C. Thomson, M. T. Williams, *Org. Biomol. Chem.* **2006**, *4*, 2337-2347.
- ⁴⁴ T. Y. S. But, P. H. Toy, *Chem. Asian J.* **2007**, *2*, 1340-1355.
- ⁴⁵ T. Y. S. But, P. H. Toy, *J. Am. Chem. Soc.* **2006**, *128*, 9636-9637.
- ⁴⁶ D. Hirose, T. Taniguchi, H. Ishibashi, *Angew. Chem. Int. Ed.* **2013**, *52*, 4613-4617.
- ⁴⁷ C. J. O'Brien, PCT Int. Appl. WO2010/118042A2.2010
- ⁴⁸ S. Davey, *Nat. Chem.* **2013**, *5*, 358.
- ⁴⁹ A) M. G. Adlington, M. Orfanopoulos, J. L. Fry, *Tetrahedron Lett.* **1976**, *17*, 2955-2958; B) V. Gevorgyan, M. Rubin, S. Benson, J.-X. Liu, Y. Yamamoto, *J. Org. Chem.* **2000**, *65*, 6179-6186.
- ⁵⁰ Competitive intramolecular cyclization through attack of the purine N-3 nitrogen on the activated 5'-alcohol results in cyclonucleoside formation, a well-known side-reaction that can plague Mitsunobu couplings, which we thought could be exacerbated at the elevated reaction temperatures required for the catalytic Mitsunobu reaction.
- ⁵¹ J. A. Buonomo, C. C. Aldrich, *Angew. Chem. Int. Ed.* **2015**, *54*, 13041-13044.
- ⁵² S. E. Cremer, R. J. Chorvat, *J. Org. Chem.* **1967**, *32*, 4066.
- ⁵³ K. D. Reichl, N. L. Dunn, N. J. Fastuca, A. T. Radosevich, *J. Am. Chem. Soc.* **2015**, *137*, 5292-5295.
- ⁵⁴ I. V. Alabugin, K. M. Gilmore, P. W. Peterson, *WIREs Comput. Mol. Sci.* **2011**, *1*, 109-141.
- ⁵⁵ Carter G. Eiden, Ph. D. Dissertation, University of Minnesota, 2017.
- ⁵⁶ S. R. Mulliken, *J. Chem. Phys.* **1955**, *23*, 1833-1840.
- ⁵⁷ Y. Zhao, D. G. Truhlar, *Theor. Chem. Acc.* **2008**, *120*, 215-241.
- ⁵⁸ M. Fianchini, *J. Org. Chem.* **2018**, ASAP

- ⁵⁹ A. Kupareva, P. Maki-Arvela, H. Grenman, K. Eranen, D. Y. Murzin, *J. Chem. Technol. Biotechnol.* **2015**, *90*, 34-43.
- ⁶⁰ J. A. Buonomo, C. G. Eiden, C. C. Aldrich, *Synthesis*, **2018**, *50*, 278-281.
- ⁶¹ E. Nicolas, A. Guerriero, V. Lyaskovskyy, M. Peruzzini, K. Lammertsma, L. Gonsalvi, J. C. Slootweg, *Inorganics*, **2016**, *4*, 34-41.
- ⁶² K. G. Andrews, D. M. Summers, L. J. Donnelly, R. M. Denton, *Chem. Commun.* **2016**, *52*, 1855-1858.
- ⁶³ K. L. Marsi, *J. Am. Chem. Soc.* **1969**, *91*, 4724-4729.
- ⁶⁴ J. A. Buonomo, C. G. Eiden, C. C. Aldrich, *Chem. Eur. J.* **2017**, *23*, 14434-14438
- ⁶⁵ C. R. Hilliard, S. Kharel, K. J. Cluff, N. Bhuvanesh, J. A. Gladysz, J. Blumel, *Chem. Eur. J.* **2014**, *20*, 17292-17295.
- ⁶⁶ L. P. Hammett, *J. Am. Chem. Soc.* **1937**, *59*, 96.
- ⁶⁷ S. Xin, C. Aitken, J. F. Harrod, Y. Mu, E. Samuel, *Can. J. Chem.* **1990**, *68*, 471-476.
- ⁶⁸ F. L. S. Tse, T. Chang, B. Finkelstein, F. Ballard, J. M. Jaffe, *J. Pharm. Sci.* **1984**, *73*, 1599; B) R. R. LeVier, M. L. Chandler, S. R. Wendel, In *The Biochemistry of Silicon and Related Problems*, Bendz, G.; Lindqvist, I., Eds.; Plenum Press: New York and London, **1978**, 473.
- ⁶⁹ C. T. Imrie, P. A. Henderson, *Chem. Soc. Rev.* **2007**, *36*, 2096.
- ⁷⁰ A) M. Lee, S. Ko, S. Chang, *J. Am. Chem. Soc.* **2000**, *122*, 12011; B) Y. Kikukawa, Y. Kuroda, K. Ymanguchi, N. Mizuno, *Angew. Chem. Int. Ed.* **2012**, *51*, 2434; C) K. Shimizu, T. Kubo, A. Satsuma, *Chem. Eur. J.* **2012**, *18*, 2226; D) A. Krüger, M. Albrecht, *Chem. Eur. J.* **2012**, *18*, 652; E) Y. Sawama, M. Masuda, N. Yasakawa, R. Nakatani, S. Nishimura, K. Shibata, T. Yamada, Y. Monguchi, H. Suzuka, Y. Takagi, H. Sajiki, *J. Org. Chem.* **2016**, *81*, 4190.
- ⁷¹ A) Y. Lee, D. Seomoon, S. Kim, H. Han, S. Chang, P. H. Lee, *J. Org. Chem.* **2004**, *69*, 1741; B) E. A. Ison, R. A. Corbin, M. M. Abu-Omar, *J. Am. Chem. Soc.* **2005**, *127*, 11938; C) T. Matsuo, H. Kawaguchi, *J. Am. Chem. Soc.* **2006**, *128*, 12362; D) T. Mitsudome, S. Arita, H. Mori, T. Mizugaki, K. Jitsukawa, K. Kaneda, *Angew. Chem. Int. Ed.* **2008**, *47*, 7938; E) B. P. S. Chauhan, A. Sarkar, M. Chauhan, A. Roka, *Appl. Organomet. Chem.* **2009**, *23*, 385; F) J. John, E. Gravel, A. Hagège, H. Li, T. Gacoin, E. Doris, *Angew. Chem. Int. Ed.* **2011**, *50*, 7533.
- ⁷² M. Sridhar, B. C. Ramanaiah, C. Narsaiah, M. K. Swamy, B. Mahesh, M. K. K. Reddy, *Tetrahedron Lett.* **2009**, *50*, 7166.
- ⁷³ A) N. W. Mitzel, A. Schier, H. Beruda, H. Schmidbaur, *Chem. Ber.* **1992**, *125*, 1053-1059; B) M. C. Harvey, W. H. Nebergall, J. S. Peake, *J. Am. Chem. Soc.* **1957**, *79*, 1437.
- ⁷⁴ Reagents were searched for commercial availability using the eMolecules database, and general supplier websites. The presence of available hydrido-chlorosilanes was investigated with a range of suppliers including: Sigma-Aldrich, Alfa-Aesar, Thermo-Fischer (includes multiple companies), Combi-Blocks, Oakwood Chemicals, Gelest Inc, Strem Inc, TCI chemicals, and Matrix Scientific.
- ⁷⁵ A) U. Patzold, G. Roewer, U. Herzog, *J. Organomet. Chem.* **1996**, *508*, 147; B) J. Binder, R. C. Fisher, M. Flock, H.-G. Sammler, A. Torvisco, F. Uhlig, *Phosphorous Sulfur Silicon Relat. Elem.* **2016**, *191*, 478.
- ⁷⁶ A) R. Hager, O. Steigelmann, G. Muller, H. Schmidbaur, *Chem. Ber.* **1989**, *122*, 2115; B) H. Schmidbaur, J. Zech, D. W. H. Rankin, H. E. Robertson, *Chem. Ber.* **1991**, *124*, 1953.
- ⁷⁷ A) A. Kunai, J. Ohshita, *J. Organomet. Chem.* **2003**, *686*, 3. B) W. Wang, Y. Tan, Z. He, Z. Zhang, *J. Organomet. Chem.* **2014**, *769*, 29.
- ⁷⁸ *Organotransition Metal Chemistry: From Bonding to Catalysis* (Ed. J. F. Hartwig), University Science Books, California, pp. 33-41.
- ⁷⁹ A Scifinder search for "Phosphine Oxide Reduction" results in over 300 hits from 2000 and beyond, 13 of which are from 2017.
- ⁸⁰ H. A. van Kalker, F. L. van Delft, F. P. J. T. Rutjes, *ChemSusChem*, **2013**, *6*, 1615-1624.
- ⁸¹ K. Andrews, R. M. Denton, *Chem. Commun.* **2017**, *53*, 7982-7985.
- ⁸² K. Zhang, L. Cai, Z. Yang, K. N. Houk, O. Kwon, *Chem. Sci.* **2018**, *9*, 1867-1872.
- ⁸³ M.-L. Schirmer, S. Adomeit, T. Werner, *Org. Lett.* **2015**, *17*, 3078-3081.

- ⁸⁴ D. L. Hughes, R. A. Reamer, J. J. Bergan, E. J. J. Grabowski, *J. Am. Chem. Soc.* **1988**, *110*, 6487-6491.
- ⁸⁵ A. D. Kosal, E. E. Wilson, B. L. Ashfeld, *Angew. Chem. Int. Ed.* **2012**, *51*, 12036-12040.
- ⁸⁶ A. Volkov, F. Tinnis, T. Slagbrand, P. Trillo, H. Adolfsson, *Chem. Soc. Rev.* **2016**, *45*, 6685-6697.
- ⁸⁷ A) F. Sandfort, M. O'Neill, M. J. Cornella, L. Wimmer, P. S. Baran, *Angew. Chem. Int. Ed.* **2017**, *56*, 3319-3323; B) K. M. M. Huihui, J. A. Caputo, Z. Melchor, A. M. Olivares, A. M. Spiewak, K. A. Johnson, *J. Am. Chem. Soc.* **2016**, *138*, 5016-5019.
- ⁸⁸ S. Das, D. Addis, S. Zhou, K. Junge, M. Beller, *J. Am. Chem. Soc.* **2010**, *132*, 1770-1771.
- ⁸⁹ S. Das, Y. Li, C. Bornschein, S. Pisiewicz, K. Jiersch, D. Michalik, F. Gallou, K. Junge, M. Beller, *Angew. Chem. Int. Ed.* **2015**, *54*, 12389-12393.
- ⁹⁰ R. F. Borch, M. D. Bernstein, H. D. Durst, *J. Am. Chem. Soc.* **1971**, *93*, 2897-2904.
- ⁹¹ I. Sorribes, K. Junge, M. Beller, *J. Am. Chem. Soc.* **2014**, *136*, 14314-14319.
- ⁹² D. Hirose, M. Gazvoda, J. Košmrlj, T. Taniguchi, *Org. Lett.* **2016**, *18*, 4036-4039.
- ⁹³ S. E. Denmark, C. S. Regens, *Acc. Chem. Res.* **2008**, *41*, 1486-1499.
- ⁹⁴ S. Ogawa, Y. Tajiri, N. Furukawa, *Bull. Chem. Soc. Jpn.* **1991**, *64*, 3182-3184.
- ⁹⁵ A. R. Mazzotti, M. G. Campbell, P. Tang, J. M. Murphy, T. Ritter, *J. Am. Chem. Soc.* **2013**, *135*, 14012-14015.
- ⁹⁶ A. P. Dieskau, B. Plietker, *Org. Lett.* **2011**, *13*, 5544-5547.
- ⁹⁷ Y.-S. Bao, C.-Y. Chen, Z.-Z. Huang, *J. Org. Chem.* **2012**, *77*, 8344-8349.
- ⁹⁸ A. K. Chakraborti, B. Singh, S. V. Chankeshwara, A. R. Patel, *J. Org. Chem.* **2009**, *74*, 5967-5974; B. T. Ramanjaneyulu, V. Reddy, P. Arde, S. Mahesh, R. V. Anand, *Chem. Asian J.* **2013**, *8*, 1489-1496.
- ⁹⁹ R. Ghosh, E. Lindstedt, N. Jalalian, B. Olofsson, *Chem. Open* **2014**, *3*, 54-57.
- ¹⁰⁰ X. Xie, S. S. Stahl, *J. Am. Chem. Soc.* **2015**, *137*, 3767-3770.
- ¹⁰¹ V. M. Uvarov, D. A. de Vekki, V. P. Reshetilovskii, N. K. Skvortsov *Russ. J. Gen. Chem.* **2010**, *80*, 35.
- ¹⁰² A. Benouargha, D. Boulahia, B. Boutevin, G. Caporiccio, F. Guida-Pietrasanta, A. Ratsimihety *Phosphorous Sulfur Silicon Relat. Elem.* **1996**, *113*, 79.
- ¹⁰³ J. D. van Beek *J. Magn. Res.* **2007**, *187*, 19.
- ¹⁰⁴ Q. Bao, J. Feng, L. Chen, F. Chen, Z. Liu, B. Jiang, C. Liu *J. Magn. Res.* **2013**, *234*, 82.
- ¹⁰⁵ W. Zhao, P. K. Yan, A. T. Radosevich *J. Am. Chem. Soc.* **2015**, *137*, 616.
- ¹⁰⁶ M. J. Pilling & P. W. Seakins *Reaction Kinetics*, 2nd Edition; Oxford Science Publications; Oxford University Press: Oxford, 1996.
- ¹⁰⁷ C. Hansch, A. Leo, R. W. Taft *Chem. Rev.* **1991**, *91*, 165.
- ¹⁰⁸ B. Osmialowski, K. Mroczynska, E. Kolehmainen, M. Kowalska, A. Valkonen, M. Pietrzak, K. Rissanen *J. Org. Chem.* **2013**, *78*, 7582.
- ¹⁰⁹ L. Wilczek, J. Chojnowski *J. Makromol. Chem.* **1983**, *184*, 77.
- ¹¹⁰ A. Kupareva, P. Maki-Arvela, H. Grenman, K. Eranen, D. Yu. Murzin *J. Chem. Technol. Biotechnol.* **2015**, *90*, 34.
- ¹¹¹ R. G. Pearson *J. Am. Chem. Soc.* **1962**, *85*, 3533.
- ¹¹² P. A. Byrne, Y. Ortin, D. G. Gilheany *Chem. Commun.* **2015**, *51*, 1147.
- ¹¹³ S. Xin, C. Aitken, J. F. Harrod, Y. Mu, E. Samuel *Can. J. Chem.* **1990**, *68*, 471-476.
- ¹¹⁴ **Gaussian 09, Revision D.01**: M. J. Frisch, G. W. Trucks, H. B. Schlegel, G. E. Scuseria, M. A. Robb, J. R. Cheeseman, G. Scalmani, V. Barone, G. A. Petersson, H. Nakatsuji, X. Li, M. Caricato, A. Marenich, J. Bloino, B. G. Janesko, R. Gomperts, B. Mennucci, H. P. Hratchian, J. V. Ortiz, A. F. Izmaylov, J. L. Sonnenberg, D. Williams-Young, F. Ding, F. Lipparini, F. Egidi, J. Goings, B. Peng, A. Petrone, T. Henderson, D. Ranasinghe, V. G. Zakrzewski, J. Gao, N. Rega, G. Zheng, W. Liang, M. Hada, M. Ehara, K. Toyota, R. Fukuda, J. Hasegawa, M. Ishida, T. Nakajima, Y. Honda, O. Kitao, H. Nakai, T. Vreven, K. Throssell, J. A. Montgomery, Jr., J. E. Peralta, F. Ogliaro, M. Bearpark, J. J. Heyd, E. Brothers, K. N. Kudin, V. N. Staroverov, T. Keith, R. Kobayashi, J. Normand, K. Raghavachari, A. Rendell, J. C. Burant, S. S. Iyengar, J. Tomasi, M. Cossi, J. M. Millam, M. Klene, C. Adamo, R. Cammi, J. W. Ochterski, R. L. Martin, K. Morokuma, O. Farkas, J. B. Foresman, and D. J. Fox, Gaussian, Inc., Wallingford CT, 2013.
- ¹¹⁵ A) C. Lee, W. Yang, R. G. Parr *Phys. Rev.* **1988**, *B37*, 785; B) A. D. Becke *J. Chem. Phys.* **1993**, *98*, 5648.

- ¹¹⁶ L. R. Domingo, M. Rios-Gutierrez, P. Perez *Molecules*, **2016**, *21*, 748.
- ¹¹⁷ J.-S. Zhang, T. Chen, J. Yang, L.-B. Han *Chem. Commun.* **2015**, *51*, 7540-7542.
- ¹¹⁸ H.-Y. Zhang, M. Sun, Y.-N. Ma, Q.-P. Tian, S.-D. Yang *Org. Biomol. Chem.* **2012**, *10*, 9627-9633.
- ¹¹⁹ L. Liu, H.-C. Wu, J.-Q. Yu *Chem. Eur. J.* **2011**, *17*, 10828-10831.
- ¹²⁰ C. A. Busacca, R. Raju, N. Grinberg, N. Haddad, P. James-Jones, H. Lee, J. C. Lorenz, A. Saha, C. H. Senanayake *J. Org. Chem.* **2008**, *73*, 1524-1531.
- ¹²¹ M. J. Petersson, W. A. Loughlin, I. D. Jenkins *Chem. Commun.* **2008**, 4493-4494.
- ¹²² G. Keglevich, T. Kovacs, F. Csatlos *Heteroatom Chemistry* **2015**, *26*, 199-205.
- ¹²³ D. E. Bergbreiter, Y.-C. Yang *J. Org. Chem.* **2010**, *75*, 873-878.
- ¹²⁴ S. E. Tunney, J. K. Stille *J. Org. Chem.* **1987**, *52*, 748-753.
- ¹²⁵ M.-Y. Jin, N. Yoshikai *J. Org. Chem.* **2011**, *76*, 1972-1978.
- ¹²⁶ J. A. S. Howell, N. Fey, J. D. Lovatt, P. C. Yates, P. McArdle, D. Cunningham, E. Sadeh, H. E. Gottlieb, Z. Goldschmidt, M. B. Hursthouse, M. E. Light *J. Chem. Soc. Dalton Trans.* **1999**, 3015-3028.
- ¹²⁷ O. J. Metters, S. J. K. Forrest, H. A. Sparkes, I. Manners, D. F. Wass *J. Am. Chem. Soc.* **2016**, *138*, 1994-2003.
- ¹²⁸ J. P. Wolfe, R. A. Singer, B. H. Yang, S. L. Buchwald *J. Am. Chem. Soc.* **1999**, *121*, 9550-9561.
- ¹²⁹ E. Ullah, J. McNulty, A. Robertson *Eur. J. Org. Chem.* **2012**, 2127-2131.
- ¹³⁰ L. M. Klingensmith, E. R. Strieter, T. E. Barder, S. L. Buchwald *Organometallics*, **2006**, *25*, 82-91.
- ¹³¹ M. Irandoust, M. Joshashani, E. Rafiee, M. Pourshahbaz *Spectrochim. Acta A Mol. Biomol. Spectrosc.* **2009**, *74*, 855-859.
- ¹³² F. L. Lin, H. M. Hoyt, H. van Halbeek, R. G. Bergman, C. R. Bertozzi *J. Am. Chem. Soc.* **2005**, *127*, 2686-2695.
- ¹³³ J. Nithyanandhan, N. Jayaraman *Tetrahedron*, **2005**, *61*, 11184-11191.
- ¹³⁴ D. L. Hughes, R. A. Reamer, J. J. Bergan, E. J. J. Grabowski *J. Am. Chem. Soc.* **1988**, *110*, 6487-6491.
- ¹³⁵ E. Saxon, J. I. Armstrong, C. R. Bertozzi *Org. Lett.* **2000**, *2*, 2141.
- ¹³⁶ W. Li, X. Wu, *Org. Lett.* **2015**, *17*, 1910-1913.
- ¹³⁷ Z. Ruan, R. M. Lawrence, C. B. Cooper, *Tetrahedron Lett.* **2006**, *47*, 7649-7651.
- ¹³⁸ N. Iranpoor, H. Firouzabadi, A. Riazi, K. Pedrood, *J. Organomet. Chem.* **2016**, *822*, 67-73.
- ¹³⁹ T. Yamakawa, H. Kinoshita, K. Miura, *J. Organomet. Chem.* **2013**, *724*, 129-134.
- ¹⁴⁰ Y. Wang, G. Du, C. Gu, F. Xing, B. Dai, L. He, *Tetrahedron* **2016**, *72*, 472-478.
- ¹⁴¹ J. M. Concellon, E. Bardales, *Org. Lett.* **2002**, *4*, 189-191.
- ¹⁴² G. Bartoli, G. Di Antonio, R. Giovannini, S. Giuli, S. Lanari, M. Paoletti, E. Marcantoni, *J. Org. Chem.* **2008**, *73*, 1919-1924.
- ¹⁴³ W. R. Perrault, B. A. Pearlman, D. B. Godrej, A. Jeganathan, K. Yamagata, J. J. Chen, C. V. Lu, P. M. Herrinton, R. C. Gadwood, L. Chan, M. A. Lyster, M. A. Lyster, M. T. Maloney, J. A. Moeslein, M. L. Greene, M. R. Barbachyn, *Org. Process Res. Dev.* **2003**, *7*, 533-546.
- ¹⁴⁴ G. Van Dyke Tiers, *Magn. Reson. Chem.* **1999**, *37*, 609-612.
- ¹⁴⁵ T. V. Nguyen, A. Bekensir, *Org. Lett.* **2014**, *16*, 1720-1723.
- ¹⁴⁶ K. A. Roper, H. Lange, A. Polyzos, M. B. Berry, I. R. Baxendale, S. V. Ley, *Beilstein J. Org. Chem.* **2011**, *7*, 1648-1655.
- ¹⁴⁷ World Health Organization. Global Tuberculosis Report 2016.
http://www.who.int/tb/publications/global_report/en/ (last accessed 7-8-18)
- ¹⁴⁸ World Health Organization. Treatment of Tuberculosis Guidelines, 4th ed.
<http://www.who.int/tb/publications/2010/9789241547833/en/> (last accessed 7-8-18)
- ¹⁴⁹ Centers for Disease Control and Prevention (CDC) (1999). Control of infectious diseases. *MMWR Morb. Mortal. Wkly. Rep.* *48*, 621-629.
- ¹⁵⁰ World Health Organization. Global Tuberculosis Report 2016.
http://www.who.int/tb/publications/global_report/en/ (last accessed 7-8-18)
- ¹⁵¹ K. Mdluli, T. Kaneko, A. Upton, *Cold Spring Hard. Perspect. Med.* **2015**, *5*, a021154

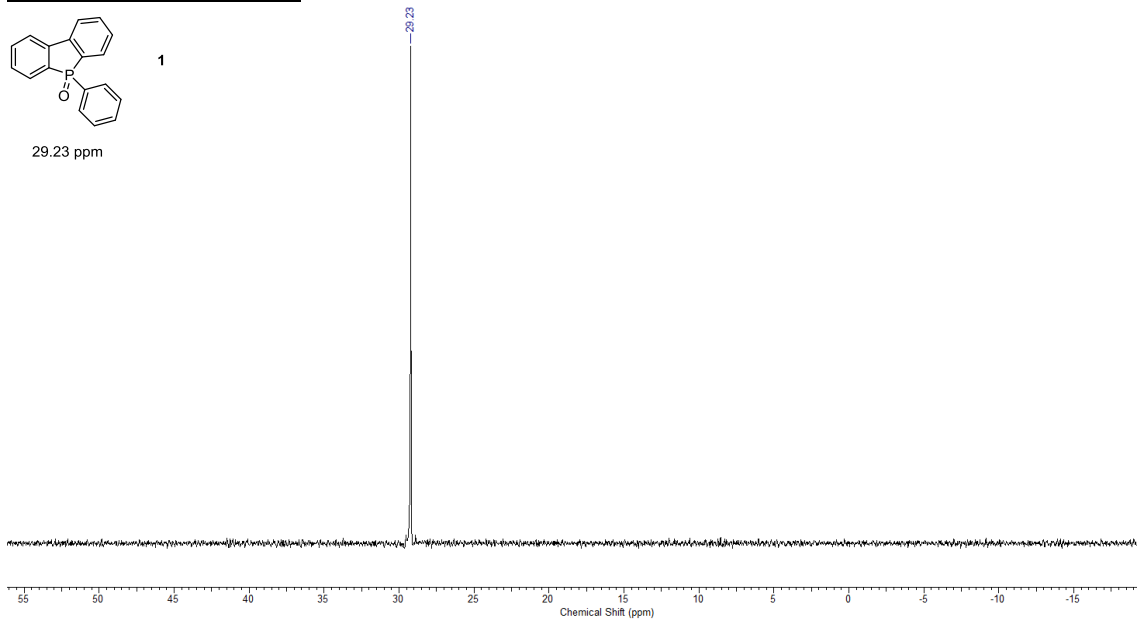
- ¹⁵² A) M. Tarshis, W. J. Weed, *Am. Rev. Tuberc.* **1953**, *67*, 391-395; B) W. McDermott, R. Tompsett, *Am. Rev. Tuberc.* **1954**, *70*, 748-754; C) K. Konno, F. M. Feldmann, W. McDermott, *Am. Rev. Respir. Dis.* **1967**, *95*, 461-469; D) N. D. Peterson, B. C. Rosen, N. A. Dillon, A. D. Baughn, *Antimicrob. Agents Chemother.* **2015**, *59*, 7320-7326.
- ¹⁵³ A) Y. Zhang, W. Shi, W. Zhang, D. Mitchison, *Microbiol. Spectr.* **2013**, *2*, MGM2-00233-2013; B) M. Stehr, A. A. Elamin, M. Singh, *Expert Rev. Anti Infect. Ther.* **2015**, *13*, 593-603.
- ¹⁵⁴ A. Scorpio, Y. Zhang, *Nat. Med.* **1996**, *2*, 662-667.
- ¹⁵⁵ A) F. I. Dessau, R. L. Yeager, F. J. Burger, J. H. Williams, *Am. Rev. Tuberc.* **1952**, *65*, 519-522; B) R. L. Yeager, W. G. Munroe, F. I. Dessau, *Am. Rev. Tuberc.* **1952**, *65*, 523-546; L. S. A. Malone, H. Lindh, D. McKenzie, J. S. Kiser, J. H. Williams, *Am. Rev. Tuberc.* **1952**, *65*, 511-518; D) L. E. Via, R. Savic, D. M. Weimer, M. D. Zimmerman, B. Prideaux, S. M. Irwin, E. Lyon, P. O'Brien, P. Gopal, S. Eum, M. Lee, J. P. Lanoix, N. K. Dutta, T. Shim, J. S. Co, W. Kim, P. C. Karakousis, A. Lenaerts, E. Nuermberger, C. E. Barry, V. Dartois, *ACS Infect. Dis.* **2015**, *1*, 203-214; E) J. P. Lanoix, R. Tasneen, P. O'Brien, J. Sarathy, H. Safi, M. Pinn, D. Alland, V. Dartois, E. Nuermberger, *Antimicrob. Agents Chemother.* **2016**, *60*, 4197-4205.
- ¹⁵⁶ R. J. Speirs, J. T. Welch, M. H. Cynamon, *Antimicrob. Agents Chemother.* **1995**, *39*, 1269-71.
- ¹⁵⁷ I. R. Montella, R. Schama, D. Valle, *Mem. Inst. Oswaldo Cruz, Rio de Janeiro*, **2012**, *107*, 437-449.
- ¹⁵⁸ B. R. Wilson, A. R. Bogdan, M. Miyazawa, K. Hashimoto, Y. Tsuji, *Trends Mol. Med.* **2016**, *22*, 1077-1090.
- ¹⁵⁹ M. S. Diarra, M. C. Lavoie, M. Jacques, I. Darwish, E. K. Dolence, J. A. Dolence, A. Ghosh, M. Ghosh, M. J. Miller, F. Malouin, *Antimicrob. Agents Chemother.* **1996**, *40*, 2610-2617.
- ¹⁶⁰ G. A. Snow, *Bacteriol. Rev.* **1970**, *34*, 99-125.
- ¹⁶¹ S. Mobashery, S. A. Lerner, M. Johnston, *J. Am. Chem. Soc.* **1986**, *108*, 1685-1686.
- ¹⁶² A. Tomasz, *Ann. Rev. Microbiol.* **1979**, *33*, 113-137
- ¹⁶³ K. Bush, *Crit. Care* **2010**, *14*, 224.
- ¹⁶⁴ K. Bush, G. A. Jacoby, *Antimicrob. Agents Chemother.* **2010**, *54*, 969-976.
- ¹⁶⁵ A) G. Zhao, M. J. Miller, S. Franzblau, B. Wan, U. Möllmann, *Bioorg. Med. Chem. Lett.* **2006**, *16*, 5534; B) S. Yan, M. J. Miller, T. A. Wencewicz, U. Möllmann, *MedChemComm* **2010**, *1*, 145-148.
- ¹⁶⁶ A. R. Flores, L. M. Parsons, M. S. Pavelka, Jr., *Microbiology*, **2005**, *151*, 521-532.
- ¹⁶⁷ A. R. Flores, L. M. Parsons, M. S. Pavelka, Jr., *J. Bacteriol.* **2005**, *187*, 1892-1900.
- ¹⁶⁸ A) H. X. Xie, J. Mire, Y. Kong, M. H. Chang, H. A. Hassaounah, C. N. Thornton, J. C. Sacchettini, J. D. Cirillo, J. Rao, *Nat. Chem.* **2012**, *4*, 802-809; B) Y. Cheng, H. Xie, P. Sule, H. Hassounah, E. A. Graviss, Y. Kong, J. D. Cirillo, J. Rao, *Angew. Chem.* **2014**, *126*, 9514-9518.
- ¹⁶⁹ T. Mazzei, P. Dentico, *Clin. Microbiol. Infect.* **2000**, *6* (Supplement 3), 53-54.
- ¹⁷⁰ A) F. Wang, C. Cassidy, J. C. Sacchettini, *Antimicrob. Agents Chemother.* **2006**, *50*, 2762-2771; B) L. W. Tremblay, F. Fan, J. S. Blanchard, *Biochemistry*, **2010**, *49*, 3766-3773.
- ¹⁷¹ PDB-ID: 3NDE; L. W. Tremblay, J. S. Blanchard, *Unpublished*
- ¹⁷² *The Organic Chemistry of β -Lactams* (Ed. T. W. G. I. Georg), VCH Publishers Inc., New York, **1993**
- ¹⁷³ K. Yu, N. Sun, S. Fang, W. Mo, B. Hu, Z. Shen, X. Hu, *Org. Process Res. Dev.* **2009**, *13*, 815-819.
- ¹⁷⁴ TubercuList World Wide Web Server <http://genolist.pasteur.fr/TubercuList/> (last accessed 7-17-18)
- ¹⁷⁵ Nicholas A. Dillon, Ph. D. Dissertation, University of Minnesota, 2017.
- ¹⁷⁶ A) S. Zhang, J. Chen, W. Shi, W. Liu, W. Zhang, Y. Zhang, *Emerg. Microbes Infect.* **2013**, *2*, e34; B) W. Shi, J. Chen, J. Feng, P. Cui, S. Zhang, X. Weng, W. Zhang, Y. Zhang, *Emerg. Microbes Infect.* **2014**, *3*, e58.
- ¹⁷⁷ N. A. Dillon, N. D. Peterson, H. A. Feaga, K. C. Keiler, A. D. Baughn, *Sci. Rep.* **2017**, *7*, 6135.
- ¹⁷⁸ A) P. Gopal, M. Yee, J. Sarathy, J. L. Low, J. P. Sarathy, F. Kaya, V. Dartois, M. Gengenbacher, T. Dick, *ACS Infect. Dis.* **2016**, *2*, 616-626; B) P. Gopal, R. Tasneen, M. Yee, J. P. Lanoix, J. Sarathy, G. Rasic, L. Li, V. Dartois, E. Nuermberger, T. Dick, *ACS Infect. Dis.* **2017**, *3*, 492-501.
- ¹⁷⁹ R. S. Jansen, K. Y. Rhee, *Trends Pharmacol. Sci.* **2017**, *38*, 393-405.
- ¹⁸⁰ Josh Thiede, Personal Communication, July 2018.

- ¹⁸¹ K. D. Revell, B. Heldreth, T. E. Long, S. Jang, E. Turos, *Bioorg. Med. Chem.* **2007**, *15*, 2453-2467.
- ¹⁸² A. M. Teitelbaum, A. Meissner, R. A. Harding, C. A. Wong, C. C. Aldrich, R. P. Rimmel, *Bioorg. Med. Chem.* **2013**, *21*, 5605.
- ¹⁸³ S. Dawadi, S. Kawamura, A. Rubenstein, R. Rimmel, C. C. Aldrich, *Bioorg. Med. Chem.* **2016**, *24*, 1314-1321.
- ¹⁸⁴ W. F. Marshall, J. E. Blair, *Mayo Clin. Proc.* **1999**, *74*, 187-195.
- ¹⁸⁵ J. E. Hugonnet, J. S. Blanchard, *Biochemistry*, **2007**, *46*, 11998-12004.
- ¹⁸⁶ K. Bush, M. C. Macielag, *Expert Opin. Ther. Pat.* **2010**, *20*, 1277-1293.
- ¹⁸⁷ W. Shi, X. Zhang, X. Jiang, H. Yuan, J. S. Lee, C. E. Barry, H. Wang, W. Zhang, Y. Zhang, *Science*, **2011**, *333*, 1630-1632.
- ¹⁸⁸ N. A. Dillon, N. D. Peterson, B. C. Rosen, A. D. Baughn, *Antimicrob. Agents Chemother.* **2014**, *58*, 7258-7263
- ¹⁸⁹ A. R. Katritzky, H.-Y. He, K. Suzuki, *J. Org. Chem.* **2000**, *65*, 8210-8213.
- ¹⁹⁰ D. Seiner, S. Hegde, J. S. Blanchard, *Biochemistry*, **2010**, *49*, 9613-9619.
- ¹⁹¹ A) P. Wu, T. E. Nielsen, M. H. Clausen, *Trends Pharmacol. Sci.* **2015**, *36*, 422-439; B) L. Munoz, *Nat. Rev. Drug Disc.* **2017**, *16*, 424-440; C) F. M. Ferguson, N. S. Gray, *Nat. Rev. Drug Disc.* **2018**, *17*, 353-377.
- ¹⁹² *Foye's Principles of Medicinal Chemistry 7th Edition* (Eds. T. L. Lemke, D. A. Williams, V. F. Roche, S. W. Zito), Lippincott Williams & Wilkins, a Wolters Kluwer Business, Baltimore, MD, **2013**.
- ¹⁹³ A) Y. Liu, M. P. Patricelli, B. F. Cravatt, *Proc. Natl. Acad. Sci. USA* **1999**, *96*, 14694; B) D. Greenbaum, K. F. Medzhradsky, A. Burlingame, M. Bogyo, *Chem. Biol.* **2000**, *7*, 569-581.
- ¹⁹⁴ A) B. F. Cravatt, A. T. Wright, J. W. Kozarich, *Annu. Rev. Biochem.* **2008**, *77*, 38-414; B) P. Yang, K. Liu, *ChemBioChem*, **2015**, *16*, 712-724.
- ¹⁹⁵ K. E. Wilke, S. Francis, E. E. Carlson, *J. Am. Chem. Soc.* **2012**, *134*, 9150-9153.
- ¹⁹⁶ A) H. C. Kolb, M. G. Finn, K. B. Sharpless, *Angew. Chem. Int. Ed.* **2001**, *40*, 2204-2021; B) C. W. Tornøe, C. Christensen, M. Meldal, *J. Org. Chem.* **2002**, *67*, 3057-3064; C) V. V. Rostovtsev, L. G. Green, V. V. Fokin, K. B. Sharpless, *Angew. Chem. Int. Ed.* **2002**, *41*, 2596-2599.
- ¹⁹⁷ E. Saxon, C. R. Bertozzi, *Science*, **2000**, *287*, 2007-2010.
- ¹⁹⁸ A. H. Lichtman, D. Leung, C. C. Shelton, A. Saghatelian, C. Hardouin, D. L. Boger, B. F. Cravatt, *J. Pharmacol. Exp. Ther.* **2004**, *311*, 441-448.
- ¹⁹⁹ A) I. Staub, S. A. Sieber, *J. Am. Chem. Soc.* **2008**, *130*, 13400-13409; B) I. Staub, S. A. Sieber, *J. Am. Chem. Soc.* **2009**, *131*, 6271-6276; C) T. Böttcher, S. A. Sieber, *Med. Chem. Commun.* **2012**, *3*, 408-417; D) S. Sharifzadeh, M. J. Boersma, O. Kocaoglu, A. Shokri, C. L. Brown, J. D. Shirley, M. E. Winkler, E. E. Carlson, *ACS Chem. Biol.* **2017**, *12*, 2849-2857.
- ²⁰⁰ A) O. Kocaoglu, R. A. Calvo, L.-T. Sham, L. M. Cozy, B. R. Lanning, S. Francis, M. E. Winkler, D. B. Kearns, E. E. Carlson, *ACS Chem. Biol.* **2012**, *7*, 1746-4753; B) O. Kocaoglu, E. E. Carlson, *Nat. Chem. Biol.* **2016**, *12*, 472-478.
- ²⁰¹ M. L. Matthews, L. He. B. D. Horning, E. J. Olson, B. E. Correia, J. R. Yates III, P. E. Dawson, B. F. Cravatt, *Nat. Chem.* **2017**, *9*, 234-243.
- ²⁰² A) P. Christen, P. K. Mehta, *Chem. Rec.* **2001**, *1*, 436-447; B) R. Percudani, A. Peracchi, *EMBO Rep.* **2003**, *4*, 850-854.
- ²⁰³ M. P. Lambert, F. C. Neuhaus, *J. Bacteriol.* **1972**, *110*, 978-987.
- ²⁰⁴ A) G. A. Prosser, L. P. S. de Carvalho, *ACS Med. Chem. Lett.* **2013**, *4*, 1233-1237; B) G. A. Prosser, L. P. S. de Carvalho, *Biochemistry*, **2013**, *52*, 7145-7149.
- ²⁰⁵ S. M. Nanavati, R. B. Silverman, *J. Am. Chem. Soc.* **1991**, *113*, 9329-9340.
- ²⁰⁶ R. Dai, D. J. Wilson, T. W. Geders, C. C. Aldrich, *ChemBioChem*, **2014**, *15*, 575-586.
- ²⁰⁷ S. Zlitni, L. F. Ferruccio, E. D. Brown, *Nat. Chem. Biol.* **2013**, *9*, 796-804.
- ²⁰⁸ E. S. Lightcap, M. H. Hopkins, G. T. Olson, R. B. Silverman, *Bioorg. Med. Chem.* **1995**, *3*, 579-585.
- ²⁰⁹ A. J. L. Cooper, O. W. Griffith, *J. Biol. Chem.* **1979**, *254*, 2748-2753

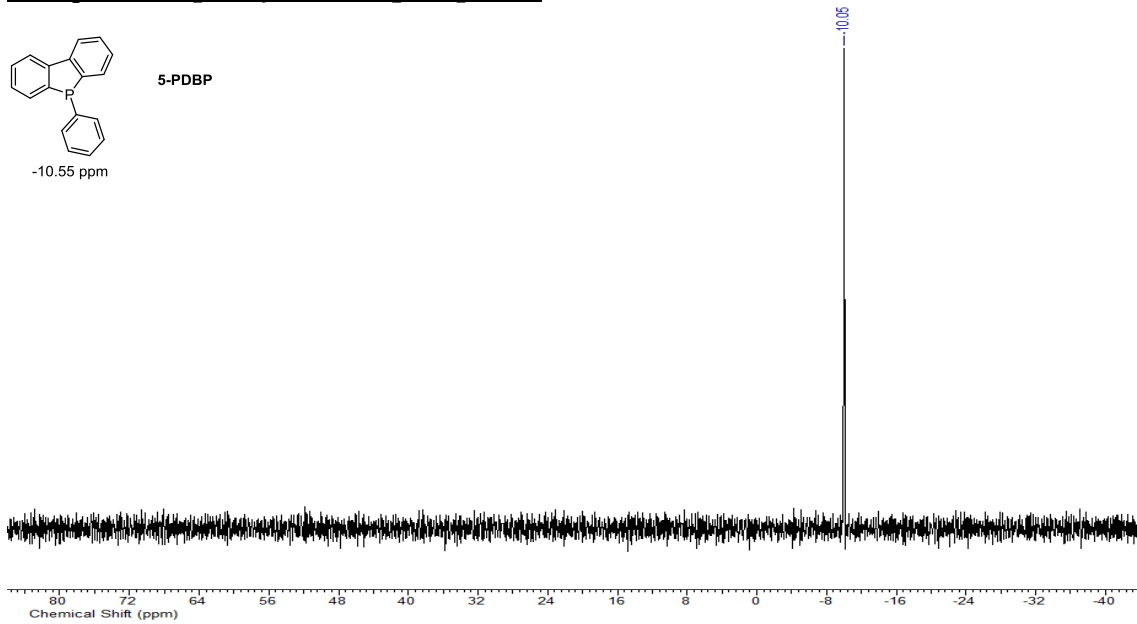
- ²¹⁰ B. Neises, W. Steglich, *Angew. Chem. Int. Ed.* **1978**, *17*, 522-524.
- ²¹¹ S. Mann, O. Ploux, *FEBS J.* **2006**, *273*, 4778-4789.
- ²¹² A) D. J. Wilson, C. Shi, B. P. Duckworth, J. M. Murtta, Y. Y. Sham, D. D. Thomas, C. C. Aldrich, *Analytical Biochem.* **2011**, *416*, 27-38; B) C. Shi, C. C. Aldrich, *J. Org. Chem.* **2012**, *77*, 6051-6058; C) R. Dai, T. W. Geders, F. Liu, S. W. Park, D. Schnappinger, C. C. Aldrich, B. C. Finzel; *J. Med. Chem.* **2015**, *58*, 5208-5217; D) C. G. Eiden, K. M. Maize, B. C. Finzel, J. D. Lipscomb, C. C. Aldrich, *J. Am. Chem. Soc.*, **2017**, *139*, 7132-7135; E) C. G. Eiden, C. C. Aldrich, *J. Org. Chem.* **2017**, *82*, 7806-7819.
- ²¹³ C. Shi, T. W. Geders, S. W. Park, D. J. Wilson, H. I. Boshoff, C. E. Barry, B. C. Finzel, C. C. Aldrich, *J. Am. Chem. Soc.* **2011**, *133*, 18194-18201.
- ²¹⁴ D. S. Bolotin, N. A. Bokach, M. Я. Demakova, V. Ю. Kukushkin, *Chem. Rev.* **2017**, *117*, 13039-13122.
- ²¹⁵ A) E. Smith, I. Collins, *Future Med. Chem.* **2015**, *7*, 159-183; B) D. P. Murale, S. C. Hong, M. M. Haque, J.-S. Lee, *Proteome Science*, **2017**, *15*, 14.
- ²¹⁶ B. P. Duckworth, K. nelson, H. I. Boshoff, C. E. Barry, C. C. Aldrich, *ACS Chem. Biol.* **2012**, *7*, 1653-1658.
- ²¹⁷ F. C. Lee-Peng, M. A. Hermodson, G. B. Kohlhaw, *J. Bacteriol.* **1979**, *139*, 339-345.
- ²¹⁸ A) T. M. A. Franco, S. Hegde, J. S. Blanchard, *Biochemistry*, **2016**, *55*, 6295-6303; B) T. M. A. Franco, L. Favrot, O. Vergnolle, J. S. Blanchard, *ACS Chem. Biol.* **2017**, *12*, 1235-1244.
- ²¹⁹ *Dye Laser Principles (Eds. F.J. Duarte, L. W. Hillman)*, Academic Publication Inc., New York, **1990**
- ²²⁰ A) E. Weerapana, A. E. Speers, B. F. Cravatt, *Nat. Protoc.* **2007**, *2*, 1414-1425; B) A. E. Speers, B. F. Cravatt, *Curr. Protoc. Chem. Biol.* **2009**, *1*, 29-41.
- ²²¹ T. B. Mete, A. Singh, R. G. Bhat *Tetrahedron Lett.* **2017**, *58*, 4709-4712.

Appendix I: NMR

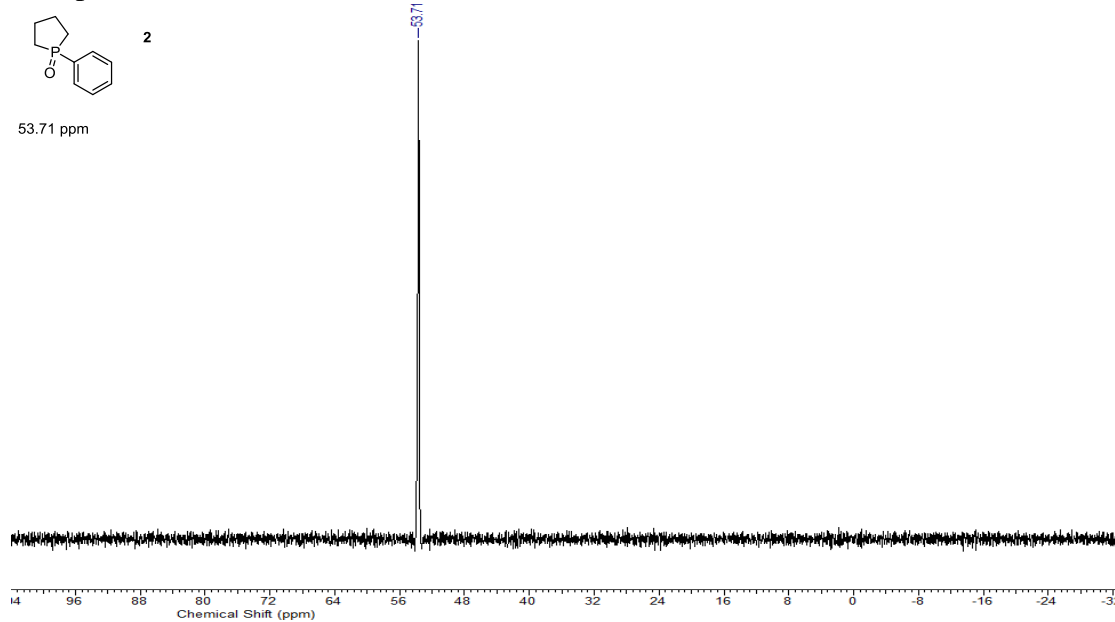
^{31}P Spectra (5PDBPO): d_8 - THF



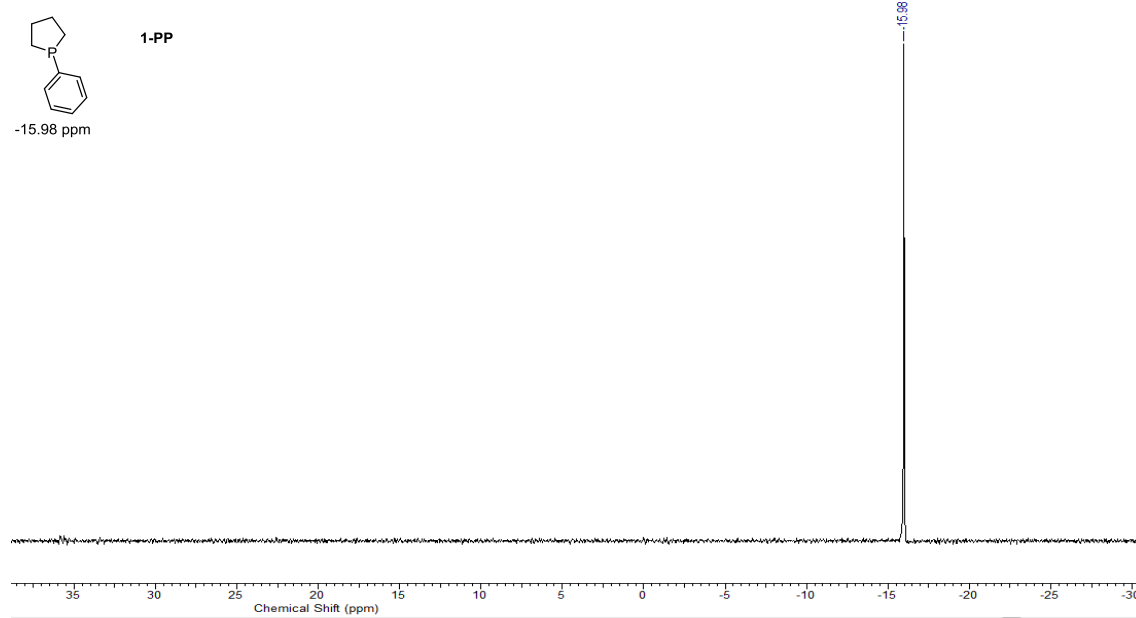
^{31}P Spectra (5-phenyldibenzophoshole): d_8 - THF



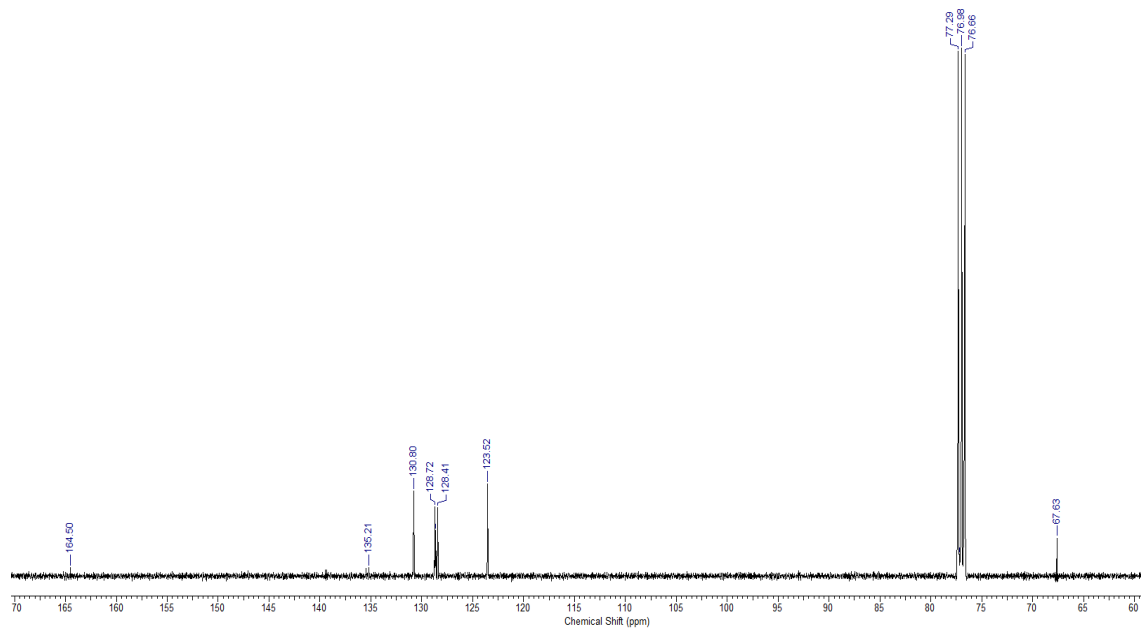
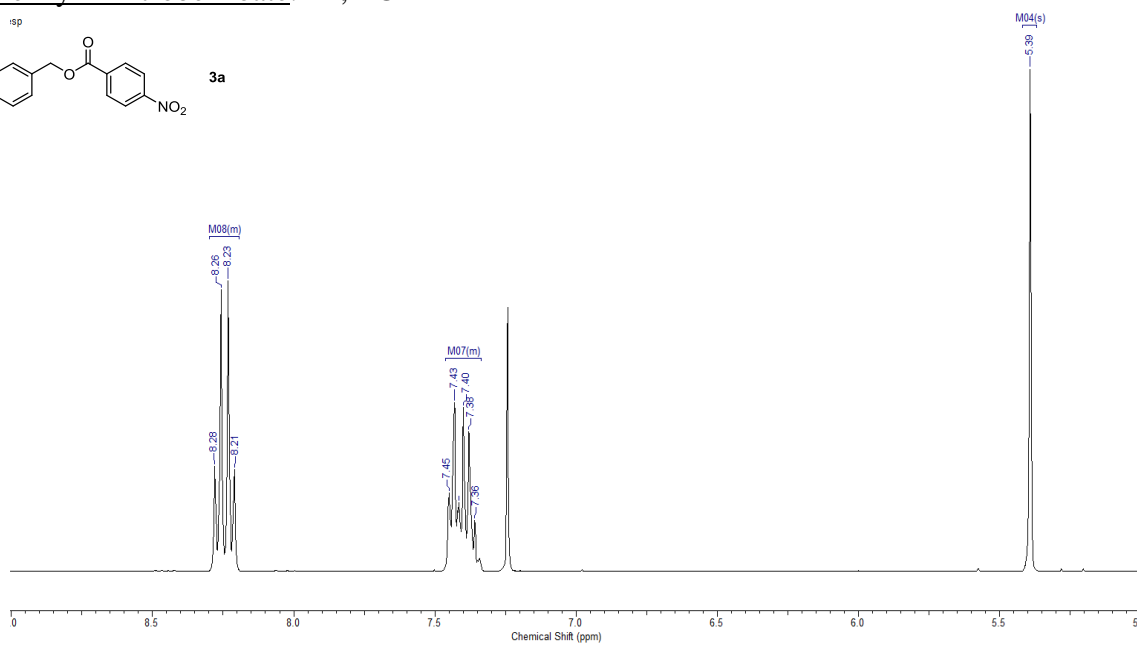
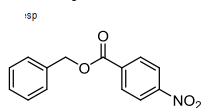
^{31}P Spectra (1PPO): d_8 - THF



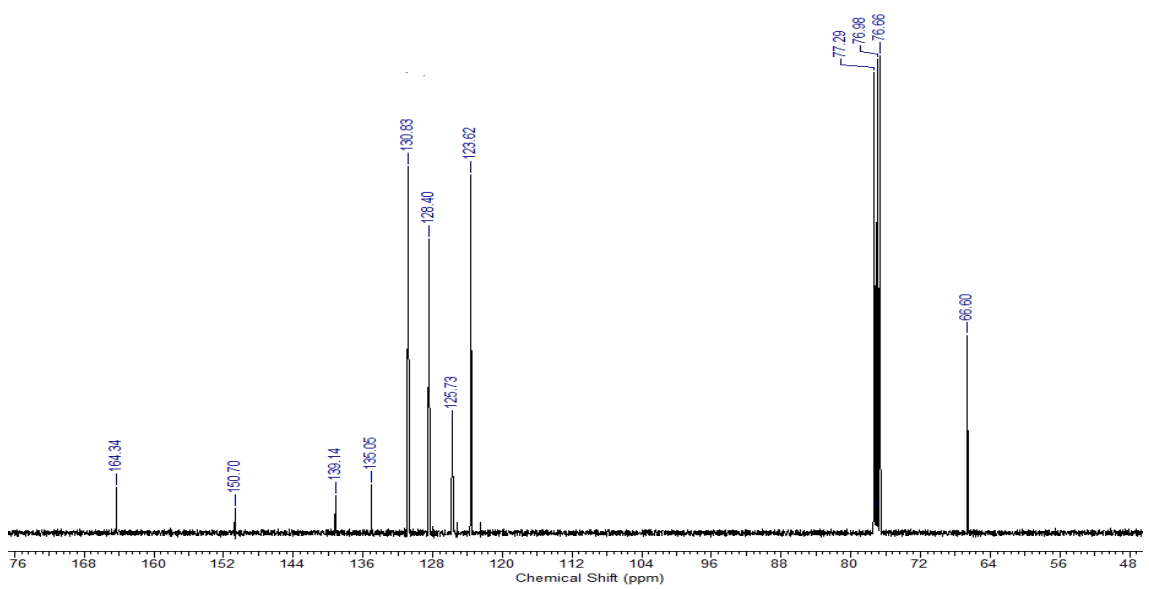
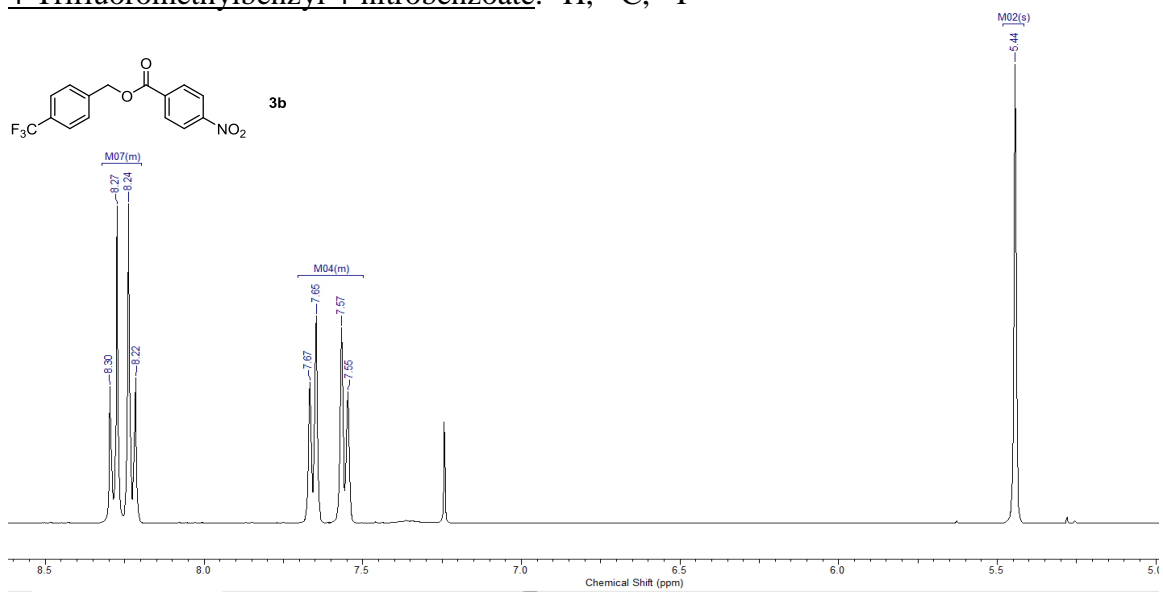
^{31}P Spectra (1-phenylphospholane): d_8 - THF

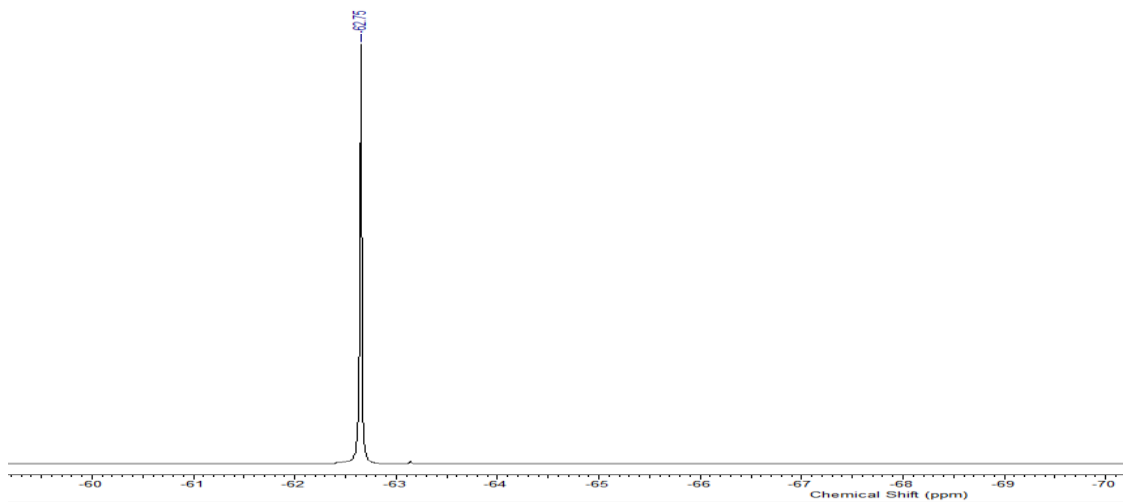


Benzyl 4-nitrobenzoate: ^1H , ^{13}C

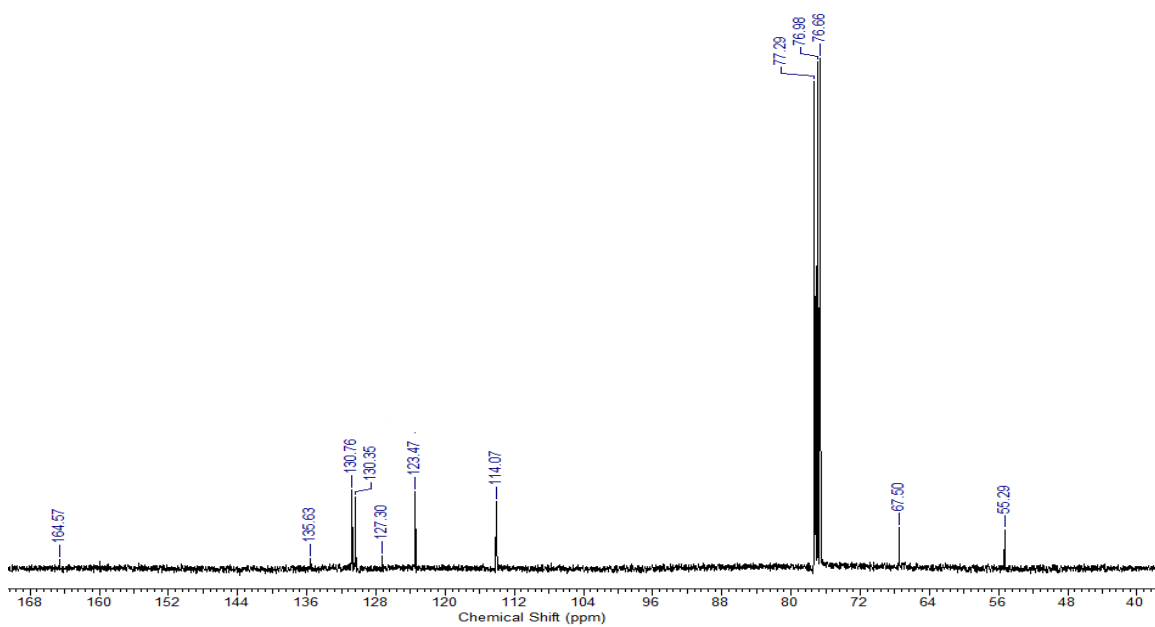
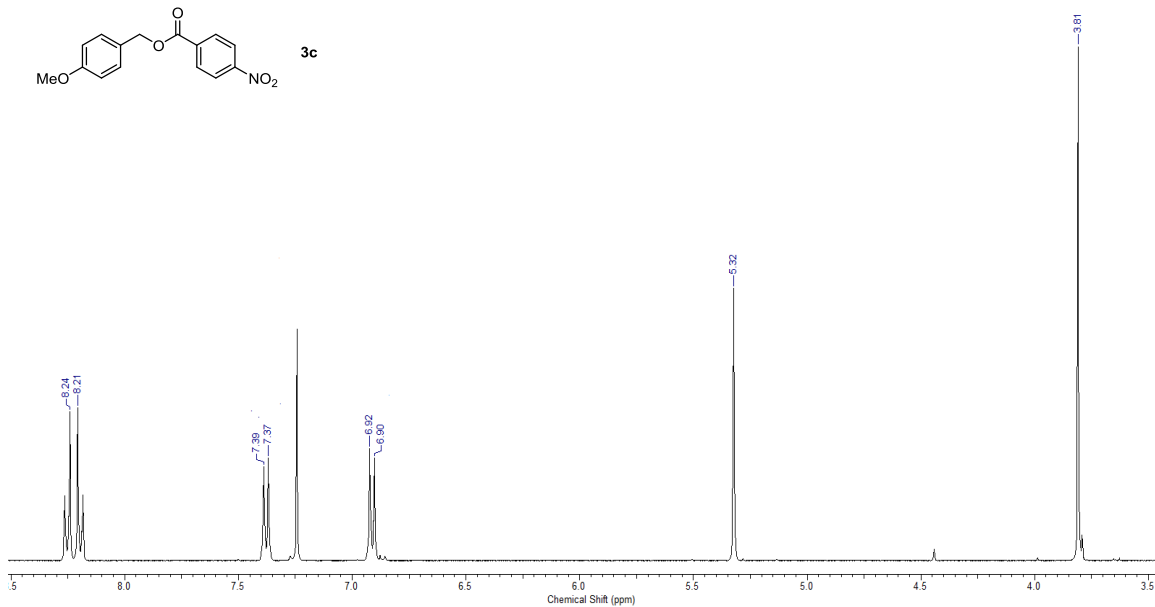
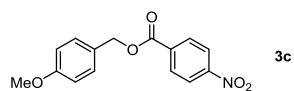


4-Trifluoromethylbenzyl 4-nitrobenzoate: ^1H , ^{13}C , ^{19}F

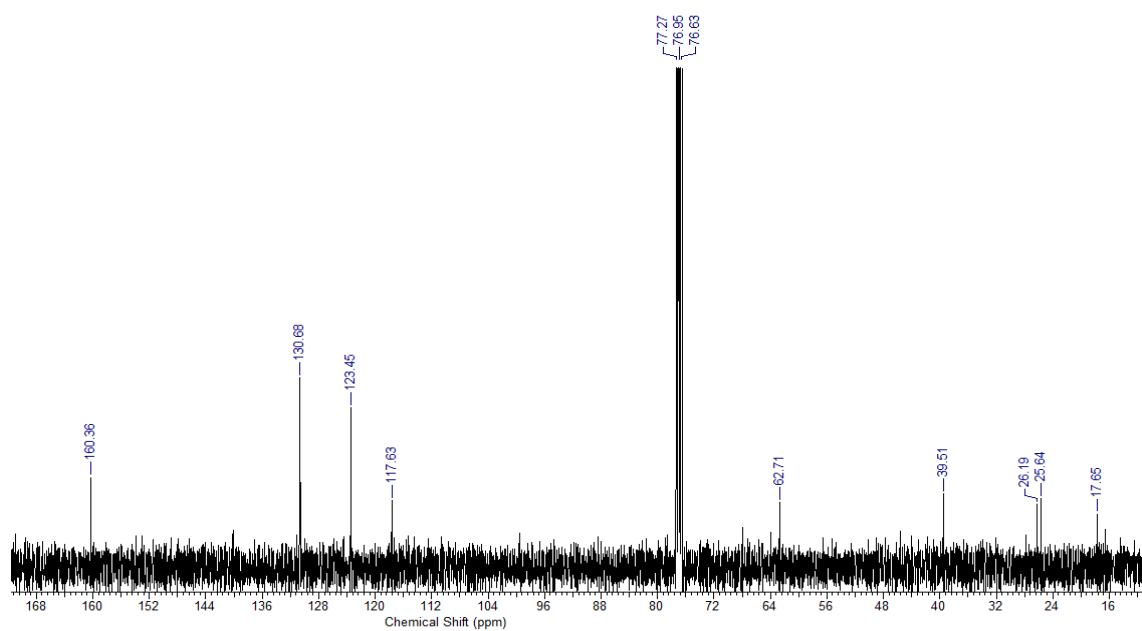
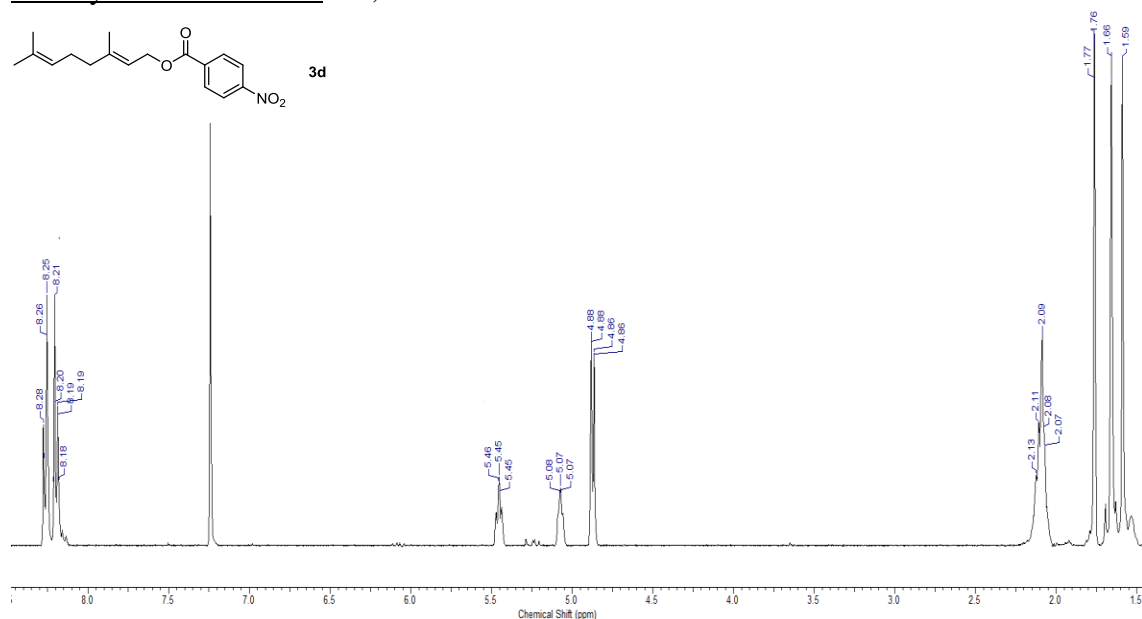
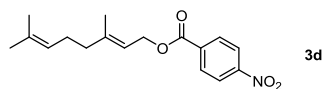




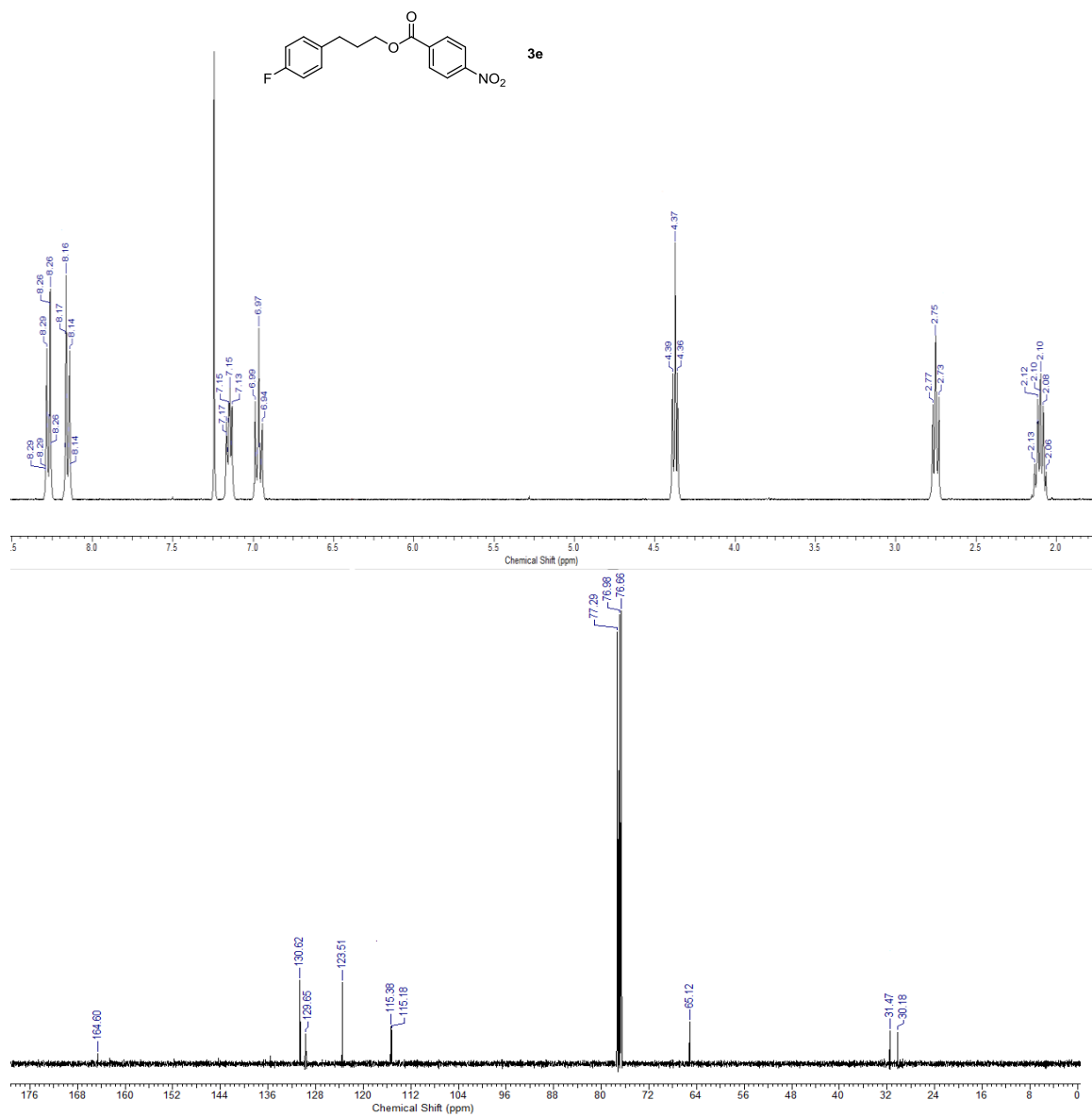
4-Methoxybenzyl 4-nitrobenzoate: ^1H , ^{13}C

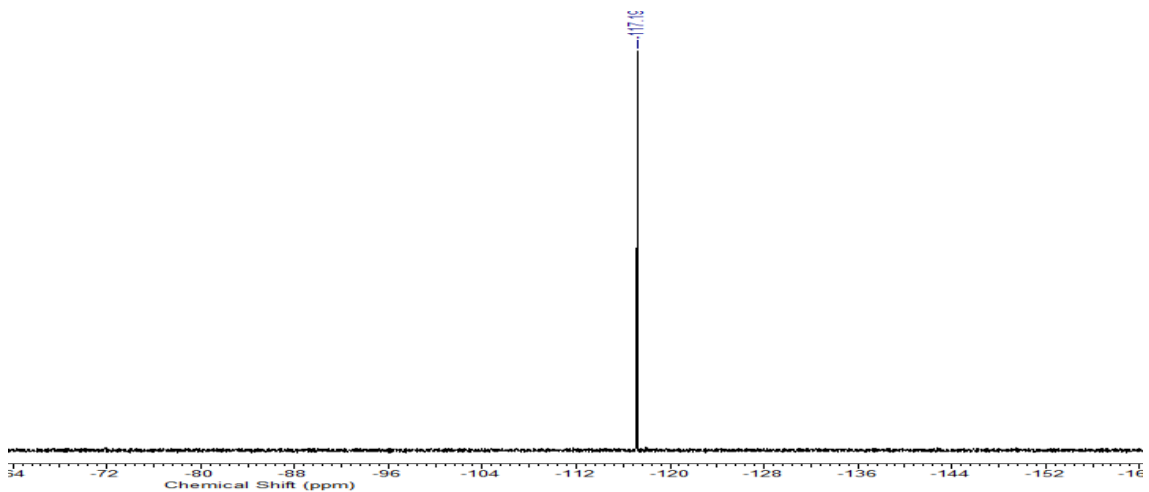


Geranyl 4-nitrobenzoate: ^1H , ^{13}C

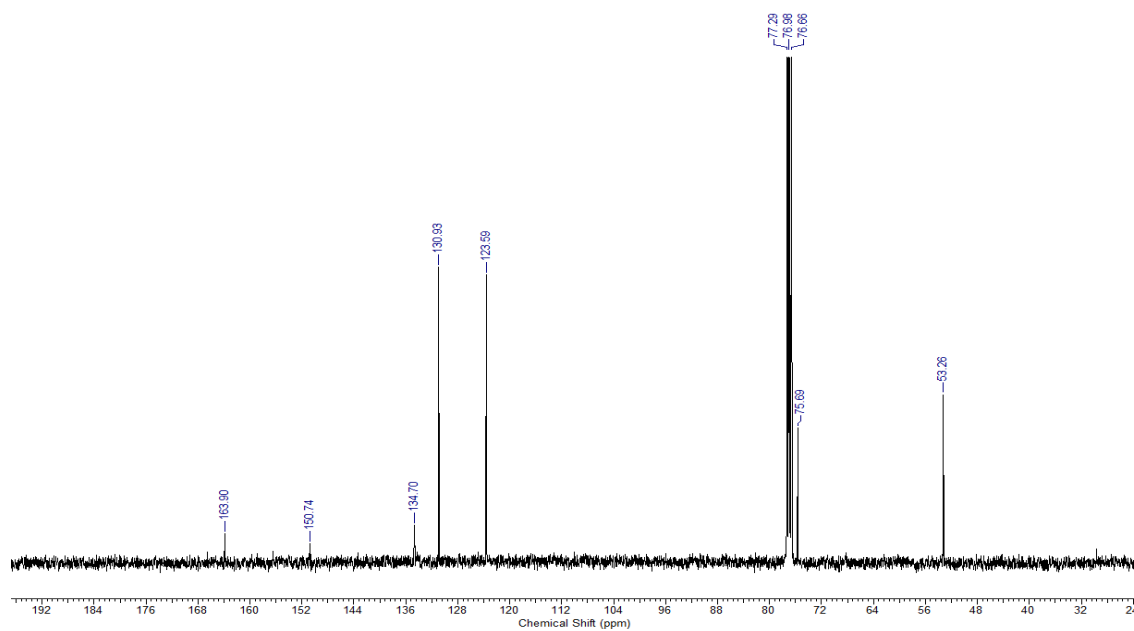
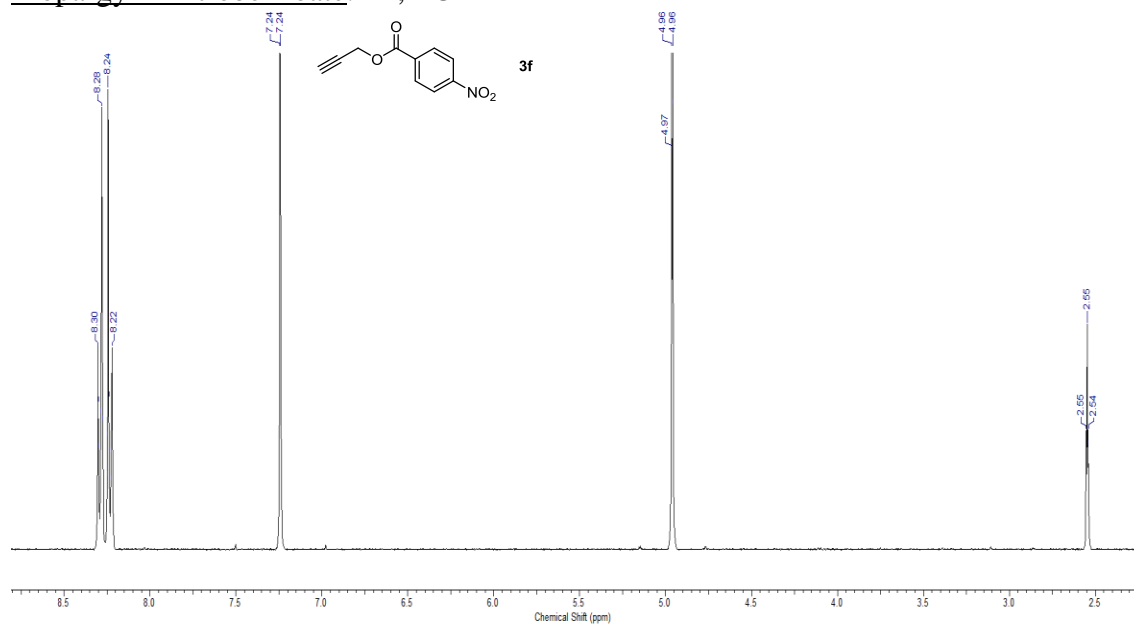


3-(4-Fluorophenyl)propyl 4-nitrobenzoate: ^1H , ^{13}C , ^{19}F

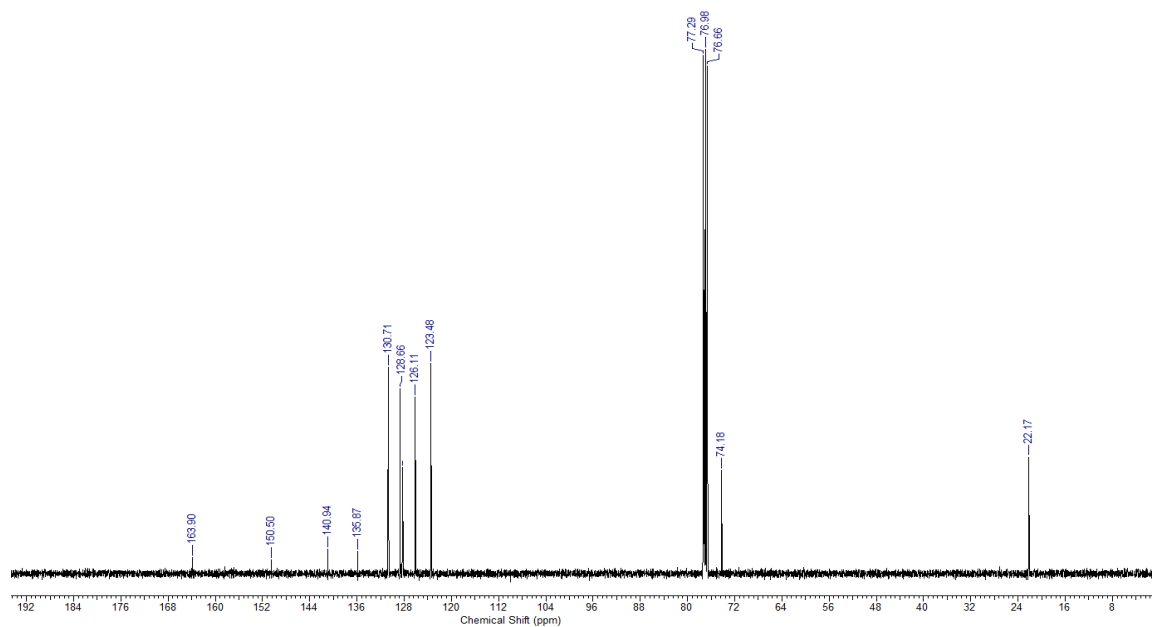
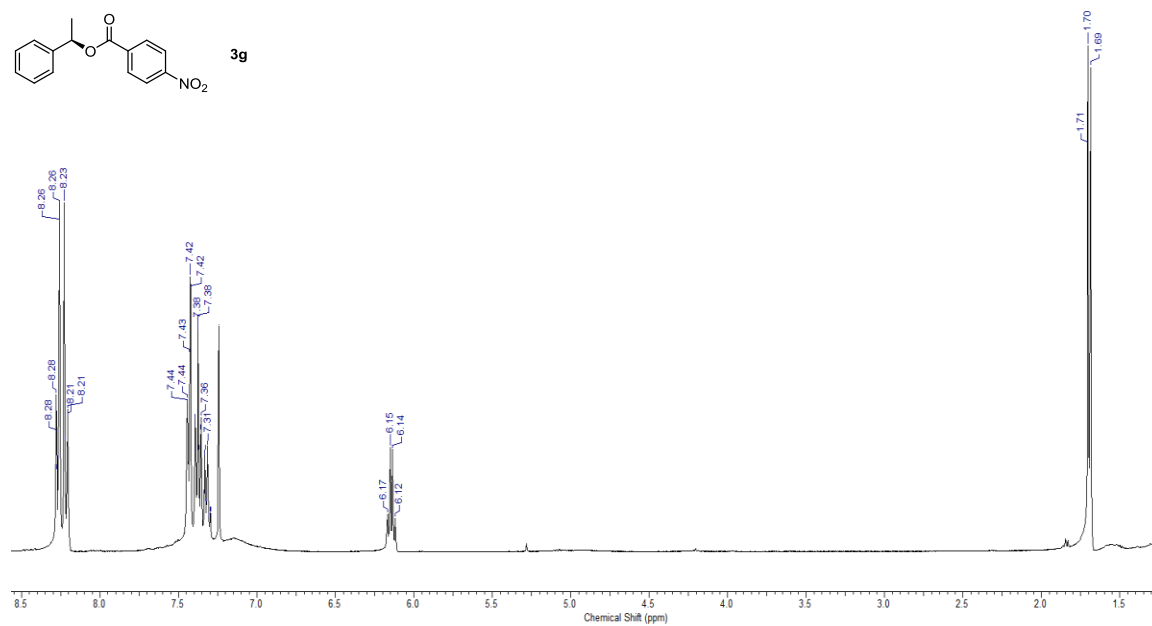
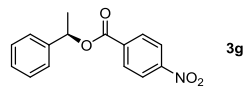




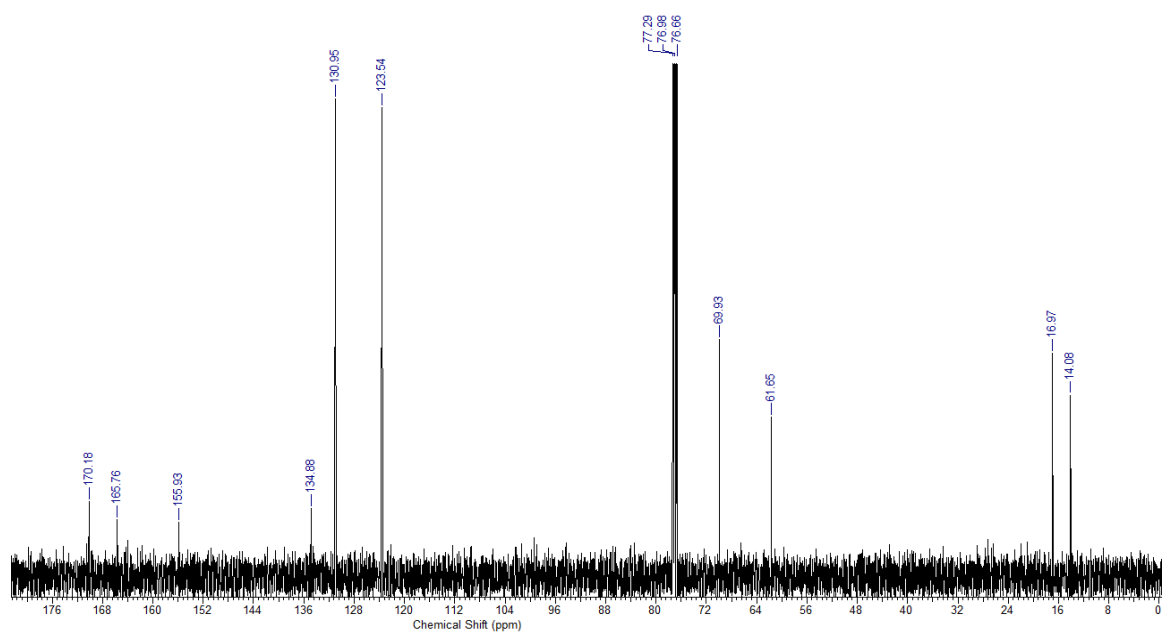
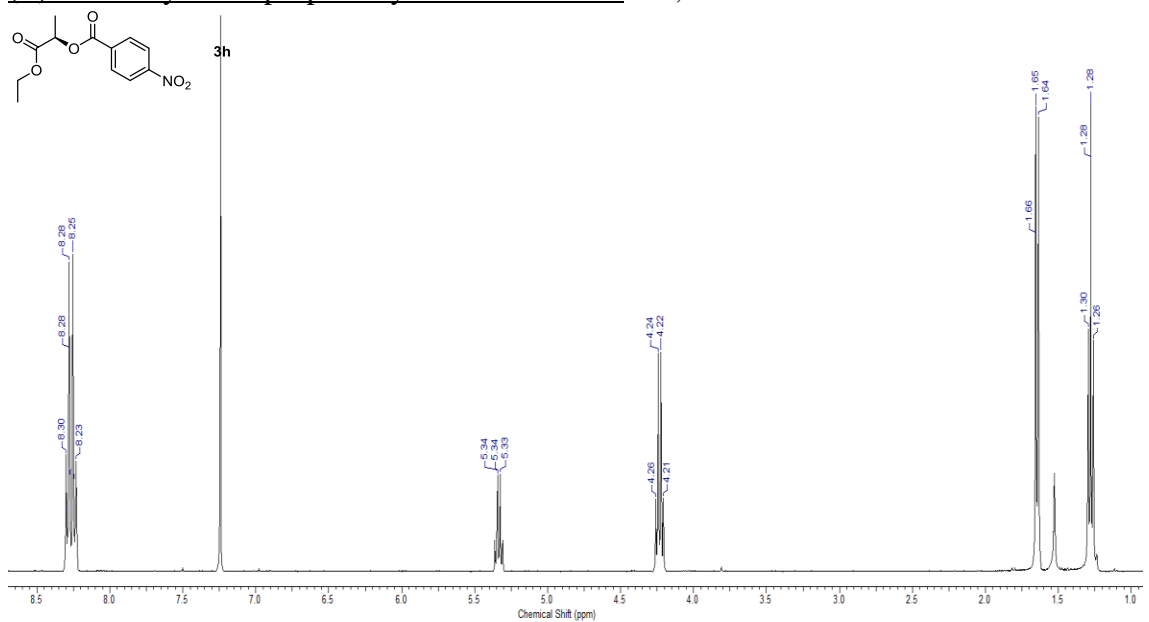
Propargyl 4-nitrobenzoate: ^1H , ^{13}C



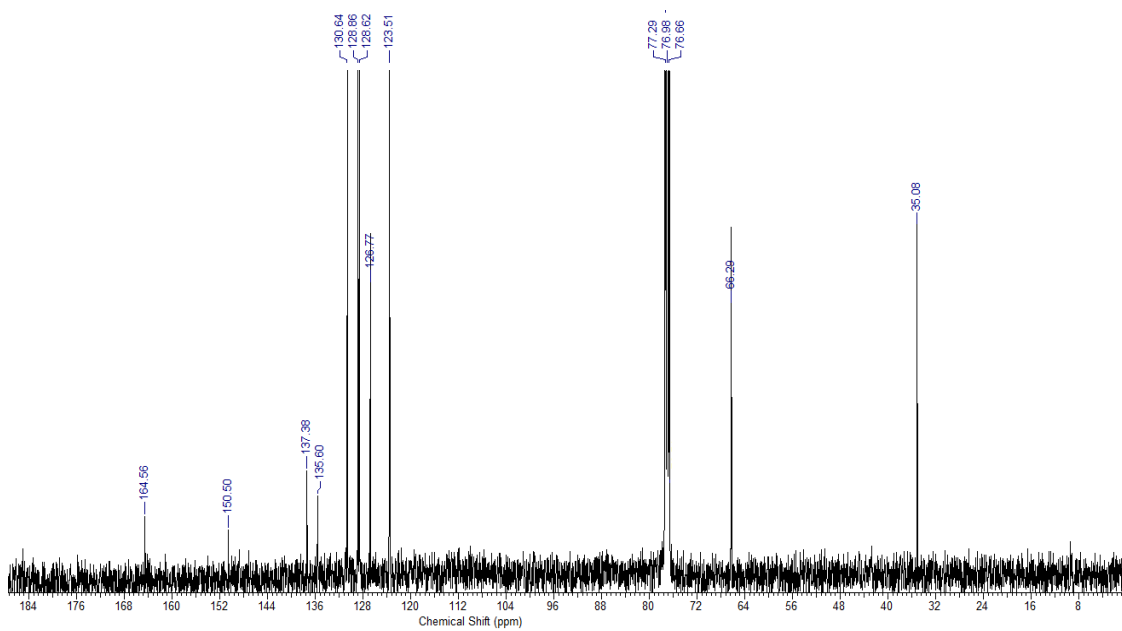
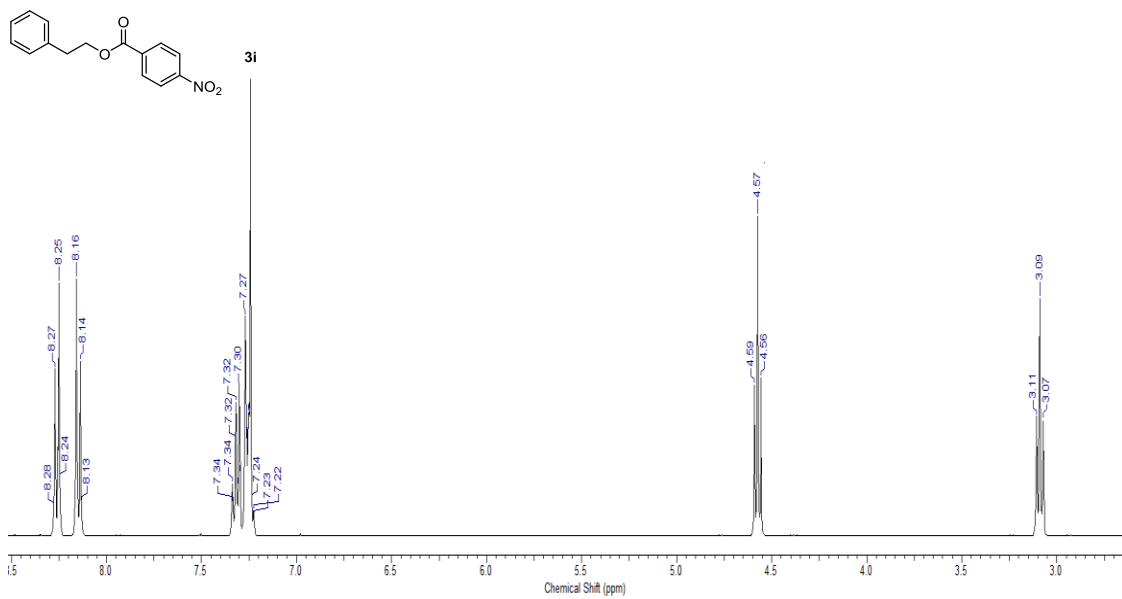
(R)-1-Phenylethyl 4-nitrobenzoate: ^1H , ^{13}C



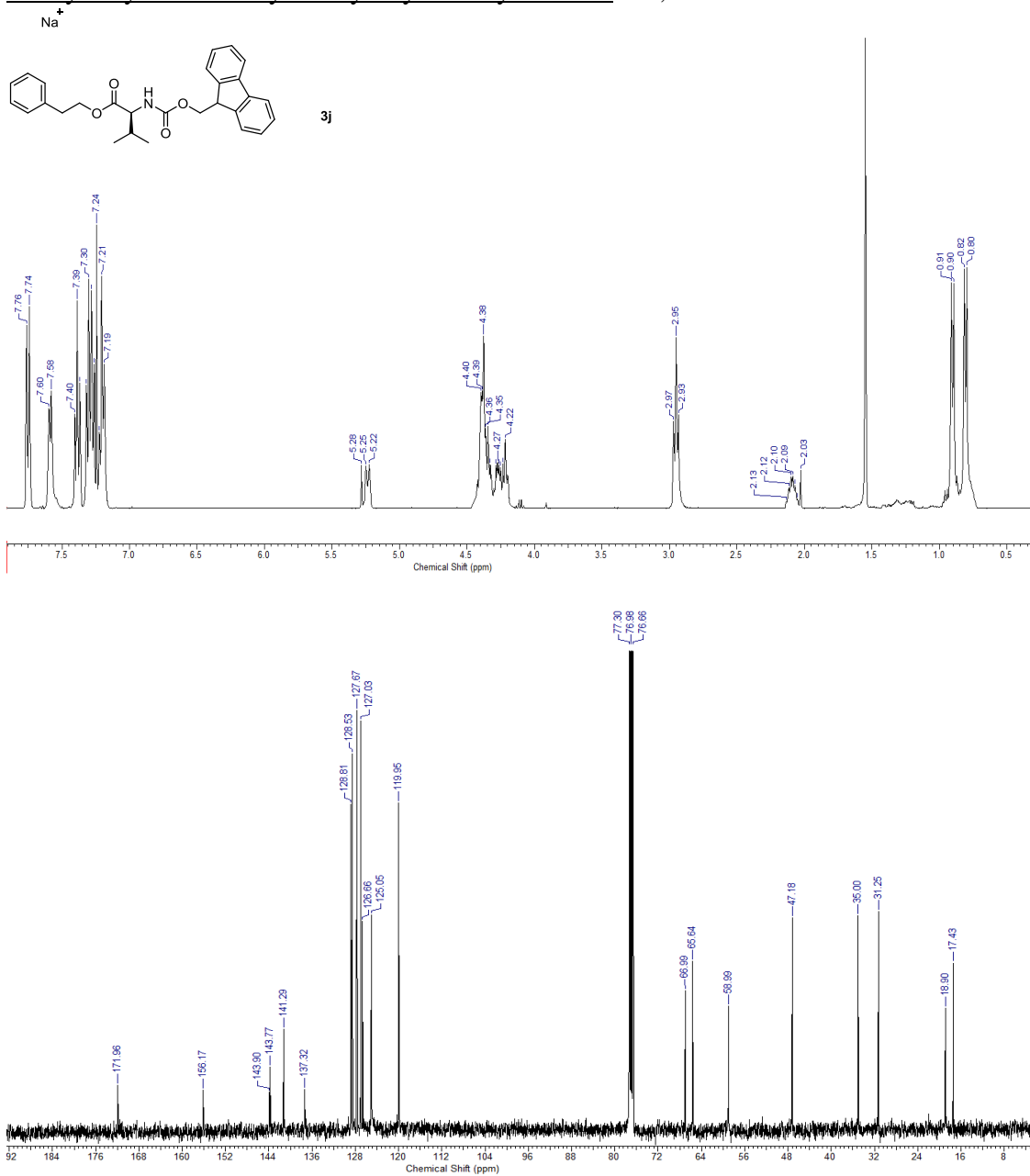
(R)-1-Ethoxy-1-oxopropan-2-yl 4-nitrobenzoate: ^1H , ^{13}C



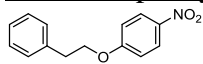
Phenethyl 4-nitrobenzoate: ^1H , ^{13}C



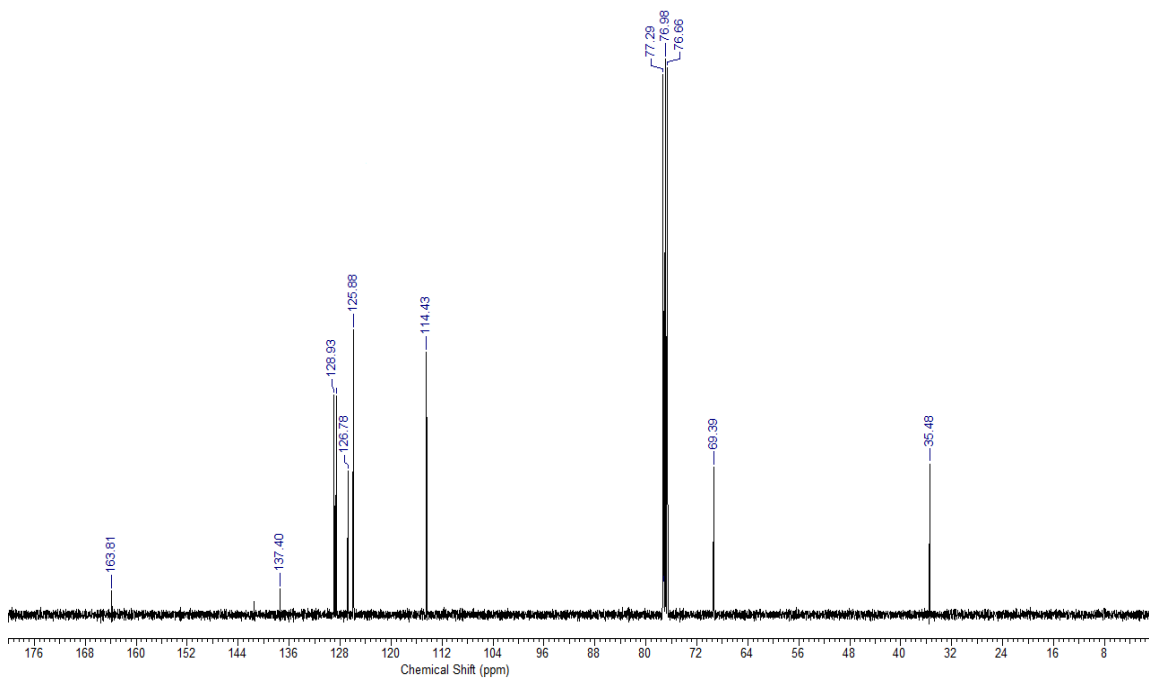
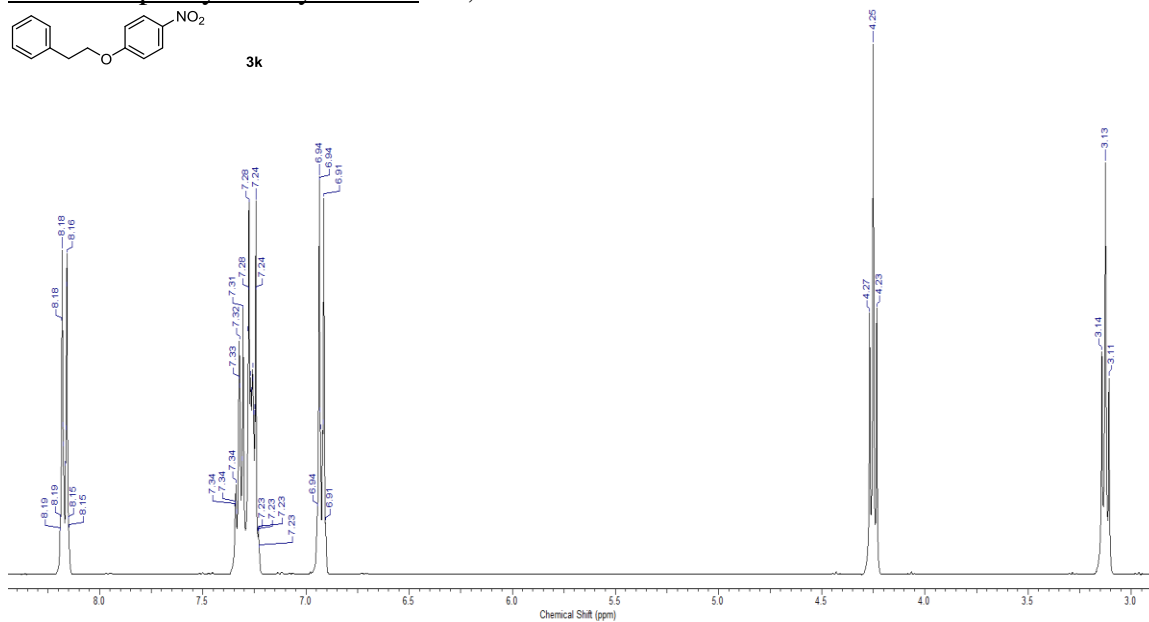
Phenylethyl *N*-fluorenylmethoxycarbonylvalinate: ¹H, ¹³C



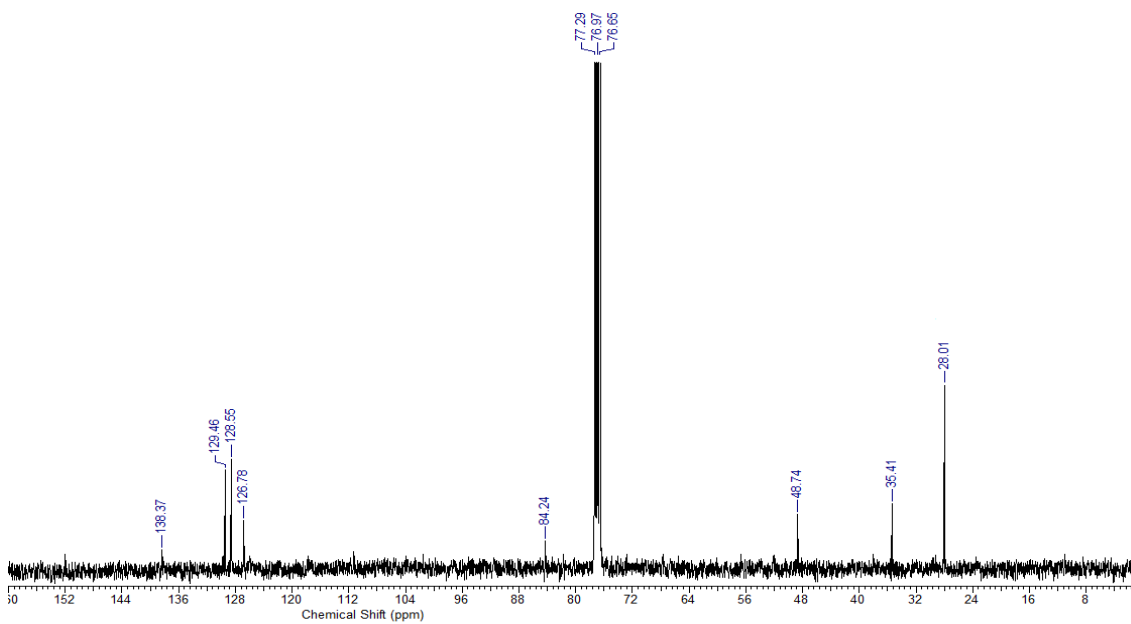
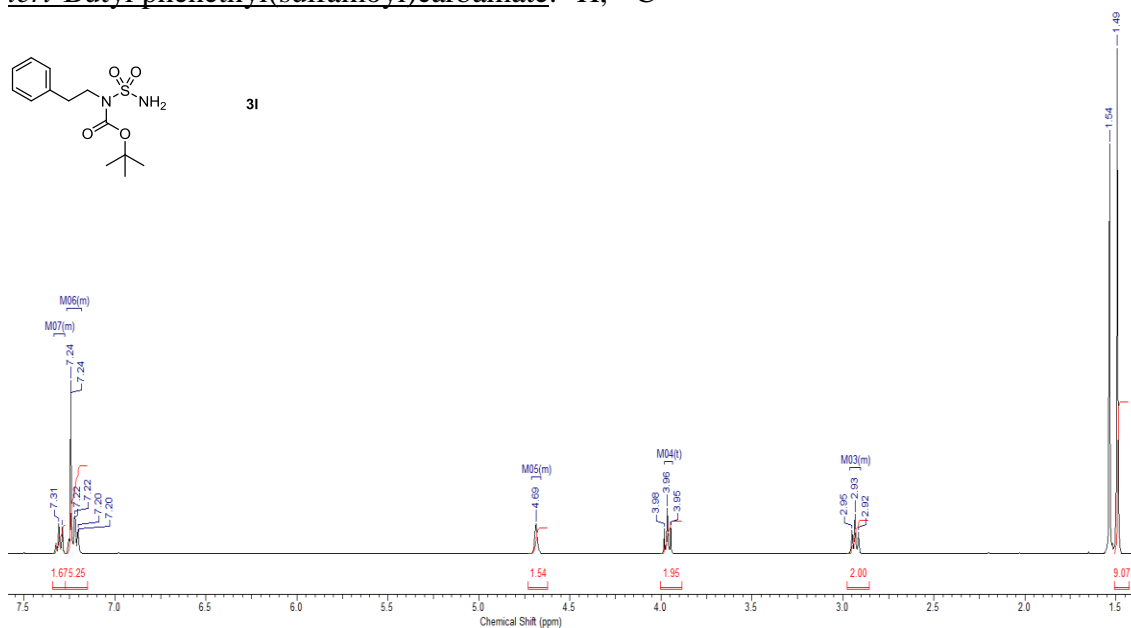
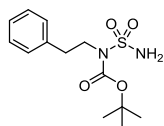
1-Nitro-4-phenylethoxybenzene: ^1H , ^{13}C



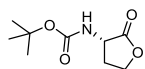
3k



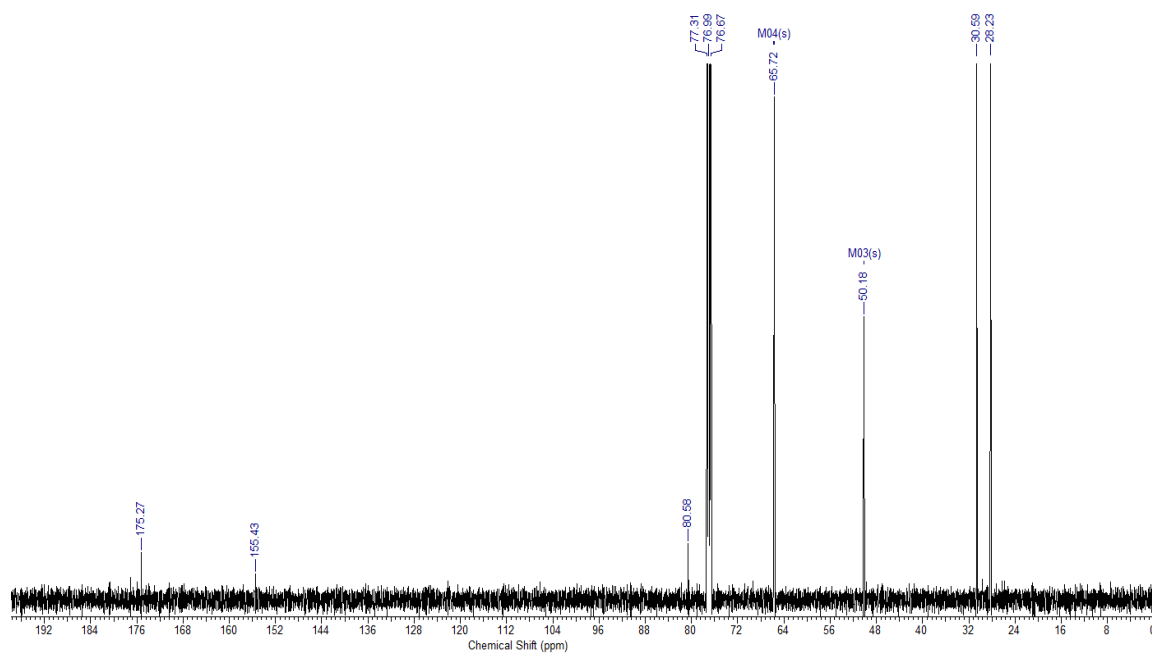
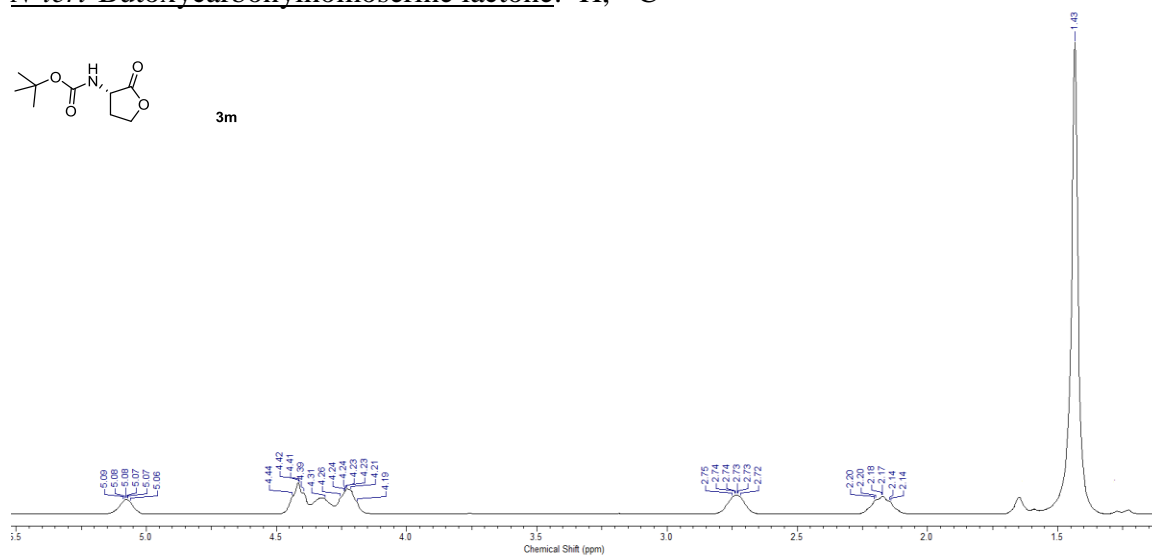
tert-Butyl phenethyl(sulfamoyl)carbamate: ^1H , ^{13}C



N-tert-Butoxycarbonylhomoserine lactone: ¹H, ¹³C

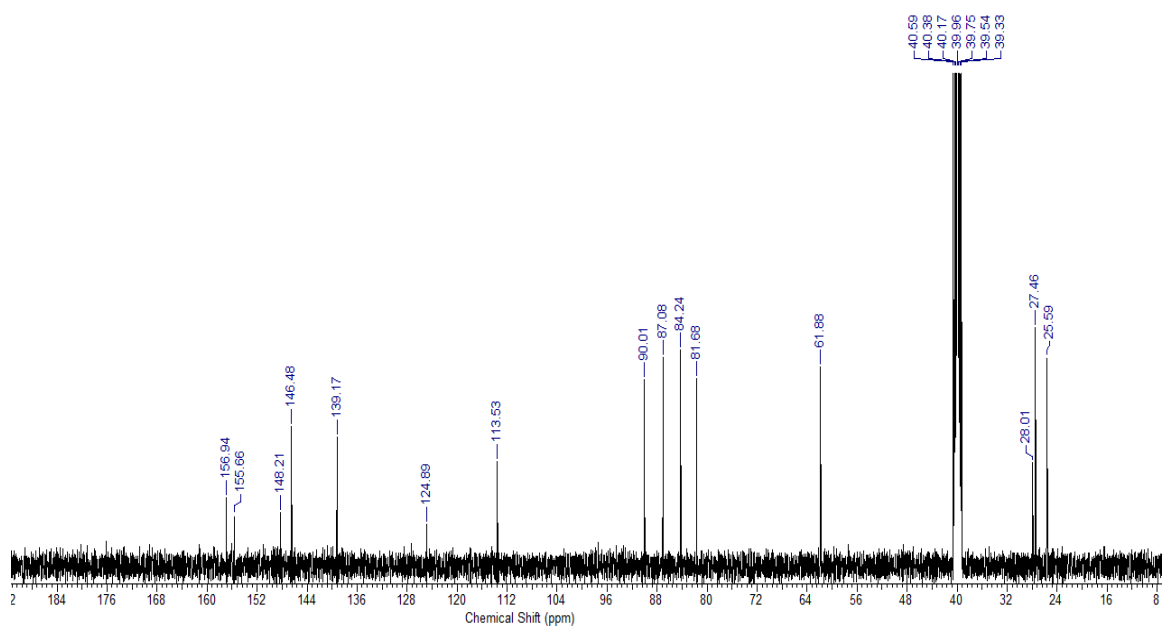
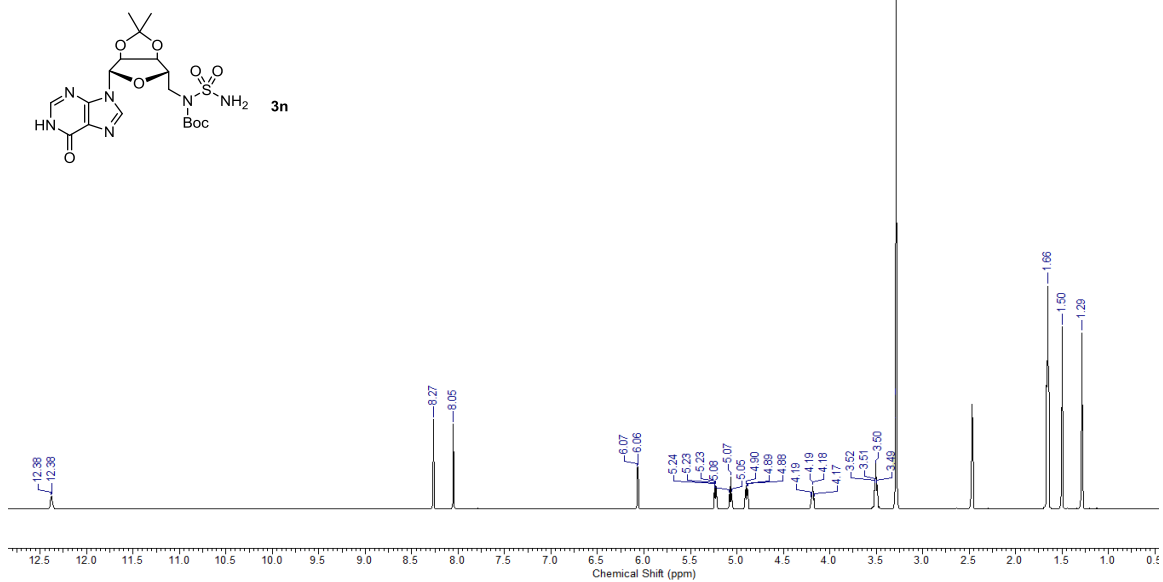


3m

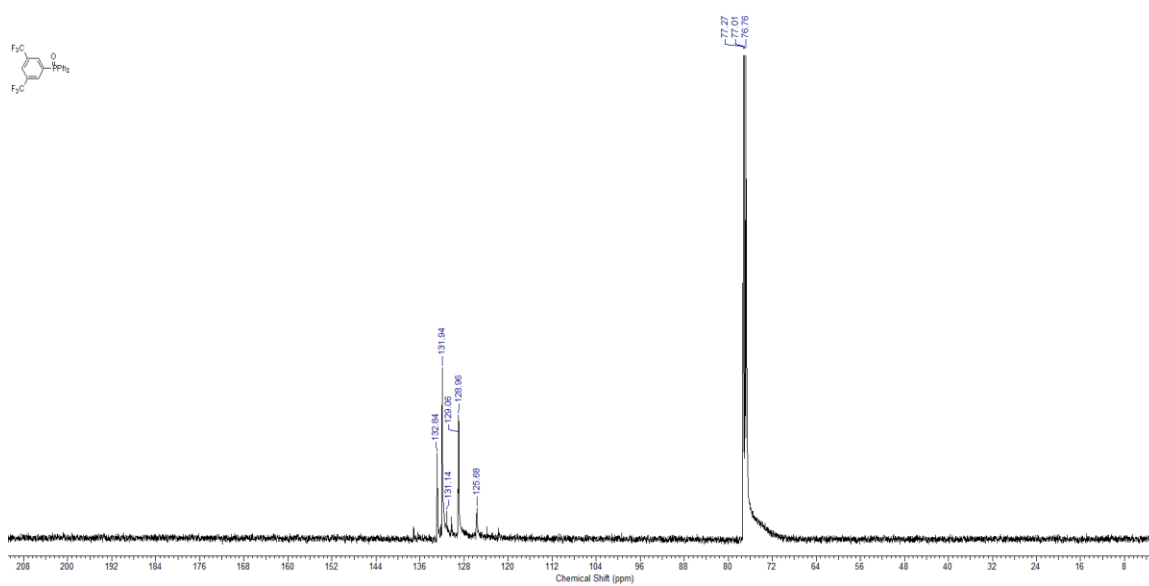
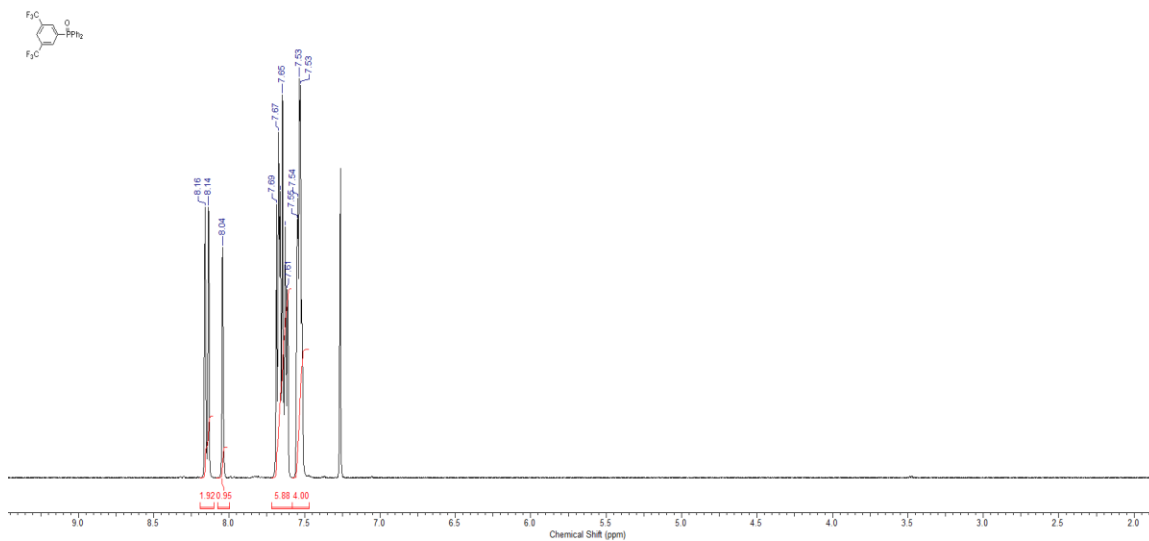


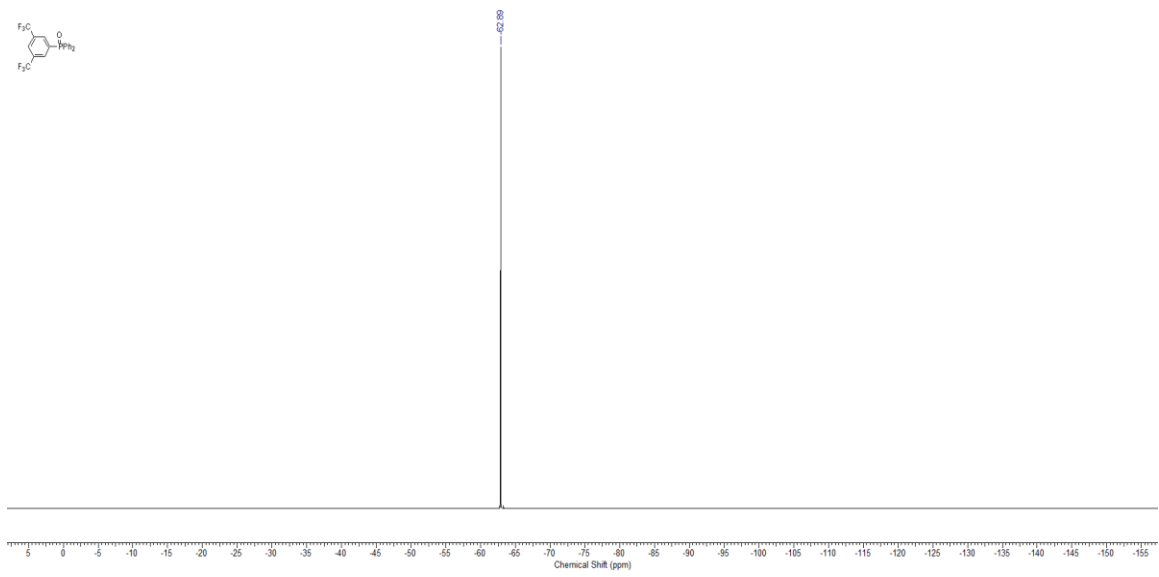
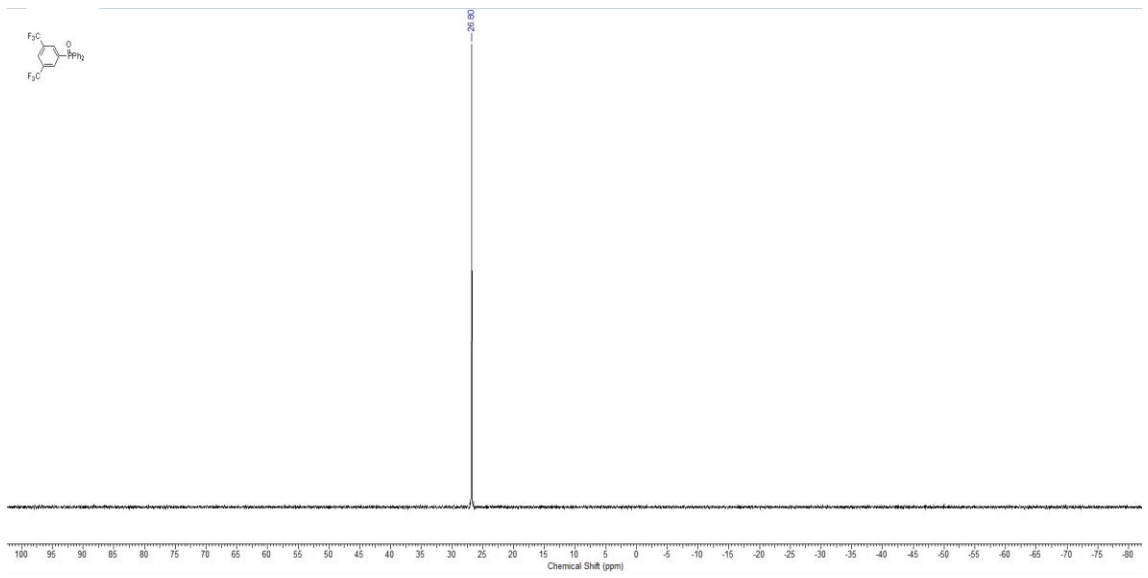
tert-Butyl (2',3'-*O*-isopropylidene-5'-deoxyinosin-5'-yl)(sulfamoyl)carbamate: ^1H , ^{13}C

702_01

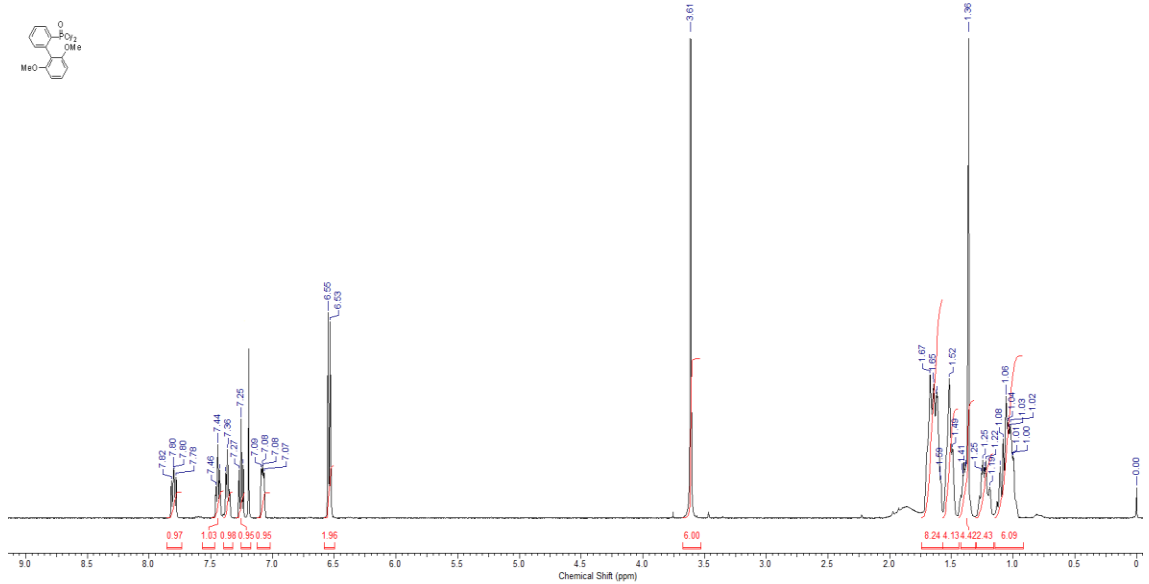


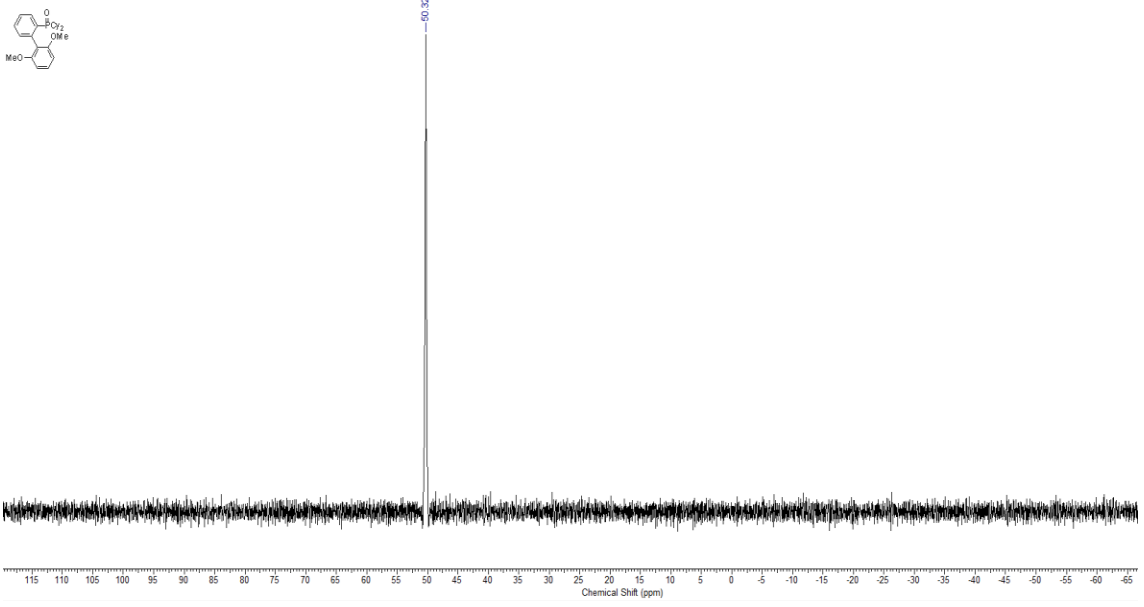
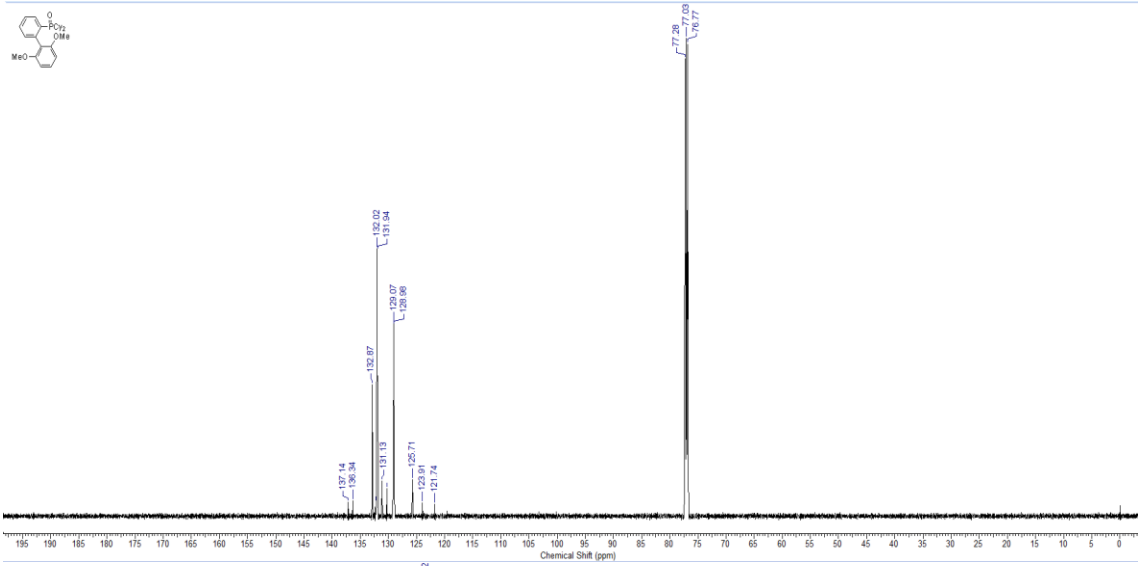
(3,5-bis(trifluoromethyl)phenyl)diphenylphosphine oxide: ^1H , ^{13}C , ^{31}P , ^{19}F NMR



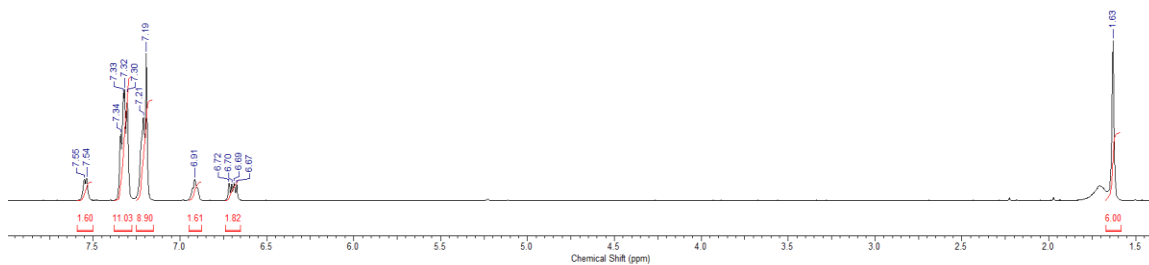


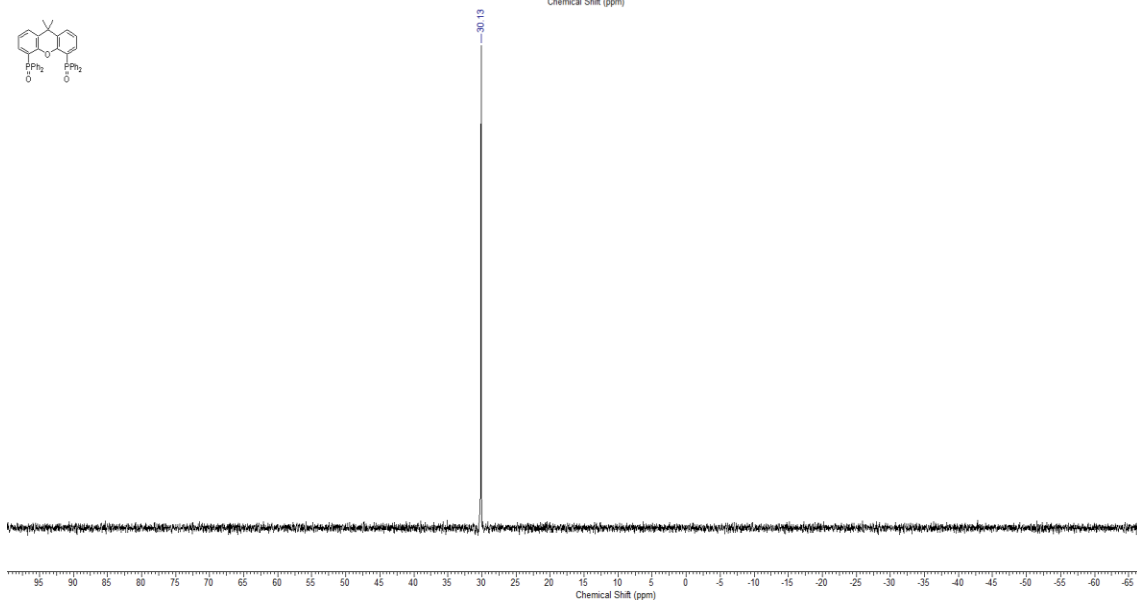
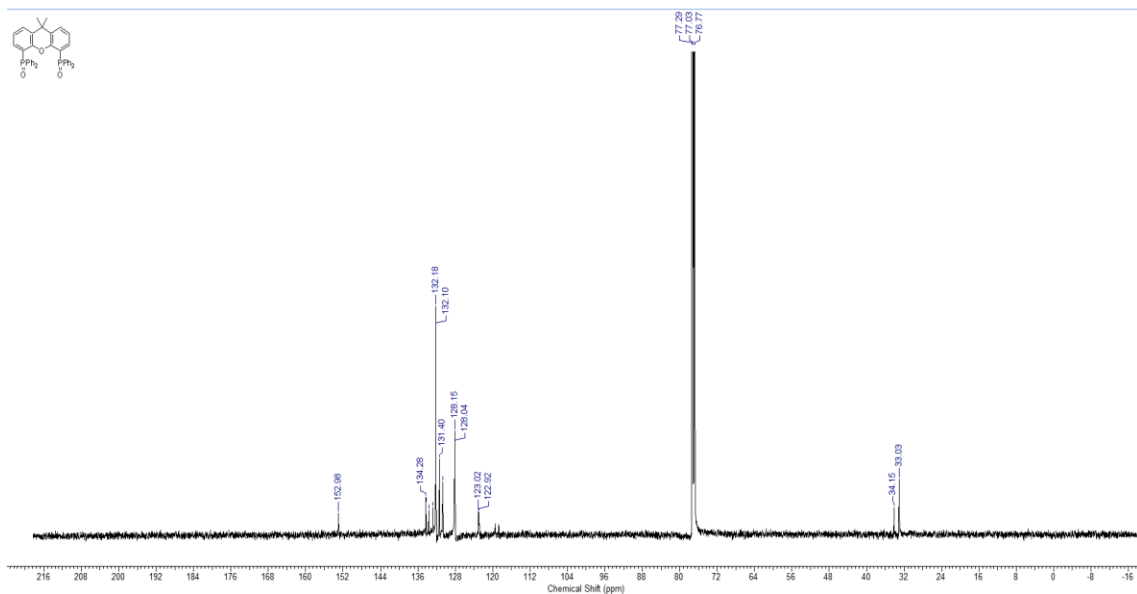
(2',6'-dimethoxy-[1,1'-biphenyl]-2-yl)dicyclohexylphosphine oxide: ^1H , ^{13}C , and ^{31}P NMR



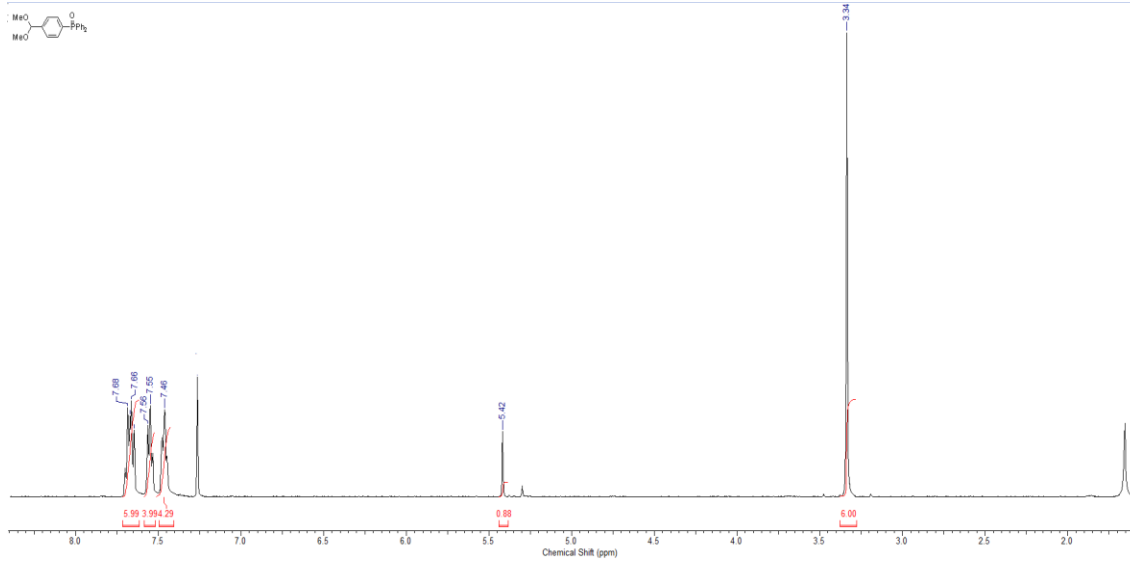


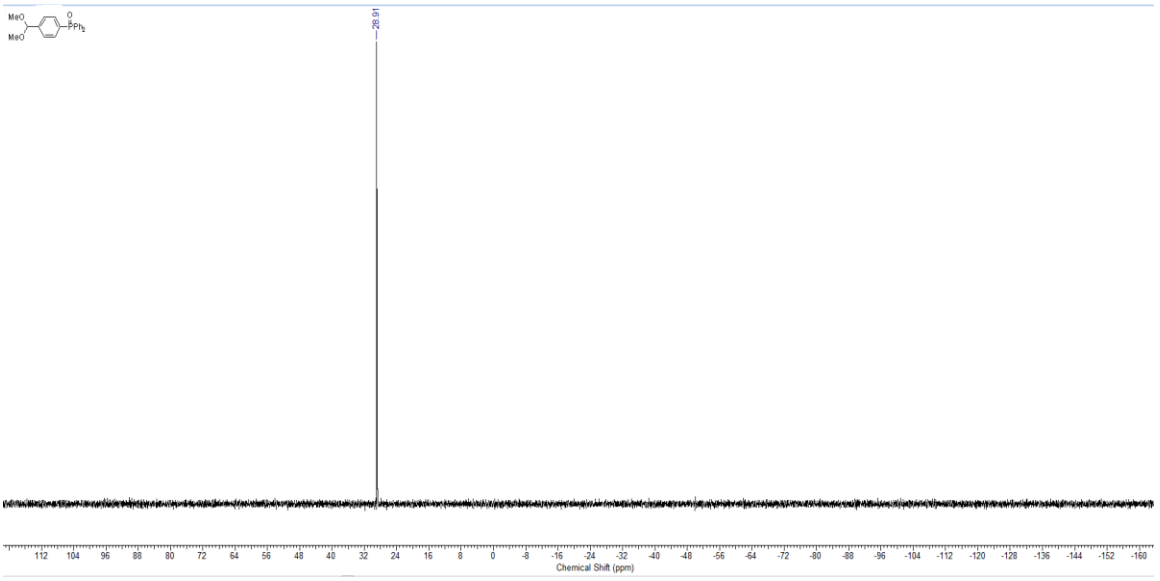
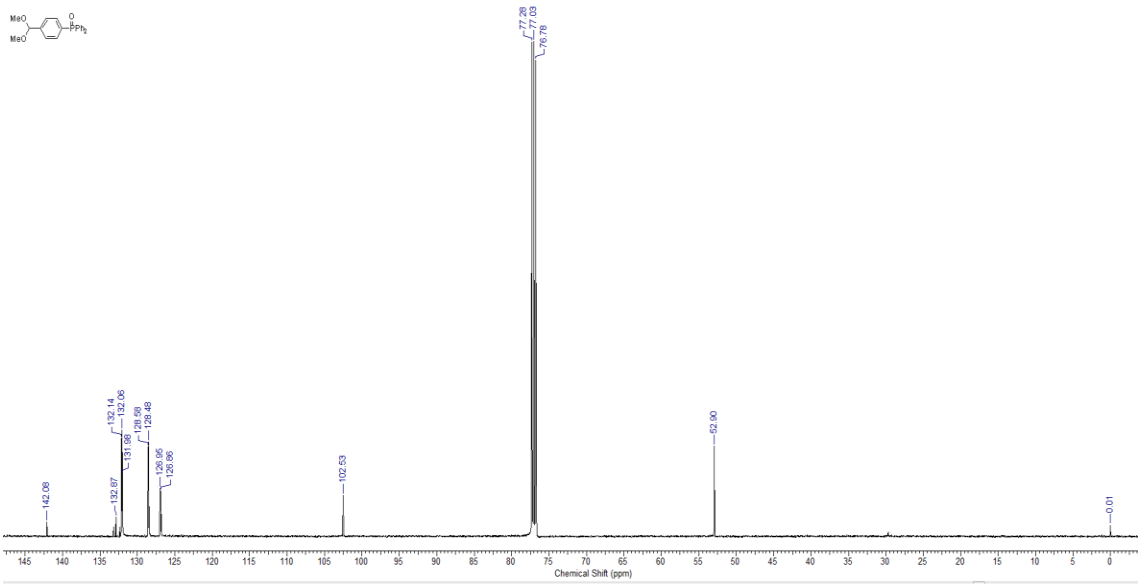
(9,9-Dimethyl-9H-xanthene-4,5-diyl)-bis-diphenylphosphine oxide: ^1H , ^{13}C , and ^{31}P NMR



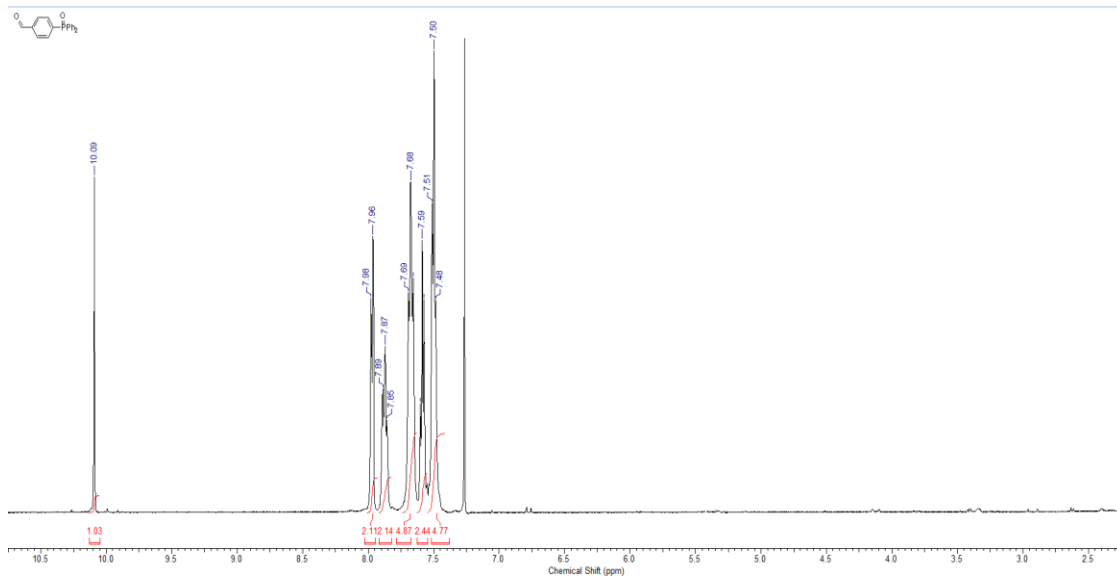


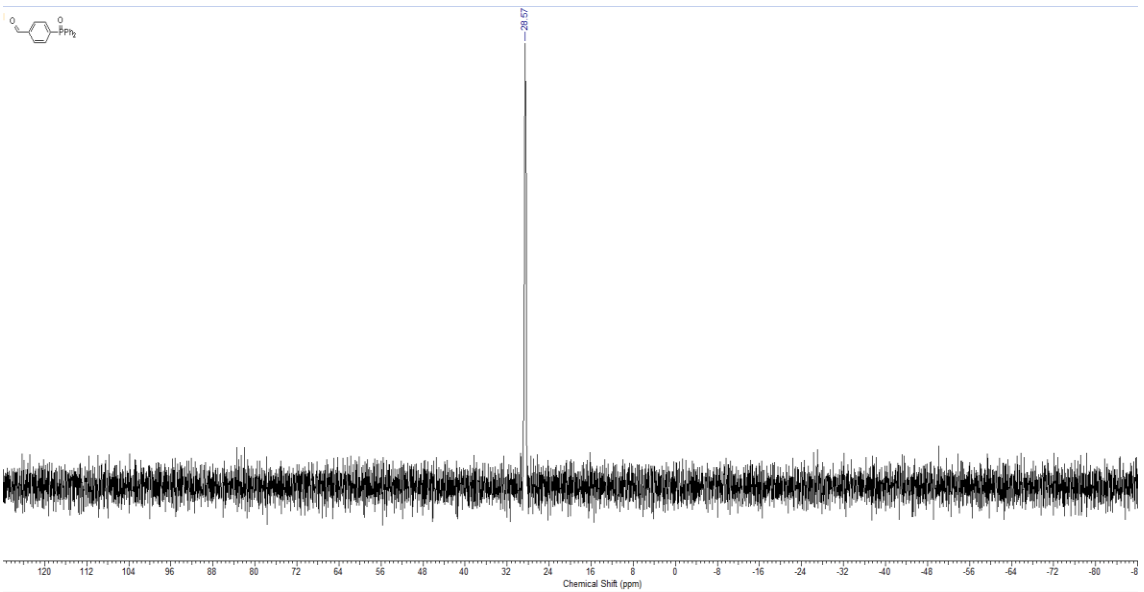
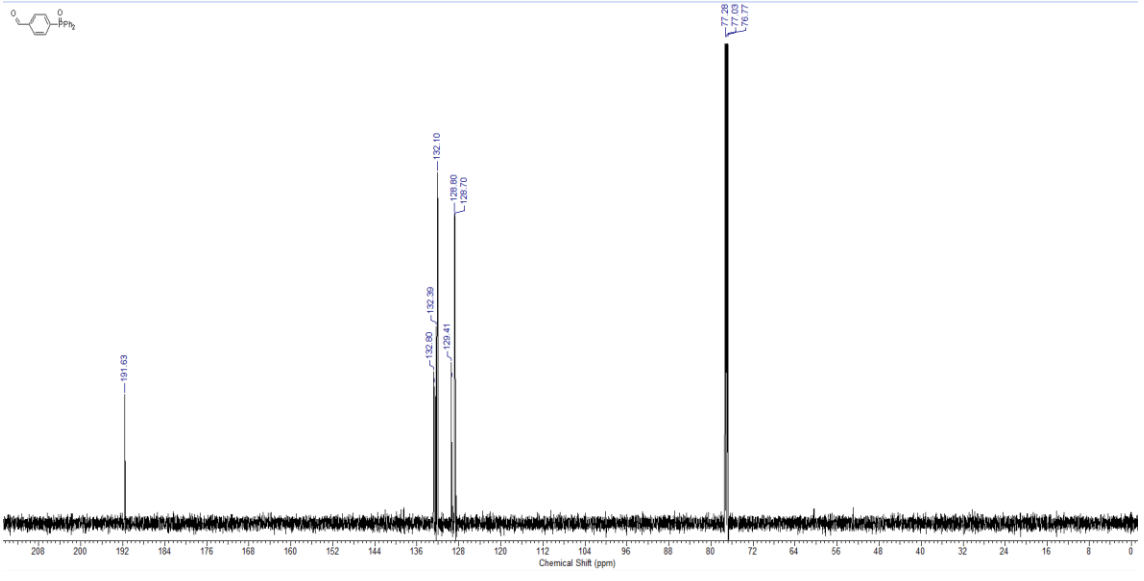
[4-(Dimethoxymethyl)phenyl]diphenylphosphine oxide: ^1H , ^{13}C , and ^{31}P NMR



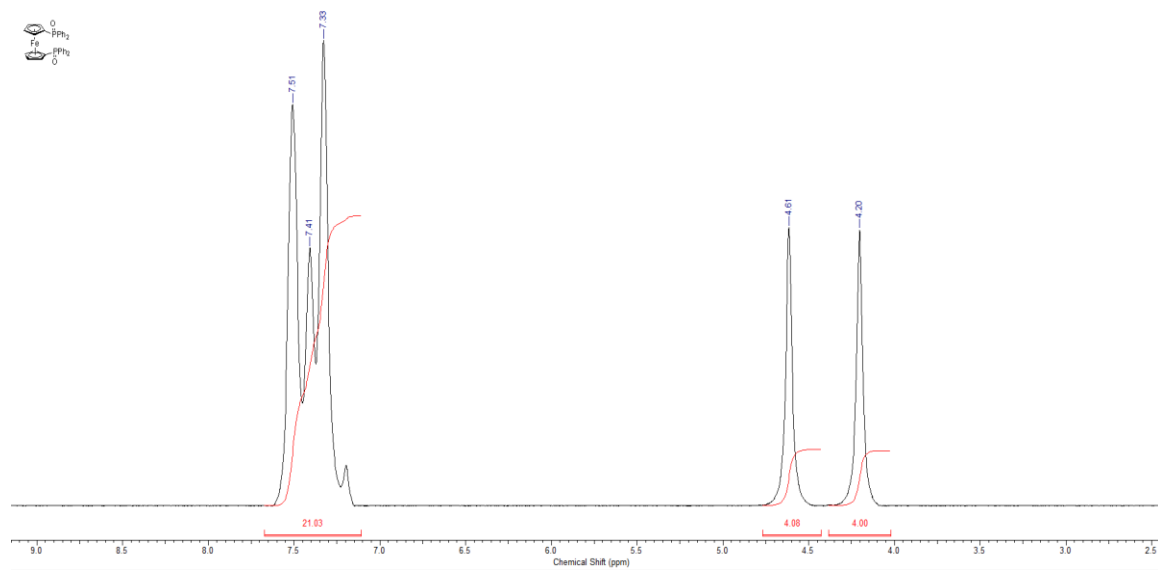


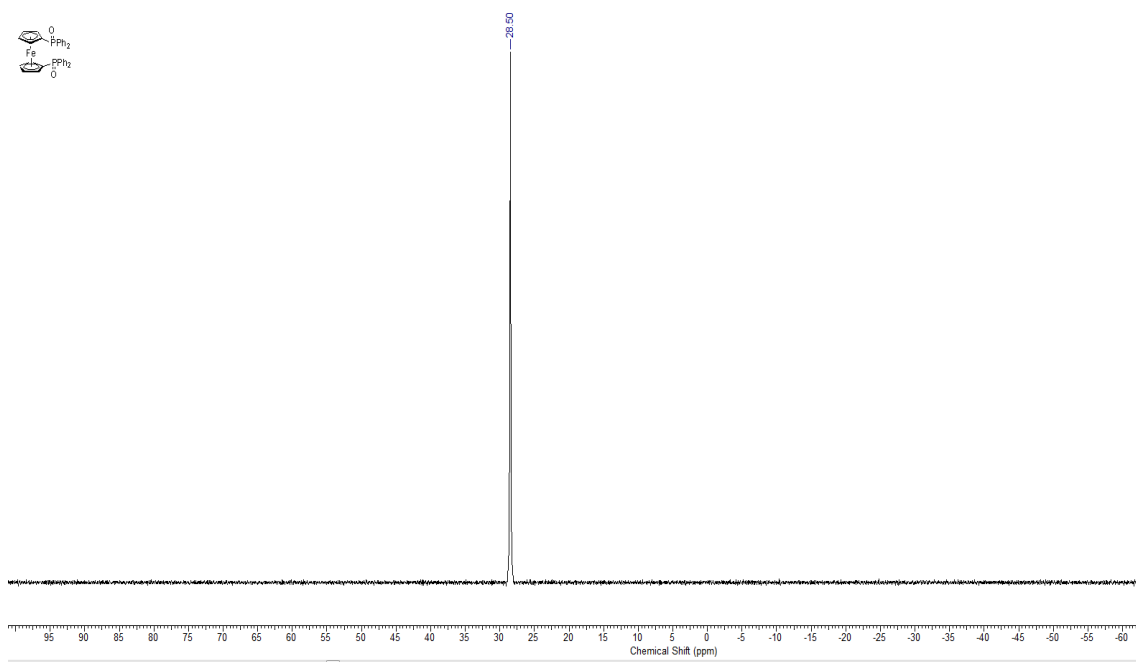
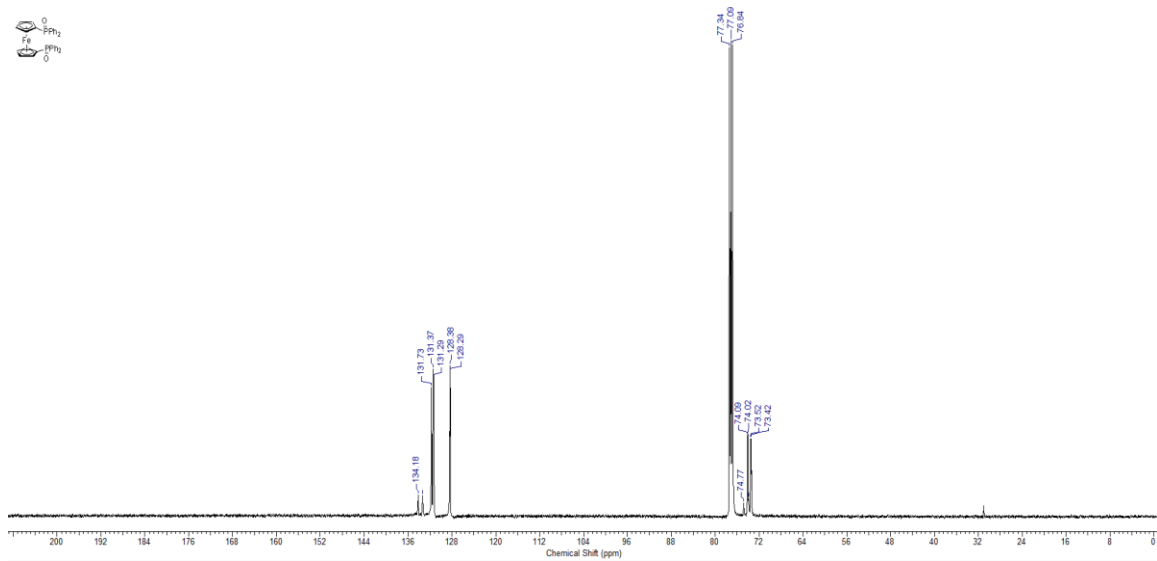
4-(Diphenylphosphine oxide)benzaldehyde: ^1H , ^{13}C , and ^{31}P NMR



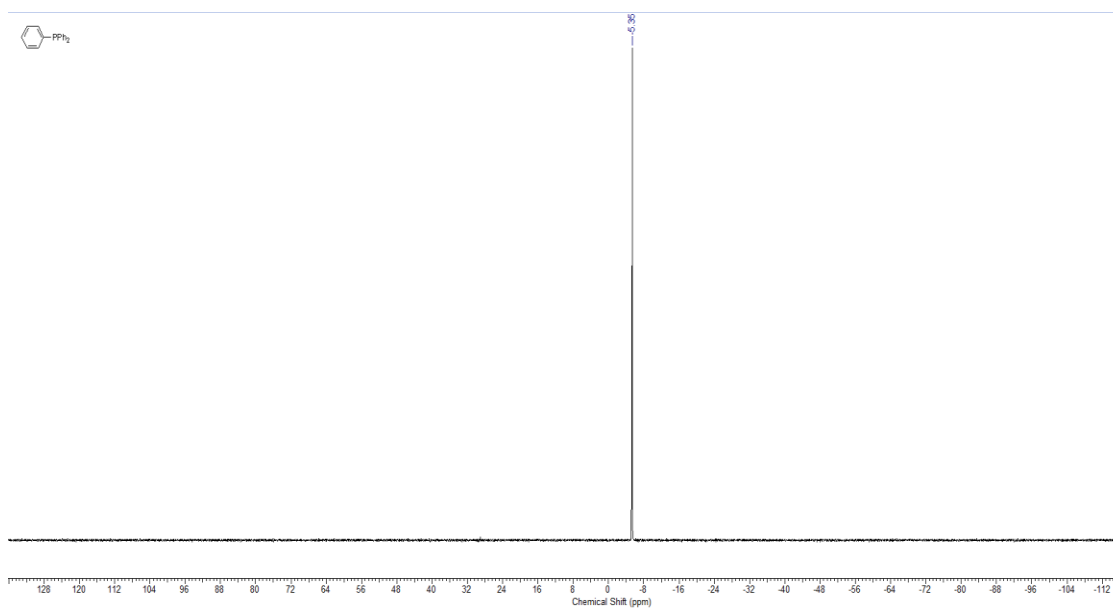
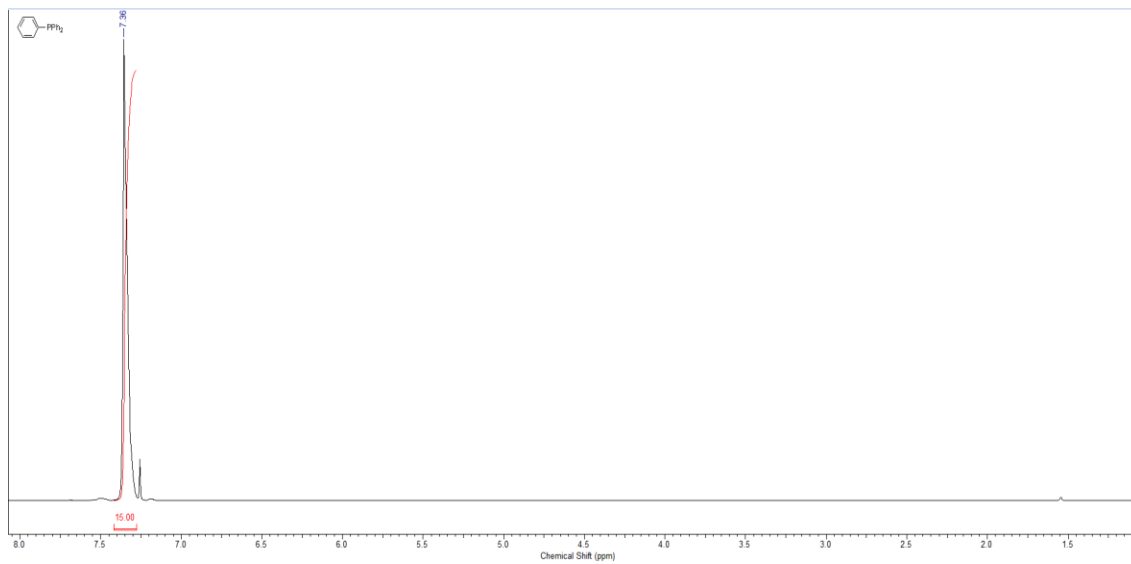


1,1'-Bis(diphenylphino oxide)ferrocene: ^1H , ^{13}C , and ^{31}P NMR

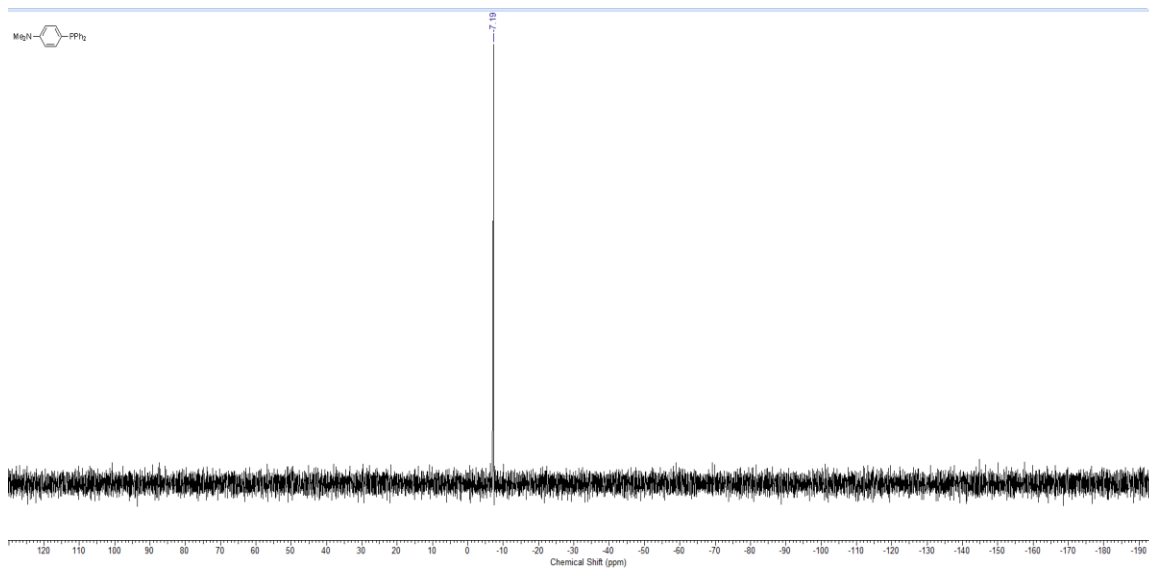
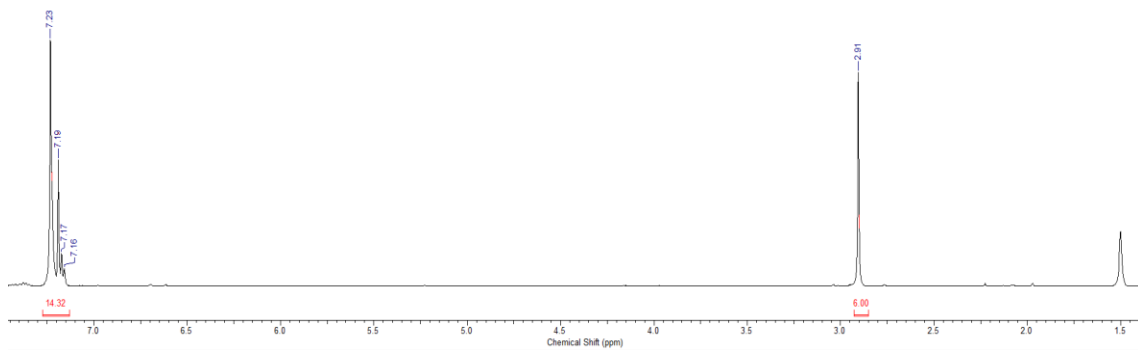




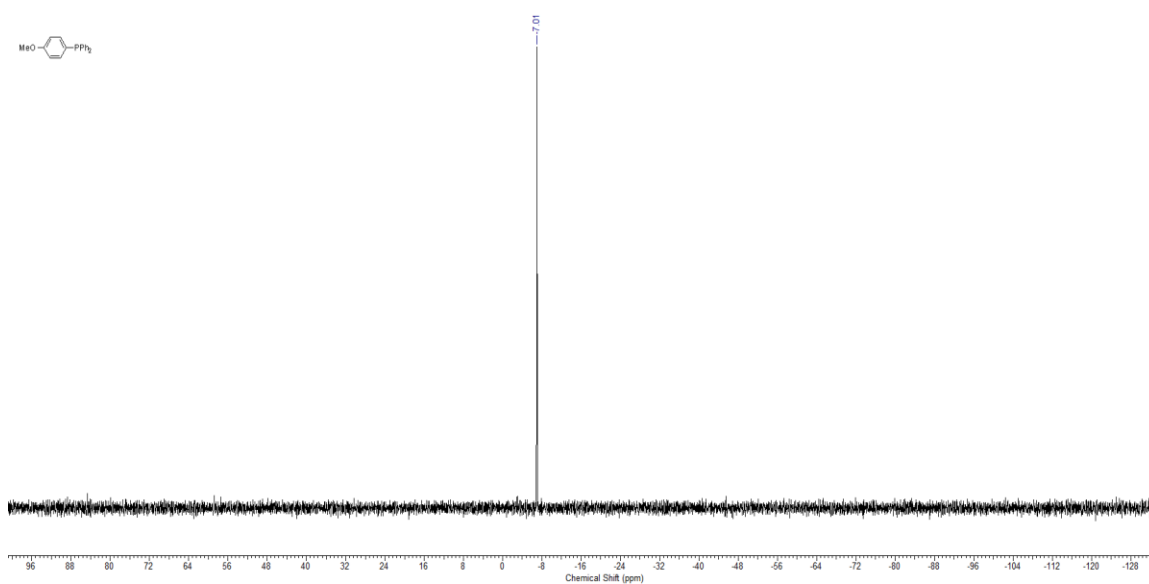
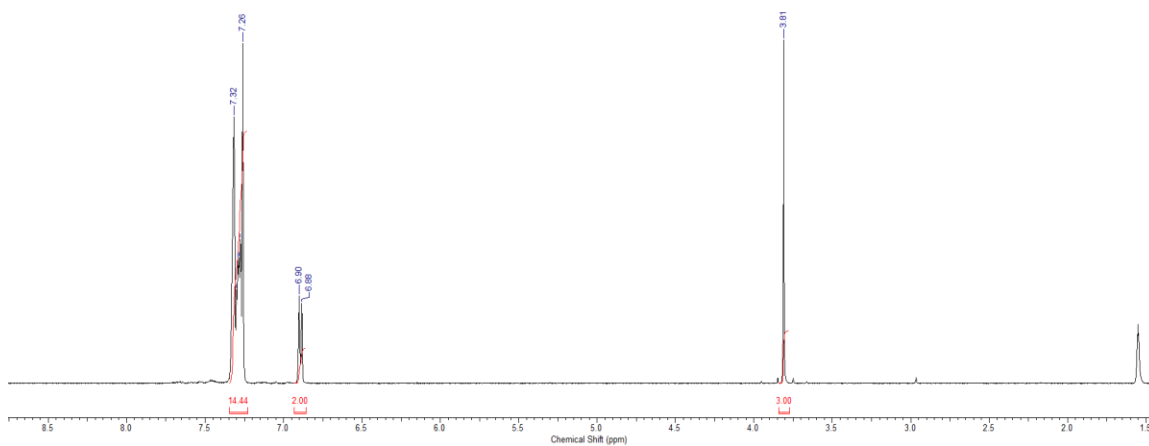
Triphenylphosphine: ^1H and ^{31}P NMR



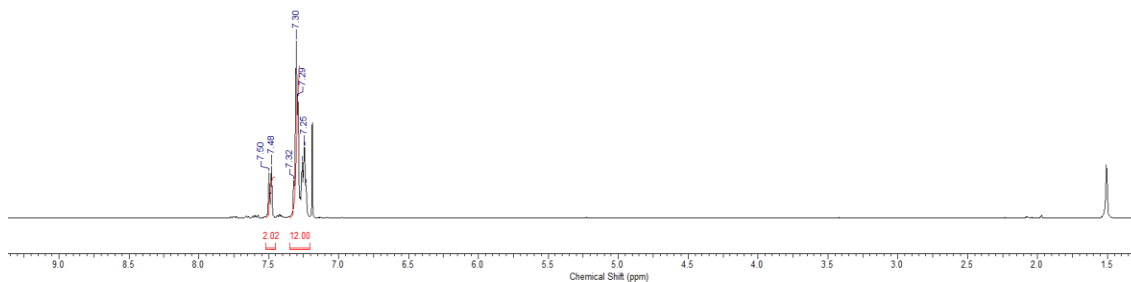
(4-(Dimethylamino)phenyl)diphenylphosphine: ^1H and ^{31}P NMR

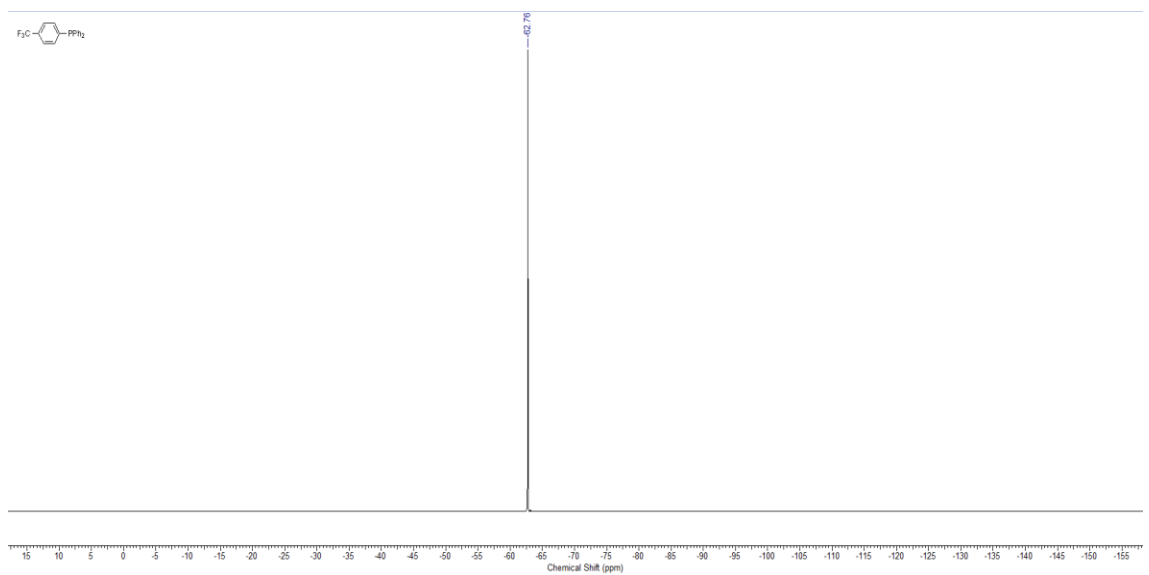
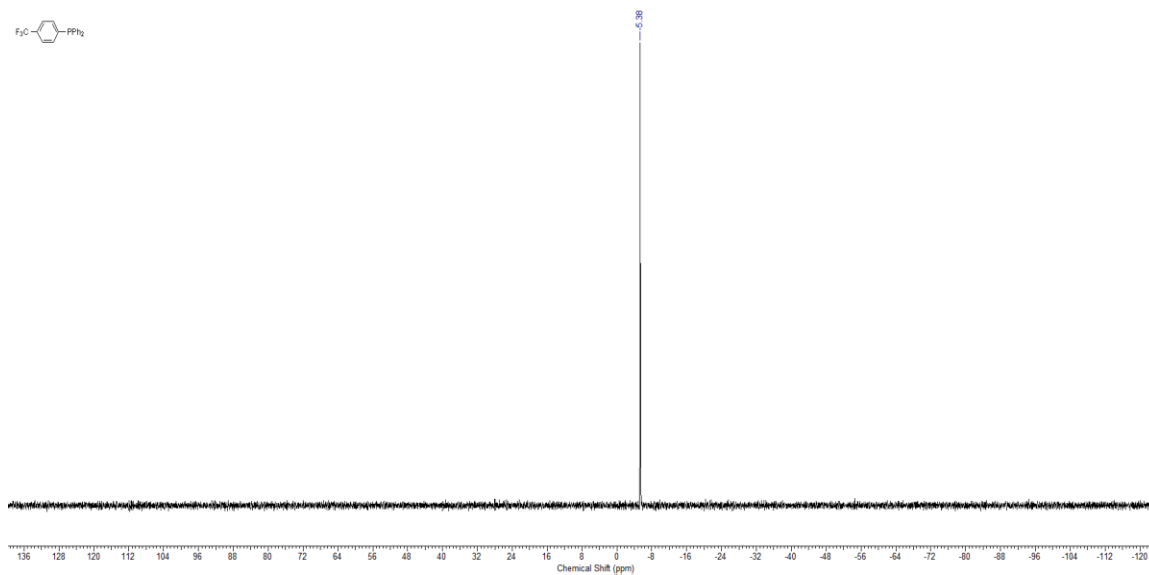


(4-(Methoxy)phenyl)diphenylphosphine: ^1H and ^{31}P NMR

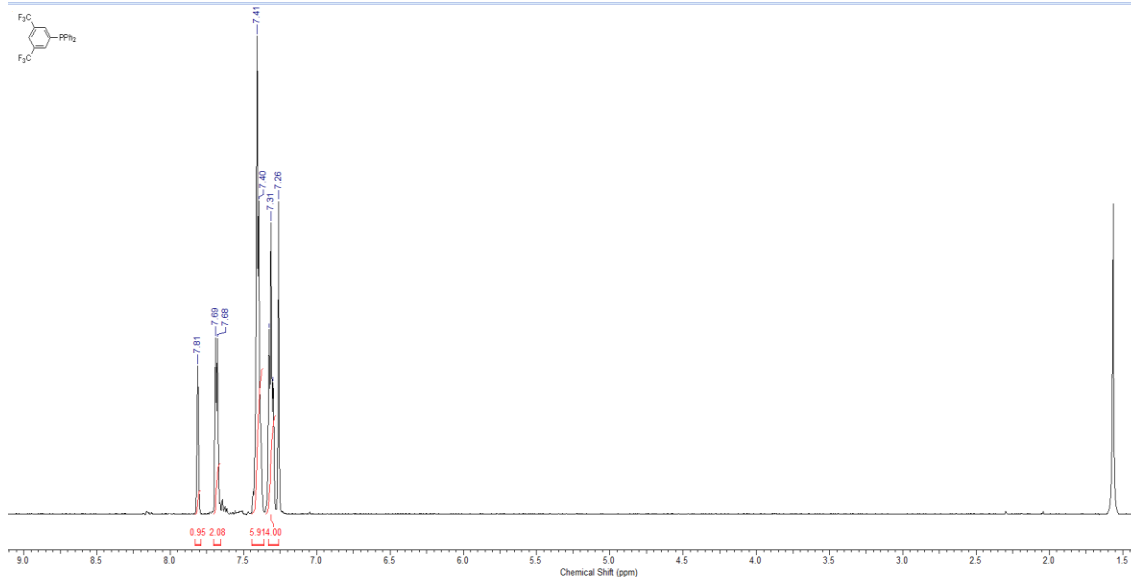


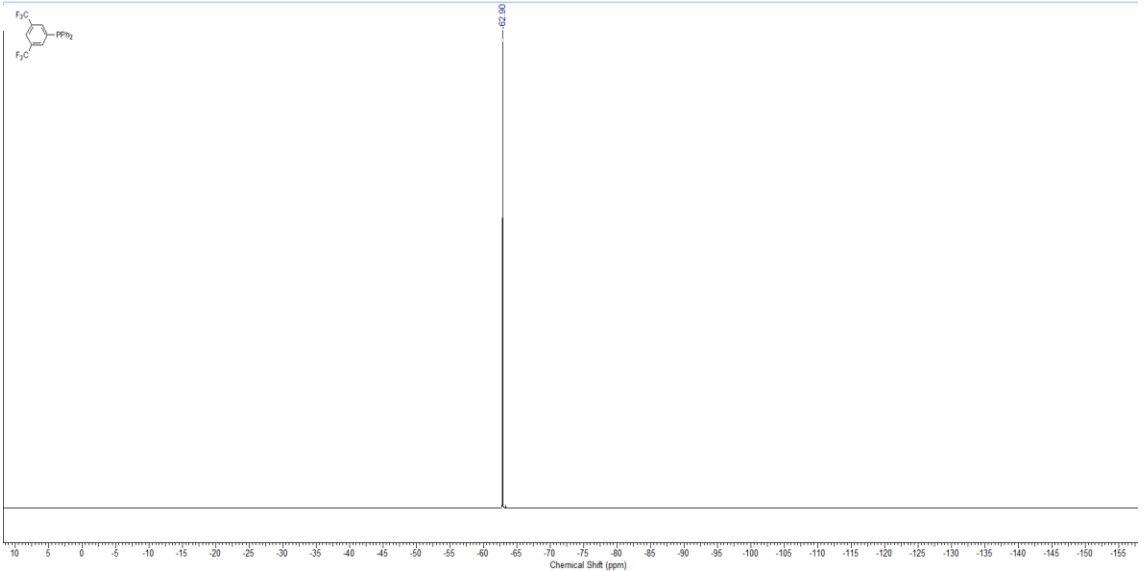
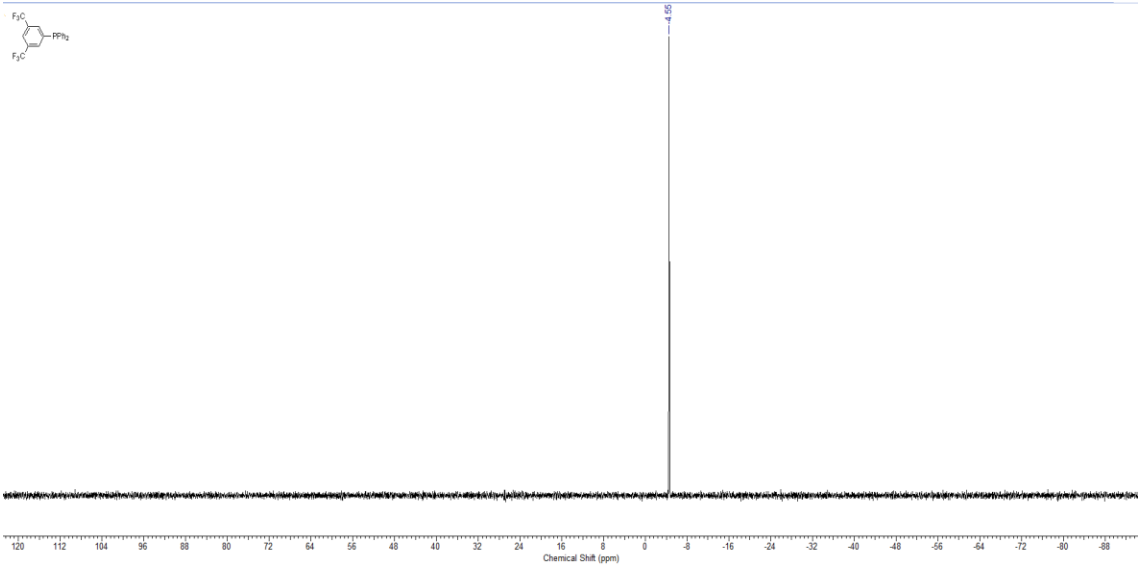
(4-(Trifluoromethyl)phenyl)diphenylphosphine: ^1H , ^{31}P , and ^{19}F NMR



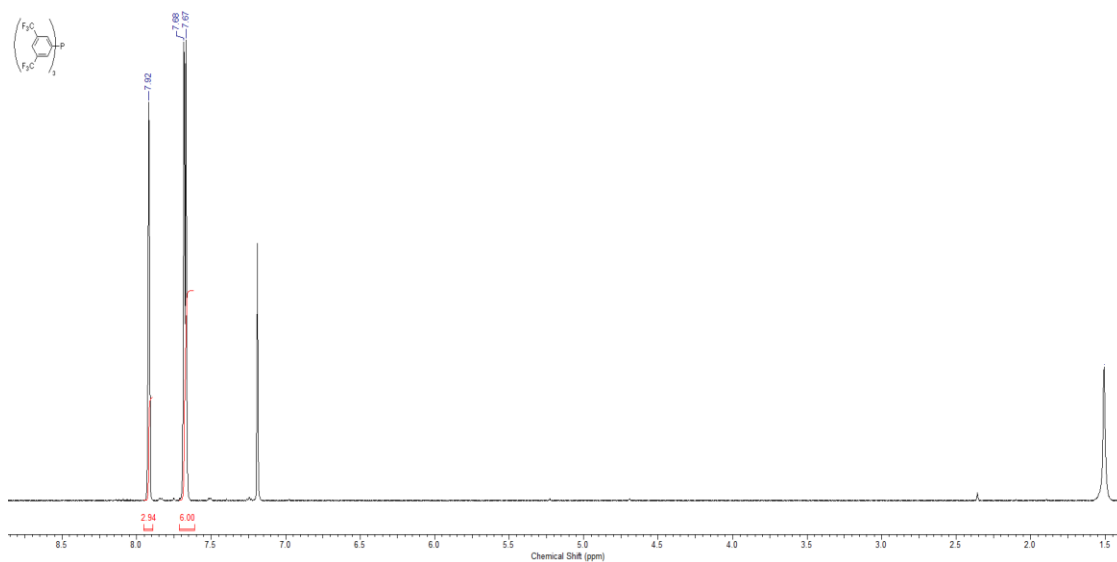


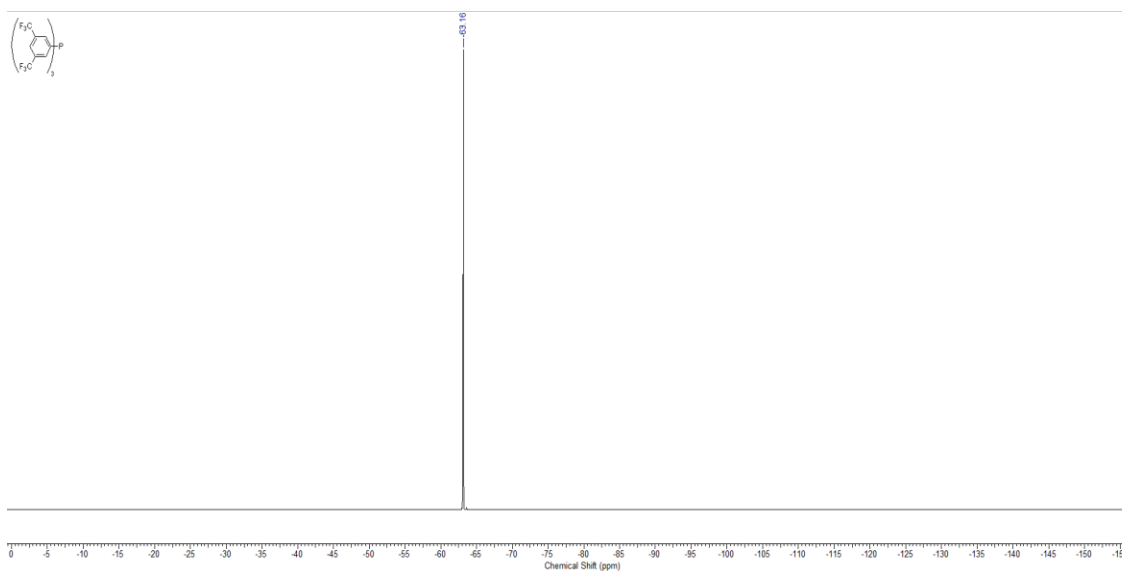
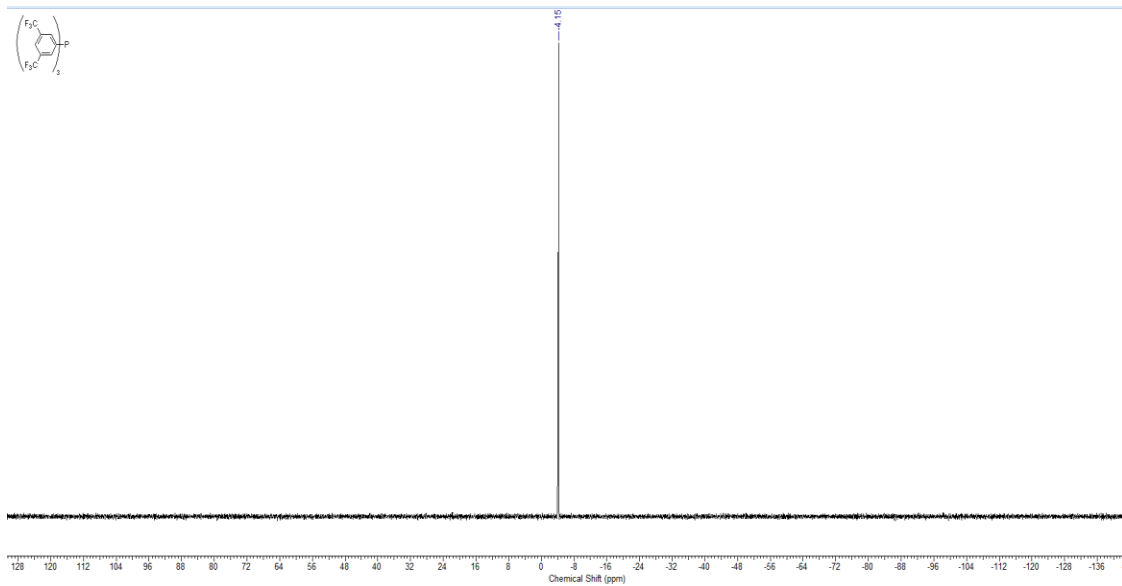
(3,5-Bis(trifluoromethyl)phenyl)diphenylphosphine: ^1H , ^{31}P , and ^{19}F NMR



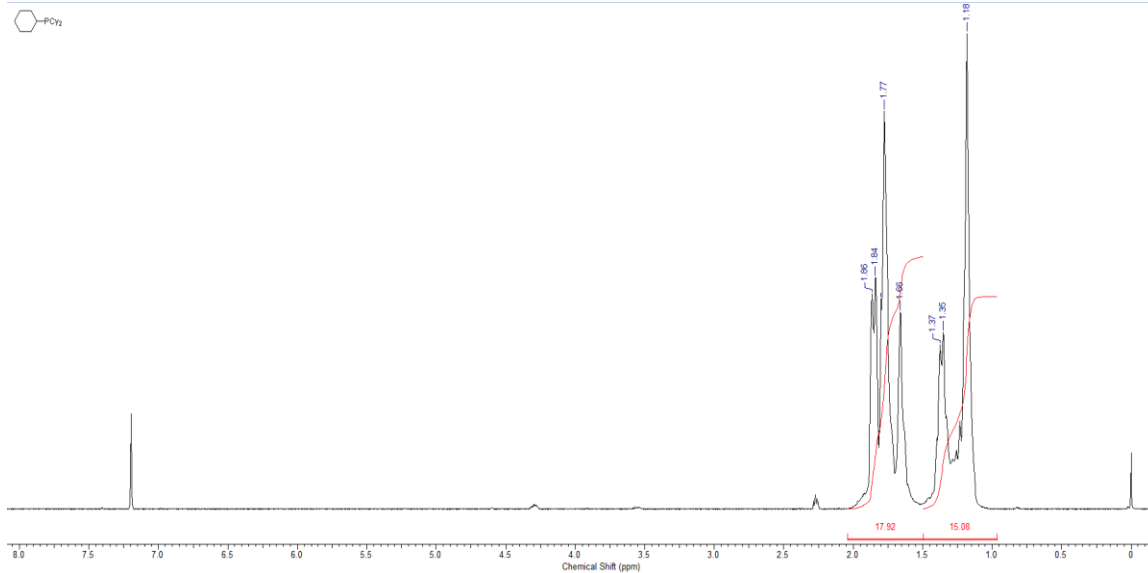


Tris-(3,5-(trifluoromethyl)phenyl)phosphine: ^1H , ^{31}P , and ^{19}F NMR

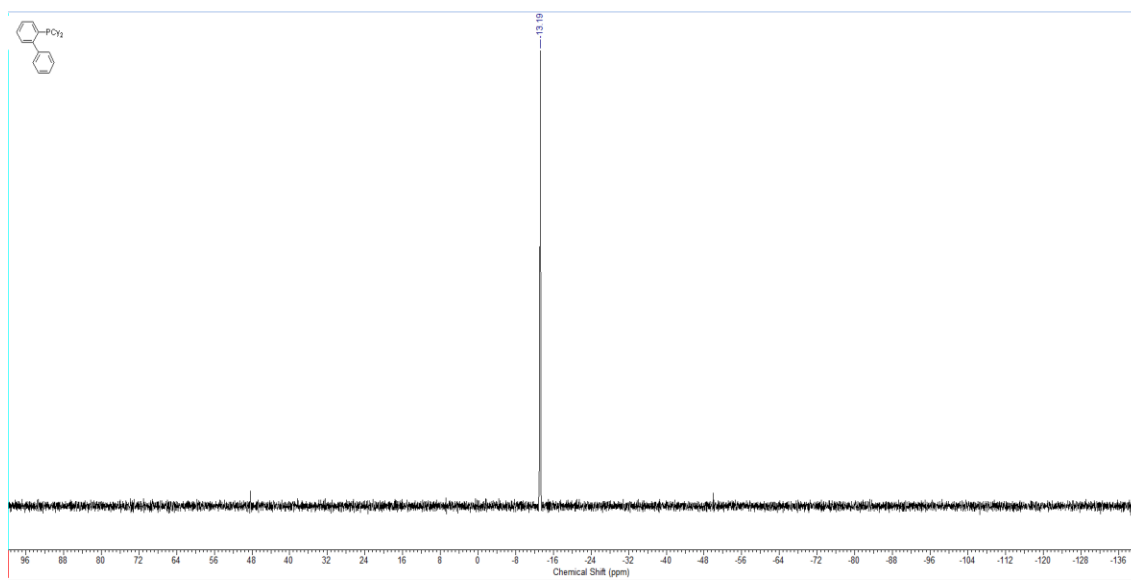
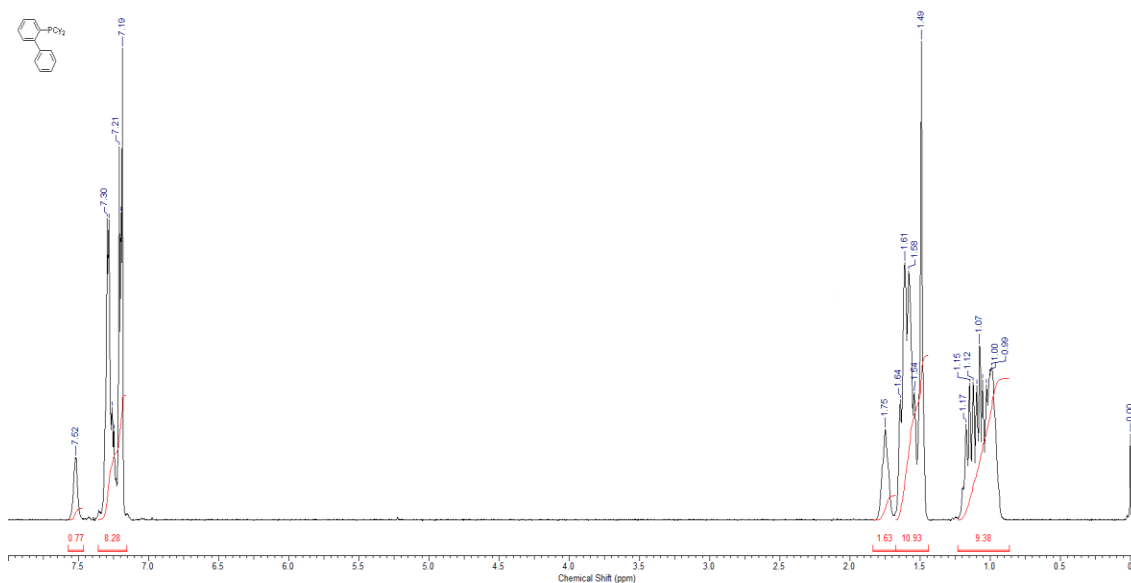




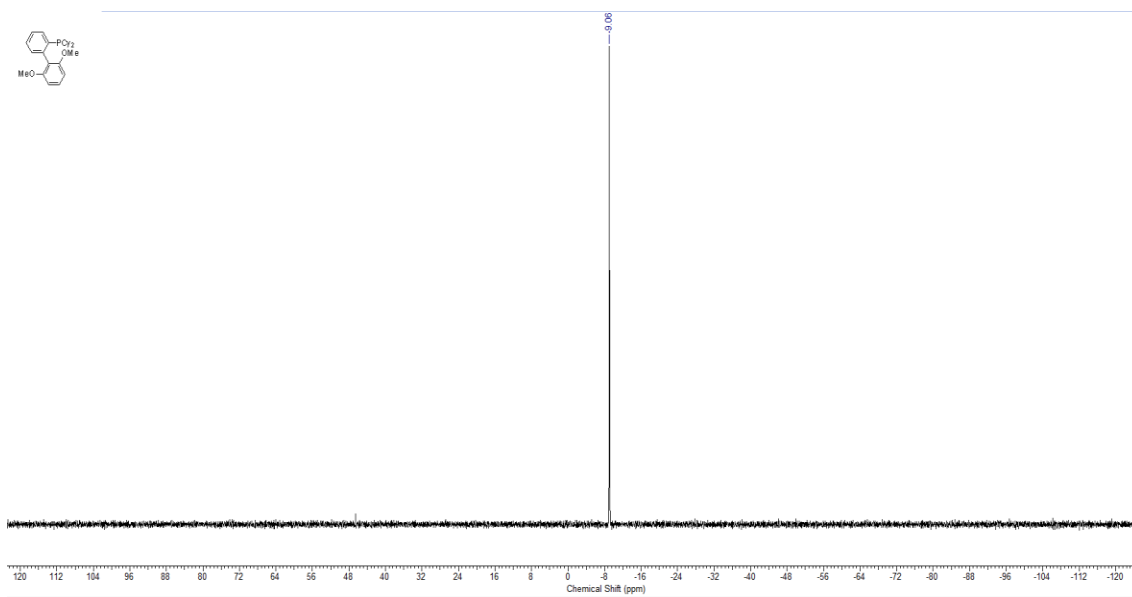
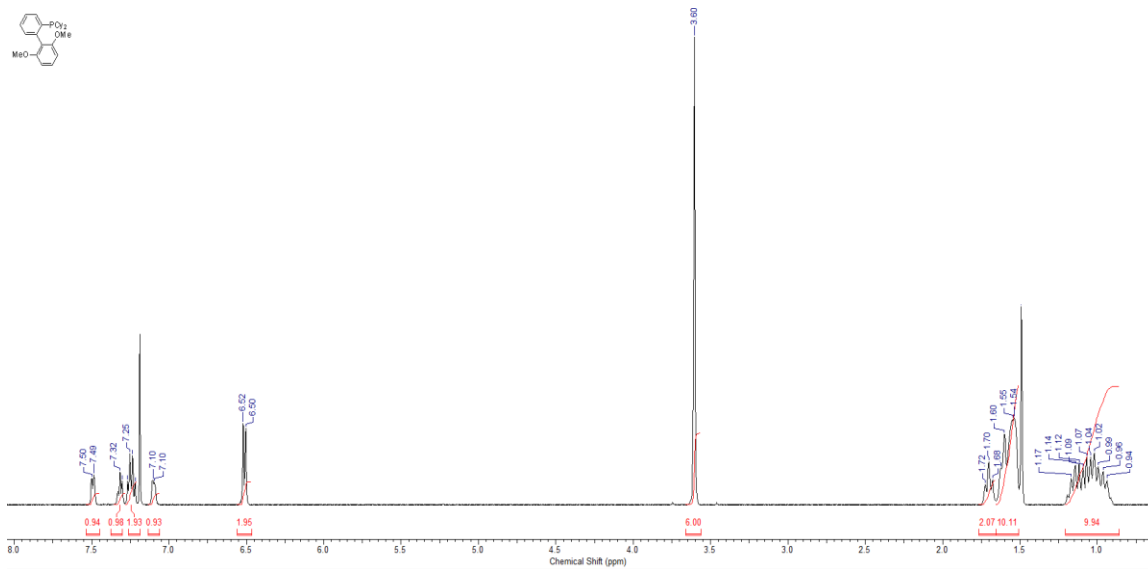
Tricyclohexylphosphine: ^1H NMR



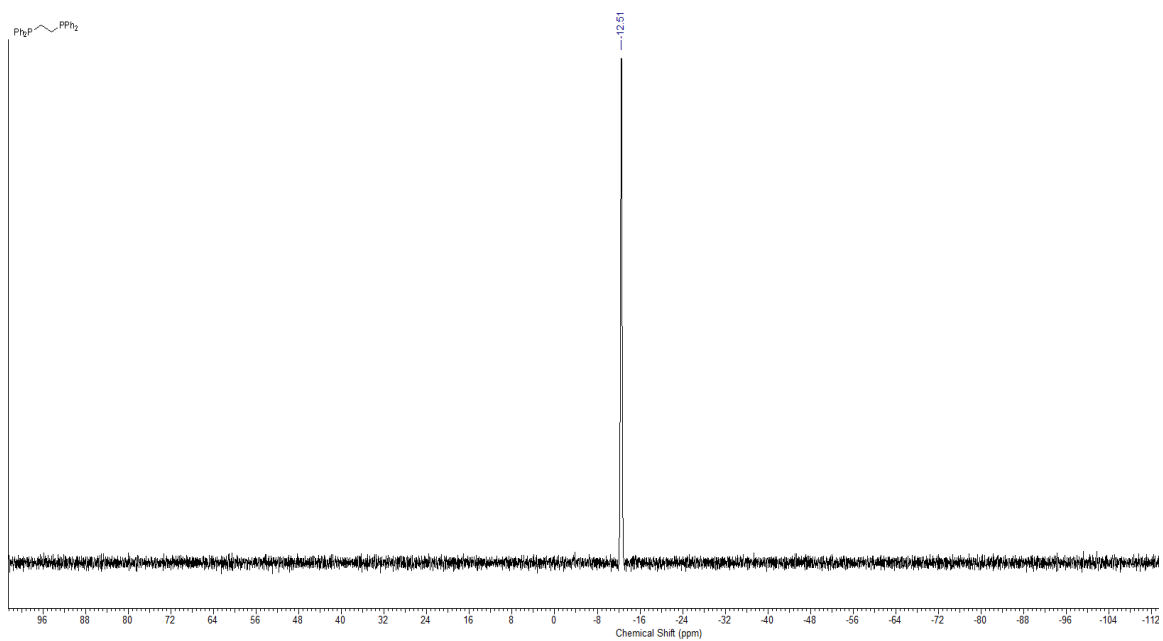
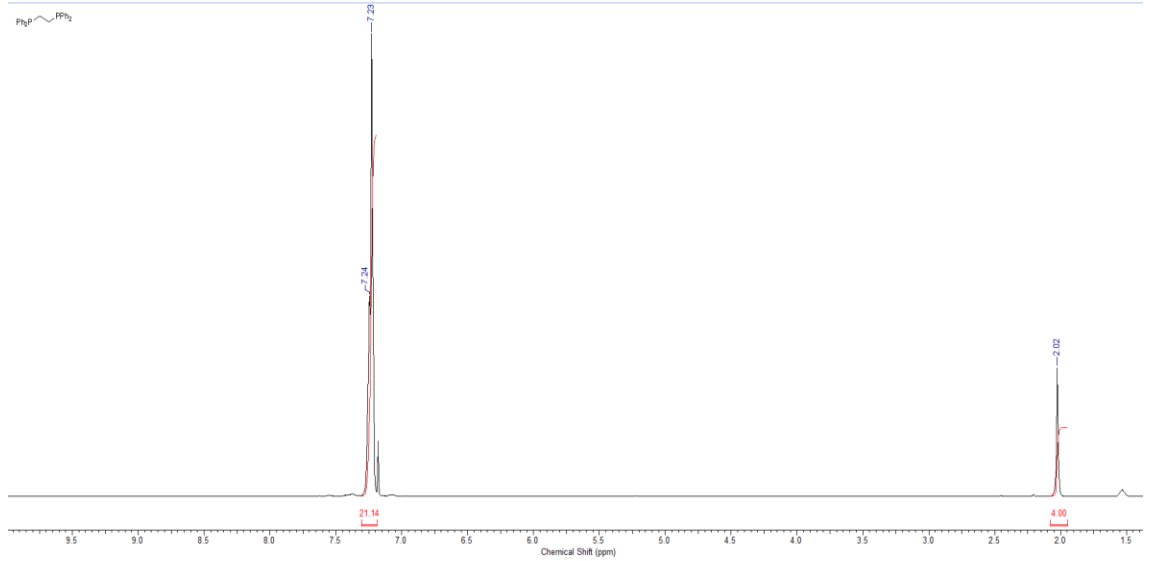
([1,1'-biphenyl]-2-yl)dicyclohexylphosphine: ^1H and ^{31}P NMR



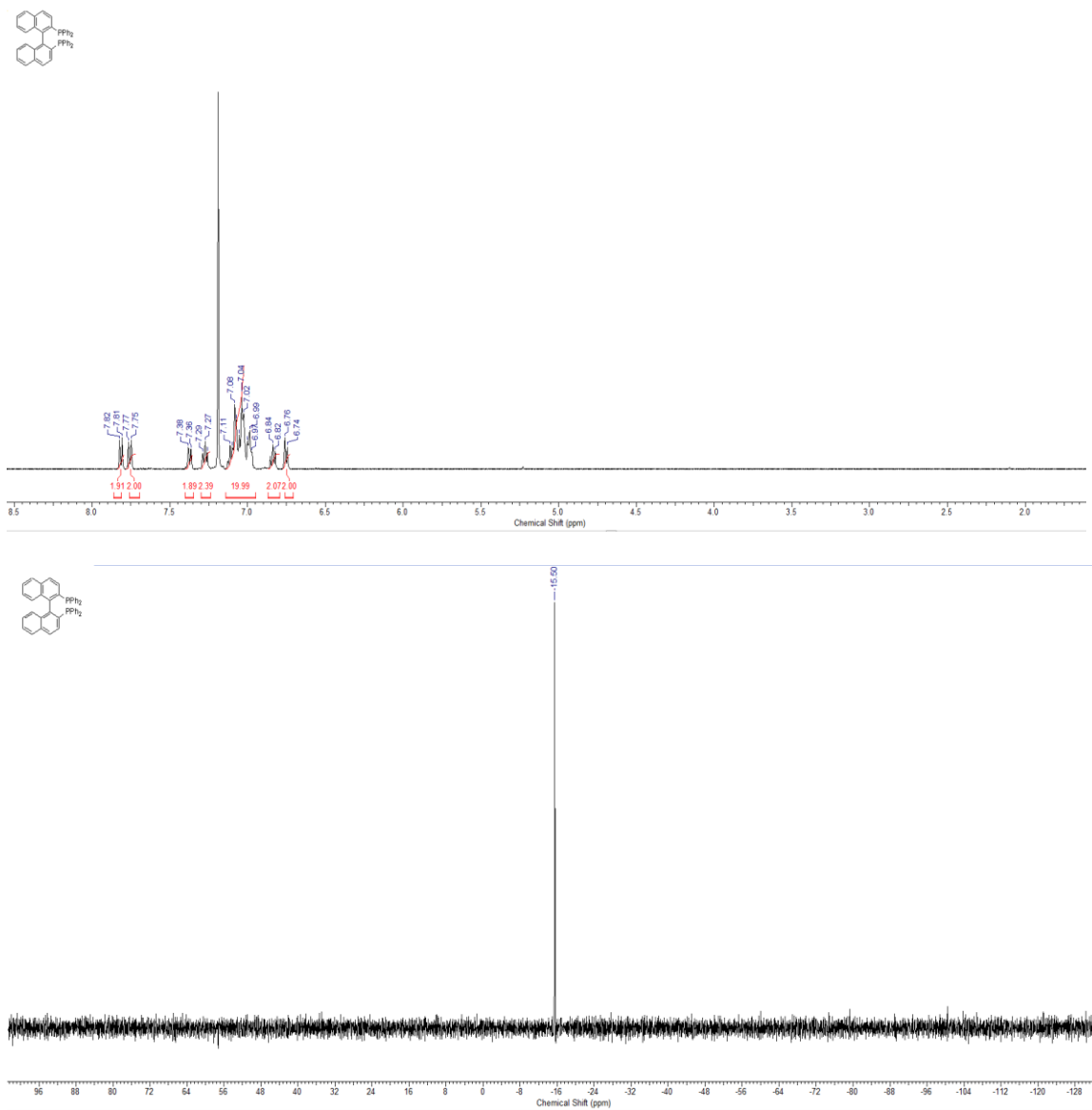
(2',6'-dimethoxy-[1,1'-biphenyl]-2-yl)dicyclohexylphosphine: ^1H and ^{31}P NMR



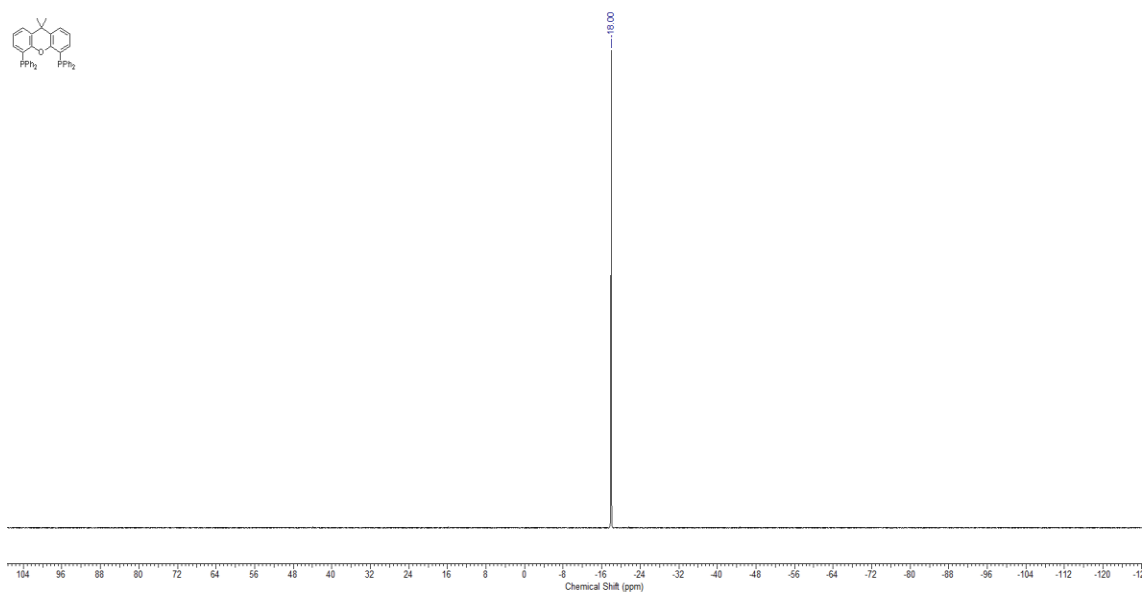
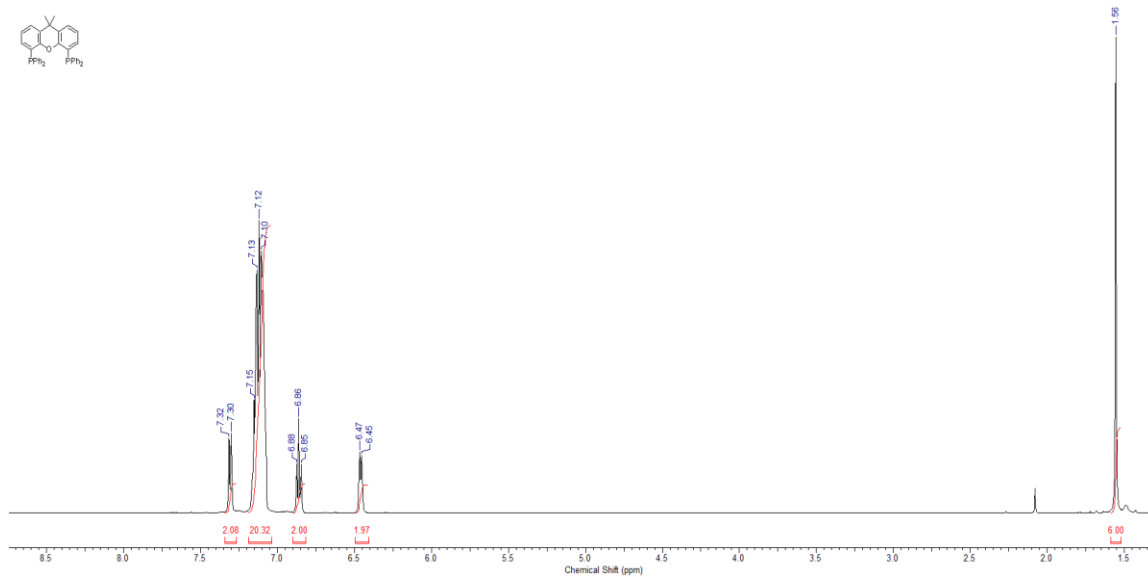
1,2-Bis(diphenylphosphino)ethane: ^1H and ^{31}P NMR



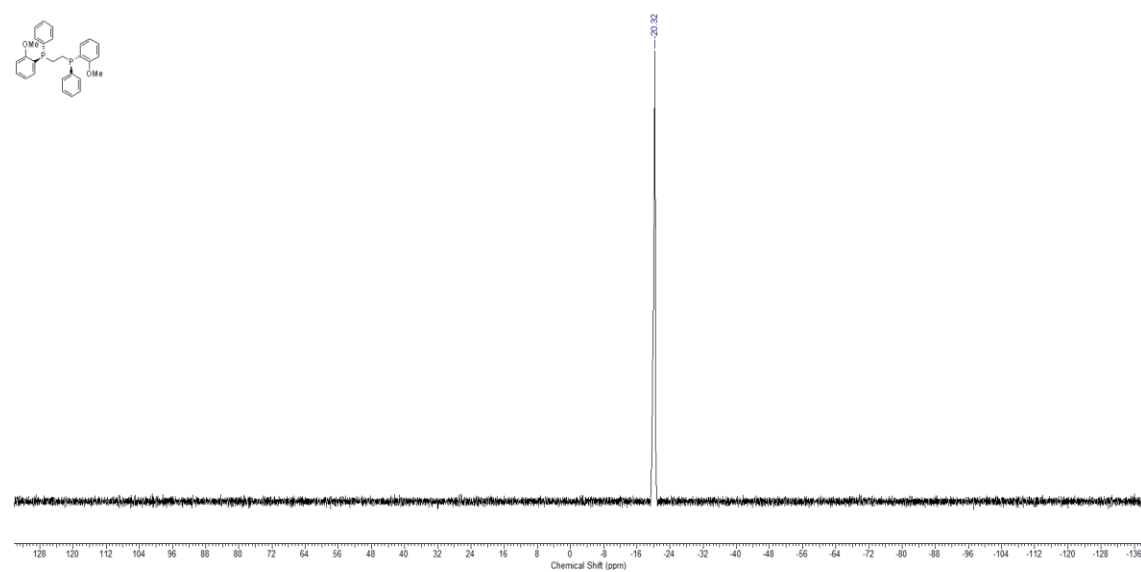
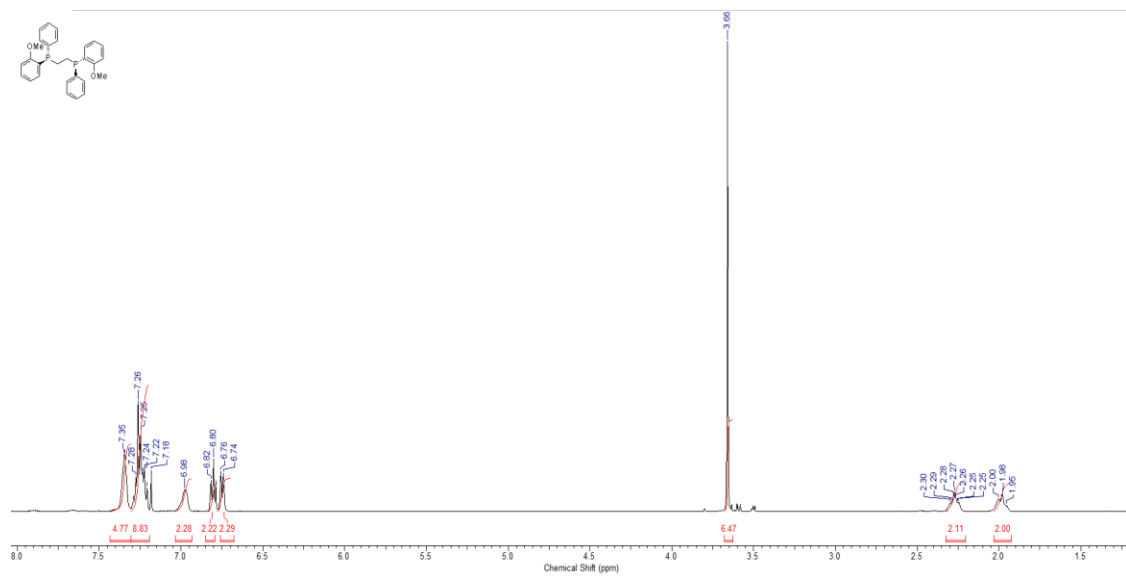
rac-2,2'-Bis(diphenylphosphino)-1,1'-binaphthene: ^1H and ^{31}P NMR



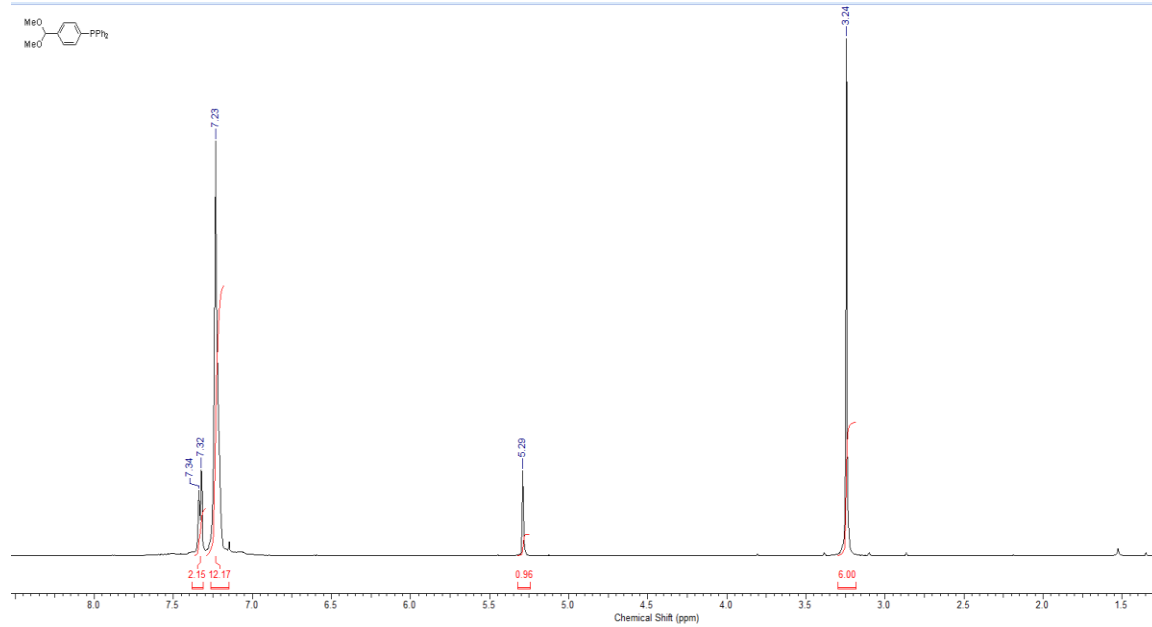
(9,9-Dimethyl-9H-xanthene-4,5-diyl)-bis-diphenylphosphine: ^1H and ^{31}P NMR

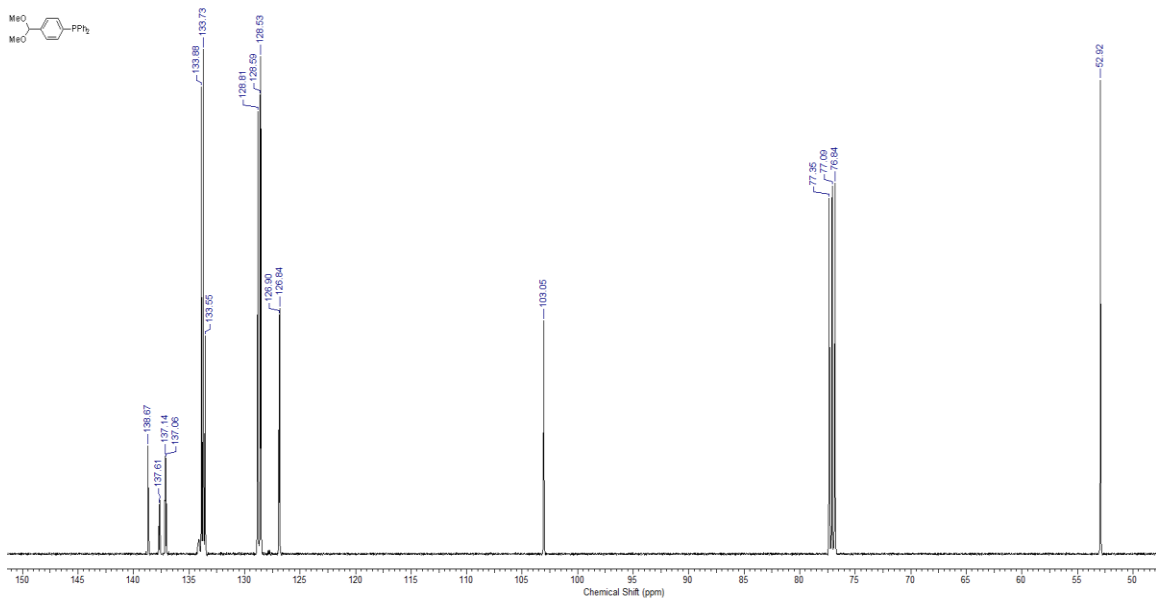
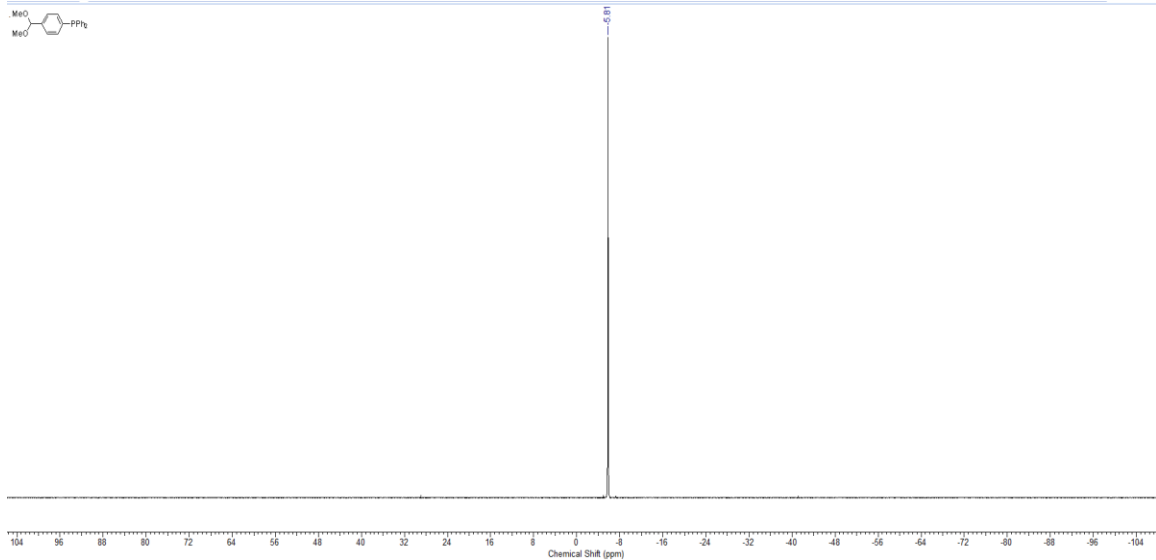


(R,R)-DIPAMP: ^1H and ^{31}P NMR

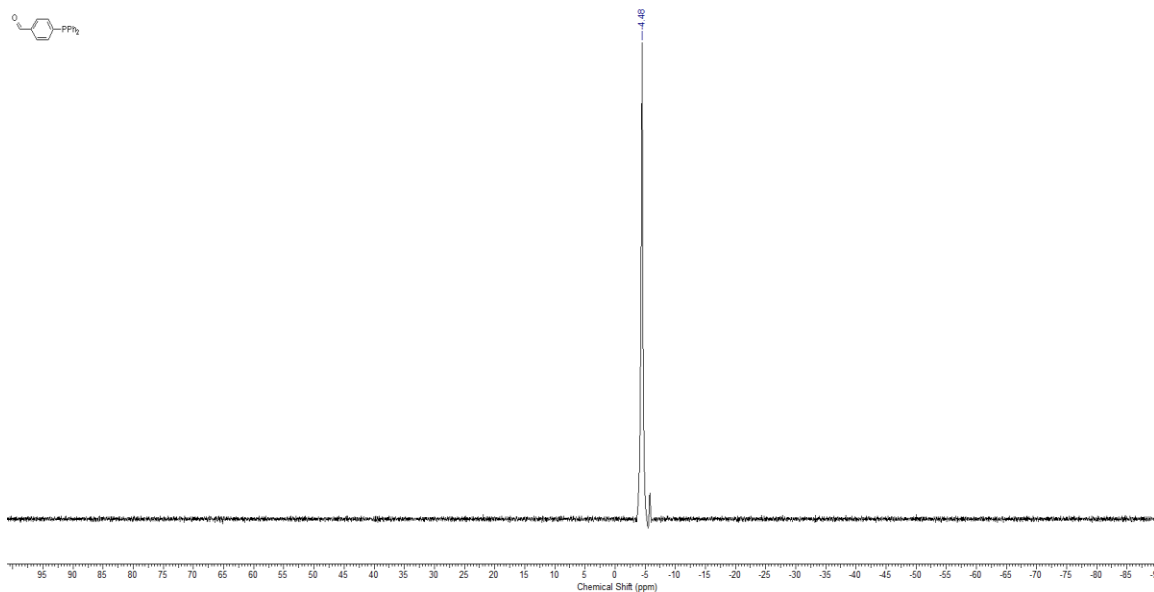


[4-(Dimethoxymethyl)phenyl]-diphenylphosphine: ^1H , ^{13}C , and ^{31}P NMR

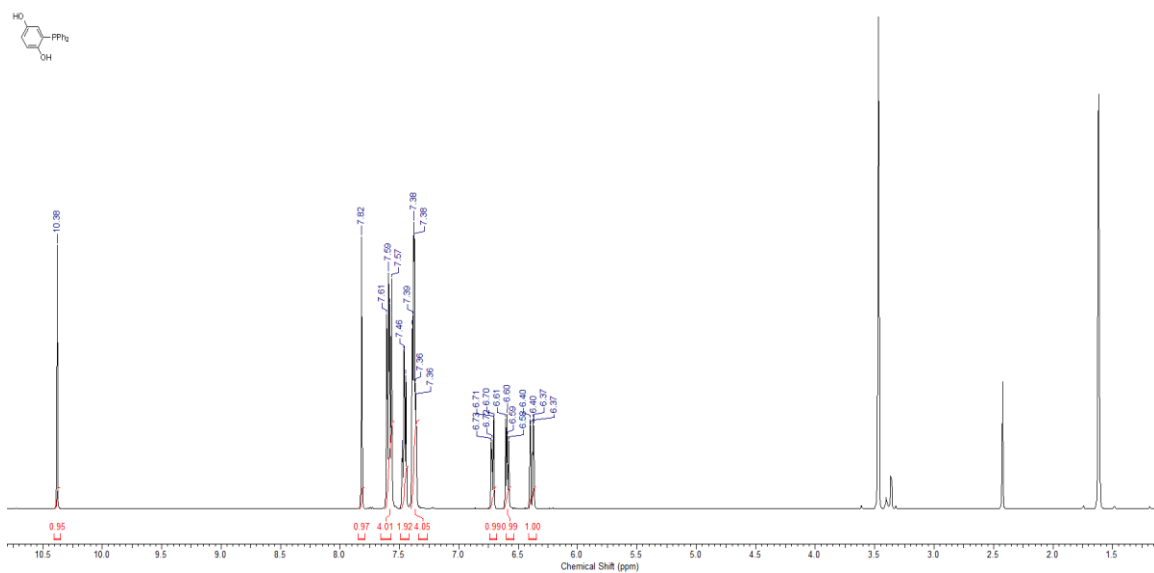


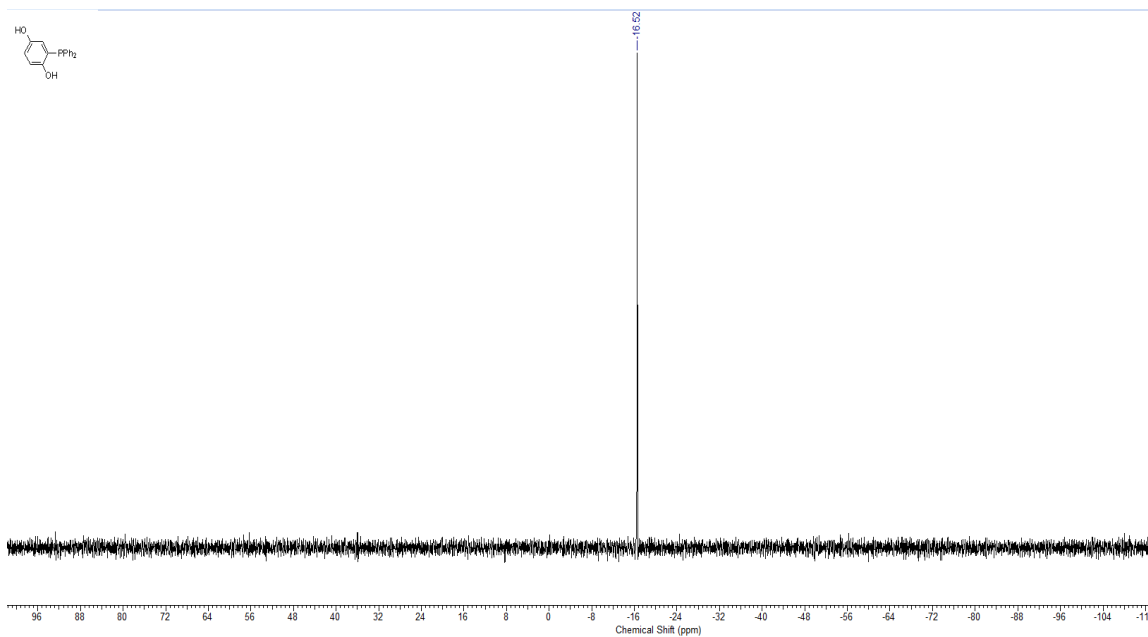
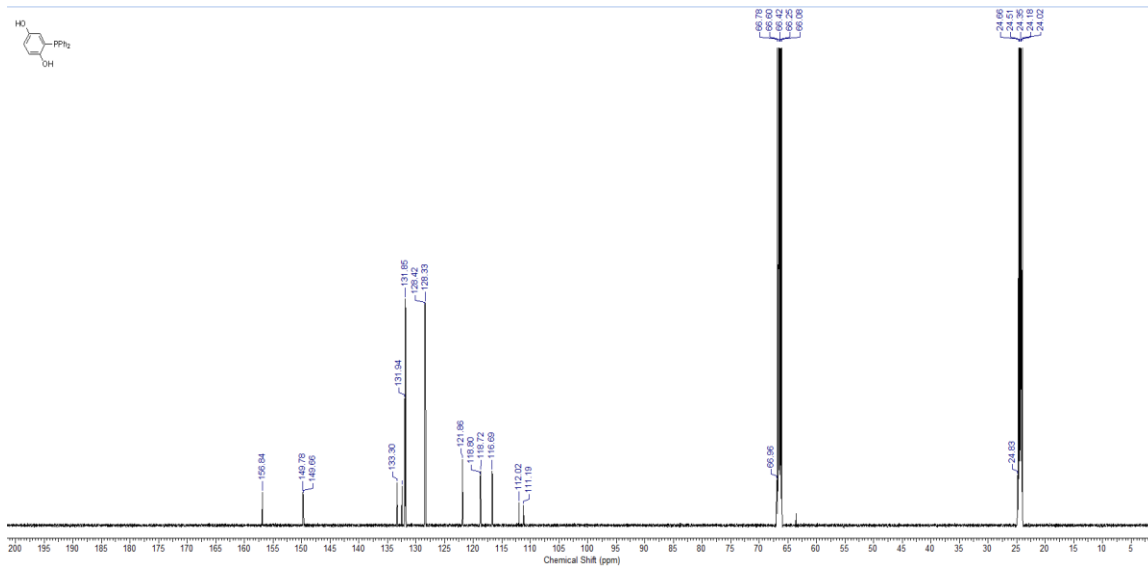


4-(Diphenylphosphino)-benzaldehyde: ^{31}P NMR

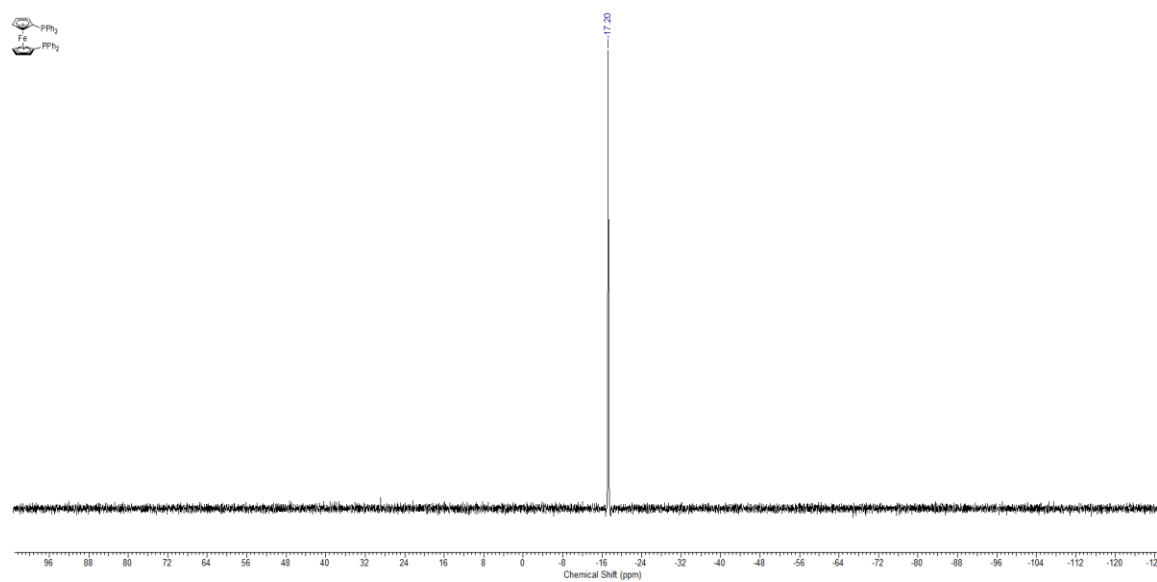
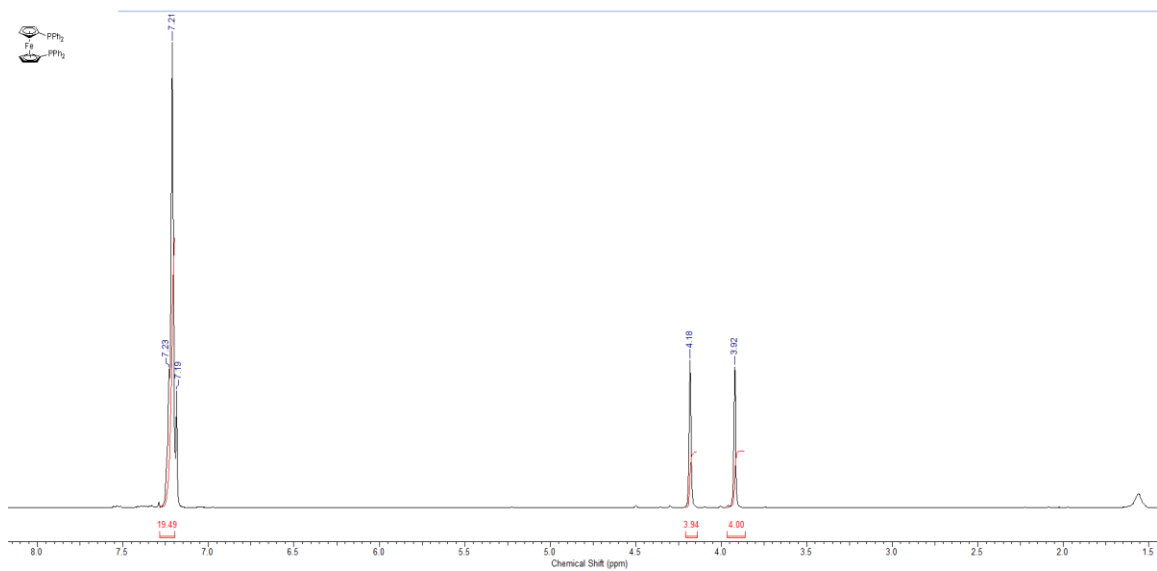


(2,5-Dihydroxyphenyl)diphenylphosphine: ^1H , ^{13}C , and ^{31}P NMR

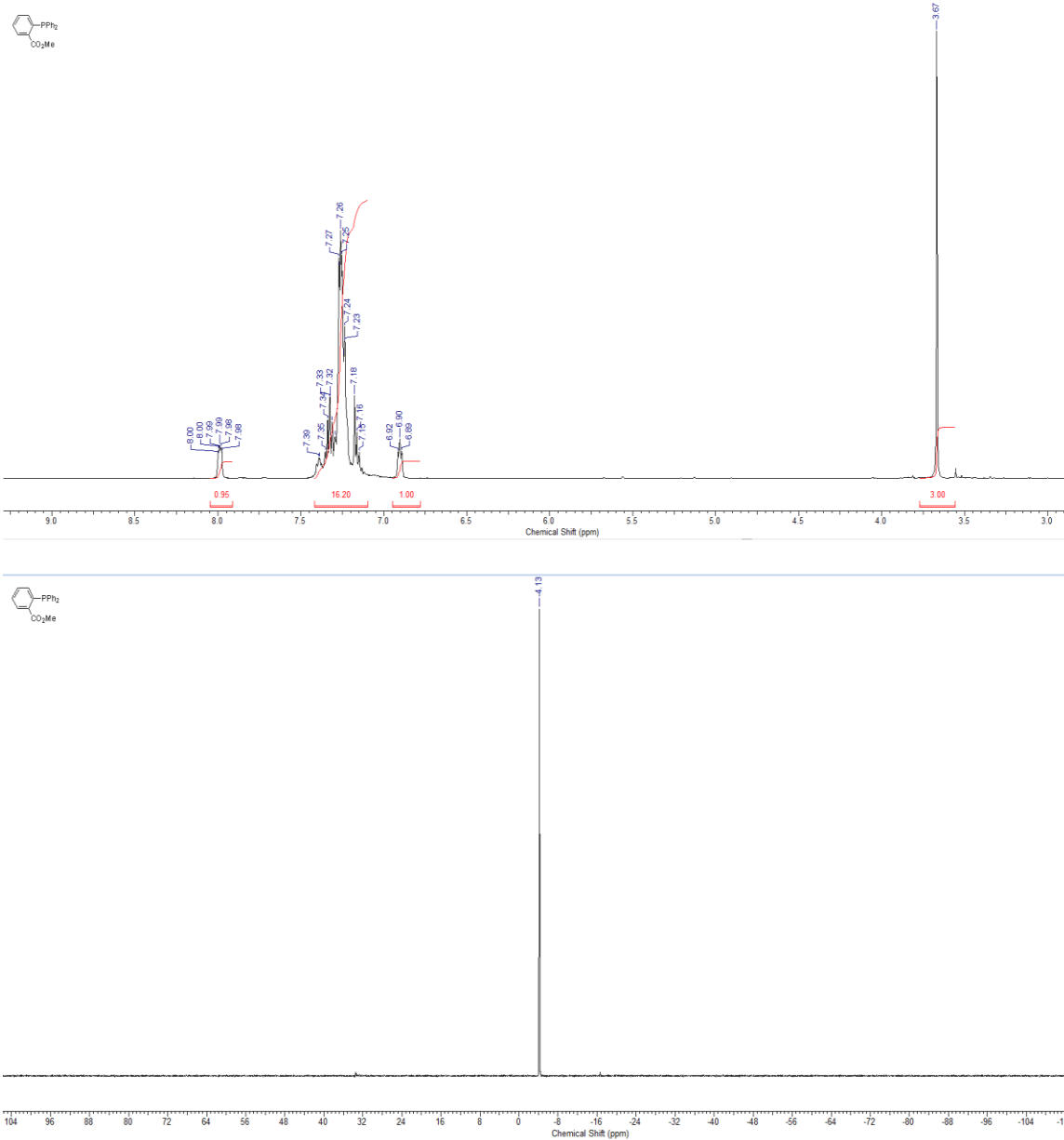




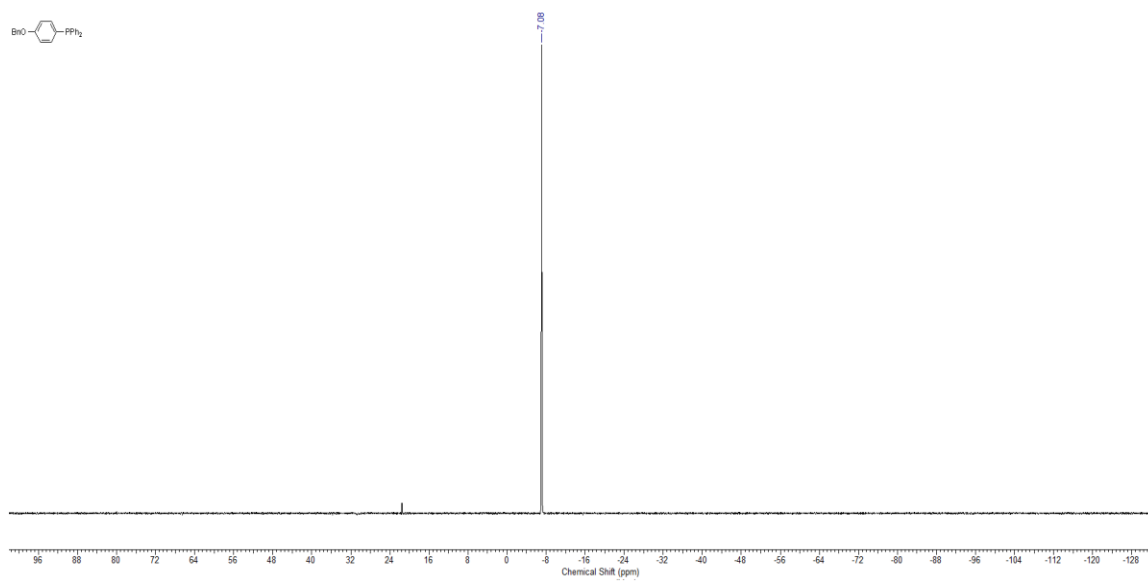
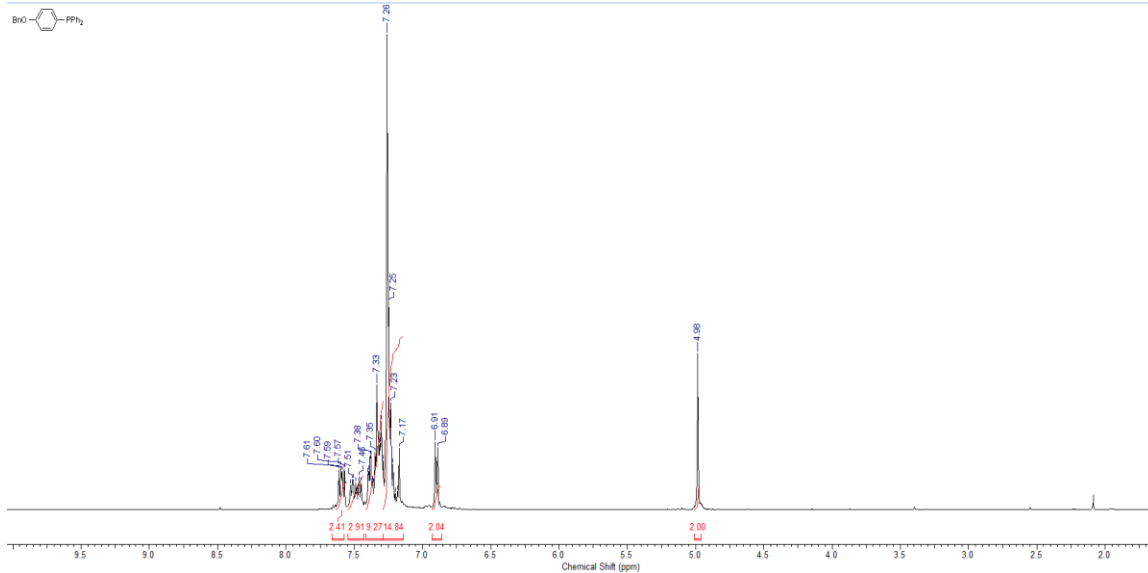
1,1'-Bis(diphenylphino)ferrocene: ^1H and ^{31}P NMR



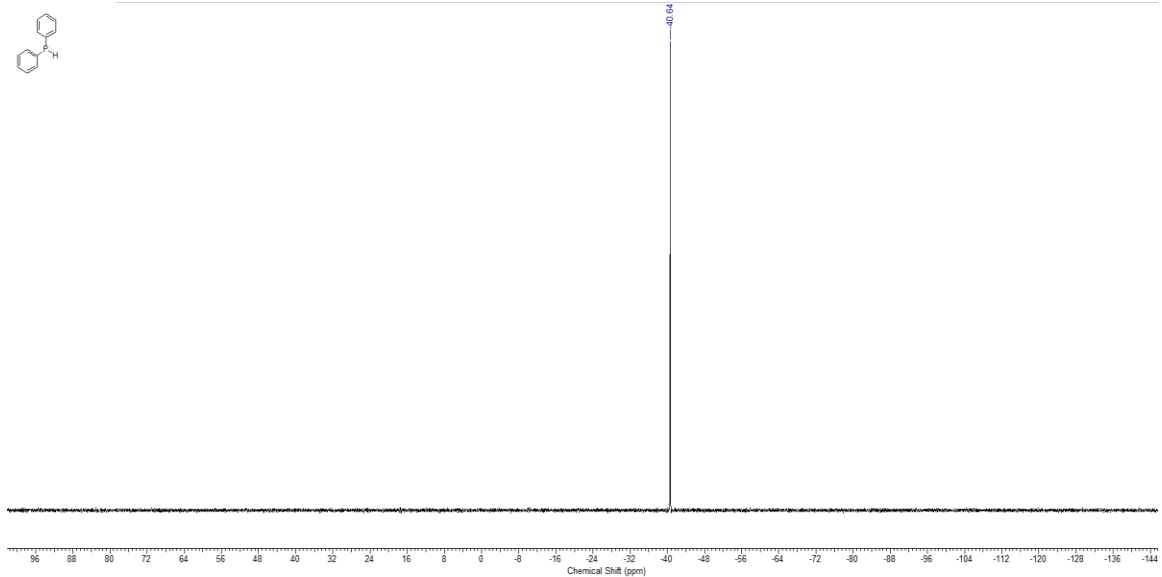
Methyl-2-(diphenylphosphino)benzoate: ^1H and ^{31}P NMR



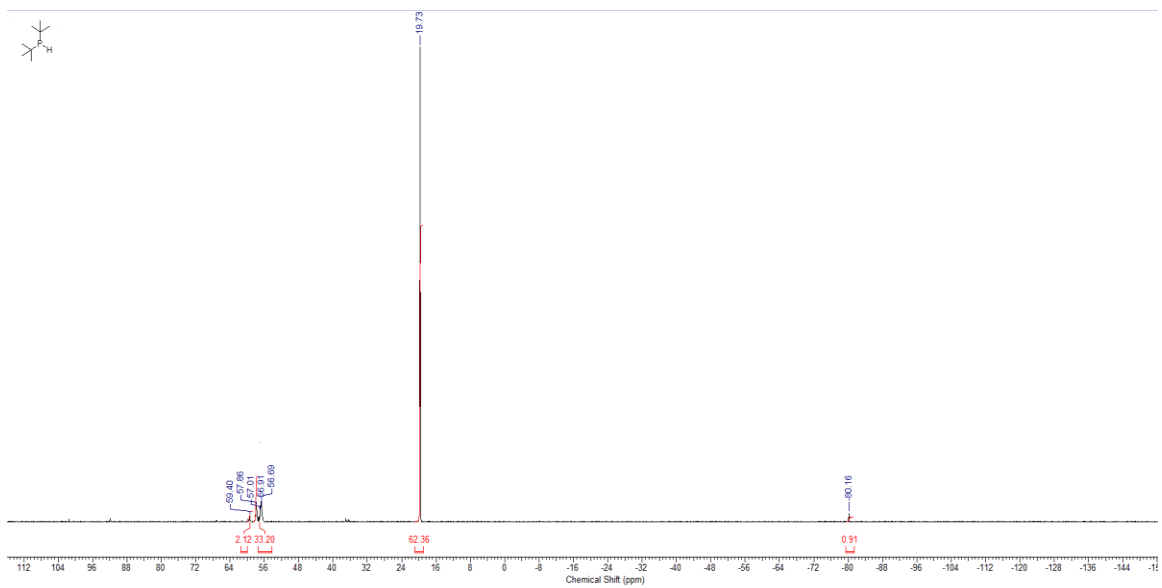
(4-(Benzyloxy)phenyl)diphenylphosphine: ^1H and ^{31}P NMR



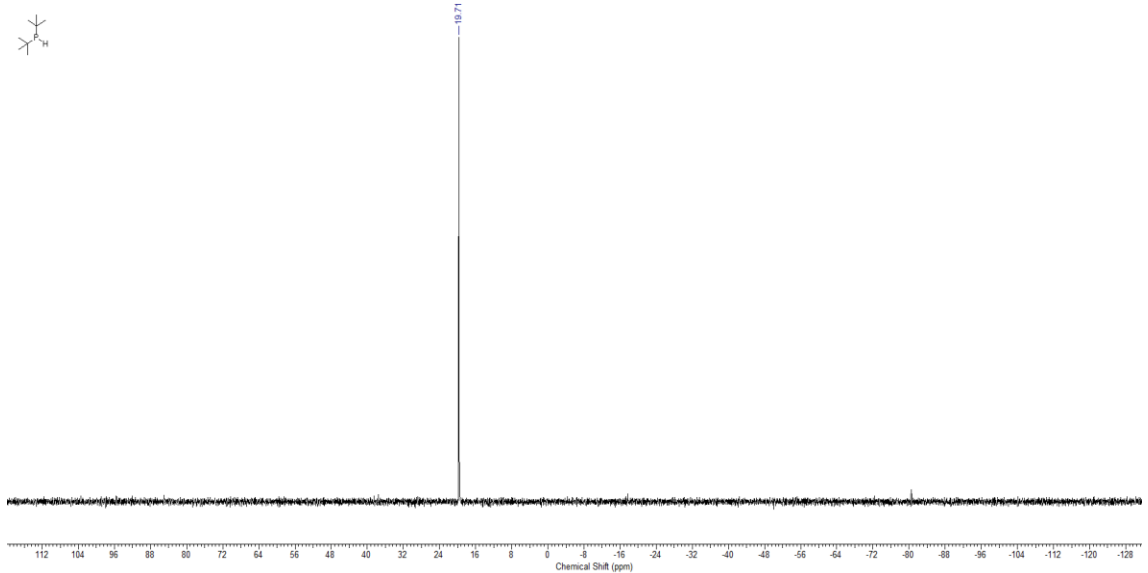
Diphenylphosphine: ^{31}P NMR



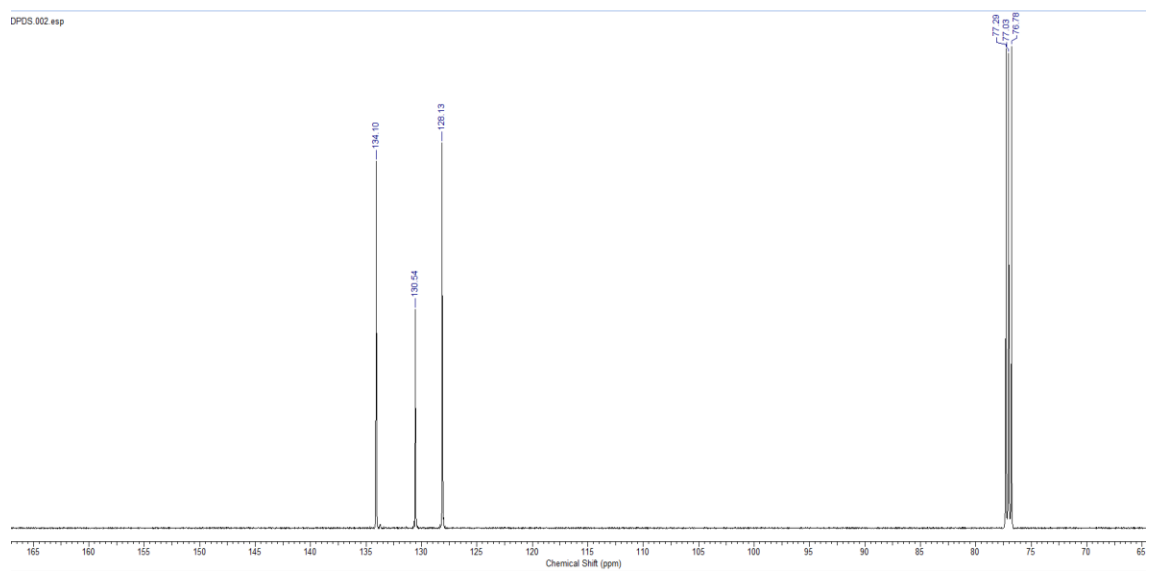
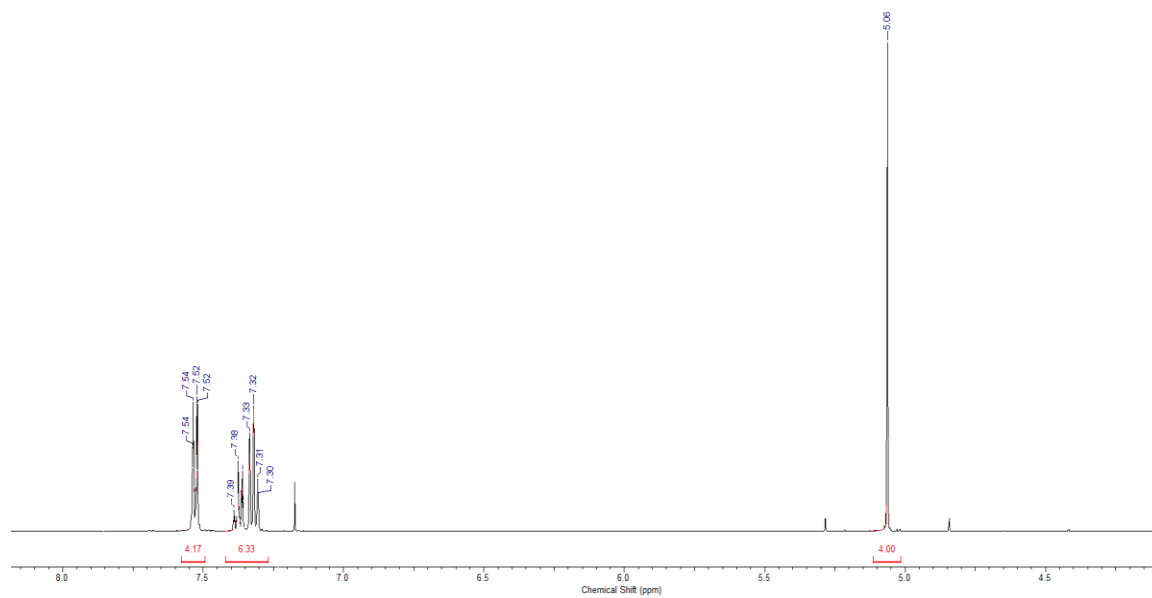
DI-*tert*-butylphosphine (@ 110 °C): ^{31}P NMR



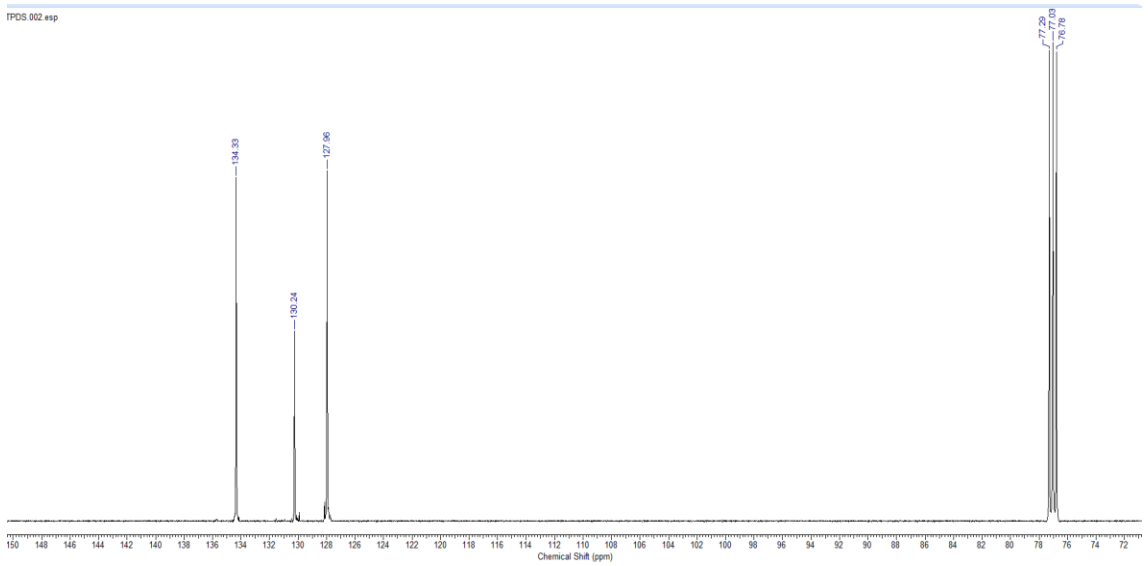
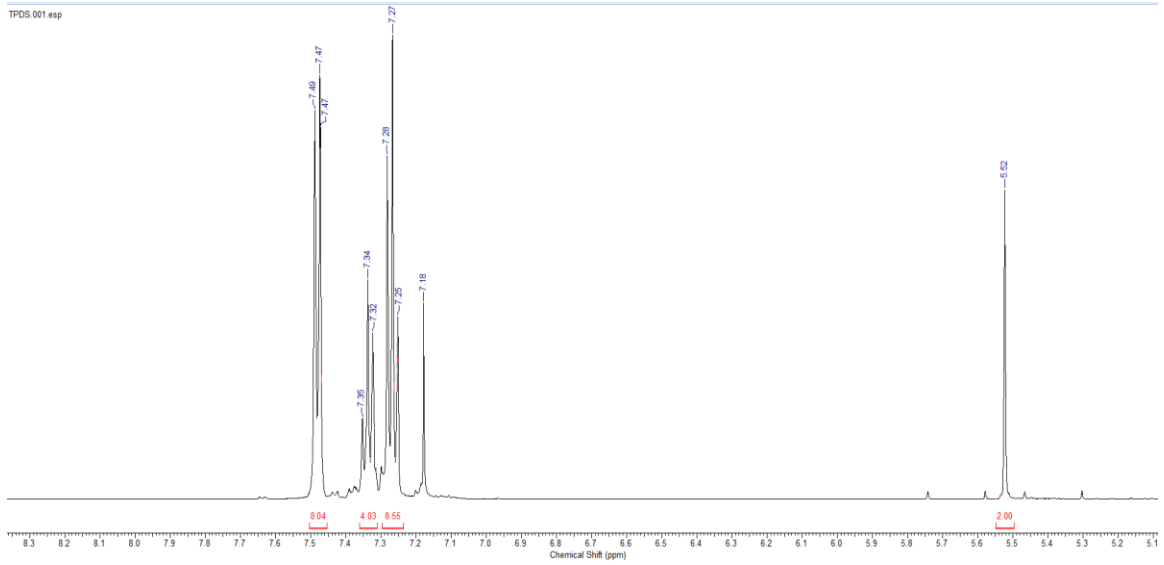
Di-tert-butylphosphine (@ 23 °C): ^{31}P NMR



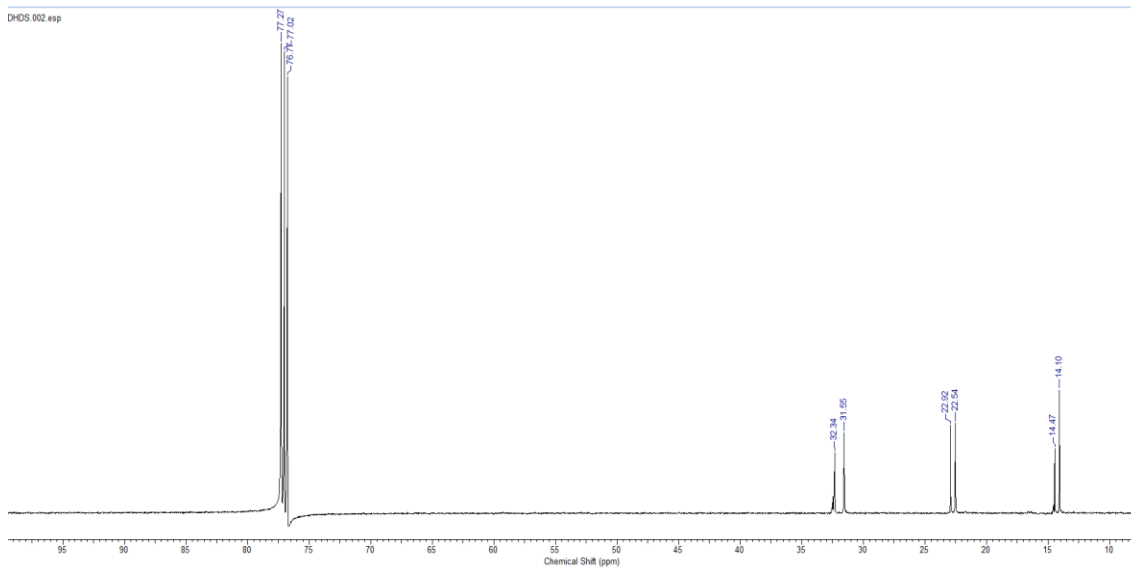
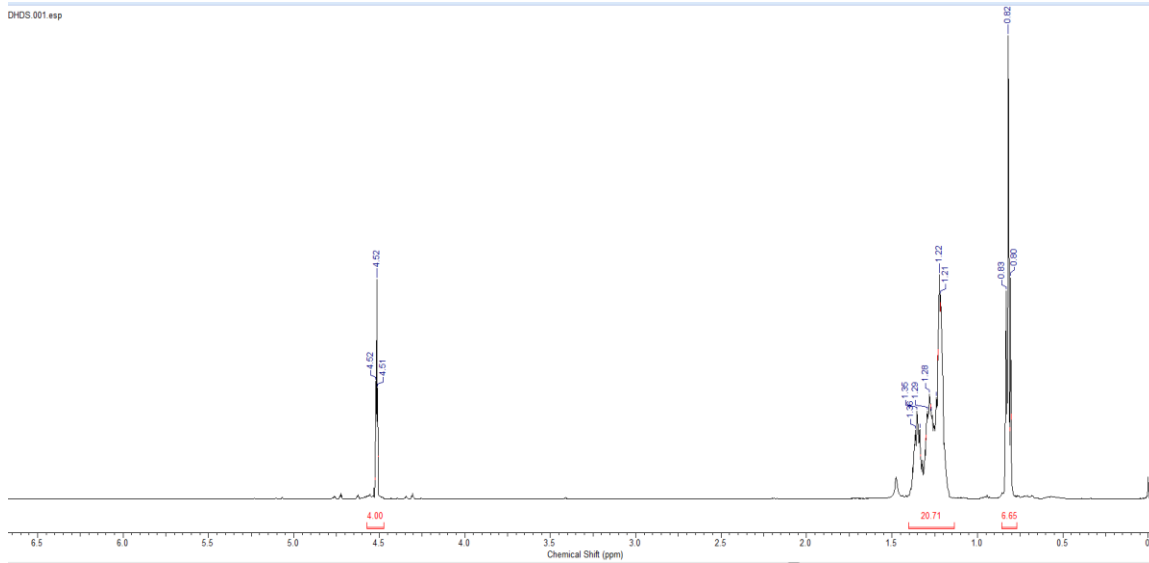
1,3-Diphenyl-disiloxane (DPDS): ^1H , ^{13}C



1,1,3,3-Tetraphenyl-disiloxane (TPDS): ^1H , ^{13}C

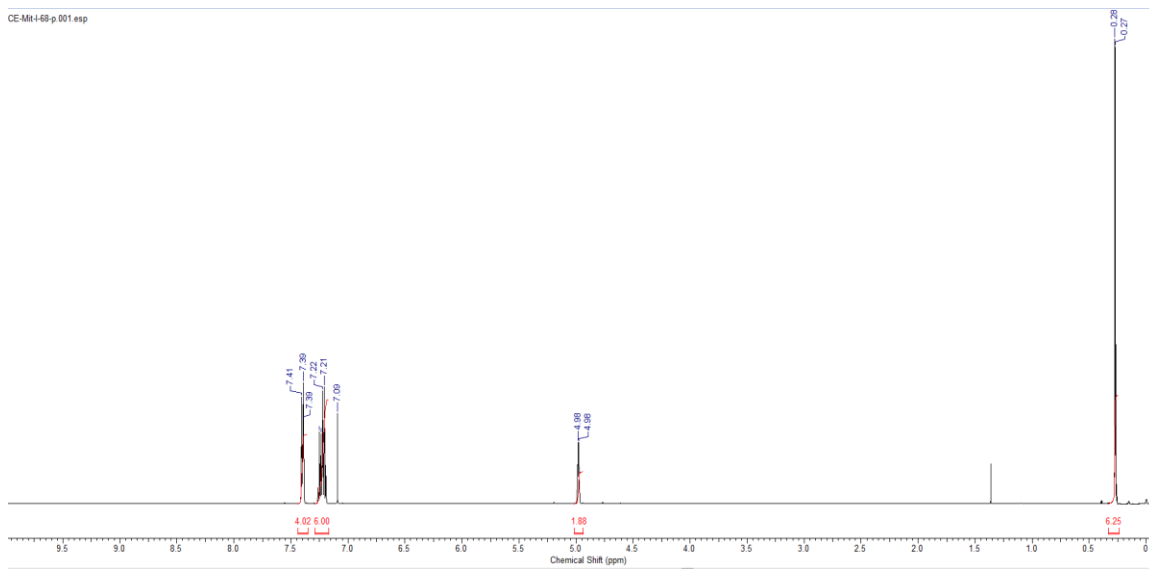


1,3-Di-*n*-hexyl-disiloxane (**DHDS**): ^1H , ^{13}C

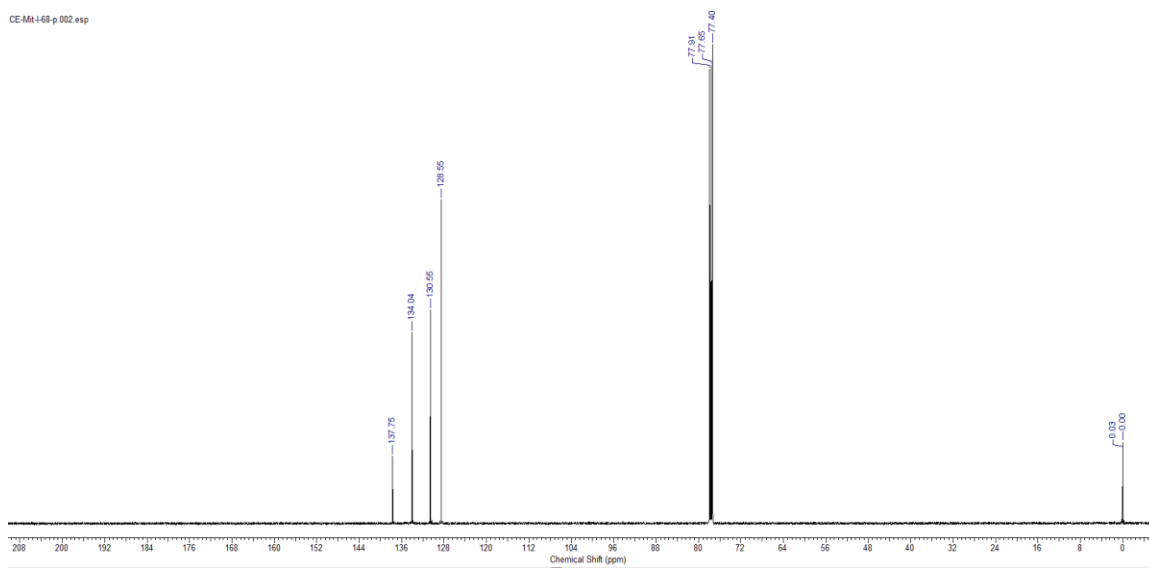


1,3-Dimethyl-1,3-diphenyl-disiloxane (DMDPDS): ^1H , ^{13}C

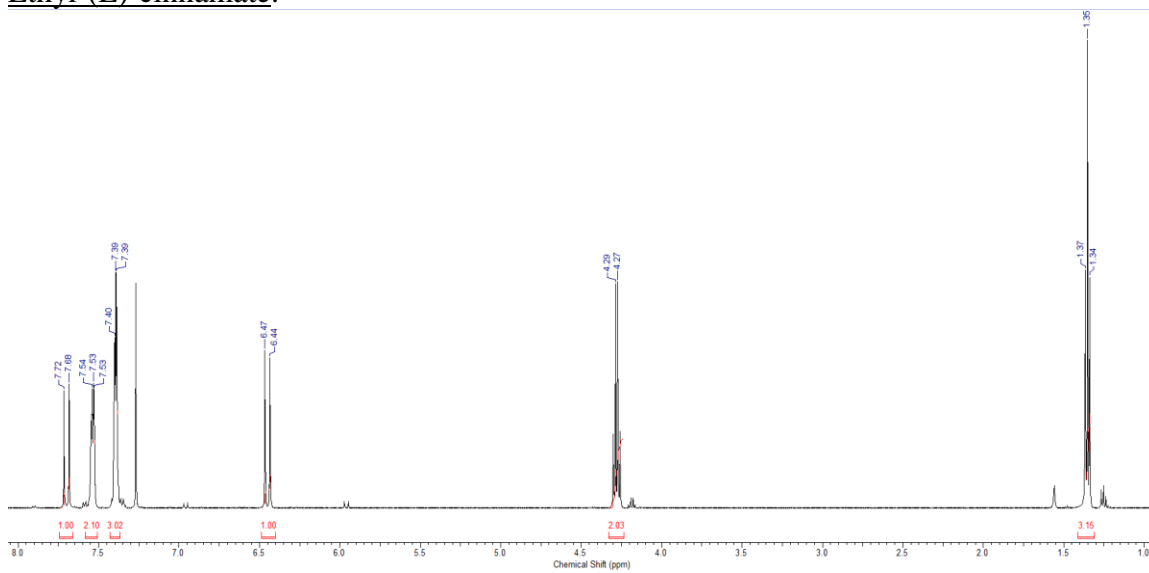
CE-Mt468 p 001 esp



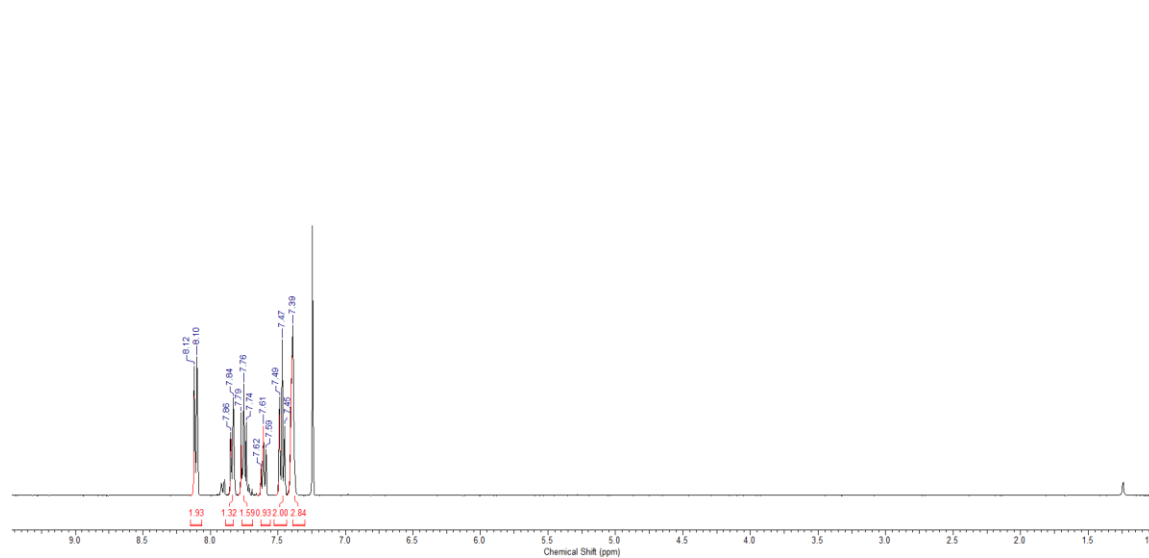
CE-Mt468 p 002 esp



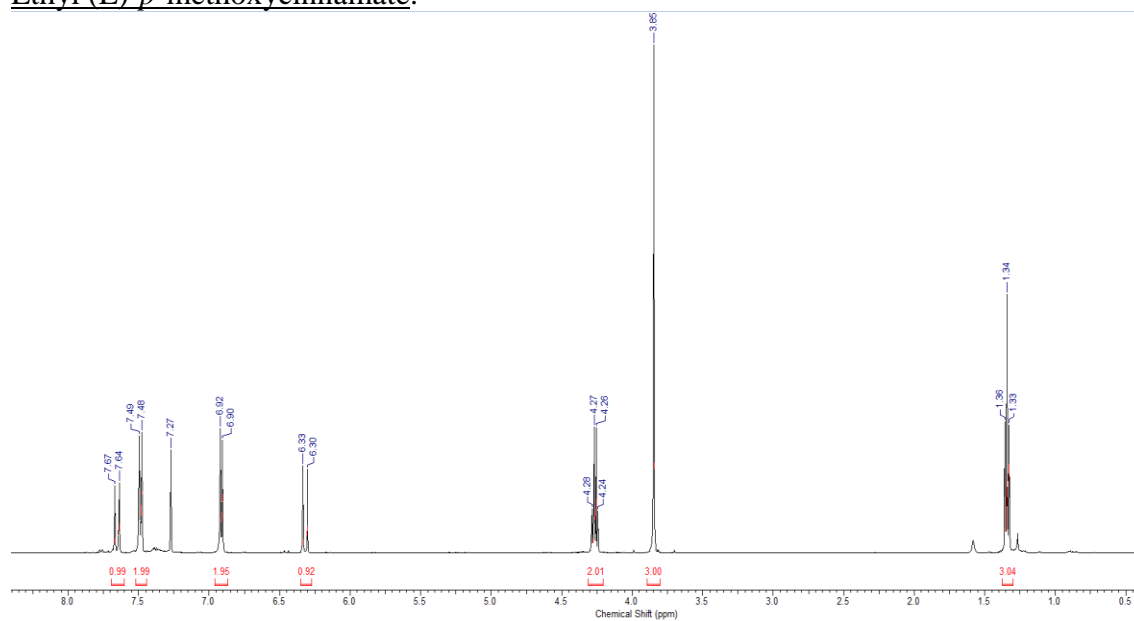
Ethyl-(E)-cinnamate:



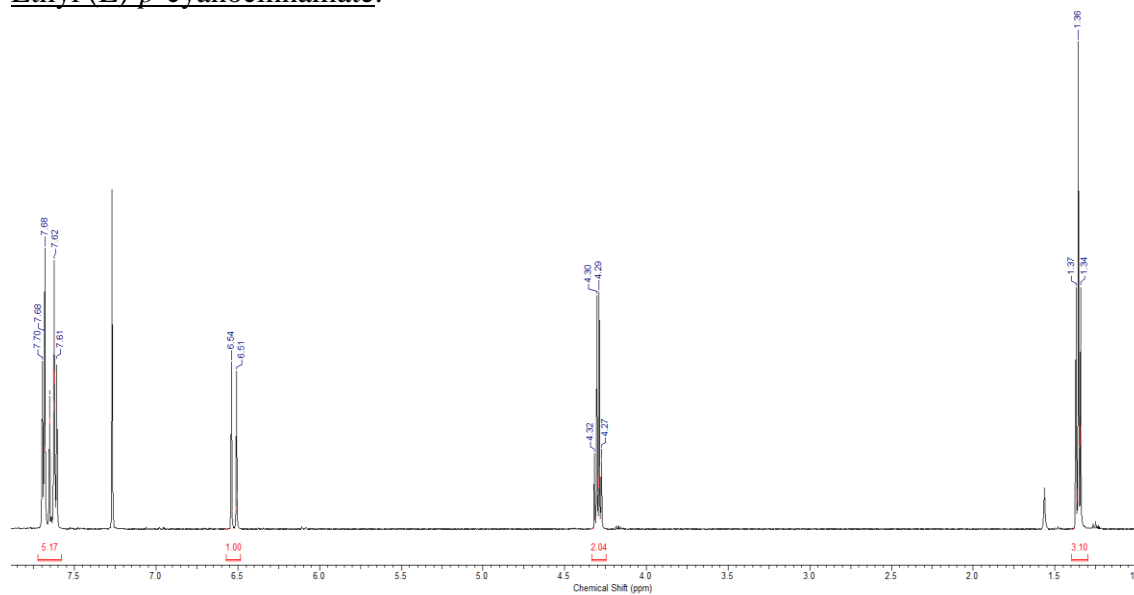
(E)-1,3-Diphenyl-propen-3-one:



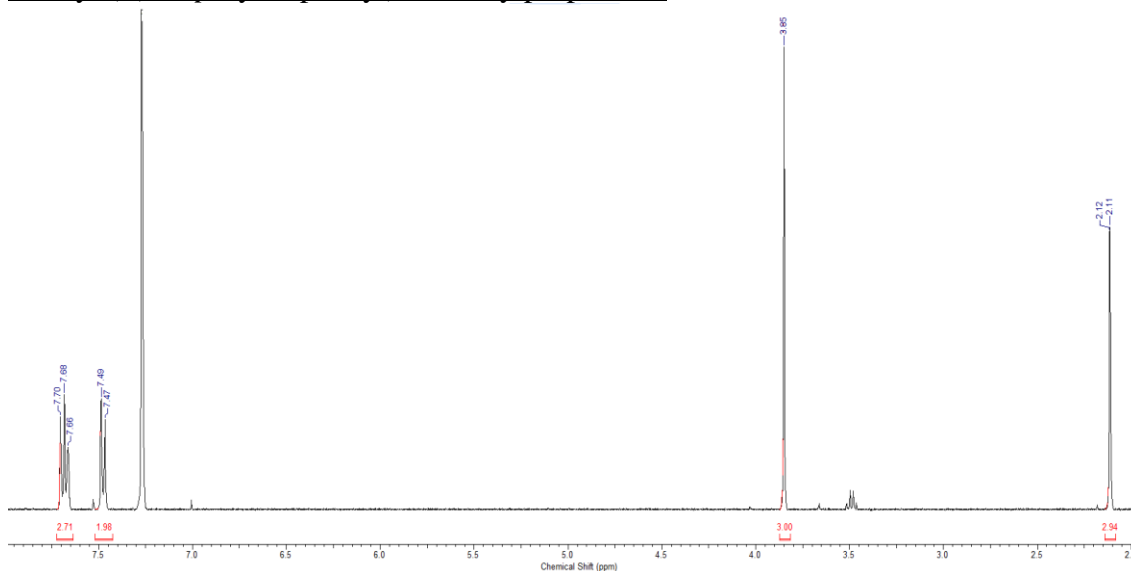
Ethyl (E)-*p*-methoxycinnamate:



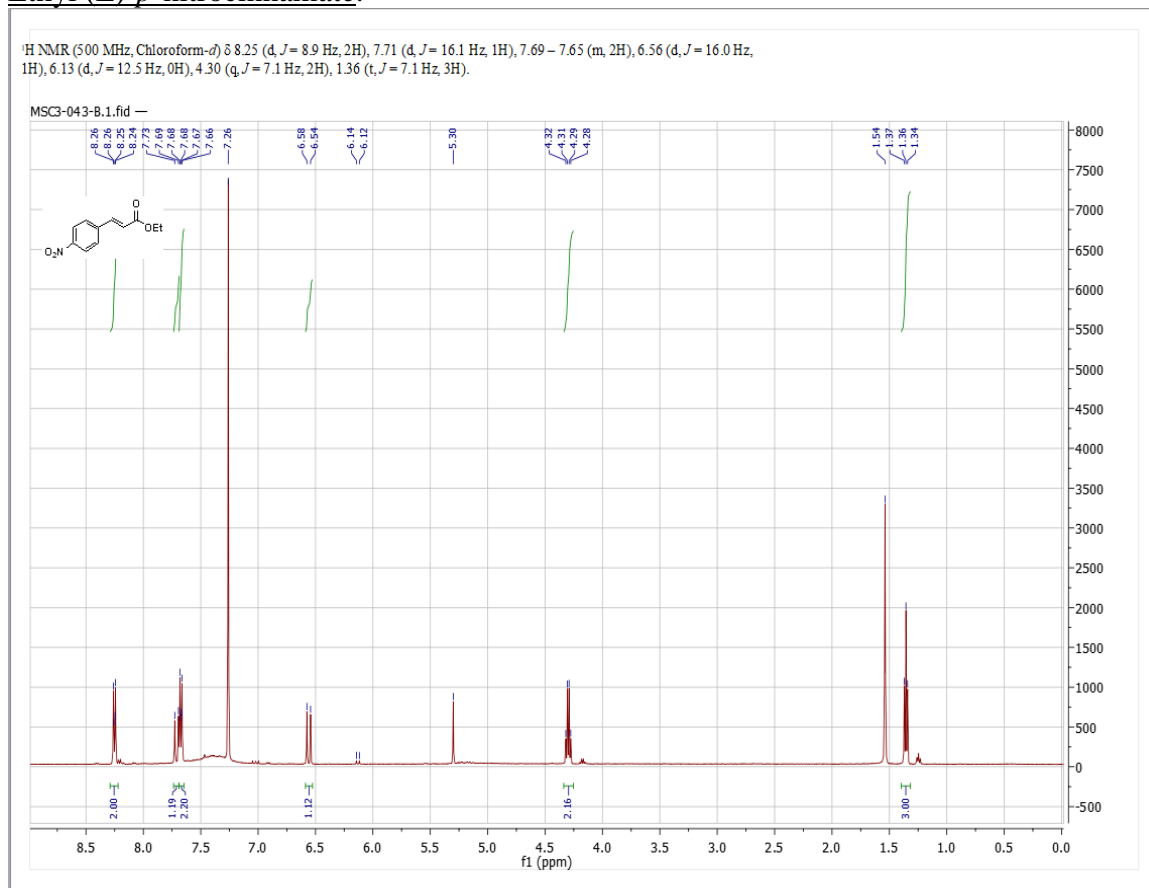
Ethyl (E)-*p*-cyanocinnamate:



Methyl (E)-3-(p-cyanophenyl)-2-methylpropenoate:

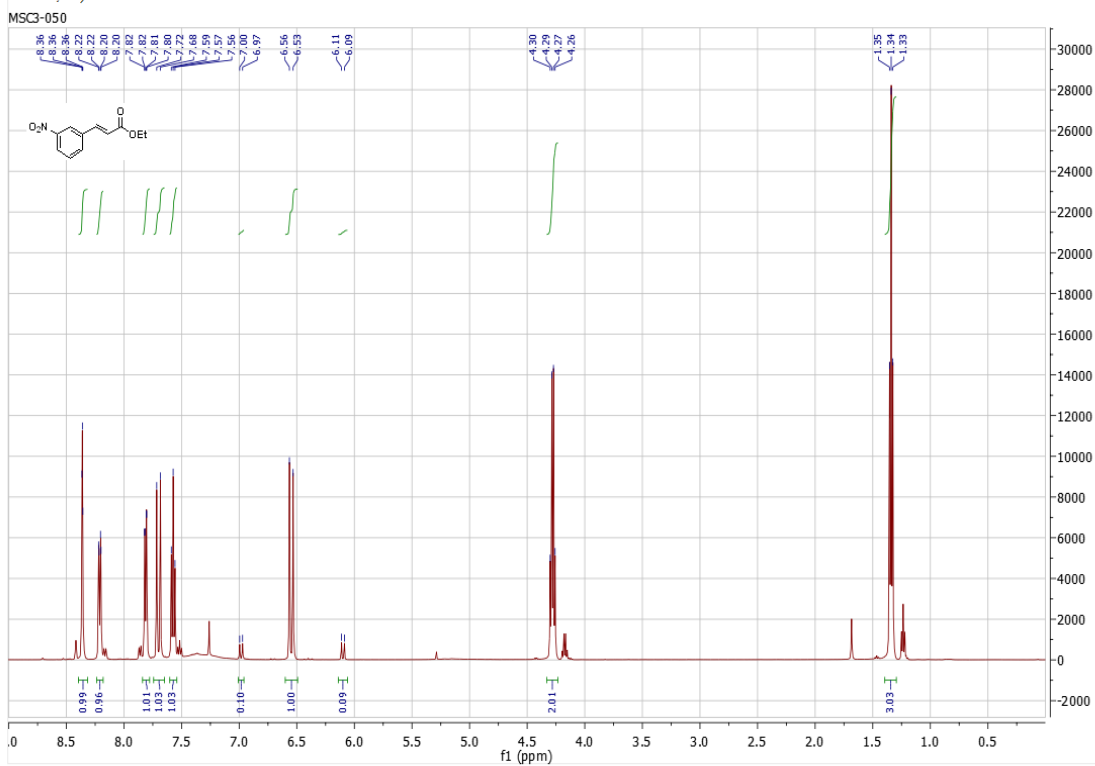


Ethyl (E)-p-nitrocinnamate:



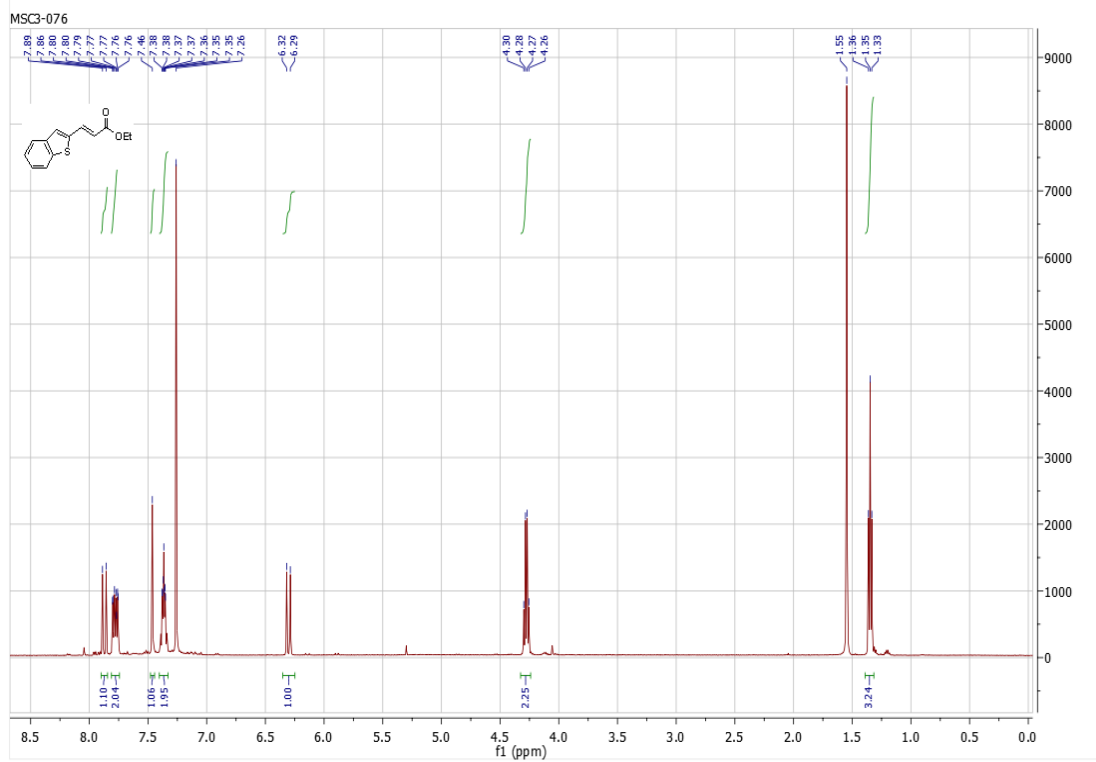
Ethyl (E)-*m*-nitrocinnamate:

¹H NMR (500 MHz, Chloroform-*d*) δ 8.36 (t, $J = 1.9$ Hz, 1H), 8.21 (dd, $J = 8.4, 2.2$ Hz, 1H), 7.84–7.78 (m, 1H), 7.70 (d, $J = 16.0$ Hz, 1H), 7.57 (t, $J = 7.9$ Hz, 1H), 6.98 (d, $J = 12.5$ Hz, 0H), 6.55 (d, $J = 16.0$ Hz, 1H), 6.10 (d, $J = 12.5$ Hz, 0H), 4.28 (q, $J = 7.1$ Hz, 2H), 1.34 (t, $J = 7.2$ Hz, 3H).

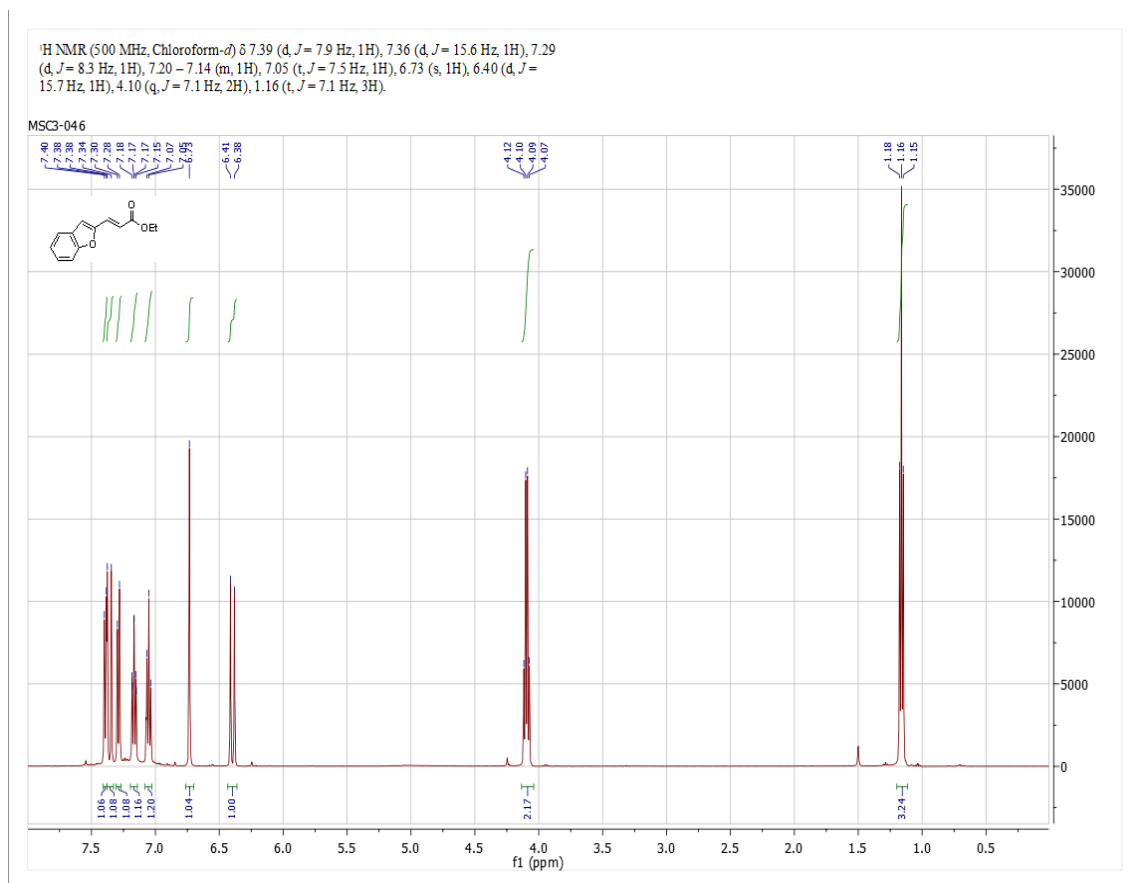


Ethyl (E)-3-(benzo[*b*]thiophen-2-yl)acrylate:

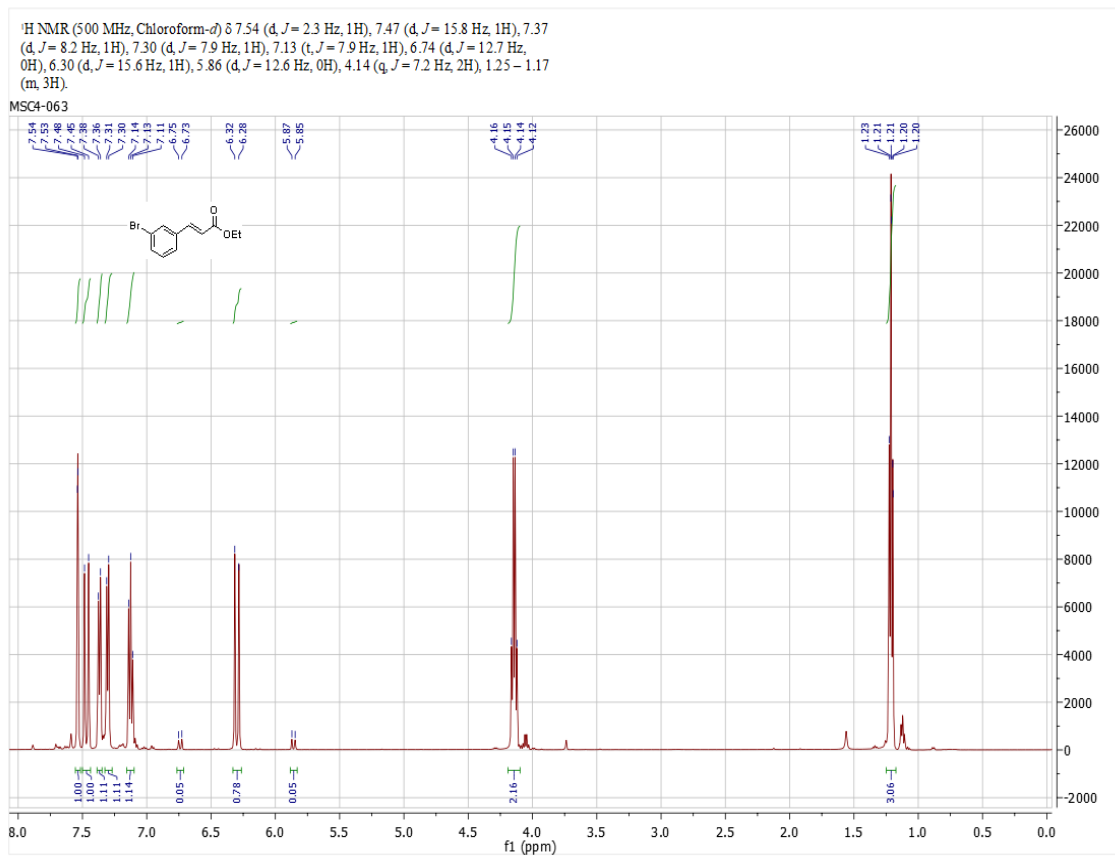
¹H NMR (500 MHz, Chloroform-*d*) δ 7.87 (d, $J = 15.6$ Hz, 1H), 7.81 – 7.74 (m, 2H), 7.46 (s, 1H), 7.37 (ddd, $J = 7.1, 5.0, 1.6$ Hz, 2H), 6.30 (d, $J = 15.6$ Hz, 1H), 4.28 (q, $J = 7.2$ Hz, 2H), 1.35 (t, $J = 7.1$ Hz, 3H).



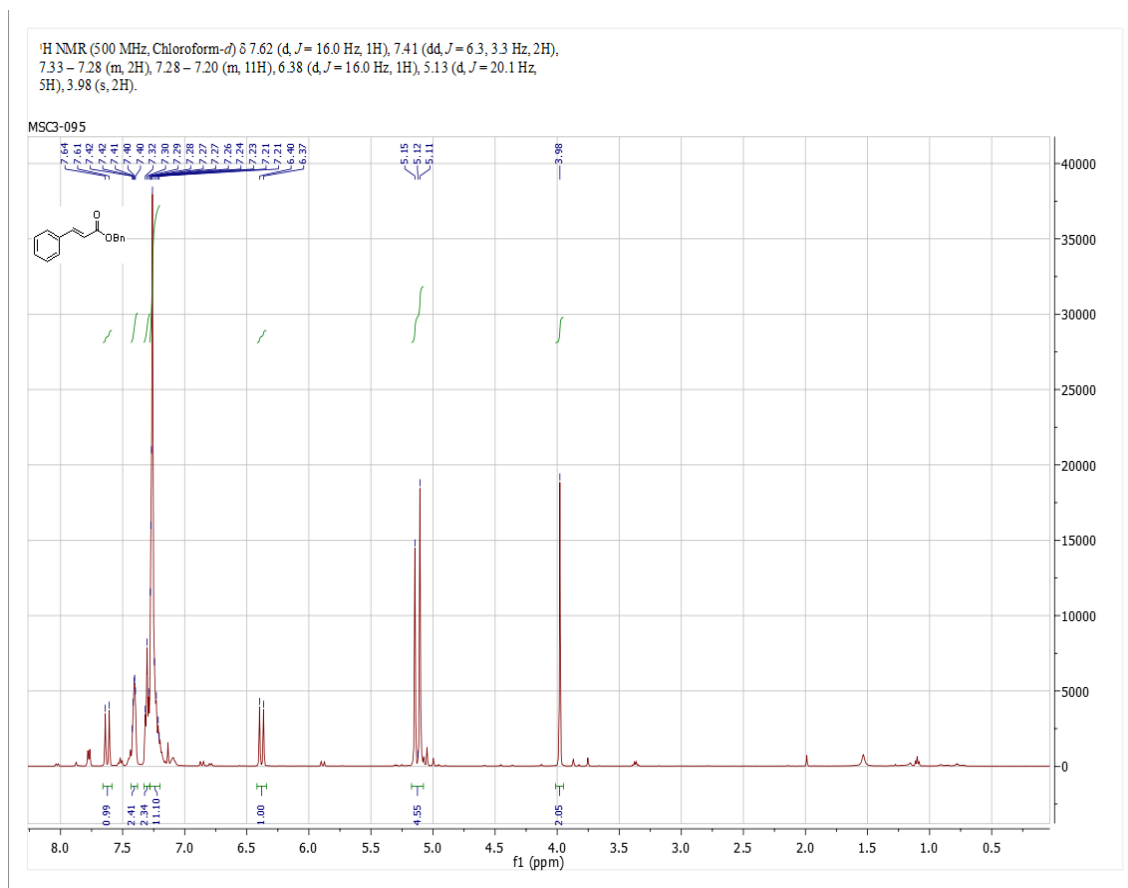
Ethyl (E)-3-(benzo[*b*]furan-2-yl)acrylate:



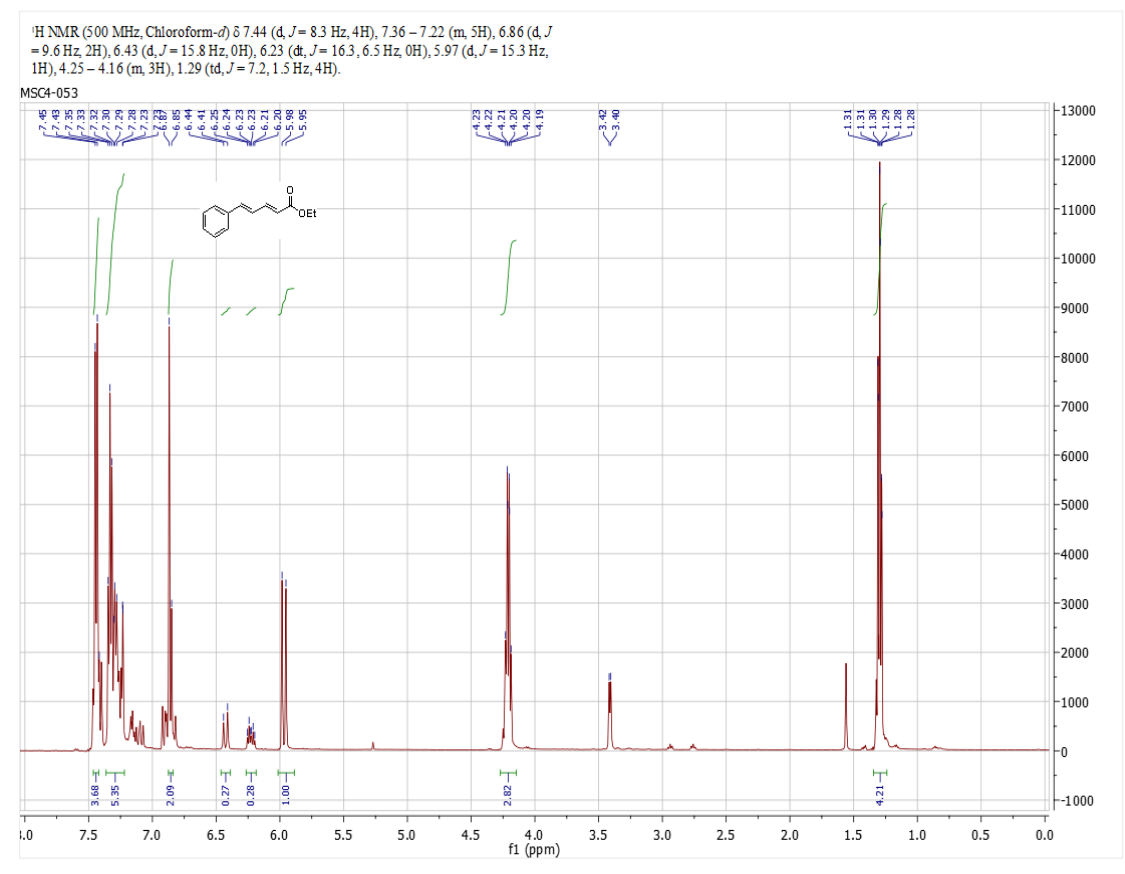
Ethyl (E)-*m*-bromocinnamate:



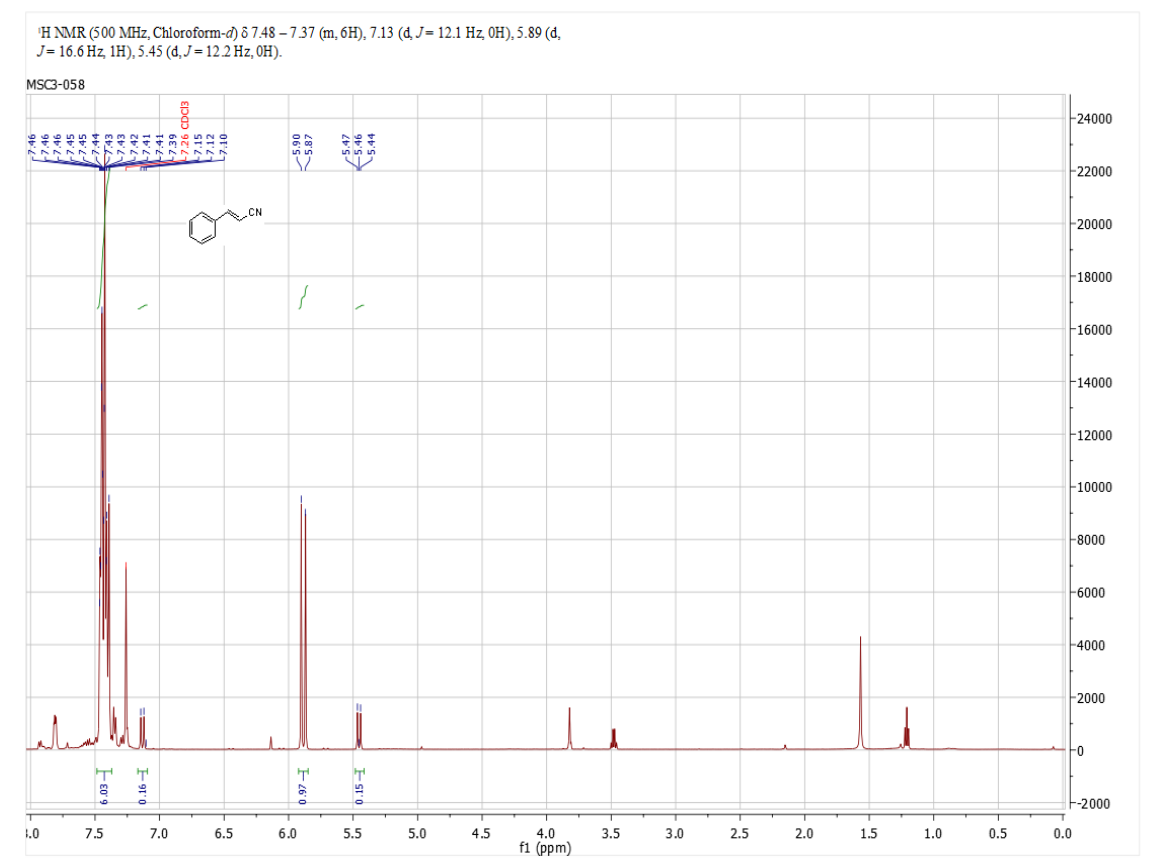
Benzyl (E)-cinnamate:



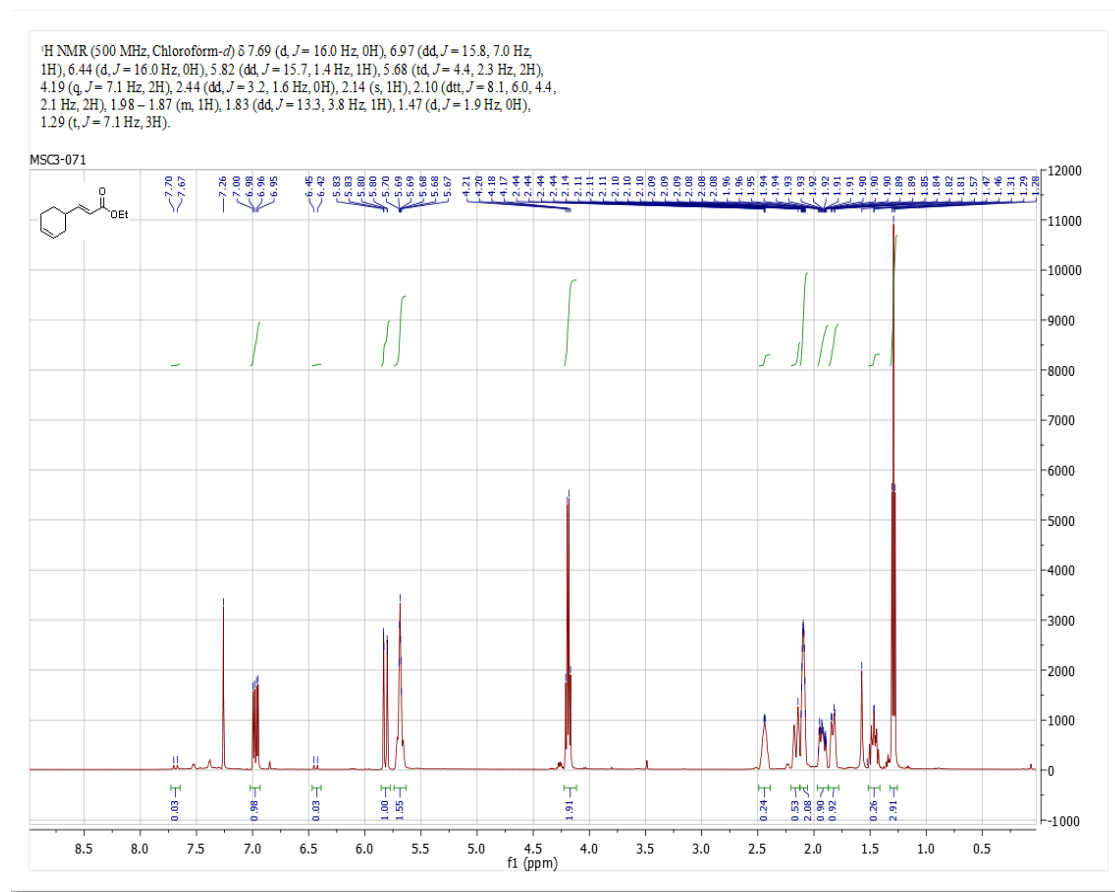
Ethyl (2E, 4E)-5-phenylpenta-2, 4-dienoate:



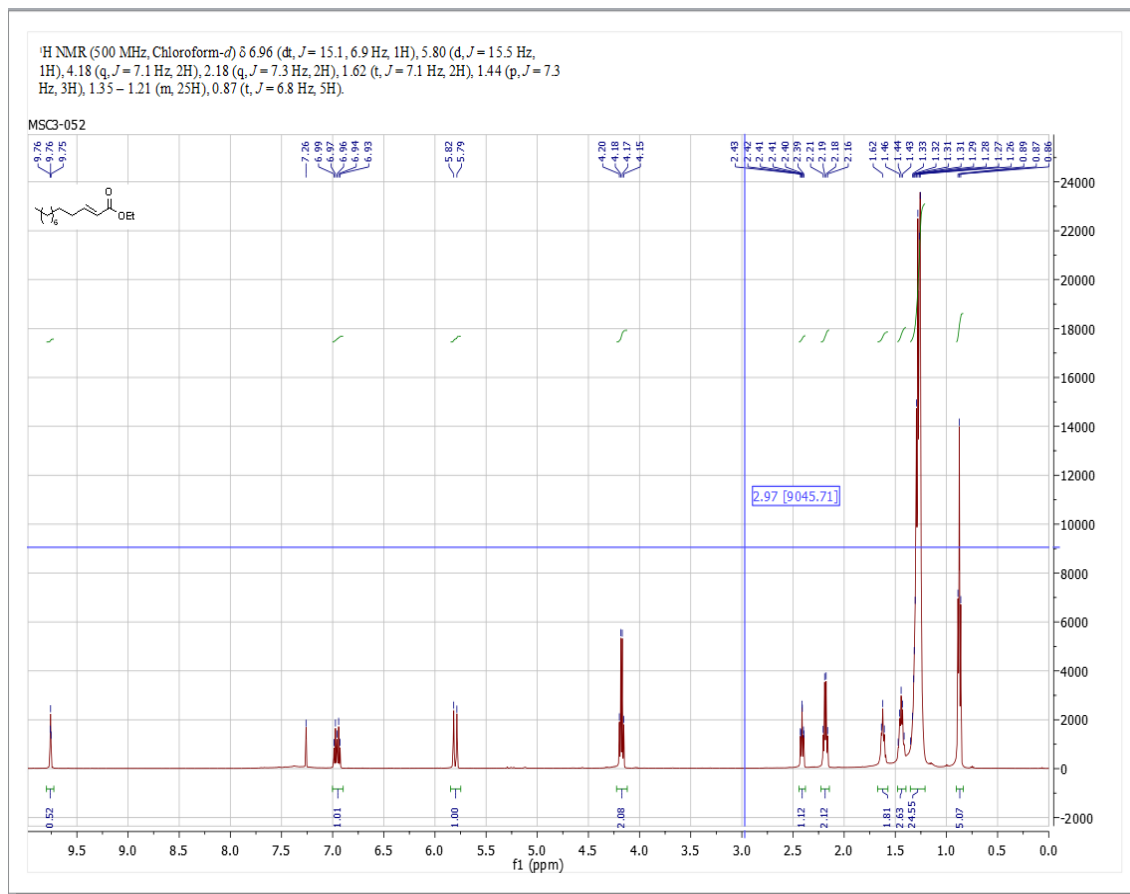
(E)-Cinnamonitrile:



Ethyl-(E)-3-(cyclohex-3-en-1-yl)acrylate:

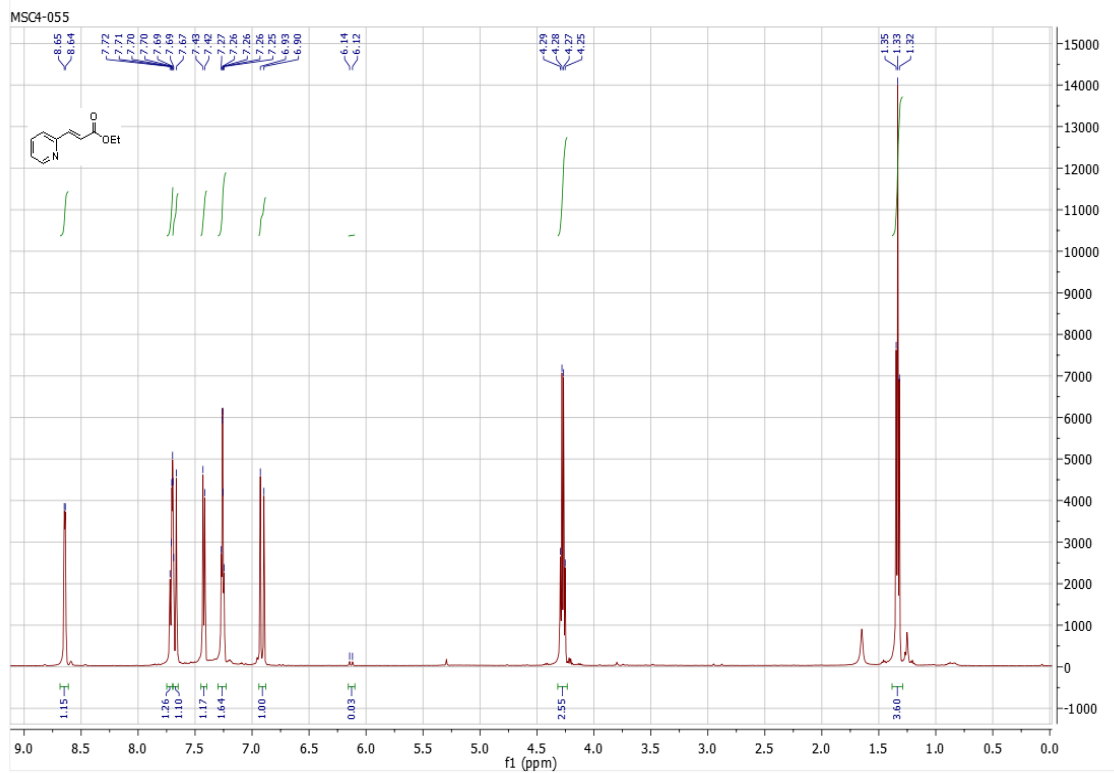


Ethyl-(E)-Dodec-2-ene:

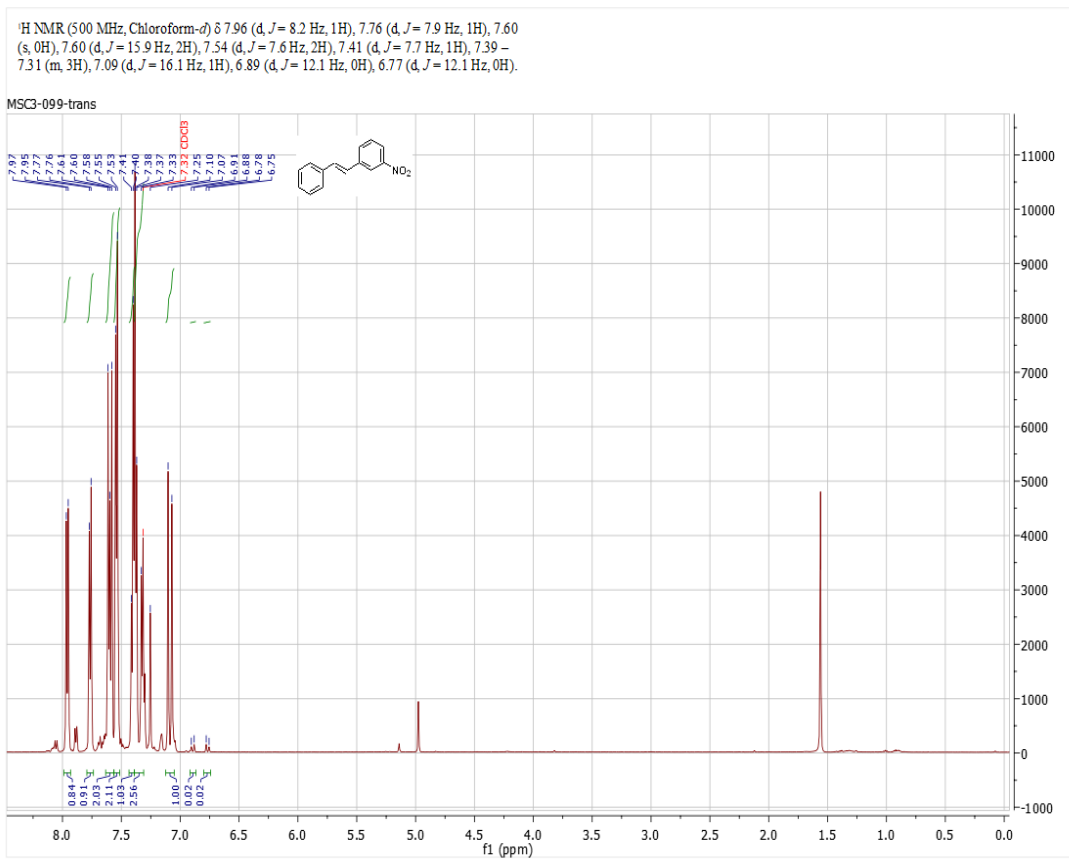


Ethyl-(E)-3-(pyridine-2-yl)acrylate:

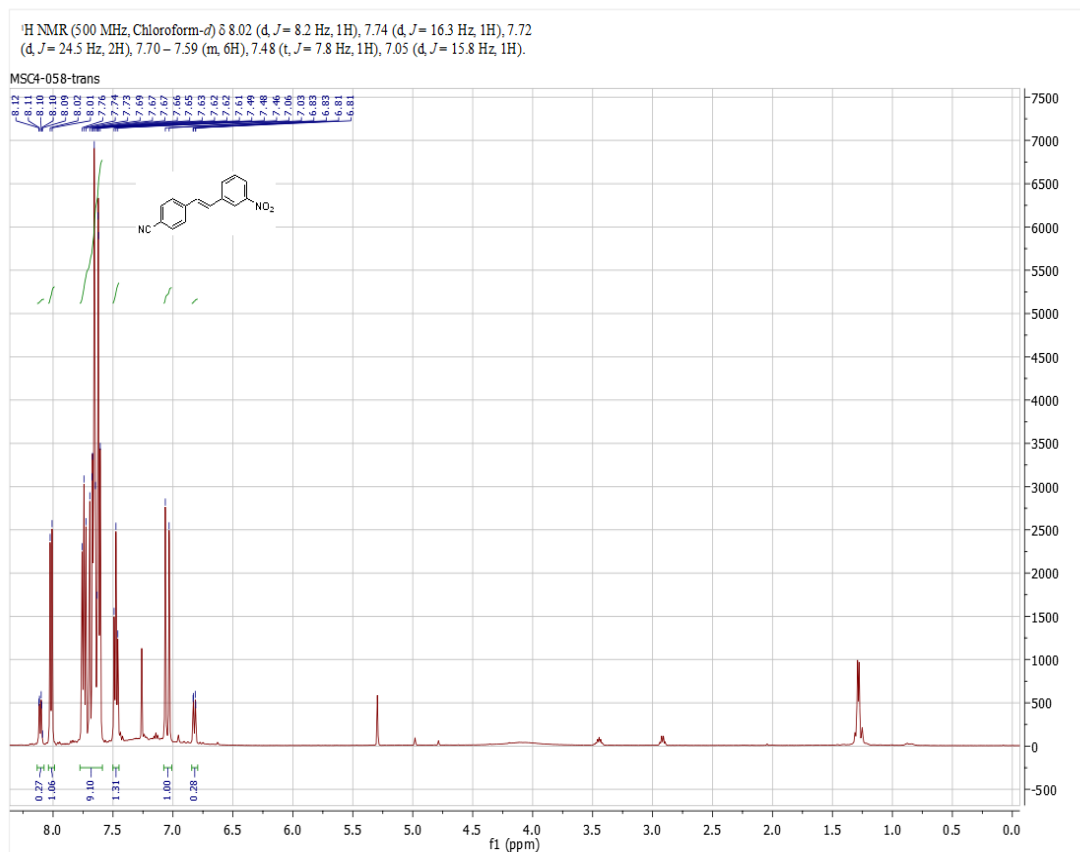
¹H NMR (500 MHz, Chloroform-*d*) δ 8.64 (d, *J* = 4.7 Hz, 1H), 7.71 (dd, *J* = 6.4, 4.7 Hz, 1H), 7.68 (d, *J* = 14.4 Hz, 1H), 7.42 (d, *J* = 7.8 Hz, 1H), 7.30 – 7.23 (m, 2H), 6.91 (d, *J* = 15.7 Hz, 1H), 6.13 (d, *J* = 12.5 Hz, 0H), 4.27 (q, *J* = 7.2 Hz, 3H), 1.33 (t, *J* = 7.2 Hz, 4H).



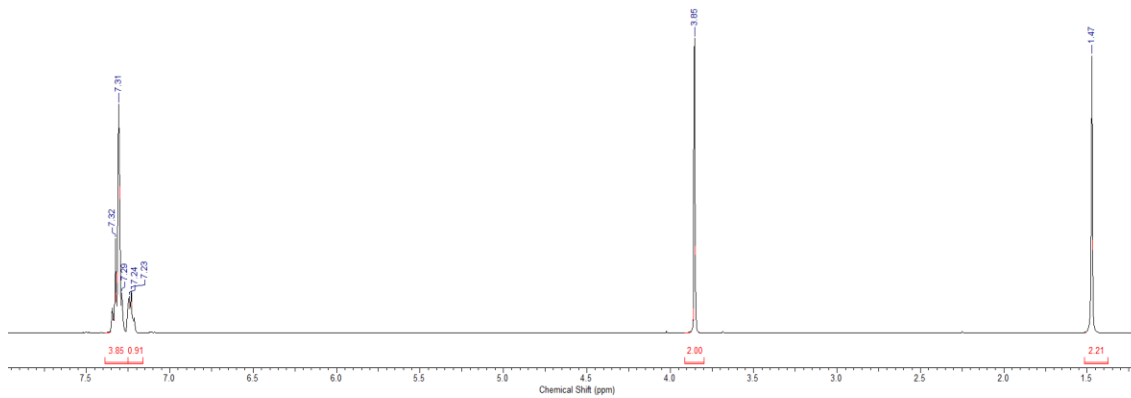
(E)-3-nitrostilbene:



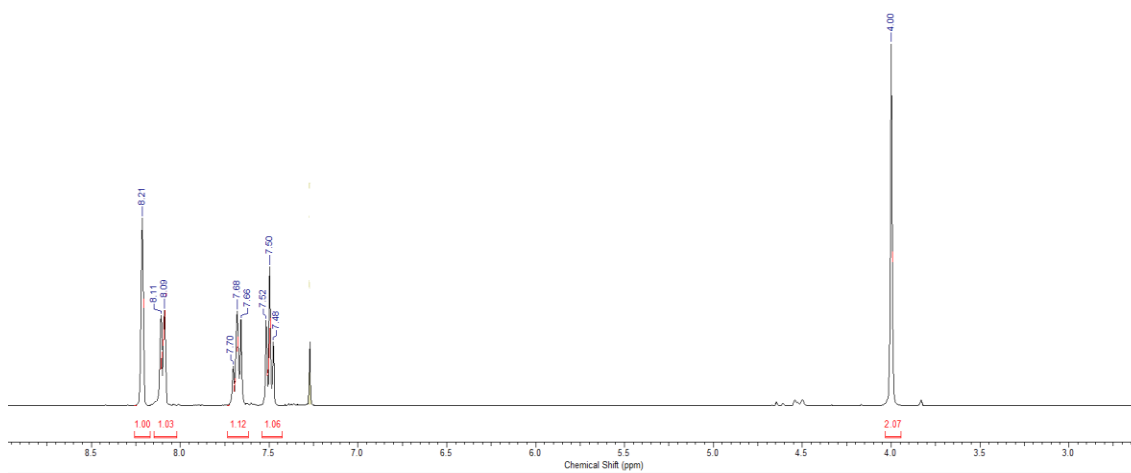
(E)-4-Cyano-3'-nitrostilbene:



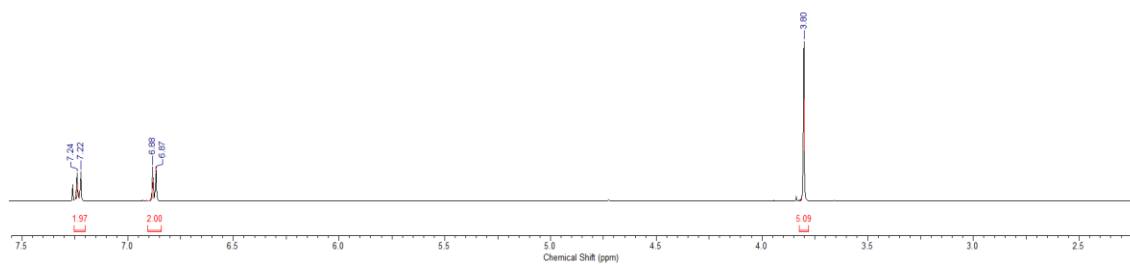
Benzylamine:



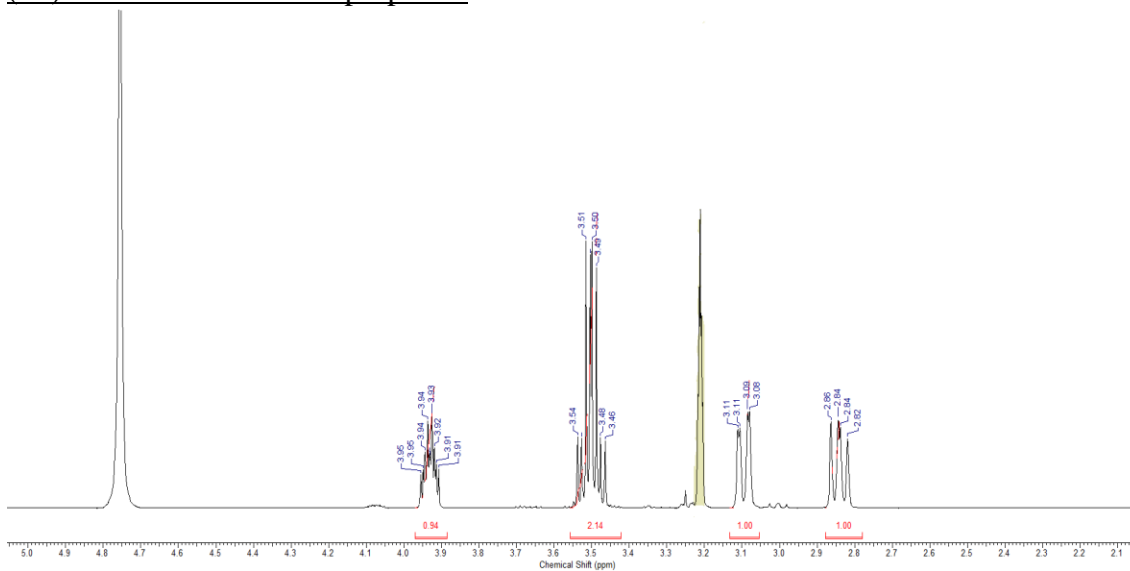
m-Nitrobenzylamine:



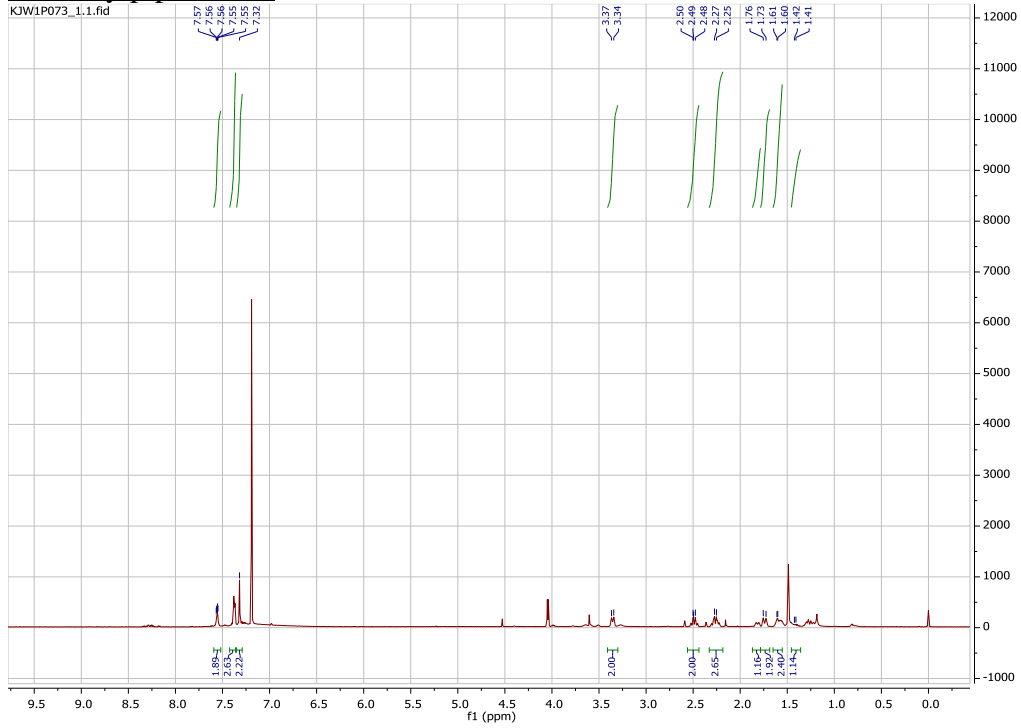
p-Methoxybenzylamine:



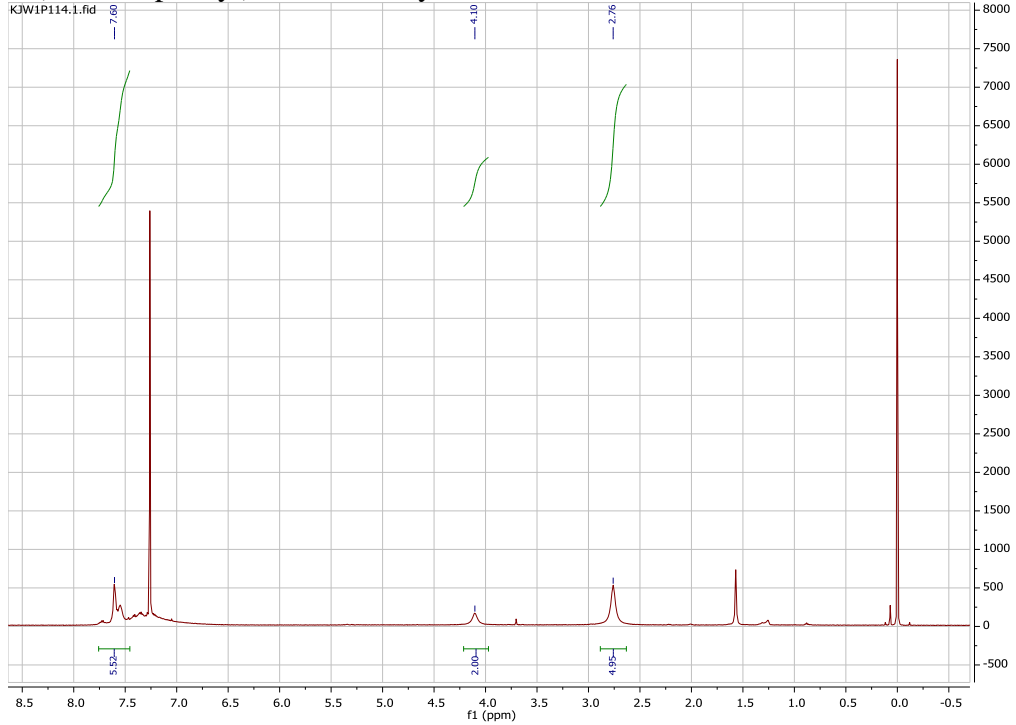
(2S)-1-Amino-3-chloro-2-propanol:



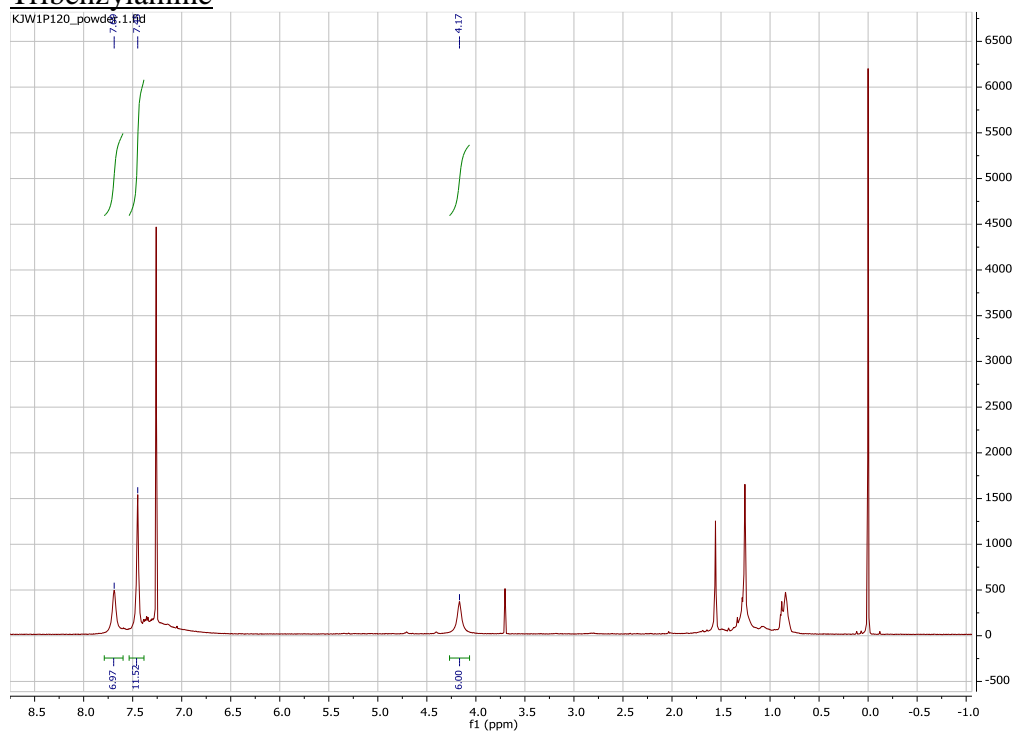
***N*-Benzylpiperidine:**



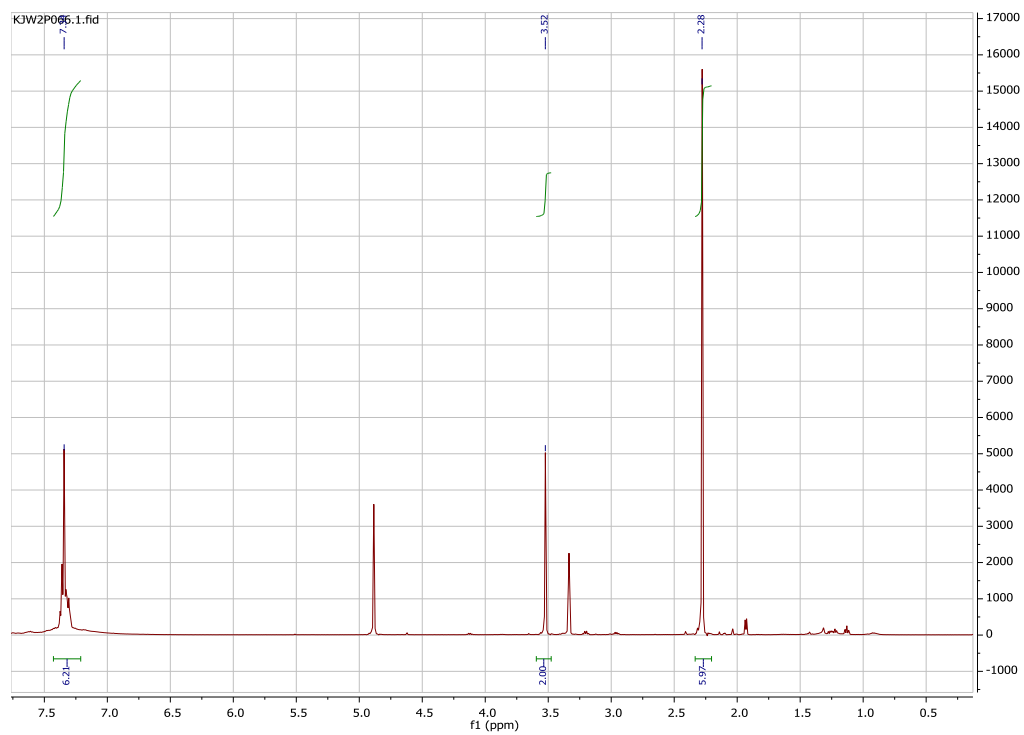
1-(4-bromophenyl)-*N,N*-dimethylmethanamine



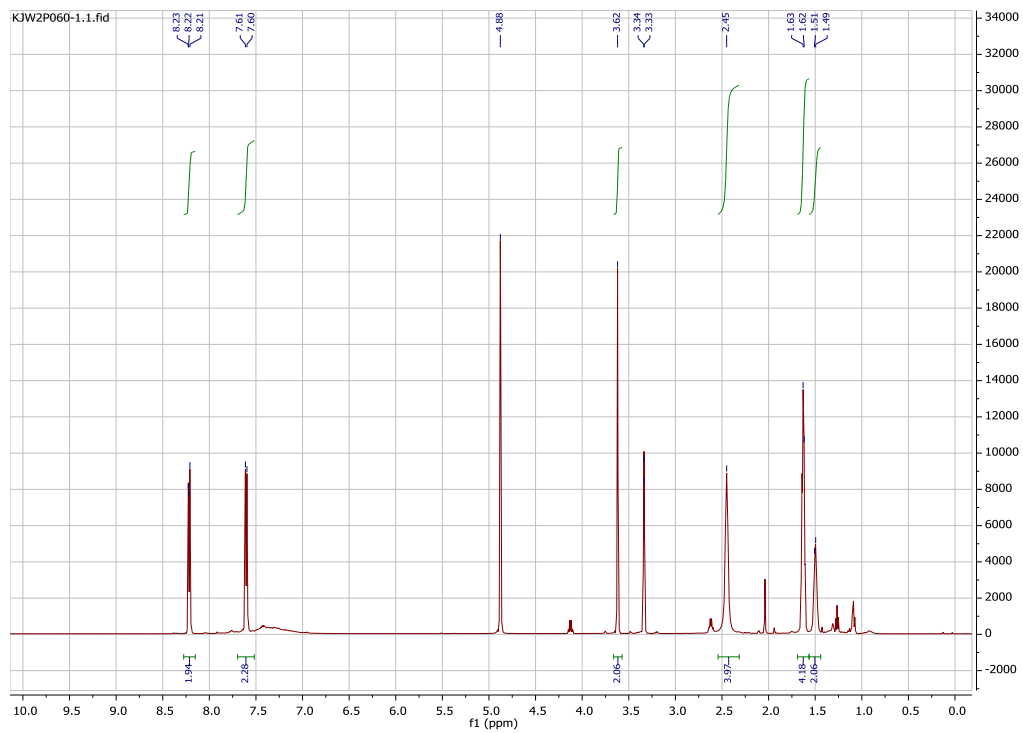
Tribenzylamine



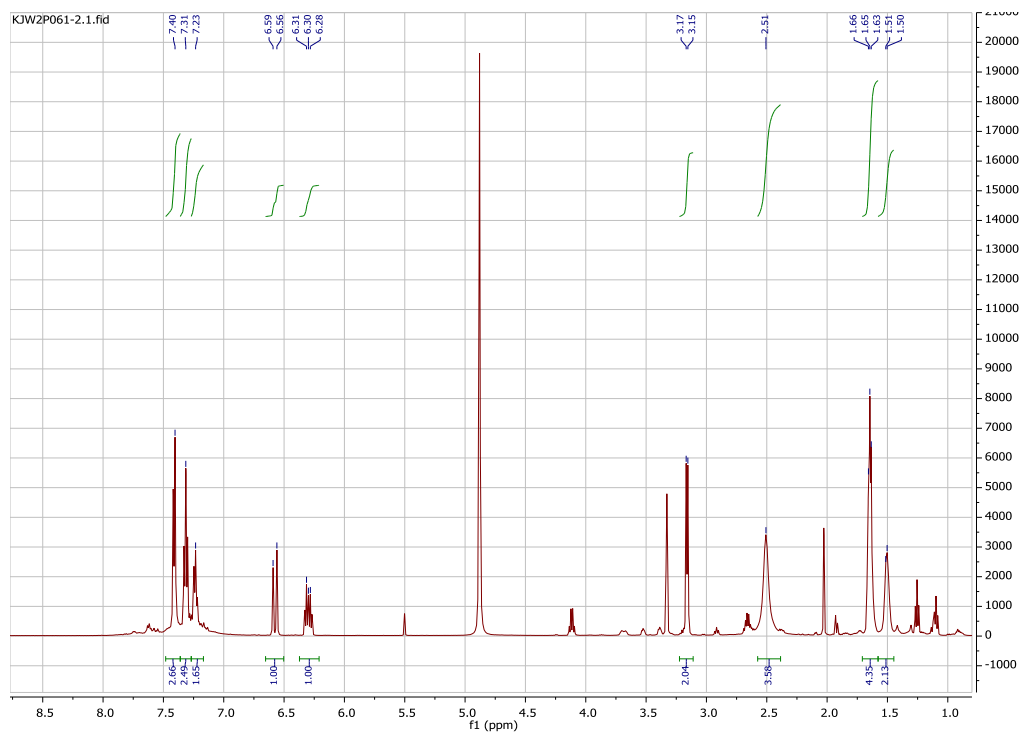
N,N-dimethylbenzylamine



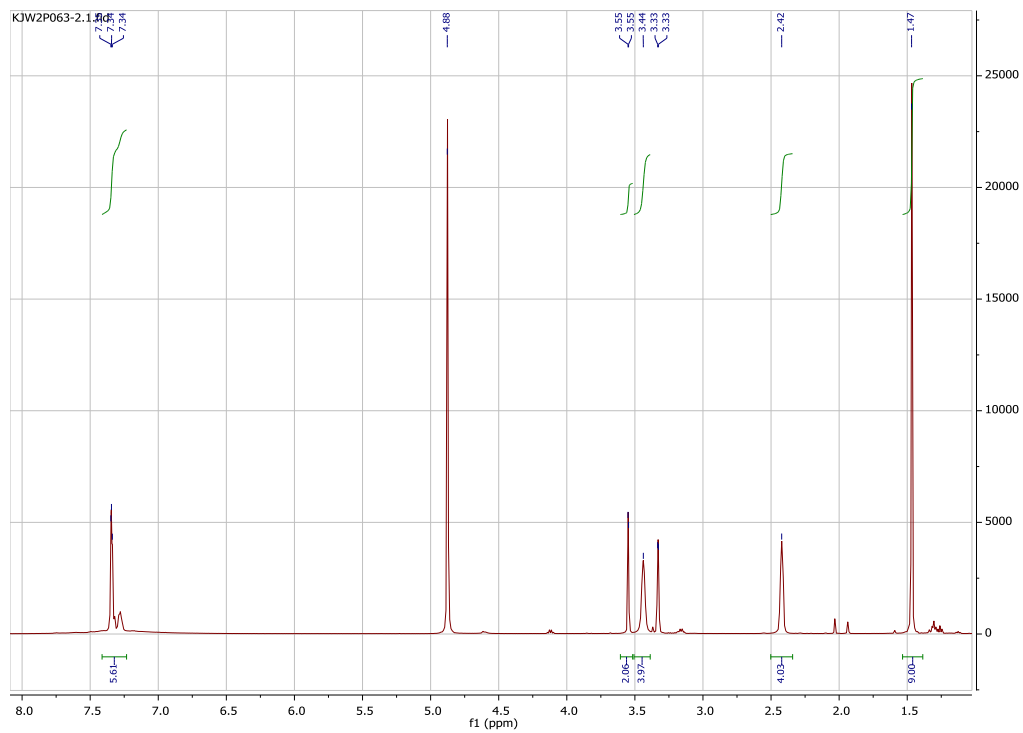
1-(4-nitrobenzyl)piperidine



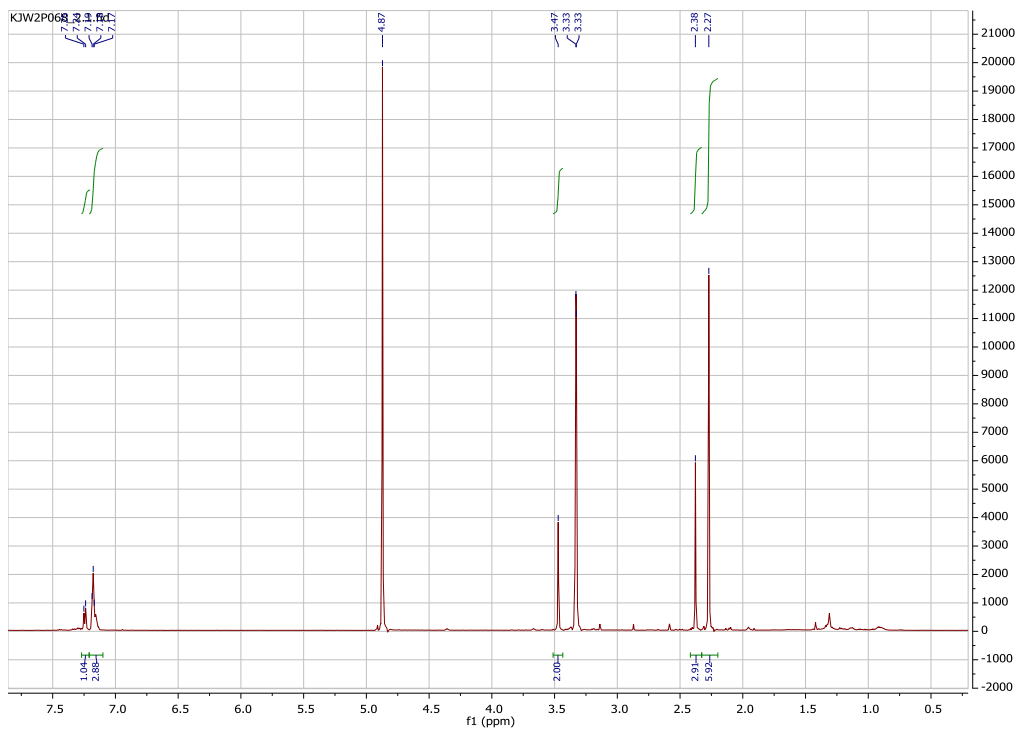
1-cinnamylpiperidine



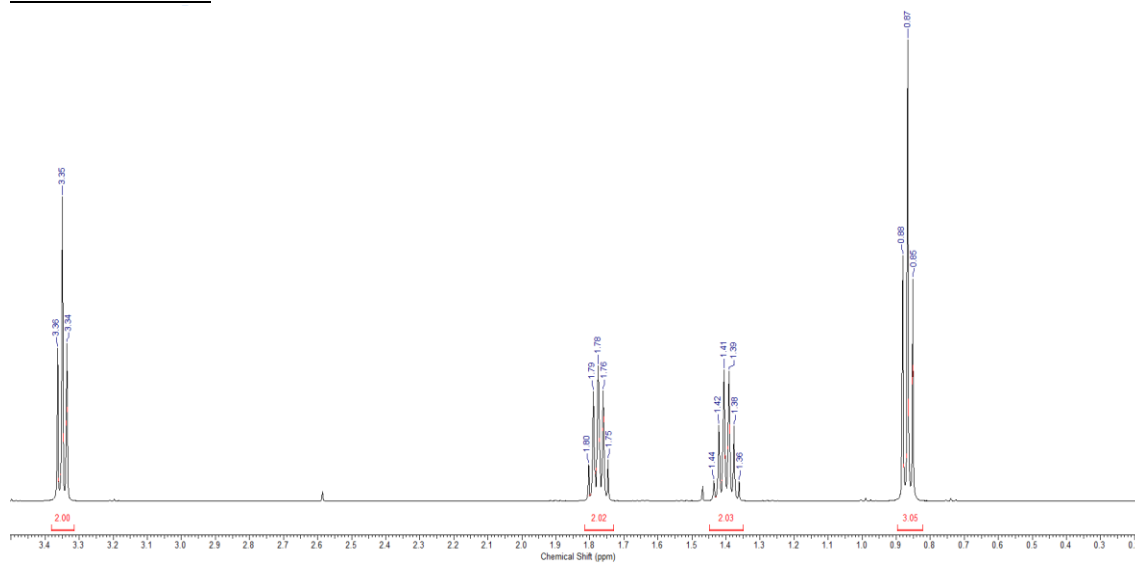
1-boc-4-benzylpiperazine



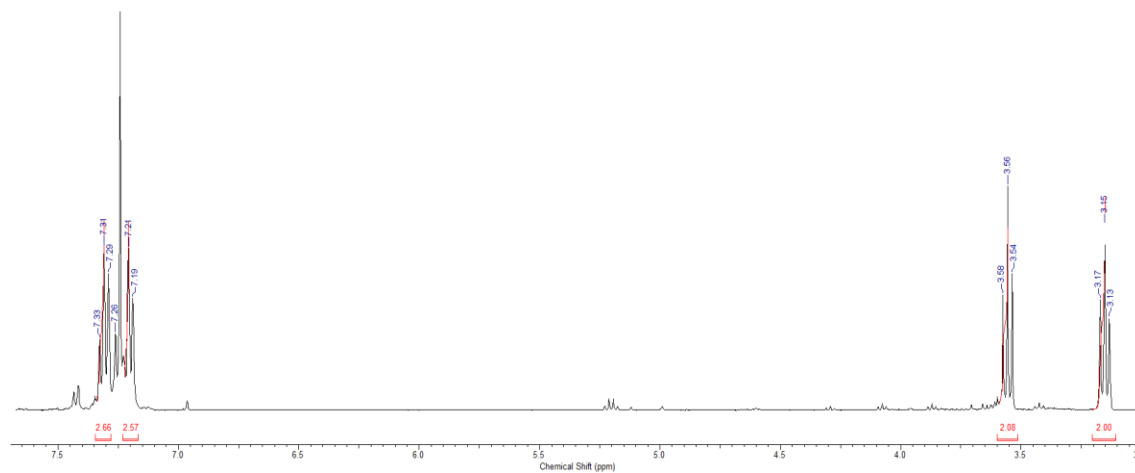
N,N-dimethyl-1-(*o*-tolyl)methanamine



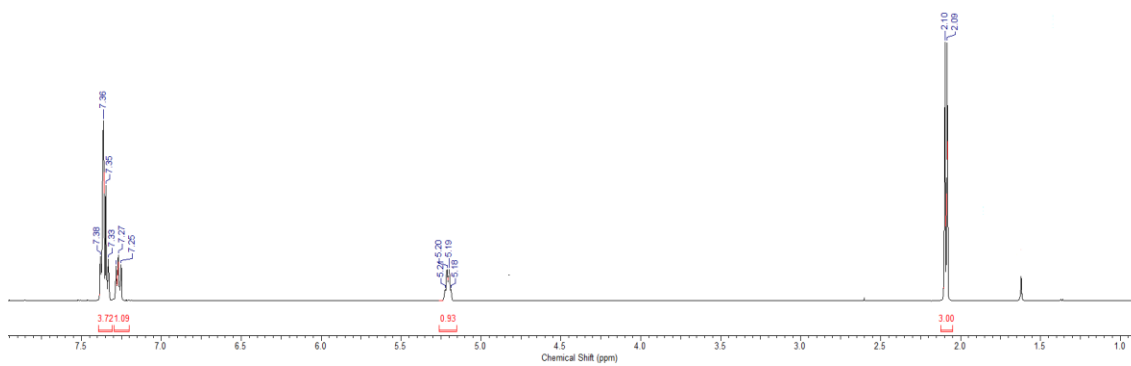
1-Bromobutane:



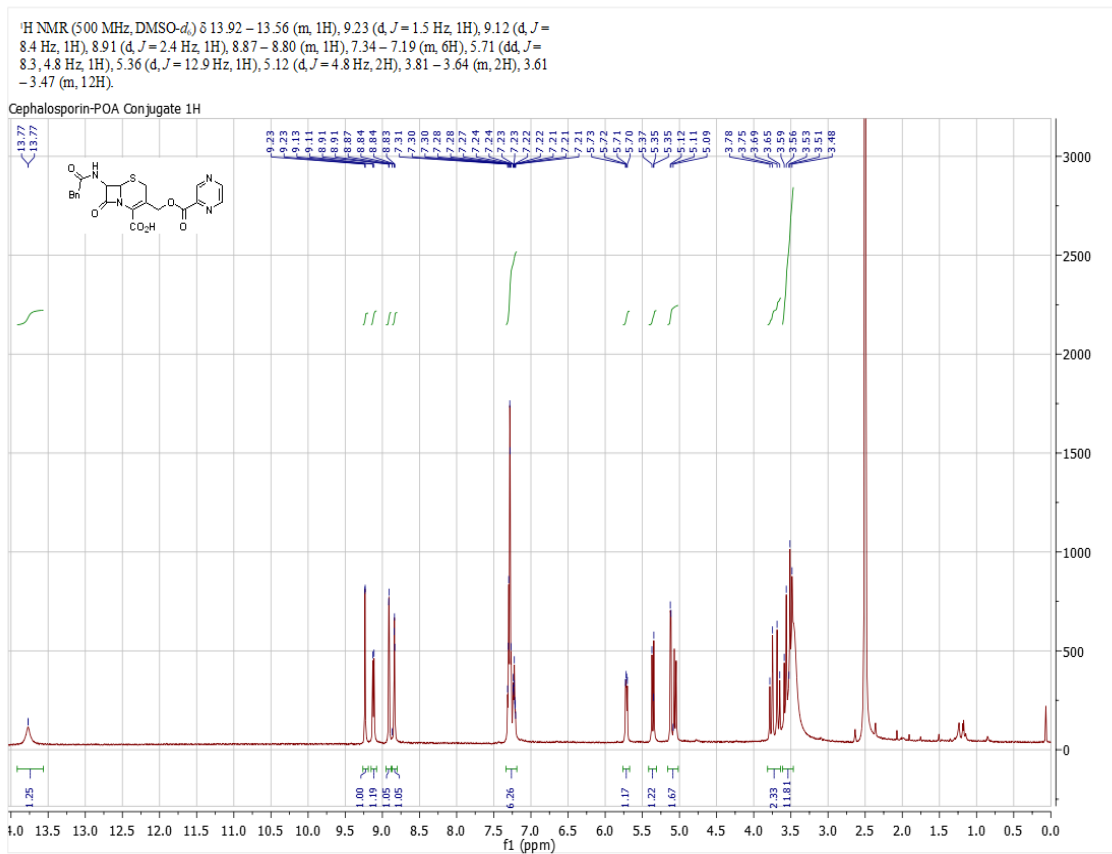
1-Bromo-2-phenylethane:



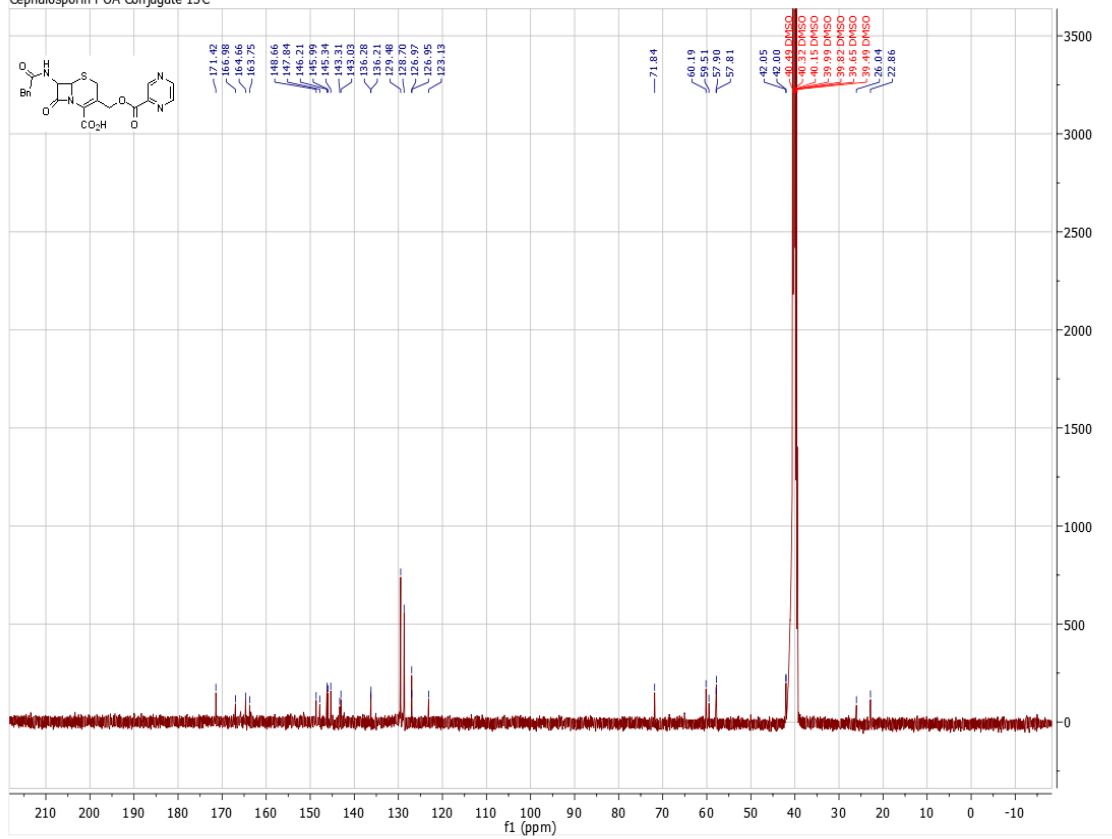
1-Bromo-1-phenylethane:



Conjugate 1:

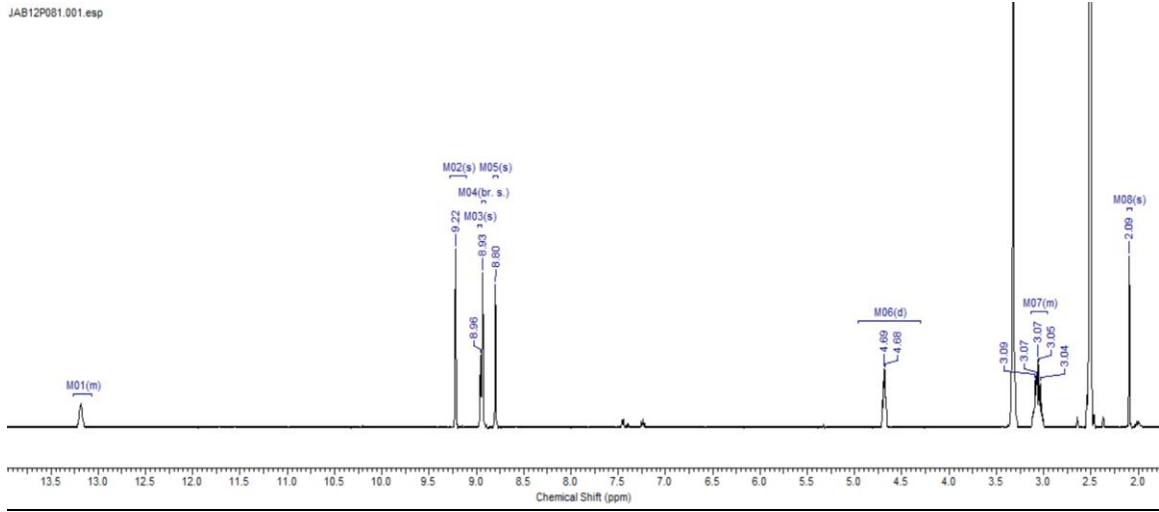


Cephalosporin-POA Conjugate 13C

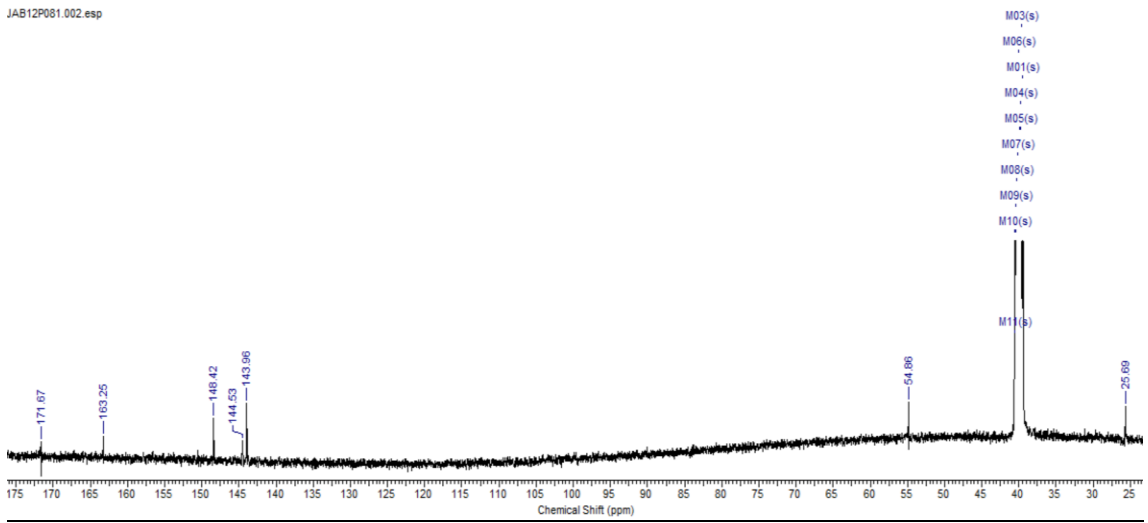


Compound 3:

JAB12P081.001.esp

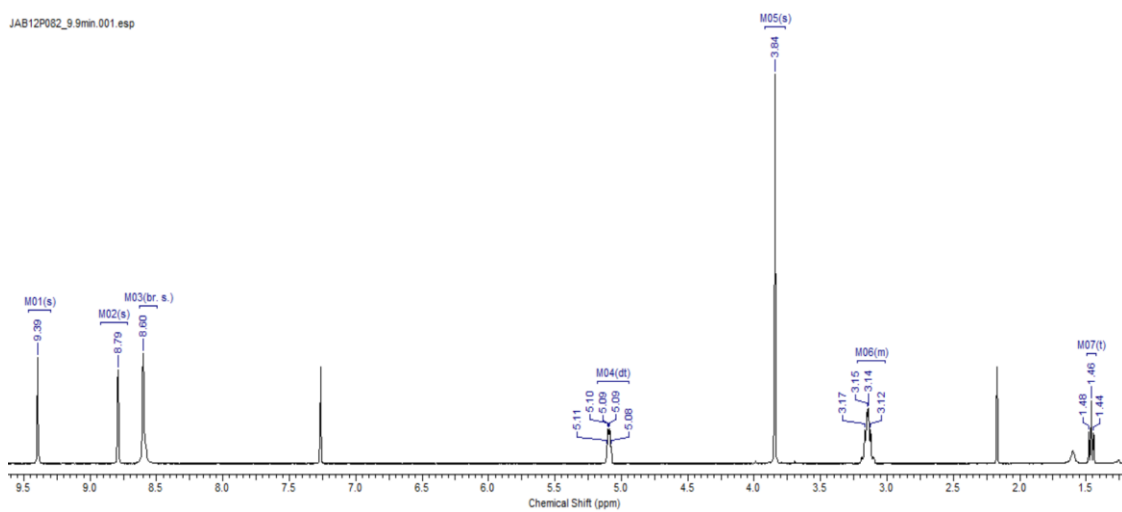


JAB12P081.002.esp

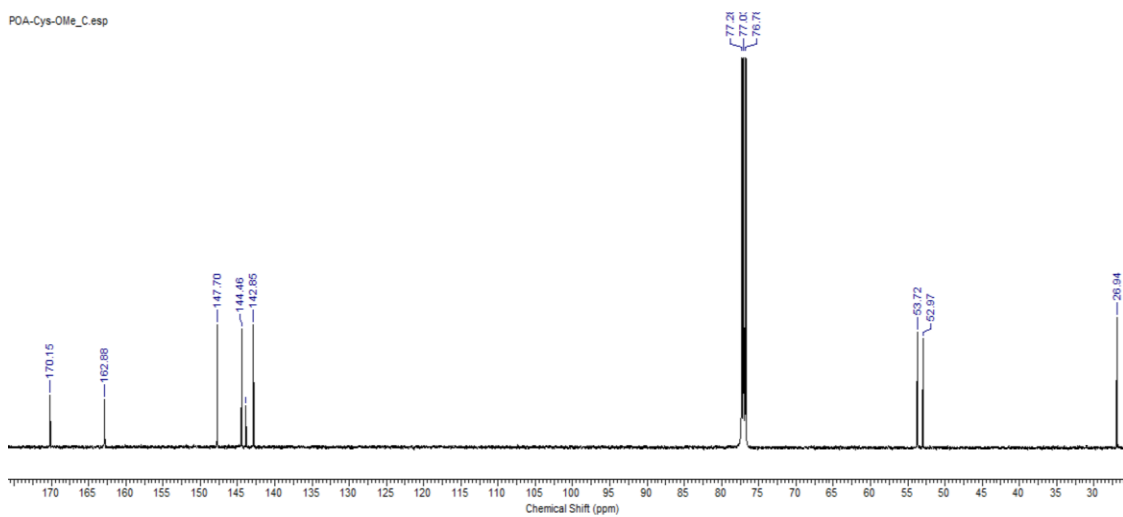


Compound 4:

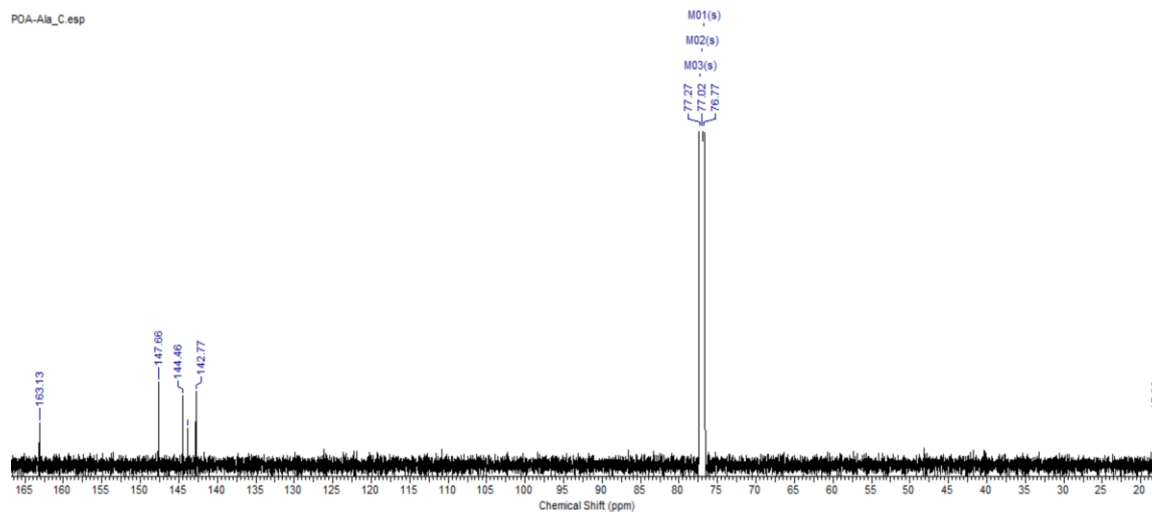
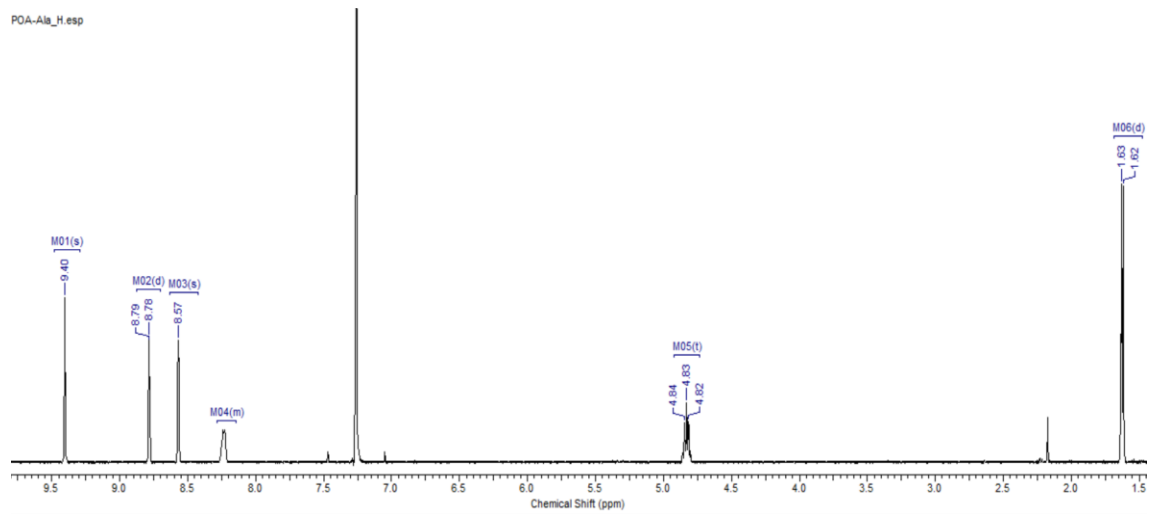
JAB12P082_9.9min.001.esp



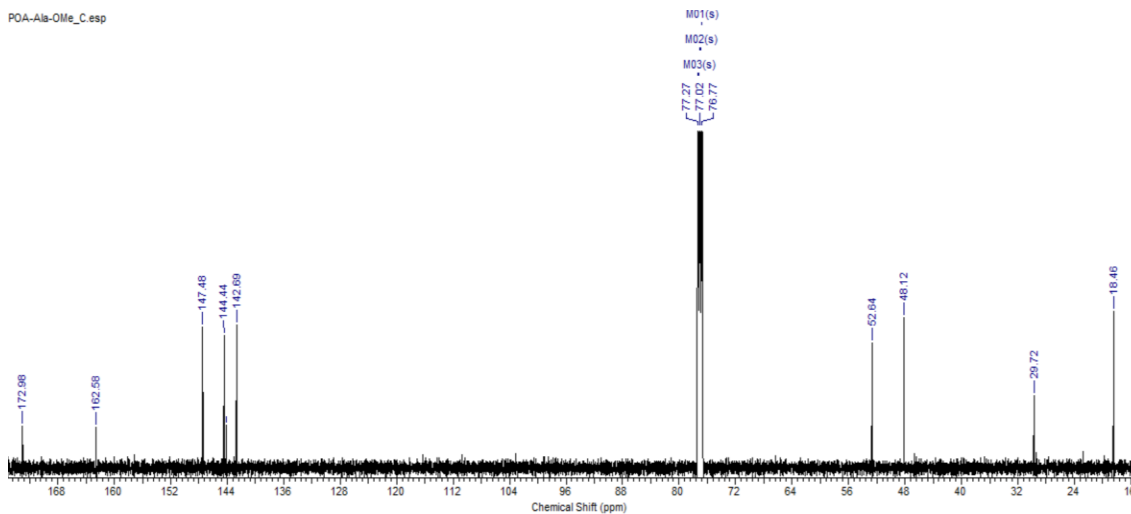
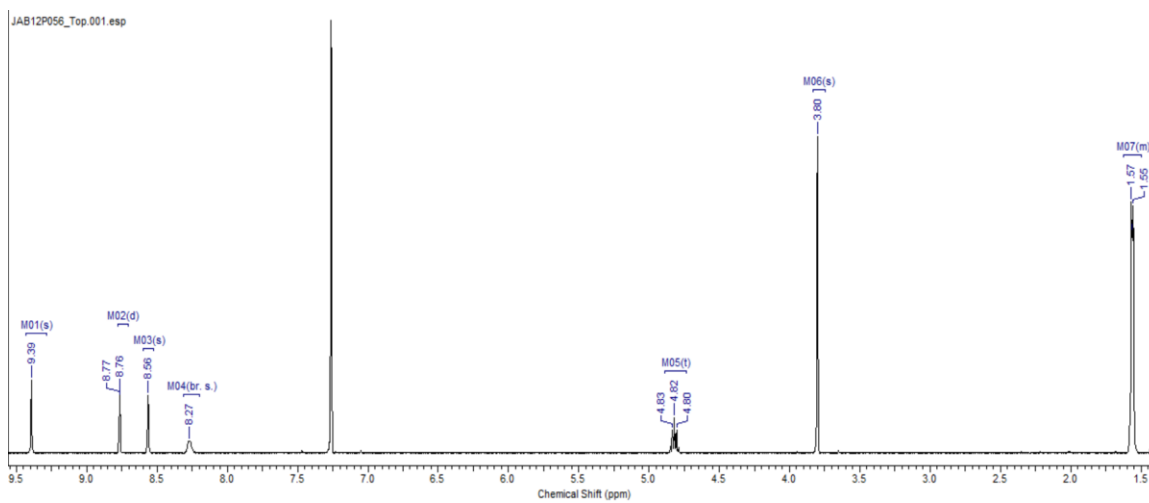
POA-Cys-OMe_C.esp



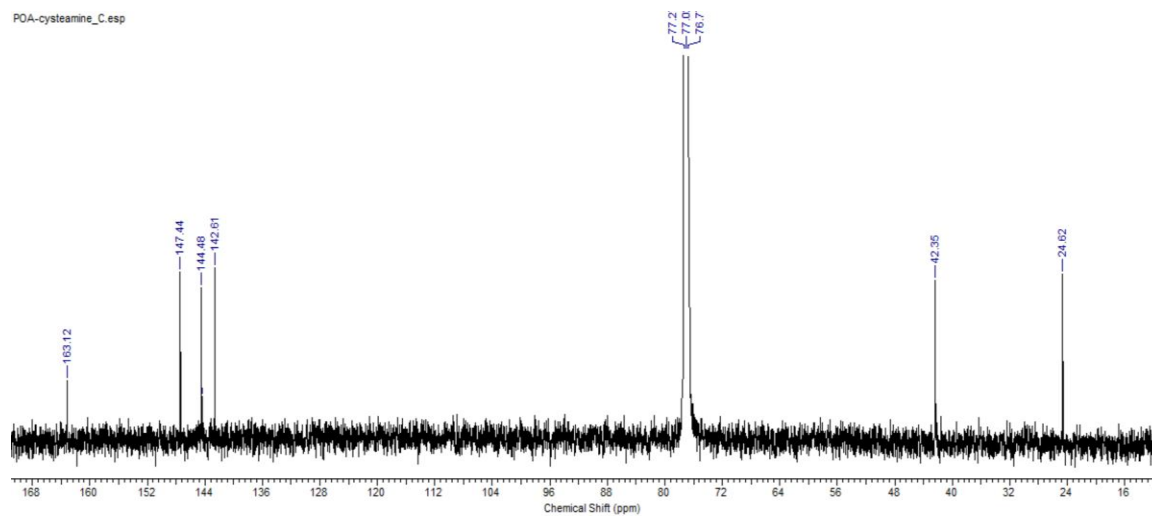
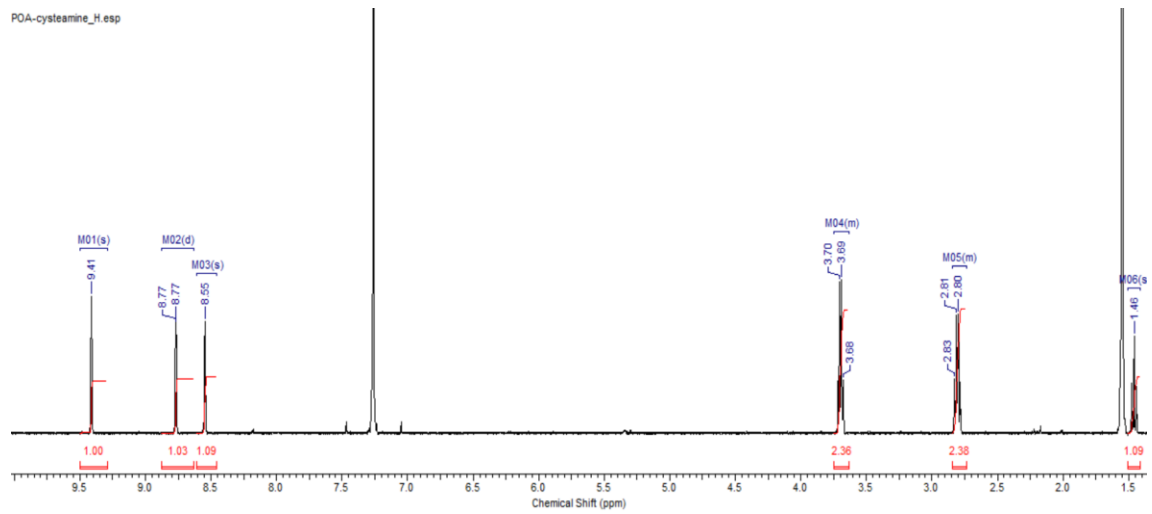
Compound 5:



Compound 6:

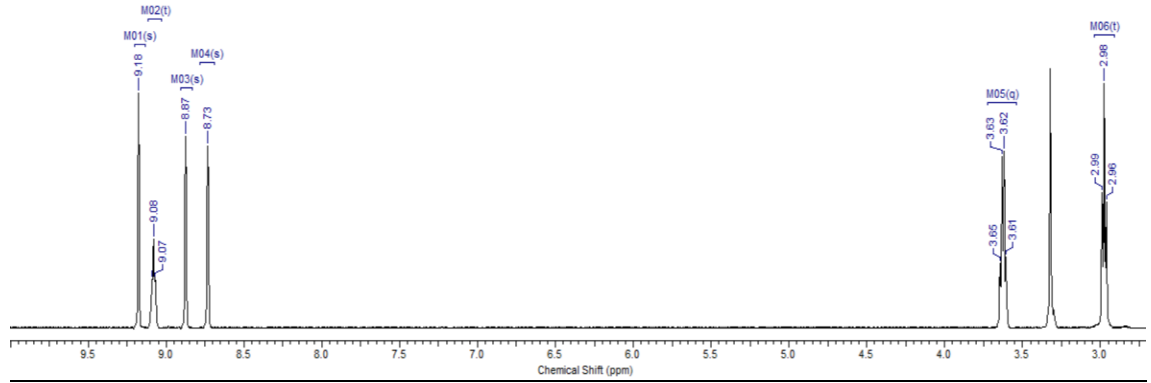


Compound 7:

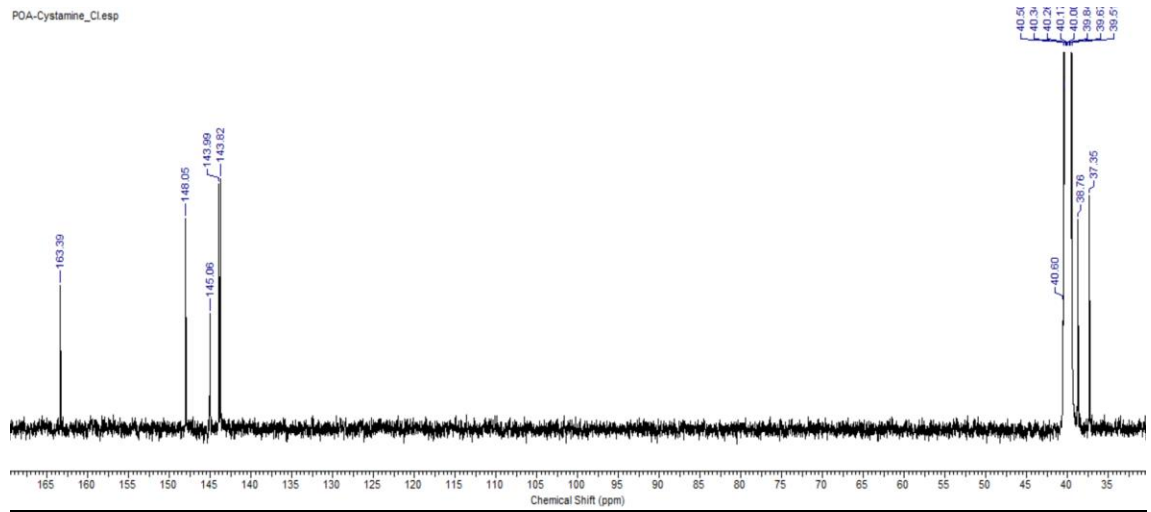


Compound 8:

POA-Cystamine_H.esp

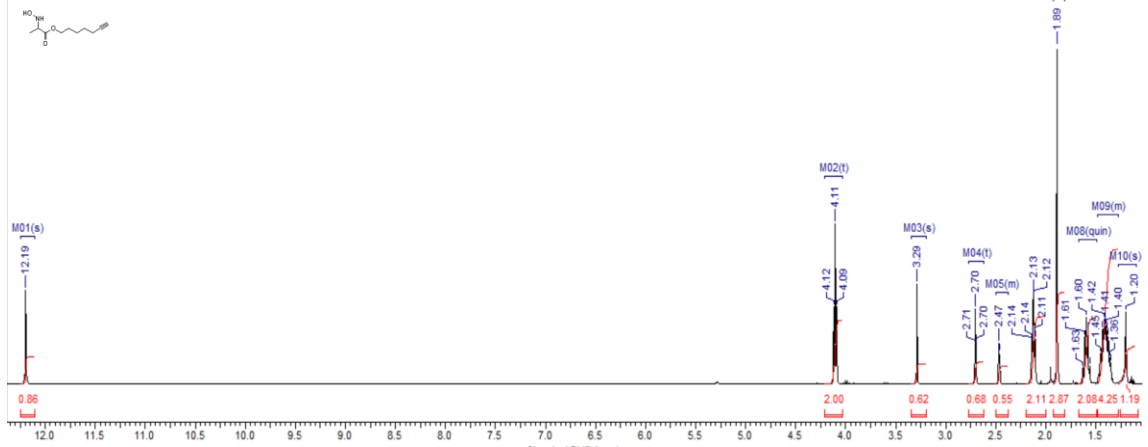


POA-Cystamine_Cl.esp

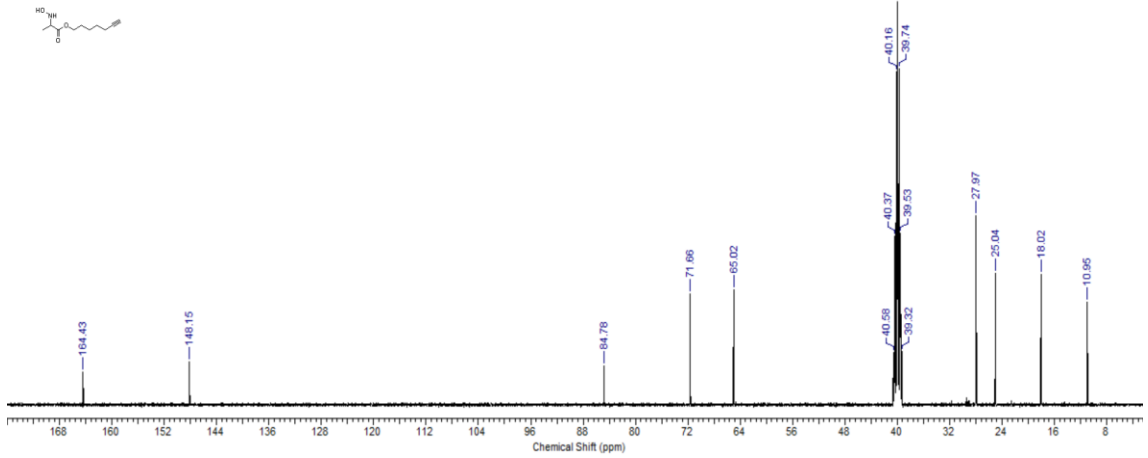


CDB-I-143:

PROTON_CDB-I-143_20150610_01

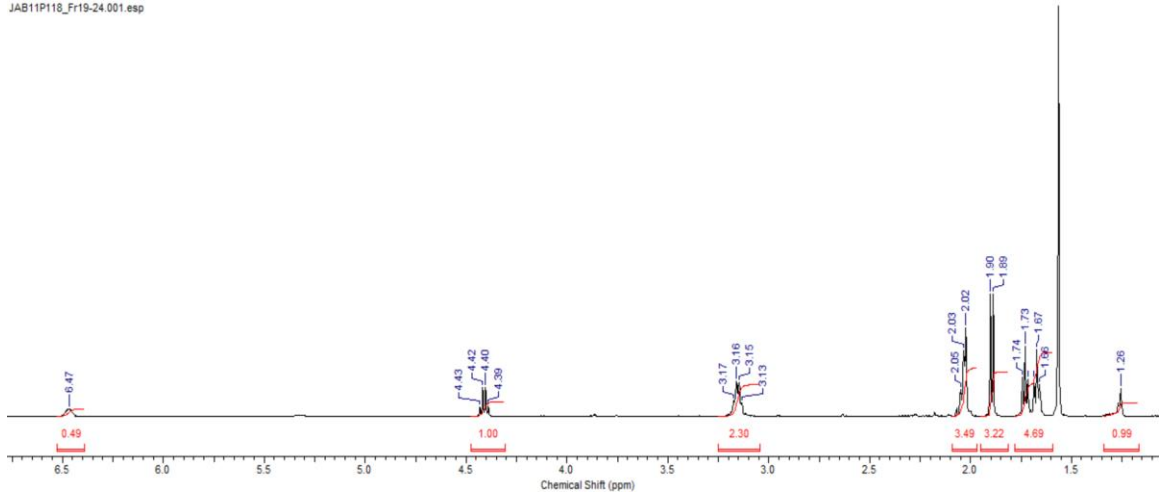


CARBON_CDB-I-143_20150611_01

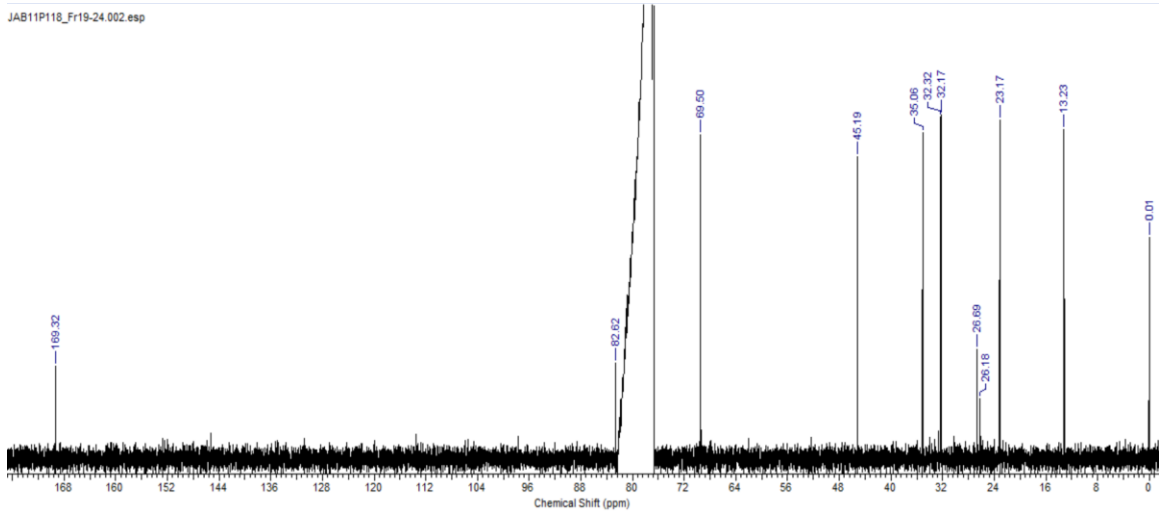


JAB11P118:

JAB11P118_Fr19-24.001.esp



JAB11P118_Fr19-24.002.esp



Appendix II: Coordinate outputs

Output information for silanes considered in the Mulliken charge study is included below.

Silane	M06-2X	B3LYP
	Si -1.2425507588 0.127348167 0.0289971408	Si 0.1561039569 -0.1896116898
	C 0.6319930165 -0.0843367981 0.1387286696	0.2385895174
	H 0.9230868103 -0.9373216261 -0.4872854261	C 1.86 74708158 -0.848891195 -
	H 1.1059095841 0.7976806231 -0.3123968678	0.2667238614
	C 1.1464584175 -0.285113758 1.5705432535	H 1.9645246471 -1.8654198963
	H 0.8916951743 0.5663405178 2.2102402769	0.139 3704164
	H 0.7069178142 -1.1785621288 2.0254284479	H 1.8840060092 -0.9639512998 -
	H 2.2344851755 -0.3995607816 1.598934147	1.360103267
	C -1.7847392138 0.108311216 -1.7814760531	C 3.067249713 0.0044 435504
	H -1.1580194659 0.8231080524 -2.3316191358	0.1855864949
	H -1.5527560336 -0.8796250393 -2.1989023219	H 3.0329546176 1.0125255671 -
triethylsilane	C -3.2668490214 0.4398378267 -1.999890046	0.243091433
	H -3.9150229915 -0.2468984774 -1.4446307967	H 3.09165 66044 0.1135337348
	H -3.498741304 1.4554194413 -1.6621364477	1.2759363936
	H -3.5458484805 0.3750729634 -3.0562066688	H 4.01927746 -0.4453031734 -
	C -1.7883619178 1.7329105393 0.8740168702	0.12051530 54
	H -1.0671483197 1.9797617523 1.6633371303	C -1.1485032846 -1.5040169584 -
	H -1.7183941451 2.5475788666 0.1402615318	0.1969506857
	C -3.2027672997 1.6776793751 1.4698439567	H -1.1014917857 -1.6801 305953 -
	H -3.9492895606 1.4152897601 0.7135432856	1.2813998663
	H -3.2638485583 0.9216487069 2.2586160747	H -0.8203352717 -2.4445787654
	H -3.4973151597 2.6380418383 1.9046883866	0.2680967609
	H -1.8954737621 -1.0110010371 0.742814592	C -2.6 019036237 -1.2070172688
	SCF E = -527.628793965	0.2172296655

	H	-2.6841481956	-1.0249072324	1.2	
					949272674
	H	-2.9960814842	-0.3231743324	-	
					0.2957389499
	H	-3.2661851459	-2.0452679612	-	
					0.0247427168
	C	-0.1818078555	1.493200529	-	
					0.5882767195
	H	0.7717199196	2.0374247162	-	
					0.6296670462
	H	-0.4616872778	1.3094668354	-	
					1.6356421494
	C	-1.2415710911	2.3822694432		
					0.0903070914
	H	-2.22351939	38	1.8985407721	
					0.1175011282
	H	-0.9637153283	2.611547588		
					1.1251634709
	H	-1.3621802184	3.3361813182	-	
					0.4370872482
	H	0.1487972128	0.0141123138		
					1.7231740421
					SCF E = -527.8236435

	Si	-1.583528264	-1.1227575522	-0.1613802168	Si	-3.6387663243	-0.2750371044		
	C	0.292863386	-1.1168763908	0.0230449061		0.0000243571			
<i>n</i> -Hexylsilane	H	0.6995250209	-2.0156857278	-0.4582233241	C	-1.992	5453245	0.6604314933	-
	H	0.7009895447	-0.2603933232	-0.5289680527		0.0000176975			
	C	0.7476677845	-1.0582330361	1.4874480748	H	-1.9775149233	1.3220152128	-	

H	0.3359219958	-0.1594855539	1.9669332964	0.877	5010954
H	0.3343401355	-1.9147184642	2.0377003488	H	-1.9775082861 1.32208381
C	2.2682719996	-1.0532254549	1.6458729698	0.8774137914	
H	2.6830687999	-1.9530207538	1.1703493001	C	-0.7407614876 -0.237 7272719
H	2.6846709692	-0.1953761856	1.0995036785	0.000012352	
C	2.7199750468	-0.9948892123	3.1037415083	H	-0.7603161053 -0.8983506374
H	2.3027114866	-0.0954509937	3.5783434621	0.8781290044	
H	2.3011161282	-1.85246854	3.6491392828	H	-0.76 03189273 -0.8984128597 -
C	4.2392232397	-0.9897659931	3.2653779095	0.8780574797	
H	4.654501326	-1.8884526696	2.7913463732	C	0.5759231068 0.5537266639 -0.000
H	4.6561024173	-0.1328776858	2.7206266648	0179642	
C	4.6747634194	-0.9312458944	4.7281589624	H	0.5982317208 1.2139272524 -
H	4.2920593309	-0.0267820018	5.2125471094	0.8792014495	
H	4.2904226779	-1.7931074202	5.2837016595	H	0.5982361926 1.213 9862069
H	5.7640683381	-0.9283712053	4.824583769	0.8791211143	
H	-1.9875514533	-1.1798512136	-1.5881478914	C	1.8264947082 -0.3351709231
H	-2.1537805749	0.1063311847	0.4458996734	0.0000087488	
H	-2.1557427547	-2.2981359125	0.5426705359	H	1.802 4617715 -0.9959535308
SCF E =	-527.6092334			0.8789932607	
				H	1.8024581931 -0.9960113482 -
				0.878	9321633
				C	3.1424786665 0.4544515536 -
				0.0000199893	
				H	3.1671197945 1.114 4177923 -
				0.8783326264	
				H	3.1671238401 1.1144752851
				0.8782493056	
				C	4.386 944257 -0.4410090335

				0.0000065078
			H	4.4082044701 -1.0886641349
				0.88468 84257
			H	4.4081997105 -1.0887228891 -
				0.8846324863
			H	5.3075295253 0.1529 353855 -
				0.0000156884
			H	-4.7855617577 0.6746962492
				0.0000305393
			H	-3.75 49159197 -1.1433794225
				1.20462227
			H	-3.7549589013 -1.1434147245 -
				1.204 5440372
				SCF E = -527.8058139
			Si	-5.8461276842 2.1662623296 -0.3588760916
			Si	1.60537400 -0.23308600 -
			O	-4.2131052954 2.0042387991 -0.1044511802
				0.38034300
			C	-6.6728021718 2.7616214055 1.2158741616
			O	-0.00031000 -0.23180600 -
			C	-6.5653592792 0.5191099859 -0.8881513988
				0.00004600
			Si	-3.2035112255 1.4845182207 1.1064352145
			C	2.58745700 -1.01444500
			C	-1.4632516945 1.4629215379 0.431335729
				1.02057300
			C	-3.7345676277 -0.22191876 1.6795758562
			C	2.17649300 1.52731900 -
			H	-6.5609182317 2.0248735503 2.0192647379
				0.72065000
			H	-7.7445775558 2.9213217434 1.0592738571
			Si	-1.60637000 -0.23052500
			H	-6.2363456631 3.7036054277 1.5607993075
				0.38034100
			H	-6.4742978778 -0.2216363953 -0.0866899941
			C	-2.58725600 -1.01912100 -
			H	-6.0458871139 0.1302321917 -1.7688134514
				1.01715400
			H	-7.6273661926 0.6170338889 -1.1361023159
			C	-2.17532000 1.53079400
			H	-3.7262452075 -0.9273667837 0.8419741669
				0.71627700

TMDSO

H	-4.744987531	-0.2102515843	2.102089591	H	2.51298400	-0.41591400
H	-3.0584493939	-0.6048489463	2.4509859037		1.93640000	
H	-1.3875448391	0.7633714066	-0.4068082848	H	3.64813300	-1.09494900
H	-0.7446052993	1.1571307987	1.1981209111		0.75378400	
H	-1.176341038	2.4544009193	0.0698912301	H	2.21975100	-2.02205200
H	-6.0214584755	3.1655352385	-1.4392468035		1.24386300	
H	-3.3022380325	2.431035496	2.2500349837	H	2.06598000	2.15716200
SCF E = -815.0141509					0.16981800	
				H	1.59396600	1.98026900 -
					1.53043900	
				H	3.23235100	1.54349700 -
					1.01682800	
				H	-2.08721100	2.15557900 -
					0.18000500	
				H	-1.57480000	1.98915900
					1.51014800	
				H	-3.22399900	1.54531100
					1.03722200	
				H	-2.48853900	-0.44051100 -
					1.94285400	
				H	-3.65274900	-1.07320000 -
					0.76389500	
				H	-2.23609700	-2.03771400 -
					1.21603100	
				H	1.78142800	-1.04947700 -
					1.61684600	
				H	-1.78302400	-1.03944700
					1.62179000	

TMDSA

			SCF E = -815.234843349
			Si 1.49089900 -0.02841900
			0.32527300
Si	-5.7770650358	2.3086951635 -0.37389337 14	
C	-6.7059311439	0.7829137101 0.210504611	C 1.54326200 1.84317800
			0.07428600
C	-6.1839006984	2.69594741 01 -2.1642847117	
Si	-3.1736358699	1.398370783 1.1115271831	C 3.01969100 -0.84448900 -
			0.41920100
C	-3.225192 3215	-0.4797023023 1.1718587765	
C	-3.900068614	2.0851707349 2.70228463	Si -1.64073900 -0.54584900 -
			0.13075200
H	-5.6408352966	3.5791518489 -2.5148231755	
H	-7.2532121998	2.89403479 03 -2.2858308419	C -2.42110700 0.71244500 -
			1.30536000
H	-5.9199725681	1.8528620481 -2.8106964859	
H	-6.47466 33588	0.5399719219 1.2529482534	C -1.94494300 -0.02874100
			1.65718700
H	-6.4424688512	-0.0843482907 -0.4036703174	
H	-7.7877437589	0.9377497308 0.1429148626	H 3.02561500 -1.92435500 -
			0.23373700
H	-2.8275487775	-0.911 2131614 0.2484983058	
H	-4.254471959	-0.8344281741 1.2906572806	H 3.93184000 -0.42520600
			0.02051600
H	-2.63 67297397	-0.8655705312 2.0109357086	
H	-3.8432946773	3.1772676478 2.719 5838351	H 3.06753600 -0.68342900 -
			1.50269000
H	-3.3672737446	1.6973670627 3.5762103198	
H	-4.9539227362	1.80 46055902 2.8090970727	H 0.65050600 2.32956100
			0.48377900
N	-4.060240633	2.0369876407 -0.2487569727	
H	-3.5 039582753	2.3451138911 -1.0379804055	H 1.60458100 2.09716700 -
			0.99028000
H	-1.762128144	1.8368264701 0.954 3728203	
H	-6.2067912565	3.4505658455 0.4813349025	H 2.41538600 2.27594000
			0.57965600
SCF E = -795.1144843			H -2.27036800 0.41909800 -
			2.35057000

	H	-1.97973000	1.70689000	-
		1.17044300		
	H	-3.50119700	0.79480800	-
		1.13187200		
	H	-1.52936600	-0.75928200	
		2.35892300		
	H	-3.02154500	0.05085500	
		1.84760900		
	H	-1.49948700	0.94709600	
		1.88286600		
	N	0.07697300	-0.75904900	-
		0.40697400		
	H	0.29521100	-1.43357800	-
		1.12091600		
	H	-2.28841800	-1.86690000	-
		0.38879700		
	H	1.47695600	-0.26992700	
		1.80000800		
		SCF E = -795.329640498		
	Si	-0.0006315725	0.0000762636	
	Si	-0.7708861101	0.9378101692	-0.1023810634
		0.5079767649		
	Cl	1.2697805422	0.9372636398	-0.0970179924
	Cl	0.8396679686	1.7489044028	-
	Cl	-1.4465564861	2.0923253242	1.4383660654
		0.1788917991		
	Cl	-1.4486198822	-0.9718560589	0.1337905344
	Cl	1.0941171253	-1.6018263364	-0
	H	-1.2583880638	1.4769269257	-1.3727675441
		.178573556		
	SCF E = -1670.6935814			
	Cl	-1.9344992608	-0.1469561861	-
		0.1809385046		

trichlorosilane

	H	-0.001787260	6	0.0002668561
		1.9745390949		
		SCF E = -1670.8340696		
	Si	0.0620036604	0.064329856	-
		0.3838372878		
	O	-0.4388187821	1.6341033532	-
		0.4277618435		
	Si	-3.7413945523	0.1666779927	-0.1508212247
	O	-3.8683715305	0.8995714352	-1.6222520963
	O	-4.9726354996	-0.8756258938	0.1416651927
	O	-2.3699970249	-0.7568515	292 -0.1128811284
	H	-3.7411494617	1.2502411817	0.8355817918
	C	-4.06440	33402	0.1320953299 -2.7986807756
	C	-4.9284866465	-2.2748323808	-0.0902648353
	C	-1.1056702872	-0.2360474599	-0.4862206712
	H	-3.9596978233	0.7	960137413 -3.6589399941
(MeO) ₃ SiH	H	-5.0684565489	-0.3073819713	-2.8104118445
	H	-3.3216513455	-0.6724321831	-2.8804687961
	H	-5.7962597139	-2.720052043	1 0.3999749843
	H	-4.0120742852	-2.7112371037	0.3177232498
	H	-4.9778552	811 -2.4931891022	-1.1634238403
	H	-0.3895801596	-1.0600894003	-0.4925616177
	H	-0.764996046	0.5204853501	0.2304984409
	H	-1.1417504537	0.21543	40365 -1.4848168354
		SCF E = -635.4314217		
		1.5247666172		
	H	2.5104812367	-1.7934450396	-
		0.212970992		
	H	1.7245634486	-1.699508309	1

		.3883035177
		H 3.2453446636 -0.8193326617
		1.0820503855
		H -2.4532473925 -2.1114250846
		1.0104376931
		H -2.3289277042 -1.6154749644 -
		0.6942635606
		H -2.8847803408 -0.4495220145
		0.537022296
		SCF E = -635.6340731
		<hr/>
	Si 0.00955900 -0.00159400 -0.96746000	Si -0.01297200 0.01074900 -
	C -0.51752600 1.69705100 -0.35516000	0.91070500
	C -1.68378600 1.88564700 0.37815400	C 0.13930900 -1.78185200 -
	H -2.31549100 1.03334200 0.61456500	0.32752100
	C -2.05166300 3.14234000 0.81763000	C 1.08387500 -2.18006000
	H -2.96550400 3.26897700 1.38879600	0.63558400
	C -1.25723200 4.23344900 0.53287700	H 1.76407800 -1.44623900
	H -1.54585200 5.22080600 0.87826300	1.05993700
	C -0.09025900 4.06674600 -0.19121300	C 1.17138600 -3.51069100
	H 0.53869400 4.92216300 -0.41515800	1.05807300
	C 0.27326000 2.81127400 -0.62861400	H 1.90929500 -3.79393900
	H 1.19690600 2.69420500 -1.19115400	1.80373500
	C -1.20236800 -1.29921400 -0.35055200	C 0.31403600 -4.47337700
	C -2.46736200 -1.42070200 -0.94522600	0.51998800
	H -2.73395200 -0.78063500 -1.78440900	H 0.38192700 -5.50788300
	C -3.39288800 -2.35073200 -0.48464400	0.84498600
	H -4.36580500 -2.42998000 -0.96016200	C -0.63056400 -4.10011600 -
	C -3.06716000 -3.18384500 0.58656700	0.44192100
		<hr/>

triphenylsilane

H -3.78751400 -3.91198700 0.94728900	H -1.29862700 -4.84407100 -
C -1.81446000 -3.08171800 1.18990000	0.86718400
H -1.55630800 -3.73060200 2.02149100	C -0.71408600 -2.76969000 -
C -0.89022600 -2.14767100 0.72286200	0.85809000
H 0.08724400 -2.08158800 1.19618500	H -1.45571000 -2.50018000 -
C 1.74397200 -0.38187400 -0.35829900	1.60728100
C 2.21112700 0.11262000 0.86146800	C 1.47294000 1.02661100 -
H 1.58348400 0.77956900 1.44894500	0.33487000
C 3.47084300 -0.22575200 1.33349900	C 2.68817200 0.96371400 -
H 3.81776300 0.16822400 2.28375300	1.04403000
C 4.28817000 -1.06428700 0.58968500	H 2.76448900 0.34274200 -
H 5.27489500 -1.32753200 0.95772100	1.93400600
C 3.84480900 -1.56168500 -0.62651900	C 3.80829400 1.68786800 -
H 4.48350000 -2.21408400 -1.21371400	0.62938400
C 2.58389900 -1.22188600 -1.09336800	H 4.73434900 1.62425000 -
H 2.24754000 -1.61833500 -2.04893900	1.19414300
H 0.01966700 -0.02879300 -2.45329700	C 3.73487300 2.49696300
SCF E = -984.751834463	0.50859400
	H 4.60368700 3.06335400
	0.83216700
	C 2.53754400 2.57840300
	1.22413300
	H 2.47160900 3.20977500
	2.10597500
	C 1.41990000 1.85192000
	0.80332700
	H 0.49423200 1.93726700
	1.36671700

	C	-1.63600100	0.76889000	-	
					0.31275700
	C	-2.20712000	0.41846700		
					0.91145600
	H	-1.73368300	-0.33611300		
					1.53317400
	C	-3.37931100	1.00529100		
					1.34824100
	H	-3.80513100	0.71595500		
					2.30395900
	C	-4.01193900	1.95528700		
					0.56622600
	H	-4.93480500	2.41398400		
					0.90681000
	C	-3.46843700	2.31389300	-	
					0.65412700
	H	-3.96409500	3.05383900	-	
					1.27478800
	C	-2.29533700	1.72679000	-	
					1.08644600
	H	-1.88563400	2.01942500	-	
					2.04945100
	H	-0.02958500	0.02748100	-	
					2.39960300
					SCF E = -985.115497490

	Si	-4.1242383804	0.5104949448	-0.4288232893	Si	-0.0000436548	1.5255080696	-
diphenylsilane	C	-4.356960299	1.8425072355	0.8745783515		0.0000024599		
	C	-3.9825727491	3.1707434579	0.6190272983	C	1.5644939705	0.4774037826	-

H	-3.5274379693	3.4293602728	-0.3351266887	0.0993995564	
C	-4.1752807896	4.1677714117	1.5729447595	C 1.6927829378	-0.5640481181 -1.
H	-3.8790202609	5.1897146432	1.3564259172	0394364524	
C	-4.7447582453	3.8512295036	2.8062546862	H 0.8690060429	-0.7933282829 -
H	-4.8928785649	4.6259725233	3.5524984836	1.7116384352	
C	-5.1179171439	2.5370593587	3.0810398569	C 2.8636916625	-1.3209612889 -
H	-5.5561322962	2.285040024	4.0420264761	1.1253057613	
C	-4.9231128613	1.5437210634	2.121777021	H 2.9398505263	-2.1194938117 -
H	-5.2127705831	0.5209173365	2.3522651264	1.8582102716	
C	-2.4819046076	0.7525322795	-1.3071418256	C 3.935572776	-1.0525363204 -
C	-1.3332875016	1.1265925684	-0.5927043545	0.2673806115	
H	-1.3982142485	1.3046448059	0.4789939638	H 4.8461611465	-1.6415713396 -
C	-0.1070658468	1.2840416654	-1.2351432141	0.3320802455	
H	0.770375669	1.5738908228	-0.664969507	C 3.8290323404	-0.0259850494
C	-0.0089433134	1.0730454944	-2.6104221257	0.6743090751	
H	0.9449558441	1.198430293	-3.1138072105	H 4.656477278	7 0.1860975481
C	-1.1393402418	0.7066480901	-3.3382468119	1.3458273529	
H	-1.0688809878	0.5472072638	-4.4099999421	C 2.6542940072	0.7292848636
C	-2.3637216006	0.5499057448	-2.6892577687	0.7548509546	
H	-3.2393404449	0.2703701211	-3.2709011069	H 2.588163033	1.5229303187
H	-5.1963706016	0.5553666075	-1.4547494557	1.4953534778	
H	-4.1913819752	-0.806357532	0.2533913602	C -1.564514033	0.4772949575 0.0
SCF E =	-753.7785699			993679465	
				C -1.6925286058	-0.5645477402
				1.0390082197	
				H -0.8685643958	-0.7940914224
				1.7108900999	
				C -2.8634000646	-1.3215197871

				1.1248784732
			H	-2.9393439976 -2.1203622099
				1.8574675189
			C	-3.9355172914 -1.052760597 7
				0.2673538608
			H	-4.8460753847 -1.6418425814
				0.3320524727
			C	-3.8292510 822 -0.0258161846 -
				0.6739390463
			H	-4.6568794916 0.1865256665 -
				1.345149 2294
			C	-2.6545483442 0.7295071444 -
				0.7544865873
			H	-2.5886291849 1.5234 555082 -
				1.4946835084
			H	-0.1350915476 2.3978120447 -
				1.198754674
			H	0.134 9463563 2.3977908303
				1.1987723872
				SCF E = -754.042198
			Si	-3.7818532169 0.2393760672 -0.117724455 Si 2.3521979515 0.0019336421
			C	-4.1908940767 1.6954890013 0.9938141541 0.0043613274
			C	-3.425035818 6 2.8703882775 0.95200676 C 0.4689756549 - 0.000507751 -
			H	-2.5722458548 2.9389558619 0.2794907951 0.0106846267
			C	-3.733882626 3.9599931835 1.7628793676 C -0.2574485157 -1.2069525393 -
			H	-3.1285409412 4.860210595 1.7 161702352 0.03068254
			C	-4.8194854669 3.8923151598 2.6358182714 H 0.268842977 -2.1586123838 -
			H	-5.0614220828 4. 739976515 3.2696781904 0.0580082356

phenylsilane

	C	-5.5904697579	2.7337579916	2.6941683964	C	-1.6546493485	-1.2102541704	-
	H	-6.4348942385	2.6753770873	3.3742792511		0.0205915872		
	C	-5.2760199428	1.6461121456	1.8794252499	H	-2.1939937777	-2.1532583328	-
	H	-5.8850327287	0.7470091805	1.9386719729		0.0376170488		
	H	-4.1001850397	0.5487941445	-1.5329243441	C	-2.3571264983	-0.001296698	
	H	-4.5820411882	-0.9314117132	0.3114820713		0.0082685519		
	H	-2.3373670202	-0.0832834976	-0.0320359165	H	-3.443458644	-0.0019778072	
	SCF E =	-522.8001768				0.014309244		9
					C	-1.6558398275	1.2071086747	
						0.0252077712		
					H	-2.1951419745	2.1501081424	
						0.0437852991		
					C	-0.2573028823	1.2047135788	
						0.0150296672		
					H	0.2704429206	2.1553813616	
						0.023901576		
					H	2.8840351887	-0.348752393	
						1.3496257742		
					H	2.8451258795	1.3561966986	-
						0.357187414		
					H	2.8809728963	-0.9937260228	-
						0.9650167595		
					SCF =	-522.9653867		
	Si	-3.7580342731	0.1459921969	-0.1884992267	Si	-3.87533400	-0.01193100	
4-	C	-4.1620878165	1.608152076	0.9254636629		0.00724200		
trifluoromethyl-	C	-3.3912771653	2.7771460053	0.8800977498				
	H	-2.539270219	2.8424817416	0.2073736744	C	-1.98682000	0.00372000	-
phenylsilane						0.00612900		
	C	-3.6900182392	3.8724519222	1.6876733919				

H	-3.087352385	4.7731421492	1.6455554232	C	-1.27175100	1.20729400	-
C	-4.7742050028	3.8007969834	2.5568278098		0.00775600		
C	-5.1281745555	4.960430028	3.4452127329	H	-1.79892100	2.15720200	-
C	-5.556673244	2.6496005241	2.6255615355		0.01106200		
H	-6.3983278532	2.6061445056	3.310632349	C	0.11454000	1.22385100	-
C	-5.2473644385	1.563374093	1.8133180068		0.00824400		
H	-5.8606428963	0.6682097747	1.8759112108	H	0.64913100	2.16637400	-
H	-4.0933443264	0.4642368092	-1.5963225169		0.01075000		
H	-4.5533510684	-1.0211201421	0.2547085587	C	0.81390100	0.02335600	-
H	-2.3114517081	-0.1619425177	-0.1068279744		0.00855600		
F	-4.2988865185	6.0034579324	3.2831027451	C	2.31553000	0.00561400	
F	-5.0875392639	4.6197098013	4.7474971812		0.00117000		
F	-6.3768590264	5.4054961167	3.2078236861	C	0.12902800	-1.18784500	-
SCF E = -859.7554511					0.00849800		
				H	0.67579900	-2.12499600	-
					0.01208100		
				C	-1.25587600	-1.19150200	-
					0.00784700		
				H	-1.77380400	-2.14580500	-
					0.01114800		
				H	-4.39307900	0.51120800	
					1.29858700		
				H	-4.34377600	-1.40787100	-
					0.17812500		
				H	-4.40391500	0.84425900	-
					1.08577700		
				F	2.85938800	1.23449300	-
					0.09074700		

	F	2.82619100	-0.72112200	-
		1.02128300		
	F	2.81352600	-0.55117700	
		1.13248800		
		SCF E = -860.023668903		

	Si	-3.8481180253	1.6798234117	-0.4499884605	Si	-4.0889650533	1.1646931178		
	O	-2.3054927126	1.1779544628	-0.0899769617		0.1860145053			
	Si	-1.1966659153	1.5870493	727	1.0779903228	O	-2.6790946397	2.007818202	
	C	-4.6708010717	2.3173613718	1.1046671395		0.3722918579			
	C	-5.013200	338	3.6696747265	1.2399264821	Si	-1.1324916362	2.54811793	53
	H	-4.8488169886	4.3543918459	0.410679486	1	0.1824963975			
	C	-5.537553069	4.1613852344	2.4341853094		C	-5.3919820236	1.7911284316	
	H	-5.7872795919	5.214429574	2.5234408416		1.3777145948			
	C	-5.7211286889	3.304762146	3.5180845928		C	-6.2304426	164	2.8705604867
	H	-6.1238657584	3.6869331028	4.4514091004		1.0373844133			
	C	-5.3848358639	1.9556312964	3.4041710446		H	-6.1331231758	3.3468719259	
	H	-5.5284689081	1.2856373126	4.2465871482		0.064327689		5	
	C	-4.8668717539	1.4687588073	2.2055587049		C	-7.1957911666	3.3448977851	
	H	-4.6068451307	0.4140848583	2.1315663246		1.9295718259			
	C	-1.5126121636	3.3420065442	1.643733792		H	-7.8324706697	4.17878319	72
	C	-1.4236717939	4.40872114	0.7356428184		1.6474420693			
	H	-1.0977678916	4.2256586799	-0.2869371339		C	-7.3443118107	2.7419661359	
	C	-1.7549752413	5.7070949007	1.1183862902		3.182544074			
	H	-1.6822813686	6.5204058552	0.4025473271		H	-8.09660707	51	3.106817888
	C	-2.1774337994	5.9596283386	2.4237100976		3.876268624			
	H	-2.4373881255	6.9702917521	2.7242740114		C	-6.5273208242	1.6646125138	
	C	-2.2679535076	4.9136547097	3.3402781		3.5382908123			
	H	-2.6080111662	5.1050592866	4.353	6617985	H	-6.6432948551	1.1901002699	

DPDS

C	-1.9411938207	3.6160805005	2.949616382	4.508704895	
H	-2.0432921522	2.804	3210868	3.6666746782	C -5.5627926702 1.1952283267 2
H	-4.5603734415	0.5110651932	-1.0077012117	.6422431269	
H	-3.8	070388243	2.7814317253	-1.440200738	H -4.9389980436 0.3529092002
H	0.1417244602	1.440009214	0.46865	25471	2.9328021714
H	-1.3338643475	0.68832055	2.2480671664		C -0.8603861624 4.0133909186
SCF E =	-1119.7243656				1.3241762424
					C 0.377684529 4.6833608377
					1.3429146238
					H 1. 1866177207 4.3562365337
					0.6919542657
					C 0.5958768793 5.7738899585 2.188
					5334797
					H 1.558767707 6.2772047916
					2.1874631328
					C -0.4262028284 6.2162 358677
					3.0350205947
					H -0.2593345839 7.0640877439
					3.6935567364
					C -1.661 9683447 5.5639932655
					3.0302957732
					H -2.4595126914 5.9032518609
					3.68561 53351
					C -1.8754476376 4.4726912569
					2.181834603
					H -2.8403193112 3.97367 3831
					2.186740535
					H -3.8261504175 -0.271335506

				0.4614782262
			H	-4.566253 77 1.344500886 -
				1.20949995
			H	-0.9109477086 2.945157455 -
				1.2343621571
			H	-0.18081412 1.4507818829
				0.5048885023
				SCF E = -1120.0552824
			Si	-1.0406073246 -3.1872188939
				0.006270775 1
	Si	-1.01323102 -3.1154552544 0.0598401994		
	H	-0.0545125237 -4.1053313226 0.5944118866		
	H	-1.2496451719 -2.0601300126 1.0803052481		
	O	-2.377738015 -3.9988947894 -0.2899024856		
	H	-3.0925555257 -3.51607756 18 -0.7235856108		
	C	-0.3873863759 -2.2650550547 -1.4822822924		
	C	0.17331 13231 -0.9825598989 -1.4303627319		
	C	-0.4679108598 -2.9048826 -2.727722249		
phenylsilanol	C	0.6532806521 -0.3618694565 -2.5809503571		
	H	0.2316027117 -0.45688 46493 -0.4793426011		
	C	0.0053400018 -2.2877288284 -3.8818635897		
	H	-0.91 15595692 -3.8961818182 -2.7938946718		
	C	0.569348848 -1.0156187668 -3.8076431047		
	H	1.0859679321 0.6323625159 -2.5227637044		
	H	-0.0647951659 -2.7962733491 -4.8387671561		
	H	0.9395127783 -0.5324711632 -4.7069657295		
		SCF E = -598.0261145		
			H	-0.1157457052 -0.416352154 -
				0.5637820117

```

C 0.2503568482 -2.3840688695 -
3.8841487885
H -0.4954331756 -4.0814712139 -
2.804394397
C 0.599308448 7 -1.0318289469 -
3.8273662681
H 0.7386402743 0.7232066998 -
2.581362793
H 0.3595602522 -2.9354825079 -
4.8144301241
H 0.9784794913 -0.53045115 -
4.7140892617
SCF E = -598.2103802

```

Output information for phosphine oxides and silanes considered in Mulliken charge study is included below.

Phosphine	M06-2X			B3LYP					
Oxide									
	P	-0.0008084087	-0.0068907536	0.961	8992374	P	-0.0045399962	-0.0311476054	0.896
	O	0.0039339112	-0.0125657455	2.4641405846	0716265				
	C	0.3332730342	1.635	4861071	0.2558908502	O	-0.0177229474	-0.1690140861	
	C	1.2364047167	2.4539375572	0.943521783	2.3974315251				
TPPO	C	-0.2510	028068	2.0874623546	-0.9312252266	C	0.1758655937	1.68	93294007
	C	1.5607107708	3.7111344611	0.439593	0707		0.2881694464		
	H	1.670682353	2.1048682857	1.8763609093		C	1.4513798852	2.2746290214	
	C	0.0770874516	3.34631357	47	-1.4338017064		0.2272502671		

H	-0.9675037889	1.4641604451	-1.4600018453	C	-0.95	03664941	2.4788899986
C	0.983162	0825	4.1559686317	-0.7502880406	0.0078096926		
H	2.2588975861	4.3452088664	0.97660433	86	C	1.5972777374	3.6192295831 -0.1177
H	-0.3803078401	3.6959956538	-2.3538750854	032797			
H	1.2344863405	5.1370515	925	-1.1411586902	H	2.3324893316	1.6809825349
C	-1.5909303028	-0.5335483066	0.2539227779	0.4516543415			
C	-1.6919	893647	-1.2425243121	-0.9470472632	C	-0.8029069155	3.8242 982636 -
C	-2.7500480058	-0.1800279441	0.953	7962232	0.3377092664		
C	-2.9466577379	-1.5832577818	-1.4513257019	H	-1.9446449355	2.0462898099	
H	-0.794998657	-1.536993457	-1.4856301466	0.0595526442			
C	-4.0016007233	-0.5230381642	0.4478776273	C	0.470	4107246	4.3954835034 -
H	-2.6630490539	0.3515214342	1.897472827	0.4036272673			
C	-4.0998320002	-1.2218514089	-0.755923106	H	2.5890276858	4.0598741203	-
H	-3.0221667561	-2.136294643	-2.3821756036	0.1622			276561
H	-4.8988225366	-0.2502304961	0.9942214287	H	-1.6820339703	4.4243919382	-
H	-5.0755292818	-1.4909331826	-1.148420922	0.5539733849			
C	1.2535585058	-1.1123911219	0.247459124	H	0.5845072354	5.441	5497765 -
C	1.5651853497	-2.2734261197	0.9630421514	0.6731894178			
C	1.8866574382	-0.8544700188	-0.9724264968	C	-1.5521110652	-0.683026001	
C	2.4955051777	-3.1766823339	0.4538058163	0.155291863			
H	1.0854825391	-2.4540121259	1.9210653279	C	-1.84	5203208	-0.6318955641 -
C	2.8157819072	-1.7615623146	-1.4801091619	1.21642734			
H	1.6633861009	0.0561794721	-1.5225595046	C	-2.4665844172	-1.2828866431	
C	3.1180391967	-2.9221712275	-0.7686171106	1.0326			810547
H	2.73862304	6	-4.074899663	1.0124014571	C	-3.033976254	-1.1776247101 -
H	3.3081018386	-1.5579580783	-2.4257115879	1.7030864731			
H	3.844856918	-3.6252732372	-1.163378335	H	-1.1543140087	-0.1	621363492 -
SCF E =	-1111.2341366						1.9103143853

C -3.6570446432 -1.8284477049
0.5433345643
H - 2.2325767069 -1.3112432023
2.0926744904
C -3.9410919492 -1.778053068 -
0.823260537
H -3.2530545531 -1.1334313465 -
2.7660971203
H -4.360232006 9 -2.2909626189
1.2299853941
H -4.8658267187 -2.2024207912 -
1.20388648 52
C 1.3794448263 -0.9767554583
0.1489508529
C 2.0470121946 -1.8841027 196
0.9842868393
C 1.7786322443 -0.8520184216 -
1.1908140302
C 3.093146 6476 -2.6635870299
0.483166595
H 1.7426739567 -1.9608823951
2.02384795 79
C 2.8231053284 -1.6324560143 -
1.6897122437
H 1.2894294125 -0.137518 4767 -
1.8464767724
C 3.4801639878 -2.5410527433 -
0.8535547717

					H	3.6060	454693	-3.3624969574	
									1.1376305685
					H	3.1272845526	-1.5276500011	-	
						2.7272			494262
					H	4.2938529764	-3.1461780427	-	
									1.2431708664
									SCF E = -1111.604154
					P	0.84349408		-0.7238328696	
									0.0513093125
					C	1.7358089776	0.	2288314588	
									1.3720260456
					C	2.611916145		1.2675391424	
									0.6374319772
					H	0.2944051285	-0.6496195924	-1.791247	4368
									0.717949038
					H	0.7405813197	-2.5917	79788	-0.3744419112
									1.35862
					H	2.1563274456	-0.694940222		1.569218088
									75245
					H	1.695263	3003	-2.3675425242	1.89963309
									1.8983901383
					H	-0.0158845238	-0.4477767656		2.70451243
									5
					H	-0.7021728103	-1.7955317792		1.7716540679
									2.0971544201
					O	-0.3108191437	1.6686390	857	0.7237572769
									2.0971544201
					C	-2.1157860324	-0.2193859384	-0.1698318499	
									3.4829524729
					C	-2.4641	599156	-1.5146631903	-0.5673889613
									1.2383162946
					H	-1.7299779297	-2.3180066445	-0.53	34791633
									2.036166
					C	-3.7553124565	-1.7848860248	-1.011681219	
									7564
					H	-4.0238980041	-2.7904403778	-1.3203569804	
									2.1853610887
					C	-4.7026216951	-0.7607913705	-1.0591298396	
									0.4619685496
					H	-5.709681289	-0.9727891897	-1.4051469062	
									3.7653752745
					C				-0.1373660189
									-
					H				0.5524215
									13
					H				3.4951887576
									1.4020945088
									-

1PPO

C -4.3580615667 0.530284957 3 -0.66508093 1.3703939723
 H -5.0954963235 1.3260639096 -0.7046078885 H 1.960992324 -0.69380794 05 -
 C -3.06423050 53 0.8031659697 -0.2213756266 2.1234372437
 H -2.7705086464 1.8029700979 0.087318611 H 1.139582102 0.8451686974 -
 SCF E = -805.2815004 1.8085815536
 O 0.94557811 97 -2.2304083404
 0.1531457457
 C -0.8982840014 -0.1573914286 -
 0.0001506 049
 C -1.2472977714 1.2022154541 -
 0.0450533061
 H -0.4783099851 1.97050 86998 -
 0.0576466989
 C -2.5898011564 1.5846227845 -
 0.0723786691
 H -2.85 12455792 2.6383172434 -
 0.1061664825
 C -3.5950509419 0.6113576358 -0.05
 647722
 H -4.639128317 0.9100511563 -
 0.0785719812
 C -3.2541442763 -0.74 28656784 -
 0.0119466038
 H -4.0320386576 -1.5007374077
 0.0011699104
 C -1 .9101322344 -1.1272139176
 0.0174565917

				H	-1.6339489691	-2.1764440766	0			
					.0557524256					
					SCF E = -805.5439601					
	C	-0.3680	912783	-0.2537178101	-0.0954935084	C	-1.3434475314	0.5620378651	-	
	C	-0.6532216827	1.2094215011	-0.540	2841819		1.5163668594			
	C	0.5716534191	1.8981823769	0.155517632		C	-1.88011906	03	1.1218400089	-
	H	-0.4990107515	1.2899	181653	-1.6237188379		0.1615255437			
	C	-2.0347196634	1.7552196306	-0.2054024443		C	-1.6033083064		-0.1471584096	
	P	1.37	55604635	0.2269963183	0.2255186193		0.74058977			79
	C	1.2300020998	3.0116156023	-0.6448	245449	H	-1.2052318961		1.9157772495	
	C	0.2743028627	2.3474799252	1.5881894419			0.1809849554			
	H	-0.8536710735	-0.486	8145545	0.8580030736	C	-3.3010939643	1.6854830	08	-
	H	-0.5775865003	-1.0511813709	-0.8111747517			0.1831855902			
	O	2.1	435856338	-0.1961421487	1.4377226602	P	-0.4159619255	-0.7436316067		-
	H	-2.111802461	2.8161570911	-0.46	66601056		0.5950049824			
	H	-2.2531429983	1.650987875	0.8616211851		C	-1.0614	682459	0.1578768754	
	H	-2.806039763	1.213	5903876	-0.7613260822		2.1372496994			
	H	1.4962590774	2.6841833582	-1.6548808919		C	-2.7927638683		-1.1185592388	
	H	2.14	09574162	3.3644835445	-0.1500894185		0.82269			32091
	H	0.545596331	3.8650644255	-0.7318	780558	H	-2.1336778379	0.0870608696		-
	H	-0.3786372874	3.2279791421	1.5792310883			2.1075946761			
	H	1.205326002	2.60785	58371	2.0990377014	H	-0.78869203	1.24999	36469	-
	H	-0.2104597133	1.566220538	2.1820894685			2.1583561931			
	C	2.322510	9323	-0.0303205544	-1.3105552244	O	-0.4182154391	-2.191774319		-
	C	3.7156545735	-0.0058052203	-1.18783	96976		1.0270487761			
	H	4.1546218985	0.1160053535	-0.201164238		H	-3.62	01302464	1.9964405132	
	C	4.5203738891	-0.16318	34057	-2.3142336172		0.8181507911			
	H	5.6010760562	-0.1436634175	-2.2130914065		H	-4.0223389935	0.9512992908	-0.555	

TMPO

C 3.938 6167018 -0.3553483383 -3.566230169 9466377
 H 4.5661772236 -0.4822529061 -4.443 0241151 H -3.351841964 2.5640318936 -
 C 2.5506021047 -0.3946362838 -3.6920392768 0.836017933
 H 2.0958317638 -0.5 575342891 -4.6641800726 H -0.1843516437 0.811 4944965
 C 1.743854038 -0.2322356573 -2.5674966877 2.1058311178
 H 0. 6637107256 -0.2768250859 -2.6788735426 H -0.779475233 -0.7619074599
 SCF E = -883.8553284 2.6617451932
 H -1.83 23196413 0.6574550351
 2.7384917626
 H -3.587443691 -0.688108529 1.44328
 28145
 H -2.4793615862 -2.0629836607
 1.2774787797
 H -3.2189590503 -1.35 66864879 -
 0.1561828869
 C 1.2863505521 -0.1485187647 -
 0.2593883786
 C 2. 2437671614 -1.1175925467
 0.0813859426
 H 1.9527625622 -2.163043184 0.11
 01887833
 C 3.5608249216 -0.7434669836
 0.3576279517
 H 4.2930544923 -1.5 021267449
 0.6182273704
 C 3.9366768431 0.6011326857
 0.2892487376
 H 4.96 18690707 0.8918808568

					0.4994580216
					C 2.9921215191 1.5711310655 -0.0593
					146187
					H 3.2816215363 2.6159524728 -
					0.1242674409
					C 1.6732135673 1.1991 327056 -
					0.3319277508
					H 0.9577809283 1.9672963965 -
					0.6089766403
					SCF E = -884.156142
					H -0.7395 619752 -0.1858195604 1.5947978028 H -0.8246886053 1.6723023183 -
					O 2.250278969 -0.5267543577 1.032145 3213 1.5088321802
					C -0.6054172617 -0.1322261176 0.5092266858 O 0.348235239 1 -1.1504883395 -
					H -1.1950542925 -0.915 5718967 0.0293694035 1.7403310826
					P 1.1881044087 0.0045467446 0.1198226131 C -0.4957015623 1.3845508352 -
					H -1.699 0716332 2.1902353002 1.7449928221 0.50454292 7
					H -2.8483556216 1.7355048497 0.48035 16972 H 0.2411850553 2.1077114616 -
					C -1.8552106794 2.1572054199 0.6625860493 0.1492702772
					H 0.6703016173 1.74339 6543 2.319495886 P -0.0644482548 -0.4156892 045 -
					C -0.7863717265 1.3162572088 -0.0218382089 0.4840374627
					C 0.700296 1524 1.7936333569 0.122579204 H -3.3064929203 1.9368591934 -
					C 1.0082854929 2.385367789 1.5000377637 0.7654399246
					H -1.8508514682 3.1860061831 0.2861256678 H -2.7025 563542 3.0005705961
					H -1.0129578759 1.2681373629 -1.0952224482 0.5114600043
					H 2.087778206 2.5136832145 1.6188003271 C -2.9373452462 1.9591142197
					H 0.5261302694 3.3638635961 1.6075974046 0.264711 0291
					C 1.1962799498 2.7103841148 -0.986394099 H -2.573387273 -0.1853631115 -
					H 0 .986949168 2.3006659854 -1.9798984909 1.9163538266

TMBPO

H	2.2748262203	2.8824863216	-0.9	056252943	C	-1.6982886184	1.0807	14716	
H	0.6989236152	3.6859567241	-0.9169002249			0.4410958443			
C	1.4276419725	-0.5121462197	-1.6229672055		C	-1.8356573547	-0.4661217723		
H	0.5062880011	-0.3244650794	-2.1894334734			0.1453380384			
H	2.208382174	0.1356709648	-2.0388272893		C	-2.780	639106	-0.7851010688	-
C	1.8520412019	-1.9825004315	-1	.7174522952		1.0251791754			
H	2.0751699542	-2.2166880621	-2.7660073587		H	-3.7514118326	1.6370843805		
H	2.7805476337	-2.1146386149	-1.1504043372			0.9243		061301	
C	0.802983114	-2.9632348878	-1.1933718483		H	-1.3546753168	1.1833242409		
H	0.6412050005	-2.7856060785	-0.1225134855			1.4784908122			
H	-0.1562455946	-2.77785404	39	-1.6969316577	H	-2.6850662582	-1.83	62996065	-
C	1.2240736549	-4.4160700622	-1.4023072178			1.3134954372			
H	1.369210	2367	-4.6325665973	-2.4659463254	H	-3.8214748967	-0.6066758459		-
H	2.1679733391	-4.62067566	-0.8870742	937		0.7306702334			
H	0.4736377676	-5.1113440394	-1.0166231048		C	-	2.1780660773	-1.3332424244	
SCF E =	-810.0741516					1.3580101233			
					H	-1.5190312625	-1.1371057758		
						2.2098093671			
					H	-2.1124083627	-2.399900482		
						1.1154466407			
					H	-3.2071778959	-1.1348095327		
						1.6842798738			
					C	1.0712037199	-0.7413157341		
						0.9367536973			
					H	0.8446555087	-0.0327093519		
						1.743345558			
					H	0.8104852744	-1.740579012	1	
						.3059111222			

	C	2.5671865216	-0.7025758886		
		0.5710538306			
	H	3.1327241229	- 1.0815529254		
		1.4329918227			
	H	2.7487937712	-1.4013301515	-	
		0.2537755393			
	C	3.1073533449	0.6838230603		
		0.1935004261			
	H	2.5933081833	1.0500113744	-0	
		.7039511358			
	H	2.8770955546	1.3964037545		
		0.9983469061			
	C	4.6184389631	0.6753536618	-	
		0.0650743127			
	H	5.170261588	0.3445782822		
		0.8229656905			
	H	4.8724129516	-0.0037268691	-	
		0.8871103432			
	H	4.9826863991	1.6731110017	-0.3	
		322900589			
		SCF E = -810.3625149			

	H	-0.8017353661	0.2493270487	1.802906784	H	-1.9017963558	0.2724671439	-	
	O	1.8799429764	-1.0431977	904	1.1122689348	2.1110259081			
	C	-0.7450146676	0.2292368982	0.7089584313	O	-0.1748266397	-2.0503666119	-	
TMPyrPO	H	-1.607680	6696	-0.3100950565	0.315343306	1.18949679			
	P	0.9581216419	-0.2618306069	0.23860693	62	C	-1.149381211	0.7190241404	-
	H	-0.88573119	2.8055686033	1.916956754	1.4516806258				
	H	-2.2087250558	2.7519133617	0.7436001114	H	-0.6170898486	1.4961881644	-	

C	-1.1210548384	2.8100721761	0.8483770338	2.0031705633				
H	1.2181030789	1.6829344266	2.3662826479	P	-0.21757263	66	-0.6486334575	-
C	-0.4521687904	1.6439498637	0.1331585651		0.6370317983			
C	1.1163970737	1.5850498027	0.1754485228	H	-3.872974448	0.9445586779		-
C	1.7055895947	2.1111564036	1.4846693015		0.57053986			89
H	-0.7924142605	3.768900787	0.4324465294	H	-3.230486862	2.5904945961		-
H	-0.7548647051	1.660996528	-0.9220532665		0.6424271371			
H	2.7653581002	1.8491473758	1.5465351455	C	-3.1855181607	1.6464867	347	-
H	1.6109521648	3.2025994382	1.5368696996		0.0878226559			
C	1.8111645582	2.2003284168	-1.0305817496	H	-3.0424009592	-1.3820722046		-
H	1.4711225176	1.7433497368	-1.9664482171		0.3662098373			
H	2.8969176009	2.0727047109	-0.9648161781	C	-1.7536581111	1.1102913322		-
H	1.6053099465	3.2772870513	-1.0821266256		0.0665627074			
N	0.8719335075	-0.8857748889	-1.3098096212	C	-1.4804230925	-0.2471611478	0.700	
C	2.0754381961	-1.5025454565	-1.9032328452		9130503			
H	2.966216056	-0.8848185503	-1.7429388478	C	-2.6544827775	-1.2368531068		
H	2.2602628214	-2.4776255397	-1.4398024593		0.6464532482			
C	1.7177730568	-1.6281119494	-3.3888971476	H	-3.5547337461	1.8391521034		
C	0.1911641428	-1.7462337192	-3.3753054863		0.9261693676			
C	-0.2023910793	-0.7393828673	-2.2927624928	H	-1.109857295	1.8755632381		
H	-0.2404103402	0.2764811158	-2.7195099737		0.3851127398			
H	-1.1781196604	-0.9569499258	-1.8484094095	H	-2.3372767112	-2.2177101296		
H	-0.2718450288	-1.5258520973	-4.3401228422		1.0131608273			
H	-0.1074539456	-2.7534587747	-3.0658783924	H	-3.4798541514	-0.8870716463	1.2	
H	2.2151520601	-2.4764262296	-3.8644721903		787857342			
H	2.0117106832	-0.7174794627	-3.923490688	C	-0.9831154368	-0.078508134		
SCF E =	-864.2095266				2.1370322627			
				H	-0.0929175211	0.5563693424		

2.1894674527
H -0.7342026048 -1.047000599
2.5852251602
H -1 .7619055604 0.3816494523
2.7595116464
N 1.3169665132 -0.0777248989 -0.
2574302562
C 2.3647325287 -1.0120755233
0.2279301363
H 1.9880070314 -1 .6649224738
1.0228385319
H 2.7055629379 -1.6537400836 -
0.5928238872
C 3.4839997196 -0.0822709574
0.7234837347
C 3.3142878387 1.1761556141 -0
.1414609889
C 1.7889843871 1.3196068231 -
0.241286699
H 1.4000454006 1. 8740530091
0.6272123332
H 1.4816907246 1.8538358618 -
1.1450650686
H 3. 7864783538 2.0647729236
0.2875719136
H 3.7380206029 1.0118319749 -1.13
8887966
H 4.472035917 -0.5417459546

0.6294279502
H 3.3282271738 0.1670 267966
1.7798406683
SCF E = -864.5044091

Geometries from the optimizations of compounds considered in the global parameters study are included below.

Compound	Geometry				
Tetracyanoethylene	C	0.6871632876	0.8886815089	-0.0000134198	
	C	2.0450027059	0.8886622932	-0.0000027056	
	C	2.7902332872	2.1153687052	0.0000272506	
	N	3.3968210987	3.0996761501	0.0000510067	
	C	2.7901996435	-0.3380651645	-0.0000169978	
	N	3.3967567709	-1.3223915416	-0.0000296466	
	C	-0.0580336478	2.1154089597	0.0000059196	
	N	-0.6645908133	3.0997353128	0.0000196097	
	C	-0.0580672917	-0.3380248964	-0.0000389695	
	N	-0.6646551409	-1.32233231	76	-0.0000599573
SCF E = -447.3674581					
S9	H	-1.0057414423	-0.018098437	-1.8453069674	
	C	-1.8347398011	0.2332053397	-1.1880447439	
	C	-3.0949394391	0.473115064	1	-1.727671561
	H	-3.2443876512	0.4160000771	-2.8013354985	
	C	-4.1653705	634	0.7850667355	-0.8868424963
	H	-5.1479886193	0.9716257971	-1.3093452	653
	C	-3.9741609596	0.8556420375	0.4910384972	
	H	-4.806677029	1.0964275	222	1.1447207023

C	-2.7110878192		0.616685127		1.0338962873
H	-2.5366893	884	0.6639819043		2.1053873208
C	-1.6389867668		0.3060218294	0.195262313	3
P	-0.0213551488		0.0330445619		0.9908729932
O	-0.1273398623		0.15050791	75	2.4823881204
C	1.098064346		1.2985424882		0.3050806489
C	1.6269618255		1.2393886675		-0.9885868398
H	1.4189593565		0.3823918209		-1.6247634509
C	2.4434760133		2.2661668219		-1.4561740733
H	2.8551654609		2.2159482564		-2.4593908534
C	2.738778566		3.3526464459		-0.6316942278
H	3.3776374089		4.150973577		-0.9969002588
C	2.2225002448		3.4091509936		0.6615810666
H	2	.4604391698	4.2492918244		1.3065067069
C	1.403744	2.3830009409		1.131394	8772
H	1.001776962		2.3997025821		2.1408069501
C	0.5847789359	-1.5380291	545		0.3336727454
C	-0.2838265832		-2.5506261066		-0.0870628384
H	-1.3566	831428	-2.3766380676		-0.0937378299
C	0.1920735111	-3.7870467409		-0.499	8075971
H	-0.5203742121		-4.5395562787		-0.8133491637
C	1.5774244442	-4.	063247194		-0.508072799
C	2.4515248168		-3.0444253357		-0.0633650966
H	3.	5207419437	-3.2118156281		-0.032586934
C	1.9577048224	-1.8154936058	0.3		442433135
H	2.6595761926		-1.0558299534		0.6803426787
N	2.0604720005	-5.	2786741526		-0.9380677047
C	1.1297934469		-6.3589937813		-1.1986655206

H	1.6878558928	-7.2376223861	-1.5213257413	
H	0.5423009493	-6.6258172256	-0.3083940762	
H	0.4360038142	-6.0911361828	-2.0024361102	
C	3.462677668	1	-5.5929922452	-0.746695361
H	3.6586677175	-6.5910346461	-1.137882941	6
H	4.0987795629	-4.8897321872	-1.294326354	
H	3.7534053058	-5.57021285	24	0.3133811028
SCF E = -1245.1434902				
H	1.9163553637	0.5754355078	-1.7311228139	
C	1.9424535647	1.4753749392	-1.1243621845	
C	2.4176469835	2.661187	568	-1.6705330967
H	2.7539361124	2.6875990514	-2.7029036451	
C	2.46	99596861	3.8201723826	-0.8897995837
H	2.8416763055	4.7465918519	-1.3	191825799
C	2.0544297735	3.7901453937	0.437020541	
H	2.1070146714	4	.6887036465	1.0446032577
C	1.5737669473	2.5993346837	0.9893012089	
H	1.259676563	2.5460089949	2.029833585	
C	1.5128618303	1.447213151	0.	209515403
P	0.7319309868	-0.01309886	0.9639068369	
O	0.8688295727	0.0009083227	2.4584382368	
C	1.4675871768	-1.4821457692	0.1907301075	
C	1.070806086	-1.9845611505	-1.0530267447	
H	0.2526452153	-1.5170677	914	-1.5984378866
C	1.7023353243	-3.1058907454	-1.5862976366	
H	1.3	93290388	-3.4869594436	-2.5554026053
C	2.7142924103	-3.743193518	-0.	8695912231
H	3.2059490965	-4.6190835629	-1.2832085691	

S10

C	3.09376886	64	-3.2619408375	0.3830345413
H	3.8657280563		-3.7738173495	0.9504074 186
C	2.4734554105		-2.1335507143	0.9128592634
H	2.7421236705	-1.75	56997742	1.8966227997
C	-0.9858556471		0.0206988441	0.3655472604
C	-1.5288068471		1.1954370554	-0.1715920398
H	-0.9028896253	2.071310284	3	-0.3185686509
C	-2.8776567648		1.252796048	-0.5161319793
H	-3.327	9601613	2.1517114818	-0.9234369803
C	-3.6790882715	0.1284013293	-0.3	438583494
C	-3.1454976277		-1.0559135246	0.1679625704
H	-3.76780238	09	-1.9415377225	0.2633552934
C	-1.8023468984		-1.1006958977	0.526688 6977
H	-1.3837282303		-2.0219290071	0.9276523944
O	-4.9893422467	0.	2190094337	-0.7435739041
C	-5.8987730401		-0.5033542036	0.0873207405
H	-6.8875738731		-0.3726278852	-0.354629348
H	-5.6546466841	-1.5711	071978	0.1259840919
H	-5.8806916752		-0.0874804409	1.1021920461
SCF E = -1225.7058254				
H	-0.3229103307		-2.146798953	0.0517436886
C	-1	.1672878583	-2.4944084473	0.6417680932
C	-2.4663733957		-2.3030520031	0 .1737427081
H	-2.6297633591		-1.81773502	-0.7832510649
C	-3.5525880754		-2.7233566042	0.9400233853
H	-4.563522027		-2.5694378188	0.5756297139
C	-3.3435881207		-3.3300189386	2.1785193691
H	-4.1900842318		-3.644939261	1 2.7803401326

S11

C	-2.0473066629		-3.524986218		2.6489684367
H	-1.86902654	02	-3.9779698917		3.6204977809
C	-0.9554758544		-3.1151268128	1.87646928	71
P	0.6968122725		-3.4500420678		2.5551694207
O	0.7359491706		-3.4368377	753	4.0517275298
C	1.8160246378		-2.2340831789		1.7984395414
C	2.4055171	674	-2.4047198226		0.5421143874
H	2.235552139		-3.3167097967	-0.02477700	76
C	3.2297301278		-1.4098246023		0.0192528725
H	3.689623784		-1.54573728	15	-0.9544080048
C	3.471464796		-0.2485423176		0.7521893139
H	4.11730149	32	0.5232750664		0.3451785062
C	2.8950973859		-0.0820414816		2.0111317575
H	3.0939597159		0.8165048079		2.586453401
C	2.069642977		-1.0734388006	2	.5366240699
H	1.6294478088		-0.9673211007		3.5244048144
C	1.1894422989	-	5.0660168211		1.8651270322
C	0.7235193334		-5.5536726815		0.6420412293
H	0.004250498		-4.9815457123		0.0617515943
C	1.1675699147		-6.7854043324	0.	1657186506
H	0.8130963448		-7.1693384146		-0.7847548084
C	2.0723175234	-	7.5246354323		0.9231010489
C	2.5305689243		-7.0549387055		2.1536513937
H	3.2290393887		-7.648613241		2.7347525643
C	2.0861563046		-5.8243961985	2.	6249674113
H	2.416666876		-5.4459592519		3.5881091662
C	2.5261894053	-8.	8770189435		0.4457025081
F	1.8299771108		-9.8692245816		1.0324921818

F	3.	8219295832	-9.0970527549	0.7275351071
F 2.373591864 -9.024706749 -0.88 07362425				
SCF E = -1448.1822637				

H		0.2375733958	-0.3749614259	0.0655597935	
C		-0.58548	50099	-0.7433103866	0.6725443356
C		-1.8972879912	-0.5945567465	0.22491	37553
H		-2.0904182875	-0.1234994577	-0.7335168129	
C		-2.9575250853	-1.0	410776987	1.0122036865
H		-3.9782251679	-0.9215176609	0.6626695231	
C	-2	.7108868599	-1.6311143353	2.2518790386	
H		-3.5377646926	-1.9665336384	2	.8695274109
C		-1.4022034745	-1.7845609611	2.7023100624	
H		-1.1954116932	-2.225413023	3.6737986733	
C		-0.3360424087	-1.3483681496	1.9080962944	
P		1.3337139564	-1.638947451	2.5577919329	
O		1.4118469623	-1.6189503274	4.0517413297	
C		2.4308880225	-0.4303912422	1.7627240507	
C		2.9408757976	-0.5830362539	0.4693183989	
H		2.7172249038	-1.4755993236	-0.1101900513	
C		3.7548817922	0.4063429155	-0.0779981762	
H		4.1523321703	0.2852216077	-1.0805630906	
C		4.0665481828	1.5432009213	0.6672727272	
H		4.7051303119	2.3104232179	0.2407950029	
C		3.5701644755	1.6907515297	1.9617977662	
H	3	.8239881582	2.5697403487	2.5454736189	
C		2.7540351702	0.7049985224	2.51	23156127
H		2.375027687	0.795349408	3.526614075	
C		1.8315385331	-3.26270	15613	1.8799051909

S12

C	1.3428272672	-3.777458029	0.6833563496
H	0.600060 6725	-3.2301617351	0.106494542
C	1.798091026	-5.0157575412	0.223700619 9
C	2.7232835913	-5.7480325766	0.9522019151
H	3.071457674	-6.710726987	0.5917335841
C	3.193709571	-5.230616808	2.161000606
C	2.7562867088	-3 .9998962507	2.630542886
H	3.1093734042	-3.6071845075	3.5800506883
C	4. 1806860586	-6.0544048942	2.9447545401
C	1.2556455771	-5.5344998677 -1.	080349776
F	1.5129981137	-4.6809953615	-2.0896266256
F	-0.0795083097 -	5.6826647346	-1.0348568763
F	1.7813296341	-6.7206581581	-1.415581112
F	3.6445987822	-7.2271347195	3.3282477101
F	4.6064631059	-5.426664859 4	.0472353523
F	5.2638170745	-6.3519773683	2.2036570579
SCF E = -1785.1345575			
H	-0.2817412749	0.635207499	0.0470855945
C	-1.1363766964	0.3125679745	0.6366215312
C	-2.4287618039	0.5225452663	0.1579477516
H	-2.5772513331	0.9988413472	-0.8060973524
C	-3.5274656069	0.1314908553	0.9220196248
H	-4.5332343817	0.2994737301	0.5493341976
C	-3.3367074303	-0.4644163162	2.1686313038
H	-4.192493512	-0.7571383038	2.7687272585
C	-2.0467262534	-0.6773584792	2.6491210993
H	-1.8817268544	-1.12291811 73	3.6264603395
C	-0.9424482513	-0.2970114535	1.8796884445

S15

P	0.7018722	621	-0.6541792527	2.5732259935
O	0.7230768162		-0.6213889385	4.07100200 98
C	1.8275120225		0.5630005121	1.8221288707
C	2.45798458		0.3638051347	0.5904646945
H	2.3161197554		-0.5684313262	0.0492542903
C	3.2841091029		1.3548367139	0.0623592978
H	3.7753281139		1.1967646311	-0.8926228862
C	3.4874129123		2.5410429029	0.7661225247
H	4.1345150082		3.3100718389	0.3 555916793
C	2.8701113103		2.7366336854	2.0015855232
H	3.038634599		3.655 0543405	2.5550069963
C	2.042603711		1.7492681131	2.5312674882
H	1.57044	90029	1.8785891382	3.5014649433
C	1.1895424093		-2.2631238352	1.8850591 287
C	0.6875555872		-2.7755841978	0.6874359701
H	-0.0678941716		-2.22651 63947	0.1307684608
C	1.1444567383		-4.0017025874	0.2053455715
H	0.74680	74495	-4.3930088927	-0.7274101863
C	2.0991766509		-4.7398846914	0.90842 78207
C	2.5871907987		-4.2220414379	2.1148207515
H	3.3238147347		-4.7888 663649	2.6790330688
C	2.1391010347		-3.0000987467	2.6025430928
H	2.5083	824861	-2.6114616584	3.5479062513
C	2.5825521897		-6.0743332312	0.40130 85687
H	3.6753897219		-6.1200218588	0.3990467673
H	2.220760503		-6.88579 93556	1.0408582944
H	2.230214029		-6.2638900728	-0.6150859785

SCF E = -1150.5275635

S13

H	0.2113406955	0.1336154119	0.0441824405
C	-0.637558461	-0.202952073	7 0.6340948345
C	-1.9335555961	-0.0085219836	0.1589009425
H	-2.0903116	483 0.4688235251	-0.8032154504
C	-3.0254065263	-0.4156316581	0.9244668 569
H	-4.0339244516	-0.2593878422	0.5543679081
C	-2.8249057067	-1.0117 277027	2.1694457021
H	-3.6756449122	-1.3161598214	2.7707181479
C	-1.53 15970309	-1.2093064917	2.6471942581
H	-1.3595913252	-1.6536949569	3.62 38416208
C	-0.4342527538	-0.8130528644	1.8755032925
P	1.2137283847	-1. 1488343618	2.5654587821
O	1.2426357595	-1.1223063279	4.0619980107
C	2. 3400635416	0.0586497048	1.8053434169
C	2.9364570417	-0.1262879787	0.55 42856385
H	2.7665383119	-1.0438374735	-0.003731958
C	3.7666203771	0.86 10576652	0.0266228596
H	4.2322504458	0.7143341659	-0.9427693986
C	4.00 7117072	2.0289239973	0.7494135149
H	4.6577254981	2.7947879923	0.338786 7737
C	3.4237451969	2.2095848673	2.003238504
H	3.6219362515	3.11317972 67	2.5708128008
C	2.5922971231	1.2257795662	2.533469895
H	2.1465967624	1.3426077981	3.5175996672
C	1.7106276893	-2.7680875572	1.8851693601
C	1.2052741954	-3.283880508	0.6890864942
H	0.4526817857	-2.7346256124	0 .1296160968
C	1.659125207	-4.5162852305	0.2236463415

H	1.2703578643	-4	.9277883746	-0.7050119669
C	2.608243402		-5.231935603	0.9541067906
C	3. 1049659277		-4.7233880686	2.1590235888
H	3.8341883312		-5.3070448032	2.7 125192155
C	2.6540836354		-3.4953741708	2.6246259188
H	3.0107999039	-3.	0909899384	3.5679139651
C	3.0808992966		-6.5451074209	0.4444378115
H	2. 6250341749		-6.8721614063	-0.5128900557
O	3.9018583366	-7.2335553101	1. 0045013495	
SCF E = -1224.5133593				

H	-0.0099554158		0.0678463549	0.0401807194
C	-0.8572737694		-0.259194651	5 0.6377673074
C	-2.1551419996		-0.0539875	0.1723354602
H	-2.3151692291		0.4222842757	-0.7898003026
C	-3.2445788151		-0.4483382244	0.9479959364
H	-4.2546058573		-0.2832478609	0.5858742549
C	-3.0395183892		-1.0427793	147 2.1929774333
H	-3.8881559943		-1.3371639134	2.802204853
C	-1.744182	8569	-1.2512702887	2.6607169246
H	-1.5680171961		-1.6942826159	3.637228 2884
C	-0.64943758		-0.8676964187	1.8791885636
P	1.0011713391		-1.215894	9543 2.5580879836
O	1.0363434894		-1.1929570195	4.0547031891
C	2.125461	6474	-0.0055049746	1.7986533967
C	2.7212588854		-0.1856584492	0.5467482 585
H	2.5531984098		-1.1027021809	-0.0127740702
C	3.5480686166		0.805614	0668 0.0207038451
H	4.0132884816		0.662647342	-0.9494704317

S14

C	3.7858292	087	1.9724627125	0.7460865841
H	4.4336667332		2.7412991546	0.3365478286
C	3.2030799312		2.1482511492	2.0008839418
H	3.3990871406		3.0511107547	2.5704505708
C	2.3753452268		1.1605138443	2.529433482
H	1.9302694453	1.	2735392728	3.5142754935
C	1.4856923521		-2.8330488132	1.8689235697
C	0.	9737047353	-3.3426992172	0.6736593048
H	0.2245564365		-2.7860480672	0.1 166604439
C	1.4100156085		-4.5789227342	0.2006321491
H	1.0012486241	-4.	9653748239	-0.7276859137
C	2.3550928572		-5.3143527587	0.9211333067
C	2	.8564872431	-4.8058706914	2.1246269168
H	3.5810141353		-5.397871447	2.6 74381708
C	2.42327422		-3.5742310189	2.5988132582
H	2.7902279811	-3.181	0185337	3.5428794514
C	2.852856233		-6.6538021961	0.4515271791
O	3.6877	3667	-7.2564723092	1.0950882728
C	2.2933596228		-7.2289929243	-0.830862 6372
H	1.2082793951		-7.3508329832	-0.7576712249
H	2.4977599331		-6.5622 55729	-1.6743147445
H	2.7595142306		-8.1971767935	-1.0092929708
SCF E = -1263.8189876				
P	0.919008922		-0.5737563929	0.413586 6799
C	1.6004317132		-1.3535856305	-1.1136455359
O	1.1601004475		-1.3106 271847	1.696162819
C	1.8210458185		1.0151114309	0.1948554459
H	1.158821	0933	1.7621577725	-0.2615200784

S16

H	2.1445323486	1.3878792961	1.16999916	54
H	2.2655106505	-2.1496462454	-0.7621490645	
H	0.818050276	-1.8084241	382	-1.7256628211
C	2.3894370568	-0.2470736678	-1.8315514047	
H	3.17046	36827	-0.6601908627	-2.4780061612
C	2.9814113222	0.6832945902	-0.75866	69578
H	1.7195456705	0.342051232	-2.4738138864	
H	3.7321719243	0.111826	4509	-0.1945191358
C	-0.8497035156	-0.2559199508	0.1281282073	
C	-1.322	6779501	0.3692469588	-1.0305221135
C	-1.7492571879	-0.6733700524	1.110	4607501
C	-2.6880213173	0.577843005	-1.2038981294	
H	-0.6280956062	0.69	43057939	-1.8031823146
C	-3.1169060823	-0.4611908294	0.9363886938	
H	-1	.3600728715	-1.1625337064	1.999363038
C	-3.5850705657	0.1630422957	-0.	2178728876
H	-3.053378783	1.0621365337	-2.1040187219	
H	-3.8158099109	-	0.7847058061	1.7012919633
H	-4.6496802534	0.3271506829	-0.3528502478	
C	3.6427966384	1.9242257963	-1.3468058803	
H	4.0552374853	2.5640608273	-	0.5613735463
H	4.4574099579	1.6522143646	-2.025530822	
H	2.9125864063	2	.5135383965	-1.9136317235
SCF E = -844.579844				
C	0.5834050177	-2.6781226672	0.60518	90628
C	0.7308048295	-1.3021508222	0.4885669607	
C	1.8104681393	-0.7426	442378	-0.2137030315
C	2.7483019961	-1.5803734533	-0.8142635475	

S17

C	2.60	10880754	-2.96300267	-0.6979243436
C	1.5299878881	-3.512855427	0.00826	61007
H	-0.2536445433	-3.0953669809	1.1578693578	
H	3.5895568936	-1.168	9352938	-1.3640918594
H	3.3318264612	-3.6189576052	-1.1607033519	
H	1.4	344571615	-4.5903541978	0.0937149595
C	1.8103302795	0.7430559528	-0.21	35343982
C	2.7480050872	1.5810961143	-0.8139101751	
C	0.7305647988	1.30	2202546	0.4888658464
C	2.6005333402	2.9636716346	-0.6972583219	
H	3.589	3328133	1.1699382202	-1.3638367593
C	0.582908139	2.6781206952	0.605798	2216
C	1.5293330536	3.5131649024	0.009060537	
H	3.3311466737	3.61986750	95	-1.1598932914
H	-0.2542173071	3.0950845458	1.1585752747	
H	1.4336014	415	4.5906265912	0.0947527548
P	-0.3570169201	-0.0001492581	1.14947997	8
O	-0.6935171666	-0.0003536695	2.6060345897	
C	-1.8476086341	-0.000163	6823	0.1090584725
C	-3.0849878133	-0.0004319508	0.7542532191	
C	-1.7803	708656	0.0000744538	-1.288096751
C	-4.258485171	-0.0004648474	-0.00055	1805
H	-3.1095547494	-0.000606042	1.8405577586	
C	-2.9527782123	0.00004	06798	-2.0368954089
H	-0.8136098389	0.0002868761	-1.7877380842	
C	-4.19	17489357	-0.000229729	-1.3919032483
H	-5.2223566109	-0.0006729949	0.49	85520391
H	-2.9035855744	0.0002259358	-3.1211523524	

H	-5.1053107466	-0	.0002551285	-1.9784834033
SCF E = -1110.0380815				
C	-0.154401145	-1.4427834093	0.9	195140769
C	0.870857369	-0.2958599296		0.9948002629
C	0.0479139143	-0.1	964812898	-1.1386577274
H	0.2683766175	-2.4217780876		1.1508254851
H	-0	.9992316773	-1.2399245298	1.5893727196
C	0.2279281727	0.7458596635	0.0	63703901
H	0.8652577422	1.6077332015		-0.1492381841
H	-0.7340691978	1.1	00040182	0.450758244
C	1.4650281441	-0.5986632097		-1.5908997412
H	1.93	66439911	0.1862431969	-2.1897730112
H	1.4571671677	-1.5328860991	-2.15	60161341
H	1.1101203487	0.0203012171		2.010621169
H	-0.5712298485	0.167	5074798	-1.9598786012
P	2.3376444039	-0.8752902118		0.0205414409
C	3.66	05905485	0.3596059808	0.211424438
C	4.730686973	-0.0210659175	1.029197	4678
C	3.6640820848	1.6258385347		-0.3838212604
C	5.7816174412	0.862721	4313	1.2633385565
H	4.7331846653	-1.0199681191		1.4566430798
C	4.717156	8318	2.5074415752	-0.1487606226
H	2.8594520181	1.932508868	-1.04614017	28
H	-6.3827073761	2.8337491272		1.0623868544
H	-5.2625668788	2.9709155	739	2.4216513406
C	5.7735247068	2.1278798667		0.6780796481
H	6.61025745	94	0.5602144088	1.8955926154
H	4.7162815809	3.486246544		-0.6177620954

S18

H	6.5945248121		2.8150945318		0.857068596
O	2.8122431143		-2.2576618309	0	.3399632551
N	-0.5699098562		-1.3887650927		-0.5074422734
S	-2.143755946	6	-1.7589904176		-0.8788091402
O	-2.2396960141		-1.7210778664	-2.3296819	145
O	-2.4679377328		-2.9392678565		-0.0956721927
C	-3.134114926		-0.4145	321569	-0.2510816958
C	-3.615628703		-0.4690518315		1.0551040683
C	-3.35	95398472	0.701994063		-1.0551517026
C	-4.3124802391		0.623762256	1.56491	32717
H	-3.4652963932		-1.3674125545		1.6457884004
C	-4.0574972942		1.784	0012817	-0.5287977708
H	-3.0120486296		0.7033589224		-2.0837239912
C	-4.	5391284802	1.7631009009		0.7859657809
H	-4.6952845624		0.5867355752	2.58	11962793
H	-4.242592048		2.6556081525		-1.1510288959
C	-5.3254430135		2.9	267126923	1.3319760952
H	-4.9625092977		3.8743641831		0.9265120808
SCF E = -1717.4562203					
P	0.4556217174		0.6166342391		0.4337161834
O	0.638942	8536	1.3466839956		1.7312480304
C	-1.3048543586		0.30175107		0.0876438353
C	-2.1677010918		0.3859479969		1.1860367498
C	-1.821779308		-0.025780812	2	-1.170571915
C	-3.528239206		0.1300244331		1.0295932444
H	-1.757020464	3	0.6706458914		2.1508243413
C	-3.1829417031		-0.280663874		-1.3246880418
H	-1.174925365		-0.0730997025		-2.0419183349

S19

C	-4.0358805904	-0.2066633	522	-0.2241761845
H	-4.1924925925	0.2001276537		1.8851893903
H	-3.57770	67442	-0.5301820017	-2.3045546955
H	-5.0964713933	-0.4030617181	-0.346	9292737
C	1.2589700079	1.3441822671		-1.0654770063
C	2.3299862698	0.294	6923381	-1.4336204158
C	1.3888932854	-0.9678044248		0.2667657702
H	1.67	87935172	2.3172546511	-0.7964856553
H	0.5387381508	1.4889825401	-1.877	0244511
C	1.6272871784	-1.0663041776		-1.2505236415
H	2.2903148463	-1.9	054856806	-1.4894789087
H	0.7144885545	-1.171238932		-1.8447540418
C	3.	4203206034	0.2395042286	-0.3370290072
H	4.3342146106	-0.2107418248	-0.	7345975137
H	3.6766155444	1.2392820272		0.0252846419
C	2.8075479277	-0.	6502117491	0.7871978546
H	3.3700063375	-1.582504325		0.8974020651
H	2.7	837864453	-0.1478066635	1.7565066881
H	2.7378094268	0.463574079	-2.433	5449334
H	0.8976275305	-1.8162881631		0.7460152253
SCF E = -882.6669597				
<hr/>				
P	0.5387299416	0.8431354194	-0.43311	2239
O	0.5757667658	2.1331691746		-1.1972699633
C	-1.1678528022	0.25709	22328	-0.1934755131
C	-1.5532257578	-0.6557531795		0.7944160039
C	-2.13	07559526	0.7818433367	-1.0613910908
C	-2.8841518478	-1.052158462	0.902	0956033
H	-0.8202320413	-1.0579864188		1.4893610333

S20

C	-3.4617021098	0.3	826515784	-0.9535543072	
H	-1.8225882392		1.5156938221	-1.8010390602	
C	-	3.83800791	-0.5354525931	0.0252707856	
H	-3.1774411044	-1.7585787535	1.	6722600988	
H	-4.2054094924		0.794474097	-1.6283994829	
H	-4.8754906763	-	0.843200344	0.1117995554	
C	1.4406660146		0.8280809877	1.1817032653	
C	2.	5824473388	-0.1883911361	0.953259066	
C	1.6078980684	-0.4878310638	-1.1	284086641	
H	0.8048649554		0.5810071999	2.0364921657	
H	1.8264317325	1.84	3199973	1.3197291879	
C	2.9623885958		-0.0402911863	-0.5345699178	
H	3.76	77076742	-0.7256697648	-0.8213909491	
H	3.2442641127		0.9794292259	-0.81	46713728
C	2.0298632405		-1.6288240667	0.9929713269	
H	2.8445906499	-2.3	423914932	1.1458076724	
H	1.3224359817		-1.7716654462	1.8165935658	
C	1.3	799280686	-1.8319091126	-0.4089671369	
H	1.9000713048		-2.621167768	-0.9	602356852
H	0.3264645258		-2.1187788042	-0.3604147819	
H	3.409975823	-0.	0290947727	1.6491378663	
H	1.5434921395		-0.5240476821	-2.2170100323	
SCF E = -882.6667364					
P	-0.2341744663		0.0033751883	0.82433	88998
O	-0.245405796		0.0092843432	2.3237611535	
C	1.4772546407		0.000326	8537	0.1859691363
C	2.4824729666		0.0038586507	1.1584803562	
C	1.8326380	335	-0.0049888461	-1.1687730298	

S22

C	3.8246865855	0.0021419429	0.78133565	23
H	2.191185389	0.0079715969	2.2051380802	
C	3.1733949563	-0.006688619	4	-1.5435355655
H	1.0694954171	-0.0078393432	-1.9423006102	
C	4.1708054	396	-0.0031048871	-0.5678418407
H	4.5986358452	0.0049379409	1.54237893	98
H	3.4398173797	-0.0108026224	-2.595783379	
H	5.2158137144	-0.0044206	079	-0.8619870129
C	-1.3039823192	-1.203013809	-0.1034266195	
C	-1.7953	932227	-0.003242078	-0.9884001641
H	-1.1881304817	-0.007061436	-1.9052	608427
C	-1.3031368696	1.2031261618	-0.1129458997	
C	-2.3626674882	1.78	5029169	0.8300993426
H	-1.8939845343	2.4986304261	1.5134467603	
H	-3.12	67984719	2.3134453223	0.2482755204
H	-2.8573521968	1.0330801264	1.4468	963613
C	-0.6548516162	2.3391335232	-0.8971807523	
H	-1.4170057732	2.85	14082623	-1.4977392388
H	-0.2114501024	3.0771428683	-0.2210141523	
H	0.	1291745758	1.9931392286	-1.5743815986
C	-3.2622300332	-0.0043324613	-1	.3987741569
H	-3.4946446124	0.8780427418	-2.0042074957	
H	-3.4953400289	-0.8914220213	-1.9970018833	
H	-3.9255679531	-0.0005332208	-0.52937895	49
C	-2.3639593909	-1.7766598955	0.8441565402	
H	-3.1283915276	-2.30921	80386	0.2665150891
H	-1.8958087004	-2.4850649694	1.5332526873	
H	-2.858	2126815	-1.0194503899	1.4548269706

C	-0.6564624127	-2.3456099612	-0.8786517917
H	-0.2136684976	-3.0786249635	-0.1966771
H	-1.4189160247	-2.8620125159	-1.4752859711
H	0.1278932581	-2.0054916595	-1.55844043
SCF E = -962.4474531			
P	1.2833389962	-0.3898539923	0.6108712025
O	1.6557526951	-1.3536806364	1.6987947776
C	-0.5169926102	-0.2712465974	0.4101326199
C	-1.18495013	0.7723293502	-0.2295435423
C	-1.271 6014757	-1.3348064421	0.9313645976
C	-2.5737746523	0.7652828261	-0.368 5597792
H	-0.636772494	1.6230193891	-0.6246668275
C	-2.6496536261	-1.356258396	0.8004420538
H	-0.7540586998	-2.1328498298	1.456509007
C	-3.3 077269944	-0.3071518594	0.1452295044
H	-3.0627897565	1.5939789628	-0.8 659070398
H	-3.2454695298	-2.1689494861	1.2020817953
C	2.0068262683	1. 3110663537	0.7052713032
C	2.9326941909	1.3700915824	-0.5287292409
C	2. 0525588733	-0.7123754124	-1.0369089244
H	2.5417569594	1.4087220378	1.6 538961051
H	1.2293953273	2.0806947913	0.6651296434
C	2.1279661583	0.69 36458344	-1.6578725499
H	2.6817628212	0.6769826376	-2.6034326297
H	1.1 536982388	1.1581661352	-1.8394901286
C	4.1172295035	0.3907527863	-0.35 23511665
H	4.9394763668	0.6680152079	-1.0180987426
H	4.5028351999	0.40 68704389	0.6711553655

S23

C	3.5387299107	-1.0048369886	-0.7375850424
H	4.0 21912453	-1.3917839172	-1.6400979769
H	3.6563522245	-1.7439562621	0.05 77075323
H	3.2525489483	2.3918257319	-0.7492055643
H	1.5355012997	-1.4 802466439	-1.6149056939
O	-4.6570114127	-0.4148909132	0.0658258491
C	-5.3690346002	0.6230279767	-0.5776614427
H	-5.0622191572	0.7220839812	-1.6253891434
H	-6.4195550812	0.3394761271	-0.5320111569
H	-5.225699215	1.5793222266	-0.061362765
SCF E = -997.1509048			
Si	-4.394258159	1.9231665752	0.1148453051
O	-3.0879792761	2.8766785482	0.4553729558
Si	-1.4920117288	3.2393777387	0.2252284964
H	-4.0617531403	0.5046621859	0.4036354297
H	-4.730511725	5 2.0375107634	-1.3271374183
H	-1.2777949024	3.6636225784	-1.1816045698
H	-0.6662778518	2.0307938744	0.4776688465
C	-0.9957991941	4.61290518	57 1.3942083858
DHDS			
C	0.4779337056	5.0144963916	1.2461150337
H	-1.1964219023	4.2875225178	2.4233018223
H	-1.6434091907	5.4804353	1.2121721726
C	0.8931303503	6.1356768216	2.1993348511
H	1.1217776759	4.1417656664	1.4 232584197
H	0.6752206966	5.3352037647	0.2137719949
C	2.3598339039	6.53 6062934	2.056492218
H	0.2554130458	7.0128300341	2.0219022656
H	0.6997774412	5.8181388734	3.2334209756

H	2.9960529595	5.6571283019	2.2325559649	
H	2.5521505025	6.8519348057	1.0213556422	
C	-5.8469187295	2.4691160868	1.1593824605	
C	-7.1076382755	1.6316458013	0.9055894408	
H	-6.0496701	697	3.5281142588	0.953117909
H	-5.5609637036	2.4091160645	2.2175791533	
C	-8.3012504477	2.0715249162	1.7540316053	
H	-7.386300597	1.6893527031	-0.1558092874	
H	-6.8986888038	0.5722614385	1.1094982125	
C	-9.55672429	2	1.2383227691	1.5059219795
H	-8.0277245617	2.0131410326	2.8167411338	
H	-8.5176593642	3.1292091053	1.5490547031	
H	-9.8282146467	1.2964230977	0.4423396463	
H	-9.3378565697	0.1805559739	1.7096755448	
C	2.7747713643	7.6559874275	3.0094135335	
C	4.2436438752	8.0453165274	2.8565112664	
H	2.5818280237	7.3392842184	4.0424426552	
H	2.1393083284	8.5331770905	2.8	321635424
H	4.5221618741	8.8468437983	3.5462967814	
H	4.8965288743	7.18	90073625	3.0555480364
H	4.4513791434	8.3910433403	1.8384648464	
C	-10.7	492711912	1.6774392444	2.3541364874
C	-11.9970669614	0.835264727	2.096599521	
H	-10.9671956946	2.73347927	2.1492630609	
H	-10.4765942224	1.6192528356	3.4157220355	
H	-12.8391246579	1.1637202637	2.7121415744	
H	-12.	302284962	0.9015582443	1.0470437073

H	-11.8083460131	-0.2197773986	2.3210304889
SCF E = -1129.3358608			
Si	-3.8518455845	1.8338312784	-0.3784287913
O	-2.3082942769	1.3888815821	0.0391177244
Si	-1.2119386955	1.72006921	49 1.2402286622
C	-4.7365041459	2.6181964685	1.0743801467
C	-4.9087968	475 4.0064548323	1.1779259728
H	-4.5575015731	4.6561999571	0.379070304
C	-5.5103168227	4.5713975845	2.3006562872
H	-5.6288320998	5.648923295	2 2.3660641312
C	-5.9403869912	3.7556342698	3.3464139087
H	-6.40431743	84 4.1960354721	4.2241856732
C	-5.772417666	2.3738363229	3.2655711932
H	-6.1051032556	1.7350239668	4.0781814724
C	-5.1808240573	1.8130969389	2.134586767
H	-5.0596005899	0.7322438271	2.0838908463
C	-1.5500299382	3.3995815941	1.9974848243
C	-1.2777029515	4.5584706278	1.2541403592
H	-0.8211072179	4.4769067611	0.2689921228
C	-1.5894951947	5.8228143397	1.7512558186
H	-1.3765080172	6.7075226557	1.1587859359
C	-2.1701497093	5.947145777	3.0129635733
H	-2.4109608924	6.9307556522	3.405555546
C	- 2.4434918275	4.8077232246	3.7682268655
H	-2.9078322872	4.900425889	4.7 455757202
C	-2.1414821736	3.5454893283	3.2606842102
H	-2.3840469195	2. 6637553729	3.8499982127
H	-4.5647017212	0.592784653	-0.7609934875

TPDS

H	0.	1231928738	1.7382854847	0.5997850825
C	-1.3518551017	0.3708556309	2.52	76208505
C	-0.6080082666	0.4142981013		3.716656375
C	-2.211617631	-0.71	66007224	2.3225857657
C	-0.721747284	-0.5930132286		4.6723224355
H	0.06	57182591	1.24864463	3.9051047102
C	-2.331666613	-1.7274687848	3.276378	7536
H	-2.7887251797	-0.774455121		1.4020391671
C	-1.5869180603	-1.6653	712767	4.4525026199
H	-0.139239324	-0.5424007957		5.5871967409
H	-3.002	1791091	-2.563321807	3.1005294708
H	-1.6780294098	-2.4511475963	5.1963	06323
C	-3.7241583142	3.0380405329		-1.8029089485
C	-4.8619679471	3.664	4173524	-2.3339344976
C	-2.4767369868	3.3403698509		-2.3651571203
C	-4.	7578662016	4.5656537708	-3.3911004667
H	-5.8438207181	3.4530228131	-1.	9134412422
C	-2.3655916787	4.2434973676		-3.4225549126
H	-1.584328139	2	.8582911031	-1.9719465658
C	-3.5066620499	4.8569174463		-3.9357026157
H	-5.6487675213	5.0418411146		-3.7891235155
H	-1.3910622519	4.465684125		-3.8469070071
H	-3.4229684808	5.5599058829	-4.7589807017	
SCF E = -1581.6893376				
Si	0.0315883496	1.5976476802		0.0391800535
C	1.5509530393	0.5236509991		-0.0813591342
C	1.5655302792	-0.6059654446		-0.912226556
H	0.672575159	4	-0.8779057673	-1.4725461632

Diphenylsilanol

C	2.704880318	-1.4002234113	-1.021988462	1
H	2.6993040088	-2.2724591895	-1.6686454626	
C	3.8494940217	-1.0759556	214	-0.294540897
H	4.7385096381	-1.6943639852	-0.3770156465	
C	3.849722	7179	0.0388124049	0.542295423
H	4.738364415	0.2887270994	1.1142323512	
C	2.7084141009	0.8329353189	0.6464381844	
H	2.7073822755	1.6961601063	1	.3069325277
C	-1.5169652757	0.5478531028	0.093228298	
C	-1.6494276297	-	0.4705877013	1.0510949367
H	-0.8446343653	-0.6490669398	1.7618786432	
C	-2.793704558	-1.2617635737	1.1034742151	
H	-2.8798890286	-2.044533935	1.8510776241	
C	-3.8285997097	-1.0497629246	0.191336788	
H	-4.720602544	-1.6679010167	0.2296008222	
C	-3.7155983608	-0.0468133714	-0.7687818382	
H	-4.518380187	0.1177663184	-1.4812726498	
C	-2.5675554964	0.745337990	8	-0.8129352875
H	-2.4889337136	1.5255864122	-1.5674873722	
H	-0.120038	7914	2.5164706081	-1.119306614
O	0.2661699057	2.4670536279	1.442180134	8
H	-0.397594949	3.1131089728	1.6988052613	
SCF E = -829.0356078				
Si	-3.591718638	-0.3152944631	0.0000166511	
C	-1.9987887992	0.660851197	-0	.0000274198
n-Hexylsilanol	H	-1.9929089514	1.3184173376	-0.8787259018
H	-1.99290499	1	.3184857716	0.8786200028
C	-0.7517804096	-0.2336694988	0.000003255	

H	-	0.7658097174	-0.8935462211	0.8785626556
H		-0.7658092366	-0.8936068997	-0.8785109
C		0.5552292969	0.5598075404	-0.0000234685
H	0.5761662775	1.	2183611771	-0.8794410115
H		0.5761676502	1.2184159033	0.8793531091
C	1.	7974019316	-0.3285323952	0.0000036681
H	1.7734372651	-0.9878383202	0.8	792864967
H	1.7734409844	-0.9878865713		-0.8792431647
C	3.1049891255	0.	4619097714	-0.0000148153
H	3.1279507104	1.1195006326		-0.8785069633
H	3	.1279469408	1.119547556	0.8784423364
C	4.3372802876	-0.4405316699	0.00	00124857
H	4.3463239016	-1.086936343		0.8839238981
H	4.3463295024	-1.08	69823635	-0.8838651714
H	5.2632777056	0.1411837651		0.0000003484
H	-3.6	667943365	-1.1915353562	1.1997293596
H	-3.6668208253	-1.1916056499	-1.	1996429624
O	-4.8420047414	0.788180053		-0.0000025212
H	-5.7493638241	0	.4735870868	0.000011693
SCF E = -602.8618275				

Entry	M06-2X	B3LYP
	Si 2.34452900 0.00060100 0.00346200	Si 2.35276400 0.00027100 0.00446300
	H 2.86396600 -0.91552800 -1.03993100	C 0.46954000 -0.00091000 -0.01056700
PhSiH ₃	H 2.82712300 1.37735800 -0.25376200	C -0.25787400 -1.20692000 -0.00765300
	C 0.46700000 0.00178900 -0.00804700	H 0.26763600 -2.15935900 -0.01688300
	C -0.25507700 1.20344700 -0.00605400	C -1.65507800 -1.20888200 0.00247400
	C -0.25352500 -1.20269500 -0.00599200	H -2.19519600 -2.15159700 0.00335900

C -1.65039400 1.20507600 0.00168400	C -2.35656200 0.00098100 0.00834700
H 0.27480000 2.15315900 -0.01287000	H -3.44289400 0.00130700 0.01438100
C -1.64688400 -1.20769600 0.00186200	C -1.65428300 1.20891400 0.00233700
H 0.27664400 -2.15296700 -0.01294300	H -2.19281100 2.15253900 0.00298500
C -2.34757100 -0.00128100 0.00633600	C -0.25574900 1.20517800 -0.00776900
H -2.19130600 2.14659300 0.00237700	H 0.27277700 2.15541000 -0.01695100
H -2.18619600 -2.15012900 0.00280700	H 2.88431000 -0.32522900 1.35615700
H -3.43331500 -0.00284400 0.01132100	H 2.84680400 1.34701600 -0.38274100
H 2.86359300 -0.45588700 1.31580100	H 2.88072300 -1.01406000 -0.94581400
Sum of electronic and thermal Free Energies= -522.715793	Sum of electronic and thermal Free Energies =
SCF E= -522.801231926	-522.860398
	SCF E = -522.940835531
Si 1.92552700 0.42998700 -0.30143000	Si 1.93173200 0.18448100 -0.44481100
H 2.38058600 0.25462900 -1.69459600	H 2.37341600 -0.69083900 -1.55844700
H 2.22569600 1.80676400 0.16316900	H 2.23832600 1.61164800 -0.75546900
O 2.77756900 -0.71970300 0.55398700	O 2.82183100 -0.36351800 0.86131700
H 2.58748000 -0.81278400 1.49324400	H 2.62971000 0.06286500 1.70925000
C 0.08119600 0.16818900 -0.12367400	C 0.07823500 0.06681700 -0.20016000
C -0.78268100 1.25077700 0.09392400	C -0.69518400 1.22713700 -0.01281100
C -0.47683100 -1.11669900 -0.22170400	C -0.58485100 -1.17588400 -0.19603200
C -2.16047800 1.06178100 0.20328200	C -2.07663300 1.15273000 0.17745300
PhSi(OH)H ₂ H -0.37730000 2.25635700 0.18491100	H -0.21374300 2.20305000 -0.02013400
C -1.85185000 -1.31253500 -0.10997500	C -1.96426600 -1.25617600 -0.00582300
H 0.17036800 -1.97569700 -0.38698000	H -0.01810200 -2.09262600 -0.34647700
C -2.69547300 -0.22123400 0.10092900	C -2.71190100 -0.09029300 0.18206700
H -2.81429000 1.91202600 0.37280000	H -2.65586500 2.06147900 0.31927600
H -2.26645300 -2.31298700 -0.18904500	H -2.45783700 -2.22457100 -0.00761200
H -3.76730500 -0.37217600 0.18792900	H -3.78721400 -0.15158900 0.32825600
Sum of electronic and thermal Free Energies= -597.967321	Sum of electronic and thermal Free energies= -
SCF E= -598.056463464	598.122058
	SCF E = -598.196438716

TPPO

P -0.00080800 -0.00689100 0.96189900	P -0.00454000 -0.03114800 0.89607200
O 0.00393400 -0.01256600 2.46414100	O -0.01772300 -0.16901400 2.39743200
C 0.33327300 1.63548600 0.25589100	C 0.17586600 1.68932900 0.28816900
C 1.23640500 2.45393800 0.94352200	C 1.45138000 2.27462900 0.22725000
C -0.25100300 2.08746200 -0.93122500	C -0.95036600 2.47889000 0.00781000
C 1.56071100 3.71113400 0.43959300	C 1.59727800 3.61923000 -0.11770300
H 1.67068200 2.10486800 1.87636100	H 2.33248900 1.68098300 0.45165400
C 0.07708700 3.34631400 -1.43380200	C -0.80290700 3.82429800 -0.33770900
H -0.96750400 1.46416000 -1.46000200	H -1.94464500 2.04629000 0.05955300
C 0.98316200 4.15596900 -0.75028800	C 0.47041100 4.39548400 -0.40362700
H 2.25889800 4.34520900 0.97660400	H 2.58902800 4.05987400 -0.16222800
H -0.38030800 3.69599600 -2.35387500	H -1.68203400 4.42439200 -0.55397300
H 1.23448600 5.13705200 -1.14115900	H 0.58450700 5.44155000 -0.67318900
C -1.59093000 -0.53354800 0.25392300	C -1.55211100 -0.68302600 0.15529200
C -1.69198900 -1.24252400 -0.94704700	C -1.84520300 -0.63189600 -1.21642700
C -2.75004800 -0.18002800 0.95379600	C -2.46658400 -1.28288700 1.03268100
C -2.94665800 -1.58325800 -1.45132600	C -3.03397600 -1.17762500 -1.70308600
H -0.79499900 -1.53699300 -1.48563000	H -1.15431400 -0.16213600 -1.91031400
C -4.00160100 -0.52303800 0.44787800	C -3.65704500 -1.82844800 0.54333500
H -2.66304900 0.35152100 1.89747300	H -2.23257700 -1.31124300 2.09267400
C -4.09983200 -1.22185100 -0.75592300	C -3.94109200 -1.77805300 -0.82326100
H -3.02216700 -2.13629500 -2.38217600	H -3.25305500 -1.13343100 -2.76609700
H -4.89882300 -0.25023000 0.99422100	H -4.36023200 -2.29096300 1.22998500
H -5.07552900 -1.49093300 -1.14842100	H -4.86582700 -2.20242100 -1.20388600
C 1.25355900 -1.11239100 0.24745900	C 1.37944500 -0.97675500 0.14895100
C 1.56518500 -2.27342600 0.96304200	C 2.04701200 -1.88410300 0.98428700
C 1.88665700 -0.85447000 -0.97242600	C 1.77863200 -0.85201800 -1.19081400
C 2.49550500 -3.17668200 0.45380600	C 3.09314700 -2.66358700 0.48316700
H 1.08548300 -2.45401200 1.92106500	H 1.74267400 -1.96088200 2.02384800
C 2.81578200 -1.76156200 -1.48010900	C 2.82310500 -1.63245600 -1.68971200
H 1.66338600 0.05617900 -1.52256000	H 1.28942900 -0.13751800 -1.84647700
C 3.11803900 -2.92217100 -0.76861700	C 3.48016400 -2.54105300 -0.85355500

H 2.73862300 -4.07490000 1.01240100	H 3.60604500 -3.36249700 1.13763100
H 3.30810200 -1.55795800 -2.42571200	H 3.12728500 -1.52765000 -2.72724900
H 3.84485700 -3.62527300 -1.16337800	H 4.29385300 -3.14617800 -1.24317100
Sum of electronic and thermal Free Energies= -1111.001265	Sum of electronic and thermal Free Energies= -
SCF E = -1111.23403536	1111.372496
	SCF E = -1111.59150273

Basic output information for pre-reaction complexes are included below:

Entry	M06-2X	B3LYP
	Si -2.9372160464 1.5657275156 1.286519953	Si -2.1893786731 0.4223200076
	C -3.3583586513 0.3896209332 -0.1100042512	1.9635231995
	C -4.2216764928 -0.6982883508 0.0992294902	C -2.7292137735 -0.8779511539
	H -4.7112578227 -0.8250982645 1.0630530563	0.7159229147
	C -4.4538184701 -1.6322511878 -0.906721593	C -3.9898712024 -1.4938616845
	H -5.1234905071 -2.4687012741 -0.7280836564	0.8216332931
	C -3.8197977763 -1.4957300099 -2.144840275	H -4.6597881988 -1.2211701723
	H -3.9883498173 -2.2317860301 -2.9251216422	1.6338815773
	C -2.9658200572 -0.4201385802 -2.3726117558	C -4.403439326 -2.4577508898 -
TPPO	H -2.4411735106 -0.3224055848 -3.317098659	0.1033083386
+	C -2.7459146841 0.5176320901 -1.3625094876	H -5.3813960072 -2.9210619717 -
PhSiH₃	H -2.0582239404 1.3382269863 -1.5499943097	0.0030629065
	H -2.2856200892 2.775907056 0.7319963516	C -3.557760776 -2.8224186595 -
	P 0.9113693008 -0.1654299419 -0.6591209267	1.1536230031
	O 0.2811895058 -0.4065128847 -1.9982295702	H -3.8756594109 -3.5708677356 -
	H -2.0217458352 0.9084360239 2.2548627288	1.8746553769
	H -4.16943196 1.948887642 2.0204027656	C -2.3009995447 -2.2208330116 -
	C 0.6598432874 1.5386672194 -0.0628103961	1.2732719793
	C 0.710423955 1.9056698818 1.2854981979	H -1.6391430738 -2.5010710185 -
	C 0.4521673942 2.5186401082 -1.0401427496	2.0884221987
	C 0.5747248561 3.2438403211 1.65105068	

H 0.8342491235 1.1486082122 2.0554063392	C -1.8871804098 -1.2579663274 -
C 0.3079230134 3.8543190597 -0.6712909753	0.3487558416
H 0.3977722425 2.2178994483 -2.0835432071	H -0.9051798306 -0.8033896272 -
C 0.3761345846 4.2176790047 0.67355869	0.4591943146
H 0.6092095624 3.5223577156 2.6996850525	H -1.9509101113 1.7419298602
H 0.1402756241 4.6101963052 -1.4319984003	1.3221988266
H 0.2629767129 5.2584605663 0.9607736853	P 2.4466094702 0.99681816 -
C 0.2837193482 -1.2705389355 0.6406869967	0.3986602994
C 0.9806752433 -1.5124341204 1.830639563	O 1.1407420249 0.2475795874 -
C -0.952478976 -1.8838639353 0.4197157307	0.5056072561
C 0.4261162672 -2.3344446561 2.8079294617	H -0.9385146707 0.0256513289
H 1.9641398918 -1.0751546374 1.9882057006	2.665219864
C -1.5024052094 -2.7086271298 1.400131853	H -3.2639000305 0.5802887772
H -1.4712171053 -1.7171227358 -0.5206330584	2.9813852312
C -0.8191960188 -2.9277304752 2.5943207203	C 2.1990765783 2.8066347864 -
H 0.9682711486 -2.5207253852 3.7296645924	0.2572302189
H -2.4656560544 -3.1775624846 1.2238096792	C 3.0733086718 3.6554963029
H -1.2493979901 -3.5701610929 3.356600168	0.4376201334
C 2.7161248142 -0.411724962 -0.6814383425	C 1.0613876252 3.3461767063 -
C 3.2007178556 -1.3773542903 -1.5702390597	0.8780808371
C 3.607304611 0.2921973736 0.1332635263	C 2.8210609097 5.028848132
C 4.5653099739 -1.6486038155 -1.6287564542	0.4965481457
H 2.501582845 -1.8962486706 -2.2204790142	H 3.9413268977 3.2486814791
C 4.9728575533 0.0171128923 0.0731569375	0.9479069101
H 3.2426247292 1.0666041619 0.8032533636	C 0.812563019 4.7184539415 -
C 5.4509185568 -0.9545516542 -0.8043835575	0.8178706376
H 4.9385424067 -2.3963200143 -2.3213993095	H 0.3693169035 2.6839792298 -
H 5.6627540251 0.5682009816 0.7045119394	1.3893879307
H 6.5149425818 -1.1645733951 -0.8525035713	C 1.6931079216 5.5615969524 -
Sum of electronic and thermal Energies = -1633.617606	0.1332234362
SCF E = -1634.04145	H 3.5000428057 5.6786683949
	1.0412212492

H	-0.0723206714	5.1272017364	-
	1.2969823395		
H	1.4959432069	6.6286257989	-
	0.0826909162		
C	3.4242725095	0.4860954015	
	1.064518058		
C	4.8262469049	0.518610822	
	1.1072557924		
C	2.7098332296	0.0360841771	
	2.1861957847		
C	5.5038305859	0.1216383931	
	2.2632278914		
H	5.3940889093	0.8365805597	
	0.237790514		
C	3.3901278248	-0.3602874434	
	3.3391594324		
H	1.6261832685	-0.0158801968	
	2.1436545217		
C	4.7868957519	-0.3148204036	
	3.380503346		
H	6.5895915071	0.1453693488	
	2.2865063749		
H	2.8298817285	-0.7101700813	
	4.2013231564		
H	5.3152810659	-0.6270026713	
	4.2768015203		
C	3.5209230223	0.7293015179	-
	1.8591608385		
C	3.4263019671	-0.5149523036	-
	2.5028357542		
C	4.4072450652	1.6962572247	-
	2.3562359947		

	C	4.2199031691	-0.7921597663	-	
		3.617220456			
	H	2.7183753361	-1.2518405592	-	
		2.1354544476			
	C	5.2007051583	1.4156351169	-	
		3.4722268927			
	H	4.4702115031	2.6738259469	-	
		1.8874543964			
	C	5.110306336	0.1713205999	-	
		4.1012634565			
	H	4.1384388595	-1.7561726526	-	
		4.1109708423			
	H	5.8810387134	2.1717079355	-	
		3.8535872152			
	H	5.7248272603	-0.0437668959	-	
		4.9707936118			
		Sum of electronic and thermal Energies=	-		
		1634.159891			
		SCF E = -1634.5783935			
	P	0.195266	0.681164	0.026755	
	O	0.704621	1.363926	1.286521	
	C	-0.260398	1.916751	-1.239665	
	C	0.446427	3.129929	-1.248072	
	C	-1.274485	1.699462	-2.184864	
	C	0.148744	4.107642	-2.199318	
	H	1.214358	3.307627	-0.501714	
	C	-1.568442	2.680112	-3.136038	
	H	-1.844191	0.775076	-2.175268	
	C	-0.856425	3.882947	-3.145299	
	H	0.696593	5.045277	-2.197682	
	H	-2.357284	2.506819	-3.862083	
	H	-1.08936	4.64587	-3.882433	
	P	-1.154953	0.145751	-0.439533	
	O	-0.334704	0.159785	-1.709285	
	C	-2.161386	1.645294	-0.286981	
	C	-2.537034	2.292664	-1.467263	
	C	-2.572903	2.146567	0.951703	
	C	-3.335359	3.432953	-1.406959	
	H	-2.185984	1.904467	-2.419448	
	C	-3.373311	3.285649	1.006757	
	H	-2.260229	1.655291	1.870532	
	C	-3.755418	3.925823	-0.172081	
	H	-3.624596	3.939748	-2.322152	
	H	-3.691916	3.677102	1.96768	
	H	-4.375462	4.815912	-0.127691	
TPPO +					
PhSiH₃					
(frequency					
only)					

C -1.294553 -0.328235 0.347294	C -0.108305 0.064102 1.039757
C -1.562896 -1.526569 -0.330723	C -0.380432 -0.777963 2.122107
C -2.196338 0.134945 1.319361	C 1.044538 0.857281 1.04057
C -2.727062 -2.246695 -0.047843	C 0.501317 -0.82465 3.200082
H -0.8632 -1.906599 -1.068797	H -1.264444 -1.410045 2.114114
C -3.357479 -0.587108 1.599174	C 1.926827 0.801554 2.115677
H -1.980237 1.051008 1.860595	H 1.266156 1.491378 0.185706
C -3.624903 -1.777205 0.91457	C 1.654343 -0.039881 3.194013
H -2.926342 -3.176043 -0.57321	H 0.296244 -1.485799 4.036134
H -4.048309 -0.225242 2.354842	H 2.834792 1.396605 2.095892
H -4.526763 -2.340381 1.136168	H 2.347252 -0.09155 4.028347
C 1.442124 -0.427565 -0.719975	C -2.283841 -1.270866 -0.332887
C 2.269226 -1.162821 0.146834	C -1.793285 -2.512779 -0.757058
C 1.599439 -0.563768 -2.10781	C -3.582914 -1.165124 0.171622
C 3.233609 -2.027512 -0.374304	C -2.605097 -3.64057 -0.668525
H 2.171645 -1.051444 1.222676	H -0.784193 -2.593457 -1.156811
C 2.566122 -1.431553 -2.623621	C -4.388906 -2.299535 0.259061
H 0.980119 0.011354 -2.789012	H -3.969711 -0.200953 0.489864
C 3.382323 -2.164593 -1.758146	C -3.899985 -3.535308 -0.16006
H 3.871552 -2.588811 0.301822	H -2.226589 -4.601542 -1.002023
H 2.684323 -1.52743 -3.698954	H -5.398791 -2.214809 0.647744
H 4.135967 -2.835509 -2.160193	H -4.530187 -4.417178 -0.096592
Si 1.531847 0.726057 4.986429	Si 2.578033 -2.013745 -0.60248
H 0.086047 0.932134 5.291468	H 2.035191 -2.167788 0.776287
H 2.049543 -0.347286 5.87541	H 3.385014 -3.216224 -0.911472
C 2.418943 2.351134 5.33894	C 3.661673 -0.478662 -0.622666
C 1.909213 3.265694 6.279017	C 4.713337 -0.332221 0.292792
C 3.629865 2.672751 4.697382	C 3.419114 0.564258 -1.52542
C 2.584695 4.453466 6.576256	C 5.496698 0.819988 0.313688
H 0.968109 3.055506 6.78359	H 4.919636 -1.124307 1.01172
C 4.307988 3.860579 4.985917	C 4.195494 1.724301 -1.506941
H 4.042414 1.991205 3.957543	H 2.603773 0.477654 -2.241078

C 3.787434 4.752395 5.929129	C 5.234797 1.853527 -0.587025
H 2.171362 5.145681 7.304966	H 6.308044 0.914893 1.029668
H 5.239609 4.090845 4.47587	H 3.990382 2.525071 -2.211465
H 4.313039 5.676305 6.154628	H 5.841541 2.754119 -0.573364
H 1.74438582 0.28420371 3.74182697	H 1.61640781 -1.9412594 -1.52955287
Sum of electronic and thermal energies = -1634.148507	Sum of electronic and thermal energies = -
SCF E = -1634.56580789	1633.612537
	SCF E = -1634.03515765
P 0.15701600 0.69676400 0.02924700	P 0.1952661685 0.6811642502
O 0.63098100 1.39920900 1.28771500	0.0267548931
C -0.28052800 1.91692800 -1.26035900	O 0.7046212082 1.3639259535
C 0.39108800 3.14926200 -1.23252800	1.2865212252
C -1.24574700 1.67663900 -2.24967500	C -0.2603983865 1.9167512539 -
C 0.11093200 4.12139500 -2.19459600	1.2396646136
H 1.11459700 3.34323500 -0.44669200	C 0.4464272402 3.1299285705 -
C -1.52235300 2.65176300 -3.21132700	1.2480715392
H -1.79386200 0.73911500 -2.26431500	C -1.2744853488 1.6994615233 -
C -0.84254400 3.87268800 -3.18638100	2.1848636843
H 0.63130800 5.07422100 -2.16516400	C 0.1487440131 4.1076424533 -
H -2.27350100 2.46066000 -3.97222400	2.199317752
H -1.06202400 4.63135900 -3.93213600	H 1.2143582578 3.3076272995 -
C -1.33503000 -0.31728900 0.32954400	0.5017135887
C -1.60706200 -1.50379100 -0.36716100	C -1.5684418076 2.6801117114 -
C -2.23337600 0.13147700 1.31080500	3.1360382103
C -2.77329800 -2.22454600 -0.09599800	H -1.844190821 0.7750758923 -
H -0.90558200 -1.87619500 -1.10780500	2.1752677877
C -3.39656100 -0.59145600 1.57910100	C -0.8564247058 3.8829472518 -
H -2.00853800 1.03542000 1.86875500	3.1452989372
C -3.66908800 -1.76802200 0.87428200	H 0.6965932122 5.0452774378 -
H -2.97539700 -3.14537500 -0.63538000	2.1976818041
H -4.08474200 -0.24128700 2.34279400	H -2.3572837389 2.5068189681 -
H -4.57257500 -2.33214600 1.08720000	3.8620829485

TPPO +
PhSi(OH)H₂

C 1.42140000 -0.41673100 -0.68204900	H -1.0893599623 4.6458702242 -
C 2.24490900 -1.12538500 0.21015800	3.8824329242
C 1.59470300 -0.58156100 -2.06488000	C -1.2945531294 -0.3282351455
C 3.22035600 -1.99377600 -0.28371600	0.3472939947
H 2.13973200 -0.98860900 1.28275100	C -1.5628964357 -1.5265691871 -
C 2.57254300 -1.45298100 -2.55188700	0.330723113
H 0.98085000 -0.02259900 -2.76448800	C -2.1963384141 0.1349446556
C 3.38421100 -2.16103600 -1.66204600	1.3193609708
H 3.85614100 -2.53412400 0.41137200	C -2.7270624754 -2.2466949351 -
H 2.70365500 -1.57057000 -3.62370000	0.0478427836
H 4.14709900 -2.83495200 -2.04135900	H -0.8631996617 -1.9065989372 -
Si 1.62381700 0.68740400 4.96594700	1.0687971067
H 0.18925200 0.83741300 5.34938900	C -3.3574789855 -0.5871082368
H 2.21784600 -0.39793300 5.78902700	1.5991741464
C 2.47387700 2.32974500 5.33194400	H -1.9802367245 1.0510076027
C 1.97994500 3.19940200 6.32104800	1.8605946406
C 3.64250100 2.70976200 4.64611000	C -3.6249034224 -1.7772054113
C 2.63030700 4.39949200 6.62323000	0.9145697996
H 1.06975800 2.94363500 6.86027900	H -2.9263416709 -3.1760433123 -
C 4.29545200 3.90989600 4.93978000	0.5732104854
H 4.03967400 2.06371300 3.86700000	H -4.0483093168 -0.2252422744
C 3.79154700 4.75624200 5.93206700	2.3548417791
H 2.22939900 5.05654200 7.39054300	H -4.5267634339 -2.3403810911
H 5.19491100 4.18544300 4.39540500	1.1361682813
H 4.29777900 5.68998300 6.16175600	C 1.4421237864 -0.4275650523 -
O 1.82793300 0.20907600 3.39364200	0.7199753389
H 1.38614400 0.71665400 2.67106600	C 2.269225929 -1.1628211085
Sum of electronic and thermal Free Energies= --	0.1468342182
1709.525079	C 1.5994391871 -0.5637677211 -
SCF E = -1709.86181457	2.1078095349
	C 3.2336087514 -2.0275119471 -
	0.3743037805

H	2.1716448862	-1.0514435551	
	1.2226761758		
C	2.5661221893	-1.4315534744	-
	2.6236211412		
H	0.9801190877	0.0113537787	-
	2.7890124019		
C	3.3823230493	-2.1645930652	-
	1.7581455358		
H	3.8715518938	-2.5888105129	
	0.3018219776		
H	2.6843225726	-1.5274303927	-
	3.6989538517		
H	4.1359673432	-2.8355091638	-
	2.1601926125		
Si	1.5318471098	0.7260571486	
	4.9864290006		
H	0.0860466226	0.9321336835	
	5.291468115		
H	2.0495434965	-0.3472861262	
	5.8754100202		
C	2.418943497	2.351134345	
	5.3389400542		
C	1.9092128192	3.2656941721	
	6.2790172335		
C	3.6298652222	2.6727507042	
	4.6973815973		
C	2.5846952772	4.453466341	
	6.5762560835		
H	0.9681088737	3.0555060352	
	6.7835896008		
C	4.3079875932	3.8605794557	
	4.9859165525		

H	4.0424142095	1.9912046036
	3.9575428758	
C	3.787433761	4.7523949357
	5.929128698	
H	2.1713621178	5.1456809021
	7.3049664023	
H	5.2396086716	4.0908454147
	4.4758702722	
H	4.313039209	5.6763047556
	6.1546275651	
O	1.795157332	0.1786536977
	3.4445171452	
H	1.3907988528	0.6642286287
	2.6834391572	
Sum of electronic and thermal Free		
Energies= -1709.532694		
SCF E=-1709.8681023		
